IVANE JAVAKHISHVILI TBILISI STATE UNIVERSITY

MIKHEIL NODIA INSTITUTE OF GEOPHYSICS

GEORGIAN GEOPHYSICAL ASSOCIATION

TECHNICAL UNIVERSITY OF GEORGIA

INSTITUTE OF HYDROMETEOROLOGY

# 2nd INTERNATIONAL SCIENTIFIC CONFERENCE

# "MODERN PROBLEMS IN GEOPHYSICS"

**Tbilisi, Georgia, October 29-31, 2026**

# PROCEEDINGS



2026 – Tbilisi

**IVANE JAVAKHISHVILI TBILISI STATE UNIVERSITY**

**Mikheil Nodia Institute of Geophysics**

**Georgian Geophysical Association**

**TECHNICAL UNIVERSITY OF GEORGIA**

**Institute of Hydrometeorology**

# 2nd INTERNATIONAL SCIENTIFIC CONFERENCE

# "Modern Problems in Geophysics"

**Tbilisi, Georgia, October 29-31, 2026**

## PROCEEDINGS

უნივერსიტეტის გამომცემლობა

**Scientific Committee and Editorial Board**

**Tamaz Chelidze:** Academician, Chairman of the Scientific Committee, Editor-in-Chief;
**Nodar Varamashvili, Jemal Kiria:** Co-Chairmans of the Scientific Committee – TSU, M. Nodia Institute of Geophysics, Georgia;
**Nana Bolashvili**: Co-Chairman of the Scientific Committee – TSU, Vakhushti Bagrationi Institute of Geography, Georgia;
**Mikheil Pipia:** Co-Chairman of the Scientific Committee – GTU, Institute of Hydrometeorology, Georgia;
**Avtandil Amiranashvili:** Deputy Editor-in-Chief;
**Aliev Vugar –** CEO & Founder, International Event Organizer Company AMIR Technical Services Azerbaijan, Azerbaijan;
**Davitashvili Magda –** I. Gogebashvili Telavi State University, Telavi, Georgia;
**Fórizs István** – Institute for Geological and Geochemical Research, Hungary;
**Ghlonti Nugzar, Melikadze George –** TSU, M. Nodia Institute of Geophysics, Georgia;
**Japaridze Nino –** Tbilisi State Medical University, Georgia;
**Kartvelishvili Liana –** National Environmental Agency, Georgia;
**Khazaradze Ketevan –** Georgian State Teaching University of Physical Education and Sport, Georgia;
**Nazaretyan Sergey –** Regional Survey for Seismic Protection, Ministry of Internal Affairs of the Republic of Armenia, Armenia;
**Rustioni Laura, Pappaccogli Gianluca –** University of Salento, Italy;
**Tatishvili Marika, Meladze Maia –** GTU, Institute of Hydrometeorology, Georgia;
**Varazanashvili Otar** – TSU, M. Nodia Institute of Geophysics, Georgia;
**Vaupotič Janja –** Jožef Stefan Institute, Slovenia.

**Organizing Committee**

**Ekaterine Mepharidze:** Chairman of Organizing Committee;
**Manana Nikolaishvili:** Deputy Chairman of Organizing Committee;
**Aleksandre Sborshchikovi, Thea Gventsadze, Sophiko Matiashvili, Dimitri Amilakhvari, Dimitri Tepnadze, Levan Laliashvili** – TSU, M. Nodia Institute of Geophysics, Georgia;
**Nino Taniashvili –** Georgian Geophysical Association, Georgia;
**Nazibrola Beglarashvili –** GTU, Institute of Hydrometeorology, Georgia;
**Inga Janelidze –** Georgian Technical University, Georgia.

© Publish Hous of Iv. Javakhishvili Tbilisi State University, 2026

ISBN 978-9941-36-562-1

ISSN 3088-4349

2nd International Scientific Conference "Modern Problems in Geophysics", Proceedings,
ISBN 978-9941-36-562-1, ISSN 3088-4349, Tbilisi, Georgia, October 29-31, 2026

# COMPARATIVE ANALYSIS OF THE 2023 SHOVI AND 2026 NEPAL CATASTROPHES

**Kereselidze Z., Varamashvili N.**

*M. Nodia Institute of Geophysics of the I. Javakhishvili Tbilisi State University, Tbilisi, Georgia*
*nodar.varamashvili@tsu.ge*

***Abstract.*** *A comparative analysis of the disasters in Shovi (Georgia, 2023) and on the Nepal-Tibet border (2026) reveals a similar genesis for the hazardous nival-glacial processes in these high-mountain regions, yet shows a stark contrast in the scale of their consequences. Shovi (2023): A catastrophic event. Intense melting of the Buba and Tbilisa glaciers – driven by climatic anomalies and exacerbated by heavy precipitation – triggered a landslide process that rapidly transformed into a destructive debris flow. Nepal (2026): Likely a cascading geological-geophysical process. The disaster began with a massive glacial collapse on Langtang Lirung Peak. An avalanche of ice and rock blocked the river channel, resulting in a sudden outburst flood and a debris flow with distinct rheological characteristics. Thus, from a rheological perspective, there is a clear resemblance between these two catastrophes. Consequently, the hydrodynamic description of the debris flow process observed at Shovi is highly likely to be applicable to modeling the catastrophic debris flow that occurred in Nepal.*

***Key Words****: Glacier, Debris-flow, Hydrodynamics, Rolling waves, Froude numbers.*

## Introduction

We believe that, during the comparative analysis, special attention should be paid to the mechanical trigger that caused the disaster in Nepal. The mechanism of ice mass detachment described for the Jankuati Glacier which is linked to the effects of global warming may prove useful in addressing this issue[1]. Therefore, it is highly probable that this mechanism, which we applied to the Shovi disaster, is also relevant on a global scale, specifically regarding the disaster in Nepal; hence, we present an excerpt from our study [2]. We believe that, similar to the issue of subglacial water reservoirs, it would be rational to take into account certain findings from other relevant publications concerning glacier studies when planning the expedition to the Tbilisi Glacier. This applies primarily to the study [1], which presents the results of a multi-decade expedition to the Djankuat Glacier. That work generalizes findings significant for the study of other glaciers in the Central Caucasus – effectively treating Djankuat as a reference glacier from a methodological standpoint. Clearly, the validity of such a statement should be assessed by a circle of specialists in the field. However, the study [1] indeed contains significant information regarding the modeling of processes affecting medium-sized glaciers. In this context, the conclusion concerning changes in the parameters of the Djankuat Glacier against the backdrop of climate change is particularly valuable. We believe it is reasonable to extrapolate this conclusion to all glaciers located in the vicinity of Djankuat. According to the study, climate change has led to a reduction in ice volume in the upper part of the Djankuat Glacier, yet the glacier's surface area has increased at elevations between 3,000 and 3,100 meters. This phenomenon is attributed to intensified ice-fall processes at the glacier's head, resulting from the reduction in ice thickness. Naturally, such an effect would lower the stability threshold at the glacier's head. If we generalize this specific case, we conclude that the warming effect likely exerts a particularly strong influence on the upper reaches of glaciers, where the terrain slope is typically steeper than in the lower sections. In the case of the Buba and Tbilisa Glacier, this implies a real possibility that catastrophic events – driven by natural mechanisms distinct from the current ones – could occur in the future within the Bubastskali and Chanchakhi valleys. Furthermore, a table illustrating the quantitative changes in the parameters of the Djankuat Glacier since the 1960s provides insight into the probable quantitative shifts in the characteristics of the Tbilisi Glacier over the same period.

## Waves modeling

To model river flow in mountain gorges, a specific system of hydrodynamic equations – the so-called shallow-water equations (Saint-Venant equations) – is employed. The hydrodynamic criteria for the applicability of these equations define the conditions under which the three-dimensional Navier-Stokes or Euler equations can be simplified to two-dimensional (or one-dimensional) equations. The physical significance of these criteria lies in the requirement that the vertical scale of the river flow (depth) must be much smaller than the horizontal scale (longitudinal channel non-uniformity or wavelength).

Among the waves generated in mountain gorges during catastrophic floods – such as the disaster in Nepal – the most destructive are known as "rolling waves." Beyond mountain gorges, they frequently occur in steep artificial channels, spillways, or during heavy rainfall runoff on roads. In specific sections of the flood channel, these waves are modeled using the shallow-water equations. The generation of rolling waves of varying intensity is mathematically governed by the Froude number, a key criterion for the hydrodynamic instability of flood flows. It is established that critically high values of this dimensionless parameter correspond to the most intense long-period rolling waves. To accurately simulate such waves, terms accounting for bed friction and turbulent viscosity must be included in the Saint-Venant equations.

For sufficiently high Reynolds numbers, following the standard transformation to dimensionless variables and hydrodynamic flow parameters, the system of simplified one-dimensional shallow-water equations consists of two equations: continuity and momentum. For flow along an incline involving a fluid characterized by generalized turbulent bed friction and Bingham rheology, the shallow-water equations in the one-dimensional approximation take the form [3, 4].

$$\frac{\partial}{\partial x}h + \frac{\partial}{\partial x}(hu) = 0\,\frac{\partial}{\partial x} \tag{1}$$

$$\frac{\partial}{\partial x}(hu) + \frac{\partial}{\partial x}\left(hu^2 + \frac{gh^2}{2}\cos\varphi\right) = gh\sin\varphi - C_w\,u^2 \tag{2}$$

where $h, u$ – average fluid depth and velocity; $\varphi$ – channel slope. The first equation represents the continuity of the medium, while the second describes the flow in an inclined channel. The single dimensionless parameter α is related to the Froude number: Fr= √α where α= tgφ/$C_w$, $C_w$- the coefficient of friction, which for simplicity is assumed to be constant, φ- channel slope.

Typically, in certain sections of virtually any flood-prone channel, the primary criterion for the applicability of shallow-water equations is amply satisfied – namely, the ratio of the characteristic flow depth to the horizontal scale (such as wavelength or the size of a channel irregularity) is small. This condition allows for reasonably accurate modeling of roll waves, even within a one-dimensional approximation. At sufficiently high Reynolds numbers, where the flow is highly turbulent, the roll wave front takes the form of a steep hydraulic jump. It should be noted that if the channel is roughly approximated as a rectangular conduit, one can utilize qualitative insights from analytical and numerical solutions derived for specific types of waves generated in river flows. This applies, in particular, to roll waves, where the Froude number plays a decisive role in determining their intensity [3, 4]. During the disaster in Nepal, this value likely exceeded the range typical of the Lhende Khola river's normal flow regime, driven by a sharp increase in flow depth and an extreme rise in velocity ***(Lhende Khola:*** *The initial debris avalanche and water surge from the glacier collapse on Langtang Lirung entered this tributary first;* ***Bhote Koshi:*** *The floodwaters fed from the Lhende Khola into the Bhote Koshi near the border area;* ***Trishuli:*** *The main destructive surge traveled along a massive 72-kilometer stretch of the Trishuli River through Rasuwa, Nuwakot, and Dhading districts;* ***Narayani / Gandak River:*** *Further downstream, the Trishuli flows into the Narayani River, crossing into India where it is known as the Gandak River and affecting downstream regions like Bihar)*, Undoubtedly, the debris flow's rheological properties were altered by the massive load of fragmented rock debris, which actively influenced the flow dynamics. This effect was likely most pronounced in the final, widest section of the gorge, where the viscoplastic nature of the debris flow fully manifested itself. In any case, the Froude number is indisputably the dimensionless hydrodynamic parameter that serves as an indicator of the destructive power of propagating long hydrodynamic waves. The following classification can be used to assess this effect: 0.3≤Fr≤ 0.5. It is known that with such a flow structure in an inhomogeneous liquid, so-called gravity (density) waves can be generated;

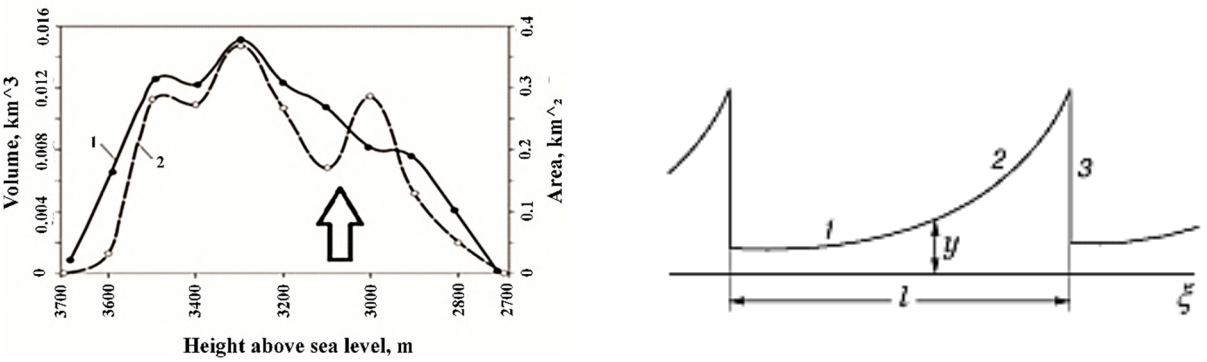
0.9<Fr<1.1 According to the Kadomtsev-Petviashvili equation, for such Froude numbers, with a balance of the influence of linear dispersion, nonlinearity and spatial effects, the generation of solitons (solitary waves) is possible.

Fr≤2. In this case, according to the shallow water equations, as a result of the effect of turbulent friction on the channel bottom, so-called linear rolling waves can be generated. For these waves, the critical value is Fr=2, which determines the threshold for the development of linear instability and a noticeable increase in amplitude;

Fr>2. At a sufficiently large Re, a nonlinear stage of increasing flow instability develops. This case corresponds to a certain critical channel depth, in which a picture of a turbulent flow arises. So-called depression waves appear in the liquid, as well as rolling waves with hydraulic jumps, which facilitate a change in the flow regime from supercritical to subcritical (section 3 in Fig.1b).

2<Fr<6. In a turbulent flow, a modulation effect may arise involving traveling packets of nonlinear rolling waves averaged over certain spatial and temporal scales.

Clearly, among the various types of waves mentioned above, giant rolling waves are of the greatest interest. A solution to the shallow-water equations exists for them, depending on the variable $\xi = x - Dt$ (where D is the wave speed). A distinctive feature of this solution is the presence of a smooth segment in the wave trajectory representing the transition from subcritical to supercritical flow (sections 1 and 2; Fig. 1b).




a. b.

**Fig. 1.** a) Area of ice zones with a thickness of 100 meters (1) and ice volume within them (2) for the Jankuat Glacier [1] and b) Rolling waves [5].

This section is defined relative to a coordinate system moving at the wave speed D and indicates the existence of a hydraulic jump (section 3; Fig. 1b) that transitions the flow from supercritical to subcritical.

## Conclusion

Two disasters – Shovi 2023 and Nepal 2026 – are strikingly comparable from geological and geophysical perspectives.

In the authors' view, the opinions expressed in the article are equally applicable to the disasters in both Shovi and Nepal. The Shovi disaster can be seen as a miniature natural laboratory for understanding the class of disasters typical of the Himalayas, rather than merely as another glacial disaster.

The paper explicitly states that the experience gained from the Shovi event should be utilized for retrospective modeling and for developing theoretical models of potential flood and debris flows in other mountain valleys.

## References


1. Lavrentev I.I., Kutuzov S.S., Petrakov D.A., Popov G.A., Thickness, subglacial topography, and ice volume of the Djankuat Glacier. // Ice and Snow, N 4, 2014, pp. 26-34. (in Russian)
2. Kereselidze Z., Varamashvili N., Possible causes of Shovi (Georgia) catastrophe. // Transactions of Mikheil Nodia Institute of Geophysics, v. LXXVI, 2023, pp. 134 -148. (in Georgian)
3. Kereselidze Z. A., Varamashvili N. D., On the Issue of Generation of Hydrodynamic Waves in the Shovi Gorge (Georgia) due to a Collapse on Glacier Tbilisa. // Journal of the Georgian Geophysical Society, v. 26(2), 2023, pp. 22 – 29.
4. Kereselidze Z. A., Varamashvili N. D., On the Issue of Modelling the Dynamic Picture of the Spread of a Mudflow in the Shovi Gorge due to a Collapse on the Glacier Buba. // Journal of the Georgian Geophysical Society, v. 27(2), 2024, pp. 48–62.
5. Lyapidevsky V.Yu., Teshukov V.M., Mathematical models of the propagation of long waves in an inhomogeneous liquid. // Novosibirsk, Publishing House SB RAS, 2000, 420 p. (in Russian)

2nd International Scientific Conference "Modern Problems in Geophysics", Proceedings,
ISBN 978-9941-36-562-1, ISSN 3088-4349, Tbilisi, Georgia, October 29-31, 2026

# SOME REASONS FOR THE INCREASE IN SEISMIC RISK OF RESIDENTIAL BUILDINGS IN ARMENIA IN 1920-2020

***Nazaretyan S., **Igityan H., ***Kazarian H., ***Harutyunyan R., ****Mirzoyan L., **Bakunts S., **Petrosyan V.**

** Territorial Survey for Seismic Protection of the Ministry of Internal Affairs of the Republic of Armenia, Yerevan, Armenia*

*** National Polytechnic University of Armenia, Yerevan, Armenia*

**** Institute of Geological Sciences of the National Academy of Sciences of Armenia, Yerevan, Armenia*

***** Yerevan State University, Yerevan, Armenia*

*snaznssp@mail.ru*

***Abstract.*** *Based on three primary causes of high seismic risk in Armenia – underestimation of seismic hazard in seismic-resistant design standards, poor construction quality, and illegal structural modifications to standard apartment buildings – the vulnerability of the main types of residential buildings is assessed, and the period of rising risk is identified. The article provides recommendations for reducing the risk of residential buildings.*

***Key words:*** *Seismic hazard, vulnerability, risk.*

## Introduction

The Spitak earthquake of 1988 (M=7.0, I=10; H=10 km) showed that at seismic intensity of 8 and 9 points by MSK-64, massive damage of the 4th (partial destruction) and 5th (complete destruction) degrees was sustained in apartment buildings of the "Stone series IA-450" and "Frame-panel series 111" structural types. The most earthquake-resistant buildings were large-panel buildings of 4-9 stories and 1-2-story stone private houses of the "midis" system on cement and lime mortar. These buildings received damage of 1-2 degrees with 9-point shaking. For example, in the city of Gyumri, where the intensity of the earthquake averaged 9 points, 7,000 people died due to the collapse of buildings of the "Frame-panel series 111" type, and in 20,000 stone private houses (of which 1,500 were 100 years old or older), which received minor damage, the number of victims was 300 people [6].

The risk depends mainly on the seismic hazard of the area and the vulnerabilities of its elements (buildings, structures, people, etc.). It is known that seismic hazard assessments (according to earthquake-resistant construction standards) and the vulnerability of buildings and structures (depending on the structural type, quality of design and construction, illegal alterations to buildings, obsolescence of the structure, etc.) have changed over time, as a result of which the seismic risk has changed. Residential buildings last for quite a long time (70–100 years); therefore, their influence on the level of seismic risk in Armenia has a long history. From this point of view, it is important to study the dynamics of changes in seismic risk and identify the causes of the high risk that has been forming over a fairly long period of time. Often, especially in developing countries, there are a considerable number of buildings that were designed on the basis of an underestimated seismic hazard value, or were built with violations of construction regulations (construction technologies were not followed, building materials did not meet the required standards, construction was carried out with deviations from the approved design, etc.), the seismic vulnerability of which is difficult to determine. Thus, the main reasons for the high seismic risk of the territory of Armenia are numerous, but the most important are the following: underestimation of seismic hazard before 2020; poor quality of design and construction of buildings and structures. In this paper, we add to these causes errors made during the operation of buildings, particularly alterations and structural damage. Our research has shown that the impact of this factor on the seismic resistance of typical buildings is quite significant [7,8,9].

## Results

### *Underestimation of seismic hazard for 1937–2020 based on standard seismic hazard maps*

From 1937 to 2020, Armenia had 8 earthquake-resistant construction standards (Table 1), on the basis of which state-sector buildings were designed and constructed. Until 1937, all buildings, including capital ones, were constructed based on centuries of construction experience. The level of seismic hazard in all building standards was underestimated. For example, in the territory of the city of Spitak, the intensity of the 1988 Spitak earthquake was 10 points according to the MSK-64 scale, and, according to the current norm, the hazard was assessed at 7 points [6]. From Table 1, it follows that, over time, the minimum level of seismic hazard in the territory of Armenia, according to construction norms, increased from 6–7 points (1937) to 8–9 points (2020). Such underestimation of seismic hazard played a major role in the vulnerability of buildings and structures, especially before 1989.

**Table 1.** Squares and quantities of seismic zones by intensity according to normative seismic hazard maps of the territory of Armenia for 1937–2020.

| Year of issuance of norms | Squares of seismic zones with a certain intensity, thousand km² | | | |
|---|---|---|---|---|
| | 6 points | 7 points | 8 points | 9 points and higher |
| 1937 | 9.1 | 12. 2 | 8. 5 | – |
| 1949 | 1.2 | 17. 1 | 11.5 | – |
| 1957 | 1.0 | 12.9 | 15.9 | – |
| 1968 | – | 5.6 | 24.2 | – |
| 1978 | – | 12.7 | 17.1 | – |
| 1989 | – | – | 3.4 | 26.4 |
| 1994 | – | 15.2 | 19.7 | 9.9 |
| 2020 | – | – | 21.4 | 8.4 |

## Quality of construction of apartment buildings

The 1988 Spitak earthquake revealed serious deficiencies in the design and construction of buildings and structures. Various commissions investigating the causes of the destruction of state sector buildings concluded that not a single typical residential building design in Armenia met the required design standards. Particularly serious violations of construction regulations were committed, the most typical being the following: failure to comply with construction technology, the use of construction materials that did not meet the required standards , construction carried out with deviations from the approved project, etc. [2,3,5,6]. Most experts believe that the main reason for the destruction of typical apartment buildings as a result of the 1988 Spitak earthquake was the poor quality of construction.

## Illegal alterations to buildings leading to a decrease in the seismic resistance of buildings

The 1988 Spitak earthquake revealed the true scale of violations of building operation standards by residents. There were especially numerous alterations to the structure of the ground floors of buildings , which led to a decrease in the seismic resistance of the entire building. Without permission from the relevant executive authorities, without the conclusion of a licensed organization, residents damaged or made "alterations" to structural elements. Among the most common violations of building operation rules were the creation of basements below the building's foundation, damage to the integrity of foundations, dismantling or moving partitions, damage to load-bearing walls and columns, "creation" of cabinets in walls by demolishing the inner layer of capital walls, etc., which significantly reduced their seismic resistance [6,9]. Research has found that in the city of Gyumri, 10% of stone buildings were destroyed due to the fault of residents due to such alterations. After the 1988 Spitak earthquake, the republic's government took a number of steps to prevent

unauthorized renovations in apartment buildings (such as tightening requirements, issuing renovation permits based on reports from licensed organizations, etc.). However, these measures prohibited new renovations without eliminating existing ones.

## Seismic vulnerability of the main types of residential buildings in Armenia

It is extremely difficult to determine the seismic vulnerability of buildings constructed with the above-mentioned deficiencies. Therefore, we propose assessing the vulnerability of such buildings based on statistical data on damage sustained during the 1988 Spitak earthquake, depending on its intensity. Table 2 presents all 8 structural types of multi-story buildings in Armenia [4] and their seismic vulnerability [7] at an earthquake intensity of 9,which corresponds to the standard hazard level of the territory of most cities in Armenia [1].

**Table 2.** The main structural types of multi-story buildings in Armenia, their brief description and probable seismic vulnerability at an earthquake intensity of 9 points (0.40 g) [7,8].

| N | Constructive type | Number of floors | Constraction period | Brief description of designs | Seismic vulnerability |
|---|---|---|---|---|---|
| 1. | Stone, individual project | 3 – 6 (mostly 4) | Before 1958 | Midis- type masonry (stone is laid on both sides; the middle is filled with lime mortar and crushed stone). Wall thickness is 60 cm. Wooden floors and ceilings , concrete stairs. | Average |
| 2 | Stone series I -451 | 4 – 5 | 1958 – 1970 | 50- cm- thick M idis walls with cement mortar and prefabricated hollow-core concrete panels are used. Anti-seismic belts are installed between floors and around the ceilings. | Average |
| 3 | Stone series IA-450 | 4 – 5 | Beginning of 1970 – beginning of 1988 | Midis-type masonry with cement mortar, constructed using prefabricated hollow-core concrete panels. Seismic barriers are installed between floors and around the ceilings. The walls are reinforced with vertical reinforced concrete elements. | High |
| 4 | Frame-panel series 111, factory-made reinforced concrete frame | 9 | 1975 – 1988 | A load-bearing reinforced concrete frame in the longitudinal direction, columns and structural panels (walls) in the transverse direction. Column cross-section is 40x40 cm. Factory-made hollow-core panels. | High |
| 5 | By the "floor lifting " method | 12 and 16 | 1970 – 1988 | Walls with a monolithic core and factory-built columns with monolithic floor panels. The floor panels are lifted into position using the columns. | High |
| 6 | Frame-braced types of Badalyan and Manukyan | Badalyan type – 12 (10) and 14 (18); Manukyan type – 12 (10) floors | 1960 – 1988 | Prefabricated reinforced concrete frames for both directions. Column cross-sections are 50x50 cm (Badalyan type) or 40x40 cm (Manukyan type). These buildings have been shown to be stronger than frame-and-panel structures due to the position of the reinforcement joints. In the Spitak earthquake zone of 1988, there were no buildings of these types | Average |
| 7 | Large-panel series 1-451KP | 5 and 9 (including 4 and 8) | 1970 G. – present day | Factory wall, reinforced concrete structure | Low |
| 8 | Monolithic reinforced concrete supporting frame | 4 and above | 1989 and after 1994 G. | The load-bearing frame is monolithic reinforced concrete, including the walls. The structures were designed based on the new seismic standards of the Republic of Armenia of 1994. The non-load-bearing walls are lightweight concrete blocks. | Low |

*Note: During a intensity 9 earthquake,* ***low-vulnerability*** *buildings sustain damage of grades 1–2 and can remain in use. Buildings with* ***moderate*** *vulnerability generally sustain damage of grade 3, their safe use is not guaranteed and these buildings must be reinforced.* ***Highly*** *vulnerable buildings sustain damage of grades 4–5, unless they are historical or architectural monuments, it is more cost-effective to demolish them.*

Fig. 1 shows the main construction periods of typical multi-apartment buildings, indicating their degree of seismic vulnerability. It is clear that the most vulnerable buildings were constructed between 1957 and 1989. Unfortunately, it was during this period that the majority of highly vulnerable buildings were constructed. This is the main reason for the high seismic risk in modern Armenia.

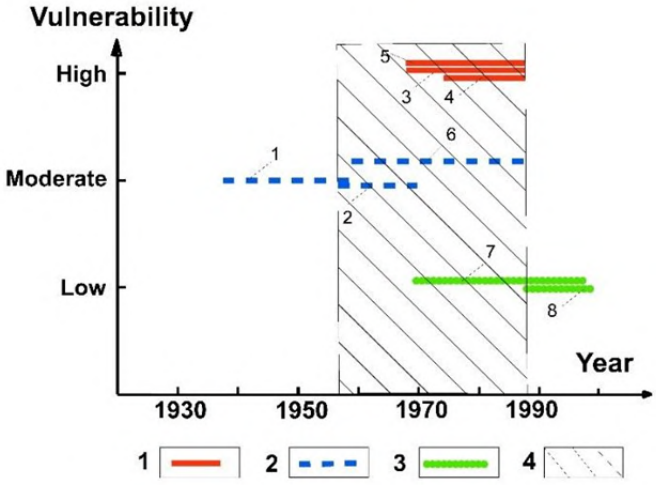



**Fig. 1.** Construction time and seismic vulnerability levels of typical multi-apartment buildings in Armenia (the numbering of building types and their vulnerability levels is presented according to Table 2). Vulnerability of buildings: 1 – highly vulnerable; 2 – moderately vulnerable; 3 – low vulnerability; 4 – construction period of highly vulnerable and moderately vulnerable building types (1957-1989).

## Conclusion

1. Three important reasons for the high seismic risk of multi-apartment buildings in Armenia are considered. These reasons include underestimation of seismic hazard according to seismic design standards, poor construction quality, and unauthorized structural modifications to standard building designs.
2. Highly vulnerable apartment buildings constructed between 1957 and 1989 contribute significantly to the high level of seismic risk in Armenia. These include the following building types: IA-450 series masonry buildings, 111 series frame-panel buildings, and structures erected using the lift-slab method. As large numbers of people reside in these buildings, the issue must be addressed through either demolition or structural reinforcement in compliance with 2020 regulatory standards.
3. The Urban Development Committee of the Republic of Armenia (UDCRA) should pay particular attention to the quality of new construction.
4. The UDCRA should pay particular attention to the quality of new construction.
5. Any unauthorized structural modifications to existing buildings must be strictly prohibited. Special commissions should inspect all apartment buildings; where structural alterations or damage are identified, appropriate remedial measures must be taken.

## References

1. Armenia: Probabilistic Seismic Hazard Assessment. // Last Updated: July 14, 2023. https://data.opendata.am/dataset/sustc-979
2. Borcherdt R.D., Results and data from seismological and geological studies of the earthquakes of December 7, 1988, near Spitak, Armenia. // USGS Publications Warehouse // Open-File Report, 1989, 189 p. DOI: 10.3133/ofr89163A

3. Cisternas A., Philip H., Arefiev S.S., Bousquet J.C., The Spitak earthquake of 7 December 1988: Field observations, seismology and tectonics. // Nature, 339, 1989, pp. 675-679. DOI: 10.1038/339675a0
4. Japan International Cooperation Agency (JICA). Project for Seismic Risk Assessment and Risk Management Planning in the Armenia. // JICA Final Report, Vol. II: Main Report, 2012, 76 p. ttps://openjicareport.jica.go.jp/pdf/12086054_01.pdf
5. Khachiyan E.E., The Spitak Earthquake of December 7, 1988: Main Seismological characteristics and analysis of its destructive Consequences. // Earthquake-resistant construction. Safe Structure, 4, 2018, pp. 9–30. (in Russian) https://bik.sfu-kras.ru/elib/view?id=PRSV-seis/2018/4
6. Nazaretyan S.N., Seismic hazard and risk of the territory of cities in the Spitak earthquake zone of 1988 (Ed. Prof. S.S. Darbinyan). // Monograph: Publishing House “Gitutyun” NAS RA. 2013, 205 p. (in Russian)
7. Nazaretyan S.N., Gevorgyan M.R., Igityan H.A., Mirzoyan L. B., Mughnetsyan E. A., Dynamics of Time Changes in the Seismic Risk of a Big City Due to the Vulnerability of Apartment Buildings (a Case Study of Yerevan). // Atmosph Ocean Physics, 58(8), 2022, pp. 867–880.
8. Nazaretyan S.N., and Igityan H.A., Assessment of the Maximum Seismic Risk for the Territory of Armenia. // Seismic Instruments, Vol. 61, No. 3, 2025, pp. 232–244. DOI: 10.3103/S0747923925700367
9. Nazaretyan S.N., Tatoyan S.S., Zakaryan N.G., Guide to identifying and excluding illegal changes in the construction of multi-apartment buildings in RA, which reduce their seismic resistance. // Monograph: Publishing House Eldorado print, Gyumri, 2022, 48 p. (in Armenian)

2nd International Scientific Conference "Modern Problems in Geophysics", Proceedings,
ISBN 978-9941-36-562-1, ISSN 3088-4349, Tbilisi, Georgia, October 29-31, 2026

# NEW APPROACHES TO SEISMIC HAZARD ASSESSMENT IN SECOND-GENERATION EUROCODE 8: FROM PGA TO SPECTRAL REPRESENTATION

**Tsereteli N.**

*M. Nodia Institute of Geophysics of the I. Javakhishvili Tbilisi State University, Tbilisi, Georgia*
*nino_tsereteli@tsu.ge*

***Abstract.*** *This paper examines the spectral representation of seismic hazard in second-generation Eurocode 8, focusing on $S_\alpha$ and $S_\beta$ and their role in defining the horizontal elastic response spectrum. Revised site parameters $v_{S,H}$ and $H_{800}$ are briefly outlined. The approach is illustrated for rock conditions in Tbilisi for the 475-year return period (approximately 10% probability of exceedance in 50 years), yielding $S_{\alpha,475}$=0.888g and $S_{\beta,475}$ = 0.181g.*

***Key Words****: Eurocode 8, seismic hazard, spectral acceleration, response spectrum.*

## Introduction

The current regulatory framework for seismic hazard assessment in Georgia continues to rely on the SZ-09 seismic zoning map incorporated in the national seismic design regulation PN 01.01-09 [1]. However, this map has significant methodological limitations and does not adequately represent current estimates of seismic hazard [5]. More recent probabilistic seismic hazard models for Georgia have been developed independently by two research teams: one led by Tbilisi State University in cooperation with European partners [5], and another involving Ilia State University and international collaborators [6]. Despite these advances, the updated hazard models have not yet been incorporated into the national regulatory framework.

At the same time, the second generation of Eurocodes introduces substantial changes in the representation of seismic hazard and in the characterisation of local ground conditions. In EN 1998-1-1:2024 [2], reference seismic hazard is specified in terms of two spectral acceleration parameters, $S_\alpha$ and $S_\beta$, rather than being represented by PGA alone. These parameters govern the principal features of the horizontal elastic response spectrum. The revised standard also introduces a site-categorisation scheme based on the shear-wave velocity profile and the depth to seismic bedrock.

The present study focuses primarily on the first of these developments: the spectral representation of seismic hazard, the definition of $S_\alpha$ and $S_\beta$, and their role in defining the horizontal elastic response spectrum. The revised approach to site characterisation is considered only briefly. The methodology is then illustrated for rock conditions at a selected site in Tbilisi for a 475-year return period, corresponding approximately to a 10% probability of exceedance in 50 years.

## Spectral Acceleration Parameters Sα and Sβ

Second-generation Eurocode 8 characterises reference seismic hazard by two spectral acceleration parameters, $S_\alpha$ and $S_\beta$ [2]. $S_\alpha$ is the maximum 5%-damped response spectral acceleration associated with the constant-acceleration range of the horizontal elastic response spectrum, whereas $S_\beta$ is the 5%-damped response spectral acceleration at the vibration period $T_\beta$, with $T_\beta$=1.0 s as the default value. The two parameters therefore constrain different parts of the spectrum and provide a more complete representation of seismic hazard than PGA alone.

For the European informative hazard maps derived from ESHM20, $S_{\alpha,475}$ and $S_{\beta,475}$ were evaluated from the median 5%-damped Uniform Hazard Spectrum (UHS) for a 475-year return period [3,4]. At each location, the period $T_{peak}$ corresponding to the maximum ordinate of the median UHS is first identified. $S_\alpha$ is then evaluated as the mean spectral acceleration over the interval $0.5T_{peak}$ to $1.5T_{peak}$:

$$0.5T_{peak} \leq T \leq 1.5T_{peak}$$
$$S_\alpha = \frac{1}{T_2 - T_1} \int_{T_1}^{T_2} S_a(T)\, \mathrm{d}T$$
$$T_1 = 0.5T_{peak}, T_2 = 1.5T_{peak}$$

For discrete UHS ordinates, the averaging is performed by trapezoidal integration. Consequently, $S_\alpha$ is not simply the peak UHS ordinate, but a representative spectral level around the short-period maximum. $S_\beta$, in contrast, is obtained directly from the UHS at the reference period:

$$S_\beta = S_a(T_\beta), T_\beta = 1.0\ \mathrm{s}$$

Together, $S_\alpha$ and $S_\beta$ provide complementary information on the spectral characteristics of seismic action: $S_\alpha$ defines the constant-acceleration level of the elastic spectrum, whereas $S_\beta$ anchors its intermediate-to-long-period range and, through the ratio $S_\beta/S_\alpha$, contributes to the definition of the spectral shape.

The use of two independent spectral acceleration parameters is particularly important because ground motions with similar PGA values may exhibit markedly different spectral shapes and therefore impose different demands on structures with different natural periods. While PGA mainly reflects the very-short-period level of ground motion, Sα and Sβ constrain the response spectrum over distinct period ranges. Their combined use therefore provides a more informative basis for representing seismic hazard in engineering applications than a single PGA value [4,6].

## Horizontal Elastic Response Spectrum and Corner Periods

The horizontal elastic response spectrum $S_e(T)$ is defined by the two spectral acceleration parameters $S_\alpha$ and $S_\beta$ together with four corner periods, $T_A$, $T_B$, $T_C$, and $T_D$ [2]. $T_A$ marks the end of the very-short-period range, $T_B$ the beginning of the constant-acceleration plateau, $T_C$ its upper corner period, and $T_D$ the transition to the constant-displacement branch.

The upper corner period of the constant-acceleration range is directly controlled by the ratio between the two hazard parameters:

$$T_C = \frac{S_\beta T_\beta}{S_\alpha}$$

For the standard spectrum, $T_B$ is related to $T_C$ through the spectral-shape parameter $\chi$, with $\chi$=4, subject to the specified bounds for $T_B$. The recommended values $T_A$=0.02s and $F_A$=2.5 define the very-short-period branch, with

$$PGA_e = \frac{S_\alpha}{F_A}$$

Between $T_A$ and $T_B$, $S_e(T)$ increases linearly from $PGA_e$ to $S_\alpha$. The spectrum remains constant at $S_\alpha$ between $T_B$ and $T_C$, decreases proportionally to 1/T between $T_C$ and $T_D$, and follows a $1/T^2$ decay beyond $T_D$. These branches correspond to the constant-acceleration, approximately constant-velocity, and constant-displacement ranges of the idealised elastic spectrum [2]. The horizontal elastic response spectrum according to the second-generation Eurocode 8 is presented in Fig. 1.

## Revised Characterisation of Local Ground Conditions

A further important change in second-generation Eurocode 8 concerns site characterisation. The classification is no longer based on $V_{S30}$ alone, but considers both the equivalent shear-wave velocity $v_{S,H}$ and the depth $H_{800}$ to the seismic bedrock formation, identified by $V_S \geq 800$ m/s [2]. The equivalent shear-wave velocity is defined as

$$v_{S,H} = \frac{H}{\Sigma \frac{h_i}{v_i}}, H = \min(30\ \mathrm{m}, H_{800})$$

where $h_i$ and $v_i$ are the thickness and shear-wave velocity of the i-th layer. If $H_{800} \geq 30$ m, $v_{S,H}$ corresponds to $V_{S30}$; when seismic bedrock occurs at a shallower depth, the equivalent velocity is evaluated only down to

$H_{800}$. The site categories A–F are therefore defined jointly in terms of the stiffness of the near-surface profile and the depth to seismic bedrock. Direct measurement of the $V_S(z)$ profile is preferred for site categorisation [2].

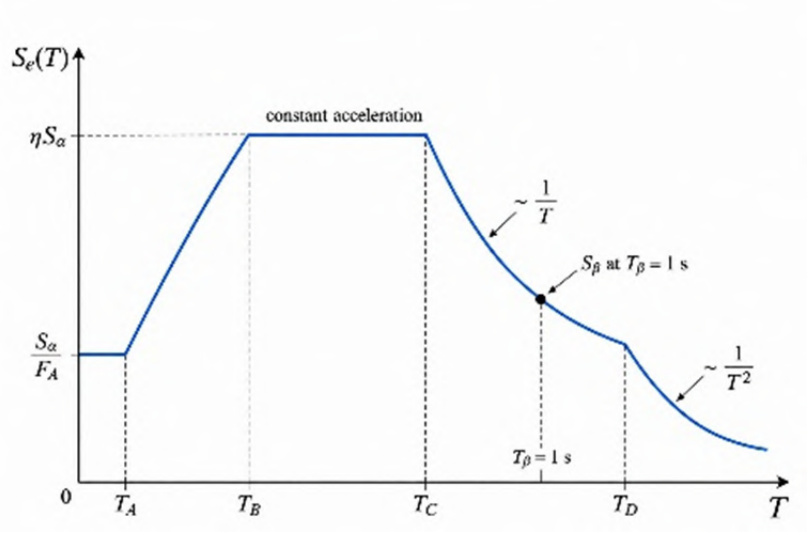



**Fig. 1.** Horizontal elastic response spectrum $S_e(T)$ and characteristic periods $T_A$, $T_B$, $T_C$, and $T_D$.

## Illustrative Application to Tbilisi

The procedure was applied to a selected site in Tbilisi under rock conditions, with $V_{S30}$=801 m/s. The analysis refers to a return period of 475 years, equivalent to approximately a 10% probability of exceedance in 50 years. The resulting spectral parameters and the corresponding elastic response spectrum are presented in Fig. 2.

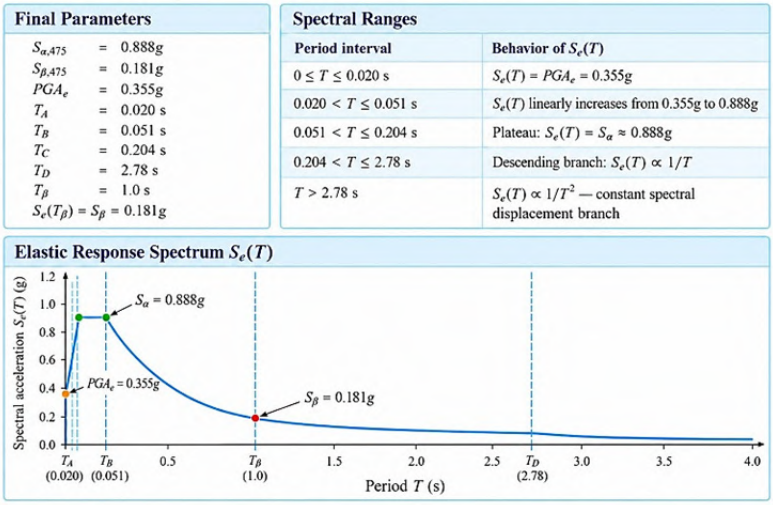



**Fig. 2.** Elastic response spectrum derived for rock conditions at the selected Tbilisi site for a 475-year return period.

For the 5%-damped UHS, the maximum spectral acceleration occurs at $T_{peak}$=0.15 s. Accordingly, $S_{\alpha,475}$ was evaluated over the interval 0.075 s≤T≤0.225 s using trapezoidal integration of the discrete UHS ordinates. The resulting spectral acceleration parameters are

$$S_{\alpha,475} = 0.888\text{g}, S_{\beta,475} = S_a(1.0\text{ s}) = 0.181\text{g}$$

Using these values and the recommended spectral parameters gives

$$PGA_e = 0.355\text{g}, T_C = 0.204\text{ s}, T_B = 0.051\text{ s}, T_D = 2.78\text{ s}$$

The example illustrates the transition from a single PGA-based descriptor to a two-parameter spectral representation in which both the short-period spectral level and the intermediate-to-long-period behaviour are explicitly constrained.

## Conclusion

Application of the methodology to the selected Tbilisi site demonstrates how $S_\alpha$ and $S_\beta$ can be derived from a 475-year UHS and used to define the corresponding Eurocode elastic response spectrum. For the analysed rock site, $S_{\alpha,475}$=0.888g and $S_{\beta,475}$=0.181g. The results demonstrate the practical applicability of the second-generation Eurocode 8 framework under Georgian conditions and the shift from a single PGA-based descriptor toward a more complete spectral representation of seismic hazard.

**Acknowledgment:** This study has been funded by project FR-23-10514 of the Shota Rustaveli National Science Foundation of Georgia (SRNSFG).

## References

1. Government of Georgia. Decree No. 71 of 15 January 2014, Technical Regulation "Seismic Resistant Construction" (PN 01.01-09), Tbilisi, Georgia.
2. CEN. EN 1998-1-1:2024, Eurocode 8 – Design of structures for earthquake resistance – Part 1-1: General rules and seismic action. European Committee for Standardization, Brussels, 2024.
3. Danciu L., Giardini D., Weatherill G., Basili R., Nandan S., Rovida A., Beauval C., Bard P.-Y., Pagani M., Reyes C.G., Sesetyan K., Vilanova S., Cotton F., Wiemer S., The 2020 European Seismic Hazard Model: overview and results. // Natural Hazards and Earth System Sciences, Vol. 24, 2024, pp. 3049–3073. DOI: 10.5194/nhess-24-3049-2024.
4. Labbé P., Paolucci R., Developments relating to seismic action in the Eurocode 8 of next generation. // In: Vacareanu R., Ionescu C. (eds.), Progresses in European Earthquake Engineering and Seismology. Springer, Cham, 2022, pp. 26–46. DOI: 10.1007/978-3-031-15104-0_2.
5. Tsereteli N., Danciu L., Varazanashvili O., Sesetyan K., Qajaia L., Sharia T., Svanadze D., Khvedelidze I. The 2020 National Seismic Hazard Model for Georgia (Sakartvelo). // In: Bonali F.L., Mariotto F.P., Tsereteli N. (eds.), Building Knowledge for Geohazard Assessment and Management in the Caucasus and Other Orogenic Regions. NATO Science for Peace and Security Series C: Environmental Security, Springer, Chapter 8, 2021, pp. 131–168. DOI: 10.1007/978-94-024-2046-3_8.
6. Onur T., Gok R., Godoladze T., Gunia I., Boichenko G., Buzaladze A., Tumanova N., Dzmanashvili M., Sukhishvili L., Javakishvili Z., Cowgill E., Bondár I., Yetirmishli G., Probabilistic Seismic Hazard Assessment Using Legacy Data in Georgia. // Seismological Research Letters, Vol. 91, No. 3, 2020, pp. 1500–1517. DOI: 10.1785/0220190331.

2nd International Scientific Conference "Modern Problems in Geophysics", Proceedings,
ISBN 978-9941-36-562-1, ISSN 3088-4349, Tbilisi, Georgia, October 29-31, 2026

# MODELLING THE EVOLUTION OF MAIN CHARACTERISTIC PARAMETERS OF THE BUBA, TBILISA, AND CHANCHAKHI GLACIERS UNDER CURRENT CLIMATE CHANGE CONDITIONS

***Amilakhvari D., **Davitashvili T.**

** M. Nodia Institute of Geophysics of Iv. Javakhishvili Tbilisi State University, Tbilisi, Georgia*
*** I. Vekua Institute of Applied Mathematics of Iv. Javakhishvili Tbilisi State University, Tbilisi, Georgia*
*ditoamilaxvari@gmail.com*

***Abstract****. This study investigates the evolution of key characteristics of the Buba, Tbilisa, and Chanchakhi (BTC) glaciers during the 21st century, using the Open Global Glacier Model (OGGM v1.6.0) and remote sensing data. The modelling workflow included the delineation of glacier outlines, reconstruction of glacier topography, identification of glacier centerlines and flowlines, simulation of mass-balance dynamics, estimation of ice thickness, and modelling of glacier flow. The results indicate that all three glaciers have been experiencing a sharp mass deficit since the 1990s. Model calculations demonstrate a substantial and accelerating reduction in both the area and volume of the BTC glaciers under the applied climate scenario: forward projections for 2020–2040 suggest that the Chanchakhi glacier will virtually disappear by 2030–2035, while the Buba and Tbilisa glaciers will lose the vast majority of their area and volume by approximately 2040. Furthermore, structural analysis revealed deep basal ice reservoirs exceeding 120 meters in thickness – located in the upper cirque of the Tbilisa glacier and the lower elevation zone of the Buba glacier. Under high subglacial water pressure and steep slope conditions, these deep reservoirs act as primary triggering and amplifying factors for high-magnitude debris flows.*

***Key words:*** *OGGM modelling, Mass balance, Glacier dynamics, Glacial hazards.*

## Introduction

Current global climate change and rising temperatures are leading to the rapid degradation of high-mountain permafrost and glacial cover worldwide [1,2]. The glaciers of the Caucasus, particularly in recent decades, have been experiencing intensive retreat and shrinkage in area (at a rate of approximately 0.5% per year) [1]. The loss of glacier mass and resulting slope instability are directly linked to the activation of catastrophic geodynamic processes, including rock-ice avalanches and glacial debris flows [1,2]. On August 3, 2023, a severe natural disaster occurred in the Oni Municipality, around the Shovi resort area [3]. A massive torrent of mud and rock moved down the bed of the Bubistskali River, spreading over an area of more than 26 hectares within approximately 15 hours and claiming 32 lives. Notably, no flood or mudflow events of comparable scale had been observed in the Bubistskali River bed over the past 100 years [1]. A global disaster with a similar cascading mechanism unfolded in August 2026 in the Nepal Himalayas (Langtang region), where high-altitude glacier and slope collapse, coupled with the instantaneous mobilization of subglacial water and debris material, generated devastating debris flows [2]. These events demonstrate that evaluating high-mountain cascading hazards is virtually impossible without full-scale glaciological investigations and numerical modeling [1,3]. The objective of this study is to perform numerical simulations of the past, present, and future evolution of the Buba, Tbilisa, and Chanchakhi (BTC) glaciers across the 1900–2100 timeframe using the Open Global Glacier Model (OGGM).

## Data and Methodology

The study is based on the **OGGM v1.6.0** modular, 1D/1.5D numerical model, which utilizes the **Randolph Glacier Inventory (RGI v6.0)** and **GLIMS** databases, the **SRTM/NASADEM DEM** for surface topography, and **CRU TS/ERA5** gridded climate datasets calibrated against local observations from the Oni meteorological station. Within the OGGM framework, geometrical centerlines are identified using the Kienholz algorithm (Kienholz et al., 2014). The surface mass balance ($m_i$) is simulated using a temperature-index melt model:

$$m_i(z) = P_f P_i^{Solid}(z) - \mu^* \max(T_i(z) - T_{melt}, 0)$$

where $P_i^{Solid}(z)$ is the solid precipitation amount at elevation z, $P_f$ is the precipitation factor, $\mu^*$ is the temperature sensitivity (melt) factor, and $T_i(z)$ and $T_{melt}$ denote the air and threshold melt temperatures, respectively. Meanwhile, the ice thickness (h) is determined by inverting mass conservation combined with Glen's flow law (n=3). The depth-integrated mean velocity (U) is calculated using the shallow ice approximation (SIA):

$$U = \frac{2A}{n+2} h\tau^n$$

Where A is the ice creep parameter, $n = 3$, $h$ is the ice thickness, and $\tau$ is the basal shear stress.

## Results of OGGM calculations

OGGM simulations revealed distinct morphometric and structural differences among the studied glaciers. Specifically, the Buba glacier features a single primary flowline and a relatively homogeneous structure, with its main and thickest ice reservoir (~100–120 m thick) located in the lower reach between 3000 and 3600 m a.s.l. In contrast, the Tbilisa glacier exhibits a complex geometry characterized by a distinct tributary, two flowlines, and its deepest basal reservoir (~120–140 m thick) confined to the upper high-altitude cirque at approximately 3800 m a.s.l. The Chanchakhi glacier is a simple valley glacier with a single centerline, where ice thickness reaches 40–60 m in its upper and lower sectors while remaining around 25–30 m throughout the central section.

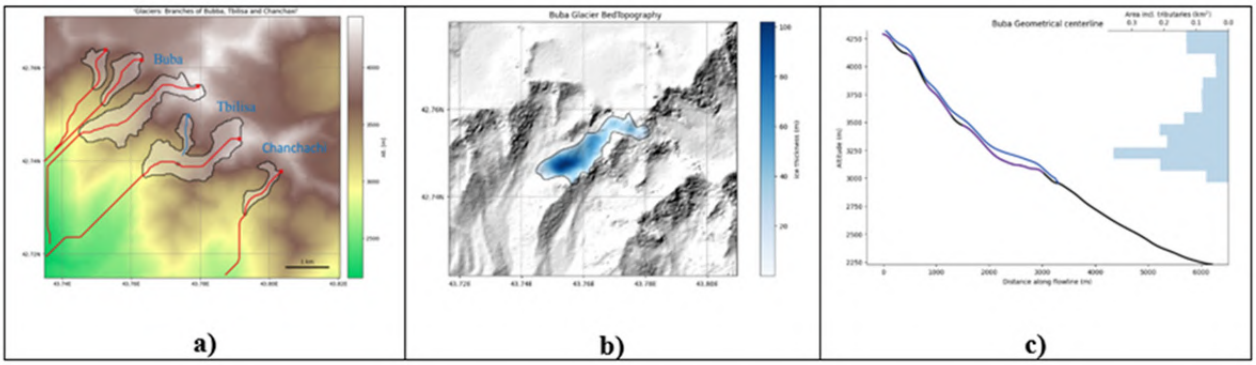



**Fig. 1.** (a) Morphometric and topographic characteristics of the studied glaciers simulated by the OGGM model: Outlines and flowlines of the Buba (single flowline), Tbilisa (two flowlines with a tributary) and Chanchakhi (single flowline) glaciers over the digital elevation model; (b) Bed topography and spatial distribution of ice thickness for the Buba glacier, showing the main overdeepened ice reservoir (~100–120 m deep) in the lower reach; (c) Longitudinal bed profile along the geometrical centerline of the Buba glacier and glacier area distribution with elevation (hypsometry).

Ice flow dynamics indicate high velocity and intensive mass displacement within the central and lower zones of the Tbilisa glacier. For the Buba glacier, modeled velocity vectors range from 5 to 50 m/yr and are directed toward the northwest, suggesting active basal sliding and vulnerability to mechanical impacts from destabilized western lateral slopes.

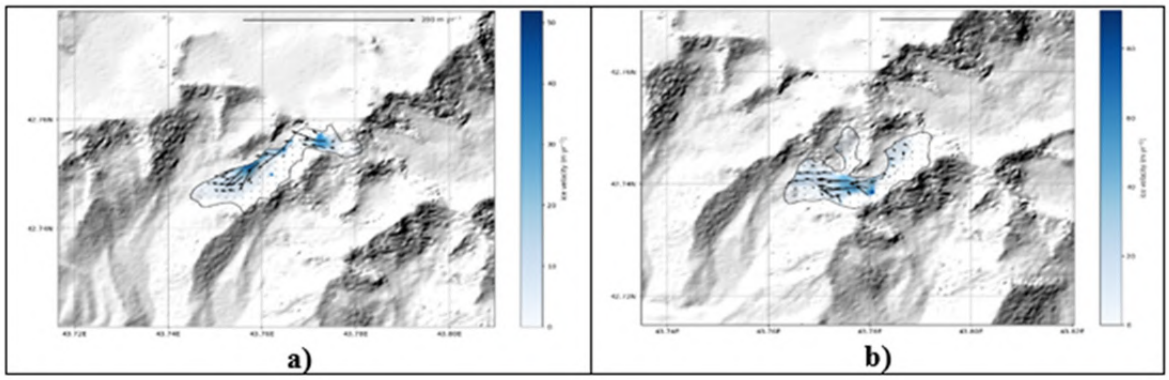



**Fig. 2.** Modeled depth-integrated ice velocity vectors and spatial distribution of surface flow speeds simulated by the OGGM model: Buba glacier, exhibiting flow velocities ranging from 5 to 50 m $yr^{-1}$ oriented northwestward toward its lateral margin, indicative of active basal sliding; Tbilisa glacier, highlighting high dynamic activity and accelerated mass displacement within its central overdeepened basin.

The long-term specific mass balance (MB) series (1900–2020) exhibits strong coherence across all three glaciers. The period from 1900 to 1985 is characterized by multi-decadal oscillations around zero that roughly coincide with 11-year solar cycles, showing pronounced local minima around 1915, 1920, and 1960. This was followed by a sharp mass gain and a marked lowering of the Equilibrium Line Altitude (ELA) between 1985 and 1990. However, after 1990, a continuous and steep upward migration of the ELA toward 3700–3800 m a.s.l. took place, culminating in 2019 when mass accumulation completely ceased on the Chanchakhi glacier even at its highest elevation of 3800 m a.s.l.

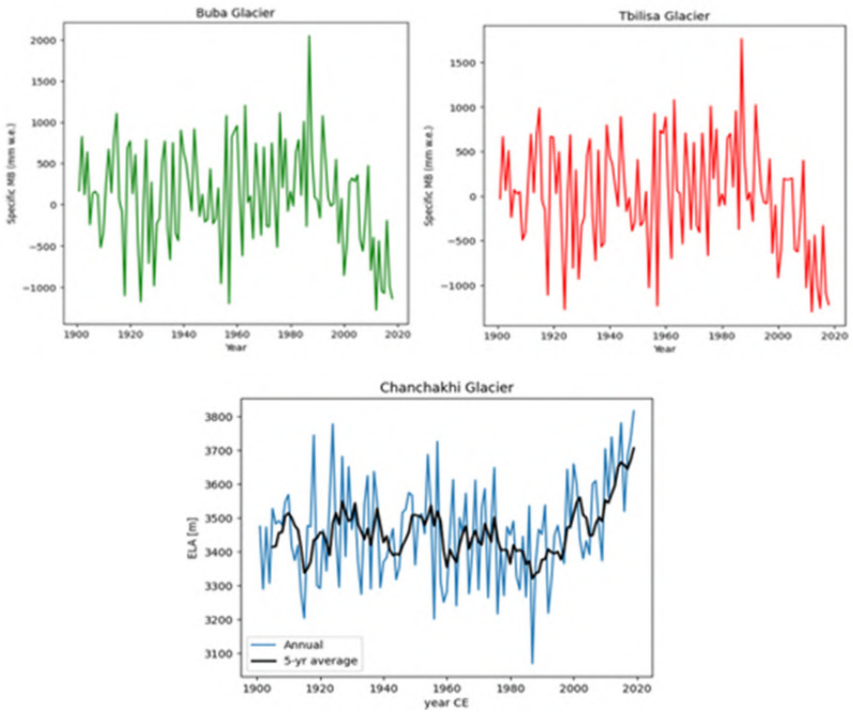



**Fig. 3.** Long-term climate-driven mass balance indicators simulated by the OGGM model (1900–2020): Annual specific mass balance (Specific MB in mm w.e.) for the Buba and Tbilisa glacier, exhibiting multi-decadal oscillations around zero prior to 1985, a prominent accumulation peak in the late 1980s, and a sharp, continuous mass deficit post-1990; Equilibrium Line Altitude (ELA in m a.s.l.) variations for the Chanchakhi glacier, showing annual values (blue line) and the 5-year moving average (black line), which highlights a pronounced, persistent upward migration toward 3700–3800 m a.s.l. since the 1990s, indicating severe ablation area expansion.

Forward simulations of glacier area (S) and volume (V) up to 2100 identify four successive evolutionary stages: a minor increase and stabilization during 1980–2000; progressive retreat during 2000–2024; **a critical collapse phase spanning 2024–2040**, during which the Buba glacier shrinks from 1.7 to 0.8 km² in area and

from 0.06 to 0.02 km³ in volume, the Tbilisa glacier drops in volume from 0.077 to 0.015 km³, and the Chanchakhi glacier virtually vanishes by 2030–2035; followed by a post-2040 stage of low-magnitude volumetric stagnation.

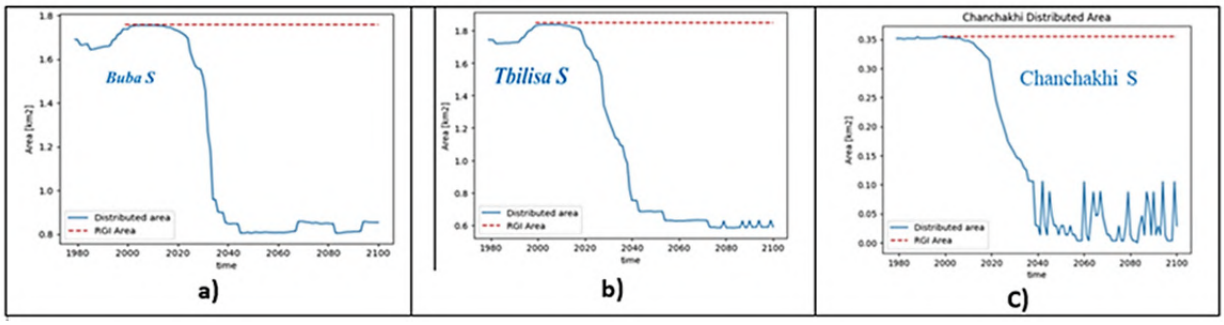



**Fig. 4.** Modeled glacier area evolution and forward projections (S in k$m^2$) from 1980 to 2100 simulated by the OGGM model: **(a)** Buba glacier, exhibiting a sharp area reduction from approximately 1.7 to 0.8 k$m^2$ during the critical 2024–2040 collapse window; **(b)** Tbilisa glacier, experiencing a dramatic contraction from 1.8 to 0.7{ k$m^2$ across the same period; **(c)** Chanchakhi glacier, undergoing rapid deglaciation post-2020 and virtually losing its permanent glacier cover by 2040. The horizontal red dashed lines denote the baseline year 2000 glacier areas extracted from the Randolph Glacier Inventory (RGI), demonstrating close agreement with the modeled distributed area.

## Conclusion

This research was motivated by the catastrophic landslide that occurred on August 3, 2023, in the Georgian resort of Shovi, which resulted in the complete destruction of the resort and the deaths of at least 32 people. The disaster was associated with the intense melting of the Buba and Tbilisa glaciers, enhanced erosional processes, rock falls at the headwaters of the glaciers, increased glacier runoff, and the formation of large debris flows. Field investigations by the National Environmental Agency (NEA) and subsequent satellite and seismic analyses confirmed that the event initiated on the steep slope of the Tbilisa glacier's right tributary (~3850 m a.s.l.) with the failure of approximately 1 million m³ (0.001$km^3$) of rock and ice. Our OGGM numerical modeling revealed that this failure site coincides with the deepest basal ice reservoir of the Tbilisa glacier (>120 m), where pressurized subglacial water underwent rapid hydraulic displacement upon impact, drastically accelerating the devastating debris-flow discharge. A remarkably identical cascading mechanism was manifested in August 2026 in the Nepal Himalayas (Langtang region), verifying that such occurrences are not isolated anomalies, but systemic geodynamic hazards driven by accelerated global climate warming. As the first comprehensive numerical assessment of the Buba, Tbilisa, and Chanchakhi glaciers using the OGGM framework, this study demonstrates an accelerating reduction in glacier area and volume, projecting the near-complete disappearance of both Buba and Tbilisa by approximately 2040. Given that the Buba glacier also harbors a massive basal reservoir in its lower reaches, continued glacial retreat, altered meltwater drainage, and destabilized slopes will maintain an elevated risk of mass-movement cascades in the Shovi area, strongly underscoring the necessity of proactive numerical modeling and long-term monitoring across the high-mountain valleys of the Caucasus.

## References

1. Davitashvili T., Samkharadze I., Amilakhvari D., Chikhradze N., Svanadze D., Rukhaia G., Study of Certain Glaciers in the Caucasus (Georgia) Based on the OGGM Modeling and Remote Sensing Data Amid Regional Climate Change. // "Universal" publishing house, UDC 551.32. D – 151, 2025, 398 p.
2. 2026 Nepal Debris Avalanche and Flash Flood ACTIVE. By Landslide Hazards Program August 27, 2026. https://www.usgs.gov/programs/landslide-hazards/science/2026-nepal-debris-avalanche-and-flash-flood
3. Davitashvili T, Amilakhvari D. // Study of dynamics of some glaciers of the Caucasus using the future-oriented OGGM model. // Proceedings of the International Conference on Future-Oriented Models of Special Education (ICFOMSE – 26), 30th – 31st January 2026, Yerevan, Armenia, 2026, pp. 34-39.

2nd International Scientific Conference "Modern Problems in Geophysics", Proceedings,
ISBN 978-9941-36-562-1, ISSN 3088-4349, Tbilisi, Georgia, October 29-31, 2026

# MUDFLOW IN TELAVI (GEORGIA) ON JULY 12, 2026

**[*]Amiranashvili A., [*]Chikhladze V., [**,***]Samkharadze I., [**]Pipia M.**

**M. Nodia Institute of Geophysics of the I. Javakhishvili Tbilisi State University, Tbilisi, Georgia*
***Institute of Hydrometeorology of Georgian Technical University, Tbilisi, Georgia*
****LEPL State Military Scientific-Technical Center "Delta", Tbilisi, Georgia*
*avtandilamiranashvili@gmail.com*

***Abstract.*** *A preliminary analysis was conducted regarding the appearance of severe mudflow and flooding triggered by heavy rainfall, which affected the city of Telavi and surrounding areas in the Kakheti region of Georgia. Radar observation data indicated that rainfall intensity near the debris-retention structures in the Telaviskhevi River gorge – located close to the entrance to Telavi – may have been significantly higher than the levels recorded at the weather station situated approximately 7 km away. A comparison was made with a similar incident that occurred on June 14, 1977.*

***Key Words:*** *Natural disasters, atmospheric precipitation, radar measurements, mudflow.*

## Introduction

Georgia experiences virtually all types of natural disasters (earthquakes, floods, hurricanes, thunderstorms, hail, droughts, landslides, mudflows, avalanches, tornadoes, forest fires, etc.), which often cause significant economic damage and lead to loss of life [1–6]. Notably, landslides and mudflows are frequently associated with heavy precipitation [5, 6]. The last such example is the mudflow process that occurred on July 12, 2026, in the Kakheti region.

On this day, according to various press sources (https://www.apsny.ge/2026/other/1783941267. php#google_ vignette; etc.), the city of Telavi and surrounding areas in Georgia's Kakheti region were hit by severe flash floods and mudflows. Exceptionally heavy rainfall caused the Telaviskhevi River to overflow its banks, dumping 57.3 mm of water – equivalent to 85% of the monthly norm – in just a few hours. Fortunately, no casualties or injuries were reported.

A critical combination of a large volume of water and solid debris generated a powerful mud-and-debris flow. Three retention structures located in the middle reach of the river (known as the Kherkheulidze retention structures) partially fulfilled their function of filtering the flow: the first captured virtually all large woody debris, the second trapped a small amount of woody material, and the third retained rock and gravel deposits. Nevertheless, due to the flow's immense volume and high energy, the debris torrent bypassed all three structures on the left side, temporarily utilized an old dirt road as a channel, damaged bank-protection structures, and caused deformation of the road surface in certain sections.

Scope of Damage Infrastructure: A powerful mudflow carrying rocks, trees, and debris completely destroyed a bridge on Kavkasioni Street, cutting the city in two. The raging waters tore up asphalt, damaged riverbank reinforcement structures, and ruined crucial irrigation systems.

Urban Areas: The floodwaters inundated Kavkasioni and Alazani avenues. The ground floors and basements of residential buildings, commercial shops, pharmacies, and a local clinic were heavily flooded, damaging property and vehicles. Utilities: Falling debris and water torrents knocked down power lines and breached the gas network, leaving thousands of residents without electricity and natural gas.

Agriculture: In nearby villages like Tsinandali, Kisiskhevi, and Kurdgelauri, the severe weather flooded agricultural lands and completely destroyed hectares of productive vineyards right before harvest.

Response and Long-Term Decisions: A specialized emergency disaster response group was immediately convened to manage the crisis. Heavy machinery and hundreds of workers were deployed to clear mud, reinforce the riverbeds, and gradually restore utility lines. By mid-August 2026, the Georgian government had allocated GEL 500000 for disaster relief.

Furthermore, an official structural assessment by the Levan Samkharauli National Forensics Bureau revealed that the disaster had compromised the integrity of nearby structures. As a result, Telavi Mayor Vazha Maghradze announced that all buildings within a 10-meter radius of the river base would be demolished, with owners offered compensation or alternative premises.

Presented below is a preliminary analysis of a powerful mudflow and flood triggered by heavy downpours that affected the city of Telavi and surrounding areas in the Kakheti region (Georgia).

## Study area, material and methods

Study area – Telavi and the Telaviskhevi River basin (Fig. 1).

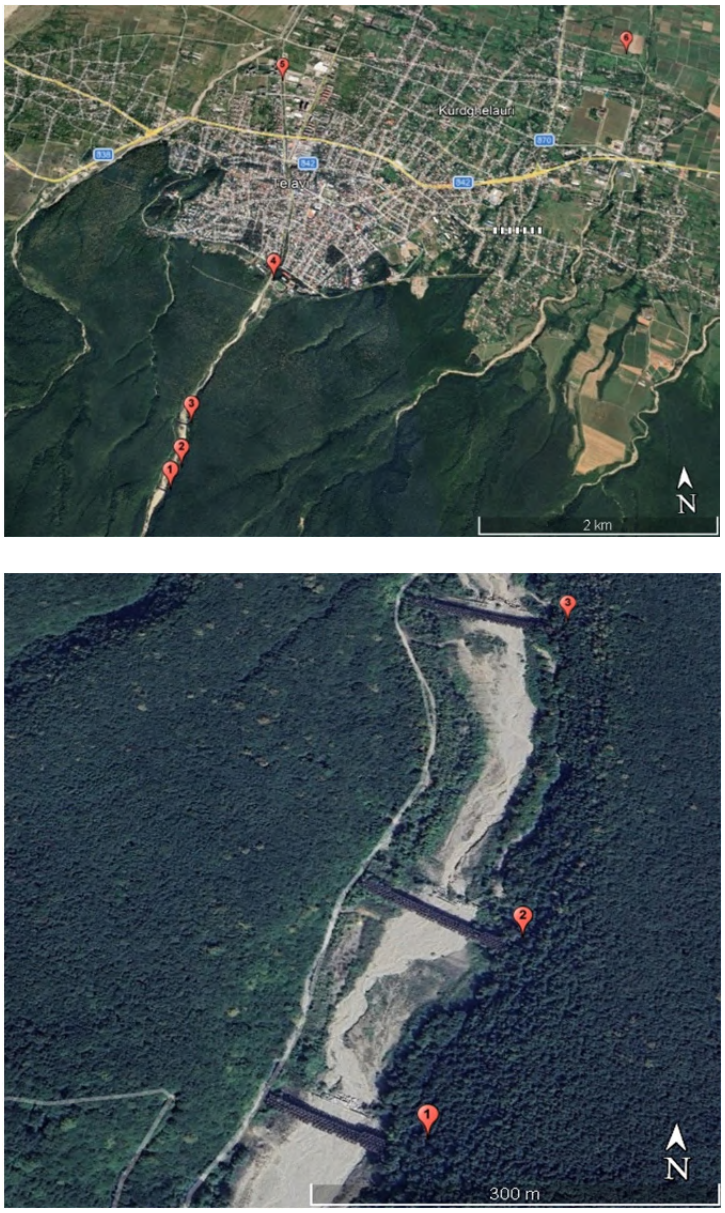



**Fig. 1.** Telavi and the Telaviskhevi river basin. 1, 2, 3 – Kherkheulidze debris-retention structures, 4 – city outskirts, 5 – destroyed bridge on Kavkasioni Street, 6 – weather station. Distance from point 2 to weather station ≈ 7 km.

Precipitation intensity was measured using meteorological radar "METEOR 735 CDP 10 – Doppler Weather Radar". Radar is established in the village Chotori of the Signagi municipality of Kakheti region of Georgia [7]. In this work radar product DPSRI(dBR) about precipitation intensity is used [8,9]. Time designation (Fig. 2), for example, t = 01 hour 26 min – 01:26 h. The data of the Georgian Environment Agency on daily sum of atmospheric precipitation and information from the press and Facebook users were also used.

## Results

Results in Fig. 2 are presented.

Fig. 2 shows radar data on precipitation intensity over Telavi (black dot) on July 12, 2026 at 01:26, 02:15, 02:30, and 02:48 hour. In particular, as shown in this Figure, the most intense precipitation occurred in the vicinity of the mudflow protection structures located near the city entrance.

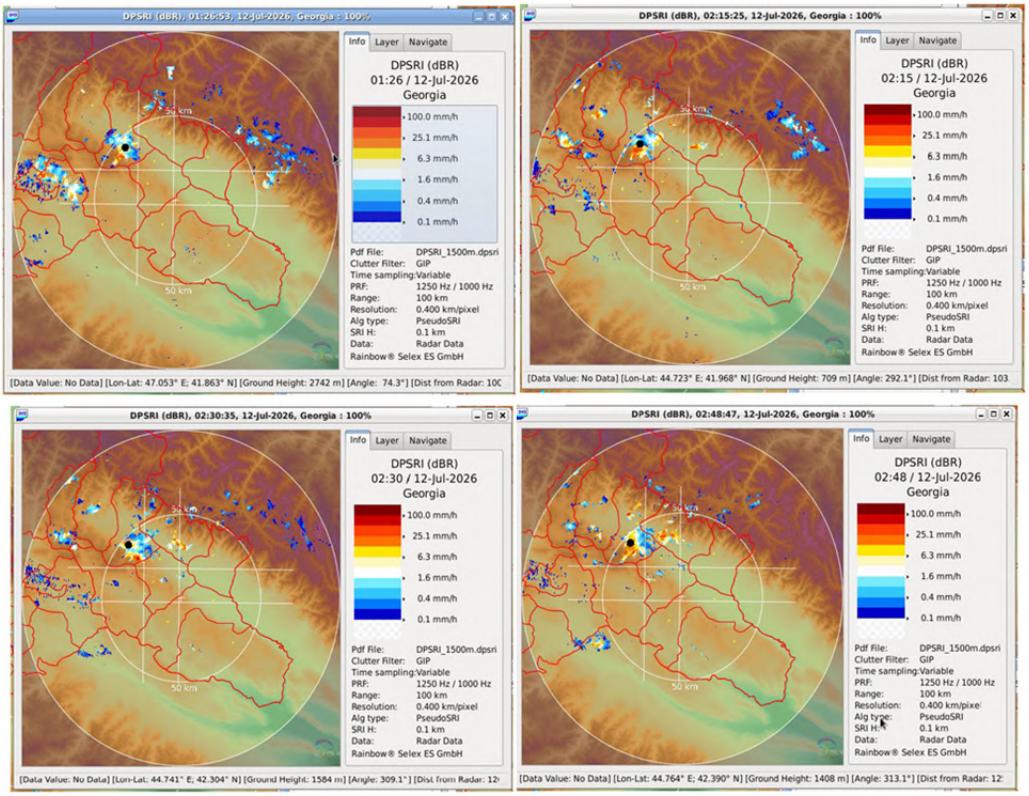



**Fig. 2.** Radar data on precipitation intensity over Telavi (black dot) on July 12, 2026 at 01:26, 02:15, 02:30, and 02:48 hour.

According to radar data, precipitation intensity reached 75–100 mm/h. These structures are situated approximately 7 km from the weather station; therefore, the precipitation amount recorded at the weather station (57.3 mm) could have been significantly lower than that at the city entrance.

For comparison, it should be noted that the mudflow in Telavi on June 14, 1977, was triggered by 72.1 mm of precipitation. At that time, the city's infrastructure was also significantly damaged over an area of approximately 0.50 km² [4].

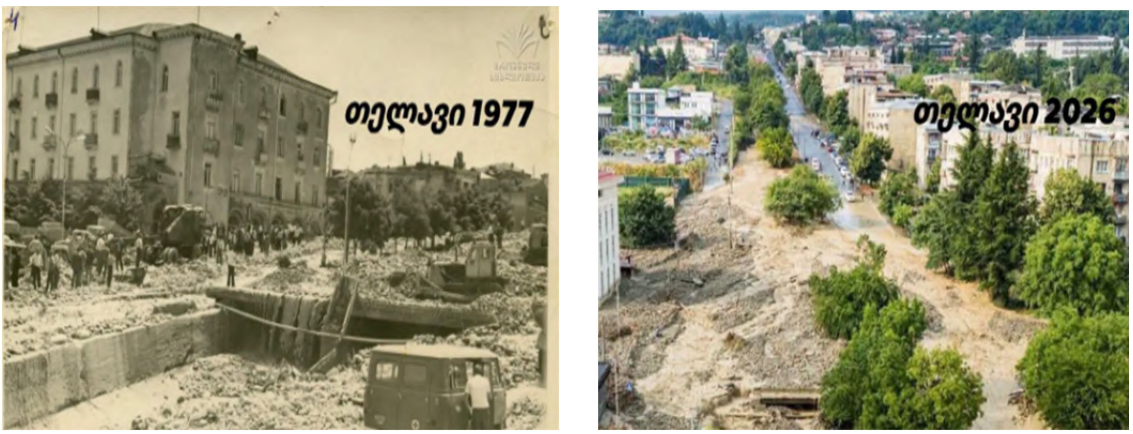



Fig. 2. Photos of the devastating mudflow in Telavi in 1977 and 2026.
[https://www.facebook.com/photo/?fbid=27454382550836762&set=a.7452689528099360]
Fig. 2 shows photos of the devastating mudflow in Telavi in 1977 and 2026.

## Conclusion

In the future, it is planned to continue these studies, including a more detailed analysis of radar data on precipitation intensity.

**Acknowledgement:** The authors thank Facebook users for the opportunity to use their photographs.

## References

1. Varazanashvili O., Tsereteli N., Amiranashvili A., Tsereteli E., Elizbarashvili E., Dolidze J., Qaldani L., Saluqvadze M., Adamia Sh., Arevadze N., Gventcadze A., Vulnerability, Hazards and Multiple Risk Assessment for Georgia. // Natural Hazards, Vol. 64, Number 3, 2012, pp. 2021-2056, DOI: 10.1007/s11069-012-0374-3, http://www.springerlink.com/content/9311p18582143662/fulltext.pdf.
2. Amiranashvili A.G., Increasing Public Awareness of Different Types of Geophysical Catastrophes, Possibilities of Their Initiation as a Result of Terrorist Activity, Methods of Protection and Fight with Their Negative Consequences. Engaging the Public to Fight Consequences of Terrorism and Disasters. // NATO Science for Peace and Security Series E: Human and Societal Dynamics, vol. 120. IOS Press, Amsterdam•Berlin•Tokyo•Washington, DC, ISSN 1874-6276, 2015, pp. 155-164.
   http://www.nato.int/science; http://www.iospress.nl http://www.springer.com
3. Gaprindashvili M., Tsereteli E., Gaprindashvili G., Kurtsikidze O., Landslide and Mudflow Hazard Assessment in Georgia. // In: Bonali, F.L., Pasquaré Mariotto, F., Tsereteli, N. (eds) Building Knowledge for Geohazard Assessment and Management in the Caucasus and other Orogenic Regions. NATO Science for Peace and Security Series C: Environmental Security. Springer, Dordrecht, 2021, https://doi.org/10.1007/978-94-024-2046-3_14
4. Varazanashvili O., Gaprindashvili G., Elizbarashvili E., Basilashvili, Ts., Amiranashvili A., Fuchs S. The First Natural Hazard Event Database for the Republic of Georgia (GeNHs). // Catalog, 2023, 270 p.
   https://openscience.ge/server/api/core/bitstreams/12d32a4e-11dc-4b5c-8878-7c1bf091039d/content;
   DOI: 10.13140/RG.2.2.12474.57286
5. Amiranashvili A., Chelidze T., Kiria T., Svanadze D., Tsamalashvili T., Varamashvili N., Retrospective Analysis of Landslides Processes in Akhaldaba (A Suburb of Tbilisi, Georgia) on June 13-14, 2015. // Journal of the Georgian Geophysical Society, e-ISSN: 2667-9973, p-ISSN: 1512-1127, Physics of Solid Earth, Atmosphere, Ocean and Space Plasma, v.29(1), 2026, pp. 50-59. https://ggs.openjournals.ge/index.php/GGS/article/view/12084
6. Amiranashvili A., Brocca L., Chelidze T., Svanadze D., Tsamalashvili T., Varamashvili N., Statistical Analysis of the Number of Damaging Landslides in Municipalities and Regions of Georgia and their Relationship with Atmospheric Precipitation in 2015-2024. // Reliability: Theory and Applications, ISSN 1932-2321, Volume 20, Special Issue No. 9 (87), November 2025, pp. 255-264.
7. Amiranashvili A.G., Chikhladze V.A., Dzodzuashvili U.V., Ghlonti N.Ya., Sauri I.P., Reconstruction of Anti-Hail System in Kakheti (Georgia). // Journal of the Georgian Geophysical Society, Issue B. Physics of Atmosphere, Ocean and Space Plasma, vol.18B, 2015, pp. 92-106.
8. Avlokhashvili Kh., Banetashvili V., Gelovani G., Javakhishvili N., Kaishauri M., Mitin M., Samkharadze I., Tskhvediashvili G., Chargazia Kh., Khurtsidze G. // Products of Meteorological Radar «METEOR 735CDP10». Trans. of Mikheil Nodia Institute of Geophysics, ISSN 1512-1135, Tb., 2016, vol. 66, pp. 60-65. (in Russian)
9. Selex ES GmbH · Gematronik Weather Radar Systems. Rainbow®5 User Guide, 464 p., www. gematronik.com

2nd International Scientific Conference "Modern Problems in Geophysics", Proceedings,
ISBN 978-9941-36-562-1, ISSN 3088-4349, Tbilisi, Georgia, October 29-31, 2026

# BUILDING BACK BETTER AFTER FLOODS: LESSONS FOR THE KURA RIVER BASIN

**Huseynov H.**

*Azerbaijan State Oil and Industry University, Baku, Azerbaijan*
*The Academy of the Ministry of Emergency Situations, Baku, Azerbaijan*
*habil.huseynov.98@gmail.com*

***Abstract.*** *Building Back Better (BBB) links post-flood recovery with the reduction of future disaster risk. This extended abstract compares selected recovery and flood-risk-management practices in the Netherlands, Germany and Japan and considers their relevance to Azerbaijan's Kura River basin. The qualitative review draws on policy frameworks, scientific literature and documented recovery experience, including the 2010 Kura floods. The cases emphasize complementary measures: river-space planning, resilient reconstruction, basin-scale protection, monitoring, warning and community preparedness. For the Kura basin, the main implication is to connect engineering rehabilitation with risk-sensitive land use and coordinated recovery planning. The findings are a comparative policy synthesis, not a quantitative assessment of recovery performance.*

***Key Words:*** *Building Back Better, flood recovery, Kura River, resilience, disaster risk reduction.*

## Introduction

Recovery after a flood can restore damaged assets without correcting the conditions that made them vulnerable. The Building Back Better (BBB) approach instead treats recovery, rehabilitation and reconstruction as an opportunity to reduce future risk. This principle is reflected in the Sendai Framework for Disaster Risk Reduction 2015–2030 and international recovery guidance [1, 2]. This paper summarizes selected international lessons and identifies their practical relevance to post-flood recovery in the Kura River basin of Azerbaijan.

## Study area, material and methods

The Kura River basin is considered through the experience of the 2010 floods and the associated recovery and risk-reduction needs [3]. A qualitative document review and cross-case comparison were used. The evidence comprises scientific literature, international frameworks, institutional reports and documented practices in the Netherlands, Germany, Japan and Azerbaijan. The comparison addresses reconstruction, river-basin and land-use planning, structural and non-structural measures, monitoring, warning and governance. No primary field survey or hydraulic modelling was undertaken; the findings therefore represent a policy and practice synthesis rather than measured differences in recovery effectiveness.

## Results and discussion

**Table 1**. summarizes the main BBB-related priorities and their relevance to the Kura River basin.

Table 1. BBB-related measures and their relevance to the Kura River basin (author's qualitative synthesis).

| Case | Main emphasis in the reviewed experience | Relevance to the Kura River basin |
|---|---|---|
| Netherlands [4, 5] | River-space measures, dike relocation and spatial adaptation. | Combine engineering protection with floodplain and land-use planning. |
| Germany [6] | Resilient reconstruction, warning arrangements and regulatory improvement. | Link rebuilding decisions to future risk and preparedness. |

| Case | Main emphasis in the reviewed experience | Relevance to the Kura River basin |
|---|---|---|
| Japan [7, 8] | Basin-scale protection, channel works and community preparedness. | Coordinate structural measures with warning and evacuation planning. |
| Azerbaijan [3, 9, 10] | Restoration after the 2010 floods, protective works and monitoring. | Connect recovery with risk zoning and coordinated basin-scale planning. |

**The Netherlands.** The Room for the River approach combines flood-safety objectives with spatial planning. Measures such as dike relocation, floodplain modification and additional space for river conveyance illustrate how protection can be linked to adaptation of land use rather than to higher defences alone [4, 5]. The intervention types shown in Fig. 1 summarize this river-space approach. For the Kura basin, the relevant lesson is the need to consider river corridors, settlements and protective infrastructure together.

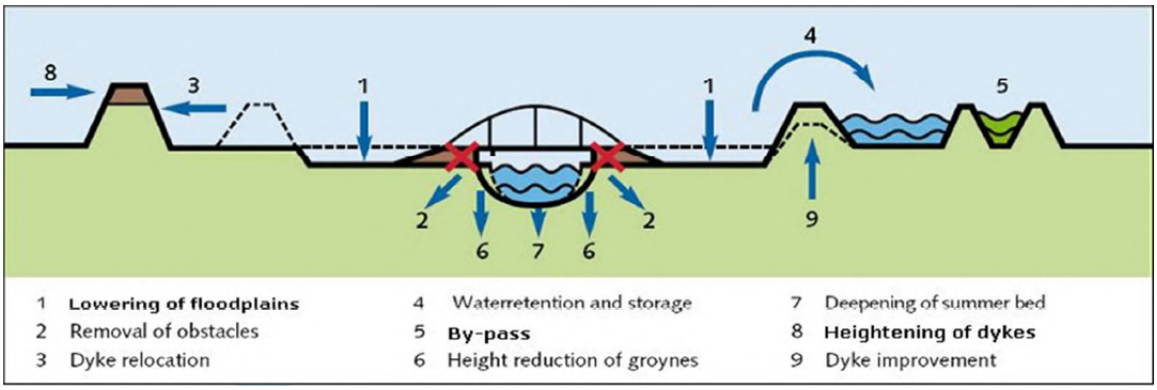



**Fig. 1.** Flood-risk-reduction measures used in the Room for the River approach (Source: [4]).

**Germany.** Experience from the 2021 floods in western Germany highlights the connection between reconstruction and future vulnerability. Flood-resilient housing, improved warning arrangements and planning or regulatory requirements are central to recovery discussions [6]. The BBB lesson is that restoring buildings and services should not be separated from decisions about their future exposure and the preparedness of users.

**Japan.** The reviewed Japanese experience combines engineering interventions with basin-scale planning and community preparedness [7]. Following the July 2018 heavy-rain disaster in the Oda River basin, the recovery discussion included river-system improvements, levee reinforcement and channel excavation, alongside evacuation planning and community-based disaster-prevention activities [7, 8]. This combination underlines the complementary roles of structural protection and preparedness.

## Implications for the Kura River basin

The 2010 Kura floods affected settlements, agricultural areas and infrastructure. The reviewed recovery experience included support for affected populations, restoration of essential services, rehabilitation of damaged areas and protective works [3, 9]. In BBB terms, these activities should form part of a longer-term process that reduces vulnerability instead of reproducing pre-flood conditions.

Three connected priorities follow from the comparison. First, engineering rehabilitation should be linked with flood-risk zoning and risk-sensitive land use. Second, hydrological monitoring, forecasting and early warning should complement protective structures and public preparedness. Third, recovery planning should connect institutional responsibilities, information management and arrangements for reviewing outcomes [2, 9, 10]. These priorities are proposed directions for application, not evidence that a complete BBB programme has already been implemented in the basin.

Recovery should also account for differences in access to information, services and temporary accommodation. Age structure and the needs of persons with disabilities are relevant to preparedness and reconstruction planning. International guidance emphasizes coordinated, inclusive recovery and the integration of disaster-risk reduction into reconstruction [2]. Measures adapted to local conditions are therefore more appropriate than the direct replication of an international project.

## Conclusion

The reviewed experience supports a common BBB principle: post-flood recovery should connect physical reconstruction with long-term risk reduction. The Netherlands emphasizes river-space and land-use adaptation; Germany highlights resilient rebuilding and warning; and Japan illustrates basin-scale protection combined with preparedness. For the Kura River basin, the principal implication is to integrate engineering measures, risk zoning, monitoring, early warning and coordinated recovery planning. The comparison provides a qualitative basis for organizing these priorities but does not establish quantitative benefits or the effectiveness of specific interventions in Azerbaijan.

## References


1. UNDRR., Sendai Framework for Disaster Risk Reduction 2015–2030. // Geneva: United Nations Office for Disaster Risk Reduction, 2015. https://www.undrr.org/publication/sendai-framework-disaster-risk-reduction-2015-2030
2. UNISDR., Words into Action Guidelines: Build Back Better in Recovery, Rehabilitation and Reconstruction. Consultative Version. // Geneva, 2017. https://www.undrr.org/publication/words-action-guidelines-build-back-better-recovery-rehabilitation-and-reconstruction
3. International Federation of Red Cross and Red Crescent Societies (IFRC). Azerbaijan: Floods. // DREF operation No. MDRAZ002, GLIDE No. FL-2010-000089-AZE. 10 December 2010.
4. Meis E., Room for the River 2.0 Programme in the Netherlands. // Ministry of Infrastructure and Water Management, 2025. https://www.inbo-news.org/wp-content/uploads/2025/05/2025_EURO-INBO_Parma_Floods_IEnW_Netherlands.pptx.pdf
5. Rijke J., van Herk S., Zevenbergen C., Ashley R., Room for the River: Delivering Integrated River Basin Management in the Netherlands. // International Journal of River Basin Management, 10(4), 2012, pp. 369–382. https://doi.org/10.1080/15715124.2012.739173
6. Birkmann J., Schüttrumpf H., Handmer J., Thieken A., Kuhlicke C., Truedinger A., Sauter H., Klopries E.-M., Greiving S., Jamshed A., Merz B., Solecki W., Kirschbauer L., Strengthening Resilience in Reconstruction after Extreme Events – Insights from Flood-Affected Communities in Germany. // International Journal of Disaster Risk Reduction, 96, 2023, 103965. https://doi.org/10.1016/j.ijdrr.2023.103965
7. Asian Disaster Reduction Center (ADRC). Building Back Better in Disaster Recovery, Rehabilitation and Reconstruction. // Kobe, Japan. https://www.adrc.asia/
8. Kanemitsu N., Yamamoto H., Watanabe Y., Murakami H., The Questionnaire Survey on Evacuation Behavior for Flood Disaster by Heavy Rain Event of July 2018 in Mabi, Kurashiki City. // Journal of Japan Society for Natural Disaster Science, 39, 2020, pp. 13–31. (in Japanese).
9. Huseynov H.A., Safarov S.H., Causes and Characteristics of Possible Flood Occasions in the Yevlax–Neftchala Zone along the Kura River Basin. // Herald of the Azerbaijan Engineering Academy, 16(3), 2024, pp. 120–127. https://doi.org/10.52171/2076-0515_2024_16_03_120_127
10. UN-Habitat., Building Climate Resilient Cities and Communities in the Republic of Azerbaijan. // United Nations Human Settlements Programme, 2024, pp. 97–101.

2nd International Scientific Conference “Modern Problems in Geophysics”, Proceedings,
ISBN 978-9941-36-562-1, ISSN 3088-4349, Tbilisi, Georgia, October 29-31, 2026

# UAV TECHNOLOGIES AS AN ADVANCED TOOL FOR GEOECOLOGICAL MONITORING IN HIGH-MOUNTAIN AREAS

**Gergokova Z.**

*Federal State Budgetary Institution "High-Mountain Geophysical Institute",*
*Nalchik, Kabardino-Balkaria, Russian Federation*
*zayna.gerg@mail.ru*

***Abstract****. This paper addresses the solutions to numerous challenges associated with the regular situational monitoring of high-mountain territories exposed to hazardous slope and channel processes. The instrumentation and methodology for addressing this issue at the modern technological level are described. Examples of the practical implementation of the presented methodology are shown. The prospects for the development of GIS technologies in solving the problems of geoecological monitoring of high-mountain territories are assessed.*

***Key words:*** *Geoecological monitoring, unmanned aerial vehicle (UAV), debris flows, landslides.*

## Introduction

Global climate changes over recent decades and the associated disruptions to the established temperature-water balance are particularly pronounced in mountain regions. A clear global trend is observed towards the activation of all types of negative processes, both natural and anthropogenic, in mountainous areas. In many cases, the situation requires constant monitoring and an adequate assessment of development prospects. This facilitates the development of optimal measures for adapting the infrastructure of populated areas to changed conditions in order to prevent or minimize possible damage.

Under these circumstances, the efficiency and quality of monitoring potentially hazardous sections of mountain landscapes are the determining factors for success in ensuring safety within the controlled territory. The aim of this work is to assess the effectiveness of applying existing advanced methods for determining spatiotemporal changes in geomorphological parameters within the monitoring zone.

## Methodology

The core concept of monitoring mountain – which generally implies inaccessible – territories using unmanned aerial vehicles (UAVs) is based on assessing the dynamics of spatiotemporal changes in landscape geomorphological parameters through comparative analysis of digital information models constructed from materials of multi-temporal aerial photography of the studied area.

Experience in applying the described methodology has been accumulated during the monitoring of hazardous natural phenomena in the mountains of the Kabardino-Balkarian Republic (Baksan, Chegem, and Cherek gorges) as part of the research work of Roshydromet "Development and improvement of methods for monitoring mudflows and mountain glaciers in the foothill and high-mountain zones" in 2021-2025.

During aerial photography, DJI Mavic Air 2 and Geoscan 401 UAVs were used. Multi-temporal (with a certain frequency, or before and after an event) surveys were conducted at approximately the same time of day, under similar weather conditions, in accordance with regulatory and technical requirements: monitoring of individually located objects – GOST R 70611-2022 [3]; cartographic processing of results – GOST R 70174-2022 [4]. Data processing was carried out in the Agisoft Metashape Professional software environment; initial data – dense point cloud. Point cloud classification was automatic. Digital terrain models (DTMs), presented as raster images, displayed the elevation values of each cell through the corresponding pixel. Office processing included stages of phototriangulation and semi-global matching. This makes it possible to obtain quantitative morphometric characteristics of the object before, after, and in the time intervals after a debris-flow event. On orthophotoplans, polygons of the site were visually identified where significant landscape transformations were observed that contributed to the development of emergency situations (Fig. 1).



**Fig. 1.** An example of an orthophotomap of one of the studied areas (Tyrnyauz tailings dump).

The volumes of eroded soil and deposited sediments were calculated for each site by approximating a plane of the DTM based on elevation values of cells located in the zone not affected by debris flow or landslide impact (Fig. 2).

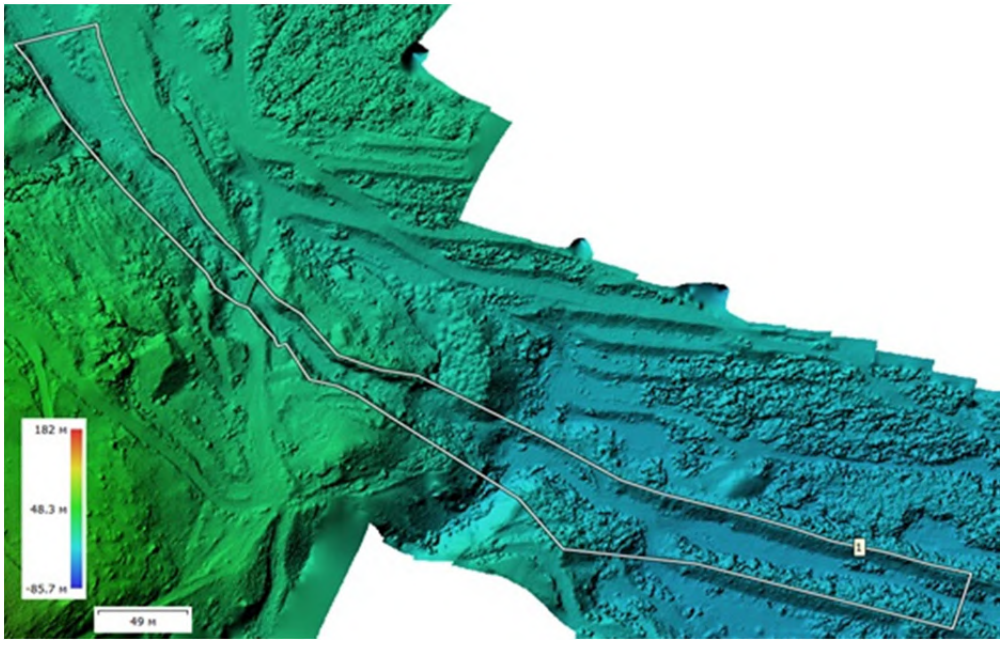



**Fig. 2.** An example of constructing plane boundaries on a digital terrain model based on the height values of cells to determine the internal volume of a drainage channel at the present time

Automatic delineation of the approximation area was based on the maximum elevation differences between adjacent cells bounded by the instrument line. To correct distortions, photographic materials were processed in Agisoft Metashape Professional software, where digital photogrammetric correction eliminated distortions caused by terrain features and survey angles through adjustments of tilt, scaling, and terrain compensation. The applied filtering, based on replacing pixel brightness values with linear smoothing filters, reduced noise and interference caused by vegetation and shadows, reducing sharp brightness contrasts. This processing ensured a relative error within 1.5–4%.

Limitations of the technical parameters of the equipment imposed certain barriers to photo processing: consumer-class drones, such as the "DJI Mavic Air 2," have hardware and software limitations that lead to

distortion aberrations, reducing the accuracy of photography and complicating the use of images for forming stereopairs. The presence of noise due to vegetation cover and shadows complicated photogrammetric processing, leading to errors in terrain modeling and distortions in calculated parameters [1, 2].

## Results and discussion

Using this methodology for monitoring natural objects (debris-flow channels, landslide slopes, etc.) during the period 2021-2025, the following information was obtained:

– data on the state of the landslide in the channel of the emergency open drainage canal within the hydraulic structure complex of the tailings dump of the Tyrnyauz Mining and Processing Plant (TMPP) [5];
– numerical values for the area of debris-flow deposits in the bed of the Gizhgit River, at the approaches to the inlet portal of drainage tunnel No. 2, and the dynamics of increasing vegetation (afforestation) area on these deposits over the specified period (TMPP hydraulic structures);
– data on the accumulation of soil-debris masses in the channel of the emergency open drainage canal (TMPP hydraulic structures);
– data on the scale of transformation of the Nalchik River bed following the passage of a debris flow in 2024 [6];
– data on the transformation of the Gerkhozhansu River bed after debris flows passed through it in 2025
– data on the area and volume of debris-flow deposits within the city of Tyrnyauz resulting from debris-flow events along the Gerkhozhansu River in the summer of 2025; and others.

## Conclusions

Based on the experience gained during the aforementioned studies, it can be concluded that the use of unmanned aerial vehicles and associated software is currently the most optimal method for conducting regular monitoring of local areas in mountainous and high-mountain territories exposed to hazardous natural phenomena.

Among the undeniable advantages of the methodology used, the following should be noted: high accuracy of calculations during analytical comparison of orthorectified images and digital models of controlled zones constructed from multi-temporal aerial photography materials (on average, the error, often due to technical features of the equipment used, is about 1.5-4%, which is a very acceptable result for this type of work); the ability to survey inaccessible high-mountain areas – obtaining such data during ground reconnaissance surveys is fundamentally impossible; the ability to obtain information in real-time, almost regardless of weather conditions (except for storm winds and heavy precipitation), which is not possible with available satellite imagery services, whose images are provided with a frequency of 3-4 days and, even when the surface is not covered by clouds, are incomparable in quality and resolution with UAV survey materials.

An equally important circumstance is that the use of UAVs ensures the safety of the research for the researchers themselves, since surveys of debris-flow or landslide areas in ground mode are often associated with significant risks, while the introduction of aerial photography allows them to remain in safe areas during the survey.

## References


1. Bilichenko I.N., The use of unmanned aerial vehicles in landscape-ecological research. // Materials of the All-Russian Scientific and Practical Conference. Application of Unmanned Aerial Vehicles in Geographical Research (Irkutsk, May 22–23, 2018). – Irkutsk: Publishing House of the Institute of Geography named after V.B. Sochava SB RAS, 2018, pp. 30-33
2. Konovalova T.I., Geosystem mapping – Novosibirsk: Academic Publishing House "Geo", 2010, 186 p.
3. GOST R 70611-2022 – Monitoring of individually located objects.
4. GOST R 70174-2022 – Cartographic processing of results.
5. Sherkhov A.Kh., Gergokova Z.Zh., Results of hardware monitoring of the emergency section of the tailings dump of the Tyrnyauz Mining and Processing Plant, // Bulletin of the Vladikavkaz Scientific Center, No. 1, 2025, pp. 72-76.
6. Sherkhov A. Kh., Gergokova Z.Zh., Akaev A.R., Determination of quantitative parameters of debris flow manifestations using UAVs. // Environmental Engineering, No. 2, 2024, pp. 83-89.

2nd International Scientific Conference "Modern Problems in Geophysics", Proceedings,
ISBN 978-9941-36-562-1, ISSN 3088-4349, Tbilisi, Georgia, October 29-31, 2026

# SAFETY EVALUATION OF OFFSHORE CO2 STORAGE IN DEPLETED LEVELS OF HYDROCARBON CULTIVATION FIELDS

**Marrazzo R., Astorri F.**

*ISPRA, Roma, Italia*
*romualdo.marrazzo@isprambiente.it*

***Abstac**t. The article is aimed at representing the activities of technical evaluation carried out by a specific Technical Working Group, supporting the CCS Technical Secretariat of the Italian ETS Committee on the examination of an experimental program for the geological storage of carbon dioxide in the depleted levels of an offshore hydrocarbon cultivation concession field. Starting from the reference standards, it is described the experimentation program and the related plants, focusing attention on the assessment of the relevant risks for the environment and health, with specific aspects related to the safety, prevention, and mitigation plans. The corrective measures of prevention and protection in case of unexpected events are specified, connected both to purely technical and plant aspects, as well as to management and organizational aspects. The discussion ends with a series of assessments about the strengths of this experimental installation, while proposing some plant and monitoring requirements, aimed at the prevention of technological accidents.*

***Key words**: Seveso, CO2, Offshore, Safety, Risk.*

## Introduction

Carbon Capture and Storage (CCS) is a key technology for reducing CO2 emissions and supporting climate goals. Increasingly stringent European greenhouse gas targets have stimulated the development of CCS projects across the energy and industrial sectors. This study examines an experimental project for the geological storage of CO2 in depleted offshore hydrocarbon reservoirs in the Adriatic Sea, Italy. The project is promoted by a multinational oil and gas company and aims to demonstrate the feasibility and safety of long-term CO2 storage. A Technical Working Group (TWG) within ISPRA evaluated the project on behalf of the Italian ETS Committee. The assessment covered capture, transport, injection, monitoring, and storage systems, with particular focus on environmental and safety risks. Potential accidental release scenarios and related mitigation measures were thoroughly analysed. The evaluation was conducted under the framework of EU Directive 2009/31/EC [1] and the Italian Legislative Decree No. 162/2011 [2]. Results provide important insights into the safe deployment of CCS technologies and their role in supporting decarbonization strategies.

## 1. The experimental project

### *1.1 Description of activities and new installations*

The experimental project presented by the Operator provides for:

1. Casalborsetti CO2 capture plant: sized to capture and treat the CO2 present in the exhaust fumes of one of the 4 existing Turbocompression units located within the Casalborsetti on – shore power plant area (an area of 44,900 m2 to the north of Ravenna, consisting of a Natural Gas compression and treatment plant). The nominal size of the capture plant will be approximately 25,000 tons of CO2 per year.
2. Compression and CO2 reception station in Casalborsetti: the Casalborsetti plant provides for the compression of the captured CO2 for sending to the pipeline. Also included in the experimental program is a system for receiving CO2 from tankers, storage, pressurization and vaporization (initially foreseen but later abandoned).
3. CO2 transport and injection system: a new 4" line will be built inside an existing gas line with a "pipe in pipe" system, for the transport of CO2 from the Casalborsetti station to the existing offshore platform and the permanent injection of CO2 into the reservoir (located in the Adriatic Sea).

4. CO2 Storage Fields: the platform will be adapted and will house the necessary equipment in order to allow the reception and subsequent injection of CO2, without any impact on the current gas production of the field.
5. CO2 monitoring system: a well, micro-seismic, soil deformation and environmental monitoring system will be created. The selection of materials for the CO2 service is functional to the water content, for the corrosion phenomena.

### *1.2 On-shore auxiliary and process units*

The interventions relating to the new plant will be carried out by the Operator in order to guarantee the operational continuity of the Casalborsetti plant and the planned production capacity. As regards the safety aspects, the following investigations were conducted by the TWG on the main units that make up the new installations: 1. Hydrogen storage. The unit consists of two packs of two hydrogen cylinders, inside the CO2 dehydration package. In any case, the storage will be carried out according to the technical data sheets of the substance, at ambient temperatures, in suitable and adequately ventilated areas and away from sources of heat, ignition and electrical discharges. 2. Chemicals. As regards chemicals, these are substances generally used in natural gas treatment plants, i.e. oxigen scavengers, pH neutralizers, amines, caustic soda. 3. Vent system (cold spark plug). The vent system will work together with a blocking and isolation system which, by means of block valves, will be able to isolate the different process units or equipment. For all the simulated scenarios there are no fallout of the CO2 concentrations at the monitored thresholds.

### *1.3 New installations in the pipeline*

As part of the experimental project, the Operator provides for the transport of CO2 between the Casalborsetti plant and the PCWC platform, through the reuse of existing pipelines in order to minimize environmental impacts and avoid new occupations of the subsoil.

The new connection can be divided into the following four sections, a brief description of which is given below: Section 1: Onshore pipeline approximately 1.5 km long which starts from the Casalborsetti gas plant up to the shoreline (guide tube: 20”). Section 2: Pipeline approximately 7.3 km long which starts from the shoreline and reaches the vicinity of the PCWT platform (guide tube: 20”). Section 3: Pipeline approximately 1.5-2.5 km long which extends from the vicinity of the PCWT platform to the foot of the PCWC platform. Section 4: ascent and transit on the PCWC.

### *1.4 New installations on the platform*

For the new CCS plant in Casalborsetti, the Operator provides for the dedicated transport of CO2 through a 4” pipeline which will connect the Casalborsetti plant to the existing platform. The installation of the new CO2 injection equipment is planned on the platform.

As regards the Electro-Instrumental Engineering, the following additions and modifications are foreseen within the project: Measurement package to measure the total CO2 flow injected into the well; Installation of SDV block valve and relative local panel; New wellhead equipped with specific automatic valves for CO2 reinjection; Control and safety instrumentation and associated systems; CO2 detection systems and related connections; Multi -cable installation of instrumentation.

In-depth analyses were carried out by the TWG on the management of the emergency: all new signals, measurements, controls related to the process, valve status and environmental sensors related to the platform will be remoted to the ground.

### *1.5 Main changes to existing plants*

At the Casalborsetti plant, the CCS project requires modifications to existing units, including turbochargers, launch traps, water circuits, and drainage systems. Particular attention was given to the integration of the CO2 capture system with the existing turbine exhaust stacks.

The heat recovery and downstream systems have been designed to minimize back pressure and avoid impacts on compressor performance, supported by the installation of an exhaust gas blower. The original stack will remain available as a bypass, ensuring continuous turbocompressor operation during maintenance or emergency shutdowns of the capture unit.

Modifications to the existing pipeline involve the removal and replacement of selected sections along onshore, coastal, and offshore stretches. The TWG assessed the new operating logic and emergency shutdown configurations, confirming that the proposed changes do not introduce additional hazard scenarios or increase the risk of accidental releases affecting the existing facilities.

## 2. Evaluation of the effects of accidental CO2 releases

### *2.1 Preliminary assessments on the marine ecosystem*

The Operator assessed potential accidental CO2 releases along the approximately 11 km pipeline connecting the onshore facility to the offshore platform.

Two scenarios were analysed: a worst-case complete rupture of the 4-inch pipeline (pipe break) and a smaller leak caused by localized corrosion near a flange (pipe leak). While a full rupture is considered highly unlikely and linked to exceptional external events, the leak scenario represents a more credible, although still improbable, event.

The analyses evaluated the dispersion of CO2 and its potential effects on environmental and human receptors. Results indicated that both scenarios would have limited spatial and temporal impacts. Consequently, the effects of accidental CO2 releases were considered negligible due to the restricted affected area and the short exposure times involved.

### *2.2 Preliminary health and environmental assessments*

Following the assessment of potential impacts on the marine environment, the Operator evaluated the consequences of accidental CO2 releases within the CCS facilities.

Since CO2 is an asphyxiant at high concentrations and may cause severe health effects [3], risk analyses were performed using the Dangerous Toxic Load (DTL) approach, based on the SLOT – Specified Level Of Toxicity – Dangerous Toxic Load (toxicity) and SLOD – Specified Level Of Death – Dangerous Toxic Load (fatality) thresholds.

Results showed that releases from the capture and compression units would not reach harmful exposure levels due to their short duration.

For the onshore pipeline, complete ruptures were not found to exceed toxicity thresholds, while small leaks could affect areas within approximately 10 m of the release point.

Similar distances were identified for offshore pipeline scenarios, although vessel stability would not be affected and discomfort levels would remain limited in time and extent.

On the offshore platform, neither toxicity nor fatality thresholds were reached, and safe evacuation routes remained available.

Thermal effects associated with CO2 releases were considered acceptable but will be further investigated through dedicated CFD analyses to determine whether additional protective measures are required.

## 3. Corrective prevention and protection measures and related safety plans

### *3.1 Instrumentation and automation*

The Operator designed the new CCS plant to operate as independently as possible from the existing facilities through a dedicated Integrated Control and Safety System (ICSS).

The ICSS consists of a Process Control System (PCS), responsible for process monitoring and operational control, and a Safety Instrumented System (SIS), dedicated to safety functions, fire and gas detection, and emergency shutdowns. The system provides continuous supervision of plant operations, alarm management, event recording, and integration with third-party control systems. The PCS enables operators to monitor and control all process units from centralized workstations. The SIS automatically brings the plant to a safe condition whenever hazardous situations are detected, preventing accidents or mitigating their consequences through predefined Safety Instrumented Functions (SIFs).

Together, these systems ensure high operational reliability and safety throughout the CCS facility.

### *3.2 Fire-fighting system and Fire & Gas detection system*

Since $CO_2$ is the primary process fluid, the Operator does not expect the CCS plant to increase the existing fire risk. Nevertheless, new fire protection measures will be integrated with the current systems to ensure safe operating conditions and minimize the consequences of potential accidents. Planned installations include fire suppression systems for electrical cabinets, portable and wheeled extinguishers, and water or water-foam firefighting systems.

The Fire & Gas (F&G) system will detect fires and hazardous gas releases, support emergency shutdown functions, activate audible and visual alarms, and provide operators with continuous monitoring through the Human Machine Interface (HMI). The system will be integrated with the Emergency Shut Down (ESD) and plant control systems to ensure rapid emergency response. Based on the identified fire scenarios, the Operator plans to install smoke detectors, hydrogen detectors in battery rooms, toxic and asphyxiating gas detectors, flame and heat detectors, manual alarm call points, sirens, and flashing lights to enhance personnel and environmental protection.

### *3.3 Electrical systems and civil structures*

The project includes new electrical systems for power distribution, protection, grounding, lighting, UPS, and emergency functions, designed to ensure efficiency, reliability, and maximum operational safety. New installations will be integrated with the existing Casalborsetti electrical and earthing network while minimizing interference with ongoing plant operations.

The TWG assessed the safety implications of power supply upgrades and possible blackout scenarios affecting both onshore and offshore facilities. In the event of a power failure, the CCS installations are designed to automatically reach a safe shutdown condition, with critical loads supported by UPS systems. Offshore facilities will also be safely secured without requiring depressurization.

Civil structures have been designed to prevent environmental contamination through concrete flooring, anti-acid coatings, and containment measures in areas handling hazardous substances. The drainage system will collect and manage amine-containing streams, acidic wastewater, boiler purge water, and potentially contaminated rainwater, ensuring proper treatment and disposal in accordance with environmental protection requirements.

### *3.4 Emergency management flows on the platform*

The Operator has reported a series of diagrams relating to the emergency management flow, for the Drilling / Workover / Completion / Simultaneous phases, also for the purpose of coordinating the parties operationally involved in the Site, differentiating them into: 1st level found externally. 2nd level. 3rd level. Civil protection emergency.

In particular, the TWG conducted in-depth analysis of the emergency management aspects, on the basis of the flow diagrams identified, with the relative support of procedures and operating instructions, in terms of men, means, methods, systems, etc. (general site emergency plan), also with reference to the reports of real emergency drillings and training sessions conducted by the Operator on the existing natural gas compression station and platform.

## Conclusions

At the conclusion of the analysis conducted by the ISPRA TWG, a series of considerations and criticalities, in terms of safety management, emerged from the technical assessment of the project are reported below. These elements, connected to the risk analysis and emergency management, resulted in particular in requests for compliance, for the Operator, for the construction of this experimental CO2 capture plant [4]:

1. In light of the results of the simulations following the releases of the various plant sections, it is necessary that:
   (a) The emergency plans will be updated taking into account the Pipeline (offshore) and Platform sections (achievement of SLOT, SLOD and discomfort values).
   (b) A CFD (Computational Fluid Dynamics) study will be carried out, in order to identify any protections shields for all sections of the system affected by thermal effects, following the release of CO2, on the platform.

2. Starting from the methods of inspection, on the pipeline, of the corrosion mechanisms, also with reference to the implemented asset integrity management procedures, the specific procedures and / or operating instructions for controlling the losses along the CO2 transport pipeline will be made available. These methods must be based on the continuous control of the process variables (pressure and flow rate), with specific attention to the management method in the event of malfunction or anomaly or failure, with the consequent blocking logic and management of the foreseen emergencies.
3. On the basis of the methods and types of waste produced following activation of the drainage system of the capture plant, the types of liquid effluent produced will be characterized, from the point of view of the characteristics of environmental hazard and / or flammability and / or of toxicity.
4. 2nd level emergency drillings will be scheduled and carried out such as to include all the accident scenarios hypothesized in those plans, in a suitable period of time (including several years), which are representative of the risk analysis conducted for the site.

## References


1. Directive 2009/31/EC of the European Parliament and of the Council of 23 April 2009 on the geological storage of carbon dioxide and amending Council Directive 85/337/EEC, European Parliament and Council Directives 2000/60/EC, 2001/80/EC, 2004/35/EC, 2006/12/EC, 2008/1/EC and Regulation (EC) No 1013/2006. OJ L 140, 5.6.2009, p. 114–135.
2. DECRETO LEGISLATIVO 14 settembre 2011, n. 162 “Attuazione della direttiva 2009/31/CE in materia di stoccaggio geologico del biossido di carbonio, nonché' modifica delle direttive 85/337/CEE, 2000/60/CE, 2001/80/CE, 2004/35/CE, 2006/12/CE, 2008/1/CE e del Regolamento (CE) n. 1013/2006”. (11G0207) GU Serie Generale n.231 del 04-10-2011.
3. EIGA Safety Info 24/11/E “Carbon Dioxide Physiological Hazards: Not just an asphyxiant!”. Prepared by the Safety Advisory Council. 2011. // EIGA – EUROPEAN INDUSTRIAL GASES ASSOCIATION AISBL. AVENUE DES ARTS 3 – 5. B-1210 BRUSSELS.
4. UK “Guidance. Post-combustion carbon dioxide capture: best available techniques (BAT). The available techniques which are the best for preventing or minimising emissions and impacts on the environment from post-combustion carbon dioxide capture”. // UK Environmental Agency. Published 2 July 2021.

2nd International Scientific Conference "Modern Problems in Geophysics", Proceedings,
ISBN 978-9941-36-562-1, ISSN 3088-4349, Tbilisi, Georgia, October 29-31, 2026

# THERMODYNAMIC ASSESSMENT OF SOME EXTREME CONVECTION EVENTS IN EASTERN GEORGIA

***Samkharadze I., **Davitashvili T., *Pipia M.**

** Institute of Hydrometeorology of the Technical University of Georgia, Tbilisi, Georgia*
*** I. Vekua Institute of Applied Mathematics of Tbilisi State University, Tbilisi, Georgia*
*inga.samkharadze562@ens.tsu.edu.ge*

***Abstract.*** *This article, based on thermodynamic characteristics, examines extreme convective phenomena that developed in the summer of 2024 in Eastern Georgia. The studies conducted showed that the development of strong convective processes is a complex nonlinear process and is not directly related to only one specific thermodynamic indicator. For effective forecasting and identification of extreme events, a complex assessment of the synoptic environment is necessary, which includes a joint analysis of humidity, vertical wind profiles, vertical velocities and thermodynamic indices (CAPE, K, TT). The complex methodology proposed in the paper allows for a clear identification and assessment of the atmospheric environment characteristic of extreme convective days, which will significantly contribute to improving the quality of forecasting of expected natural events in the region of Eastern Georgia.*

***Key words:*** *Convection, thermodynamic instability, atmospheric physics.*

## Introduction

Over the past two decades, against the backdrop of dramatic climate change, the frequency and intensity of extreme hydrometeorological events in Georgia have increased significantly. Namely, in the spring-summer period, strong convective processes often develop in the territory of Eastern Georgia, which are accompanied by abundant precipitation, hail, strong winds, and in some cases, tornadoes. These events cause significant damage to the infrastructure, agriculture, and population of the region [1,4,7]. Thus, the study of the mechanisms of development of extreme convective events and the improvement of their forecasting methods is one of the most important tasks of modern applied meteorology and climatology. In assessing the strength of convective instability and expected processes, a decisive role is assigned to thermodynamic and atmospheric indices. Parameters such as Convective Available Potential Energy (CAPE), Total Totals Index (TT), K Index, and total moisture content of the atmospheric air column (TCW) allow for a comprehensive assessment of air mass instability, moisture distribution, and the potential for the development of updrafts [6]. However, the analysis of individual indices alone is often not sufficient for the accurate identification of local, high-intensity events (for example, tornadoes). For this, it is necessary to consider thermodynamic indices in conjunction with the vertical structure of the atmosphere, wind shear, and vertical velocities. The main objective of this study is to conduct a detailed analysis of the thermodynamic and synoptic conditions of extreme convective days observed in the territory of Eastern Georgia. The study discusses ERA5 reanalysis data, based on which the change in instability indices, vertical profiles, and the correlations between them are studied in order to identify the specific atmospheric environment characteristic of the formation of extreme events [1-3] .

## Study area, material and methods

The study used the European Centre for Medium-Range Weather Forecasts (ECMWF) Global Reanalysis Data ERA5. ERA5 provides high temporal and spatial (0.25° x 0.25° grid) resolution of atmospheric parameters. The following main thermodynamic indices and meteorological parameters were calculated and analyzed to assess instability and convective potential [2,5]:
Convective Instability Potential Energy (CAPE) – represents the potential energy of air rising from the lower layers of the atmosphere from the level of free convection (LFC) to the equilibrium level (EL) [4,6,7].

Total Totals Index (TT) – is used to determine the probability of instability and thunderstorms in the middle and lower layers of the atmosphere:

$$TT = T850 + Td850 – 2 * T500$$

(where T is the temperature in °C, and Td is the dew point temperature at the respective 850 hPa and 500 hPa levels).

K Index (K)- takes into account the vertical temperature gradient (850–500 hPa), low-level humidity (850 hPa), and mid-level air dryness (700 hPa):

$$K = (T850 – T500) + Td850 – (T700 – Td700)$$

Total water content of the atmospheric air column (TCW) – characterizes the total amount of water vapor and liquid/solid phase (kg/m²) present in the entire column of the atmosphere (Table 1).

**Table 1.** Limit values of thermodynamic indices.

| Index | Value / Range | Atmospheric Condition |
|---|---|---|
| CAPE (J/kg) | 0 | Stable atmosphere |
| | 0 – 1000 | Weak instability |
| | 1000 – 2500 | Moderate instability |
| | 2500 – 3600 | High instability |
| | > 3600 | Extreme instability |
| TT Index | < 44 | Stable condition, weak convection |
| | 45 – 50 | Moderate instability, local thunderstorms |
| | > 50 | High instability, strong convection |
| K Index | 20 – 30 | Weak convection |
| | 30 – 40 | Moderate instability |
| | > 40 | High instability |
| TCW (kg/m²) | < 20 | Dry air mass |
| | 20 – 30 | Moderate moisture |
| | 30 – 40 | Heavy precipitation potential |
| | > 40 | Extremely strong convection |

To determine the spatiotemporal structure of convective processes, the following parameters were analyzed on isobaric surfaces (850 hPa, 700 hPa, 500 hPa) and vertical sections: wind speed and direction, relative humidity (RH), vertical velocity – to determine the intensity of ascending and descending flows. In addition, a correlation analysis was performed to assess the relationship between the obtained indices and meteorological parameters.

## Results

Three cases of strong convective processes observed in the territory of Eastern Georgia in June 2024 were selected for the study.

June 1, 2024 – On June 1, a large-scale convective process developed in Eastern Georgia, covering Telavi, Kvareli, Sagarejo, Gurjaani, Sighnaghi and Dedoplistskaro. The main direction of the process was from west to east (Fig. 1).

Thermodynamic indices: The maximum values of CAPE in the areas of Telavi and Gurjaani reached 1000–1700 J/kg, which indicates moderately high instability. TT index values between Gurjaani and Tbilisi exceeded 50, while K index increased to 32–35, indicating a high probability of heavy convective precipitation and thunderstorms. Humidity and wind profile: Total column humidity (TCW) in the southeastern part reached 31–36 kg/m². Analysis of vertical wind profiles revealed a sharp shift in height between 850 hPa and 500 hPa, which facilitated the organized development of convective clouds.

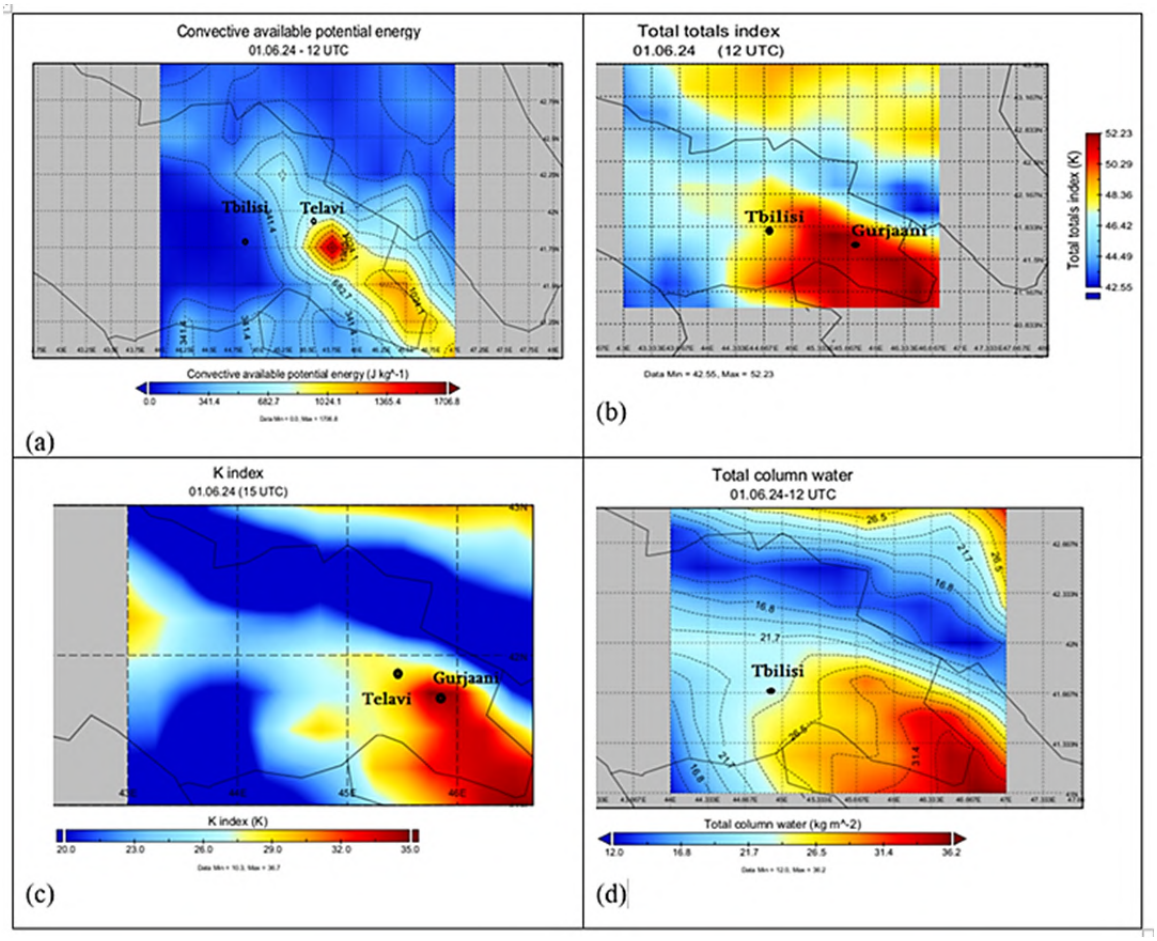



**Fig. 1.** Spatial distribution of atmospheric instability indices and moisture parameters over Georgia on June 1, 2024: (a) Convective Available Potential Energy (CAPE) at 12:00 UTC; (b) Total Totals index at 12:00 UTC; (c) K index at 15:00 UTC; (d) Total column water at 12:00 UTC.

June 17, 2024 case – On June 17, local, but intense convective processes were observed in the Kakheti region, namely in Telavi and Gurjaani. The CAPE index varied within the range of 900–1300 J/kg. The TT index was 47–49, and the K index was within the range of 28–31. Thermodynamic indicators showed that the process was of a local nature. The main concentration of moisture was in the lower 850 hPa layer of the atmosphere, while the presence of a relatively dry air mass was observed in the middle layer (Fig.2).

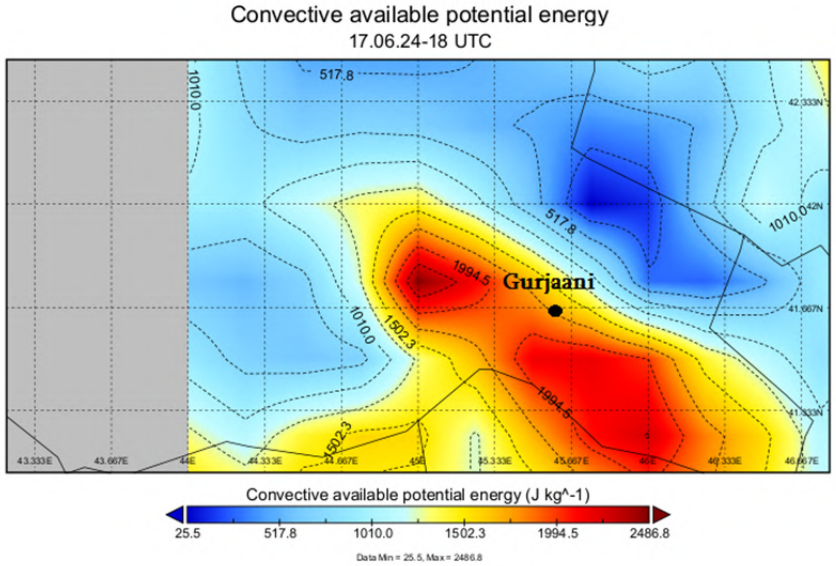



**Fig. 2.** Spatial distribution of Convective Available Potential Energy (CAPE) on June 17, 2024, at 18:00 UTC.

June 25, 2024 Event (Tornado) – On June 25, a particularly extreme convective event developed in Telavi and Akhmeta municipalities, which was accompanied by the formation of a tornado (Fig.3). CAPE values in the Telavi region reached 1500–1880 J/kg. The K index and TT index were within the limits of 30–33 and 49–52, respectively. Vertical analysis conducted on the Telavi-Akhmeta section revealed strong upward air flows. Vertical velocity (omega) ranged from -0.4 to -0.6 Pa/s (which is an upward velocity equal to approximately 7 cm/s). Relative humidity in the lower layers (850–900 hPa) exceeded 78–80%, and vertical wind shear created a strong cyclonic circulation, which led to the formation of a tornado (Table 3).

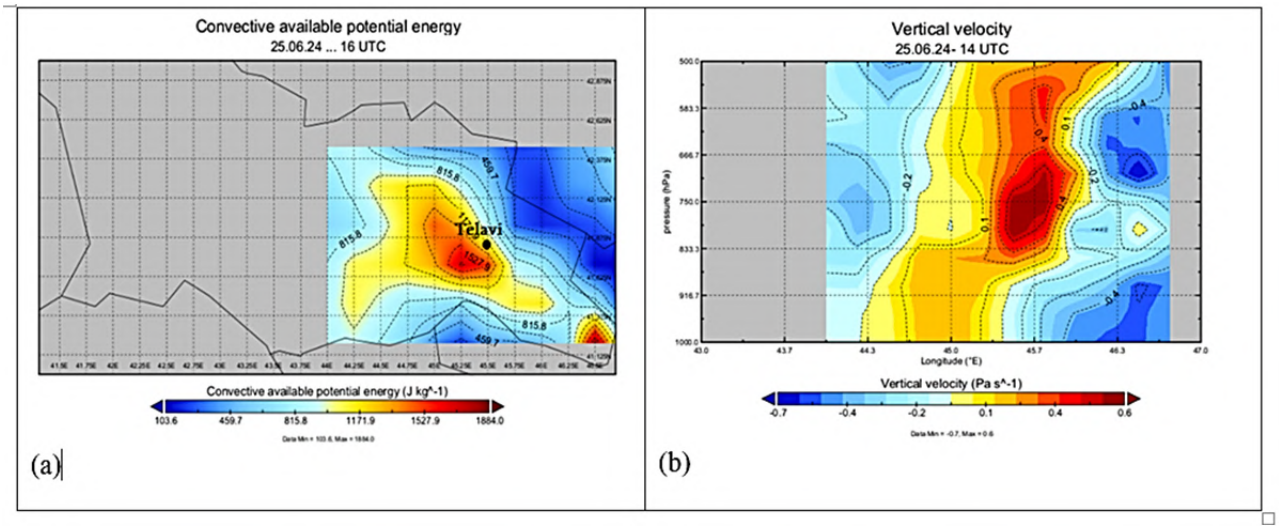



**Fig. 3.** Atmospheric conditions on June 25, 2024: (a) Spatial distribution of Convective Available Potential Energy (CAPE) at 16:00 UTC; (b) Vertical velocity cross-section at 14:00 UTC.

**Table 2.** Maximum thermodynamic parameters recorded on the study days.

| Date | Location | CAPE (J/kg) | TT Index | K Index | TCW (kg/m²) | Extreme Event |
|---|---|---|---|---|---|---|
| **01.06.2024** | Telavi, Gurjaani | 1000 – 1700 | > 50 | 32 – 35 | 31 – 36 | Heavy convective precipitation |
| **17.06.2024** | Telavi, Gurjaani | 900 – 1300 | 47 – 49 | 28 – 31 | 25 – 28 | Local thunderstorm |
| **25.06.2024** | Telavi, Akhmeta | 1500 – 1880 | 49 – 52 | 30 – 33 | 32 – 38 | Tornado |

Statistical and correlation analysis conducted between thermodynamic indices and meteorological parameters revealed several important patterns:

- A strong and close correlation was recorded between the K and TT indices (r = 0.8 – 0.9). This indicates that both indices similarly reflect the temperature gradient and moisture conditions in the lower and middle layers of the atmosphere.
- The correlation between CAPE and the TT index was found to be low (0.3). This confirms that convective available potential energy on extreme days is a more independent parameter and requires separate evaluation.
- High moisture content at the 850 hPa level, strong vertical updrafts, and vertical wind shear with height were observed on the analyzed extreme days. On relatively calm days, these indices were significantly lower, and vertical streams were weak and uniform.

**Table 3.** Correlation Relationship Between Thermodynamic Indices.

| Index | Correlation coefficient (r) | Connection |
|---|---|---|
| **K Index – TT Index** | 0.8 – 0.9 | Strong correlation |
| **CAPE – TT Index** | ≈ 0.3 | Weak correlation |

## Conclusion

The conducted research has shown that the development of strong convective processes and vortices (tornadoes) in Eastern Georgia is not associated with only one specific thermodynamic index. For effective forecasting and identification of extreme events, a complex assessment of the synoptic environment is necessary – a joint analysis of humidity, vertical wind profiles, vertical velocities, and thermodynamic indices (CAPE, K, TT). The proposed comprehensive methodology allows us to clearly identify and assess the atmospheric environment characteristic of extreme convective regional events. Advance knowledge of such extreme days will help improve the quality of forecasting expected natural phenomena in the region.

## References


1. Kunz M., The skill of convective parameters and indices to predict isolated and severe thunderstorms. // Nat. Hazard Earth Syst. 7, 2007, pp. 327–342.
2. Cornel Soci, Hans Hersbach, Adrian Simmons. The ERA5 global reanalysis from 1940 to 2022". // Quarterly Journal of the Royal Meteorological Society 150(764), 2024. 4014-4048. DOI: 10.1002/qj.4803
3. Pruppacher H.R., Klett J.D., Microphysics of Clouds and Precipitation. // Springer: Cham, The Netherlands, 2010, 954 p.
4. Davitashvili T., Samkharadze I., Megreladze L., Kvatadze R., Using modern technology to protect vineyards from hail amid climate change. // E3S Web of Conferences, 2020. www.e3sconferences.org/articles/e3sconf/abs/2021/10/e3sconf_icies2020_00034/e3sconf_icies2020_00034
5. Hersbach H., Bell B., Berrisford P., Hirahara S., The ERA5 global reanalysis. // Quarterly Journal of the Royal Meteorological Society. June 2020, 146(730), 2020.
6. Davitashvili T., Samkharadze I., Amiranashvili A., Modelling Extreme Meteorological Processes Posing a Risk to Agriculture Under Modern Climate Change. // Reliability: Theory&Applications 20 (SI 9 (87)), 2025, pp. 619-628.
7. Davitashvili T., Samkharadze I., Monitoring of Aeolian Mineral Dust Transport from Deserts to the South Caucasus (Georgia) Under Complex Orography Conditions Using Modern Models and Satellite Images. // Processes 13, 2277, 2025. https://doi.org/10.3390/pr13072277

2nd International Scientific Conference "Modern Problems in Geophysics", Proceedings,
ISBN 978-9941-36-562-1, ISSN 3088-4349, Tbilisi, Georgia, October 29-31, 2026

# CALCULATED ASSESSMENT OF THE PARAMETERS OF VULNERABLE SECTIONS OF THE HYDRAULIC STRUCTURES OF THE TYRNYAUZ TAILINGS STORAGE FACILITY

**Sherkhov A.**

*Federal State Budgetary Institution "High-Mountain Geophysical Institute",*
*Nalchik, Kabardino-Balkaria, Russian Federation*
*fff.ddd.11@mail.ru*

***Abstract.*** *The paper assesses the conformity of the characteristics of selected sections of the hydraulic structures of the Tyrnyauz tailings storage facility with the changing conditions of their operation. Based on a comparative analysis of geoecological monitoring data collected for the facility over the past five years, numerical values of their geomorphological parameters were determined, and calculated characteristics of selected parameters were obtained.*

***Key words:*** *Drainage tunnel, debris-flow deposits, flow conveyance capacity, emergency channel.*

## Introduction

The Tyrnyauz Mining and Processing Plant (Tyrnyauz GOK) tailings storage facility has been the subject of close attention from specialists of relevant organizations (the Main Directorate of the Ministry of Emergency Situations of Russia for the Kabardino-Balkarian Republic, the Federal State Budgetary Institution "High-Mountain Geophysical Institute", "Sevkavvodkhoz", the Ministry of Natural Resources of the Kabardino-Balkarian Republic, and others) for several decades. The hydraulic structures (HS) of the enterprise, which until recently had no responsible owner, are currently in a deteriorated condition and do not correspond to the present natural and climatic conditions of the Gizgit River basin, where the facility was designed and constructed in the 1950s–1960s. Changes in the temperature and moisture balance caused by global climate transformations have resulted in the development of floods exhibiting debris-flow characteristics, for which the hydraulic structures of the facility were not originally designed.

The scenario of greatest concern to specialists is one in which a debris flow moving along the Gizgit River blocks the intake opening of Drainage Channel No. 2 of the tailings storage facility, followed by the flow entering the settling reservoir and subsequently reaching the tailings beach. This may result in water saturation of the stored material and failure of the main tailings dam, with potentially catastrophic consequences. To prevent such a scenario, an emergency open drainage channel was constructed in the early 2000s to ensure the safe conveyance of flow along the right end of the tailings dam into the Baksan River. The channel is 1.6 km long. At present, a landslide mass has developed along the right side of the channel in its upper third, substantially filling the channel over a length of 75 m. A detailed description of the monitoring zones and the infrastructure of the tailings storage facility as a whole was previously presented by the author [1]. The purpose of this study is to provide an up-to-date assessment of the situation based on the parameters of potentially hazardous sections and their conformity with the prevailing conditions.

## Methodology

The initial calculation data for the monitored facilities were obtained through digitization of aerial survey materials covering the tailings storage facility for 2021–2025. Analytical processing of the generated orthophotos and digital surface models makes it possible to determine their morphometric characteristics with high accuracy; the error in parameter determination was approximately 1.5–3.8%. The areas of the investigated zones and other initial data required for the calculations were determined using Agisoft Metashape Professional. The calculations of landslide stability and channel flow conveyance capacity in the section obstructed by the landslide were performed in accordance with regulatory documents and methodological sources [2–6], using different methods for different hydrological situations and flood-flow regimes.

## Results

Thus, for the section of debris-flow deposits approaching the intake portal of Drainage Tunnel No. 2, processing of orthorectified images acquired in different years in specialized geographic information applications made it possible to determine the following parameters: the total area of the deposits was 22,000 m²; the total area of the deposits covered by woody and shrubby vegetation was 9,400 m², accounting for 48% of the total area occupied by the deposited material; and the dynamics of vegetation development on the deposits over the period 2021–2025 were assessed, with an increase of 22%.

Since the format of the present paper does not allow all the details of the various calculation methods to be discussed, only the calculation results and their comparative analysis are presented below. It should be noted that the calculation results are preliminary. More accurate data would require extensive engineering surveys, laboratory testing, drilling, and other investigations, which were not performed in the present study. Typical calculated characteristics of loose clastic soil, including water-saturated soil, were adopted from tabulated normative values corresponding to the geological characteristics of the study area. Below, in figure 1, is a photo of the area under study.




**Fig. 1.** A landslidesectionin the channel of an openemergencyspillway. The bluelineindicates the drainagechannel, the dotted line is a fragment of the riverbedblocked by a landslide. Photofrom the quadcopter 06/03/2026.

Calculations of the stability coefficient of the landslide mass within the open emergency drainage channel were performed using the methods of three independent sources [2–4] for three types of conditions/scenarios: A – natural conditions; B – water-saturated conditions; C – water saturation combined with groundwater backwater. According to the orthophotos and the digital terrain models of the landslide section, the slope angle was 18°; the area of the landslide body was 32,000 m².

The calculation results are presented in the consolidated Table 1.

**Table 1.** Calculated values of the stability coefficient of the landslide section within the open emergency drainage channel

| Scenario | SP 116 | Dynamic Geomorphology | GOST R 54257 | Status |
|---|---|---|---|---|
| A – natural conditions | 7,85 | 1,75 | 1,46 | Stable |
| B – water saturation | 3,63 | 1,10 | 0,91 | Conditionally stable / risk |
| C – water saturation + groundwater backwater | 3,28 | 0,74 | 0,62 | Unstable |
| Threshold (Class I) | ≥ 1,25 | ≥ 1,10 | ≥ 1,25 | – |

The flow conveyance capacity of the channel specified during its construction was 245 m³/s at a 0.1% exceedance probability. According to the digital terrain models, the mean channel gradient in this section was 1.20°, while the mean residual cross-sectional area of the channel along the obstructed section was 48 m². The cross-section was assumed to be trapezoidal. Calculations were performed using three methods, including the Manning method for sediment-water and debris-flow conditions, with consideration of the relevant regulatory documents [2, 5]. The flow was considered either as a sediment-water flow or as a potential debris flow.

The results of the flow conveyance capacity calculations for the partially obstructed section of the water passage are presented in Table 2.

**Table 2.** Calculated flow conveyance capacity of the channel in the landslide-affected section

| Method. Flow regime | Conveyance capacity |
|---|---|
| Manning. Sediment-water flow | ~277 m³/s |
| Manning. Debris-flow regime | ~166 m³/s |

The calculated flow conveyance capacities presented above should be regarded as approximate, since a number of assumptions were made. These include, for example, the assumption of a regular trapezoidal cross-section and averaged values of the solid-phase concentration for sediment-water and mud-rock flows. These parameters should be refined through a more detailed hydrogeological investigation of the facility.

## Conclusions

The numerical assessment based on the analysis of multi-temporal aerial survey data and spatial-temporal changes in the morphometric parameters of hydraulic-structure zones of the Tyrnyauz Mining and Processing Plant tailings storage facility that are susceptible to emergency situations confirms the presence of additional risks associated with debris-flow activity along the Gizgit River.

The area of debris-flow deposits in the Gizgit River channel section adjacent to the intake head of the drainage tunnel was refined and found to be 22,000 m². An increase of 22% in the area occupied by woody and shrubby vegetation on the deposits was identified for the period 2021–2025. This is an adverse factor, since it substantially increases the probability of blockage of the drainage tunnel intake portal in the event of a debris flow along the Gizgit River.

Calculations of landslide-slope stability performed using three independent methods demonstrate substantial differences in the stability coefficient depending on hydrological conditions. Under natural soil conditions, the slope has a sufficient stability margin. Under water-saturated conditions, which may occur during a flood period in the Gizgit River basin, the parameter approaches the threshold values; when combined with a high groundwater level, it enters a high-risk zone. In the latter case, there is a high probability of channel blockage and complete loss of its conveyance capacity. Such a scenario is particularly hazardous because the channel is the only reserve water-conveyance structure available in the event of failure of the drainage tunnel.

Calculations of the conveyance capacity of the emergency channel show that, at present, in the section partially blocked by the landslide body, the channel is capable of conveying a sediment-water flood at the limit of its capacity, with a minimal safety margin, while localized erosion remains possible. However, in the event of a debris-rich mud-rock flow, the conveyance capacity will apparently be insufficient, which is highly likely to result in rapid reduction of the effective flow cross-section and the formation of a temporary blockage dam followed by its breach.

## References


1. Sherkhov A.Kh., Gergokova Z.Zh., Results of instrumental monitoring of the emergency section of the Tyrnyauz Mining and Processing Plant tailings storage facility. // Vestnik Vladikavkazskogo Nauchnogo Tsentra, Bulletin of the Vladikavkaz Scientific Center, No. 1, 2025, pp. 72–76.
2. SP 116.13330.2012. Engineering Protection of Territories against Hazardous Geological Processes.
3. Educational and Methodological Manual. Dynamic Geomorphology: Landslide Processes and Their Regional Characteristics.
4. GOST R 54257-2010. Reliability of Building Structures and Foundations.
5. SP 100.13330.2016. Hydraulic Design of Open Channels.
6. Gegiev K.A., Sherkhov A.Kh., Gergokova Z.Zh., On the analysis of existing methods for determining debris-flow velocity. // Debris Flows: Disasters, Risk, Forecast, Protection. Proceedings of the 5 th International Conference. Tbilisi, Georgia, October 1–5, Tbilisi: Universal, 2018, pp. 308–312.

2nd International Scientific Conference "Modern Problems in Geophysics", Proceedings,
ISBN 978-9941-36-562-1, ISSN 3088-4349, Tbilisi, Georgia, October 29-31, 2026

# STATISTICAL ANALYSIS OF ANNUAL PRECIPITATION SUM WITH DIFFERENT PROVISIONS IN GEORGIA

***Amiranashvili A., *Chelidze T., *Elizbarashvili I., *Kiria T., **Tsamalashvili T., *Varamashvili N.**

**M. Nodia Institute of Geophysics of I. Javakhishvili Tbilisi State University, Tbilisi, Georgia*
***A. Janelidze Geological Institute of I. Javakhishvili Tbilisi State University, Tbilisi, Georgia*
*avtandilamiranashvili@gmail.com*

***Abstract.*** *Data on calculated annual atmospheric precipitation with 1% provision for 83 meteorological stations in Georgia are presented. A comparative statistical analysis of minimum, maximum and mean annual precipitation sums with annual sums precipitation with different provision for the territory of Georgia as a whole, as well as for its regions and eastern and western parts is conducted. Correlation and regression relationships between the parameters under study have been established.*

***Key Words****: Atmospheric precipitation, precipitation with different provision, statistical analysis.*

## Introduction

In recent years, the M. Nodia Institute of Geophysics, TSU has conducted research on landslide processes in Georgia, including their links to atmospheric processes [1–12]. We have investigated the impact of precipitation on landslide activation across time scales ranging from tens of minutes [1, 2] to several days [3–5], months [6–10], and years (climatic time scale) [11]. Additionally, data on 5-day moving precipitation sums with a 1% provision were used to map the stationary hazard of slope processes in Georgia, accounting for the triggering effect of precipitation [12].

To assess the long-term risks of landslide reactivation driven by precipitation, data on annual precipitation sums with varying provision are required. Such data for 83 meteorological stations in Georgia are available in the handbook [13]. Given that this source lacks information on annual precipitation sums with a 1% provision, we performed the necessary calculations to supplement the existing data.

In addition, we conducted a comparative statistical analysis of minimum, maximum and mean annual precipitation sums with annual precipitation sums with different provisions for the territory of Georgia as a whole, as well as for its regions and eastern and western parts. The results of the analysis are presented below.

## Study area, material and methods

Study area – 12 region of Georgia: 1. Autonomous Republic of Abkhazia (Abkh); 2. Samegrelo-Zemo Svaneti (S-ZS); 3. Guria (Gur); 4. Autonomous Republic of Adjara (Adj); 5. Samtskhe-Javakheti (S-J); 6. Kvemo Kartli (KK); 7. Tbilisi (Tb); 8. Kakheti (Kakh); 9. Mtskheta-Mtianeti (MM); 10. Shida Kartli (Sh K); 11. Imereti (Im); 12. Racha-Lechkhumi and Kvemo Svaneti (RLKS). Data of the handbook [13] on annual sum of atmospheric precipitation, as well as data on annual precipitation sums with provision (95%, 90%, 80% ... 20%, 10%, 5% and 2%) for 83 meteorological stations in Georgia in 1961-1990 are used. The annual precipitation sum with a 1% provision was calculated by extrapolating data available in this handbook. The standard statistical methods are used [14]. The following designations will be used below: Pmin, Pmax, Pmean – minimal, maximal and mean annual sums of precipitation respectively; P(95%)… P(1%) – the annual precipitation sum with corresponding provision; St Dev – standard deviation; R2 – coefficient of determination; R – coefficient of linear correlation; R' – index of correlation for nonlinear relationships. The degree of correlation was determined in accordance with [14]: very high correlation ($0.9 \leq R \leq 1.0$); high correlation ($0.7 \leq R < 0.9$); moderate correlation ($0.5 \leq R < 0.7$); low correlation ($0.3 \leq R< 0.5$); negligible correlation ($0 \leq R < 0.3$).

The dimension of atmospheric precipitation (mm) is often omitted from the text below.

## Results

Results in Fig. 1-4 and Tables 1-5 are presented. Fig. 1 and Table 1 present data on the distribution of P(1%) across the territory of Georgia.

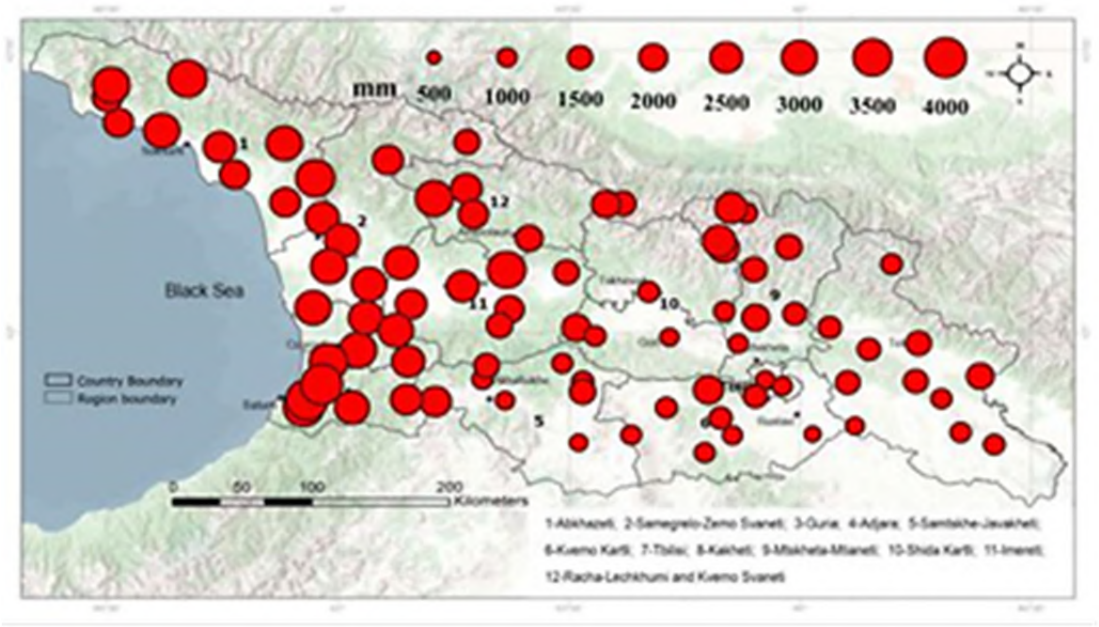



**Fig. 1.** Distribution of P(1%) on territory of Georgia.

**Table 1.** Annual precipitation sum with 1% provision for 83 stations in Georgia.

| Station | P(1%) | Station | P(1%) | Station | P(1%) | Station | P(1%) |
|---|---|---|---|---|---|---|---|
| Abastumani | 1085 | Gori | 905 | Lentekhi | 2300 | Pskhu | 3508 |
| Ambrolauri | 1803 | Gudauta | 3050 | Mamisoni_pass | 1635 | Keda | 2793 |
| Anaseuli | 3232 | Gudauri | 2246 | Manglisi | 2118 | Kobuleti | 3461 |
| Akhalgori | 1109 | Gurjaani | 1469 | Martvili | 2822 | Kutaisi | 2531 |
| Akhalkalaki | 835 | Dedoplistskaro | 1091 | Mestia | 1631 | Kazbegi | 2471 |
| Akhaltsikhe | 923 | Dmanisi | 1073 | Sabueti_m | 1982 | Kvareli | 1588 |
| Akhmeta | 1328 | Dusheti | 1867 | Mukhrani | 1001 | Shiraki | 1126 |
| Babushera | 2170 | Zekari_pass | 1562 | Omalo | 1142 | Shovi | 1949 |
| Batumi_Air | 3847 | Zestafoni | 2034 | Ochamchire | 2241 | Chakvi | 4060 |
| Batumi | 4060 | Zugdidi | 2924 | Sagarejo | 1472 | Chokhatauri | 2915 |
| Bakuriani | 1207 | Tbilisi, Digomi | 950 | Samgori | 993 | Tsageri | 2162 |
| Barisakho | 1663 | Tetritskaro | 1310 | Samtredia | 2354 | Tskhinvali | 1180 |
| Bakhmaro | 2573 | Telavi | 1321 | Sachkhere | 1595 | Tskhratskaro | 1663 |
| Bichvinta | 2153 | Tianeti | 1359 | Senaki | 2934 | Tsalka | 1167 |
| Bolnisi | 985 | Torsa | 3116 | Sokhumi | 2513 | Tsipa | 1671 |
| Borjomi | 1055 | Kvezani | 3512 | Stephantsminda | 1152 | Tsnori | 1070 |
| Gagra | 2195 | Kojori | 1399 | Tkibuli | 3444 | Khaishi | 2269 |
| Gagra_ridge | 3240 | Lagodekhi | 1804 | Udabno | 872 | Khashuri | 1136 |
| Gali | 2773 | Lata | 3072 | Paravani | 1037 | Khulo | 2387 |
| Gardabani | 722 | Lanchkhuti | 2898 | Pasanauri | 1628 | Jvari_pass | 2607 |
| Goderdzi_pass | 2342 | Lebarde | 3279 | Poti | 3066 | | |

As follows from Fig. 1 and Table 1 value of P(1%) change from 722 (Gardabani) to 4060 (Batumi).

In Table 2 data about average values of $P_{mean}$ and P(1%) by regions of Georgia is presented. $P_{mean}$ change from 600 (Tbilisi) to 2074 (Adjara) and P(1%) – from 1114 (Tbilisi) to 3279 (Adjara).

**Table 2.** Average values of $P_{mean}$ and P(1%) by regions of Georgia.

| Region | Abkh | S-ZS | Gur | Adj | S-J | KK | Tb | Kakh | MM | ShK | Im | R-L KS |
|---|---|---|---|---|---|---|---|---|---|---|---|---|
| $P_{mean}$ | 1653 | 1644 | 1820 | 2074 | 734 | 628 | 600 | 730 | 996 | 613 | 1335 | 1143 |
| P(1%) | 2766 | 2755 | 2905 | 3279 | 1115 | 1229 | 1114 | 1298 | 1777 | 1082 | 2147 | 1970 |

Linear regression P(1%) with $P_{mean}$ averaged by regions of Georgia (Table 2) is: $P(1\%) = 1.5188 \cdot P_{mean} = 184.92$ (R = 0.99, very high correlation).

The regression equations for the spatial (two-dimensional) distribution of the values $P_{mean}$ and P(1%) across the territory of Georgia (Table 3, Fig. 2; x – latitude, y – longitude) are as follows:

$$P_{mean} = a+b/x+c\cdot\log(y)+d/x^2+e\cdot\log(y)^2+f\cdot\log(y)/x+g/x^3+h\cdot\log(y)^3+i\cdot\log(y)^2/x+j\cdot\log(y)/x^2,\ R'=0.88.$$

$$P(1\%) = a+b/x+c\cdot y+d/x^2+e\cdot y^2+f\cdot y/x+g/x^3+h\cdot y^3+i\cdot y^2/x+j\cdot y/x^2,\ R'=0.86$$

(high correlation for both distributions).

**Table 3.** Regression equation coefficients of spatial distribution (two-dimensional) of $P_{mean}$ and P(1%) on territory of Georgia

| Coeff. | a | b | c | d | e | f | g | h | i | j |
|---|---|---|---|---|---|---|---|---|---|---|
| $P_{mean}$ | -5.7E+08 | 8.6E+09 | 4E+08 | 1.08E+11 | -8.8E+07 | -5.9E+09 | 3.53E+10 | 5871930 | 9.68E+08 | -2.93E+10 |
| P(1%) | -2.8E+07 | -6.3E+08 | 2329002 | 4.15E+10 | -50568.6 | -1.6E+07 | 1.22E+11 | 248.8119 | 818633.1 | -1.2E+09 |

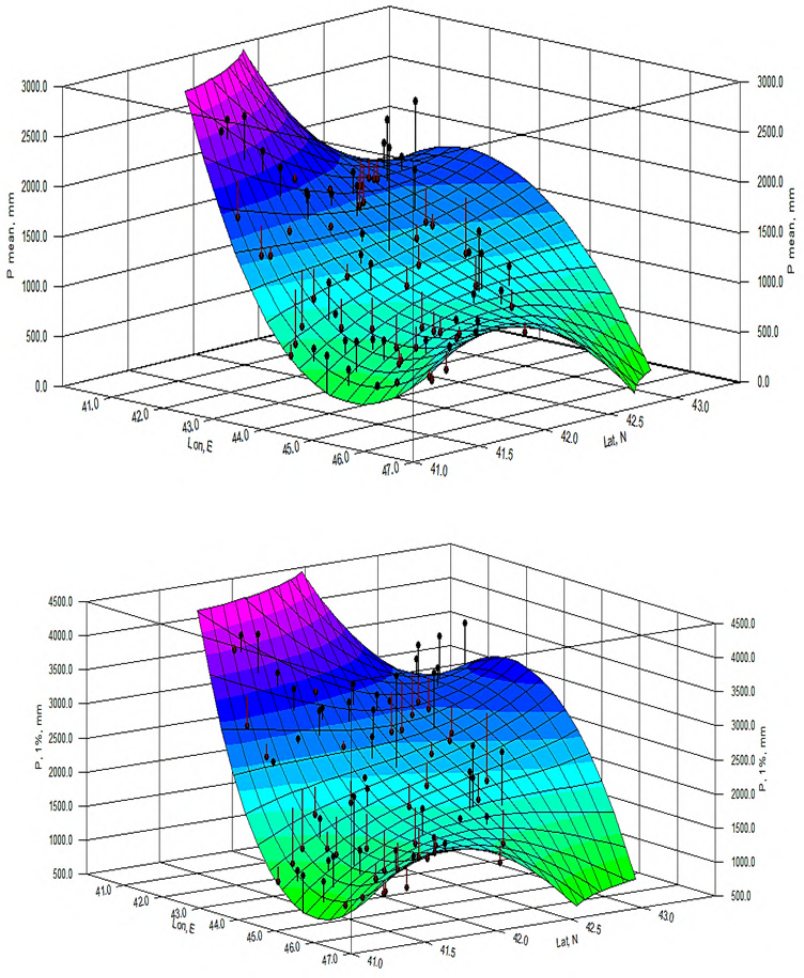



**Fig. 2.** Calculation model (two-dimensional) of distribution of $P_{mean}$ (on the left) and P(1%) (on the right) on territory of Georgia.

Fig. 3 shows the vertical distributions of $P_{mean}$ and P(1%) in Eastern and Western Georgia.

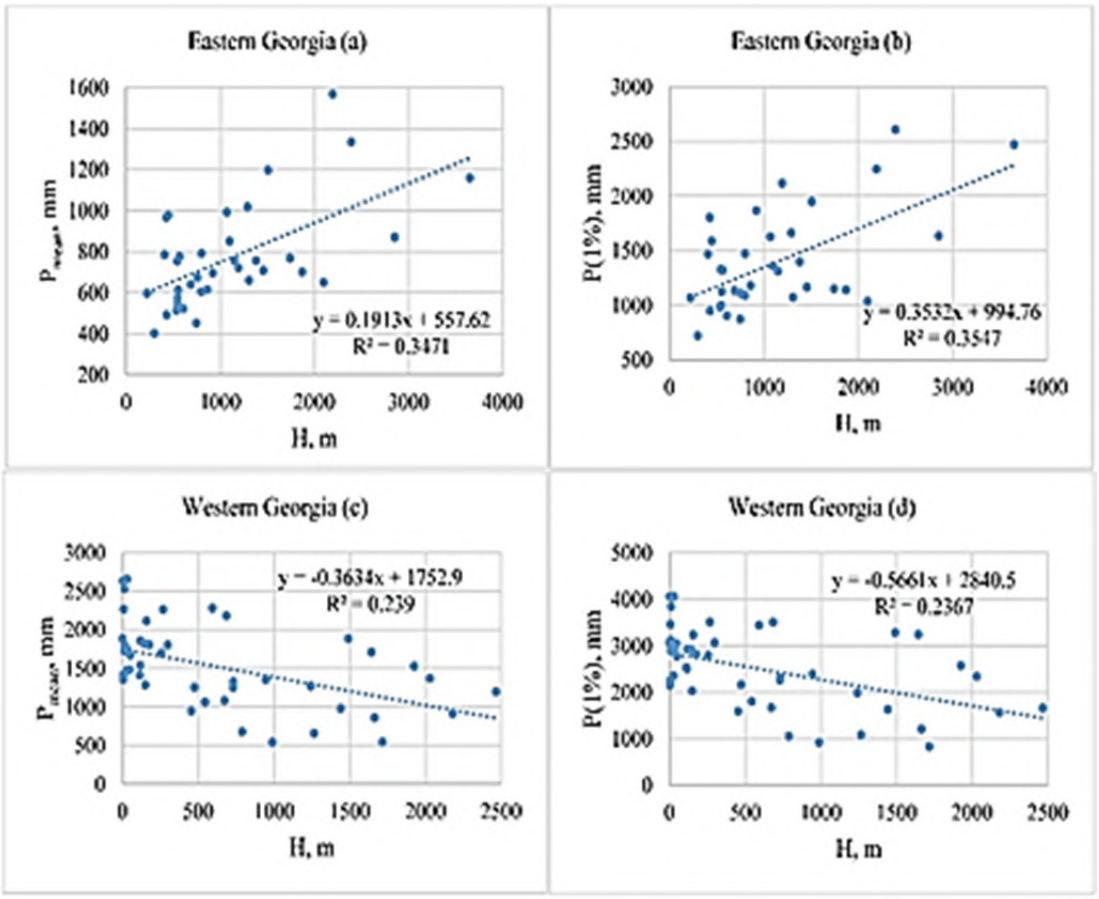



**Fig. 3.** Vertical distributions of $P_{mean}$ and P(1%) in Eastern and Western Georgia.

In Eastern Georgia, the values of P and P(1%) increase linearly with terrain elevation (R = 0.59 and 0.60; Figs. 3a and 3b, respectively; moderate correlation). In Western Georgia, the values of P and P(1%) decrease linearly with terrain elevation (R = -0.49 for both distributions; Figs. 3c and 3d, respectively; low correlation).

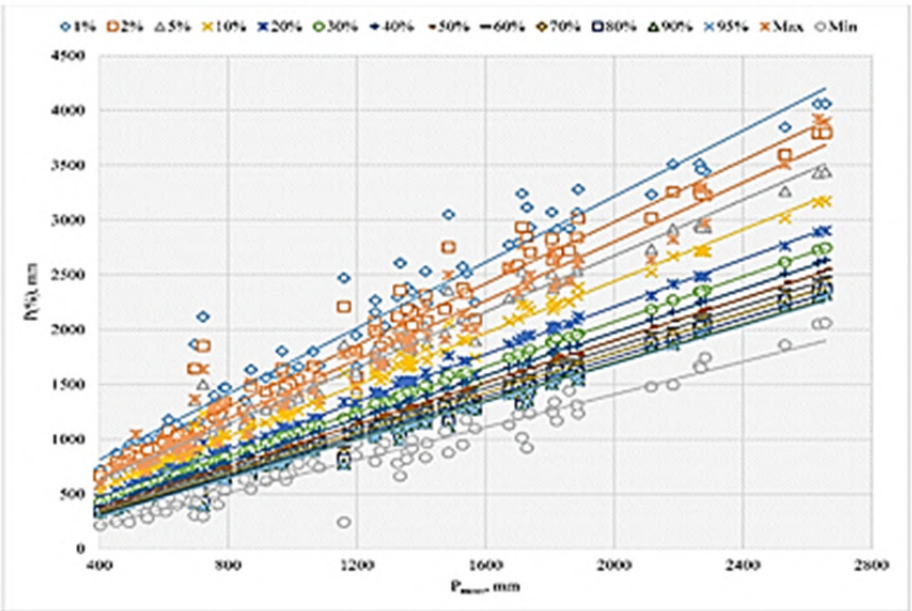



**Fig. 4.** Linear regression $P_{mean}$ with $P_{max}$, $P_{min}$ and P(1%)…P(95%) in Georgia.

**Table 4.** Coefficients of linear regression $P_{mean}$ with $P_{max}$, $P_{min}$ and P(1%)…P(95%) in Georgia. $R_{min}$ = 0.971(very high correlation).

| Variable | a | b | Variable | a | b |
|---|---|---|---|---|---|
| P(1%) | 1.501171 | 211.4135 | P(60%) | 0.932551 | -26.2474 |
| P(2%) | 1.4049 | 171.1538 | P(70%) | 0.911184 | -35.2248 |
| P(5%) | 1.277657 | 117.9949 | P(80%) | 0.892621 | -42.9789 |
| P(10%) | 1.181378 | 77.72143 | P(90%) | 0.876215 | -49.7691 |
| P(20%) | 1.085131 | 37.52975 | P(95%) | 0.868741 | -52.9978 |
| P(30%) | 1.028787 | 13.99394 | $P_{max}$ | 1.34626 | 108.5561 |
| P(40%) | 0.988923 | -2.85269 | $P_{min}$ | 0.74778 | -86.761 |
| P(50%) | 0.957835 | -15.6498 | | | |

Fig. 4 and Table 4 present data on linear regression $P_{mean}$ with $P_{max}$, $P_{min}$ and P(1%)…P(95%) in Georgia. It should be noted that the high level of correlation between the parameters under study makes it possible to estimate the values of $P_{max}$, $P_{min}$, and P(1%)…P(95%) for any weather station – even one with a short observation record that is not included in the handbook [13] – based solely on $P_{mean}$ values.

Finally in Table 5 statistical characteristics of $P_{mean}$, $P_{max}$, $P_{min}$ and and P(1%)…P(95%) in Georgia is presented.

**Table 5.** Statistical characteristics of $P_{mean}$, $P_{max}$, $P_{min}$ and and P(1%)…P(95%) in Georgia.

| Variable | Max | Min | Average | St Dev | Variable | Max | Min | Average | St Dev |
|---|---|---|---|---|---|---|---|---|---|
| $P_{mean}$ | 2657 | 403 | 1201 | 570 | P(50%) | 2550 | 379 | 1135 | 547 |
| P(1%) | 4060 | 722 | 2014 | 879 | P(60%) | 2480 | 363 | 1094 | 533 |
| P(2%) | 3793 | 661 | 1858 | 817 | P(70%) | 2420 | 349 | 1059 | 521 |
| P(5%) | 3439 | 581 | 1652 | 737 | P(80%) | 2369 | 337 | 1029 | 511 |
| P(10%) | 3171 | 520 | 1497 | 677 | P(90%) | 2323 | 327 | 1003 | 503 |
| P(20%) | 2904 | 459 | 1341 | 620 | P(95%) | 2302 | 322 | 990 | 499 |
| P(30%) | 2747 | 423 | 1250 | 587 | $P_{max}$ | 3925 | 585 | 1725 | 784 |
| P(40%) | 2636 | 398 | 1185 | 564 | $P_{min}$ | 2062 | 213 | 811 | 439 |

In particular, maximum values of parameters under study change from 2062 to 4060, minimum – from 213 to 722 and average – from 811 to 2014.

## Conclusion

In the near future, the results of this work will be used to study climate change in Georgia and to assess the risk of various natural disasters (including landslides) driven by extreme precipitation, covering Georgia as a whole as well as its individual regions and settlements.

**Acknowledgment:** This work was supported by Shota Rustaveli National Science Foundation of Georgia (SRNSFG), Grant number FR-23-5466, “Machine Learning Approach to the Landslide Activation Prediction in Georgia”.

## References

1. Amiranashvili A., Chelidze T., Svanadze D., Tsamalashvili T., Tvauri G., Abnormal Precipitation Before the Landslide in Akhaldaba (A Suburb of Tbilisi, Georgia) on June 13, 2015 According to Radar Measurements. // Journal of the Georgian Geophysical Society, e-ISSN: 2667-9973, p-ISSN: 1512-1127, Physics of Solid Earth, Atmosphere, Ocean and Space Plasma, v. 26(1), 2023, pp. 30–41. https://ggs.openjournals.ge/index.php/GGS/article/view/6959
2. Amiranashvili A., Chelidze T., Kiria T., Svanadze D., Tsamalashvili T., Varamashvili N., Retrospective Analysis of Landslides Processes in Akhaldaba (A Suburb of Tbilisi, Georgia) on June 13-14, 2015. // Journal of the Georgian

Geophysical Society, e-ISSN: 2667-9973, p-ISSN: 1512-1127, Physics of Solid Earth, Atmosphere, Ocean and Space Plasma, v.29(1), 2026, pp. 50-59. https://ggs.openjournals.ge/index.php/GGS/article/view/12084

3. Amiranashvili A., Brocca L., Chelidze T., Kiria T., Svanadze D., Tsamalashvili T., Varamashvili N. Assessment of the Relationship Between Daily and Total Multi-Day Precipitation Sums and Landslide Activation in the Regions of Georgia. // Journal of the Georgian Geophysical Society, e-ISSN: 2667-9973, p-ISSN: 1512-1127, Physics of Solid Earth, Atmosphere, Ocean and Space Plasma, v.29(1), 2026, pp. 27-49. https://ggs.openjournals.ge/index.php/GGS/article/view/12083
4. Chelidze T., Amiranashvili A., Svanadze D., Tsamalashvili T., Tvauri G., Terrestrial and satellite-based assessment of rainfall triggered landslides activity in Georgia, Caucasus. // Bull. Georg. Nat. Acad. Sci., vol. 17, no. 2, 71-77, 2023, http://science.org.ge/bnas/vol-17-2.html
5. Chelidze T., Kiria T., Amiranashvili A., Svanadze D., Tsamalashvili T., Varamashvili N., Landslide Hazard Maps of Georgia Using Machine Learning Approach. // Bull. Georg. Nat. Acad. Sci., ISSN: 0132 – 1447, vol. 20(194), no. 2, 2026, pp. 23-29. http://science.org.ge/bnas/t20-n2/03_Chelidze_Geophysics.pdf
6. Amiranashvili A., Brocca L., Chelidze T., Kiria T., Svanadze D., Tsamalashvili T., Varamashvili N., Intra-Annual Distribution of Landslide Recurrence in Georgia and its Relationship with Monthly and Cumulative Multi-Month Sums of Precipitation. // Journal of the Georgian Geophysical Society, e-ISSN: 2667-9973, p-ISSN: 1512-1127, Physics of Solid Earth, Atmosphere, Ocean and Space Plasma, v.28(2), 2025, pp. 25-30. https://ggs.openjournals.ge/index.php/GGS/article/view/10453
7. Amiranashvili A., Brocca L., Chelidze T., Kiria T., Svanadze D., Tsamalashvili T., Varamashvili N., Statistical Analysis of the Relationship Between Monthly and Cumulative Multi-Month Sums of Precipitation with the Number of Landslides in the Regions of Georgia. // Transactions of Mikheil Nodia Institute of Geophysics, ISSN 1512-1135, vol. LXXVIII, Publish House of Ivane Javakhishvili Tbilisi State University, Tbilisi, 2025, pp. 49-66. http://dspace.gela.org.ge/bitstream/123456789/10809/1/7_Tr_IG_78_2025.pdf
8. Amiranashvili A., Brocca L., Chelidze T., Svanadze D., Tsamalashvili T., Varamashvili N., Statistical Analysis of the Number of Damaging Landslides in Municipalities and Regions of Georgia and their Relationship with Atmospheric Precipitation in 2015-2024. // Reliability: Theory and Applications, ISSN 1932-2321, Volume 20, Special Issue No. 9 (87), November 2025, pp. 255-264. https://doi.org/10.24412/1932-2321-2025-987-255-264
9. Amiranashvili A., Brocca L., Chelidze T., Kiria T., Svanadze D., Tsamalashvili T., Varamashvili N., Peculiarities of Intra-Annual Distribution of Landslide Recurrence in Adjara and Guria Regions (Western Georgia) and in Eastern Georgia and their Relationship with Monthly Sums of Precipitation. // Journal of the Georgian Geophysical Society, e-ISSN: 2667-9973, p-ISSN: 1512-1127, Physics of Solid Earth, Atmosphere, Ocean and Space Plasma, v.29(1), 2026, pp. 60-68. https://ggs.openjournals.ge/index.php/GGS/article/view/12085
10. Amiranashvili A.G., Brocca L., Chelidze T.L., Svanadze D.T., Tsamalashvili T.N., Varamashvili N.D., Statistical Analysis of Annual and Semi-Annual Sum of Atmospheric Precipitation Data for 59 Municipalities (11 Regions) of Georgia with Landslide Hazard Zones from 2015 to 2024. // Journal of the Georgian Geophysical Society, e-ISSN: 2667-9973, p-ISSN: 1512-1127 Physics of Solid Earth, Atmosphere, Ocean and Space Plasma, v.28(1), 2025, pp. 50 – 63. https://ggs.openjournals.ge/index.php/GGS/article/view/9249
11. Amiranashvili A., Chelidze T., Svanadze D., Tsamalashvili T., Tvauri G., Some results of a study of the relationship between the mean annual sum of atmospheric precipitation and re-activated and new landslide cases in Georgia taking into account of climate change. // Journal of the Georgian Geophysical Society, e-ISSN: 2667-9973, p-ISSN: 1512-1127, Physics of Solid Earth, Atmosphere, Ocean and Space Plasma, v. 25(2), 2022, pp. 38–48. https://openjournals.ge/index.php/GGS/article/view/5959
12. Chelidze, T., Tsamalashvili, T., Fandoeva, M., Mass-movement stationary hazard maps of Georgia including precipitation triggering effect: fuzzy logic approach. // Bull. Georg. Nat. Acad. Sci., vol. 16, no. 2, 56-63, 2022, http://science.org.ge/bnas/t16-n2/07_Chelidze_Geophysics.pdf
13. Sakartvelos sametsniero-gamoqenebiti klimaturi tsnobari. // Gamomtsemloba "Universali", ISBN 978-9941-26-798-7, Tbilisi, 2020, 307 p.
14. Hinkle D. E., Wiersma W., Jurs S. G., Applied Statistics for the Behavioral Sciences. // Boston, MA, Houghton Mifflin Company, 2003.

2nd International Scientific Conference "Modern Problems in Geophysics", Proceedings,
ISBN 978-9941-36-562-1, ISSN 3088-4349, Tbilisi, Georgia, October 29-31, 2026

# ESTIMATION OF THE ANNUAL DAMAGE LANDSLIDES NUMBER IN GEORGIA IN RELATION TO AVERAGE ANNUAL EXTREME PRECIPITATION SUMS OF DIFFERENT PROVISION

**[*]Amiranashvili A., [*]Chelidze T., [*]Kiria T., [**]Tsamalashvili T., [*]Varamashvili N.**

*[*]M. Nodia Institute of Geophysics of I. Javakhishvili Tbilisi State University, Tbilisi, Georgia*
*[**]A. Janelidze Geological Institute of I. Javakhishvili Tbilisi State University, Tbilisi, Georgia*
*avtandilamiranashvili@gmail.com*

***Abstract.*** *An assessment estimation of the annual damage landslides number (DLSN) in Georgia in relation to average annual extreme precipitation sums with 10%, 5%, 2% and 1% provision is conducted. In particular, mean annual value of DLSN may vary from 1177 to 2790 for mean annual sum of atmospheric precipitation with provision 10% and 1% respectively.*

***Key Words****: Damage landslides number, extreme precipitation with different provision, statistical analysis.*

## Introduction

Landslides are a type of natural disaster occurring almost everywhere [1], including in Georgia, a country characterized by diverse terrain [2]. They inflict immense damage on infrastructure, the economy, and the environment, disrupting people's daily lives [3, 4].

The triggering of landslides is driven by a combination of natural and anthropogenic factors: heavy and prolonged precipitation, as well as the rapid melting of seasonal snow cover or glaciers, which leads to soil saturation and a consequent significant reduction in soil strength and stability; the presence of steep slopes, specific rock compositions, inclined bedding, and fracturing; fluctuations in groundwater levels and surface water hydrological regimes; earthquakes and tectonic movements capable of triggering the collapse of unstable slopes; improper construction and mining practices, slope destabilization during road construction, excessive soil removal, and large-scale deforestation that weakens the stabilizing function of plant root systems; and the region's general climatic conditions, which determine the likelihood and intensity of processes conducive to landslide formation [5, 6].

Therefore, long-term forecasting of landslide reactivation – especially when taking into account the multitude of factors mentioned above – is extremely difficult. In particular, we employed statistical forecasting methods for this purpose in studies [7, 8].

The paper [7] presents the results of a study of the variability features of the annual number of registered landslides (LS) in Georgia in 1995-2024 and their expected change up to 2030. The stability of the time series of LS values was studied by determining their correlation links over time (linear correlation, Kendall and Spearman rank correlation). The level of autocorrelation in the time series of LS values was determined. The periodicity of these time series was studied. Interval forecasting of LS values up to 2030 was carried out, taking into account the periodicity in the observation series.

In paper [8], some results of statistical analysis of long-term variations of annual amount of atmospheric precipitation for 21 meteorological stations of Georgia (P) located in areas with landslides, average annual sum of precipitation for these stations ($P_a$), relationship between the $P_a$ and number of re-activated and new cases of landslides, and the estimated values of LS up to 2045 using predictive data on $P_a$ are presented. Data from the Environmental Agency of Georgia on the P in period 1936 – 2020 and data on LS in period 1996 – 2018 are used.

The forecast of $P_a$ using the AAA version of the Exponential Smoothing (ETS) algorithm was carried out. The forecast of the $P_a$ value up to 2040 were estimated taking into account the periodicity of precipitation variability, which is 11 years. A cross-correlation analysis of the time series of the $P_a$ and LS values

showed that the best correlation between the indicated parameters is observed with a five-year advance of precipitation data. With this in mind, a linear regression equation was obtained between the five-year moving average of the $P_a$ and the five-year moving average of the LS values. Using this equation and predictive $P_a$ data, five-year moving averages of re-activated and new landslides cases up to 2045 were estimated.

This work is a continuation of previous studies [7, 8]. An assessment estimation of the annual damage landslides number in Georgia in relation to average annual extreme precipitation sums with 10%, 5%, 2% and 1% provision is presented below.

## Study area, material and methods

Study area – Georgia. Data of the Geological bulletins [9] about average annual sum of precipitation from 25 meteorological stations and annual damage landslides number (DLSN) in Georgia in the period from 2015 to 2024 are used.

The following designations will be used below P – average annual sum of precipitation for 25 meteorological stations; P(10%), P(5%), P(2%), P(1%) – corresponding average provision for mean annual sum of atmospheric precipitation 25 meteorological stations; P_67%Low, P_67%Upp, P_99%Low, P_99%Upp – lower and upper levels of confidence interval of average values with indicted probability; $R^2$ – coefficient of determination; R' – index of correlation for nonlinear relationships. Data about P(10%), P(5%), P(2%) and P(1%) taken from [10,11]. In the proposed work the analysis of data is carried out with the use of the standard statistical analysis methods [12].

The dimension of atmospheric precipitation (mm) is often omitted from the text below.

## Results

Results in Fig. 1, 2 and Tables 1, 2 are presented.

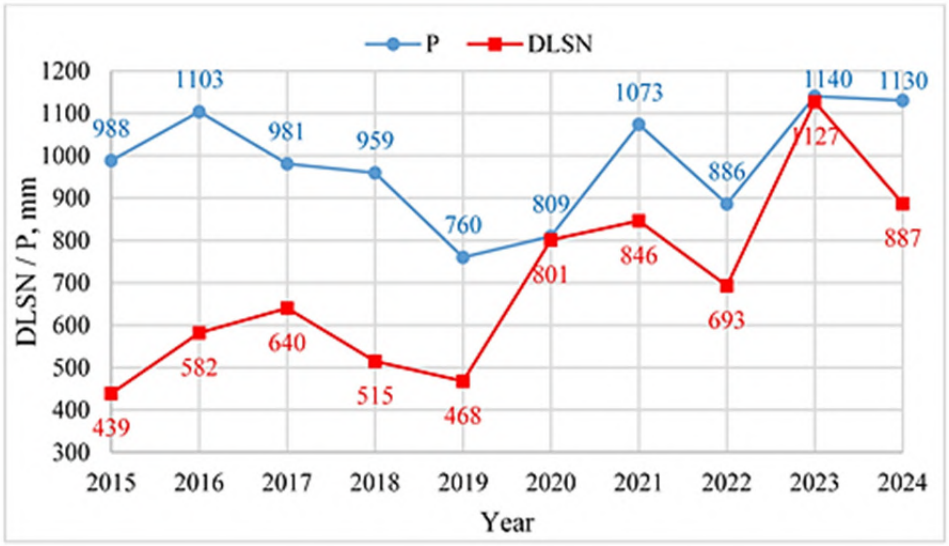



**Fig. 1.** Variability of annual damage landslides number (DLSN) and mean annual sum of atmospheric precipitation (P) in Georgia in 2015-2024.

Fig. 1 present variability of annual damage landslides number and mean annual sum of atmospheric precipitation (P) in Georgia in 2015-2024. P – average for 25 meteorological stations. As follows from this figure value of P change from 760 (2019 year) to 1140 (2023 year) mm, and value of DLSN – from 439 (2015 year) to 1127 (2023 year).

The average annual precipitation across 25 weather stations in Georgia ranges from 1239 to 1687 mm, with precision ranging from 10% to 1% (Table 1). This same table presents data on the lower and upper limits of the mean values P(10%)…P(1%), which range from 1187 (P_67%Low) to 1753 mm (P_67%Upp) and from 1104 (P_99%Low) to 1858 mm (P_99%Upp).

**Table 1.** Average annual precipitation sum for 25 meteorological stations in Georgia – including upper and lower values – at various provision.

| Provision | P | P_67%Low | P_67%Upp | P_99%Low | P_99%Upp |
|---|---|---|---|---|---|
| P(10%) | 1239 | 1187 | 1291 | 1104 | 1374 |
| P(5%) | 1374 | 1317 | 1430 | 1228 | 1520 |
| P(2%) | 1552 | 1490 | 1614 | 1392 | 1712 |
| P(1%) | 1687 | 1620 | 1753 | 1516 | 1858 |

The relationship between the number of damage landslides and the mean annual sum of atmospheric precipitation has the form:

$$DLSN = a+b\cdot\log(P)+c\cdot\log(P)^2,\ R^2 = 0.392,\ R' = 0.63$$ (moderate correlation [12]).

This relationship is shown graphically in the bottom-left part of Fig. 2.

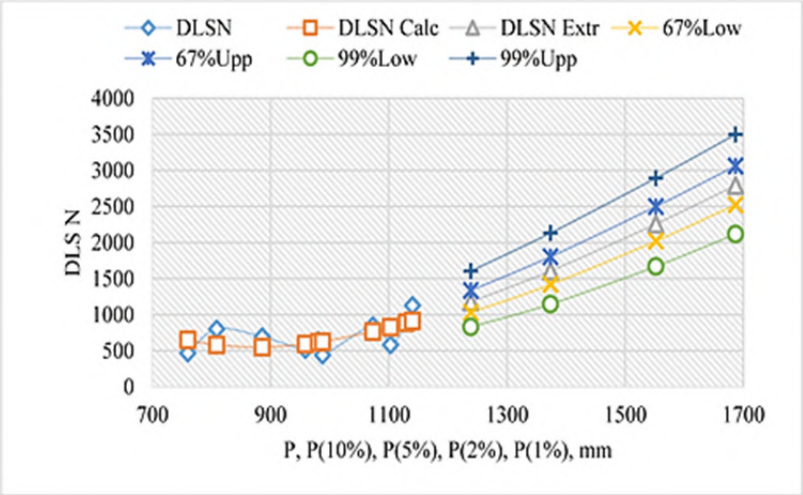



**Fig. 2.** Extrapolation of damage landslides number for mean annual sum of atmospheric precipitation with different provision.

The upper right part of Fig. 2 shows DLSN values extrapolated using the formula mentioned above, based on the precipitation data presented in Table 1.

Numerical data on extrapolated damage landslides number for mean annual sum of atmospheric precipitation – including upper and lower values – with different provisions in Table 2 is presented.

**Table 2.** Data on extrapolated damage landslides number (DLSN) for mean annual sum of atmospheric precipitation – including upper and lower values – with different provision (Fig. 2).

| Provision | P | Damage Landslides Number (DLSN) | | | | |
|---|---|---|---|---|---|---|
| | | Extrapolation | 67%Low | 67%Upp | 99%Low | 99%Upp |
| P(10%) | 1239 | 1177 | 1031 | 1336 | 829 | 1606 |
| P(5%) | 1374 | 1607 | 1419 | 1805 | 1146 | 2133 |
| P(2%) | 1552 | 2257 | 2022 | 2499 | 1669 | 2893 |
| P(1%) | 1687 | 2790 | 2524 | 3061 | 2118 | 3499 |

In particular, mean annual value of DLSN may vary from 1177 to 2790 for mean annual sum of atmospheric precipitation with provision 10% and 1% respectively.

## Conclusion

Going forward, as new data is accumulated, there are plans to continue such studies for specific regions and localities in Georgia.

**Acknowledgment:** This work was supported by Shota Rustaveli National Science Foundation of Georgia (SRNSFG), Grant number FR-23-5466, "Machine Learning Approach to the Landslide Activation Prediction in Georgia".

## References

1. Li H., Samsudin N. A. A, Systematic Review of Landslide Research in Urban Planning Worldwide. // Nat Hazards, 121, 2025, pp. 6391–6411. https://doi.org/10.1007/s11069-024-07064-4
2. Amiranashvili A., Elizbarashvili E., Gaprindashvili G., Varazanashvili O., Fuchs S., Statistical Analysis of Parameterized Landslide Data in Georgia from 1900 to 2022. // Reliability: Theory and Applications, ISSN 1932-2321, Special Issue № 6 (81), Part-2, Vol. 19, 2024, pp. 812 – 818. https://doi.org/10.24412/1932-2321-2024-681-812-818
3. Froude M., Petley D., Global Fatal Landslide Occurrence from 2004 to 2016. // Nat. Hazards Earth Syst. Sci., 18, 2018, pp. 2161–2181.
4. Amiranashvili A., Chelidze T., Kiria T., Svanadze D., Tsamalashvili T., Varamashvili N., Retrospective Analysis of Landslides Processes in Akhaldaba (A Suburb of Tbilisi, Georgia) on June 13-14, 2015. // Journal of the Georgian Geophysical Society, e-ISSN: 2667-9973, p-ISSN: 1512-1127, Physics of Solid Earth, Atmosphere, Ocean and Space Plasma, v.29 (1), 2026, pp. 50-59. https://ggs.openjournals.ge/index.php/GGS/article/view/12084
5. Dalğıç S., Karimov E., Investigation of Landslide Mechanism in the Balaban Landslide Area using 3D Numerical Modelling. // Int. Journal of Sustainability and Risk Control, Vol.1, No 2(2), Baku, Azerbaijan, September 2025, pp. 31-35.
6. Amiranashvili A., Brocca L., Chelidze T., Svanadze D., Tsamalashvili T., Varamashvili N., Statistical Analysis of the Number of Damaging Landslides in Municipalities and Regions of Georgia and their Relationship with Atmospheric Precipitation in 2015-2024. // Reliability: Theory and Applications, ISSN 1932-2321, Volume 20, Special Issue No. 9 (87), November 2025, pp. 255-264.
7. Amiranashvili A., Brocca L., Chelidze T., Svanadze D., Tsamalashvili T., Varamashvili N., Variability of the Annual Number of Registered Landslides and Mudflows in Georgia in 1995-2024 and their Expected Change up to 2030. // Transactions of Mikheil Nodia Institute of Geophysics, ISSN 1512-1135, vol. LXXVIII, Publish House of Ivane Javakhishvili Tbilisi State University, Tbilisi, 2025, pp. 67-74. http://dspace.gela.org.ge/bitstream/123456789/10808/1/8_Tr_IG_78_2025.pdf
8. Amiranashvili A., Chelidze T., Svanadze D., Tsamalashvili T., Tvauri G., Some Results of a Study of the Relationship Between the Mean Annual Sum of Atmospheric Precipitation and Re-Activated and New Landslide Cases in Georgia Taking into Account of Climate Change. // Journal of the Georgian Geophysical Society, e-ISSN: 2667-9973, p-ISSN: 1512-1127, Physics of Solid Earth, Atmosphere, Ocean and Space Plasma, v. 25(2), 2022, pp. 38–48. https://openjournals.ge/index.php/GGS/article/view/5959
9. Geological bulletins. 2016-2025. (in Georgian) https://nea.gov.ge/c/Departments/Geology
10. Sakartvelos sametsniero-gamoqenebiti klimaturi tsnobari. // Gamomtsemloba "Universali", ISBN 978-9941-26-798-7, Tbilisi, 2020, 307 p. (in Georgian)
11. Amiranashvili A., Chelidze T., Kiria T., Tsamalashvili T., Varamashvili N., Statistical Analysis of Annual Precipitation Sum with Different Provision in Georgia. // 2nd International Scientific Conference „Modern Problems in Geophysics", Proceedings, ISSN 3088-4349, Tbilisi, Georgia, October 29 – 31, 2026.
12. Hinkle D. E., Wiersma W., Jurs S. G., Applied Statistics for the Behavioral Sciences. // Boston, MA, Houghton Mifflin Company, 2003.

2nd International Scientific Conference "Modern Problems in Geophysics", Proceedings,
ISBN 978-9941-36-562-1, ISSN 3088-4349, Tbilisi, Georgia, October 29-31, 2026

# MAIN RESEARCH RESULTS OF THE PROJECT "MACHINE LEARNING APPROACH TO THE LANDSLIDE ACTIVATION PREDICTION IN GEORGIA" (2023-2026)

**[*]Chelidze T., [*]Amiranashvili A., [**]Brocca L., [*]Kiria T., [*]Svanadze D., [***]Tsamalashvili T., [*]Varamashvili N.**

*[*]M. Nodia Institute of Geophysics of the I. Javakhishvili Tbilisi State University, Tbilisi, Georgia*
*[**]Research Institute for Geo-Hydrological Protection, Perugia, Italy*
*[***]A. Janelidze Geological Institute of I. Javakhishvili Tbilisi State University, Tbilisi, Georgia*
*avtandilamiranashvili@gmail.com*

***Abstract.*** *This work presents the main scientific results of the project "Machine Learning Approach to the Landslide Activation Prediction in Georgia," supported by Shota Rustaveli National Science Foundation of Georgia (SRNSFG), Grant number FR-23-5466.*

***Key Words:*** *Natural catastrophe, landslides, atmospheric precipitation, statistical analysis, machine learning.*

## Introduction

From 2020 to 2023, research was conducted at the M. Nodia Institute of Geophysics (Tbilisi State University) under the project "Assessment of Landslide and Mudflow Hazards for Georgia using Stationary and Satellite Rainfall Data," supported by the Shota Rustaveli National Science Foundation of Georgia (SRNSFG), Grant No. FR-19-8190.

Specifically, the following results were obtained.

A database of geodynamic processes in Georgia was compiled by integrating existing data, and a static hazard zoning map (for landslides and mudflow) was created in accordance with pan-European standards.

Ground-based, satellite, and radar-based precipitation monitoring methods used in Georgia were systematized, and the resulting data underwent statistical processing.

Century-long precipitation data were compared against the map used to generate the landslide hazard map, taking static precipitation patterns into account.

By comparing the spatiotemporal distribution of precipitation with the intensity of geodynamic processes, critical precipitation thresholds for triggering geodynamic activity across Georgia and in specific regions were estimated.

A dynamic geoinformation system for geodynamic hazards (landslides and mudflow) in Georgia was developed based on regular analysis of satellite precipitation data, accounting for regional characteristics (critical thresholds) and employing fuzzy logic and pattern recognition methods. The proposal envisioned using this system as the foundation for a specialized service capable of forecasting catastrophic landslide events in Georgia.

This study – the results of which have been published [1–15], accepted [16, 17], and are currently being prepared for publication [18, 19] – complements and extends previous research. It is based on the analysis of a more extensive and detailed dataset covering precipitation (ground-based and satellite observations), landslides [20–22], topography, hydrology, land cover, and geological conditions [17], utilizing both traditional statistical methods and modern machine learning techniques.

## Study area, material and methods

Study area – Georgia, its individual parts, regions, municipalities, and settlements. The following databases were used: data of the Georgian National Environment Agency and Department of Geology about daily,

monthly, annual sums of precipitation, annual precipitation sum with different provision etc. [14,20,21]; three-minute meteorological radar precipitation data [12]; half-hourly satellite precipitation data [**Error! Hyperlink reference not valid.**]; daily, monthly and annual landslide data [21,22]. Terrain elevation (meter), slope (degree), aspect (degree), curvature, forest (binary), distance to river and slope (meter), distance to fault (meter), soil type (categorical), lithology (categorical), Topographic Wetness Index (TWI). The data have a spatial resolution of 20x20 m (a total of 175 million values for each parameter) [17]. Stationary Susceptibility and Dynamic Landslide Hazard Forecasting System for Georgia was conducted Using ERA5, Fuzzy Logic and Hybrid Machine Learning [18].

## Results

Representativeness of data from meteorological stations in Georgia for monthly sum of atmospheric precipitation around of these stations was installed [1]. Comparison of Satellite and Ground-Based Data on Semi-Annual and Annual Sum of Atmospheric Precipitation for 26 Points in Georgia in 2001-2020 was conducted [3]. Statistical Analysis of Annual and Semi-Annual Sum of Atmospheric Precipitation Data for 59 Municipalities (11 Regions) of Georgia with Landslide Hazard Zones from 2015 to 2024 was conducted [4]. Data on calculated annual atmospheric precipitation with 1% provision for 83 meteorological stations in Georgia are presented. A comparative statistical analysis of minimum, maximum and mean annual precipitation sums with annual precipitation sums with different provision for the territory of Georgia as a whole, as well as for its regions and eastern and western parts is conducted. Correlation and regression relationships between the parameters under study have been established [14].

It was studied variability of the annual number of registered landslides and mudflows in Georgia in 1995-2024 and their expected change up to 2030 [7,8].

A detailed statistical analysis was conducted of the three-minute, daily, monthly, and annual precipitation totals associated with landslide processes [2,5,6,9,11-13,15,16]. In particular, the following results were obtained.

The article [12] presents the results of an analysis of radar measurements of precipitation intensity preceding a series of small landslides in the Akhaldaba region (a suburb of Tbilisi, Georgia) on June 13-14, 2015.

The dependence of the cumulative landslide sum on the cumulative precipitation with a one-hour lead time is obtained, which has the form of a third-degree polynomial. A rapid increase in the number of landslides is observed with increasing accumulated precipitation (with a one-hour lead time).

This study once again demonstrates that radar measurements of precipitation intensity can be an effective tool for studying the role of precipitation in landslide occurrence, as well as for short-term forecasting of their activation, especially in areas where ground-based precipitation measurements are unavailable.

In article [2] the results of the analysis of the precipitation regime that caused the landslide in Nergeeti (Imereti, Georgia) on February 7, 2024 are presented (day with landslide and 3, 5, 7, 10, 20 and 30 days before its onset for meteorological stations Kutaisi and Zestaponi). These data were compared with similar generalized data for 75 landslide cases in Imereti. In particular, it was found that the heavy precipitation regime that triggered the landslide in Nergeeti was observed quite rarely in the Imereti region – in 12% of cases out of 75 for the amount of precipitation on the day with the landslide and only in 8% of cases for the accumulated amount of precipitation over 30 days.

A detailed statistical analysis of the relationship between daily and accumulated multi-daily precipitation sums and the number of landslides in 12 regions of Georgia is presented in [11]. Landslide data with a known days of activation were used (a total of 519 landslide events from 1968 to 2022). For the analysis, the precipitation sum for the day of landslide activation (P1) was determined, as well as the accumulated precipitation sum for 3 days (P3), 5 (P5), 7 (P7), 10 (P10), 20 (P20) and 30 days (P30) prior to landslide occurrence (including the day with landslide).

The relationship between average precipitation values (threshold values) and daily precipitation duration during the day of landslide activation and before 3, 5...30 days of landslides activation in Georgia and its individual regions was determined. It was found that, overall, in eastern Georgia (including the Samtskhe-Javakheti region), landslide activation occurs with significantly lower precipitation sums than in western

Georgia. The average P1 values are 8.8 and 11.9 mm, respectively, and the P30 values are 75.2 and 156.6 mm. The linear correlation between the number of landslides and the P1…P30 values across the regions of Georgia is high for P1,P3,P20 and P30 and moderate for P5,P7 and P10. For Georgia the sum of precipitation associated with landslides exceeds the general long-term mean daily precipitation sum by approximately 95%. For Georgia as a whole and its Eastern and Western parts, the dependence of the number of landslides on the P1 ... P30 values have the form of a third-degree polynomial (sequentially: slight increase – plateau – strong increase). For P1 values, the precipitation sum plateau, after which a strong increase in the number of landslides begins, covers the range from 6.3 to 30.8 mm, and for P30 – from 62.4 to 189.5 mm (the total relative number of landslides is ≈ 42.1–43.3%).

In [5] the correlation and regression relationship between the intra-annual distribution (%) of the number of landslides (LS) and the precipitation sums in the month when the landslide occurred and the accumulated sums for the month and 1...11 months before the landslide, P(1)…P(12), respectively, were studied. In particular, it was found that the intra annual distribution of landslides across the territory of Georgia is rather uneven. The highest number of landslides occurs in July and September (11.7% and 11.0%, respectively), while the lowest occur in January and November (5.3% and 5.6%, respectively). A moderate correlation is observed between the intra-annual distribution of LS with the intra-annual distributions of P(9)…(12). For the pairs LS – P(1) and LS – P(8), the correlation is low. For the remaining cases, the correlation is negligible. Linear regression equations between the parameters under study are presented.

For the regions of Adjara and Guria (Georgia), and Eastern Georgia the intra-annual distribution of landslides across the studied territories of Georgia is quite uneven [13]. The highest relative number of landslides in Adjara and Guria occurs in October (18.7%), and the lowest in August (3.4%). The highest relative number of landslides in Eastern Georgia occurs in June (12.4%), and the lowest in July (6.4%). In Adjara and Guria in the linear approximation, correlation coefficient R between intra-annual distribution of the recurrence of landslides and mean sum of precipitation during the month of their activation is moderate (R=0.62), and in the case of approximation by a third-degree polynomial – index of correlation R' is high (R'=0.80). In Eastern Georgia between specified parameters mostly linear correlation is observed (R=0.60, moderate correlation). The level of nonlinear relationships does not go beyond moderate correlation.

A detailed statistical analysis of the relationship between monthly and accumulated multi-month precipitation sums and the number of landslides in 12 regions of Georgia is presented in [6]. Landslide data with a known month and year of activation were used (a total of 788 landslide events from 1961 to 2022). For the analysis, the precipitation sum for the month of landslide activation (P1) was determined, as well as the accumulated precipitation sum for the month of activation and for 1 month (P2), 2 months (P3), …, and 11 months (P12) prior to landslide occurrence.

The relationship between average precipitation values (threshold values) and monthly precipitation duration during the month of landslide activation and before landslide activation in Georgia and its individual regions was determined. It was found that, overall, in eastern Georgia (including the Samtskhe-Javakheti region), landslide activation occurs with significantly lower precipitation sums than in western Georgia. The average P1 values are 76 and 156 mm, respectively, and the P12 values are 684 and 1588 mm. The linear correlation between the number of landslides and the P1…P12 values across the regions of Georgia is low for P1 and moderate for P2…P12. The sum of precipitation associated with landslides exceeds the general long-term average monthly precipitation by approximately 16%. For Georgia as a whole, the dependence of the number of landslides on the P1 and P12 values has the form of a fifth-order polynomial (sequentially: slight increase – plateau – strong increase). For P1 values, the precipitation sum plateau, after which a strong increase in the number of landslides begins, covers the range from 62 to 149 mm, and for P12 – from 914 to 1588 mm (the number of landslides is ≈ 108–114).

In the work [9] the results of statistical analysis of the number of re-activated and new cases of damaging landslides in 11 regions of Georgia and 59 municipalities included in them, as well as the relationship of landslide processes with atmospheric precipitation in the period from 2015 to 2024 are presented. Based on the number of landslides in year, normed to 100 km² (LS100), it is proposed to introduce the following five danger categories: “Low” (LS100 = 0.02÷1), “Moderate” (LS100 = >1÷2), “High” (LS100 = >2÷3), “Very High” (LS100 = >3÷4), “Extreme” (LS100 = >4). It was found that 28 municipalities belong to the landslide hazard category "Low", 10 municipalities – to the category "Moderate", 9 municipalities – to the category

"High ", 6 municipalities – to the category "Very High " and 6 municipalities – to the category "Extreme". As the average annual amount of precipitation increases, the number of landslides also increases. Connection of LS100 values with mean annual sum of atmospheric precipitation by municipalities and regions of Georgia have a power-law function.

Paper [16] presents the results of a statistical analysis of 1636 landslides in 12 regions of Georgia from 1900 to 2022, as well as the relationship between landslide processes and precipitation. Based on landslide area (LS) data, the landslide risk for each region was determined using five hazard categories: "Small" (LS $\geq$0.0002 ÷ <0.002 km$^2$), "Medium" (LS $\geq$0.002 ÷ <0.02 km$^2$), "Large" (LS $\geq$0.02 ÷ <0.2 km$^2$), "Very Large" (LS $\geq$0.2 ÷ $\leq$2 km$^2$), and "Huge" (LS = >2 km$^2$). It was found that the highest recurrence of landslide hazard in one region falls on the category "Medium" (Tbilisi, 49.1 %), in eight regions on the category "Large" (Imereti – 34.9%, Kakheti – 50.0%, Kvemo Kartli – 47.8%, Mtskheta-Mtianeti – 44.3%, Racha-Lechkhumi and Kvemo Svaneti – 55.8%, Samegrelo-Zemo Svaneti – 47.8%, Samtskhe-Javakheti – 49.0%, Shida Kartli – 45.0%), in one region on the categories "Large" and "Very large" (Abkhazeti – 34.5 and 34.9%), and in two regions on the category "Very large" (Adjara – 69.3%, Guria – 33.3%. Overall, in Georgia, the highest frequency of landslide hazard occurs in the "Large" and "Very Large" categories – 35.6% and 36.3%. As average annual precipitation increases, so does the landslide hazard level. In particular, for the categories "Very Large" and "Huge" this relationship has the form of a third-degree polynomial.

In work [15] an assessment estimation of the annual damage landslides number (DLSN) in Georgia in relation to average annual extreme precipitation sums with 10%, 5%, 2% and 1% provision is conducted. In particular, the mean annual value of DLSN may vary from 1177 to 2790 for the mean annual sum of atmospheric precipitation with provision 10% and 1% respectively.

Statistical data on landslides (LS) in Georgia are of relatively low quality, a three-stage methodology was applied for assessing LS probability [10]. First, an initial statistical assessment of LS hazard was performed using 11 weighted objective factors. Second, the initial statistical model was compared with the map of observed LS on the territory of Georgia. Third, machine learning (ML) methods were applied to assess LS probability for obtaining the final LS hazard map. The obtained results indicate a good correlation between the model predictions and the observed data, which confirms the reliability and robustness of the proposed model, even in the case of unbalanced data.

Study [18] presents a methodology for the static and dynamic assessment of LS hazard for the territory of Georgia. The proposed dynamic approach is based on the spatial-temporal extension of a previously developed static LS susceptibility map [10]. The static model is used as a background assessment of LS susceptibility, while the rainfall trigger component is added using the cumulative precipitation indices (R_24), (R_3), (R_5), and (R_30), calculated from ERA5 hourly reanalysis data.

The approach combines static LS susceptibility, a rainfall-trigger index, retrospective event analysis and established machine-learning algorithms. For 309 LS events recorded during 2010–2022, the manuscript reports antecedent precipitation indices, S_static, I_dyn and their difference. In the analytical formulation, the positive change in the dynamic index is imposed by the rainfall modulation and must not be interpreted as independent evidence of predictive performance or as a quantified increase in disaster risk.

The final evaluation sample consists of 309 LS events and 309 susceptibility-matched controls. With training on 2010–2020 and testing on 2021–2022, the Random Forest model without coordinates achieved reported values of AUC = 0.754, F1 = 0.740 and MCC = 0.432. These values describe performance within the adopted sampling and temporal split. They do not independently establish spatial transferability, the benefit of fuzzy inference, calibrated natural-frequency event probabilities or robustness to class imbalance.

The study provides a retrospective framework for combining static susceptibility with rainfall-related information in Georgia. The reported model performance is conditional on the adopted event inventory, matched controls and temporal split. Further work should quantify precipitation and inventory uncertainty, assess regional transferability, document the complete implementation and evaluate any operational warning configuration prospectively. The current assessment does not estimate exposure, vulnerability or economic losses.

The map of 6 scenarios of dynamic landslide risk in Georgia is presented at https://ig-geophysics.ge/-dynamic_6.html

## Conclusion

Research results approach provides a basis for the further development of LS early warning systems in Georgia. At the next stage, regional calibration of rainfall thresholds, comparison of ERA5 data with ground-based meteorological stations and weather radar observations, as well as operational testing of the model in a near-real-time forecasting mode are recommended.

The summarized results of the aforementioned studies will soon be published in the monograph [19].

**Acknowledgment:** This work was supported by Shota Rustaveli National Science Foundation of Georgia (SRNSFG), Grant number FR-23-5466, "Machine Learning Approach to the Landslide Activation Prediction in Georgia".

## References

1. Amiranashvili A., Chelidze T., Svanadze D., Tsamalashvili T., Varamashvili N., About the Representativeness of Data from Meteorological Stations in Georgia for Monthly Sum of Atmospheric Precipitation Around of These Stations. // Journal of the Georgian Geophysical Society, e-ISSN: 2667-*9973,* p-ISSN*:* 1512-1127, Physics of Solid Earth, Atmosphere, Ocean and Space Plasma, v. 27(1), 2024, pp. 52–57. https://ggs.openjournals.ge/index.php/GGS/article/view/7983
2. Amiranashvili A., Brocca L., Chelidze T., Svanadze D., Tsamalashvili T., Varamashvili N., Analysis of the Precipitation Regime that Triggered the Landslide in Nergeeti (Imereti, Georgia) on February 7, 2024. // Int. Sc. Conf. "Complex Geophysical Monitoring in Georgia: History, Modern Problems, Promoting Sustainable Development of the Country", Proceedings, ISBN 978-9941-36-272-9, Publish House of Iv. Javakhishvili Tbilisi State University, Tbilisi, Georgia, October 17-19, 2024, pp. 155 – 158. http://dspace.gela.org.ge/bitstream/123456789/10619/1/39_MM-180.pdf
3. Amiranashvili A., Chelidze T., Svanadze D., Tsamalashvili T., Varamashvili N., Comparison of Satellite and Ground-Based Data on Semi-Annual and Annual Sum of Atmospheric Precipitation for 26 Points in Georgia in 2001-2020. // Int. Sc. Conf. "Complex Geophysical Monitoring in Georgia: History, Modern Problems, Promoting Sustainable Development of the Country", Proceedings, ISBN 978-9941-36-272-9, Publish House of Iv. Javakhishvili Tbilisi State University, Tbilisi, Georgia, October 17-19, 2024, pp. 159 – 163. http://www.openlibrary.ge/bitstream/123456789/10618/1/40_MM-180.pdf
4. Amiranashvili A.G., Brocca L., Chelidze T.L., Svanadze D.T., Tsamalashvili T.N., Varamashvili N.D., Statistical Analysis of Annual and Semi-Annual Sum of Atmospheric Precipitation Data for 59 Municipalities (11 Regions) of Georgia with Landslide Hazard Zones from 2015 to 2024. // Journal of the Georgian Geophysical Society, e-ISSN: 2667-9973, p-ISSN: 1512-1127 Physics of Solid Earth, Atmosphere, Ocean and Space Plasma, v.28(1), 2025, pp. 50 – 63. https://ggs.openjournals.ge/index.php/GGS/article/view/9249
5. Amiranashvili A., Brocca L., Chelidze T., Kiria T., Svanadze D., Tsamalashvili T., Varamashvili N., Intra-Annual Distribution of Landslide Recurrence in Georgia and its Relationship with Monthly and Cumulative Multi-Month Sums of Precipitation. // Journal of the Georgian Geophysical Society, e-ISSN: 2667-9973, p-ISSN*:* 1512-1127, Physics of Solid Earth, Atmosphere, Ocean and Space Plasma, v.28(2), 2025, pp. 25-30. https://ggs.openjournals.ge/index.php/GGS/article/view/10453
6. Amiranashvili A., Brocca L., Chelidze T., Kiria T., Svanadze D., Tsamalashvili T., Varamashvili N., Statistical Analysis of the Relationship Between Monthly and Cumulative Multi-Month Sums of Precipitation with the Number of Landslides in the Regions of Georgia. // Transactions of Mikheil Nodia Institute of Geophysics, ISSN 1512-1135, vol. LXXVIII, Publish House of Ivane Javakhishvili Tbilisi State University, Tbilisi, 2025, pp. 49-66. http://dspace.gela.org.ge/bitstream/123456789/10809/1/7_Tr_IG_78_2025.pdf
7. Amiranashvili A., Brocca L., Chelidze T., Svanadze D., Tsamalashvili T., Varamashvili N., Statistical Analysis of the Annual Number of Registered Landslides and Mudflows in Georgia in 1995-2024. // 1st International Scientific Conference "Modern problems in Geophysics". Proceedings, ISBN 978-9941-36-434-1, ISSN 3088-4349, Tbilisi, Georgia, November 6-8, 2025. Publish House of Iv. Javakhishvili Tbilisi State University, Tbilisi, 2025, pp. 35-38. http://dspace.gela.org.ge/bitstream/123456789/10789/1/9_Conf_MPG_2025.pdf
8. Amiranashvili A., Brocca L., Chelidze T., Svanadze D., Tsamalashvili T., Varamashvili N., Variability of the Annual Number of Registered Landslides and Mudflows in Georgia in 1995-2024 and their Expected Change up to 2030. // Transactions of Mikheil Nodia Institute of Geophysics, ISSN 1512-1135, vol. LXXVIII, Publish House of Ivane Javakhishvili Tbilisi State University, Tbilisi, 2025, pp. 67-74. http://dspace.gela.org.ge/bitstream/123456789/10808/1/8_Tr_IG_78_2025.pdf
9. Amiranashvili A., Brocca L., Chelidze T., Svanadze D., Tsamalashvili T., Varamashvili N., Statistical Analysis of the Number of Damaging Landslides in Municipalities and Regions of Georgia and their Relationship with Atmos-

pheric Precipitation in 2015-2024. // Reliability: Theory and Applications, ISSN 1932-2321, Volume 20, Special Issue No. 9 (87), November 2025, pp. 255-264. https://doi.org/10.24412/1932-2321-2025-987-255-264
10. Chelidze T., Kiria T., Amiranashvili A., Svanadze D., Tsamalashvili T., Varamashvili N., Landslide Hazard Maps of Georgia Using Machine Learning Approach. // Bulletin of the National Academy of Sciences of Georgia, ISSN: 0132 – 1447, vol. 20(194), no. 2, 2026, pp. 23-29. http://science.org.ge/bnas/t20-n2/03_Chelidze_Geophysics.pdf
11. Amiranashvili A., Brocca L., Chelidze T., Kiria T., Svanadze D., Tsamalashvili T., Varamashvili N., Assessment of the Relationship Between Daily and Total Multi-Day Precipitation Sums and Landslide Activation in the Regions of Georgia. // Journal of the Georgian Geophysical Society, e-ISSN: 2667-9973, p-ISSN*:* 1512-1127, Physics of Solid Earth, Atmosphere, Ocean and Space Plasma, v.29(1), 2026, pp. 27-49. https://ggs.openjournals.ge/index.php/GGS/article/view/12083
12. Amiranashvili A., Chelidze T., Kiria T., Svanadze D., Tsamalashvili T., Varamashvili N., Retrospective Analysis of Landslides Processes in Akhaldaba (A Suburb of Tbilisi, Georgia) on June 13-14, 2015. // Journal of the Georgian Geophysical Society, e-ISSN: 2667-9973, p-ISSN: 1512-1127*,* Physics of Solid Earth, Atmosphere, Ocean and Space Plasma, v.29(1), 2026*,* pp. 50-59. https://ggs.openjournals.ge/index.php/GGS/article/view/12084
13. Amiranashvili A., Brocca L., Chelidze T., Kiria T., Svanadze D., Tsamalashvili T., Varamashvili N., Peculiarities of Intra-Annual Distribution of Landslide Recurrence in Adjara and Guria Regions (Western Georgia) and in Eastern Georgia and their Relationship with Monthly Sums of Precipitation. // Journal of the Georgian Geophysical Society, e-ISSN: 2667-9973, p-ISSN*:* 1512-1127*,* Physics of Solid Earth, Atmosphere, Ocean and Space Plasma, v.29(1), 2026, pp. 60-68. https://ggs.openjournals.ge/index.php/GGS/article/view/12085
14. Amiranashvili A., Chelidze T., Kiria T., Tsamalashvili T., Varamashvili N., Statistical Analysis of Annual Precipitation Sum with Different Provision in Georgia. // 2nd International Scientific Conference „Modern problems in Geophysics", Proceedings, Tbilisi, Georgia, October 29 – 31, 2026.
15. Amiranashvili A., Chelidze T., Kiria T., Tsamalashvili T., Varamashvili N., Estimation of the Annual Damage Landslides Number in Georgia in Relation to Average Annual Extreme Precipitation Sums of Different Provision. // 2nd International Scientific Conference „Modern problems in Geophysics", Proceedings, Tbilisi, Georgia, October 29 – 31, 2026.
16. Kiria T., Amiranashvili A., Brocca L., Chelidze T., Svanadze D., Tsamalashvili T., Varamashvili N., Landslide Risk Assessment in the Regions of Georgia and its Relationship with Atmospheric Precipitation. // Ecology & Safety, ISSN 1314-7234, Vol. 20, 2026. (in press)
17. Kiria T., Amiranashvili A., Brocca L., Chelidze T., Svanadze D., Tsamalashvili T., Varamashvili N., A Database for Creating Static and Dynamic Models of Landslide Processes in Georgia Using Machine Learning Methods. // Ecology & Safety, ISSN 1314-7234, Vol. 20, 2026. (in press)
18. Kiria T., Chelidze T., Brocca L., Amiranashvili A., Svanadze D., Varamashvili N., Tsamalashvili T., Stationary Susceptibility and Dynamic Landslide Hazard Forecasting System for Georgia Using ERA5, Fuzzy Logic and Hybrid Machine Learning. // GeoHazards, ISSN: 2624-795X, 7(4), 119, 2026, 23 p. https://doi.org/10.3390/geohazards7040119.
19. Chelidze T., Amiranashvili A., Brocca L., Varamashvili N., Svanadze D., Kiria T., Tsamalashvili T., Landslide Processes in Georgia and Their Forecasting Using Machine Learning. Monograph, 2026 (in preparation for publication).
20. Sakartvelos sametsniero-gamoqenebiti klimaturi tsnobari. // Gamomtsemloba "Universali", ISBN 978-9941-26-798-7, Tbilisi, 2020, 307 p.
21. Geological bulletins. 2016-2025. (in Georgian) https://nea.gov.ge/c/Departments/Geology
22. Varazanashvili, O., Gaprindashvili, G., Elizbarashvili, E., Basilashvili, Ts., Amiranashvili, A., Fuchs, S., The First Natural Hazard Event Database for the Republic of Georgia (GeNHs) – Catalog, 2023, 270 p. http://dspace.gela.org.ge/handle/123456789/10369; DOI: 10.13140/RG.2.2.12474.57286

2nd International Scientific Conference "Modern Problems in Geophysics", Proceedings,
ISBN 978-9941-36-562-1, ISSN 3088-4349, Tbilisi, Georgia, October 29-31, 2026

# UNPRECEDENTED PRECIPITATION IN BATUMI ON SEPTEMBER 19, 2026

[*]Amiranashvili A., [**]Chikhladze V., [*,**] Pipia M.

[*]*Mikheil Nodia Institute of Geophysics of Ivane Javakhishvili Tbilisi State University, Tbilisi, Georgia*
[**]*Institute of Hydrometeorology of Georgian Technical University, Tbilisi, Georgia*
*avtandilamiranashvili@gmail.com*

***Abstract:*** *In this work, some results of heavy precipitation analysis in Batumi on September 19, 2026 based on ground-level measurements are presented.*

***Key Words:*** *Atmospheric precipitation, flooding, flood.*

## Introduction

Atmospheric precipitation, as one of the most important climate-forming factors, directly affects the state of the environment. Therefore, in Georgia, as in other countries, special attention has been and continues to be paid to studying the intensity and spatiotemporal distribution of precipitation [1–3]. The relevance of this research has grown even further against the backdrop of ongoing global warming [3]. Intense and prolonged precipitation leads to floods, landslides, mudflows, and damage to infrastructure and vegetation [4–11]. In some cases, anomalous precipitation results in loss of life [4, 5, 7, 11]. Floods and landslides triggered by heavy precipitation occur most frequently in Western Georgia, although these phenomena are also common in the eastern part of the country, including Tbilisi [4–11]. For instance, heavy rains lasting several days triggered a landslide that caused fatalities in the village of Nergeeti (Imereti region) on February 7, 2024 [7]. A heavy downpour in the Adigeni and Chokhatauri municipalities on July 21, 2025, led to the flooding of large areas, damage to infrastructure, and the triggering of landslides [9].

Heavy precipitation occurred along the Adjara coast and in adjacent areas from the course of September 19 through the morning of September 20, 2026. Consequently, street flooding and temporary strain on urban infrastructure occurred in certain districts of Batumi. Rain fell continuously in Batumi for 21 hours, with a total accumulation of 275 mm – an amount exceeding 90% of the monthly climatic norm. Notably, 20% of this total – 52.5 mm – fell within a single hour (between 21:00 and 22:00 on September 19). According to the National Environmental Agency, the 24-hour rainfall recorded at the Batumi station (273 mm) is unprecedented for September and represents a "1-in-100-year" weather event. Furthermore, data from the agency's meteorological stations indicate the following rainfall totals for September 19–20: • Kobuleti station: 134.5 mm; • Kokhi (Kobuleti): 58.5 mm; • Mtirala National Park: 93 mm; • Sindieti station (Khelvachauri): 50.8 mm [https://www.apsny.ge/2026/pol/1789917819.php].

This work is a continuation of previous research. Presented below are some results from the analysis of intense precipitation that occurred in Batumi on September 19, 2026, based on ground-based measurement data.

## Study area, material and methods

Study area – Batumi. The following information is used.

Data of Georgian National Environmental Agency about the daily sum of atmospheric precipitation is used [https://www.apsny.ge/2026/pol/1789917819.php]. Extrapolation of daily precipitation provision for Batumi on September 19, 2026, based on calculated data regarding maximum daily precipitation in September with provision once in 1.6, 5, 10, 20, 50, and 100 years [12] was conducted.

In the proposed work the analysis of data is carried out with the use of the standard statistical analysis methods.

## Results and discussion

Results in Fig. 1,2 and Table 1 are presented.

In Fig. 1 (left part) and Table 1 calculated values on max daily precipitation of various provision in September for Batumi (according to data 1961-1990), Batumi Airport and Kobuleti according to data 1961-1990 and 1961-2010 [12] are presented.

As noted above, 273 mm of precipitation fell in Batumi on September 19, 2026. Extrapolating the data for the Batumi weather station indicates that such an amount of precipitation occurs once every 850 years (Fig. 1, right panel).

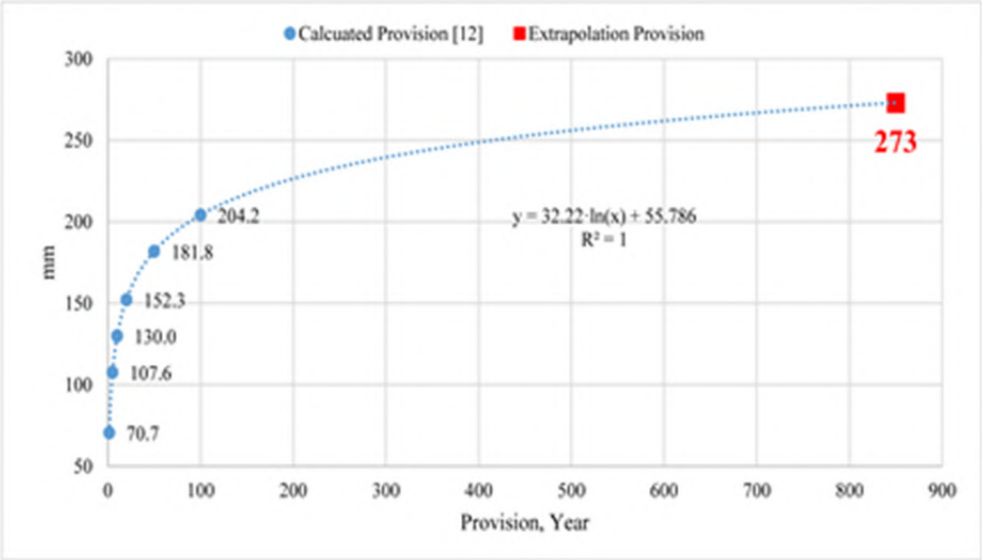



**Fig. 1.** Extrapolation of daily precipitation provision for Batumi on September 19, 2026, based on calculated data regarding to max daily precipitation in September with provision once in 1.6, 5, 10, 20, 50, and 100 years [12].

**Table 1.** Calculated values on max daily precipitation of various provision in September for Batumi Airport and Kobuleti according to data 1961-1990 and 1961-2010 [12].

| Station | Period of observation | Provision, once in years | | | | | |
|---|---|---|---|---|---|---|---|
| | | 1.6 | 5 | 10 | 20 | 50 | 100 |
| Batumi Airport 1 | 1961-1990 | 72.5 | 112.1 | 136 | 159.9 | 191.6 | 215.5 |
| Batumi Airport 2 | 1961-2010 | 77.3 | 124.8 | 153.5 | 182.2 | 220.1 | 248.9 |
| Kobuleti 1 | 1961-1990 | 62.7 | 106.1 | 132.3 | 158.5 | 193.2 | 219.4 |
| Kobuleti 2 | 1961-2010 | 64.7 | 105.7 | 130.5 | 155.3 | 188.1 | 212.9 |

For the Batumi Airport weather station, the calculated 100-year precipitation amount is 215.5 mm based on 1961–1990 data, whereas it is 248.9 mm based on 1961–2010 data (an increase in precipitation due to climate change). The situation is the opposite for the Kobuleti weather station: the calculated 100-year precipitation amount is 219.4 mm based on 1961–1990 data and 212.9 mm based on 1961–2010 data (a decrease in precipitation due to climate change) [12]. Notably, while the calculated 100-year precipitation amount at the Batumi Airport station was lower than at Kobuleti based on 1961–1991 data, it became significantly higher than at Kobuleti based on 1961–2010 data. Based on data from the Batumi Airport weather station, the extrapolated precipitation figures for Batumi are as follows: once every 530 years according to 1961–1990 data, and once every 180 years according to 1961–2010 data. In other words, climate change significantly alters the methodology for calculating expected maximum precipitation over a given period – a methodology that relies on the assumption of stationarity in climatic observation series.

It should be noted that, according to the National Environmental Agency, a daily rainfall of 273 mm in Batumi in September is a once-in-a-century event – a figure that does not quite align with our estimates. Nevertheless, the rainfall in Batumi on September 19, 2026, was highly anomalous in any case.

As for Kobuleti, where 134.5 mm of precipitation fell, the amount was not anomalous (Table 1). No anomalous precipitation levels were recorded at nearby weather stations either (see Introduction). Thus, Batumi found itself at the epicenter of the rainfall on that day.

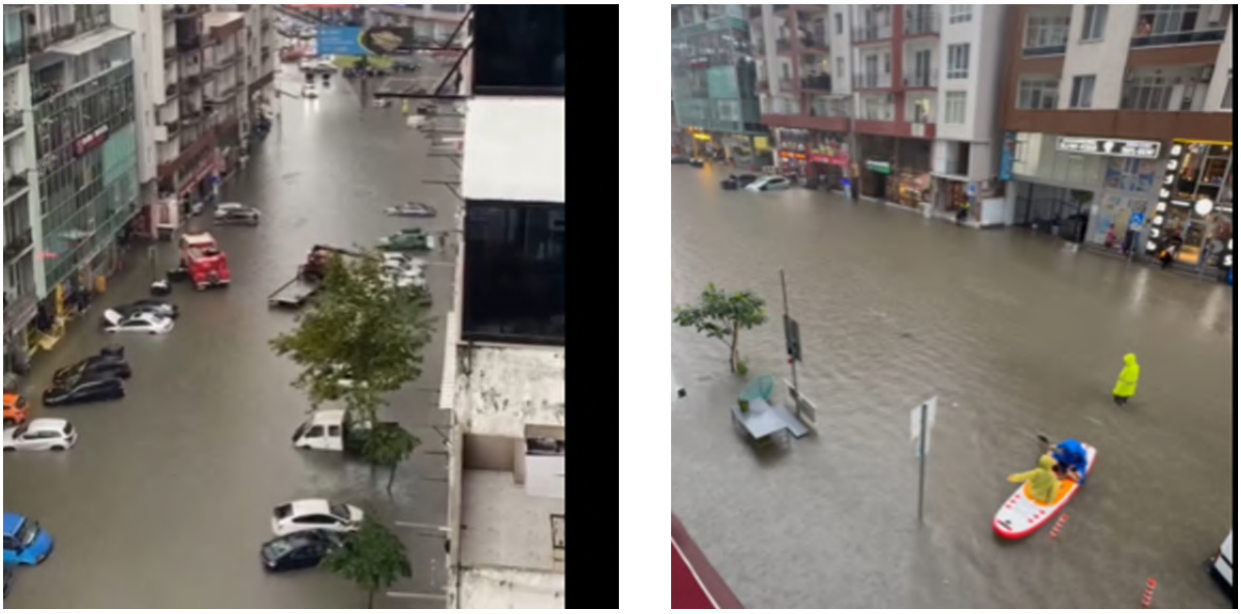


**Fig. 2.** An examples of the negative consequences of a heavy rainfall on two locations in Batumi on September 19, 2026. (https://www.facebook.com/reel/2868463793528181; https://www.facebook.com/reel/1799018547784182).

Fig. 2 shows photographs of flooded streets in Batumi by way of illustration.

## Conclusion

Estimates of the probability of maximum precipitation occurring once every a certain number of years are based on the analysis of climatic observation series (spanning at least 30 years) that are assumed to be stationary. In the context of climate change, the database must be continuously updated to ensure that these estimates remain representative for practical applications.

In the future, we plan to continue similar studies for different regions of Georgia using ground-based and satellite measurement data against the backdrop of climate change.

**Acknowledgement:** The authors thank Facebook users for the opportunity to use their photographs.

## References

1. Khvedelidze Z., Amiranashvili A., Dolidze J., Chitaladze D., Pavlenishvili N., Statistical Structure of Diurnal Precipitation Distribution on the Territory of Eastern Georgia. // Proc. of I. Javakhishvili Tbilisi State University, Physics, N 357, ISSN 1512-1461, Tbilisi University Press, Tbilisi, 2004, pp. 79-87.
2. Amiranashvili A.G., Special Features of Changeability of Daily Sum of Precipitation in Tbilisi in 1957-2006. // Journal of the Georgian Geophysical Society, Issue B. Physics of Atmosphere, Ocean and Space Plasma, v.18B, Tbilisi, 2015, pp.81-91.
3. Kartvelishvili L., Tatishvili M., Amiranashvili A., Megrelidze L., Kutaladze N., Weather, Climate and their Change Regularities for the Conditions of Georgia. // Monograph, Publishing House "UNIVERSAL", Tbilisi 2023, 406 p., https://doi.org/10.52340/mng.9789941334658
4. Amiranashvili A., Kereselidze Z., Mitin M., Khvedelidze I., Chikhladze V., Alarming factors of the Microclimate of the Vere River Valley and their Influence on the Floods Intensity. // Trans. of Mikheil Nodia Institute of Geophysics, ISSN 1512-1135, v. 69, Tbilisi, 2018, pp. 204-218. (in Georgian)
5. Amiranashvili A., Chelidze T., Svanadze D., Tsamalashvili T., Tvauri G., Abnormal Precipitation Before the Landslide in Akhaldaba (A Suburb of Tbilisi, Georgia) on June 13, 2015 According to Radar Measurements. // Journal of the Georgian Geophysical Society, e-ISSN: 2667-9973, p-ISSN: 1512-1127, Physics of Solid Earth, Atmosphere, Ocean and Space Plasma, v. 26(1), 2023, pp. 30–41. https://ggs.openjournals.ge/index.php/GGS/article/view/6959;

DOI: https://doi.org/10.48614/ggs2620236959
6. Beglarashvili N., Jamrishvili N., Janelidze I., Pipia M., Tavidashvili Kh., Analysis of Strong Precipitation in Tbilisi on August 29, 2023. // International Scientific Conference "Geophysical Processes in the Earth and its Envelopes", Proceedings, Tbilisi, Georgia, November 16-17, 2023, pp. 154-158.
7. Amiranashvili A., Brocca L., Chelidze T., Svanadze D., Tsamalashvili T., Varamashvili N., Analysis of the Precipitation Regime that Triggered the Landslide in Nergeeti (Imereti, Georgia) on February 7, 2024. Int. Sc. Conf. "Complex Geophysical Monitoring in Georgia: History, Modern Problems, Promoting Sustainable Development of the Country", Proceedings, ISBN 978-9941-36-272-9, Publish House of Iv. Javakhishvili Tbilisi State University, Tbilisi, Georgia, October 17-19, 2024, pp. 155 – 158.
http://dspace.gela.org.ge/bitstream/123456789/10619/1/39_MM-180.pdf
8. Beglarashvili N., Jamrishvili N., Janelidze I., Pipia M., Tavidashvili Kh., Some Results of Analysis of Heavy Precipitation in Tbilisi on July 7, 2024 Based on Ground-Level and Satellite Measurements. Int. Sc. Conf. "Complex Geophysical Monitoring in Georgia: History, Modern Problems, Promoting Sustainable Development of the Country", Proceedings, ISBN 978-9941-36-272-9, Publish House of Iv. Javakhishvili Tbilisi State University, Tbilisi, Georgia, October 17-19, 2024, pp. 164 – 167.
http://dspace.gela.org.ge/bitstream/123456789/10617/1/41_MM-180.pdf
9. Beglarashvili N., Elizbarashvili I., Jamrishvili N., Janelidze I., Pipia M., Tavidashvili Kh., Analysis of Heavy Precipitation in the Adigeni and Chokhatauri Municipaliities on July 21, 2025 Based on Satellite Measurements. 1st International Scientific Conference "Modern problems in Geophysics". Proceedings, ISBN 978-9941-36-434-1, ISSN 3088-4349, Tbilisi, Georgia, November 6-8, 2025. Publish House of Iv. Javakhishvili Tbilisi State University, Tbilisi, 2025, pp. 125-128.
http://dspace.gela.org.ge/bitstream/123456789/10766/1/32_Conf_MPG_2025.pdf
10. Beglarashvili N., Elizbarashvili I., Jamrishvili N., Janelidze I., Megrelidze L., Pipia M., Tavidashvili Kh., Some Results of Investigation of the Effects of Heavy Precipitation on the Environment in Some Regions of Georgia Using Ground-Level and Satellite Measurements. Materials of International Scientific Conference "Study and sustainable use of natural ecosystems in the conditions of modern climate change", Tbilisi, Georgia, December 11, 2025, Scientific Reviewed Proceedings of the Institute of Hydrometeorology of the GTU, ISSN 1512 – 0902, # 137, 2025, p. 34, Doi.org/10.36073/1512-0902-137, http://openlibrary.ge/bitstream/123456789/10799/1/Vol-137.pdf
11. Amiranashvili A., Chelidze T., Kiria T., Svanadze D., Tsamalashvili T., Varamashvili N., Retrospective Analysis of Landslides Processes in Akhaldaba (A Suburb of Tbilisi, Georgia) on June 13-14, 2015. // Journal of the Georgian Geophysical Society, e-ISSN: 2667-9973, p-ISSN: 1512-1127, Physics of Solid Earth, Atmosphere, Ocean and Space Plasma, v.29(1), 2026, pp. 50-59.
https://ggs.openjournals.ge/index.php/GGS/article/view/12084
12. Sakartvelos sametsniero-gamoqenebiti klimaturi tsnobari. // Gamomtsemloba "Universali", ISBN 978-9941-26-798-7, Tbilisi, 2020, 307 p.

2nd International Scientific Conference "Modern Problems in Geophysics", Proceedings,
ISBN 978-9941-36-562-1, ISSN 3088-4349, Tbilisi, Georgia, October 29-31, 2026

# WATERSPOUT IN KOBULETI (GEORGIA) AND PENSACOLA (FLORIDA, USA) ON SEPTEMBER 07, 2026

**Amiranashvili A., Chikhladze V., Jamrishvili N., Tavidashvili Kh.**

*M. Nodia Institute of Geophysics of the I. Javakhishvili Tbilisi State University, Tbilisi, Georgia*
*avtandilamiranashvili@gmail.com*

***Abstract.*** *The article presents an analysis of atmospheric stability levels and the characteristics of the thunderstorms that led to the formation of waterspouts in Kobuleti (Georgia) and Pensacola (Florida, USA) on September 7, 2026.*

***Key Words:*** *Natural disasters, hurricane winds, tornadoes, waterspouts, TT index.*

## Introduction

Tornadoes and waterspouts occur in many countries around the world [1–3], including Georgia [4–7]. These natural phenomena often cause significant damage to a country's agro-economic and other infrastructure and can result in human casualties [2]. Specifically, study [5] examines, as a case study, a tornado that struck the terminal complex in the city of Poti on September 25, 2021, causing substantial damage to one of the cargo terminals.

Studies [6, 7] present findings from a field survey of the path taken by a tornado in Kakheti on June 25, 2024. The damage sustained by Alaverdi Cathedral and the surrounding area was analyzed in detail, yielding important information. The damage caused by the tornado along its path was also investigated. The present study builds upon this previous research. Below, we present an analysis of atmospheric stability levels and the characteristics of the thunderstorms that led to the formation of waterspouts in Kobuleti (Georgia) and Pensacola (Florida, USA) on September 7, 2026.

## Study area, material and methods

Study area – Kobuleti (Georgia) – Latitude: 41.81 N; Longitude: 41.78 E and Pensacola (Florida, USA) – Latitude: 30.33 N; Longitude: -87.14 W (Fig. 1). The straight-line distance between Kobuleti and Pensacola is approximately 10395 kilometers (about 6459 miles). Information from Facebook users regarding waterspouts in these cities on September 7, 2026, was used.




**Fig. 1.** Locations of Kobuleti (Black Sea coast) and Pensacola (the Emerald Coast of the Gulf of Mexico).

Data on vertical atmospheric sounding [https://www.ready.noaa.gov/index.php] for calculating the Indexes of Stability of the Atmosphere [http://weather.uky.edu/about_totl.htm].

In this work, the Total Index (TT) of atmospheric stability is used.

$$\mathbf{TT} = \mathbf{T}_{850} + \mathbf{T}_{d850} - \mathbf{2}\cdot\mathbf{T}_{500} \text{ in degrees C.}$$

where **T** represents temperature and $\mathbf{T}_d$ represents dew point temperature at the indicated level (500, 700, and 850 hPa).

## Results

Results in Fig. 2-3 and Tables 1-2 are presented.

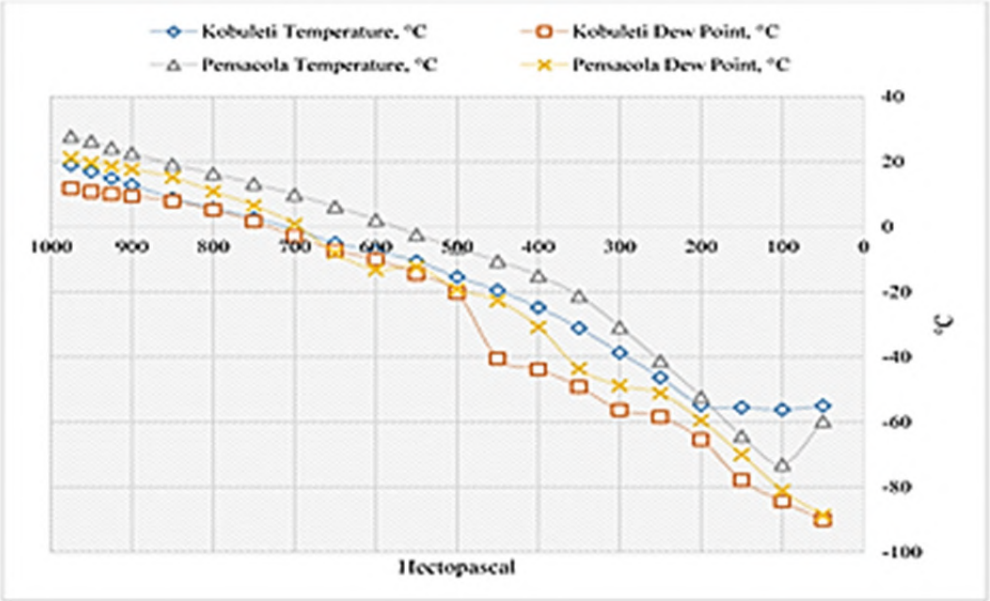



**Fig. 2.** Vertical distribution of air temperature and dew point over Kobuleti (Georgia) and Pensacola (Florida, USA) on 07.09.2026 at 13:00 local time.

Fig. 2 shows the vertical distribution of air temperature and dew point over Kobuleti (Georgia) and Pensacola (Florida, USA) in 07.09.2026 at 13:00 on local time. As shown in this Figure, the values of the indicated parameters over Kobuleti are significantly lower than over Pensacola.

**Table 1.** Statistical characteristics of air temperature and Dew Points over Kobuleti and Pensacola in the altitude range 975-500 hPa in 07.09.2026 at 13:00 on local time (°C).

| Location | Kobuleti | | Pensacola | |
|---|---|---|---|---|
| Variable | Temperature | Dew Point | Temperature | Dew Point |
| Max | 19.0 | 11.8 | 27.8 | 21.2 |
| Min | -15.4 | -20.3 | -6.6 | -19.2 |
| Range | 34.4 | 32.1 | 34.4 | 40.4 |
| Average | 3.5 | 0.2 | 13.3 | 4.8 |
| St Dev | 11.4 | 11.0 | 11.5 | 14.7 |

For instance, in the 975–500 hPa altitude range over Kobuleti, the mean air temperature is 3.5°C and the dew point is 0.2°C, whereas over Pensacola they are 13.3°C and 4.8°C, respectively (Table 1).

Over Kobuleti, at the 975 hPa level (390 m a.s.l.), the air temperature is 19.0°C and the dew point is 11.8°C; at the 500 hPa level (5740 m a.s.l.), the air temperature is -15.4°C and the dew point is -20.3°C. Over Pensacola, at the 975 hPa level (346 m a.s.l.), the air temperature is 27.8°C and the dew point is 21.2°C; at the 500 hPa level (5899 m a.s.l.), the air temperature is -6.6°C and the dew point is -19.2°C (Table 1).

**Table 2.** TT Index for study regions in 07.09.2026 on local time.

| Hour. min | TT Index | | Stability of the Atmosphere | |
|---|---|---|---|---|
| | Kobuleti | Pensacola | Kobuleti | Pensacola |
| 7.00 | 44.8 | 47.2 | Scattered Thunderstorms | Scattered Thunderstorms/ Isolated Severe |
| 10.00 | 44.9 | 46.0 | Scattered Thunderstorms | |
| 13.00 | 47.5 | 47.6 | Scattered Thunderstorms/ Isolated Severe | |
| 16.00 | 45.4 | 47.7 | Scattered Thunderstorms | Scattered Thunderstorms/ Isolated Severe |

Despite the significant difference in the values of the specified parameters over the study locations, the TT index values for Kobuleti and Pensacola differed little throughout the day on September 7, 2026. The level of atmospheric stability ranged from "Scattered Thunderstorms" to "Scattered Thunderstorms/Isolated Severe" (Table 2). In other words, conditions conducive to the formation of a waterspout (a localized tornado) were present in both locations. The occurrence of a waterspout at the study sites on the same day is particularly interesting, given that the distance between them exceeds 10000 km.

It is also worth noting that during the devastating tornado that passed through the territory of the terminal in Poti on September 25, 2021, the Total Totals (TT) index ranged from 50 to 53 (Stability of the Atmosphere: “Scattered Thunderstorms / Few Severe / Isolated Tornadoes” ÷ “Numerous Thunderstorms / Scattered Tornadoes”) [5]. On June 25, 2024, in Kakheti, a tornado traveled a distance of approximately 6 km over a period of about 20 minutes – from its estimated time of formation until it dissipated. Throughout the day, in Kakheti the TT index varied within the same range as in Poti on September 25, 2021 [5].

Thus, the TT index satisfactorily describes the atmospheric conditions conducive to the formation of powerful tornadoes, whereas for waterspouts, this correspondence is rather approximate and requires other approaches [8, 9].

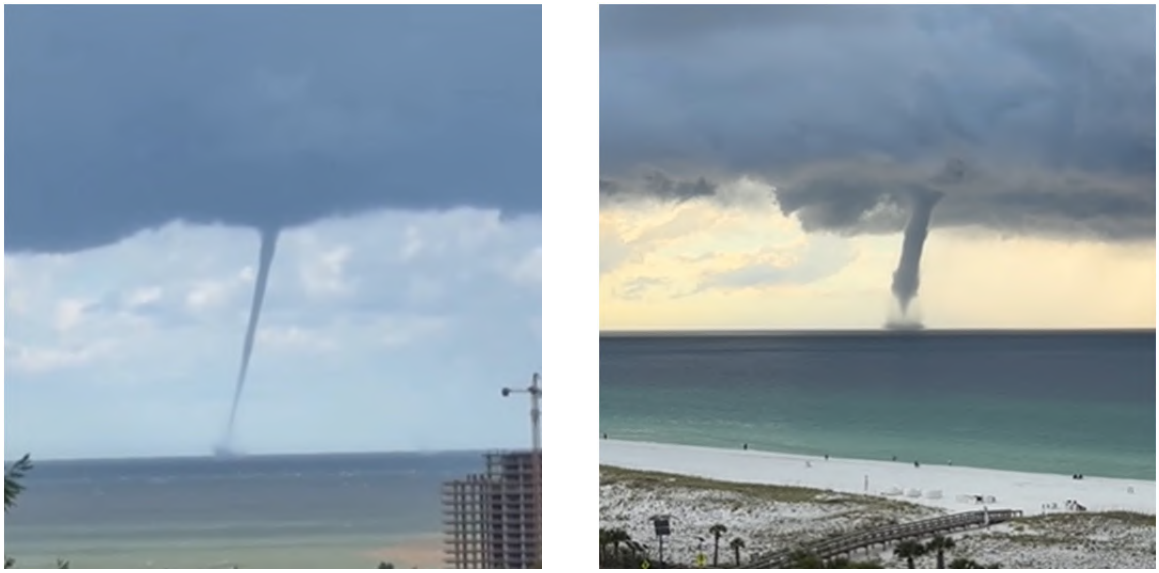


**Fig. 3.** Photos of a waterspout in Kobuleti (left) and Pensacola (right), September 7, 2026.
(Kobuleti – https://www.facebook.com/reel/1124559020511618;
Pensacola – https://www.facebook.com/reel/945950251902074)

Finally, Figure 3 presents, by way of illustration, photographs of a waterspout in Kobuleti (left) and Pensacola (right), taken on September 7, 2026.

## Conclusion

Plans are in place to continue this research in the future as new data accumulates.

**Acknowledgments**

The authors thank Facebook users for the opportunity to use their photographs of waterspouts and information about these natural phenomena in Kobuleti and Pensacola.

## References


1. Firdaus I.M., Yamazaki T., Abdillah M.R., Riawan E., Indonesia Tornado Database: Tornado Climatology of Indonesia. // Natural Hazards and Earth System Sciences, 25(11), 2025, pp. 4331-4341.
2. Gunter W.S., White L.ϭ Ledbetter C. Tornado Emergency! A Review of Their History, Climatology, and Associated Tornadoes. // Weather, Climate, and Society, 18(4), 2026, pp. 979-989.
3. Bărăscu A., Antonescu B., Ene D., Ionita M., Rusz O., Kühne T., Bell A., An Updated Tornado Climatology for Romania. // Monthly Weather Review, 154(4), 2026, pp. 625-642.
4. Chikhladze V., Jamrishvili N., Tavidashvili Kh., Tornadoes in Georgia. // Int. Sc. Conf. „Natural Disasters in the 21st Century: Monitoring, Prevention, Mitigation“, Proceedings, ISBN 978-9941-491-52-8, Tbilisi, Georgia, December 20-22, 2021, pp. 23-26.
5. Chikhladze V., Amiranashvili A., Gelovani G., Tavidashvili Kh., Laghidze L., Jamrishvili N., Assessment of the Destructive Power of a Tornado on the Territory of the Poti Terminal on September 25, 2021. // II International Scientific Conference “Landscape Dimensions of Sustainable Development Science – Carto/GIS – Planning – Governance”, Dedicated to the 75th Anniversary of Professor Nikoloz (Niko) Beruchashvili, Proceedings, 12-16 September 2022, Tbilisi, Georgia, Ivane Javakhishvili Tbilisi State University Press, 2022, ISBN 978-9941-36-030-5, pp. 275-281. (in Georgian)
   http://www.dspace.gela.org.ge/handle/123456789/10120
6. Amiranashvili A., Chikhladze V., Pipia M., Varamashvili N., Some Results of an Expeditionary Study of the Tornado Distribution Area in Kakheti on June 25, 2024. // Journal of the Georgian Geophysical Society, e-ISSN: 2667-9973, p-ISSN: 1512-1127, Physics of Solid Earth, Atmosphere, Ocean and Space Plasma, v. 27(1), 2024, pp. 67 – 76
7. Amiranashvili A., Chikhladze V., Kekenadze E., Pipia M., Samkharadze I., Telia Sh., Varamashvili N., Meteorological Conditions for the Tornado Formation in Kakheti (Georgia) on June 25, 2024. // Int. Sc. Conf. “Complex Geophysical Monitoring in Georgia: History, Modern Problems, Promoting Sustainable Development of the Country”, Proceedings, ISBN 978-9941-36-272-9, Publish House of Iv. Javakhishvili Tbilisi State University, Tbilisi, Georgia, October 17-19, 2024, pp. 168 – 171.
   http://www.openlibrary.ge/bitstream/123456789/10616/1/42_MM-180.pdf
8. Renko T., Kozarić T., and Tudor M., Waterspout Forecast Indexes over the Adriatic Sea Computed from Operational ALADIN Model Data. // Conference: 5th HyMEX Workshop At: Menorca, Spain, May 2011.
9. Leung, Y.T., Lam, K.F., Lau, T.K., Chan, Y.W. and Chan, P.W., Meteorological indices for potential occurrence of waterspout/tornado in Hong Kong. Meteorol. Z, 34, 2025, pp.81-91.

2nd International Scientific Conference "Modern Problems in Geophysics", Proceedings,
ISBN 978-9941-36-562-1, ISSN 3088-4349, Tbilisi, Georgia, October 29-31, 2026

# ANALYSIS OF THE DESTRUCTIVE EFFECT OF THE KAKHETI HURRICANE BASED ON REAL DATA ON THE DIMENSIONS OF THE ALAVERDI CATHEDRAL

**Kereselidze Z., Khvedelidze I., Chkhitunidze M.**

*M. Nodia Institute of Geophysics of the I. Javakhishvili Tbilisi State University, Tbilisi, Georgia*
*marina_chxitunidze@yahoo.com*

***Abstract.*** *On June 25, 2024, a powerful tornado in Kakheti damaged the Alaverdi Cathedral's dome and cross. This paper analyzes the mechanical causes behind the cross's dislodgement using its actual parameters. The study reveals that static wind pressure alone was likely insufficient to cause the damage. Instead, critical dynamic effects, such as vibrations and resonance induced by the tornado, played a decisive role in compromising the structural integrity of the historic monument.*

***Key words:*** *Tornado, Alaverdi Cathedral, dome cross, dynamic load, resonance, wind impact.*

## Introduction

A tornado represents one of the most complex and energetic manifestations of atmospheric circulation. Although its area of impact is typically local, its destructive effects often significantly exceed the damage caused by conventional storm winds. Tornados are characterized by the rapid rotation of air masses, intense turbulence, and continuous changes in flow direction.

As a result of the tornado recorded in the Kakheti region on June 25, 2024, the conical roof covering of the Alaverdi Monastery dome was damaged, and the cross mounted on top of the dome was dislodged. This event brought to the forefront the question of what type of mechanical processes could have caused such damage. This issue was investigated in a study, which utilized the parameters of a model cross made of brass: height $L = 2.7m$, width $D = 0.63 \cdot L = 1.7m$, diameter D = 0.15 m, thickness $Z = 0.007$m, It is assumed that by means of a vertical frame and anchors, the cross was rigidly connected to the load-bearing part of the dome (presumably to wooden beams) and was covered with a concrete slab of thickness $H = 0.3$m [1].

## Structural Characteristics of the Alaverdi Cross

Based on the investigation of the pre-disaster state, it was possible to reconstruct the primary parameters of the cross.

The total height of the cross from its base was approximately 160 cm, while the width of its horizontal arms was approximately 155 cm. The cross was fabricated from a rectangular cross-section copper alloy profile with transverse dimensions of 4 × 2 cm. The ends were decoratively flattened, which increased both the visual effect and the effective wind-exposed surface area.

The cross was embedded into a stone base to a depth of approximately 25–30 cm. The stone base, in turn, rested upon and was connected to earlier stone elements integrated into the upper part of the brick-built dome cone. The base of the cross was additionally covered with a sheet metal made of the same copper alloy.

The construction of the conical dome roof covering is of particular interest. It consisted of sheet metal plates secured onto wooden battens (laths). Such a system is relatively lightweight; however, under high wind conditions, it can generate additional vibrational effects, which are subsequently transmitted through the structural joints to the supporting base of the cross [2].

## Wind Load Assessment

During a tornado, the primary mechanical factor acting on a structure is the dynamic pressure of the airflow. It is determined by the expression:

$$q = \frac{\rho V^2}{2} \quad (1)$$

Where: $q$ is the dynamic pressure, $\rho$ is the air density, $V$ is the wind speed.

If the characteristic speed of the tornado fluctuated within the range of 40–50 m/s , the dynamic pressure would reach several kilopascals. Such a load produced both a horizontal force and a bending moment relative to the cross.

Unlike conventional wind, a tornado flow is not characterized by a constant direction. Air masses continuously change their direction of motion, causing the structure to experience a variable, pulsating load. It is precisely these loads that create conditions for dynamic instability.

**Stability Analysis of the Cross**

The Alaverdi cross can be considered a cantilevered elastic system with a fixed lower part and a free upper part. For an element with a rectangular cross-section, the resistance to bending is determined by the geometric moment of inertia:

$$I = \frac{bh^3}{12} \quad (2)$$

where $b$ and $h$ are the dimensions of the cross-section.

In the case of a $4 \times 2$ cm cross-section, the obtained value indicates that the profile of the cross was sufficiently durable against the impact of normal wind. Copper alloys are also distinguished by high corrosion resistance and satisfactory mechanical strength.

Therefore, plastic deformation of the cross due to a single static load alone appears highly unlikely.

## Dynamic Effects and the Possibility of Resonance

During the disaster, the most critical factor may not have been the average wind speed, but rather its rapidly fluctuating pulsations. Rotational flows of various scales are generated inside a tornado. They periodically alter the magnitude and direction of the load. If the frequency of such an external impact happens to be close to one of the natural vibration frequencies of the structure, resonance develops.

Under resonant conditions, the amplitude of the load increases significantly. In such a scenario, multiple oscillatory processes can develop at the base of the cross, progressively weakening the connections:

- Between the cross and the stone base;
- Between the stone base and the brickwork/masonry of the dome;
- Between the upper part of the dome and the roofing elements.

Furthermore, the conical roof covered with sheet metal plates could itself transfer into a vibrational mode under the influence of the wind, further increasing the dynamic loads.

## Probable Damage Mechanism

The analysis of the structural layout indicates that the tearing away of the cross was likely not the result of a single mechanical factor.The following scenario is more realistic:

- The tornado caused a partial deformation of the conical roof covering of the dome;
- The system of wooden battens and sheet metal plates transitioned into an intense vibration mode;
- These vibrations were transmitted to the supporting joint of the cross;
- In parallel, a variable aerodynamic force acted on the cross;
- As a result of repeated oscillations, the connection between the stone base and the supporting part weakened;
- Ultimately, the integrity of the system was compromised, and the cross was torn away.

This type of mechanism aligns more closely with the nature of the recorded damage than the action of a static wind force alone.

**Dynamic Calculation for Resonance**

The fundamental (lowest) frequency of vibration of a cross, or equivalently, a cantilever beam, in engineering mechanics is determined by the following expression [1]:

$$\Omega_1 = \frac{0.56}{H^2}\sqrt{EI/m} \tag{3}$$

where $m$ represents the linear mass of a 27 kg brass cross, $E$ – the modulus of elasticity of the cross material, $I$ – the geometric moment of inertia at the base of the cross.

There is an alternative variant of formula (7), in which the cross is approximated as a vertical cantilever beam, whose first, or fundamental, frequency of bending-induced vibrations is:

There is formula in which the cross is approximated as a vertical cantilever beam, whose first, or fundamental, frequency of bending-induced vibrations is:

$$\Omega_1 = \frac{3.5}{2\pi L^2}\cdot\left(E\cdot\frac{I}{\rho A}\right)^{\frac{1}{2}} \tag{4}$$

where $\rho \approx 2500$ kg.m$^3$ is the density of brass, $A = L\cdot t$ is the cross-sectional area of the rectangular frame of the cross (cantilever), $I = L\cdot t^3/12$ is the moment of inertia of the frame, and $t = 0.007$m is the tube thickness.

Using the set of parameters for the cross, formula (4) yields: $\Omega_1 \approx 0.53$ Hz, meaning the fundamental period of bending vibration of the cross is $T \approx 1.88$ s, Practically the same result is given by formula (3), according to which $\Omega_1 \approx 0.6$Hz. The numerical coefficient characterizing the natural vibrations of various structures is determined from the corresponding differential equation (see Note). Its solution must satisfy, for instance, within the harmonic vibration approximation, the relevant boundary conditions of the body as a whole, or of its elastic contour. According to the theory of natural mechanical vibrations, for cross-type structures, resonance may occur between the vortex shedding frequency and the fundamental frequency, or one of the nearby overtones, of the natural vibration spectrum of the cross. This phenomenon can develop if the condition $\Omega_1 \leq 4$Hz is met. If the frequency is $\Omega_1 < 4.0$ Hz enhancing the stability of the cross against resonance is possible by altering the tube diameter or by installing special dampers. A damper is an elastic device designed to dissipate the energy of impact loads and suppress vibrations.

**Note.** Natural vibrations associated with the effect of bending (elastic deformation) are a fundamental phenomenon that determines the dynamic characteristics of a specific engineering structure (Fig. 1).

In general, the differential equation for the free vibrations of any body is of the fourth order. The natural vibration frequency spectrum of a beam-assembled structure, to which the cross belongs, is determined from the equation:

$$EI\left(\frac{\partial^4\Omega}{\partial x^4}\right) + \rho A\left(\frac{\partial^2\Omega}{\partial t^2}\right) = 0, \tag{5}$$

where the notations given above are applied.

Equation (5) is solved using the method of separation of variables: $\Omega(x,t) = \Omega(x)\cdot sin(\omega t)$, which leads to a fourth-order ordinary differential equation, whose vibration spectrum represents an infinite series of overtones of $\Omega(x)$ – where each component frequency corresponds to a different mode of deformation of the structure. For example, for the case of a vibrating cantilever beam, there is a general equation:

$$\Omega_n = ((\beta_n L)^2 / (2\pi L^2)) \times (EI/m)^{1/2} \tag{6}$$

where $\Omega_n$ is the overtone frequency, and $(\beta_n L)^2$ is the eigenvalue (coefficient) depending on the boundary conditions of equation (6). For instance, for a cantilever beam, the ratio of the numerical coefficients is $\Omega_2/\Omega_1 = 6.27$ meaning that the partial frequencies do not form a harmonic series.



**Fig. 1.** Tornado phenomenon.

## Conclusion

According to the assessments obtained for the model cross, the analysis conducted on the basis of the actual geometric and structural parameters of the cross located on the dome of the Alaverdi Cathedral shows that the structure represented a relatively rigid system consisting of a cross made of a rectangular copper alloy profile, a stone base, and the upper stone masonry of the dome.

It was found that the static pressure of the wind alone was, in all probability, insufficient to tear the cross away. A combined action of dynamic processes appears more credible, encompassing structural vibrations, pulsating wind impacts, roof vibrations, and potential resonant effects.

Consequently, in the case of the Alaverdi Cathedral, the destructive effect of the tornado must be viewed as the result of a combined impact of aerodynamic, dynamic, and structural factors, which ultimately led to the failure of the supporting joint of the dome cross.

## Acknowledges

We would like to express our gratitude to the LEPL National Agency for Cultural Heritage Preservation of Georgia for providing information regarding the geometric parameters of the cross on the dome of the Alaverdi Cathedral, as it existed prior to the natural disaster on June 25, 2024.

## References

1. Kereselidze Z., Zhonzholadze N., Chkhitunidze M., Modeling of the destructive action of a tornado in Kakheti on the example of Alaverdi cathedral. // Journal of the Georgian Geophysical Society, 2026, submitted for printing.
2. Amiranashvili A. G., Chikhladze V. A., Pipia M. G., Varamashvili N. D., Some Results of an Expeditionary Study of the Tornado Distribution Area in Kakheti on June 25, 2024. // Journal of the Georgian Geophysical Society, e-ISSN: 2667-9973, p-ISSN: 1512-1127 Physics of Solid Earth, Atmosphere, Ocean and Space Plasma, v. 27(1), 2024, pp. 67 – 76.

2nd International Scientific Conference "Modern Problems in Geophysics", Proceedings,
ISBN 978-9941-36-562-1, ISSN 3088-4349, Tbilisi, Georgia, October 29-31, 2026

# ANGSTROM FIRE INDEX FOR BOLNISI (GEORGIA)

**[*]Bliadze T., [**]Beglarashvili N., [***]Janelidze I., [*]Mepharidze E., [*]Tchankvetadze A.**

[*]*Mikheil Nodia Institute of Geophysics of Ivane Javakhishvili Tbilisi State University, Tbilisi, Georgia*
[**]*Institute of Hydrometeorology of Georgian Technical University, Tbilisi, Georgia*
[***]*Georgian Technical University, Tbilisi, Georgia*
teimuraz.bliadze@gmail.com

***Abstract.*** *The paper presents data on intraannual distributions of average monthly mean and monthly max values of the Angstrom Fire Index (AFI_mean and AFI_max), and also the distribution of the number of daily mean and maximum values of AF by month in Bolnisi in 2018-2023. The intraannual distributions of mean monthly values of AFI in Bolnisi has the form of a sixth-degree polynomial. The highest fire danger is observed in July and August based on AFI mean data (category "High") and from June to August based on AFI_max data (category "Extreme"). On average, for the mean daily values of AFI with the category "Extreme", the largest number of days is observed in August (6 days), and for the maximum daily values of AFI – from May to September (10, 20, 26, 25 and 16 days, respectively).*

***Key Words:*** *Angstrom Fire Index, temperature, fire.*

## Introduction

The issue of fires, including forest fires, is a pressing concern for many countries worldwide [http://www.sasquatchstation.com/Fire_Weather.php;
http://www.forestservice.gr/meteo/fwi1.html], including Georgia [1].

In recent decades, this problem has become particularly acute due to rapid global and local warming [2], which contributes to increased fire risk [3]. Notably, as of August 1, 2026, forest and landscape fires had affected 112.3 million hectares globally – an area roughly comparable to the territory of South Africa [https://naked-science.ru/community/1209262].

Various countries employ different indicators to assess forest fire risk [3–6]. These indices are mathematical formulas that formalize the influence of factors such as air temperature and humidity, precipitation, the moisture content of forest fuels, lightning activity, and so forth. The simple Swedish Angstrom Fire Index [4,5] is frequently used, featuring either a four-range [http://www.forestservice.gr/meteo/fwi1.html] or five-range
[http://www.sasquatchstation.com/Fire_Weather.php] scale. In addition to providing climatological and operational data on fire risk levels, forecasting of these levels is also conducted [https://www.weather.gov/fire].

In Georgia, efforts to assess fire risk using the Angstrom Fire Index (AFI) [4, 5] began in 2019, starting with a case study of Tbilisi [7]. Similar studies were extended to the cities of Telavi and Kutaisi, the Russian cities of Nalchik and Kislovodsk, and Azerbaijani capital, Baku [10–14].

Specifically, it was found that extreme fire danger occurs in Baku and Tbilisi for an average of 75 days per year; however, the overall level of fire danger in the forests of Tbilisi is higher than in Baku. A direct linear correlation exists between the mean daily and mean monthly AFI values for Baku and Tbilisi [14].

This study builds upon previous research. Presented below are the results of a statistical analysis of daily values of the Angström Fire Index (AFI) for the city of Bolnisi (Georgia), based on a five-level scale and covering the period from 2018 to 2023.

## Study area, material and methods

Study area is Bolnisi (Georgia). The work used data from the Georgian National Environment Agency on average daily and urgent (at 4 p.m. local time) values of air temperature T and relative humidity R in the period 2018-2023 [http://www.pogodaiklimat.ru/archive.php?id=ru&region=07]. The Swedish Angstrom

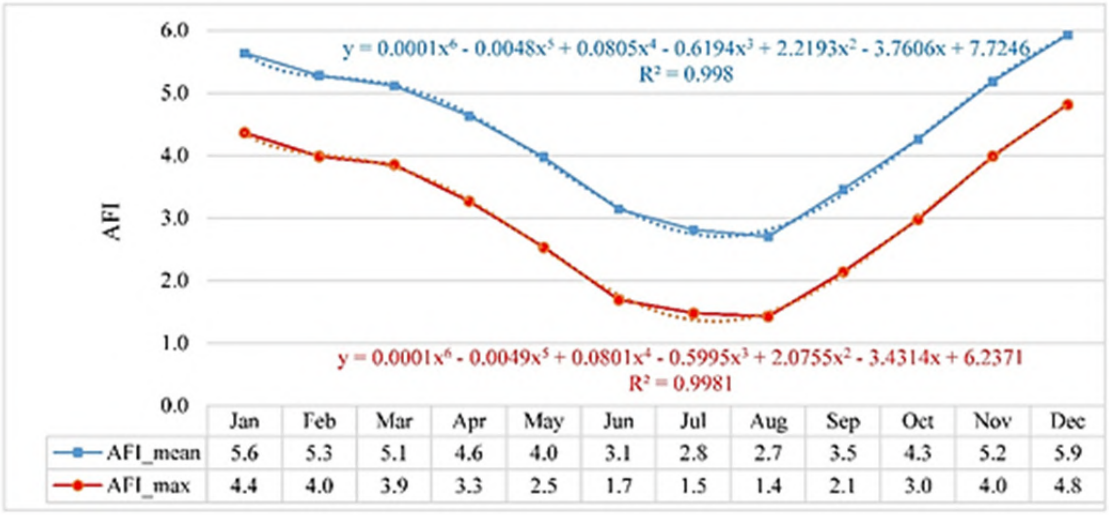
Index (AFI) is calculated from the formula: AFI = (R/20) + (27-T)/10 [4,5]. The gradations of the values of AFI are as follows [http://www.sasquatchstation.com/Fire_Weather.php]: I. AFI ≥ 4.1 – Low, II. AFI = 4.0 ÷ 3.0 – Moderate, III. AFI = 2.9 ÷ 2.5 – High, IY. AFI = 2.4 ÷ 2.0 – Very High, Y. AFI = <2.0 – Extreme.

The standard statistical methods are used. AFI_mean and AFI_max – daily average and daily maximum Angstrom Fire Index, respectively.

## Results and discussion

Results in Fig. 1 – Fig.3 are presented.

Fig. 1. Present the intraannual diatributions of mean monthly values of AFI in Bolnisi in 2018-2023.

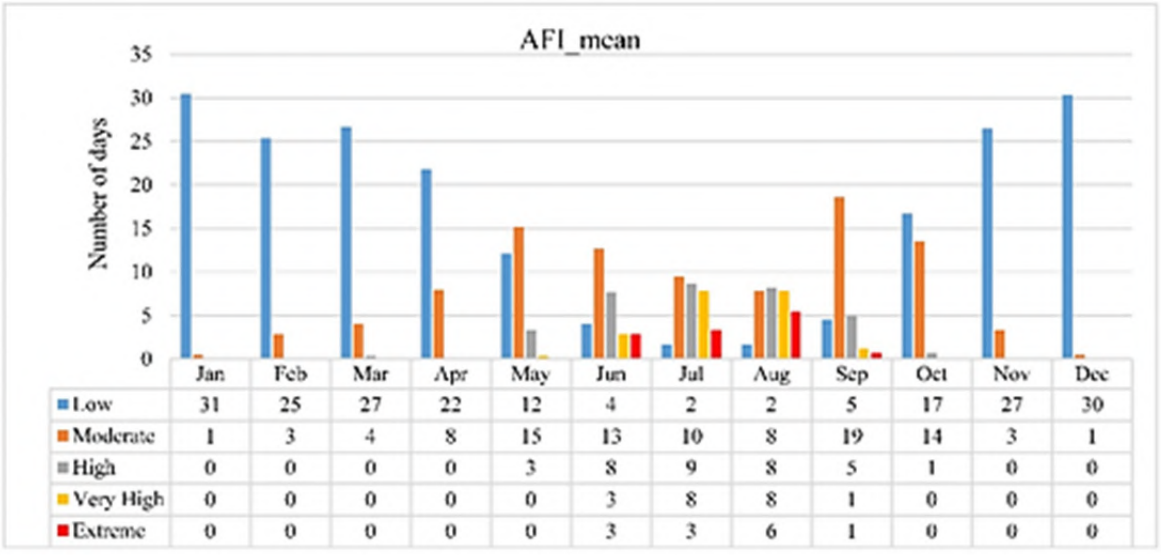



| | Jan | Feb | Mar | Apr | May | Jun | Jul | Aug | Sep | Oct | Nov | Dec |
|---|---|---|---|---|---|---|---|---|---|---|---|---|
| AFI_mean | 5.6 | 5.3 | 5.1 | 4.6 | 4.0 | 3.1 | 2.8 | 2.7 | 3.5 | 4.3 | 5.2 | 5.9 |
| AFI_max | 4.4 | 4.0 | 3.9 | 3.3 | 2.5 | 1.7 | 1.5 | 1.4 | 2.1 | 3.0 | 4.0 | 4.8 |

**Fig. 1.** The intraannual diatributions of mean monthly values of AFI in Bolnisi in 2018-2023.

The intraannual diatributions of mean monthly values of AFI in Bolnisi has the form of a sixth-degree polynomial (Fig. 1). The highest fire danger is observed in July and August based on AFI_mean data (category "High") and from June to August based on AFI_max data (category "Extreme").

In Fig. 2 data about mean number of days with different categories of AFI_mean in Bolnisi from January to December are presented.

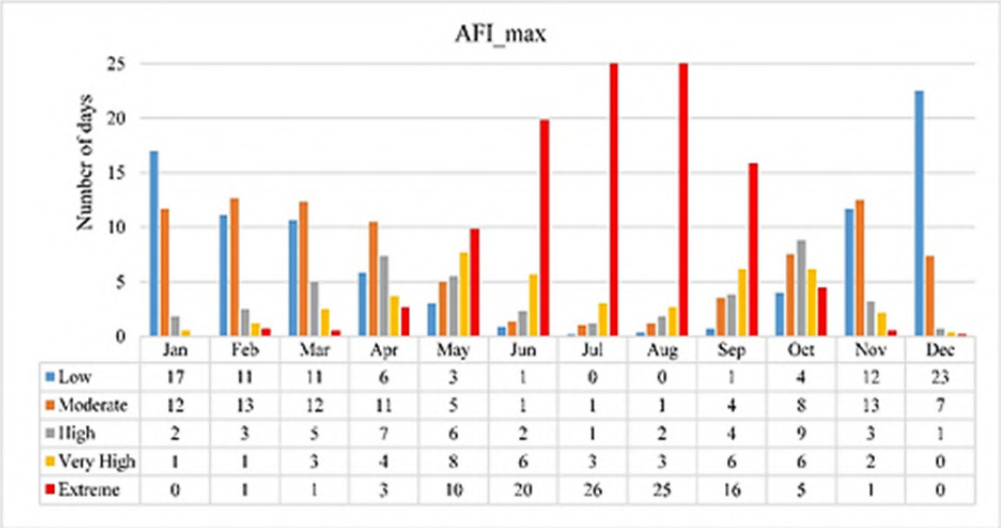



| | Jan | Feb | Mar | Apr | May | Jun | Jul | Aug | Sep | Oct | Nov | Dec |
|---|---|---|---|---|---|---|---|---|---|---|---|---|
| Low | 31 | 25 | 27 | 22 | 12 | 4 | 2 | 2 | 5 | 17 | 27 | 30 |
| Moderate | 1 | 3 | 4 | 8 | 15 | 13 | 10 | 8 | 19 | 14 | 3 | 1 |
| High | 0 | 0 | 0 | 0 | 3 | 8 | 9 | 8 | 5 | 1 | 0 | 0 |
| Very High | 0 | 0 | 0 | 0 | 0 | 3 | 8 | 8 | 1 | 0 | 0 | 0 |
| Extreme | 0 | 0 | 0 | 0 | 0 | 3 | 3 | 6 | 1 | 0 | 0 | 0 |

**Fig. 2.** Mean number of days with different categories of AFI_mean in Bolnisi from January to December.

In particular, as follows from Fig. 2, on average during the year for mean daily values of AFI_mean with the "Extreme" category, the greatest number of days is observed in August (6 days), etc.

In Fig. 3 data about mean number of days with different categories of AFI_max in Bolnisi from January to December are presented.




| | Jan | Feb | Mar | Apr | May | Jun | Jul | Aug | Sep | Oct | Nov | Dec |
|---|---|---|---|---|---|---|---|---|---|---|---|---|
| Low | 17 | 11 | 11 | 6 | 3 | 1 | 0 | 0 | 1 | 4 | 12 | 23 |
| Moderate | 12 | 13 | 12 | 11 | 5 | 1 | 1 | 1 | 4 | 8 | 13 | 7 |
| High | 2 | 3 | 5 | 7 | 6 | 2 | 1 | 2 | 4 | 9 | 3 | 1 |
| Very High | 1 | 1 | 3 | 4 | 8 | 6 | 3 | 3 | 6 | 6 | 2 | 0 |
| Extreme | 0 | 1 | 1 | 3 | 10 | 20 | 26 | 25 | 16 | 5 | 1 | 0 |

**Fig. 3.** Mean number of days with different categories of AFI_max in Bolnisi from January to December.

In particular, as follows from Fig. 3, on average during the year for max daily values of AFI_max with the "Extreme" category, the greatest number of days are observed from May to September (10, 20, 26, 25 and 16, respectively).

## Conclusion

It is planned to continue this research in the near future, taking into account the rapid warming of the climate in recent years.

**Acknowledgement:** The authors are grateful to the chief of the atmospheric physics department of M. Nodia Institute of Geophysics A. Amiranashvili, for assistance in the fulfillment of this work.

## References

1. Bliadze T., Statistical Analysis of the Weekly Fire Alerts Count in Georgia and its Regions in 2012-2023.// Int. Sc. Conf. "Complex Geophysical Monitoring in Georgia: History, Modern Problems, Promoting Sustainable Development of the Country", Proceedings, ISBN 978-9941-36-272-9, Publish House of Iv. Javakhishvili Tbilisi State University, Tbilisi, Georgia, October 17-19, 2024, pp. 101 – 104. http://109.205.44.60/bitstream/123456789/10632/1/26_MM-180.pdf
2. Kartvelishvili L., Tatishvili M., Amiranashvili A., Megrelidze L., Kutaladze N. Weather, Climate and their Change Regularities for the Conditions of Georgia. // Monograph, Publishing House "UNIVERSAL", ISBN: 978-9941-33-465-8, Tbilisi 2023, 406 p., https://doi.org/10.52340/mng.9789941334658
3. Ullah M.R., Liu X.D., Al-Amin M., Spatial-Temporal Distribution of Forest Fires and Fire Weather Index Calculation from 2000 to 2009 in China. // Journal of Forest Science, 59, 2013 (7), pp. 279–287.
4. Skvarenina J., Mindas J., Holecy J., Tucek J., Analysis of the Natural and Meteorological Conditions During Two Largest Forest Fire Events in the Slovak Paradise National Park. // Forest fire in the wildland-urban interface and rural areas in Europe: an integral planning and management challenge. Athens. 2003.
5. Lukić T., Marić P., Hrnjak I., Gavrilov M.B., Mladjan D., Zorn M., Komac B., Milošević Z., Marković S.B., Sakulski D., Jordaan A., Đorđević J., Pavić D., Stojsavljević R., Forest Fire Analysis and Classification Based on a Serbian Case Study. // Acta Geographica Slovenica, 57-1, 2017, pp. 51–63.
6. Klassifikatsiya prirodnoy pozharnoy opasnosti lesov. // Prikaz Rosleskhoza ot 5 iyulya 2011 g. № 287, 6 s., dokument s sayta aviales.ru
7. Bliadze T., Kirkitadze D., Samkharadze I., Tsiklauri Kh.. Statistical Characteristics of Angstrom Fire Index for Tbilisi. // Int. Sc. Conf. "Natural Disasters in Georgia: Monitoring, Prevention, Mitigation". Proc., ISBN 978-9941-13-899-7, Publish House of Iv. Javakhishvili Tbilisi State University, December 12-14, Tbilisi, 2019, pp.86-90.

8. Bliadze T., Kirkitadze D., Samkharadze I., Tsiklauri Kh.. Statistical Characteristics of Angstrom Fire Index for Telavi (Georgia). // International Scientific Conference „Modern Problems of Ecology“,Proceedings, ISSN 1512-1976, v. 7, Tbilisi-Telavi, Georgia, 26-28 September, 2020, pp.64-67.
9. Bliadze T., Gekkieva S., Kirkitadze D. Comparison of Angstrom Fire Index for Nalchik (Kabardino-Balkaria, Russian Federation) and Telavi (Georgia). // International Scientific Conference „Modern Problems of Ecology“,Proceedings, ISSN 1512-1976, v. 7, Tbilisi-Telavi, Georgia, 26-28 September, 2020, pp.68-72.
10. Bliadze T., Povolotskaya N., Senik I., Comparison of Angstrom Fire Index for Tbilisi (Georgia) and Kislovodsk (Russia). // Int. Sc. Conf. „Natural Disasters in the 21st Century: Monitoring, Prevention, Mitigation“. Proceedings, ISBN 978-9941-491-52-8, Tbilisi, Georgia, December 20-22, 2021. Publish House of Iv. Javakhishvili Tbilisi State University, Tbilisi, 2021, pp. 158 – 162.
11. Bliadze T., Amiranashvili A., Chkhitunidze M., Laghidze L., Statistical Analysis of Angstrom Fire Index for Kutaisi, Georgia. // II International Scientific Conference “Landscape Dimensions of Sustainable Development Science – Carto/GIS – Planning – Governance”, Dedicated to the 75th Anniversary of Professor Nikoloz (Niko) Beruchashvili, Proceedings, 12-16 September 2022, Tbilisi, Georgia, Ivane Javakhishvili Tbilisi State University Press, 2022, ISBN 978-9941-36-030-5, pp. 270-274. http://www.dspace.gela.org.ge/handle/123456789/10119
12. Amiranashvili A., Bliadze T., Japaridze N., Khazaradze K., Revishvili A., Angstrom Fire Index as a Bioclimatic Indicator (Using the Example of the Impact on the Spread of Covid-19 in Tbilisi). // Int. Sc. Conf. "Geophysical Processes in the Earth and its Envelopes". Proceedings, ISBN 978-9941-36-147-0, Publish House of Iv. Javakhishvili Tbilisi State University, November 16-17, 2023, pp. 328-331.
http://openlibrary.ge/handle/123456789/10467
13. Amiranashvili A., Bliadze T., Davitashvili M., Khakhiashvili M., Variability of the Angstrom Fire Index in Kakheti due to Climate Change. // Transactions of Mikheil Nodia Institute of Geophysics, ISSN 1512-1135, vol. LXXV, 2022, pp. 117-136. (in Georgian)
http://openlibrary.ge/handle/123456789/10298
14. Aliyev V., Bliadze T., Chikhladze V., Davitashvili M., Tatishvili M., Comparison of Angstrom Fire Index for Baku (Azerbaijan) and Tbilisi (Georgia). // 1st International Scientific Conference “Modern problems in Geophysics”. Proceedings, ISBN 978-9941-36-434-1, ISSN 3088-4349, Tbilisi, Georgia, November 6-8, 2025. Publish House of Iv. Javakhishvili Tbilisi State University, Tbilisi, 2025, pp. 171-174.
http://dspace.gela.org.ge/bitstream/123456789/10754/1/44_Conf_MPG_2025.pdf

2nd International Scientific Conference "Modern Problems in Geophysics", Proceedings,
ISBN 978-9941-36-562-1, ISSN 3088-4349, Tbilisi, Georgia, October 29-31, 2026

# INVESTIGATION OF AROMATIC HYDROCARBON POLLUTION IN SOILS NEAR LAKE BOYUKSHOR ABSHERON PENINSULA

**[*]Hajiyeva S., [**]Mustafayev I., [*]Aliyeva T., [***]Huseynov E.**

[*]*Baku State University, Baku, Azerbaijan*
[**]*Azerbaijan University of Architecture and Construction, Baku, Azerbaijan*
[***]*Azerbaijan State University of Oil and Industry, Baku, Azerbaijan*
*taranaaliyeva2024@gmail.com*

***Abstract.*** *This study presents the results of an environmental assessment of soil contamination by volatile aromatic hydrocarbons (BTEX compounds) in the vicinity of Lake Boyukshor. Soil samples were collected from four monitoring points and analyzed for benzene, toluene, ethylbenzene, and xylene isomers. The obtained results demonstrated spatial variability in pollutant distribution. The highest concentrations of BTEX compounds were detected in sample S1, where p-xylene (10.3197 µg/kg), toluene (5.2204 µg/kg), and benzene (1.8347 µg/kg) predominated. In the remaining samples, the concentrations were either below detection limits or detected at very low levels. Comparative analysis with maximum permissible concentrations (MPC) indicated that the measured values did not exceed established environmental standards for soils. However, localized accumulation of BTEX compounds may be associated with anthropogenic impacts, including oil industry activities and historical hydrocarbon contamination characteristic of the Absheron Peninsula. The results indicate the necessity for continuous environmental monitoring of soils in the Lake Boyukshor area to prevent potential ecological risks and ensure ecosystem stability.*

***Key words:*** *BTEX, soil contamination, aromatic hydrocarbons, environmental monitoring, Lake Boyukshor.*

Lake Boyukshor is the largest lake among the Absheron lakes in terms of surface area and is characterized by a severe ecological condition. According to the mineralization level of its water, Lake Boyukshor belongs to the group of saline lakes, and the mineralization of its water exceeds the maximum permissible concentration (MPC) many times over. The oxygen regime of the lake is completely disturbed. One of the main reasons for the low concentration of dissolved oxygen in the lake water is the intensification of biological processes resulting from the oxidation of pollutants. Consequently, the biochemical oxygen demand in Lake Boyukshor exceeds the norm several times.

Under the influence of natural factors and wastewater discharged into the lake, not only does the mineralization of Lake Boyukshor increase, but the concentrations of cations and anions in the water also rise sharply. Thus, the concentrations of calcium, magnesium, and chlorides exceed sanitary standards many times, while sulfates are several times higher than the permissible limits. The concentrations of petroleum products and phenols, which are the main pollutants of the lake, significantly exceed the MPC. Synthetic detergents are also present in concentrations above the norm. Among heavy metals, copper, cadmium, iron, zinc, and manganese exceed the MPC several times [1–5].

During June–August 2025, water samples from Lake Boyukshor, wastewater discharged into the lake, bottom sediments, and soil samples from the surrounding area were collected and analyzed by us according to various parameters.

Soil samples were collected from different depths using the drilling method. Higher levels of contamination were observed in the upper soil layers. Soil samples collected from the vicinity of Lake Boyukshor were analyzed for volatile aromatic hydrocarbons including benzene, toluene, ethylbenzene, and xylene isomers (BTEX compounds). The obtained concentrations are presented in Table 1 and Fig. 1.

**Table 1.** Concentration of BTEX compounds in soil samples

| Compound | Unit | S1 | S2 | S3 | S4 | MPC |
|---|---|---|---|---|---|---|
| Benzene | µg/kg | 1.8347 | <0.0400 | <0.0400 | <0.0400 | 0.3 mg/kg |
| Toluene | µg/kg | 5.2204 | 0.3323 | <0.0400 | 0.4073 | 0.3 mg/kg |
| Ethylbenzene | µg/kg | 0.2342 | <0.0400 | <0.0400 | <0.0400 | 0.1 mg/kg |
| p-Xylene | µg/kg | 10.3197 | 0.0548 | <0.0400 | 0.1300 | 6 mg/kg |
| m-Xylene | µg/kg | <0.0400 | <0.0400 | <0.0400 | <0.0400 | 6 mg/kg |
| Total BTEX | µg/kg | 17.6090 | 0.3871 | <0.0400 | 0.5373 | |

The results indicate that sample S1 exhibited the highest concentrations of all detected BTEX compounds, suggesting localized hydrocarbon contamination in this area. Among the analyzed pollutants, p-xylene showed the maximum concentration (10.3197 µg/kg), followed by toluene (5.2204 µg/kg) and benzene (1.8347 µg/kg).

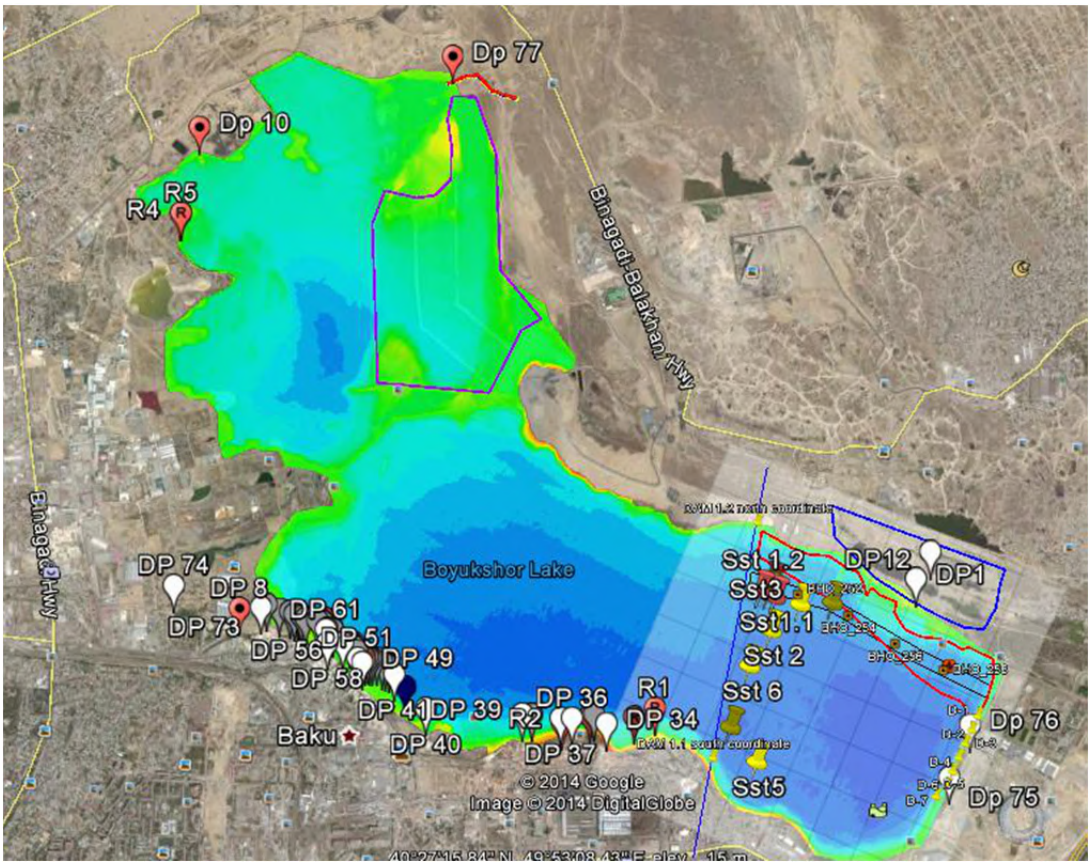



**Fig. 1.** Sampling stations.

In samples S2, S3, and S4, most compounds were either below the detection limit or detected at very low concentrations. Sample S3 demonstrated the lowest contamination level, where all analyzed parameters were below the analytical detection limit.

Although BTEX compounds were detected in several soil samples, the measured concentrations were significantly lower than the maximum permissible concentrations (MPC) established for soils. Therefore, according to the obtained analytical data, the investigated soils cannot be classified as heavily polluted by aromatic hydrocarbons.

However, the elevated BTEX concentrations observed in sample S1 may indicate the influence of localized anthropogenic activities associated with petroleum production, industrial discharge, or historical oil contamination, which are characteristic environmental problems in the Absheron Peninsula region.

The spatial variability of pollutant distribution suggests that hydrocarbon contamination around Lake Boyukshor is uneven and depends on local environmental and technogenic factors. Continuous environmental monitoring is therefore recommended to assess potential risks to soil quality and ecosystem health.

## References


1. Hajiyeva S.R., Aliyeva T.I., Yusifova M.M., The ecological state of Boyuk Shor lake of Azerbaijan. // Environmental Monitoring and Assessment, V.192, N 780, 2020, pp.1-11.
2. Mustafayev I.I., Mammadov V.Y., Salmanov M.A., Huseynov S.Y., Absheron Lakes. Baku: "Rüzgar" Ecological Society, 2001, 52 p.
3. Hajiyeva S.R., Aliyeva T.I., Huseynova P.V., Anthropogenic pollution sources of Lake Boyukshor. // VI Republican Scientific Conference "Actual Problems of Ecology and Soil Science in the XXI Century", 2017, pp. 28–30.
4. Gadzhiyeva S.R., Aliyeva T.I., Gadzhiyeva Kh.F., Huseynova P.V., Alizadeh B.F., Ecological condition and pollution of Lake Boyukshor. // Journal of Postgraduate and Doctoral Students, 2017, pp. 59–61.
5. Hajiyeva S.R., Aliyeva T.I., Bayramov Q.I., Huseynova P.I., Ecological assessment of Lake Boyukshor. // International Scientific Conference "Coordination Compounds Chemistry: Actual Problems of Analytical Chemistry" dedicated to the 85th anniversary of Academician Rafiqa Alirza gizi Aliyeva, 2017, p. 184.

2nd International Scientific Conference "Modern Problems in Geophysics", Proceedings,
ISBN 978-9941-36-562-1, ISSN 3088-4349, Tbilisi, Georgia, October 29-31, 2026

# HYDROECOLOGICAL ASSESSMENT OF HYDROCARBON CONTAMINATION IN BOTTOM SEDIMENTS OF LAKE GU, ABSHERON PENINSULA

**Aliyeva T.**

*Baku State University, Baku, Azerbaijan*
*taranaaliyeva2024@gmail.com*

***Abstract.*** *This study presents an environmental assessment of petroleum hydrocarbon contamination in bottom sediments of a lake system in the Absheron Peninsula. Sediment samples were collected from three stations (St15–St17) and analyzed for total petroleum hydrocarbons (TPH) and polycyclic aromatic hydrocarbons (PAHs). The results demonstrated significant accumulation of hydrocarbons at all sampling points. TPH concentrations ranged from 1750 to 2510 mg/kg (GC analysis), while total extractable hydrocarbons reached up to 5250 mg/kg. The dominant fractions were heavy hydrocarbons ($C_{21}$–$C_{35}$), indicating long-term and weathered petroleum pollution. PAH analysis revealed strong spatial variability, with the highest total concentration recorded at St16 (26.48 mg/kg). High-molecular-weight PAHs such as benz[a]anthracene and chrysene were dominant at this site. The results confirm severe anthropogenic impact and the presence of localized pollution hotspots. Continuous monitoring is recommended for ecological risk assessment and environmental management.*

***Key words:*** *Petroleum hydrocarbons, TPH, PAHs, bottom sediments, environmental pollution, Absheron Peninsula, sediment quality.*

The Absheron Peninsula is one of the most industrially impacted regions in Azerbaijan, where long-term oil extraction, refining activities, and urban wastewater discharge have significantly altered natural ecosystems. Aquatic systems in this area are especially vulnerable to petroleum-derived pollution due to continuous anthropogenic pressure.

Bottom sediments act as a major sink for hydrophobic organic contaminants, including total petroleum hydrocarbons (TPH) and polycyclic aromatic hydrocarbons (PAHs). These compounds are persistent, toxic, and capable of long-term accumulation in aquatic environments. TPH represents a broad mixture of petroleum-derived substances, while PAHs are a group of organic pollutants formed through incomplete combustion and petroleum degradation processes. Due to their stability and toxicity, PAHs are considered priority pollutants in environmental monitoring programs. High-molecular-weight PAHs are particularly dangerous because of their carcinogenic and mutagenic properties [1-5].

The aim of this study is to assess the levels, composition, and spatial distribution of TPH and PAHs in bottom sediments of a lake system in the Absheron Peninsula in order to evaluate the degree of anthropogenic impact and identify pollution hotspots.

Bottom sediment samples were collected from three stations (St15, St16, St17) located within a lake system of the Absheron Peninsula. The stations were selected to represent areas with different levels of anthropogenic influence. Sediment samples were collected from the upper sediment layer using a grab sampling method. This layer is considered the most active zone for pollutant accumulation and exchange with the overlying water column. Samples were placed in pre-cleaned containers and transported to the laboratory under cooled conditions. Total petroleum hydrocarbons (TPH) were determined using gas chromatography (GC) across the $C_7$–$C_{40}$ range. Additionally, total extractable hydrocarbons were measured to estimate the overall petroleum contamination load.

Polycyclic aromatic hydrocarbons (PAHs) were analyzed using chromatographic techniques. The following compounds were identified: naphthalene, acenaphthylene, anthracene, fluoranthene, phenanthrene,

pyrene, benz[a]anthracene, chrysene, and others. All concentrations were expressed in mg/kg. Spatial distribution patterns were evaluated through comparative analysis between sampling stations. The obtained concentrations are presented in Table 1and Table 2.

**Table 1.**

| Bottom sediments | | St15 | St16 | St17 |
|---|---|---|---|---|
| **Field number** | **Unit** | 104 | 105 | 110 |
| **TPH** | **Qu** | | | |
| $C_7H_{16}$ | mg/kg | <10 | <10 | <10 |
| $C_8H_{18}$ | mg/kg | <10 | <10 | 20 |
| $C_9H_{20}$ | mg/kg | <10 | <10 | <10 |
| $C_{10}H_{22} + C_{11}H_{24}$ | mg/kg | <10 | <10 | 200 |
| $C_{12}H_{26} + C_{15}H_{32}$ | mg/kg | 200 | 50 | 200 |
| $C_{16}H_{34} + C_{20}H_{42}$ | mg/kg | 50 | <10 | 120 |
| $C_{21}$-$C_{30}$ | mg/kg | 1000 | 1700 | 1000 |
| $C_{30}$-$C_{35}$ | mg/kg | 400 | 560 | 300 |
| $C_{35}$-$C_{40}$ | mg/kg | 100 | 200 | 120 |
| **Total TPH by GC** | mg/kg | **1750** | **2510** | **1960** |
| **Total extractable hydrocarbons** | mg/kg | **3880** | **4660** | **5250** |

**Table 2.**

| Bottom sediments | | St15 | St16 | St17 |
|---|---|---|---|---|
| **Field number** | **Unit** | 104 | 105 | 110 |
| **PAH** | | **Qu** | | |
| Naphthalene | mg/kg | 0.2004 | <0.0040 | 0.1021 |
| Acenaphtylene | mg/kg | <0.0040 | <0.0040 | <0.0040 |
| Anthracene | mg/kg | 0.0653 | <0.0040 | 0.0510 |
| Fluoranthene | mg/kg | <0.0040 | <0.0040 | <0.0040 |
| Naphthalene,2-bromo- | mg/kg | 0.1352 | 0.0862 | 0.0707 |
| Flurene | mg/kg | 0.0186 | <0.0040 | 0.0118 |
| Phenanthrene | mg/kg | <0.0040 | <0.0040 | <0.0040 |
| Acenaphthene | mg/kg | <0.0040 | <0.0040 | <0.0040 |
| Pyrene | mg/kg | <0.0040 | 2,4843 | <0.0040 |
| Benz[a]anthracene | mg/kg | <0.0040 | 16.9430 | <0.0040 |
| Chrysene | mg/kg | <0.0040 | 6,9695 | <0.0040 |
| Total | mg/kg | **0.2191** | **26.4830** | **0.2356** |

The analysis revealed high levels of petroleum hydrocarbon contamination in all sediment samples. TPH concentrations ranged from 1750 mg/kg (St15) to 2510 mg/kg (St16). Total extractable hydrocarbons were even higher, reaching 5250 mg/kg at St17. The dominant hydrocarbon fractions were heavy components ($C_{21}$–$C_{35}$), which are typically associated with weathered crude oil and long-term petroleum contamination. The high abundance of these fractions indicates chronic pollution rather than recent input.

PAH concentrations showed strong spatial variability across the studied stations. The highest total PAH concentration was recorded at St16 (26.48 mg/kg), while St15 and St17 exhibited significantly lower levels (0.22–0.23 mg/kg). At St16, the dominant compounds were benz[a]anthracene (16.94 mg/kg) and chrysene (6.97 mg/kg), which are high-molecular-weight PAHs associated with combustion processes and petroleum residues. Lower molecular weight PAHs were mostly below detection limits, indicating aged and weathered contamination. The results clearly indicate that bottom sediments in the studied lake are significantly impacted by petroleum-derived pollutants. The dominance of heavy hydrocarbon fractions and high-molecular-weight PAHs suggests long-term accumulation under anaerobic sediment conditions. Station St16 represents

a clear pollution hotspot, likely influenced by historical industrial discharge, wastewater input, or oil-related activities typical for the Absheron Peninsula region.

The study demonstrates severe petroleum hydrocarbon contamination in bottom sediments of a lake system in the Absheron Peninsula. High concentrations of TPH and PAHs indicate long-term anthropogenic pressure on the aquatic environment. The predominance of heavy hydrocarbon fractions ($C_{21}$–$C_{35}$) and toxic PAHs such as benz[a]anthracene and chrysene confirms chronic pollution and sediment accumulation processes. Spatial variability suggests the presence of localized contamination hotspots, particularly at station St16. The results highlight the necessity for continuous environmental monitoring and implementation of pollution control measures to reduce ecological risks and protect aquatic ecosystems in the region.

## References


1. Hajiyeva S.R., Aliyeva T.I., Yusifova M.M., The ecological state of Boyuk Shor lake of Azerbaijan. // Environmental Monitoring and Assessment, V.192, N 780, 2020, pp.1-11.
2. Mustafayev I.I., Mammadov V.Y., Salmanov M.A., Huseynov S.Y., Absheron Lakes. Baku: "Rüzgar" Ecological Society, 2001, 52 p.
3. Hajiyeva S.R., Aliyeva T.I., Huseynova P.V., Anthropogenic pollution sources of Lake Boyukshor. // VI Republican Scientific Conference "Actual Problems of Ecology and Soil Science in the XXI Century", 2017, pp. 28–30.
4. Gadzhiyeva S.R., Aliyeva T.I., Gadzhiyeva Kh.F., Huseynova P.V., Alizadeh B.F., Ecological condition and pollution of Lake Boyukshor. // Journal of Postgraduate and Doctoral Students, 2017, pp. 59–61.
5. Hajiyeva S.R., Aliyeva T.I., Bayramov Q.I., Huseynova P.I., Ecological assessment of Lake Boyukshor. // International Scientific Conference "Coordination Compounds Chemistry: Actual Problems of Analytical Chemistry" dedicated to the 85th anniversary of Academician Rafiqa Alirza gizi Aliyeva, 2017, p. 184.

2nd International Scientific Conference "Modern Problems in Geophysics", Proceedings,
ISBN 978-9941-36-562-1, ISSN 3088-4349, Tbilisi, Georgia, October 29-31, 2026

# COMPOUNDS OF MANGANESE, COPPER, AND MOLYBDENUM IN THE BOTTOM SEDIMENTS OF THE TEREK RIVER

**Atabieva F., Selina V.**

*Federal State Budgetary Institution "High-Mountain Geophysical Institute",*
*Nalchik, Kabardino-Balkaria, Russian Federation*
*atabieva0812@mail.ru*

***Abstract****. Recently, heavy metals have become a serious problem in terms of water and sediment pollution and are now considered a serious global issue. The most dangerous form of heavy metals in water and sediments from an ecological perspective is their dissolved form, as it is considered more bioavailable. This article presents the results obtained from analyzing the level of heavy metal compounds (Mo, Mn, Cu) in the bottom sediments of the Terek River in the foothill zone, where anthropogenic impact is insignificant, and in the estuarine part, based on the results of studies conducted in 2025. The measurements were carried out using an atomic absorption spectrometer with electrothermal atomization "MGA-915M"; fractions smaller than 1 mm were analyzed. The maximum concentrations of manganese and copper compounds, amounting to 696.2 and 30.9 (mg/kg), respectively, were found in the bottom sediments of the second layer of the Terek River in the foothill zone; molybdenum concentrations were 0.83 mg/kg in the upper layer, also in the foothill zone. The period of rising floodwaters (May) was characterized by a decrease in the concentrations of the studied metals throughout the entire thickness of the bottom sediments (both in the upper and lower layers). The powerful flow of meltwater from glaciers intensifies the erosion of surface sediments, the transport of silt fractions, and the significant dilution of the water in the Terek River. The periods of low water (March) and the decline of the flood (September) lead to a decrease in the flow velocity, which, in turn, intensifies the sedimentation of the studied metal compounds and results in an increase in their concentrations in the bottom sediments.*

***Key words:*** *Bottom sediments, manganese, copper, molybdenum.*

## Introduction

One of the areas of environmental monitoring of water bodies is the study of bottom sediments (BS). The water and bottom sediments of some areas may be characterized by elevated concentrations of various metals. From an ecological perspective, the most dangerous form of heavy metals in BS is the so-called "bioavailable" form [1, 2]. The form in which a metal is present in water (ionic, in a complex with organic substances, or as part of particles) is strongly influenced by various factors (pH, water hardness, etc.). It is the dissolved forms of metal compounds that are usually considered more bioavailable and toxic [3, 4, 5].
In surface waters within the West Caspian Basin District, the river waters of almost the entire Terek Basin are characterized by natural concentrations of aluminum, iron, copper, and manganese exceeding the maximum permissible concentration (MPCs) for fisheries water bodies [6]. The maximum concentrations of dissolved forms of manganese compounds in the rivers of the Terek River basin in the middle and lower reaches for the period 2022-2024 reached 45.02 micrograms/dm$^3$ [7], copper-6.79 micrograms/dm$^3$ [8], in the water of some rivers there was an excess of the standard values of molybdenum compounds, and the level of dissolved forms of chromium, nickel, lead and cadmium were below the maximum permissible concentration (MPCs) for fisheries water bodies [9]. Therefore, it is of interest to study the bottom sediments of the Terek River in terms of the content of manganese, copper, and molybdenum compounds, as one of the ways to investigate the ecological state of water bodies-a reflection of their current condition and containing information about the pollution of the water body in the study area.

## Methods for analyzing water and bottom sediment samples

Water and bottom sediment sample collection points are located in the foothill and plain parts of the Terek River, within the territories of the republics of Kabardino-Balkaria and North Ossetia-Alania (Table 1).

**Table 1.** Water sample collection points on the Terek River, 2025.

| Water body, (length) | Distance from the source, km | northern latitude; eastern longitude | Sampling point |
|---|---|---|---|
| the Terek River (578 км) | 151 | 43.315448; 44.212947 | the village of Elkhotovo |
| | 230 | 43.681515; 44.368029 | the village of Alexandrovskaya |

Section I for the river was located in the foothill zone, and section II was in the plain part. Samples of bottom sediments were collected during the winter low‑water period, during the rise of the flood, and during the recession of the flood from two layers: the 1st layer at a depth of 0-5 cm, the 2nd layer at a depth of 20-30 cm. Under laboratory conditions, the concentrations of manganese, copper, and molybdenum compounds dissolved in the water were measured in all the collected samples. The measurements were carried out using an atomic absorption spectrometer with electrothermal atomization, "MGA-915M". In the bottom sediments, fractions smaller than 1 mm were analyzed in accordance with the methodology.

## Results and discussion

The following patterns were observed for the spatio‑temporal changes in the concentration of manganese compounds in the bottom sediments of the Terek River: during the low‑water period (March), high concentrations of manganese (Fig. 1) were characteristic throughout the entire thickness of the bottom sediments. In the first layer (a), the content of manganese compounds in the foothill part was about 568 mg/kg, and in the plain part-580 mg/kg. In the second layer (b), a similar situation was observed, with an increase in values: 696 mg/kg for the foothill part of the river, and 673 mg/kg for the plain part. During the rise of the flood period (May), there was a sharp decrease in the content of manganese compounds in all horizons. In the first layer (a), the concentration dropped to 370 mg/kg in the foothill part and to the annual minimum of 198 mg/kg on the plain. In the second layer (b), the decline was repeated: 322 mg/kg in the foothill part and the minimum values of 179 mg/kg for the plain part. This decline is likely due to the dilution of water, which erodes the bottom sediments, but during the flood recession (September), the concentration of manganese compounds increases almost twofold in the foothill part and threefold in the plain part. In the first layer (a), the concentration in the foothill area dropped to a minimum (221 mg/kg), while on the plain there was a slight increase in manganese concentration to 227 mg/kg. At the same time, in the second layer (b), a strong autumn accumulation was recorded: in the foothill area, the concentration increased to 542 mg/kg, and in the plain zone, peak values of 672 mg/kg were reached, which are close to the maximum values typical of the low‑water period (Fig. 1).

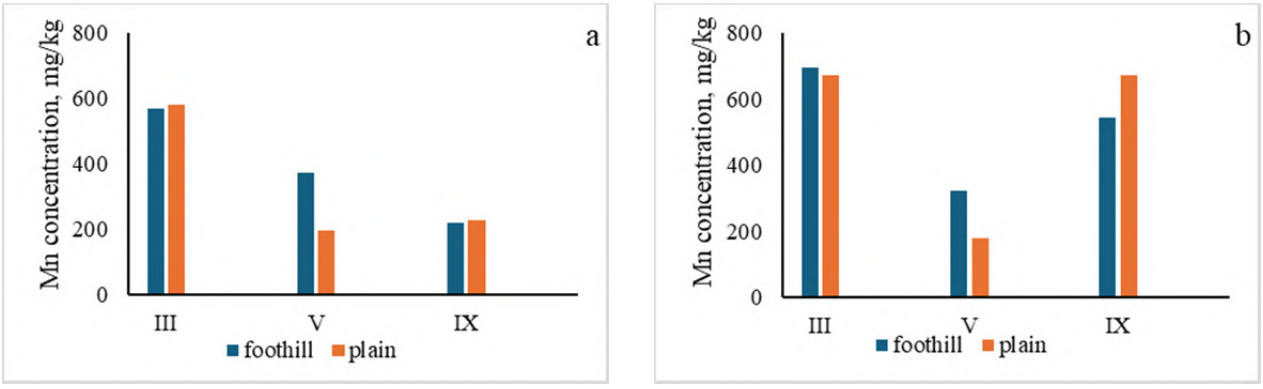



**Fig. 1.** Concentration of manganese in the first (a) and second (b) layers of bottom sediments in the foothill and plain zones of the Terek River during different phases of the water regime: III – March; V – May; IX – September.

Changes in the level of molybdenum compound content in the bottom sediments of the Terek River (Fig. 2) also depend on the river's hydrological regime (Fig. 2). During the low‑water period (March), consistently high concentrations of molybdenum compounds were observed, especially in the foothill zone. In the first layer (a) in the foothill part of the river, the concentrations reached their annual maximum-about 0.83 mg/kg, exceeding the values for the plain zone (0.24 mg/kg) by more than three times. In the second layer (b), a sim-

ilar trend was maintained: 0.78 mg/kg for the foothill part, while for the plain part it was 0.37 mg/kg. The high values are associated with the low water level and minimal flow velocity during low water, which contributed to intensive sedimentation of suspended particles that had sorbed molybdenum compounds. With the onset of active glacier melting (May) and an increase in the river water level, a pronounced decline in concentration was observed throughout the entire thickness of the bottom sediments (Fig. 2).

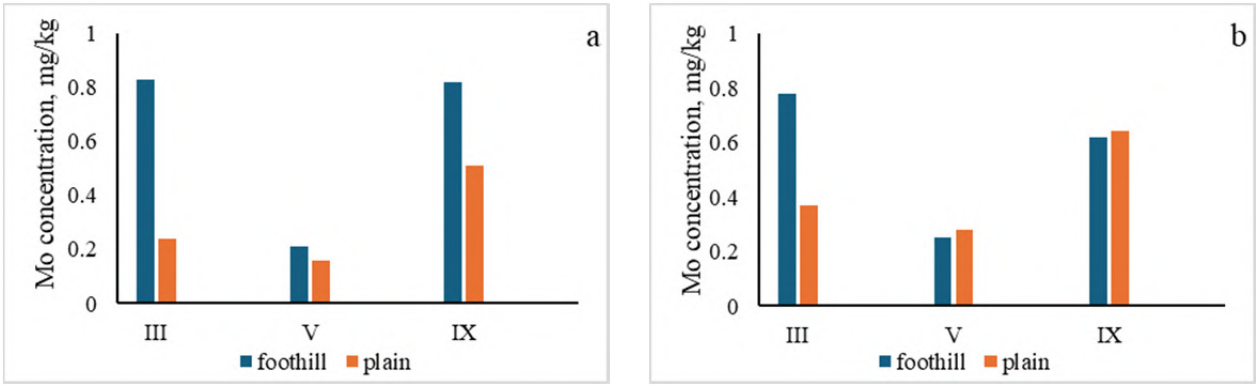



**Fig. 2.** Concentration of molybdenum in the first (a) and second (b) layers of bottom sediments in the foothill and plain zones of the Terek River during different phases of the water regime: III – March; V – May; IX – September.

Spatiotemporal changes in the concentration of copper compounds (Fig. 3) in the bottom sediments of the Terek River also revealed a relationship between their distribution and the hydrological seasons of the year. During the low-water period (March), the concentration of copper compounds in the surface layer (a) was about 5.5 mg/kg in the foothill part and 5.8 mg/kg in the plain part. In the second layer (b): in the foothill area, the concentration was approximately 5.7 mg/kg, while in the plain area, a slight decrease was observed-to 4.3 mg/kg. During the flood rise period (May), the minimum copper concentrations were recorded. During the flood decline period (September), the distribution pattern changed dramatically, and the values reached their maximum throughout the entire thickness of the bottom sediments. In the first layer (a) of the foothill part, there was a sharp increase in copper content-up to 22.5 mg/kg, while in the plain part it reached 12.5 mg/kg. In the second layer (b), this peak is even more pronounced: in the foothill part, the concentration reached 31.0 mg/kg, and on the plain it increased to 1.8 mg/kg. This powerful autumn peak is due to the recession of the flood: the drop in flow velocity triggers the mass deposition of suspended particles that have absorbed copper compounds, which were actively leached from rock formations or possibly came from anthropogenic sources.

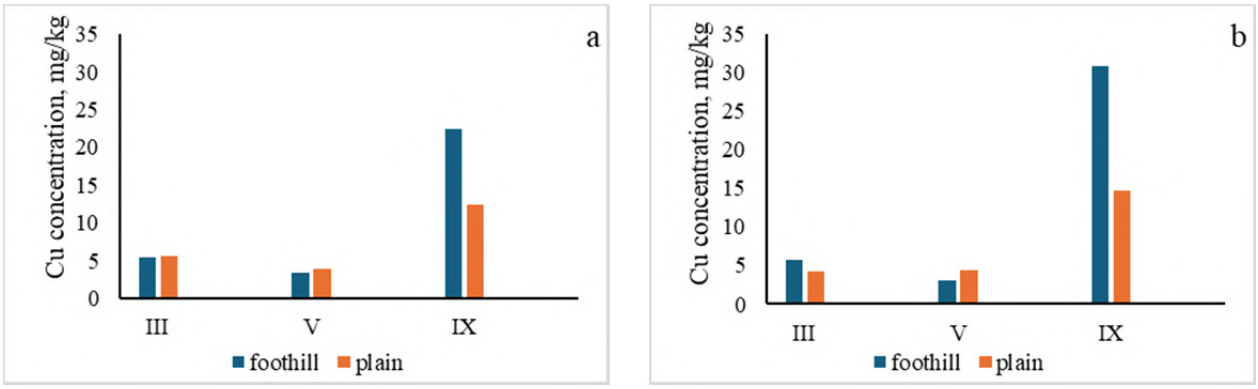



**Fig. 3.** Concentration of copper in the first (a) and second (b) layers of bottom sediments in the foothill and plain zones of the Terek River during different phases of the water regime: III – March; V – May; IX – September.

## Conclusions

One of the main factors influencing the concentrations of the studied metal compounds is the phase of the river's water regime. The period of rising floodwaters (May) was characterized by a decrease in the concentrations of molybdenum, manganese, and copper throughout the entire thickness of the bottom sediments

(both in the upper and lower layers). The powerful flow of glacial meltwater activates the erosion of surface sediments, the transport of silt fractions, and the strong dilution of river water. The periods of low water (March) and the decline of the flood (September) lead to a decrease in the flow velocity, which in turn activates the sedimentation of the compounds of the studied metals and results in an increase in their concentrations in bottom sediments.

## References


1. Moiseenko T. I., Gashkina N. A, Dinu M. I., Distribution of metal forms and assessment of their bioavailability in the land waters of the Arctic region (proposals for water quality standards). // Geochemistry, T. 66, No. 7, 2021, pp. 630-645.
2. Baba N. H., Garbunga G.Y., Bioavailability of metals in the biosphere, Department of Chemical Sciences, Federal University Wukari, P.M.B. 1020 Katsina-Ala Road Wukari, Taraba State, Nigeria Published: 30.03.2024.
3. Magalhaes D., Marques M, Baptista D., Forsin D, Buss D., Metal bioavailability and toxicity in freshwaters. Environ. // Chem. Lett., 13, 2015, pp. 69-87.
4. Merrington G., Peters A., Schlekat C.E., Accounting for metal bioavailability in assessing water quality: a step change? // Environ. Toxicol. Chem., 35(2), 2016, pp. 257-265.
5. Drozdova O. Yu., Demin V. V., Makarova M. A., Karpukhin M. M., Lapitsky S. A., Changes in the forms of copper occurrence in surface waters with increasing anthropogenic load © 2022. // Reports of the Russian Academy of Sciences. Earth Sciences, Vol. 504, No. 2, 2022, pp. 200-204.
6. Yanin E.P., Kuzmich V.N., Ivanitsky O.M., Regional natural heterogeneity of the chemical composition of surface waters on land and the need to take it into account when assessing their ecological state and the intensity of anthropogenic pollution. // Problems of the Environment and Natural Resources, No. 6, 2016, pp. 3-72.
7. Atabieva F.A., Alita S.L., On the need to introduce regional maximum permissible concentrations of manganese in water bodies of the Terek River basin. // Bulletin of the Udmurt University. Series: Biology, Earth Sciences. Vol. 35, Issue 3, 2025.
8. Atabieva F. A., Otarova A. S., Selina V. V,. On copper compounds in the Terek River basin and the need to introduce regional maximum permissible concentrations. // Water Management in Russia: Problems, Technologies, Management. 2026. No. 2. Pp. 122–132. https://doi.org/10.35567/1999-4508-2026-2-, EDN: XVTSCU.
9. Alita S.L., Atabieva F.A., Regional maximum permissible concentrations of molybdenum for water bodies in the Terek River basin. // Water Management in Russia: Problems, Technologies, Management., No. 3, 2025, pp. 64-73. https://doi.org/10.35567/19994508 2025-3.

2nd International Scientific Conference "Modern Problems in Geophysics", Proceedings,
ISBN 978-9941-36-562-1, ISSN 3088-4349, Tbilisi, Georgia, October 29-31, 2026

# SENSITIVITY OF AN ISOTOPE-ENABLED WATER BALANCE MODEL TO GLOBAL INPUT DATA IN THE DATA-SCARCE ALAZANI RIVER BASIN, EASTERN GEORGIA

***Chikviladze E., **Ortega L., ***Watson A., **Miller J., ****Birkel C., *Melikadze G., *****,******Bong H., *******Kralisch S.**

**M. Nodia Institute of Geophysics, Ivane Javakhishvili Tbilisi State University, Tbilisi, Georgia*
***Isotope Hydrology Section, International Atomic Energy Agency, Vienna, Austria*
****School for Climate Studies, Stellenbosch University, Stellenbosch, South Africa*
*****Leibniz Institute of Freshwater Ecology and Inland Fisheries (IGB), Berlin, Germany*
******Institute of Industrial Science, The University of Tokyo, Tokyo, Japan*
*******NASA Goddard Institute for Space Studies (GISS), New York, United States of America*
********Flood Prediction Centre, State Office for Environment, Mining and Nature Conservation, Jena, Germany*
*elene.chikviladze@tsu.ge*

***Abstract****. A dual-isotope ($\delta^{18}O$, $\delta^{2}H$) J2000-iso model was applied to the data-scarce Alazani River basin, eastern Georgia, for 2012–2019, comparing ERA5 and IsoGSM forcing as provided with forcing corrected against regional stations. Uncorrected forcing gave about three times the observed streamflow (best KGE −0.50); corrected forcing gave about two thirds (KGE 0.29) but missed the May snowmelt peak, as the corrected forcing lacked the increase of precipitation with elevation.*

***Key Words****: Isotope hydrology, J2000-iso, ERA5, IsoGSM.*

## Introduction

Streamflow records are the basis for building and calibrating hydrological models, yet gauge networks in many regions are sparse, and Georgia is no exception. Where discharge records are short or incomplete, additional constraints on the catchment water balance are needed. Stable water isotopes ($\delta^{18}O$, $\delta^{2}H$) are natural tracers of water sources, mixing and evaporation, and carry information that is not contained in streamflow alone. Isotope-enabled versions of the J2000 rainfall-runoff model, implemented in the Jena Adaptable Modelling System (JAMS) [1], use these tracers to constrain flow partitioning and storage. Isotope-based calibration alone can, however, give solutions of inconsistent quality [2], and model performance depends strongly on the input data sources used [3].

In data-scarce basins, both meteorological and isotope forcing often have to come from global products, such as the ERA5 reanalysis [4] and the Isotope-enabled Global Spectral Model (IsoGSM) [5]. These products are continuous in time, but their coarse grids smooth the strong elevation gradients of mountain catchments, and they are commonly bias-corrected against the few available stations before use.

This study applies a dual-isotope J2000-iso model to the upper Alazani River basin in eastern Georgia and compares two forcing setups: global products used as provided, and the same products corrected against regional station observations. To our knowledge, this is the first isotope-enabled J2000 water balance model for Georgia. The aim is to show how strongly simulated streamflow depends on the choice and correction of input data.

## Study area

The Alazani River originates at 2,600–2,800 m a.s.l. on the southern slopes of the Greater Caucasus and flows south-east through the Alazani Valley into the Mingachevir Reservoir in Azerbaijan [6]. This study covers the upper-to-middle part of the basin in Georgia (about 4,000 $km^2$), with the Shakriani gauging station

(41.99°N, 45.58°E) as the calibration point (Fig. 1). The climate is semi-arid to dry continental; annual precipitation in the lowlands is 300–500 mm, with a maximum in May [6]. The river is fed by groundwater (~40%), rainfall (~31%) and snowmelt (~29%), and spring floods in May–June carry 35–40% of annual runoff [6]. The valley hosts extensive, interconnected aquifers that sustain river flow throughout the year [7].

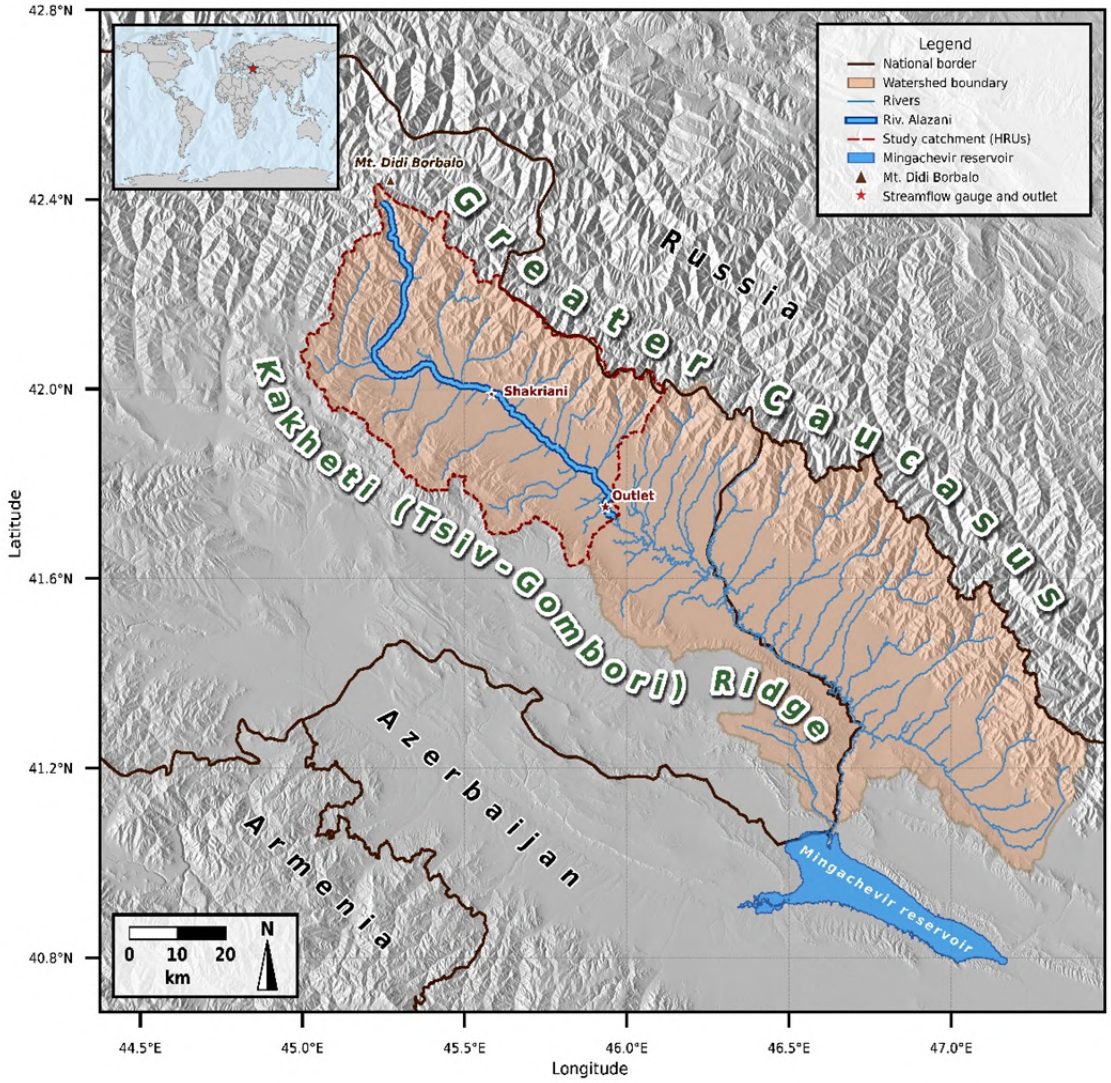



**Fig. 1.** Alazani River basin and the study catchment above the model outlet, with the Shakriani streamflow gauge.

## Data and methods

J2000-iso is a process-based, distributed model in which hydrological response units route water through snow, soil and two groundwater storages (RG1, RG2) and track $\delta^{18}O$ and $\delta^{2}H$ through each storage [1,2]. The model was run at daily time step for 2012–2019.

Precipitation isotopes come from GNIP stations and river-water isotopes at Shakriani from GNIR [8]; meteorological observations come from GNIP and NOAA stations [9] (Fig. 2). Because these records are short and do not overlap fully in time, gridded products were used as continuous forcing at 15 grid points: ERA5 for precipitation and temperature, and IsoGSM for precipitation isotopes. Two setups were compared (Table 1). Setup A used the products as provided. In setup B, precipitation was taken from IsoGSM and scaled with one monthly climatological factor, the ratio of the regional mean observed (GNIP, NOAA) to the regional mean IsoGSM precipitation; ERA5 temperature was shifted by a monthly offset equal to the difference between the regional observed and regional ERA5 means; and IsoGSM $\delta^{18}O$ and $\delta^{2}H$ were shifted by a monthly offset equal to the difference between the regional GNIP and regional IsoGSM means, computed for each month with GNIP data and interpolated over the remaining months. In all cases, the same factor or offset was applied to all 15 grid points.

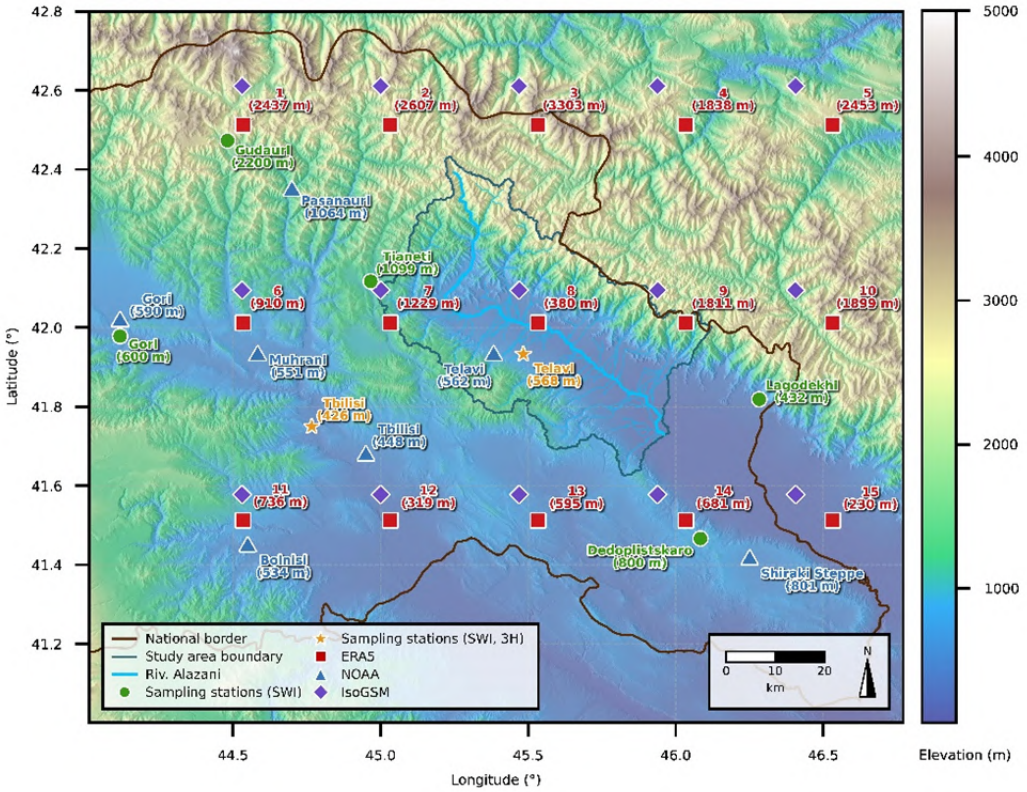



**Fig. 2.** Input data: isotope sampling stations (circles; stars also tritium), NOAA meteorological stations (triangles), ERA5 (squares) and IsoGSM (diamonds) grid points, with elevations.

**Table 1.** Input data in the two model setups.

| Variable | Setup A (as provided) | Setup B (corrected) | Correction in setup B |
|---|---|---|---|
| Precipitation | ERA5 | IsoGSM, scaled | × one monthly factor: regional observed / regional IsoGSM mean |
| Temperature | ERA5 | ERA5, shifted | + one monthly offset: regional observed − regional ERA5 mean |
| $\delta^{18}O$, $\delta^{2}H$ | IsoGSM | IsoGSM, shifted | + monthly offset: regional GNIP − regional IsoGSM mean |
| Reference data | GNIP and NOAA stations; streamflow and river isotopes (GNIR) at Shakriani | same | – |

For each setup, 5,010 parameter sets were sampled by Monte Carlo simulation. Streamflow at Shakriani was evaluated with the Kling–Gupta efficiency (KGE), and river-water isotopes with efficiencies for $\delta^{18}O$ and $\delta^{2}H$. To retain only hydrologically realistic runs, three criteria were applied jointly: both isotope efficiencies exceeded −0.41, the mean-flow benchmark of KGE [10]; groundwater (RG1+RG2) contributed 50–70% of total runoff, reflecting the groundwater-dominated regime of the middle basin, where groundwater contributions exceed 60% [6]; and KGE was among the best 20% of all runs. This left 423 runs in setup A and 15 in setup B. Simulated daily flows were aggregated to monthly means and compared with observed monthly means (June 2017 excluded).

## Results

Precipitation forcing differed strongly between the setups. Averaged over the 15 grid points, annual precipitation in 2012–2019 was 1,062 mm in setup A and 375 mm in setup B. The correction reduced points above 1,500 m from 1,387 to 357 mm and lower points from 777 to 391 mm, so that corrected precipitation

no longer increases with elevation. Three pairs of grid points carry identical corrected series, reflecting the coarser IsoGSM grid.

Observed streamflow at Shakriani peaks in May (~57 m³/s), with winter baseflow of about 11 m³/s (Fig. 3). With setup A, the model overestimates flow throughout the year: the median flow of the selected runs was 3.1 times the observed, and winter flows of 30–40 m³/s exceed observations about threefold, although the spring rise is reproduced. With setup B, the model underestimates flow (0.64 times the observed median); the spring peak reaches only ~17 m³/s, about 30% of the observed, and occurs in June instead of May, while late-summer and autumn baseflow is closer to observations. The best KGE of the selected runs was −0.50 in setup A, below the mean-flow benchmark of −0.41 [10], and 0.29 in setup B. The corrected inputs thus improve the overall fit despite the underestimated volumes, although only 15 runs met all criteria.

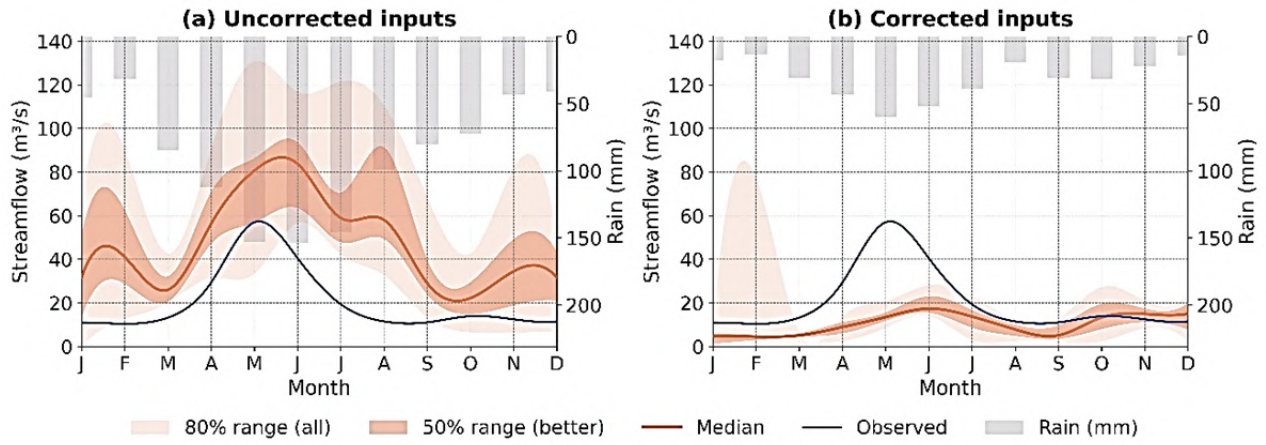



**Fig. 3.** Seasonal streamflow at Shakriani, 2012–2019: observed (blue, median of monthly means across years) and simulated with (a) uncorrected and (b) corrected inputs. Light band: 10–90% of the selected runs; dark band and line: 25–75% and median of the best quarter of the selected runs (by KGE). Grey bars: mean monthly input rainfall over the 15 grid points.

The two setups bracket the observations: the uncorrected global forcing is too wet and the corrected forcing too dry. Two features of the corrected forcing probably explain the missed snowmelt peak. First, the observation stations lie mostly between 430 and 1,100 m, while the grid points average about 1,430 m; scaling to the regional station mean pulls precipitation towards lowland values, and the coarse IsoGSM grid does not reproduce the orographic increase. Second, the additive temperature offset transfers the elevation difference between stations and grid points to all points, warming the high-elevation cells and reducing snow accumulation. The isotope criterion was passed by 98% of runs in setup A and 85% in setup B, so that run selection was controlled mainly by the groundwater and KGE criteria. The small number of runs retained in setup B (15) also limits the robustness of its uncertainty bands. Because all inputs were changed together, the contribution of each cannot be separated here.

## Conclusion

A dual-isotope J2000-iso model was set up for the upper Alazani basin with ERA5 and IsoGSM forcing supplemented by sparse station data. Uncorrected ERA5 precipitation (about 1,060 mm/yr at the grid points) led to about three times the observed streamflow. Replacing ERA5 precipitation with IsoGSM and correcting the inputs with regional factors and offsets derived from low-elevation stations reduced streamflow to about two thirds of the observed and removed the May snowmelt peak, but improved the best KGE from −0.50 to 0.29. In mountain catchments, input corrections derived from low-elevation stations should be applied with caution, as they may not represent conditions at higher elevations. Follow-up work will test each input correction separately and extend the evaluation to all water balance components.

**Acknowledgements:** This study was carried out within an internship at the Isotope Hydrology Section of the International Atomic Energy Agency (IAEA), Vienna. The M. Nodia Institute of Geophysics, Ivane Javakhishvili Tbilisi State University, provided the hydrological and isotope data and carried out the field work.

## References


1. Krause P., Kralisch S., “The hydrological modelling system J2000 – knowledge core for JAMS”, Proc. MODSIM 2005 Int. Congress on Modelling and Simulation (ZERGER, A., ARGENT, R.M., Eds). // Modelling and Simulation Society of Australia and New Zealand, 2005, pp. 676–682.
2. Watson A., et al., Advancing isotope-enabled hydrological modelling for ungauged calibration of data-scarce humid tropical catchments. // Hydrol. Process, 38 (2), 2024, e15065.
3. Watson A., et al., Evaluating input data sources for isotope-enabled rainfall-runoff models. // Hydrol. Process, 38 (9), 2024, e15276.
4. Hersbach H., et al., The ERA5 global reanalysis, // Q. J. R. Meteorol. Soc. 146, 730, 2020, pp. 1999–2049.
5. Yoshimura K., Kanamitsu M., Noone D., OKI, T., Historical isotope simulation using reanalysis atmospheric data, J. Geophys. Res. Atmos. 113 (2008) D19108.
6. Shotadze M., Barnovi E., Rapid Assessment of the Rioni and Alazani–Iori River Basins of Georgia. // Technical Report, 2011.
7. Melikadze G., Gventsadze A., Kapanadze N., Vepkhvadze S., Todadze M., Support in the Delineation and Characterization of Groundwater Bodies and the Design of a Groundwater Monitoring Network in the Alazani–Iori Basin Districts in Georgia. // EUWI+ Report ENI/2016/372-403, EU Member State Consortium, Vienna, 2019.
8. INTERNATIONAL ATOMIC ENERGY AGENCY, WORLD METEOROLOGICAL ORGANIZATION, Global Network of Isotopes in Precipitation (GNIP) and Global Network of Isotopes in Rivers (GNIR), WISER database, https://nucleus.iaea.org/wiser (accessed 2025).
9. NATIONAL OCEANIC AND ATMOSPHERIC ADMINISTRATION, NCEI Climate Data Online, https://www.ncei.noaa.gov/maps/daily/ (accessed 2025).
10. Knoben W.J.M., Freer J.E., Woods R.A., Technical note: Inherent benchmark or not? Comparing Nash–Sutcliffe and Kling–Gupta efficiency scores. // Hydrol. Earth Syst. Sci. 23, 10, 2019, pp. 4323–4331.

2nd International Scientific Conference "Modern Problems in Geophysics", Proceedings,
ISBN 978-9941-36-562-1, ISSN 3088-4349, Tbilisi, Georgia, October 29-31, 2026

# CURRENT STATE OF THE SOIL COVER

**[*]Dakhova O., [**]Kerefova Z., [**]Khuchunaeva L.**

*[*]Kabardino-Balkarian State University named after H.M. Berbekov,*
*Nalchik, Kabardino-Balkaria, Russian Federation*
*[**]Federal State Budgetary Institution "High Mountain Geophysical Institute",*
*Nalchik, Kabardino-Balkaria, Russian Federation*
*dakhva@rambler.ru*

***Abstract.*** *Soil is a strategically important natural resource that underpins food security, ecological balance and sustainable development of territories. With a number of key ecosystem functions, from providing nutrients to water filtration and carbon sequestration, soil acts as a link between animate and non-living nature. At the same time, soil resources belong to the category of conditionally renewable: the processes of soil formation proceed extremely slowly. In the 21st century, the state of soil cover in many regions of the world is characterized by increasing negative trends. Among the most common degradation processes are erosion, compaction, salinization, desertification, loss of organic matter and pollution by pollutants. The scale of these problems is such that they are internationally recognized. In Russia, which has vast soil resources, there are also significant areas of land subject to some form of degradation, which directly affects agricultural productivity and ecosystem stability. This paper examines the state of the soil cover of the Kabardino-Balkarian Republic (KBR).*

***Key words:*** *Wind erosion, soil types, pollution, residential areas, heavy metals.*

## Introduction

Anthropogenic impact remains a key factor in the deterioration of soil condition. Intensive farming, irrational use of agrochemicals, deforestation, urbanization and industrial development of territories lead to a violation of the natural mechanisms of soil self-regulation. At the same time, the consequences of degradation go far beyond the agricultural sphere: they affect water and air quality, biodiversity, climate stability and even human health.

The relevance of assessing the current state of soils is due to the need to develop scientifically based measures for their conservation and restoration. This requires a comprehensive analysis of current fertility indicators, the identification of dominant degradation factors and an assessment of regional features of the dynamics of soil properties. Modern monitoring methods play an important role in this process, from traditional field surveys to remote sensing technologies and digital mapping, which provide objective and comparable data.

## Purpose of the Study

The purpose of this article is to summarize information on the current state of soils, to characterize the main trends in their change under the influence of natural and anthropogenic factors, as well as to identify the key areas of research and practical measures aimed at the rational use and protection of soil resources. This approach provides a holistic view of the current state of the soil cover and identifies priorities to ensure the long-term sustainability of the soil stock.

## Research Materials and Methods

In the work, the methods of observation, descriptive, comparative, statistical and cartographic methods of research were used. The information base of the study was fund, reference and literary materials.

The Kabardino-Balkarian Republic is located in the central, highest mountainous (up to 5000 m above sea level and above) part of the Greater Caucasus, on its northern slopes, in the basin of the left tributaries of the Terek River.

The republic occupies part of the Ciscaucasian plain. The southern border of Kabardino-Balkaria is the state border of Russia with Georgia. In the east and south-east, the republic borders on the Republic of North Ossetia-Alania. In the north, the republic borders on the Stavropol Territory, and in the west on the Karachay-Cherkess Republic. (Fig. 1).

The total area of the republic is 12.5 thousand km2, which is 0.7% of the area of the Russian Federation and 2.9% of the area of the North Caucasus region. Kabardino-Balkaria is a mountainous republic [1, 2, 4].

According to the features of its structure and the nature of the relief, the territory of Kabardino-Balkaria is divided into three parts: plain (33%), foothill (16%) and mountainous (51%).




**Fig. 1.** Map of Kabardino-Balkaria.

The Kabardino-Balkarian Republic is located in the southern part of the temperate climatic zone. In terms of the combination of heat and moisture, it is located in two climatic regions: in the Ciscaucasia and the High Mountain Caucasus.

Located in relatively low southern latitudes (between 42,051' and 44,001' north latitude), the territory of the republic receives significant amounts of solar radiation, which determines the abundance of sunlight and heat. The maximum amounts of radiation arrive in May-July at the highest altitudes of the sun and the length of the day.

On the territory of the KBR, according to the conditions of heat supply and humidity, the following types of climates can be distinguished: continental (steppe zone, north-eastern part); moderately continental (foothill part); high-mountain (mountainous part) [3, 5].

In Kabardino-Balkaria, 9 main types of soils have been formed: dark chestnut, meadow-chernozem and meadow soils of the steppes, pre-Caucasian chernozems, mountain-forest, mountain-meadow, alluvial, mountain chernozems, mountain-tundra soils.

In the north-eastern part (Prokhladnensky and Tersky districts) dark chestnut soils with a content of 3-4% humus is widespread. They contain a sufficient amount of nutrients that have a good structure. With irrigation and proper agricultural techniques on dark chestnut soils, high yields of cereals, technical, melons and grapes are obtained.

On the banks of the Malka River of the Prokhladnensky District with the villages of Karagach, Altud, Novo-Poltavka and others, in the Urvansky, Maysky districts and the settlements of Planskoye, Deyskoye, Arik of the Tersky District, meadow-chernozem and meadow soils of the steppes have been formed. In some places in these areas, there are salts that are harmful to plants, so the cultivation of corn and garden crops requires limited watering.

Black soils are distributed in Kabardino-Balkaria on the lands of Upper Kurp, Lower Kurp, Upper Akbash, Old Lesen, Second Lesen, Lower Cherek, Old Cherek, Nalchik, Chegem First, Chegem Second, Second Kyzburun, Kishpek, Baksanenok, Staraya Kreposti, Psynadakho, Zalukokoazhe.

High yields of wheat, corn and other crops are grown on chernozem soils. Since the republic's relief, climate and parent rocks are diverse, black soils are represented by the following prototypes:

– Ciscaucasian carbonate black soils, the humus horizon has a dark gray color, its thickness is from 80 to 100 cm;
– Caucasian chernozems are weakly leached, prevail to the south of carbonate chernozems, the amount of humus in these soils ranges from 5 to 8%;
– Ciscaucasian chernozems are leached, cover the strip of foothills, they contain up to 10% of humus, the thickness reaches 100-150 cm.

In the treeless areas of the Pasture and Rocky Ranges, mountain black soils are formed. The humus horizon of these soils is up to 50 cm. It contains a lot of humus – 12-14%, while the soil has a dark color.

In the mountains covered with broad-leaved forests, the soils are brown mountain-forest, sometimes they have a brownish-gray color, lumpy structure, and a small thickness of the fertile layer. These are relatively young soils.

They are suitable not only for growing high-quality wood, but also for the development of vegetable growing and horticulture.

Above 2000 m, in the zone of subalpine and alpine vegetation, the soils are mountain-meadow. They have a different thickness of the dark layer – from 20 to 60 cm, contain 12-13% humus. Pastures and hayfields of the republic are located on these soils. Their largest massifs are located in the northwest, where the Zolsky and Nagornye pastures are located.

Mountain-tundra soils of the KBR are found on the Main and Lateral ridges, near glaciers and snowfields. The soil cover up to 5 cm thick is represented mainly by poorly decomposed peat.

In river valleys, a special type of soil is distinguished – alluvial or floodplain. These are rich and fertile soils.

## Research Results and Discussion

The area of agricultural land in the Kabardino-Balkarian Republic, according to the information provided by the Federal State Budgetary Institution "Station of Agrochemical Service "Kabardino-Balkaria"", is 627.1 thousand hectares, including arable land of 289.3 thousand hectares. Out of 290 thousand hectares of arable land, 220.0 thousand hectares of soils of the Prokhladnensky, Tersky, Chegemsky, Chereksky and Elbrus districts have a low content of humus (about 3.6%), and medium and high – on 70.0 thousand hectares. determining its properties and crop yields.

The humus content in the soils of the arable land of the republic has decreased by almost 0.6% over 45 years of observations. Every year, the content of nutrients (potassium, phosphorus) in soils decreases.

In the composition of agricultural land, the area of acidic soils is 107.2 thousand hectares, or 22%, including arable land of 9.4 thousand hectares, or 6.2%, perennial plantations of 2.7 thousand hectares (18.9%), hayfields of 13.9 thousand hectares (36.8%) and pastures of 81.2 thousand hectares (41%).

Arable lands of the Zolsky, Prokhladnensky, Tersky and Cherek districts are more subject to water and wind erosion.

Soil salinity is registered on an area of 14200 hectares, waterlogged and swampy soils are 33100 hectares, stony soils – 11100 hectares.

About 80% of mountain pastures are erosion-hazardous. Poisonous and weedy plants are found on one-third of the area of these lands. Constant, and sometimes unsystematic exploitation of mountain pastures has led to a great sparseness. Impoverishment of the geobotanical composition of the herbage, almost complete displacement of leguminous high-protein grasses by weeds is manifested.

Geobotanical surveys have shown that in the Aursentkh and Khaimashi tracts, the areas of eroded and knocked down pastures are 40 and 25%, respectively, and 45-50% of path-like pastures. At present, there is practically no tract in the republic, the agrobotanical condition of which could be considered satisfactory.

Thus, unregulated grazing in wet weather destroys the turf more intensively, contributing to the formation and increase of erosion centers and subsequent erosion.

## Soil contamination

In the process of control and supervisory activities of the Rospotrebnadzor Territorial Administration, laboratory control of the level of soil contamination is carried out. During the year, samples were taken on the territory of residential areas:

– for microbiological indicators – 236;
– for sanitary and chemical indicators – 291;
– parasitological indicators – 959;

Including on the territory of children's institutions:

– for microbiological indicators – 145;
– for sanitary and chemical indicators – 156;
– parasitological indicators – 794.

In the sanitary protection zones of water supply sources, the following were selected:

– samples for microbiological indicators – 60;
– samples for sanitary and chemical indicators – 47;
– tests for parasitological indicators – 58.

The share of soil samples that do not meet hygienic standards according to microbiological indicators in 2024 is 10% according to the CBR. Compared to the previous 2023, a single soil pollution was detected in the Chegem district and insignificant in the city of Nalchik. In terms of sanitary and chemical indicators, 2 samples out of 388 or 0.5% do not meet hygienic standards.

## Conclusion

Monitoring of the content of heavy metals in the soil of municipalities of the republic, carried out for a number of years, did not reveal their presence in any of the samples in 2023, and in 2024, only 0.6% of the analyzed soil samples of the city of Nalchik showed the presence of metals above the established hygienic standards.

Outside the residential zone, the source of pollution of soils and vegetative mass of agricultural crops with metals (lead, zinc, cadmium, copper) is road transport. Their high content was found within a radius of 7 km around the city of Nalchik and extends in arable soils at a distance of 50 meters along the highways in the direction of Vladikavkaz and Pyatigorsk.

The soils of the Prokhladnensky District are the most polluted, which may be due to the intensively developing poultry farming, animal husbandry and agriculture.

Thus, there is a tendency to increase microbiological contamination of soils in the Prokhladnensky municipal district and the KBR as a whole, against the background of a decrease in the city of Nalchik. The soil in the municipalities of the KBR does not have an epidemic significance for the development of infectious diseases among the population

## References


1. Dakhova O. O. Study of Pollution of Anthropogenic Landscapes by Motor Transport and Industrial Enterprises. // III International Scientific and Practical Conference "Young Scientists in Solving Actual Problems of Science" (May 18-20, 2012), Vladikavkaz, Part 2, 2012, pp. 64-68.
2. Dakhova O. O., Assessment of the state of urban anthropogenic landscapes. // Izvestiya KBNTS RAN No6 (50). – Nalchik, 2012, pp. 77-81.
3. Dakhova O. O., Khuchunaev B. M., Mustafaeva Z. A., Kupovykh G. V., Daov I. S.. Ecological problems of the Kabardino-Balkarian Republic. // Izvestiya vysshikh uchebnykh zavedenij Severo-Kavkazskii region, series: Natural Sciences, No4, 2018, pp. 72-76.
4. Dakhova O.O., Pashtova L.R., Tatarenko N.V., Sabanova R.K., Some types of urban landscape pollution. // Collection of scientific works of the national university scientific and practical conference, timed to the 85th anniversary of the foundation of Kabardino-Balkarian State University Nalchik, 2018, pp. 53 – 58.
5. Dakhova O. O., Khuchunayev B.M., Daov I. S., Bekkiyeva S.A., Khatefova L.V., Khuchunayeva S.B., Gekkiyeva S.O., Miskarova R.G., Integral Estimate of Ecological Status of Nalchik. // The European Proceedings of Social & Behavioural Sciences EpSBS, 01 – 03 November, T 177, 2018, pp. 58-62.

2nd International Scientific Conference "Modern Problems in Geophysics", Proceedings,
ISBN 978-9941-36-562-1, ISSN 3088-4349, Tbilisi, Georgia, October 29-31, 2026

# NUMERICAL MODELING OF WIND WAVES BASED ON THE SPECTRAL MODEL SWAN IN THE GEORGIAN COASTAL ZONE OF THE BLACK SEA

**[*,**] Demetrashvili D., [*] Kukhalashvili V., [*,***] Kvaratskhelia D.**

[*] *M. Nodia Institute of Geophysics, I. Javakhishvili Tbilisi State University, Tbilisi, Georgia*
[**] *Institute of Hydrometeorology, Georgian Technical University, Tbilisi, Georgia*
[***] *Business and Technology University, Tbilisi, Georgia*
*demetr_48@yahoo.com*

***Abstract.*** *The paper presents a wind wave modeling and forecasting system based on the third- generation numerical spectral model SWAN implemented in the easternmost part of the Black Sea, covering the Georgian sector and adjacent waters. The SWAN model, often used for coastal waters of various seas, is based on solving the wave energy balance spectral equation using the finite-difference method. Its implementation for the Georgian coastal zone is performed in a spherical coordinate system using MATLAB. Using a nested method, in the first stage, the model is run over a large area covering the Black and Azov Seas using a coarse grid, but in the final stage, high-resolution calculations are performed for the Batumi-Poti-Anaklia coastal zone. The calculations are illustrated by the example of forecasting significant wave heights and directions.*

***Key words:*** *Modeling system, spectral model, significant wave height, forecasting period.*

## Introduction

Wind waves are an interesting natural phenomenon, the study and prediction of which is one of the most important tasks of operational oceanography. This problem is particularly relevant for coastal/shelf zones, which often experience high anthropogenic pressure. The Georgian Black Sea coastal zone, and in particular the Batumi-Poti-Anaklia coastal waters, are characterized by intensive economic activity. The seaports of Batumi and Poti, as well as important recreational centers, are located here. Therefore, modeling and forecasting wind waves, studying wave regime, and assessing wave parameters in the Black Sea Georgian coastal zone are becoming increasingly relevant.

Currently, third-generation spectral models, such as SWAN, WAM, WW3, STWAVE, and others, have been developed for modeling and forecasting surface wind waves in oceans and individual seas, as well as for studying wave regimes [1-9]. Among spectral wave models, the SWAN (Simulating Waves Nearshore) model, which was developed in the 90s of the last century in the Netherlands (Delft University of Technology), provides a relatively complete description of the processes of wave formation and transformation in coastal/shelf zones. The spectral model SWAN is widely used to calculate wave parameters for various regions of the world's oceans – the Baltic Sea, the Mediterranean Sea, the Gulf of Mexico, the Portuguese continental nearshore, etc.

In some studies, SWAN was used for coastal water areas of the Azov-Black Sea basin [2, 4]. In [2], wave processes for the Blue Bay were modeled. Wind data, as an atmospheric forcing, were taken from well-known atmospheric dynamics models MM5 (Fifth-Generation Penn State/NCAR Mesoscale Model) and SKIRON (http://forecast.uoa.gr) with a spatial resolution of 10 km. A 4-step nested grid algorithm was used. In the initial stage, waves were modeled for the entire Azov-Black Sea basin at a resolution of 5 km, and in the final stage, wave fields were modeled for the Blue Bay waters at a resolution of 20 meters in latitude and 15 meters in longitude. The model was validated by comparison with measurement data obtained on an experimental oceanographic platform.

In [4], numerical simulation of wind waves near Tuzla Island in the Kerch Strait is considered. A rectangular grid with a resolution of 150 m was used to implement the model. Calculations were performed for 24 storm situations. The calculations revealed that the wave fields had significant spatial heterogeneity due to

the influence of bottom topography and refraction. In the case of southerly winds, the island had a blocking effect on wave propagation in a northerly direction.

Within the Shota Rustaveli National Science Foundation grant project, the Sea and Atmosphere Dynamics Modeling Sector at the Mikheil Nodia Institute of Geophysics of Ivane Javakhishvili Tbilisi State University in 2025 conducted a study on the implementation of the well-known SWAN spectral wind wave model in the Georgian Black Sea coastal zone.

The objective of this work is to present a wind wave modeling system based on the SWAN model in the Georgian coastal zone of the Black Sea and to illustrate some of the wave modeling results.

## Materials and methods

The SWAN wind wave spectral model is based on solving the wave energy balance spectral equation using the finite-difference method. In the Cartesian coordinate system, the equation is as follows:

$$\frac{\partial N}{\partial t} + \frac{\partial}{\partial x}(c_x N) + \frac{\partial}{\partial y}(c_y N) + \frac{\partial}{\partial \sigma}(c_\sigma N) + \frac{\partial}{\partial \theta}(c_\theta N) = S/\sigma \quad , N = E/\sigma$$

The following notations are used here: E is the wave energy spectrum, N is the action density spectrum, σ, θ are the frequency and angular coordinates, $C_x$, $C_y$, $C_\sigma$ , $C_\theta$ are the rates of transport of N along the spatial and frequency-angular coordinates. The right-hand side of the equation is a source function, that describes the generation of waves by the wind, the nonlinear spectral interaction between harmonics and the dissipation of wave energy [10, 11].

The input data for SWAN are the wind field at a height of 10 m above the sea surface and the seabed topography. The model calculates the significant wave height (SWH) and wave direction. SWH is the average height of the 1/3 of the largest waves in the wave spectrum over a given time period and in a given area. SWH approximately corresponds to the height of the waves perceived by a person visually.

SWAN was applied to the Black Sea, focusing on the coastal zone of Georgia in a spherical coordinate system using MATLAB. The model, using a nested method, is implemented at 3 computational levels, or stages. In the first stage, wave parameters are calculated for the entire Black Sea basin and the sea of Azov. In the second stage, the model is implemented in a regional domain, including the Georgian sector of the Black Sea and the adjacent waters. In addition, the wave parameters calculated at the first level are used at the regional liquid boundary as boundary conditions. In the final third stage, wave parameters are determined in the Batumi-Poti-Anaklia waters. Furthermore, the results obtained in the second stage are used as boundary conditions at the liquid boundary.

## Results and discussion

The spatial resolution for the entire Black Sea was $0.08^0$ x $0.08^0$ , and the number of grid points was 176 x 76. The spatial resolution for the Georgian sector of the Black Sea was $0.01^0$ x $0.02^0$, and the number of grid points was 245 x152. The Georgian sector of the Black Sea is separated from the open part by a conditional liquid boundary, which approximately coincides with the $39.06^0$E meridian. In the third stage, wave parameters for the Batumi-Poti-Anaklia water area are calculated with the highest spatial resolution $0.002^0$ x$0.001^0$ and number of nodes 408x476. The wind field was provided from the Copernicus reanalysis data ERA5
(https://cds.climate.copernicus.eu/datasets/reanalysis-era5-single-levels?tab=download) at an altitude of 10 m above sea level with a spatial resolution of $0.025^0$ x $0.25^0$ and temporal resolution of 3 h. The angular coordinate step is $10^0$. In the spectral space, 30 logarithmically spaced frequencies between 0.05 Hz and 1.0 Hz were considered. The time integration step was Δt = 10 min.

We were able to compare our **SWAN** modeling results with the results obtained with the **Wavewatch III v.3.14** spectral model for the entire Black Sea basin. The forecast period was 00:00 GMT, November 2-6, 2025. We compared the modeling results every 3 hours. The comparative analysis shows that the modeling results are generally in good agreement with each other both qualitatively and quantitatively.

This study presents the results of wave field modeling for the forecast period 12-15 Decmber, 2025. The starting time of the forecast was 00:00 GMT, December 12, 2025. The selection of this forecast interval is

due to the fact that, according to the information of the Adjara Regional Meteorological Observatory of the National Environmental Agency, during this interval, there were high waves in the Batumi nearshore according to visual observations.

Wind field analysis showed that the wind direction and speed underwent significant changes during the considered time interval. Wind speed increased sharply on December 13, reaching 14-15 m/s over most of Georgian waters. Strong winds were partially maintained on December 14 as well. Strong winds were observed approximately in the interval: 03:00 PM, December 13 – 06:00 AM, December 14. Significant wave heights exceeded 3 m/s between 06:00 PM, 13 December – 03:00 AM, 14 December (according to coarse-grid modeling over the entire sea basin). Fig.1 illustrates simulated wind wave direction amd significant wave height in three time ponts in the Georgian sector of the Black Sea and in Batumi-Poti-Anaklia water area, where waves are calculated with higher resolution. The Figure shows that the significant wave height gradually increases from the shore to the open sea. For example, by 9 pm, on

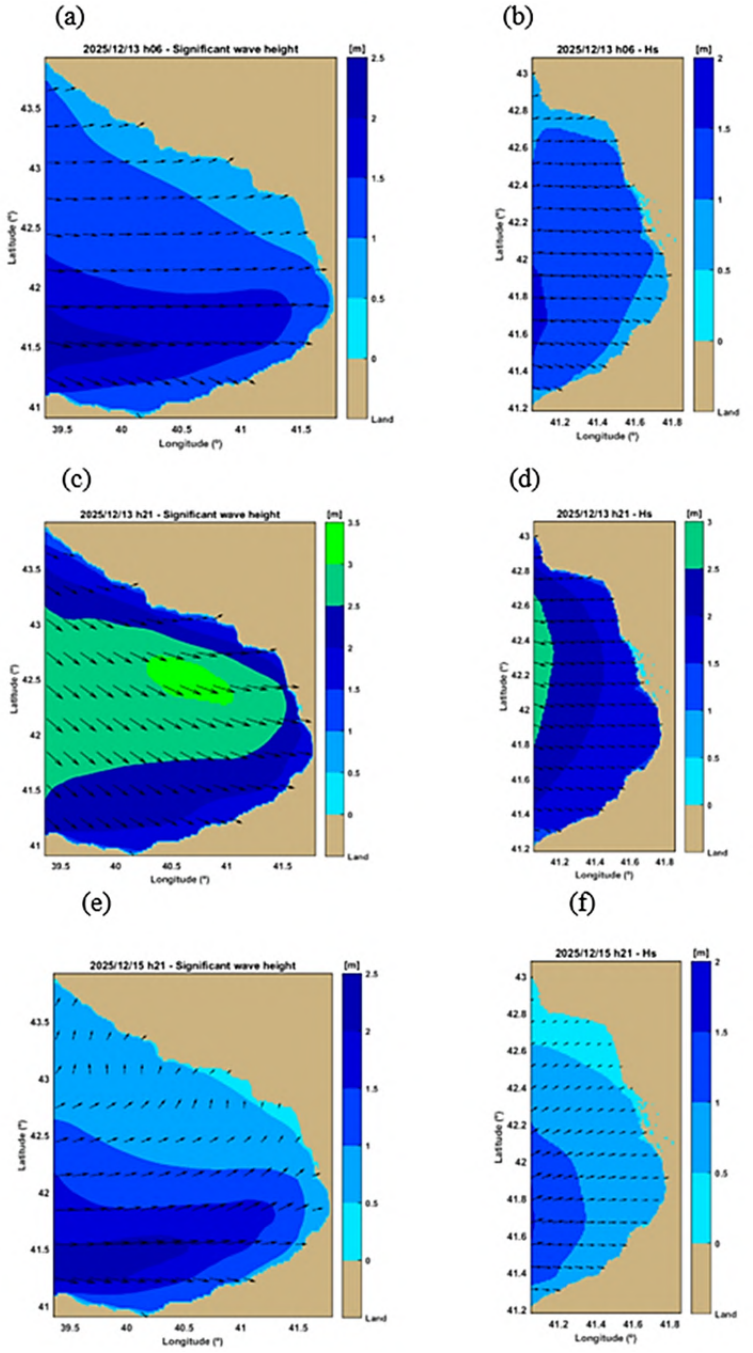



**Fig.1.** Simulated significant wave height and direction for the Georgian sector of the Black Sea (left panels) and for Batumi-Poti-Anaklia nearshore (right panels) at the following points in time in 2025: (a), (b) – 06:00 GMT, December 13; (c), (d) – 21:00 GMT, December 13; (e), (f) – 21:00 GMT, December 15.

December 13, significant wave heights in nearshore waters were up to 2.5 meters, and then increased to 3-3.5 meters offshore (Fig.1c and Fig.1d).

## Conclusion

A wind wave modeling and forecasting system has been implemented for the Georgian coastal area for the first time, which allows us to calculate significant wave height and direction based on the well known third generation SWAN spectral model.

The next step in the development of the wave modeling system is related to the integration of an operational atmospheric model into the system, which provides wind field forecasts.

**Acknowledgment:** Authors are grateful to Corresponding member of Romanian Academy of Sciences, Professor Eugen Rusu and Professor Liliana Rusu for their assistance in implementing the wind wave model SWAN in the Black Sea coastal zone of Georgia.

## References

1. Polonsky A. B., Fomin V. V., Garmashov A. V., Characteristics of wind waves of the Black Sea. // Reports of the National Academy of Sciences of Ukraine., ISSN 1025-6415, № 8, 2011, pp.108-112. (in Russian)
2. Mihaylichenko S. Yu., Fomin V. V. Calculations of unsteady wind waves in the waters of the Blue Bay on the basis of the model SWAN. // Ecological Safety of coastal and shelf zones and comprehensive use of shelf resources. Collected scientific papers. Sevastopol, Iss. 25, vol. 2, 2011, pp. 275-280. (in Russian)
3. Gippius F. N., Arkhipkin V. S., Surkova G. V., Regime of wind waves on the Black Sea according to hindcast computations. // In: Komplexsnie issledovania morey Rossii: operativnaia okeanografia i expedicionnye issledovania, 2016, pp. 265-270. (in Russian)
4. Fomin V., V., Ivanov V. A., Numerical modeling of wind wave near the Tuzla bar island. // Ecological Safety of coastal and shelf zones and comprehensive use of shelf resources. Sevastopol, Iss. 10, 2004, pp.233-242. (in Russian)
5. Rusu E., Rusu L., Soares C. G., Prediction of extreme wave conditions in the Black Sea with numerical models // Proceeding of 9th International workshop on wave hindcasting and forecasting. September, 2006.
6. Rusu E., Strategies in using numerical wave models in ocean/coastal applications. // Journal of Marine Science and Technology., vol.19, No.1, 2011, pp. 58-75.
7. Rusu L., Bernardino M., Soares C. G., Wind and wave modeling in the Black Sea. // Journal of Operational Oceanography, Vol.7, No 1., 2014, pp.5-20.
8. Jose-Henrique G. M. Alves, Yung Y. Chao, Hendrik L. Tolman., The Operational North Atlantic Hurricane Wind-Wave Forecasting System at NOAA/NCEP. // Technical Note. 2005, 53 p.
9. Hoque Md. A., Perrie W., Solomon S. M., Application of SWAN model for storm generated wave simulation in the Canadian Beaufort Sea. // Journal of Ocean Engineering and Science, №5, 2020, pp.19-34.
10. SWAN Scientific and Technical Documentation. https://swanmodel.sourceforge.io/download/zip/swanuse.pdf

2nd International Scientific Conference "Modern Problems in Geophysics", Proceedings,
ISBN 978-9941-36-562-1, ISSN 3088-4349, Tbilisi, Georgia, October 29-31, 2026

# PRECIPITATION EFFECTS ON A BRANCH OF THE INGIRISHI MAIN FAULT AND RELATED HYDROLOGICAL AND GEODYNAMIC PROCESSES

***Kiria J., *Dovgali N., *Davitashvili L., *Tsaguria T., **Sakvarelidze E.**

**M. Nodia Institute of Geophysics, Ivane Javakhishvili Tbilisi State University, Tbilisi, Georgia*
***Ivane Javakhishvili Tbilisi State University, Tbilisi, Georgia*
*kiria51@yahoo.com*

***Abstract.*** *This paper examines the possible relationship between the temporal distribution of precipitation and changes in the subsurface hydrological parameter (H) in the context of investigating a branch of the Ingirishi Main Fault (Fig. 1). Particular attention is paid to data from February 2023 and the Ozurgeti earthquake (M = 4.3), which occurred on 11 February. The aim is to assess whether hydrological changes caused by precipitation infiltration and the seismic event may be associated with deformation processes at the study site. According to data for 1–28 February 2023, total precipitation was 135.4 mm. The maximum daily precipitation – 48.4 mm – was recorded on 20 February. After that day, the value of (H) increased sharply over the following days. This temporal sequence raises the hypothesis of a possible relationship between precipitation and the hydrological response. However, the available data do not, by themselves, confirm that the observed changes are directly related to deformation of the Ingirishi Fault branch or to the Ozurgeti earthquake. A joint analysis of deformation, seismological, and hydrological data is required to investigate this issue.*

***Key words:*** *Ingirishi Main Fault, fault branch, precipitation, pore pressure, deformation, Ozurgeti earthquake, temporal correlation.*

## Introduction

The study of contemporary geodynamic processes in active tectonic fault zones requires the joint consideration of tectonic, seismic, and hydrological factors. Precipitation infiltration may alter soil and rock water content, groundwater regime, and pore pressure. Under suitable geological conditions, these changes may affect the effective stress acting on fault surfaces.

The Ozurgeti earthquake (M = 4.3), which occurred on 11 February 2023, provides an opportunity to compare the date of the seismic event, the distribution of precipitation, and observations from the branch of the Ingirishi Main Fault in the time domain.

However, temporal coincidence between events does not imply a causal relationship. It is therefore necessary to distinguish the possible hydrological influence of precipitation, the deformation response associated with the earthquake, and other natural or technical factors [1-4].

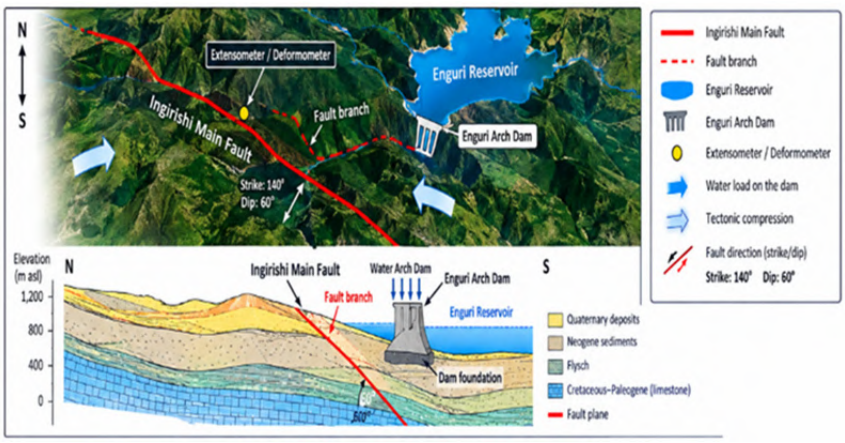



**Fig. 1.** Location of the Ingirishi Main Fault and its branch, the Enguri HPP, and the extensometer/deformometer. Geological-geophysical scheme with the fault geometry and dam foundation (plan view and geological cross-section).

## Aim and Objectives of the Study

The aim of the study is to assess the temporal relationship between precipitation, changes in (H), and the Ozurgeti earthquake in February 2023, and to identify the need for additional deformation data.
The main objectives are:

1. Quantitative analysis of the precipitation and (H) time series.
2. Comparison of the date of the 11 February earthquake with changes in precipitation and (H).
3. Assessment of the possible time lag between precipitation and the hydrological response.
4. Examination of a possible deformation mechanism associated with precipitation and changes in pore pressure.
5. Development of a methodology for distinguishing seismic and hydrological effects on the basis of deformation data.

## Data and Methods

Daily precipitation and (H) values for 1–28 February 2023 were used for the analysis (Fig. 2).

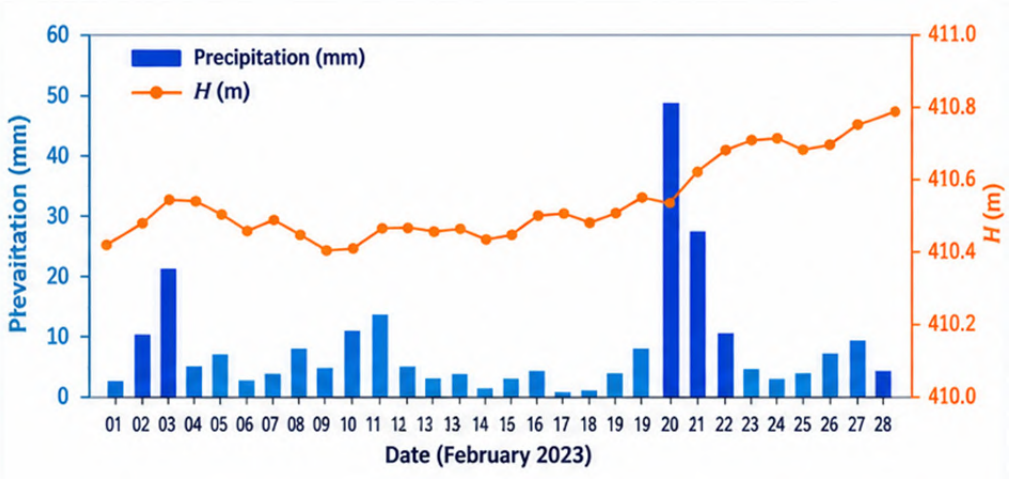



**Fig. 2.** Daily precipitation and H variation (1-28 February 2023).

## Formula for calculating total precipitation

The total precipitation over a given period is calculated by summing the precipitation recorded on each day:

$$\boxed{P_{\Sigma} = \sum_{i=1}^{N} P_i}$$

where:

- $P_{\Sigma}$ – total precipitation, mm;
- $P_i$ – precipitation measured on day i, mm;$i$
- $N$ – number of observation days.

For our data, for 1–28 February 2023:

$$P_{\Sigma} = \sum_{i=1}^{28} P_i$$

$$\boxed{P_{\Sigma} = 135.4 \text{ mm}}$$

## Formula for calculating the change in H

If H denotes the water level or another monitoring parameter, its change between the initial and final times is calculated as follows: $H$

$$\boxed{\Delta H = H_{\text{final}} - H_{\text{initial}}}$$

where:

- $H_{\text{initial}}$ – value at the beginning of the observation period;
- $H_{\text{final}}$ – value measured at the end of the period;
- $\Delta H$ – change in the parameter.

For our data:

$$H_{\text{initial}} = 410.49 \text{ m}$$
$$H_{\text{final}} = 411.61 \text{ m}$$

Accordingly,

$$\boxed{\Delta H = +1.12 \text{ m}}$$

A positive sign indicates an increase in H.

## Formula for assessing the relationship between precipitation and H.

The Pearson correlation coefficient is used for an initial assessment of the linear relationship between precipitation and H:

$$\boxed{r_{PH} = \frac{\sum_{i=1}^{N}(P_i - \bar{P})(H_i - \bar{H})}{\sqrt{\sum_{i=1}^{N}(P_i - \bar{P})^2 \sum_{i=1}^{N}(H_i - \bar{H})^2}}}$$

where the terms represent the mean values of the corresponding datasets.$\bar{P}\ \bar{H}$

If the effect of precipitation occurs with a delay, the following can be used:

$$\boxed{r(\tau) = \text{corr}[P, (t)H(t+\tau)]}$$

The resulting correlations should be interpreted as indicators of statistical association, not as evidence of causation. The results may be affected by a temporal trend, seasonality, autocorrelation in the data, and other hydrological factors (Fig. 3).

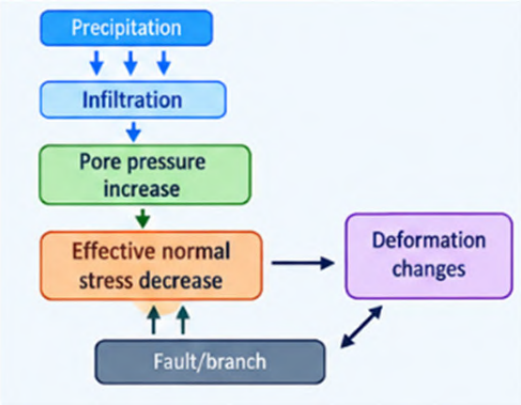



**Fig. 3.** Possible mechanism of the influence of precipitation on deformation.

To assess the possible influence of the Ozurgeti earthquake, deformation data obtained before and after the earthquake need to be compared. If the coordinates or deformation plots for monitoring points 3 and 5 are available, the time series X(t), Y(t), and ΔD(t) can be analysed.

## Results and Discussion

Total precipitation in February 2023 was 135.4 mm. The maximum daily precipitation, 48.4 mm, was recorded on 20 February.

The minimum value of (H) was 410.27 m on 15 February, while the maximum value was 411.61 m on 28 February. From the beginning to the end of the month, (H) increased by 1.12 m.

The period from 20 to 24 February is particularly noteworthy. On 20 February, (H) was 410.31 m, while on 24 February it was 411.35 m. Thus, an increase of approximately 1.04 m was recorded over this interval.

This change followed a period of intense precipitation, supporting the hypothesis of a possible relationship between precipitation and the hydrological response. Nevertheless, these observations alone cannot establish what proportion of the change in (H) was due to precipitation, or whether the change is directly associated with deformation of the fault branch.

Assessing the possible influence of the earthquake that occurred on 11 February requires a comparison of deformation time series recorded before and after the event. The presented precipitation and (H) table does not contain direct deformation measurements; therefore, at this stage, neither an immediate nor a residual deformation caused by the earthquake can be confirmed.

## Possible Physical Mechanism

The precipitation-influence hypothesis can be represented by the following sequence:
Precipitation → infiltration → change in pore pressure → change in effective stress → possible deformation response.

Effective normal stress is expressed by the following formula:

Effective normal stress is the normal stress acting on the granular framework of a rock and accounts for an important part of the rock's resistance to compression and frictional stability along a fault surface. Pore-fluid pressure reduces the load transferred to the granular framework. For a saturated porous rock, according to the conventional effective-stress principle:

$$\boxed{\sigma_n' = \sigma_n - P_f}$$

where:

- $\sigma_n'$ – effective normal stress, Pa or MPa;
- $\sigma_n$ – total normal stress on the rock or fault plane;
- $P_f$ – pore-fluid pressure.

If precipitation infiltration increases pore pressure within a fault zone, effective normal stress may decrease under appropriate conditions, potentially changing the frictional stability of the fault surface.

This mechanism is a physically plausible hypothesis. However, applying it specifically to the Ingirishi Fault branch requires consideration of rock permeability, groundwater regime, fault geometry, and deformation observations.

## Conclusion

The February 2023 data show an increase in (H) following intense precipitation, particularly during 20–24 February. This temporal sequence indicates a possible relationship between precipitation and hydrological changes.

The possible influence of the 11 February 2023 Ozurgeti earthquake (M = 4.3) on deformation of the Ingirishi Main Fault branch requires separate investigation. The available data do not provide a basis for attributing the change in (H) to the earthquake or directly to fault deformation.

The main hypothesis of the study is that hydrological changes caused by precipitation may affect the stress–strain state of the fault zone. Confirmation of this hypothesis requires a joint analysis of precipitation, groundwater, seismic events, and direct deformation measurements over a longer period.

## References


1. Chelidze T., Kiria J., Tsaguria T., Kiria T., Dovgali,N., & Davitashvili L., Study of processes in a crack located on the right bank of the Enguri Dam based on preliminary data from a two-coordinate laser extensometer. // Proceedings of the M. Nodia Institute of Geophysics, Vol. LXX, 2019.
2. Kiria J., Tsaguria T., Sakvarelidze E., Dovgali N., Davitashvili L., & Kutelia G., Influence of the strong earthquake in Turkey on the Enguri arch dam and its surrounding area. // Transactions of the Mikheil Nodia Institute of Geophysics, ISSN 1512-1135, Vol. LXXVI, 2023.
3. Gvinieria A., et al., Tectonics of the Ingirishi Fault (Georgia). // Bulletin of the Geological Society of America, 2018.
4. Zhang Y., Precipitation–groundwater interactions in seismic regions. // Journal of Hydrology, 2019.

2nd International Scientific Conference "Modern Problems in Geophysics", Proceedings,
ISBN 978-9941-36-562-1, ISSN 3088-4349, Tbilisi, Georgia, October 29-31, 2026

# INTEGRATED GEOPHYSICAL AND MICROBIAL BIOMONITORING OF METALLURGICAL CONTAMINATION IN SOIL AND GROUNDWATER

**[*]Jandieri G., [**]Janelidze I., [***]Zivzivadze O.**

[*]*Rafiel Dvali Institute of Machine Mechanics, Tbilisi, Georgia; Independent Investigator, Leipzig, Germany*
[**]*Georgian Technical University, Tbilisi, Georgia*
[***]*Akaki Tsereteli State University, Kutaisi, Georgia*
*gigo.jandieri@gmail.com*

***Abstract.*** *This review paper proposes an integrated environmental monitoring concept combining electrical resistivity tomography (ERT), induced polarization (IP), hydrochemical measurements and subsurface microbial biomonitoring. The central hypothesis is that migration of metallurgical contaminants changes the physicochemical conditions of soil and groundwater and consequently affects indigenous microbial activity and electron-transfer processes. These biological changes may contribute to measurable electrochemical and geophysical responses. The proposed system uses geophysical methods to identify and track anomalous subsurface zones, microbial measurements as an indicator of biological response, and conventional chemical analysis for identification and quantitative confirmation of contaminants. The approach is intended as an early-warning system for metallurgical industrial areas and as a potential basis for future bioelectrochemical remediation. The proposed framework may be recommended as a supplementary early-warning tool in environmental monitoring programs for metallurgical sites.*

***Key words****: Environmental geophysics; metallurgical contamination; microbial and bioelectrochemical monitoring.*

## Introduction

Metallurgical production is associated with substantial environmental pressures generated during extraction, processing and high-temperature treatment of mineral raw materials [1, 2]. Previous work by the authors focused mainly on greenhouse-gas emissions and the environmental efficiency of carbon utilization in ferrous and non-ferrous metallurgy. Particular attention was given to the technological utilization of metallurgical dusts and sludges and to methods for reducing environmental losses [3-5].

However, metallurgical environmental impact extends beyond atmospheric emissions. Solid and liquid technogenic residues may remain in industrial areas for long periods and can act as secondary sources of potentially hazardous elements. Rainwater infiltration and interaction with these materials can mobilize soluble components and transport them through the soil profile toward groundwater. Thus, an environmental problem initially associated with a metallurgical production site may develop into a subsurface contamination problem: metallurgical source → soil contamination → infiltration → groundwater contamination → contaminant plume.

Groundwater contamination is particularly difficult to monitor because the contaminant distribution is heterogeneous and cannot be observed directly from the surface. Conventional monitoring based on wells and chemical analyses provides reliable information at individual sampling points but may not adequately describe the spatial development of a contaminant plume [6].

Geophysical methods, particularly ERT and IP, provide complementary spatial information about subsurface electrical and electrochemical properties [7]. At the same time, microorganisms naturally present in soil and groundwater respond to changes in pH, redox conditions, ionic composition and contaminant concentrations.

The combination of these two approaches provides a basis for a new monitoring concept in which geophysics describes the spatial structure of the subsurface anomaly, while microbial activity provides an additional biological indicator of changing environmental conditions.

Based on the considerations outlined above, the objective of this paper is to synthesize current knowledge on geophysical and microbial indicators and to propose a conceptual framework for their integrated application in metallurgical industrial areas.

## Metallurgical Contamination of Soil and Groundwater

Metallurgical dusts, sludges, slags and tailings may contain significant quantities of metal-bearing mineral phases. Depending on the raw materials and production technology, elements such as Fe, Mn, Cu, Zn, Ni, Cr, Pb, Cd and others may be present [1]. The environmental significance of these materials depends not only on their total concentration but also on their chemical form, solubility and interaction with the surrounding soil and groundwater.

A simplified contamination pathway is: technogenic residue → rainfall and infiltration → dissolution/desorption → migration through soil → groundwater → contaminant plume

The migration process depends on soil permeability, water saturation, mineralogy, pH, redox conditions and groundwater flow. This means that the same metallurgical residue may remain relatively stable under one set of conditions but become a source of mobile contaminants under another.

The environmental monitoring problem is therefore fundamentally a coupled geological, hydrological, chemical and biological problem.

**Geophysical Monitoring:** *Electrical Resistivity Tomography and Induced Polarization*

In modern studies [8], ERT is proposed as the principal method for spatial mapping of subsurface electrical anomalies. Electrical resistivity depends on pore-water conductivity, saturation, porosity, mineral composition and other properties of the subsurface. Changes associated with contaminant migration may therefore produce measurable resistivity anomalies. ERT can be used to: identify anomalous zones, determine their approximate geometry and depth, monitor contaminant migration, compare contaminated and background areas, perform repeated time-lapse surveys.

The principal advantage is that ERT provides spatial information between conventional sampling points.

However, resistivity alone cannot uniquely identify a particular contaminant. Similar anomalies may result from increased moisture, salinity, clay content or other geological factors. Consequently, ERT should be interpreted together with hydrochemical and geological information.

IP provides complementary information related to electrochemical polarization processes in the subsurface.

The combined use of ERT and IP can therefore provide [9]:

ERT → spatial electrical structure
IP → electrochemical/polarization response.

This combination is potentially more informative than resistivity measurements alone, particularly in heterogeneous contaminated environments.

## Subsurface Microbial Biomonitoring

Soil and groundwater contain indigenous microbial communities that participate in mineral transformation and geochemical cycling.

Contamination can modify microbial activity through changes in: pH, oxidation-reduction conditions, dissolved ions, electron donors and acceptors, metal toxicity, availability of organic substrates et al. [10].

The proposed approach treats microorganisms primarily as biological indicators of changes in the subsurface environment.

The conceptual mechanism is: Contaminant migration → Geochemical change → Microbial response → Change in metabolic/electron-transfer activity → Electrochemical response.

Certain microorganisms are capable of extracellular electron transfer. This property provides a basis for microbial electrochemical sensors and bioelectrochemical monitoring systems. Such systems should not initially be regarded as direct substitutes for chemical analysis. Their principal function is to detect a biological/electrochemical response that can indicate a change requiring further investigation.

## Integrated Monitoring Concept

Based on the analysis of existing approaches, we propose a monitoring concept in which two widely used geophysical methods (ERT and IP) are integrated, and a third approach, – chemical monitoring- is com-

bined with them to form a unified diagnostic framework.

Consequently, the monitoring concept includes three complementary approaches that together form a unified diagnostic structure:

1. Geophysical monitoring – ERT + IP/SIP: Determines where the subsurface anomaly occurs and how it changes with time.
2. Microbial monitoring – Indigenous microorganisms / biofilms / bioelectrochemical sensors: Determines whether the biological system exhibits a significant response.
3. Chemical monitoring – Groundwater and soil sampling: Determines what contaminant is present and at what concentration.

The complete monitoring chain can therefore be expressed as: Metallurgical Waste → Soil → Infiltration → Groundwater → ERT/IP Anomaly • Microbial Response → Chemical Confirmation → Early Warning.

The central principle is that no individual method is expected to provide a complete diagnosis. Instead, confidence increases when independent geophysical, biological and chemical observations demonstrate consistent changes.

## Proposed Experimental Validation

The concept requires experimental validation before field application. The first stage should consist of laboratory characterization of representative metallurgical residues and soil materials, Fig. 1. The following parameters should be determined: elemental composition, mineralogical composition, leachable fraction, pH, electrical conductivity, redox potential.

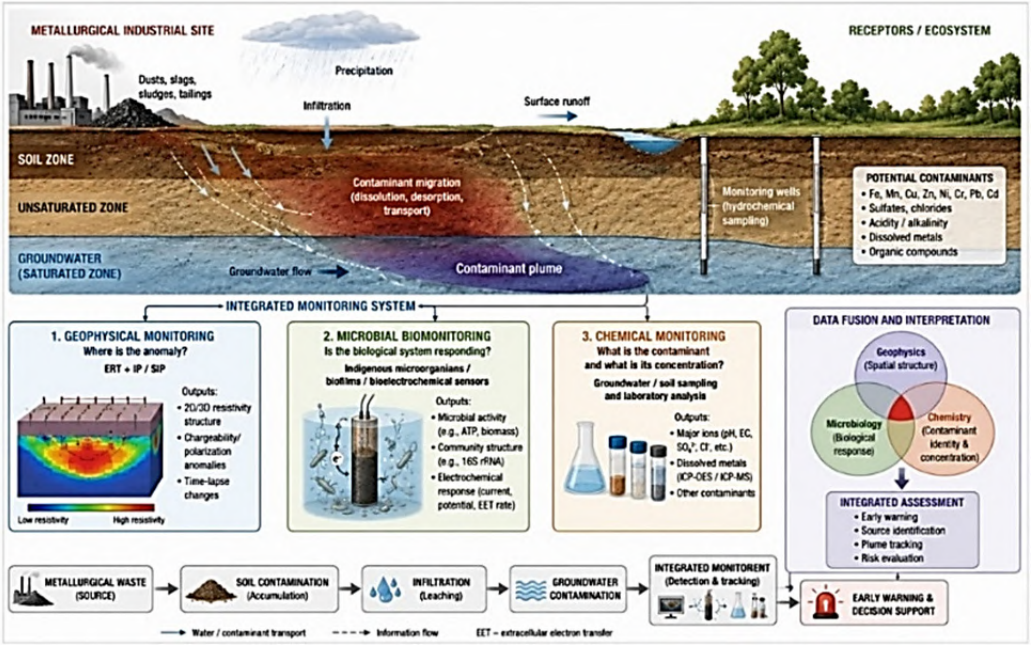



**Fig. 1.** Conceptual framework of integrated geophysical and Microbial biomonitoring for detection and tracking of metallurgical contamination in soil and groundwater.

The second stage should employ controlled soil-column experiments. Electrodes should be installed in representative soil material and measurements performed simultaneously with controlled contaminant migration. The following parameters should be monitored: ERT/IP + pH + Eh + EC + dissolved metals + microbial activity + electrochemical response.

The objective is to determine whether reproducible relationships exist between contaminant migration, microbial response and electrical properties. Only after laboratory validation should the system be tested at a selected metallurgical industrial site. A field monitoring network could consist of: ERT/IP profiles + monitoring wells + microbial electrochemical sensors + periodic chemical sampling.

Repeated measurements would allow changes in the subsurface system to be identified before or during development of a significant groundwater contaminant plume.

## Discussion

The proposed concept does not introduce ERT, IP or microbial electrochemical technologies as completely new individual methods. Their scientific foundations have already been established. The proposed innovation is their integration into a single monitoring framework specifically directed toward metallurgical contamination of soil and groundwater. The main advantage is the combination of spatial and point-based information.

Conventional sampling answers: What is the contaminant concentration at this point?

Geophysics adds: Where is the anomalous zone and how is it changing?

Microbial monitoring adds: Is the biological system responding to the changing geochemical conditions?

Together these observations can provide a more complete picture of subsurface contamination. At the same time, several limitations must be recognized. Geophysical responses are non-unique, and microbial activity is affected by many environmental factors. Therefore, microbial and geophysical anomalies cannot automatically be interpreted as evidence of a particular metal concentration. Chemical analysis remains necessary for final identification and quantification.

The proposed system should consequently be regarded as an integrated early-warning approach, rather than a replacement for conventional environmental analysis.

A further development could involve the transition from monitoring to remediation. Microbial electrochemical systems are being investigated not only for sensing but also for transformation or removal of contaminants in groundwater. This creates the possibility of combining: detection → monitoring → remediation within a single technological framework.

## Conclusions

Metallurgical wastes can serve as long‑term sources of soil and groundwater contamination in industrial areas. Rainfall, infiltration and geochemical reactions may mobilize potentially hazardous components and transport them from surface residues into the subsurface and groundwater.

Preventive monitoring and sustainable control of this problem require the integration of traditional, but spatially limited, chemical monitoring methods with geophysical techniques such as ERT and IP. Such integration provides complementary spatial and temporal information about subsurface anomalies associated with contaminant migration.

Future laboratory and field experiments should establish quantitative relationships between contaminant mobility, microbial activity and geophysical response. The long-term objective is the development of an integrated environmental control system: Prevention → Detection → Early Warning → Remediation.

This approach may provide a practical basis for environmental monitoring of metallurgical industrial areas where long-term contamination of soil and groundwater represents a significant environmental risk.

## References


1. Jishkariani G., Jandieri G., Sakhvadze D., Tavadze G., Oniashvili G., Zakharov G. and Aslamazishvili Z., Ecological Problems Related to Mining-Metallurgical Industries and Innovatory, Energy-Efficient Ways of Solving Them. // Engineering, 4 (2), 2012, pp. 83-89. https://doi.org/10.4236/eng.2012.42011
2. Harpprecht C., Xicotencatl B.M., Nielen S., Meide M., Li Ch., Li Zh., Tukker A., Steubing, B., Future environmental impacts of metals: // A systematic review of impact trends, modelling approaches, and challenges. Resources, Conservation and Recycling, 205, 2024, 107572. https://doi.org/10.1016/j.resconrec.2024.107572
3. Jandieri G. Sakhvadze D., Smelting of aluminum silicomanganese from technogenic and secondary resources of the mining and smelting industry of Georgia. // Scientific Proceedings X International Congress «Machines, technologies, materials», 1, 2013, pp. 107–110.
4. Jandieri G., Portyanko O., Recycling – a modern solution for improving the operational efficiency of the mining and metallurgical enterprises. // International Conference “The Development of Mining and Geology is the Precondition for the Revival of Economy”, Book of Abstracts, 2021, pp. 42-46. http://msgeorgia2012.com/files/SUL%20BOLO%20TEZISEBI2021.pdf#page=4213.
5. Jandieri G., Janelidze I., On Climate Change Mitigation Measures in Ferrous and Non-Ferrous Metallurgy (General Analysis). // International Scientific Conference „Natural Disasters in the 21st Century: Monitoring, Prevention,

Mitigation“. Proceedings. Tbilisi, Georgia, 20-22, 2021. Publish House of Iv. Javakhishvili Tbilisi State University, Tbilisi, 2021, pp. 42-45. URL:http://openlibrary.ge/bitstream/123456789/9574/1/12_Conf_ND_2021.pdf

6. Narimani R., Murgulet I., Murgulet D. Emerging Contaminants in Groundwater: Challenges, Management, and Policy Perspectives. // In: Zandaryaa, S., Fares, A., Eckstein, G. (eds) Emerging Pollutants. Advances in Water Security. Springer, Cham., 2025. https://doi.org/10.1007/978-3-031-71758-1_9
7. Xia T., Li M., Slater L., Hu X., Binley A., Ma X., & Mao D. The evolving roles of electrical geophysical methods for in situ remediation assessment. // Progress and perspectives. Water Resources Research, 62, 2026, e2025WR043172. https://doi.org/10.1029/2025WR043172
8. Arboleda-Zapata M., Osterman G., Li X., Sasidharan S., Dahlke H.E., Bradford S.A., Time-lapse ensemble-based electrical resistivity tomography to monitor water flow from managed aquifer recharge operations. // Journal of Hydrology, 659, 2025, 133282. https://doi.org/10.1016/j.jhydrol.2025.133282
9. Chao Ch., Ma X., Liu Sh., Zheng Ch., Mao D., Characterization of solid waste deposit using electrical resistivity tomography and time domain induced polarization. Journal of Environmental Management, 366, 2024, 121854, https://doi.org/10.1016/j.jenvman.2024.121854
10. Jandieri G., Sakhvadze D., Schukin B., Underground Development of Mineral Subsoil Using Microorganisms: A Mini-Review. Mikrobiolohichnyi Zhurnal [Microbiological Journal], 85(4), 2023, pp. 66-71. https://doi.org/10.15407/microbiolj85.04.066

2nd International Scientific Conference "Modern Problems in Geophysics", Proceedings,
ISBN 978-9941-36-562-1, ISSN 3088-4349, Tbilisi, Georgia, October 29-31, 2026

# WATER REACTION INTO ONI WELL ON EARTHQUAKES IN 2026

**Kobzev G., Melikadze G., Jimsheladze T., Chelidze T., Tchankvetadze A., Goguadze N., Kiria T.**

*M. Nodia Institute of Geophysics of the I. Javakhishvili Tbilisi State University, Tbilisi, Georgia*
*tamar.jimsheladze@tsu.ge*

***Abstract.*** *The well at Oni responds well to distant earthquakes. The azimuths of these earthquakes often fall within a relatively narrow sector.*

***Key Words:*** *Earthquakes, azimuth.*

## Introduction

The Oni well, located in the Caucasus Mountains, shows a distinct response to earthquakes. Some of the results obtained using it are presented below. Additional information can be found in [1].

**Well coordinates: 42.573° N 43.437° E, Georgia, Caucasus.**

**Well parameters: Length 255 m, screen 70-250 m. Static water level 9.1 m.**

**Confined sub-artesian aquifer; fractured shale and basalts. Well's resonance period: P=32 sec**.

The water level in Oni well was recorded every 1 minute. Device XR5-SE-M and program LogXR used.

Five earthquakes are depicting on fig.1. The moment of the earthquake announced as the starting (zero) time. Graph time (x-axis) is in format HH:MM (Hours: Minutes). Y-axis is in cm. Below is water reaction in Oni well on remote earthquakes in 2026.

## Sensitivity of well

The azimuths of the observed earthquakes fall within the 82°–125° range.

The focal depths of the earthquakes ranged from 6 to 20 km.

Distance to earthquakes in the east direction, in degrees, is 70- 87 °; the distance in the west direction is 98°.

For comparison, the inaccessible (shadow) area for P-waves of earthquakes is 90°-150°.

The strongest response 13.8 cm was triggered by an earthquake M=7.4 with an azimuth 92° and distance (in degrees) 70°.

The weakest earthquake with M=6.6 has azimuth 82.6° and distance 70.4°.

**Table 1.** Water level reaction in Oni well on earthquakes in 2026.

| NN | Date | Magnitude | Distance, km/° | Depth, km | Azimuth, degree | Earthquake's place | Reaction, cm |
|---|---|---|---|---|---|---|---|
| 1 | 20/04/2026, 07:52 | 7.4 | 7785/ 70° | 11 | 92 | Near East Coast of Honshu, Japan | 13.84 |
| 2 | 7/06/2026, 23:37 | 7.8 | 8894/ 80.4° | 57 | 116.7 | Mindanao, Philippines | 6.1 |
| 3 | 19/06/2026, 06:52 | 6.6 | 7829/ 70.4° | 6 | 82.6 | Off East Coast of Kamchatka | 2.68 |
| 4 | 24/06/2026, 22:05 | 7.5 | 10944/ 98.4° | 10 | -108.1 | Carabobo, Venezuela | 5.55 |
| 5 | 14/08/2026, 21:58 | 7.7 | 9663/ 86.9° | 20 | 125.5 | Flores region, Indonesia | 2.68 |

## Results

Results in Fig. 1 – Fig.5 and Table 1 are presented.

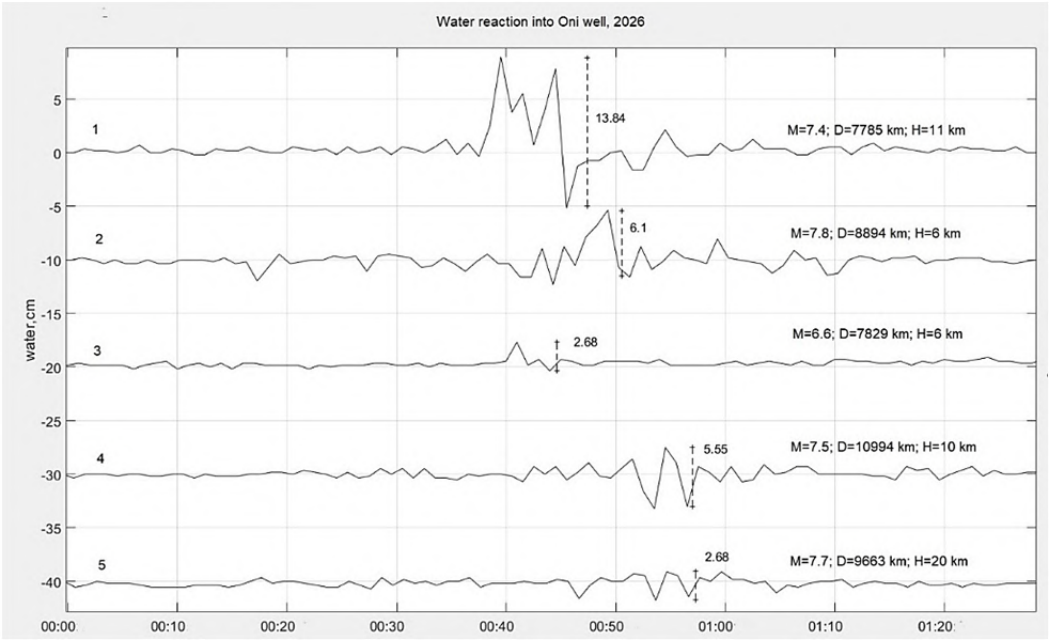
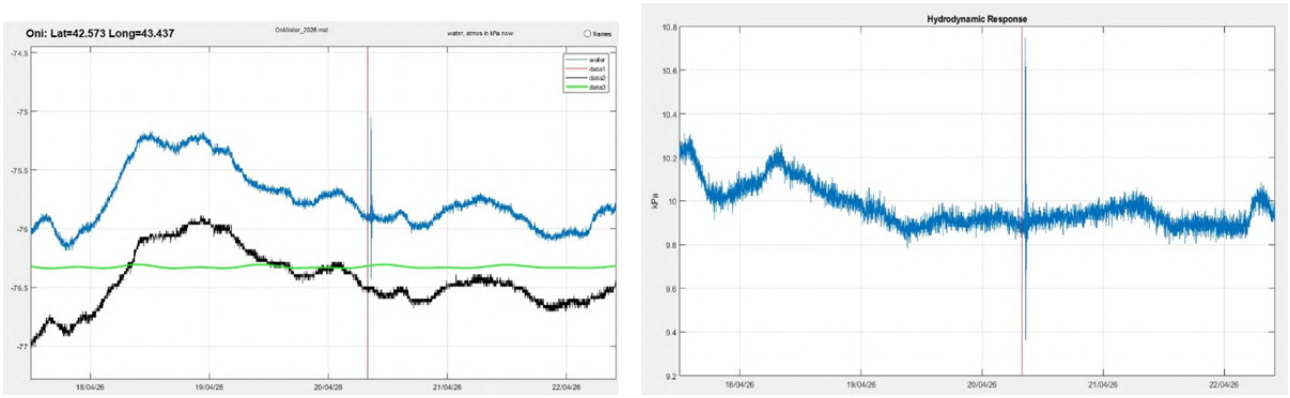
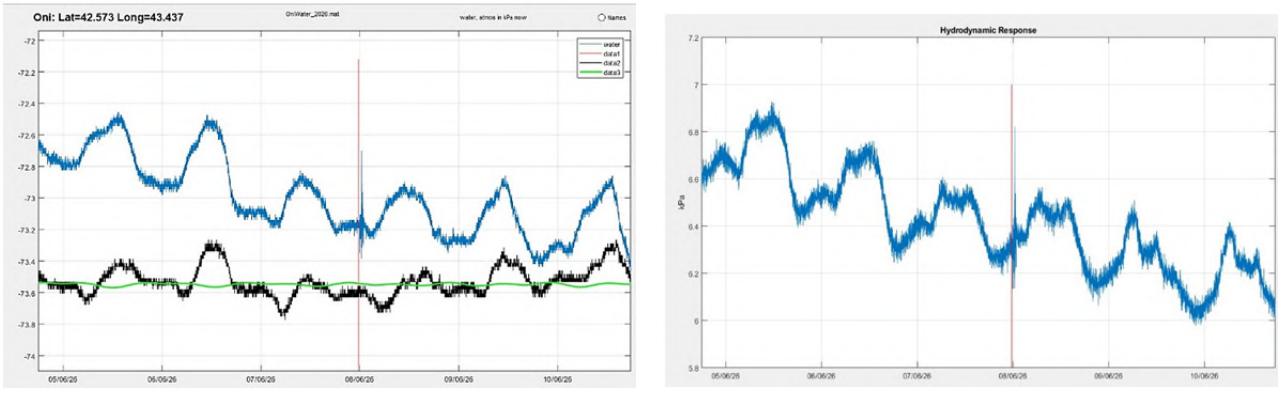



**Fig.1.** Oni, water reaction on the earthquakes in 2026. Earthquakes started at HH:MM=00:00.



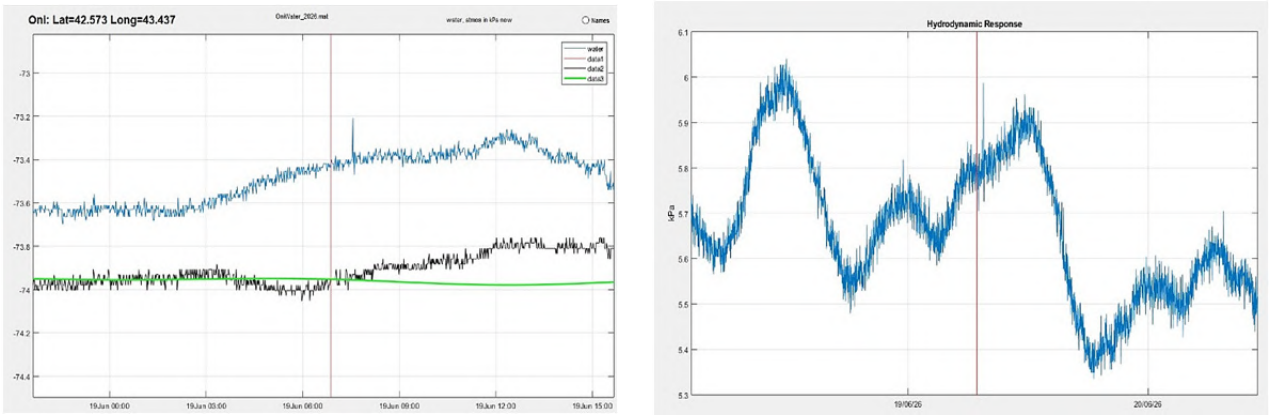

a. b.

**Fig. 2.** Oni, water reaction on the earthquake in 20/04/2026, 07:52, Mag=7.4. a – Water level, atmospheric pressure and tidal variations at the Oni borehole. The vertical line marks an earthquake. On abscise axis time is in hours. b- Hydrodynamic Response.



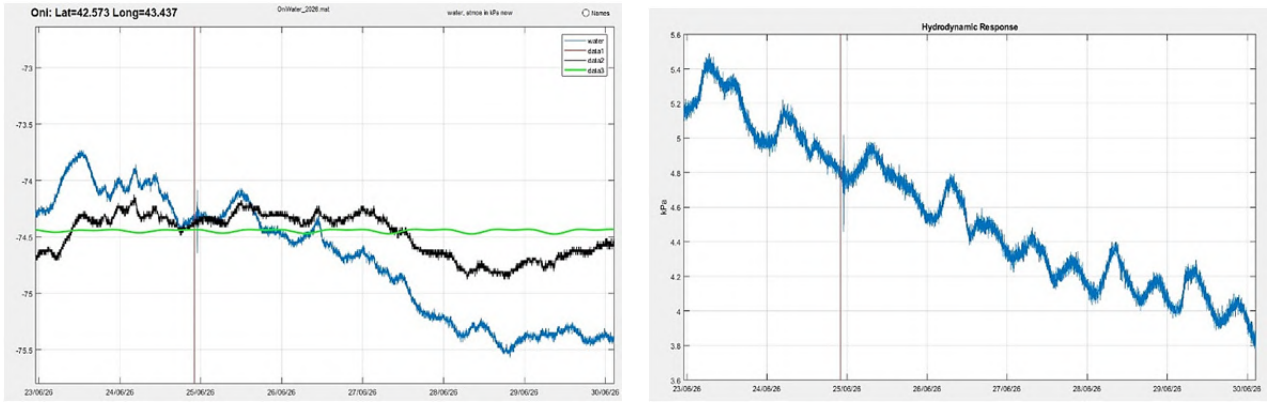

a b

**Fig. 3.** Oni, water reaction on the earthquake in 7/06/2026, 23:37, Mag=7.8. a – Water level, atmospheric pressure and tidal variations at the Oni borehole. Vertical line marks an earthquake. On abscise axis time is in hours. b- Hydrodynamic Response.



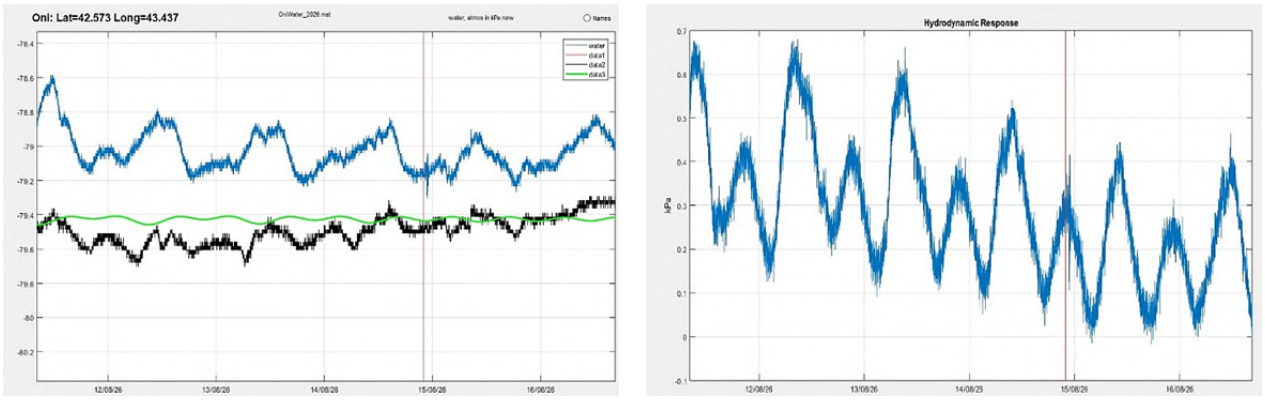

a b

**Fig. 4.** Oni, water reaction on the earthquake in 19/06/2026, 06:52, Mag=6.6. a – Water level, atmospheric pressure and tidal variations at the Oni borehole. Vertical line marks an earthquake. On abscise axis time is in hours. b- Hydrodynamic Response.




a b

**Fig. 5.** Oni, water reaction on the earthquake in 24/06/2026, 22:05, Mag=7.5. a – Water level, atmospheric pressure and tidal variations at the Oni borehole. Vertical line marks an earthquake. On abscise axis time is in hours. b- Hydrodynamic Response.




a b

**Fig. 6.** Oni, water reaction on the earthquake in 14/08/2026, 21:58, Mag=7.7. a – Water level, atmospheric pressure and tidal variations at the Oni borehole. Vertical line marks an earthquake. On abscise axis time is in hours. b- Hydrodynamic Response.

## Conclusion

Located in Georgia, Caucasus, the Oni well demonstrates high sensitivity to the distant earthquake of 2026. It responds more strongly when the earthquake's azimuth falls within a specific sector.

**Acknowledgement:** This work was supported by the Shota Rustaveli National Science Foundation of Georgia (SRNSFG), Grant number FR24-17839.

## References


1. Kobzev G., Melikadze G., Jimsheladze T., Karel R., Tchankvetadze A., Oni Water Reaction on Earthquake in 2021. // International Scientific Conference „Natural Disasters in the 21st Century: Monitoring, Prevention, Mitigation“ Proceedings, ISBN 978-9941-491-52-8, Tbilisi, Georgia, December 20-22, 2021, pp.10-12.
2. Melikadze G. I., Jimsheladze T. J., Kobzev G. N., & Tchankvetadze A. S., Revealed of Hydrodynamic Anomalies in Boreholes of Georgia Caused by Earthquakes. // Journals of Georgian Geophysical Society, 24(2), 2021. https://doi.org/10.48614/ggs2420213317

2nd International Scientific Conference "Modern Problems in Geophysics", Proceedings,
ISBN 978-9941-36-562-1, ISSN 3088-4349, Tbilisi, Georgia, October 29-31, 2026

# REVISITING THE TBILISI GEOTHERMAL SYSTEM: HYDROCHEMICAL AND STABLE-ISOTOPE EVIDENCE AND THE NEED FOR A MULTI-TRACER APPROACH

**Kapanadze N., Melikadze G., Tsutskiridze E., Todadze M., Chikviladze E., Tchankvetadze A.**

*M. Nodia Institute of Geophysics, Ivane Javakhishvili Tbilisi State University, Tbilisi, Georgia*
*ninokapanadze@gmail.com*

***Abstract****. Hydrochemical and stable-isotope ($\delta^{18}O$, $\delta^{2}H$) data from the Tbilisi geothermal system were re-evaluated with historical records. Five waters form two groups: A-1, L-5 and L-6 (Na–Cl type) and the distinct SO-4 and Q-1. Paired 2022 and 2026 samples shift towards higher δ values, most strongly at Q-31/Q-1, where a low $\delta^{2}H/\delta^{18}O$ slope suggests water–rock exchange. Causes remain unresolved; the PHDF-25-3232 project will add age, recharge and water–rock tracers.*

***Key Words****: Tbilisi geothermal system, hydrochemistry, stable isotopes, multi-tracer approach.*

## Introduction

Major-ion chemistry and stable water isotopes ($\delta^{18}O$, $\delta^{2}H$) are standard tools for characterizing geothermal waters: the former describes water type and geochemical evolution, the latter groundwater origin and recharge conditions [1]. Neither, however, uniquely resolves residence time, mixing or water–rock interaction, and similar compositions can result from different processes [1,2]. Tracers such as $^{3}H$, $^{14}C$-DIC, $\delta^{13}C$-DIC, dissolved noble gases, $\delta^{34}S$-$SO_4$, $^{87}Sr/^{86}Sr$ and $^{234}U/^{238}U$ provide complementary constraints [1,2].

The Tbilisi geothermal system in eastern Georgia comprises thermal-water occurrences and deep boreholes in the Lisi–Saburtalo, Central Tbilisi and Samgori–Sartichala sectors, with strong spatial variability in depth, temperature, mineralization and ionic composition [3–6]. Historical and more recent investigations have provided important information on these waters, and historical hydrochemical records offer a longer-term context for evaluating contemporary observations. Nevertheless, the relationships among the principal sectors, and the relative roles of recharge, circulation, mixing and water–rock interaction, remain poorly constrained.

This study combines historical records with quantitative hydrochemistry and stable-isotope data to characterize spatial variability in the system and to assess how far these data can constrain relationships among its sectors. The remaining uncertainties define the multi-tracer programme of the ongoing PHDF-25-3232 project.

## Study area, data and methods

The system is divided into three domains (Fig. 1): the Lisi–Saburtalo sector in western and north-western Tbilisi, where several wells exceed 2 km in depth and historical temperatures are about 54–64 °C; Central Tbilisi, including shallow and deep thermal waters of the Abanotubani balneological area; and the south-eastern sector towards Phonichala and Samgori–Sartichala [3,5,7]. Thermal groundwater occurs within several stratigraphic units and productive intervals, with substantial differences in borehole depth and water temperature. It circulates in permeable sedimentary formations interbedded with less permeable units and cut by faults [4,5]. Historical records show predominantly Na-rich waters with varying proportions of sulfate, chloride and bicarbonate [3,6]. This heterogeneity provides the spatial framework for comparing the geothermal waters considered here.

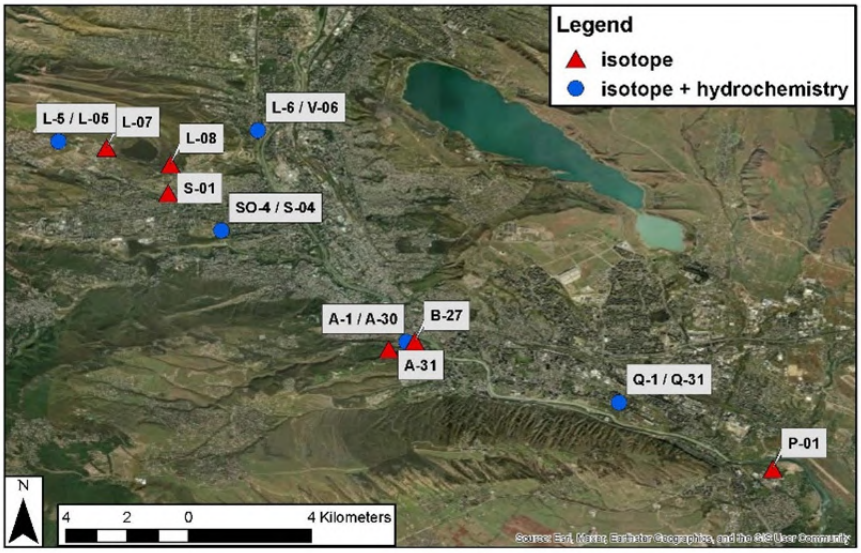



**Fig. 1.** Tbilisi geothermal system with the three study domains (Lisi–Saburtalo, Central Tbilisi, south-eastern sector towards Samgori–Sartichala) and the sampling sites with hydrochemical and/or stable-isotope data. Inset: location of Tbilisi in Georgia.

The dataset combines historical borehole and hydrochemical records, previously acquired $\delta^{18}O$ and $\delta^{2}H$ measurements from two sampling periods (2022 and 2026), and five quantitative hydrochemical analyses (SO-4, Q-1, A-1, L-5, L-6) evaluated within PHDF-25-3232. Historical records were used to provide hydrogeological context and to characterize broad hydrochemical patterns. The isotope measurements predate the current project; their original sampling information and well associations were retained and re-evaluated within the present hydrogeological framework. Because well identifiers differ between historical and recent records, wells were cross-referenced by location, depth, productive interval, temperature and local designation. Major ions ($Na^+$, $K^+$, $Ca^{2+}$, $Mg^{2+}$, $Cl^-$, $SO_4^{2-}$, $HCO_3^-$, $CO_3^{2-}$) and $SiO_2$ were converted to meq/L; all five analyses met a charge-balance criterion of ±5%. Isotope compositions are reported in ‰ relative to VSMOW. The map was prepared in Google Earth Engine and the diagrams in Python (Matplotlib).

## Results

In the Piper diagram (Fig. 2a), A-1, L-5 and L-6 plot close together, with $Na^+$+$K^+$ dominating the cations and $Cl^-$ the anions. SO-4 and Q-1 plot apart from this group, with higher proportions of $HCO_3^-$+$CO_3^{2-}$. The Schoeller diagram (Fig. 2b) confirms similar profiles for A-1, L-5 and L-6, while SO-4 has higher $HCO_3^-$+$CO_3^{2-}$ and Q-1 has higher $Ca^{2+}$ and $Mg^{2+}$ concentrations. Both diagrams thus show measurable differences in relative major-ion composition and concentration patterns among the five samples.

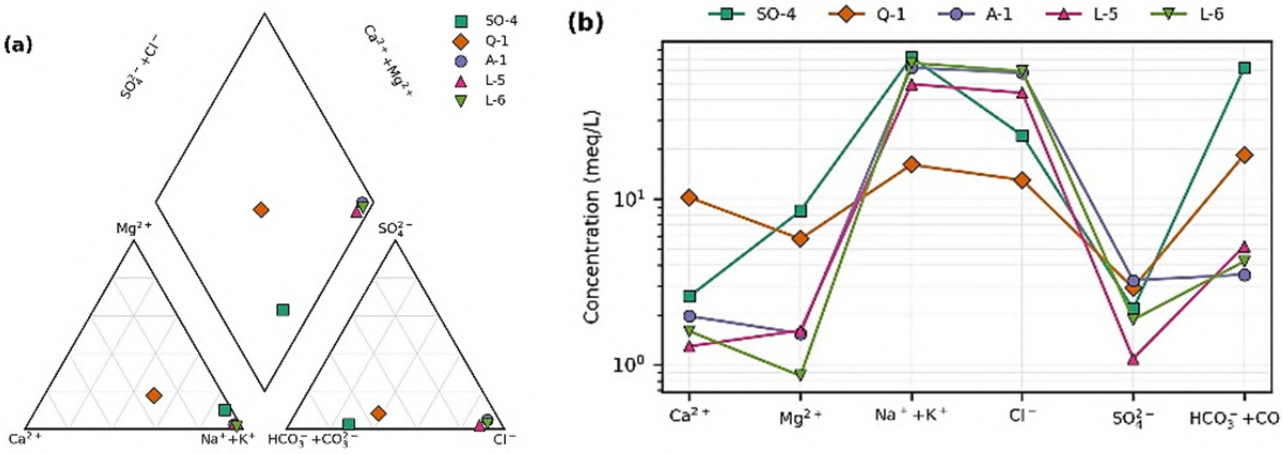



**Fig. 2.** Major-ion composition of the five geothermal waters: (a) Piper diagram (meq% of major cations and anions); (b) Schoeller diagram (meq/L, logarithmic scale).

Stable-isotope compositions differ among samples and between 2022 and 2026 (Fig. 3). For the pairs S-04/SO-4, L-05/L-5, V-06/L-6 and A-30/A-1, the 2026 samples are shifted towards higher $\delta^{18}O$ and $\delta^{2}H$ relative to 2022 by remarkably similar amounts ($\Delta\delta^{18}O$ = +2.97 to +3.31‰, $\Delta\delta^{2}H$ = +12.9 to +14.2‰; slopes 4.2–4.3). The Q-31/Q-1 pair plots separately and shows the largest shift, from $\delta^{18}O$ = −2.49‰ and $\delta^{2}H$ = −42.5‰ in 2022 to +3.12‰ and −27.0‰ in 2026 ($\Delta\delta^{18}O$ = +5.61‰, $\Delta\delta^{2}H$ = +15.5‰). The ratio $\Delta\delta^{2}H/\Delta\delta^{18}O$ is thus about 2.8, far below the slope of about 8 of the GMWL.

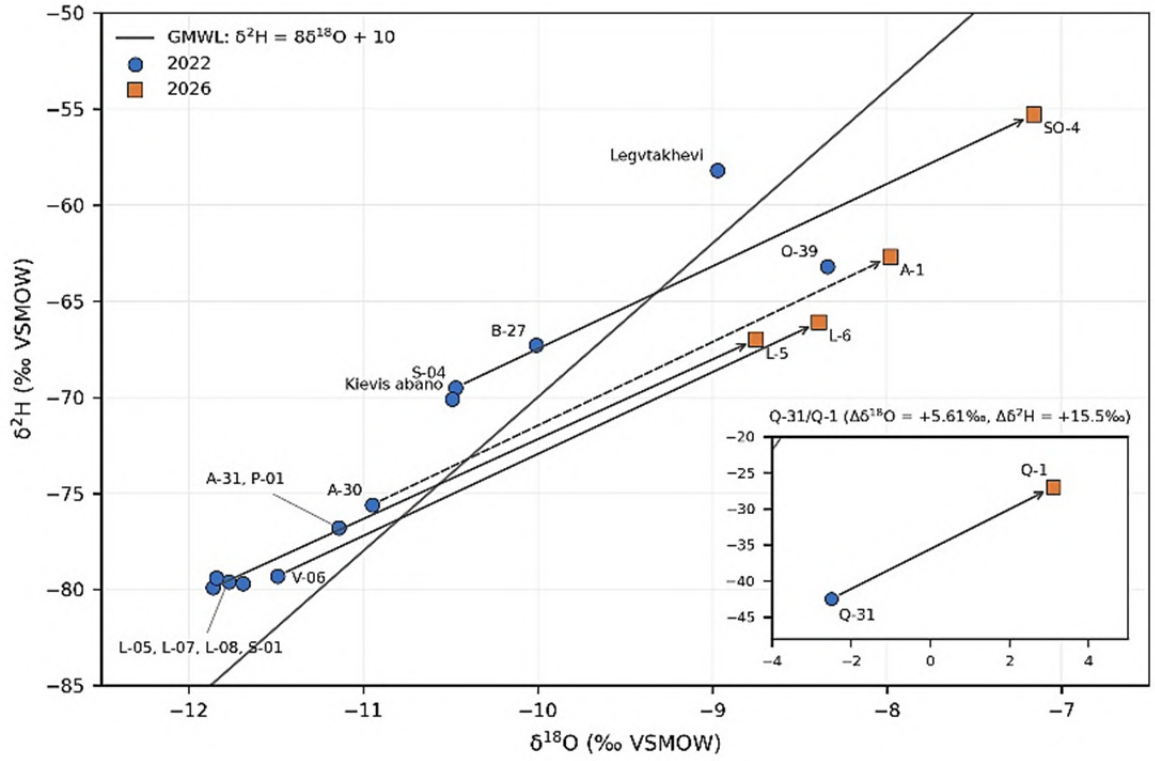



**Fig. 3.** $\delta^{18}O$ and $\delta^{2}H$ of the Tbilisi geothermal waters relative to the GMWL (‰ VSMOW). Arrows connect cross-identified sampling locations from 2022 to 2026 (not flow directions); the dashed arrow marks the provisional A-30/A-1 association. All 2022 samples are shown; the Q-31/Q-1 pair is shown in the inset.

## Discussion

Two hydrochemical groups are distinguished, indicating spatial variability in major-ion composition within the sampled waters. However, with only five analyses, similarity in major-ion composition does not establish hydraulic connection between wells. The isotope shift between 2022 and 2026 is consistent in direction, but two sampling periods cannot establish a systematic temporal evolution, and the data cannot distinguish real changes in the system from differences in sampling conditions or other hydrogeochemical processes.

The near-identical shift of the four main pairs, although the wells differ in depth, temperature and chemistry, may indicate an analytical offset between the 2022 and 2026 measurements rather than a change in the system; inter-laboratory comparison of standards is needed to test this. The Q-31/Q-1 pair differs from the other pairs in both magnitude and slope of its shift. Its $\delta^{18}O$ increases by 5.61‰ while $\delta^{2}H$ increases by only 15.5‰, a slope of about 2.8, far below the meteoric slope of about 8. A predominantly oxygen shift of this kind is characteristic of isotope exchange between thermal water and rock at elevated temperature [1], because rocks contain abundant oxygen but little hydrogen. The present data, however, cannot exclude mixing with an isotopically distinct water or differences in sampling conditions, so this interpretation remains tentative.

The PHDF-25-3232 project will therefore add $^{3}H$, $^{14}C$-DIC, $\delta^{13}C$-DIC, $\delta^{34}S$-$SO_4$, $^{87}Sr/^{86}Sr$, $^{234}U/^{238}U$ and dissolved noble gases (He, Ne, Ar, Kr, Xe). Combined with repeated hydrochemical and isotope sampling, these tracers will constrain groundwater age, recharge conditions, and water–rock interaction, and allow the alternative explanations for the observed patterns to be tested.

## Conclusion

Major-ion chemistry distinguishes a Na–Cl group (A-1, L-5, L-6) from the distinct waters SO-4 and Q-1. Paired isotope samples show a consistent shift towards higher $\delta^{18}O$ and $\delta^{2}H$ from 2022 to 2026, largest at Q-31/Q-1, but two sampling periods do not demonstrate systematic temporal change. At Q-31/Q-1, the low $\Delta\delta^{2}H/\Delta\delta^{18}O$ slope of about 2.8 points to possible high-temperature water–rock exchange, which remains to be tested. Hydrochemistry and stable isotopes alone therefore identify spatial and apparent temporal patterns without constraining their causes; the multi-tracer programme of PHDF-25-3232 is designed to resolve them.

**Acknowledgement:** This research was conducted within the framework of the Individual PhD Research Grant PHDF-25-3232, funded by the Shota Rustaveli National Science Foundation of Georgia (SRNSFG).

## References

1. Clark I.D., Fritz P., Environmental Isotopes in Hydrogeology. // CRC Press/Lewis Publishers, Boca Raton, FL, 1997.
2. Faure, G., Mensing T.M., Isotopes. // Principles and Applications, 3rd edn, Wiley, Hoboken, NJ, 2005.
3. Buachidze G.I., Vardigoreli O., Vashakidze B., Iainishvili T., Kotikadze N., Tsertsvadze L., Thermal Waters of Georgia. // Epoka Publishers, Tbilisi, 1998,130 p.
4. Buntebarth G., Kapanadze N., Kobzev G., Melikadze G., "Re-assessment of the geothermal potential of Tbilisi region: the hydrodynamic digital model project". // Association of Academies of Sciences in Asia Workshop on Environment and Resources, Izmir, Turkey, 2009, pp. 154–161.
5. Kapanadze N., Melikadze G.I., Kobzev G., "Modeling of the Tbilisi (Georgia) geothermal deposit under climate change conditions". // Climate Change and its Effects on Water Resources: Issues of National and Global Security, Springer, 2011, pp. 277–284. https://doi.org/10.1007/978-94-007-1143-3_30
6. Kapanadze N.A., Melikadze G.I., Forizs I.V., Vepkhvadze S.G., Todadze M.S., Chikviladze E.V., Ghlonti L.E., Chemical survey and reservoir temperature estimations of Tbilisi geothermal deposit by application of silica-enthalpy mixing method. // J. Georgian Geophys. Soc. 22, 2, 2020, pp. 10–15.
7. Kapanadze, N., Melikadze G., Todadze M., Tsutskiridze E., Forizs I., Assessment of geothermal potential in the Tbilisi geothermal reservoir. // EGU General Assembly 2022, Vienna, EGU22-4374, 2022. https://doi.org/10.5194/egusphere-egu22-4374

2nd International Scientific Conference "Modern Problems in Geophysics", Proceedings,
ISBN 978-9941-36-562-1, ISSN 3088-4349, Tbilisi, Georgia, October 29-31, 2026

# ASSESSMENT OF WATER QUALITY AND ECOLOGICAL STATUS OF SOME SMALL RIVERS IN THE COASTAL ZONE OF ADJARA

*, **Kiknadze N., *Gvarishvili N., *Tavdgiridze G., ***Khakhutaishvili A., **Kharazi N.

* *Batumi Shota Rustaveli State University, Batumi, Georgia*
** *Institute of Agrarian and Membrane Technologies, Batumi, Georgia*
*** *"Legi" Testing Laboratory, Batumi, Georgia*
*nino.kiknadze@bsu.edu.ge*

***Abstract.*** *Small rivers flowing near towns and cities are particularly vulnerable to anthropogenic pressures, which affect their ecological status and biodiversity. This study aims to assess the ecological status of the waters of three small rivers in the Adjara region – Bartskhana, Korolistskali, and Mejinistskali. The study included an assessment of the organoleptic characteristics of river waters, analysis of physicochemical and multi-element parameters, and microbiological investigations. The results showed deterioration in water quality in the lower reaches of the Bartskhana and Korolistskali Rivers, associated with pollution caused by sewage, domestic, industrial, and agricultural waste. Relatively stable water-quality indicators were recorded in the Mejinistskali River basin. The obtained data indicate the need for systematic monitoring of these rivers and implementation of ecological restoration measures, which will contribute to the sustainable management of water resources and the preservation of ecosystem functions in the Adjara region.*

***Key words:*** *Small rivers; chemical composition; microbiological analysis; ecological assessment.*

## Introdaction

Small rivers are important components of natural ecosystems and the human living environment, particularly in regions such as Adjara, characterized by complex terrain, intensive precipitation, and high biodiversity. They provide water resources, regulate erosion and nutrient cycling, and support aquatic habitats. Increasing urbanization, inadequate sewage systems, agricultural intensification, chemical pollution, and climate-related changes pose growing threats to their ecological sustainability [1, 3, 7].

The present study examines three small rivers of Adjara – Bartskhana, Korolistskali, and Mejinistskali – which are important hydrological units of the Black Sea basin and differ in geographical characteristics and anthropogenic pressure. Monitoring these rivers is important for public health, rational use of water resources, and environmental management [2, 3, 7].

The **Bartskhana River**, located in Khelvachauri Municipality, is 8.2 km long and has a drainage basin of 19 km². Its source is on the northwestern slope of the Meskheti Range. It is a mountain river that rapidly enters the coastal lowland and urban area of Batumi before flowing into the Black Sea. The river is fed by rainfall and groundwater, and its mean annual discharge is 0.6 m³/s [7]. Within Batumi, major anthropogenic pressures include urban and construction waste, inadequate se9wage systems, road and stormwater runoff, industrial wastewater, and oil-related infrastructure. The Batumi oil terminal and facilities associated with oil storage and transportation represent additional potential sources of pollution [1, 2].



**Fig. 1.** Bartskhana River.

The **Korolistskali River**, located north of Batumi, originates on the northern slope of Mount Chinkadze at 1,306.8 m above sea level. It is a mountain river with a length of 29.5 km, a drainage basin of 159 km², and a mean discharge of 3.8 m³/s. Major pressures include land-use changes, agricultural intensification, agrochemical runoff, domestic wastewater, stormwater, solid waste, and sand and gravel extraction. These pressures may increase nutrient concentrations, turbidity, total suspended solids (TSS), and hydromorphological disturbance [1, 2].



**Fig. 2.** Korolistskali River.

The **Mejinistskali River** is 9 km long and originates in the Kakhaberi Lowland, flowing into the Black Sea between Batumi Airport and the city. Approximately 7.9 km of the river lies within Batumi's administrative territory. Its water quality is affected by urbanization, domestic and agricultural runoff, wastewater, solid waste, stormwater, car-washing facilities, transport, and construction activities [1, 2].

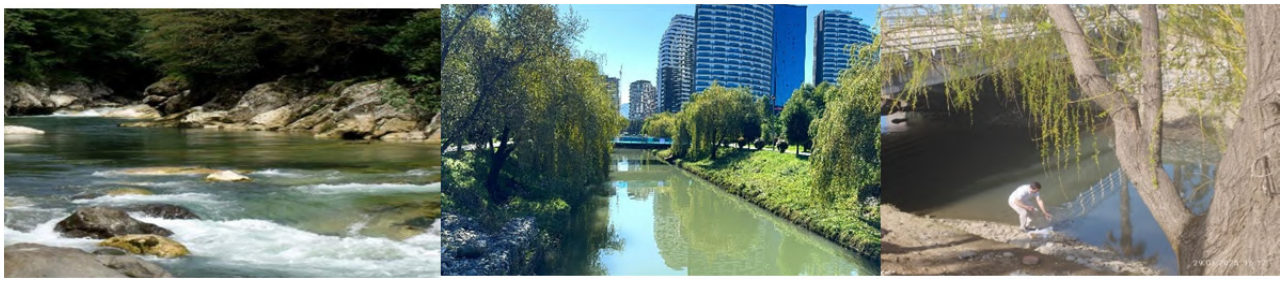


**Fig. 3.** Mejinistskali River.

## Materials and Methods

Water samples were collected at two locations for each river: (a) near the headwaters and (b) near identified pollution sources. Field observations included organoleptic characteristics and in situ measurements of physical parameters. Laboratory analyses included physicochemical, multi-element, and microbiological investigations. Nitrogen and phosphorus compounds were determined spectrophotometrically, pH potentiometrically, and multi-element composition using inductively coupled plasma atomic emission spectrometry (ICP-AES) [5, 6, 8]. Phosphorus determination followed ISO 6878:2004 [5], while nitrate determination was based on ISO 7890-3 [8]. Water-quality terminology was based on ISO 6107 [9]. Microbiological analyses were performed using culture-based methods to determine saprophytic microorganisms and *Escherichia coli*. The research was conducted using the facilities of the Institute of Agrarian and Membrane Technologies, Batumi Shota Rustaveli State University.

## Results and Discussion

Water near the headwaters of the Bartskhana and Korolistskali Rivers was transparent, with temperatures of 11.0–16.0°C, no visible floating particles, and an odor intensity of 0 points. At polluted sites, water quality deteriorated markedly: odor intensity reached 4 points in Bartskhana and 2 points in Korolistskali, while the Bartskhana water contained a visible oil film and floating particles Table 1). The polluted-site temperature reached 27°C. At the Mejinistskali site, odor intensity was 4–5 points, with abundant floating particles and turbidity. Headwater waters had near-neutral pH values of 6.5–6.8, whereas polluted sites showed an acidic shift. The most pronounced value was recorded in Bartskhana, where pH reached 3.0.

**Table 1.** Field Measurement Results of River Water.

| *Location* | *Odor, points* | *T, °C* | *Floating particles* | *Transparency* | *pH* |
|---|---|---|---|---|---|
| Bartskhana (near the headwaters) | 0 | 11,0 | - | Transparent from the surface | 6,7 |
| Bartskhana (near the pollution source) | 4 | 20,0 | Oil film and other floating particles on the water surface | Turbid | 3,0 |
| orolistskali (near the headwaters) | 0 | 15,0 | - | Transparent from the surface | 6,5 |
| Korolistskali (near the pollution source) | 2 | 27,0 | Floating particles on the water surface | Slightly turbid | 4,8 |
| Mejinistskali (near the headwaters) | 0 | 19,5 | - | Transparent from the surface | 6,8 |
| Mejinistskali (near the pollution source) | 4-5 | 23,0 | Abundant floating particles on the water surface | Turbid | 5,3 |
| ***Standard*** | ***0-2*** | | ***No floating particles should be present within the 0–20 cm surface layer*** | ***The water should be transparent from the surface*** | ***6.5-8.5*** |

Nitrite concentrations increased substantially at polluted sites. In Bartskhana, the concentration was 8.5 times higher than at the headwater site and 2.2 times above the limit established by Resolution No. 425 of the Government of Georgia. In Korolistskali, nitrite concentration was 6.4 times higher than at the headwater site and 1.48 times above the established standard. The Mejinistskali sample showed the highest concentration, 33.74 mg/L, corresponding to 10.22 times the established surface-water standard (Table 2). Phosphate concentrations at polluted sites were 2.80, 4.13, and 7.35 times higher than at the corresponding headwater sites of Bartskhana, Korolistskali, and Mejinistskali, respectively. In Mejinistskali, the phosphate concentration was 1.09 times above the established standard.

**Table 2.** Concentrations of Inorganic Biogenic Nutrients in River Waters.

| Location | $PO_4^{3-}$, mg/L | $NO_3^-$, mg/L | $NO_2^-$, mg/L |
|---|---|---|---|
| Bartskhana (near the headwaters) | 0.08 | 2.85 | 0.85 |
| Bartskhana (near the pollution source) | 0.33 | 4.7 | 7.26 |
| orolistskali (near the headwaters) | 0.05 | 1.65 | 0.77 |
| Korolistskali (near the pollution source) | 0.14 | 2.75 | 4.9 |
| Mejinistskali (near the headwaters) | 0.52 | 2.73 | 1.25 |
| Mejinistskali (near the pollution source) | 3.82 | 5.4 | 33.74 |
| ***Standard*** | ***3.5*** | ***45*** | ***3.3*** |

Multi-element analysis showed that most macroelements remained below the applicable surface-water standards. Potassium was not detected in Bartskhana and Korolistskali headwater samples. At polluted sites, macroelement concentrations increased but remained below the established limits. Among microelements, Cu, Cd, Mo, and Zn were not detected. Boron was detected at low concentration in Mejinistskali, while aluminum occurred at polluted sites of Korolistskali and Mejinistskali (Table 3). Silicon exceeded the maximum permissible concentration (MPC) in polluted-site samples from Bartskhana and Mejinistskali.

**Table 3.** Concentration of Microelements, mg/L.

| Location | Fe | Si | B | Al | Mn |
|---|---|---|---|---|---|
| Bartskhana (near the headwaters) | 0.0018 | 3.91 | - | - | <0.0001 |
| Bartskhana (near the pollution source) | 0.0318 | 10.61 | - | - | 0.0019 |
| orolistskali (near the headwaters) | 0.0031 | 3.99 | - | - | <0.0003 |

| | | | | | |
|---|---|---|---|---|---|
| Korolistskali (near the pollution source) | 0.0621 | 4.03 | - | 0.159 | 0.0025 |
| Mejinistskali (near the headwaters) | 0.0029 | 2,87 | - | - | <0.0002 |
| Mejinistskali (near the pollution source) | 0.0555 | 11.67 | 0.0049 | 0.0141 | 0.0385 |
| ***MPC, mg/L*** | ***0.3*** | ***10*** | ***0.5*** | ***1.0*** | ***0.25*** |

Among the trace and potentially toxic elements, Co, Cr, Ni, Hg, Ti, and Be were not detected in the water samples. The concentrations of Se, As, Ba, and Sb at the river pollution sites were below the maximum permissible concentrations (MPCs). The concentrations of V and Li in the river water samples collected from the polluted locations exceeded the maximum permissible concentrations (MPCs) (Table 4). The occurrence of elevated V and Li may reflect a combination of natural geochemical processes and anthropogenic influences; however, source attribution requires additional investigation.

**Table 4.** Concentrations of Trace and Potentially Toxic Elements, mg/L.

| Location | Se | V | As | Li | Ba |
|---|---|---|---|---|---|
| Bartskhana (near the headwaters) | - | 0.0006 | - | - | - |
| Bartskhana (near the pollution source) | - | 0.0018 | <0.0022 | 0.1251 | 0.0009 |
| orolistskali (near the headwaters) | - | 0.0008 | - | - | - |
| Korolistskali (near the pollution source) | <0.0007 | 0.0018 | - | 0.1460 | 0.0013 |
| Mejinistskali (near the headwaters) | - | 0.0007 | - | - | - |
| Mejinistskali (near the pollution source) | <0.0004 | 0.00242 | <0.0013 | 0.1863 | 0.007 |
| ***MPC, mg/L*** | ***0.001*** | ***0.001*** | ***0.05*** | ***0.05-0.1*** | ***0.1*** |

Microbiological analysis showed that saprophytic microorganisms and *E. coli* were within the established limits near the headwaters of Bartskhana and Korolistskali, whereas both parameters exceeded permissible levels at polluted sites Table 5). The most significant result was the elevated abundance of *E. coli*, exceeding the established limits by 9.3 times in Bartskhana, 31 times in Korolistskali, and 80 times in Mejinistskali, indicating substantial fecal contamination.

**Table 5.** Results of the Determination of Saprophytic Microorganisms and *E. coli.*

| **Location** | **Parameter, unit of measurement** | |
|---|---|---|
| | **Total number of saprophytic microorganisms, CFU/1 mL** | **Number of lactose-positive coliform bacteria (*E. coli*), CFU/1 L** |
| Bartskhana (near the headwaters) | 65 | 260 |
| Bartskhana (near the pollution source) | 180 | 2800 |
| orolistskali (near the headwaters) | 70 | 300 |
| Korolistskali (near the pollution source) | 280 | 9300 |
| Mejinistskali (near the headwaters) | 70 | 260 |
| Mejinistskali (near the pollution source) | 350 | 24000 |
| ***Standard*** | ***Not more than 100 CFU/1 mL*** | ***Not more than 300 CFU/1 L*** |

## Conclusion

The study demonstrated clear deterioration of water quality at anthropogenically impacted sites of the investigated small rivers. Bartskhana showed particularly pronounced pollution, characterized by an oil film, strongly acidic pH (3.0), and elevated nitrite concentrations. Increased nitrite and phosphate concentrations were also recorded in Korolistskali and Mejinistskali. Multi-element analysis revealed elevated concentrations of Si and, at certain polluted sites, V and Li. Microbiological analysis demonstrated substantial fecal contamination, with *E. coli* exceeding permissible levels by 9.3, 31, and 80 times in Bartskhana, Korolistskali, and Mejinistskali, respectively. The results emphasize the need for systematic monitoring, identifica-

tion and control of pollution sources, improved wastewater and waste management, and ecological restoration of riverbanks and riverbeds.

**Practical Recommendations:**

- Implement systematic monitoring of river water quality;
- Strengthen control of wastewater discharge and solid-waste management;
- Prevent pollution from petroleum products and agrochemicals;
- Identify and control major pollution sources;
- Implement ecological restoration measures in riverbanks and riverbeds;
- Conduct regular microbiological and multi-element monitoring.

## References


1. Government of Georgia. Resolution No. 425 of the Government of Georgia. On Approval of the Technical Regulation for the Protection of Surface Waters of Georgia from Pollution. Tbilisi, 2014. https://www.gov.ge/files/276_39952_103569_425311213.pdf
2. Consortium of European Union Member States. Annex to the Chorokhi–Adjaristskali River Basin Management Plan: Coastal and Transitional Waters. European Union Water Initiative Plus for the Eastern Partnership Countries (EUWI+), Results 2 and 3, ENI/2016/372-403. Tbilisi, 2021. https://www.rec-caucasus.org/wp-content/uploads/2021/04/122.pdf?utm
3. Kiknadze N., Gvarishvili N., Surmanidz G., Spatial and Temporal Assessment of Physicochemical Water Quality Parameters in Selected Rivers of Georgia. // II GLOBAL SYMPOSIUM on Chemistry, Biochemistry and Health Sciences, 23-24 July, 2026, pp.151-156. https://journals.4science.ge/index.php/chemistry https://journals.4science.ge/index.php/chemistry/article/view/4987/5045
4. World Bank. Georgia Solid Waste Sector Assessment Report. Washington, DC: International Bank for Reconstruction and Development/The World Bank, 2021. https://documents1.worldbank.org/curated/en/535371622781111161/pdf/Georgia-Solid-Waste-Sector-Assessment-Report.pdf
5. Water quality – Determination of phosphorus – Ammonium molybdate spectrometric method. Geneva: International Organization for Standardization, ISO 6878:2004, 2004. https://standards.iteh.ai/catalog/standards/cen/39d283f0-512e-4b93-a064-9a52b0f23214/en-iso-6878-2004?srsltid=AfmBOor_YYzipmETwG-FvGfhRa7aKODRuuFfzuKx1rZPHoVnDd37wohc
6. Simultaneous ICP Atomic Emission Spectrometer ICPETM-9820. https://www.shimadzu.com/an/sites/shimadzu.com.an/files/pim/pim_document_file/applications/application_note/14064/an_04-ad-0238-en.pdf?fbclid=IwAR0cu6DEBot6nD5Z0tLutpxheNAewsLpmE89ObND5QpOSNIJxCMDrMJGGck
7. Environmental Protection of International River Basins. Surface Water Delineation Report: Water Body Identification and Typology, Chorokhi-Adjaristskali Pilot Basin, Georgia. Activity 2.2. March 2013. https://doczz.net/doc/3153707/surface-water-delineation-report---environmental-protecti...?utm
8. Water quality – Determination of nitrate – Part 3: Spectrometric method using sulfosalicylic acid. Geneva: International Organization for Standardization, ISO 7890-3:1988. https://www.iso.org/obp/ui/#iso:std:iso:7890:-3:ed-1:v1:en
9. Water quality – Vocabulary. Geneva: International Organization for Standardization, ISO 6107. https://www.iso.org/obp/ui/en/#iso:std:iso:6107:ed-1:v1:en

2nd International Scientific Conference "Modern Problems in Geophysics", Proceedings,
ISBN 978-9941-36-562-1, ISSN 3088-4349, Tbilisi, Georgia, October 29-31, 2026

# RESULTS OF SOIL RESEARCH IN CHIATURA MUNICIPALITY AND MAP OF SOIL MANGANESE CONTAMINATION

***Shavliashvili L., *Kuchava G., *Shubladze E., **Rikadze Z., ***Gavardashvili G., *Tabatadze M.**

** Institute of Hydrometeorology, Georgian Technical University,Tbilisi, Georgia*
*** National Environmental Agency, Ministry of Environmental Protection and Agriculture of Georgia, Tbilisi, Georgia*
**** Tsotne Mirtskhulav Institute of Water Management, Georgian Technical University, Tbilisi, Georgia*
*gkuchava08@gmail.com, shavliashvililali09@gmail.com*

***Abstract.*** *Manganese production is intensively underway in Chiatura Municipality. Ore mining and processing began in 1879, which causes significant damage to the environment and the local population, especially when the deposit is developed in an open-cast manner. The aim of the study is to conduct a complex scientific field study in Chiatura Municipality, to assess the risks of pollution in ecosystems with manganese and some heavy metals (Cu, Zn, Pb, Cd, Co, Ni); based on the data obtained, a map of manganese pollution of soils in Chiatura Municipality was compiled to identify vulnerable points of pollution; ways to minimize the causes of soil degradation will be outlined. To solve the set tasks, soil samples were taken from the area surrounding the pollution source, from various villages and background areas of Chiatura at a depth of 0-5, 5-30 cm, as well as suspended solids and bottom sediments of the Kvirila River. The following were determined in the samples: pH, heavy metals: Cu, Zn, Pb, Cd, Ni, Co and the total form of manganese. The analyses were conducted using modern methods and equipment that meet and comply with European standards.*
*The following conclusions were reached:*

- *Villages of Chiatura Municipality are divided into high, medium and low pollution zones according to the manganese content in the soil.*
- *In villages with high pollution, the manganese content ranges from 11.09 to 147.43; in medium – 4.65 – 9.09 and in low – 0.12 – 1.64 g/kg.*
- *A map of manganese pollution in the soil of some villages of Chiatura Municipality has been compiled;*
- *The content of heavy metals in the soil is less than the MPC, only in some cases does the concentration of zinc and cadmium exceed the permissible norm;*
- *The concentration of manganese in the suspended solids and sediments of the Kvirila River in all cases exceeds the MPC, which once again indicates the pollution of the Kvirila River.*

***Key words:*** *Soil pollution; pollution map; heavy metals; suspended solids; sediments.*

## Introduction

Manganese mining is intensively carried out in Chiatura Municipality. Ore mining and processing began in 1879. On the one hand, it is a source of income and new job creation. However, it causes significant damage to the environment and the local population [1-3], especially when the deposit is developed in an open-cast manner. Due to its high profitability, this method is widely used in many countries of the world and currently, 80-85% of the ore is extracted by this method [4].

The manganese deposit is divided by the Kvirila River into two main parts – north-western and south-eastern. Each of them, in turn, is divided into separate uplands: Darkveti, Mgvimevi, Sarek, Tabagrebi, Zeda Rgani, Rgani, Merevi, Shukruti, Perevisa and others, on which the villages of the same name are located at an altitude of 500-800 m above sea level [4].

In Chiatura Municipality, the company "Georgian Manganese" carries out mining operations for manganese concentrate using the mine method, but licenses have also been issued to small private companies. There are approximately 20 deposits in the municipality, of which 9 are mine shaft and 11 are open-carier type. https://socialjustice.org.ge

Damage or contamination of soil and ground, and hence soil degradation, is expected during the quarry opening process. Industrial wastewater, which is generated during the ore woshing, contains large amounts of suspended solids, heavy metals, and manganese compounds and is discharged into the Kvirila River without treatment. During manganese mining, manganese oxide is released into the atmosphere in the form of dust. Wind and precipitation contribute to its spread and deposition in the territory of municipality [5]. Manganese is one of the most common chemical elements. It makes up about 0.1% of the Earth's crust. Manganese occurs in free form in nature. It is contained in the soil. Often, manganese is found in combination with iron and other minerals. Manganese is a gray-white metal that resembles iron. In a compact state, manganese is light gray, and in powder form it is grayish-black.

The main extraction of manganese ore is pyrolusite – $MnO_2$. Manganese is widely used in metallurgy, electrical and chemical industries, medicine, paint and varnish production, ceramics, glass, leather production, and photography. Manganese is also used as a mineral fertilizer in agriculture.

Manganese does not cause acute poisoning. It is a cumulative poison and causes the following occupational diseases: manganism, conjunctivitis, bronchial asthma, eczema, and allergic dermatitis [6].

## Study area and methods

In Chiatura Municipality, Raw calcareous soils developed on the weathering products of limestones and carbonate sandstones predominate. Yellow-brown forest soils are common from 400-500 m to 800-1000 m above sea level. Brown forest acid and Brown forest weakly unsaturated soils occur at altitudes of 800(900)-1800(2000) m above sea level. Alluvial soils are found on the lower terraces of the Kvirili River and its tributaries [7].

The paper presents the physico-chemical characteristics of the surrounding areas and village soils of the manganese processing enterprises of the Chiatura municipality, as well as the characterization of river Kvirila suspended solids and Bottom sediments.

To solve the set tasks, soil samples were taken from the area surrounding the pollution source; from various villages and background areas of Chiatura at a depth of 0-5, 5-30 cm; GPS was used during soil sampling.

The collected soil samples were processed: dried, pulverized, sieved, and the following were determined: pH, heavy metals: Cu, Zn, Pb, Cd, Ni, Co, and total manganese [8].

Samples of water, suspended solids and bottom sediments from the Kvirila River were also taken, in which the total manganese content was determined.

The analyses were conducted using modern methods and equipment that meet and comply with European standards:

1. Plasma emission spectrometer – ICP-OES; Epa method 200.8;
2. Soil digester – Milestone – Start D Microwave system;
3. pH-Meter – Milwaukee-Mi 150.

## Discussion of Results

Table 1 shows the Mn content in the soil of Chiatura Municipality, 2024-2026.

As can be seen from Table 1, the villages of Chiatura Municipality are divided into high, medium and low pollution zones according to the manganese content in the soil. The corresponding coordinates are indicated at each soil sampling point. In the villages with high pollution, the manganese content ranges from 11.09 to 147.43; in the medium – 4.65 – 9.09 and in the low – 0.12 – 1.64 g/kg. The following villages stand out with high manganese concentrations: village Buligauri – 71.70 (20.5 MPC); village Darkveti diversion-65.30 (18.7 MPC); village Sarkveltubani – 48.43 (13.8 MPC) and Tabagrebi – 37.60 (10.7 MPC) g/kg; medium concentration: village Kvemo Rgani – 9.62 (2.8 MPC); village Darkveti – 9.09 (2.6 MPC); village Tsirkvali – 7.33 (2.1 MPC) and village Perevisa – 5.21 (1.5 MPC) g/kg; and low concentration: village Kvemo Chalovani – 1.64 (0.5 MPC); village Tsinsofeli – 1.27 (0.4 MPC); village Kalauri -1.13 (0.3 MPC) g/kg, etc. (Fig. 1).

As studies show, the concentration of manganese in the territory of Chiatura Municipality varies, depending on the amount of ore in the soil profile. Accordingly, in areas with high manganese content, investor interest is also high.

In villages with high and medium manganese content, intensive mining activities are underway and there are many quarries. This was our goal to identify pollution hotspots and create a manganese pollution map of Chiatura Municipality (Fig.2).

**Table 1.** Mn content in the soil of some villages of Chiatura Municipality, 2024-2026.

| N | Sampling location | Coordinates | Analysis result |
|---|---|---|---|
| | | | g/kg |
| | **High pollution** | | |
| 1 | Village Darkveti 30 cm | X-363037 Y-4686104 | 65.30 |
| 2 | 100 m above Ltd "Jruchula" ,, | X-363795 Y-4686866 | 30.35 |
| 3 | Village Tabagrebi ,, | X-356605 Y-4692800 | 37.60 |
| 4 | Village Buligauri ,, | X-358606 Y-4683906 | 71.70 |
| 5 | Village Sarkveltubani ,, | X-356364 Y-4684674 | 48.43 |
| 6 | Chiatura, Chavchavadze Street ,, | X 0358386 Y 4682947 | 147.43 |
| 7 | Chiatura, Dekanozishvili Street ,, | X 0358873 Y 4683484 | 17.84 |
| 8 | Chiatura, Agmashenebeli Street ,, | X 0358991 Y 4683292 | 11.09 |
| | **Medium pollution** | | |
| 1 | Village Darkveti 30 cm | X-362421 Y-4687181 | 9.09 |
| 2 | Village Shukruti ,, | X-362827 Y-4680355 | 4.65 |
| 3 | Village Perevisa ,, | X-361622 Y-4681729 | 5.21 |
| 4 | Village Tsirkvali ,, | X-358474 Y-4687359 | 7.33 |
| 5 | Village Kvemo Rgani ,, | X-356721 Y-4687266 | 9.62 |
| | **Low pollution** | | |
| 1 | Village Tsinsofeli 30 cm | X-357360 Y-4681512 | 1.27 |
| 2 | Village Kalauri | X-362248 Y-4680674 | 1.13 |
| 3 | Village Sveri | X-360164 Y-4676148 | 0.31 |
| 4 | Village Mandaeti | X-362081 Y-4671019 | 0.53 |
| 5 | Village Tskhrukveti | X-357488 Y-4677652 | 0.07 |
| 6 | Village Skindori | X-357488 Y-4677652 | 0.12 |
| 7 | Village Zemo Chalovani | X-358396 Y-4688387 | 0.42 |
| 8 | Village Kvemo Chalovani | X-356895 Y-4691823 | 1.64 |
| 9 | Village Zemo Rgani | X-357349 Y-4686328 | 0.69 |

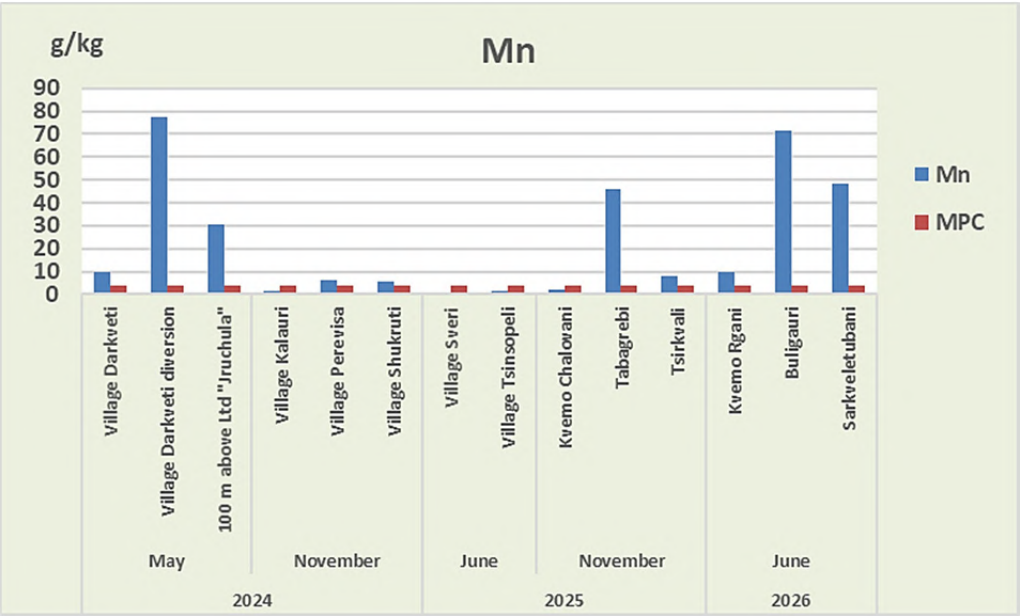



**Fig.1.** Manganese content in soils of Chiatura Municipality in 2024-2026.

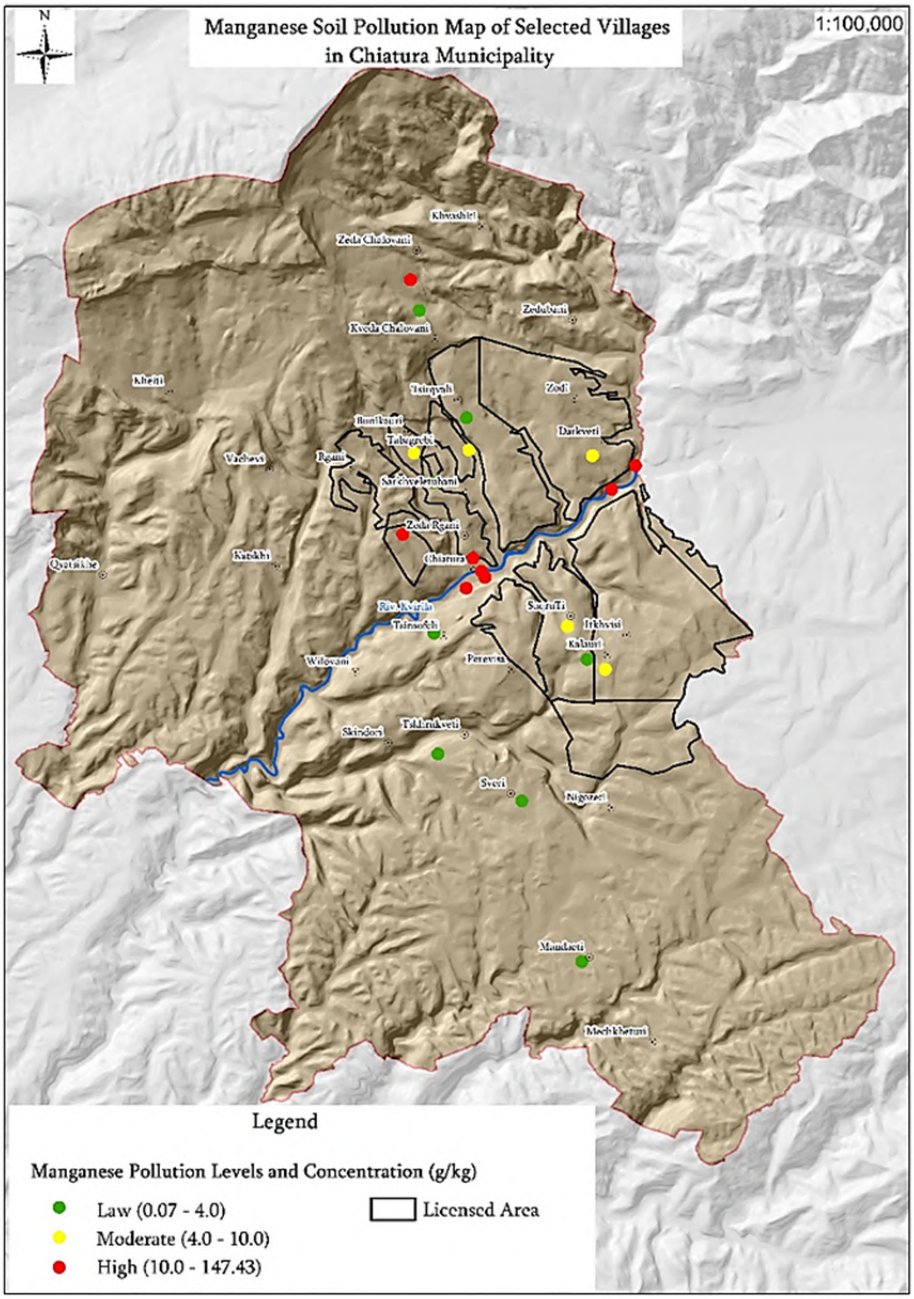
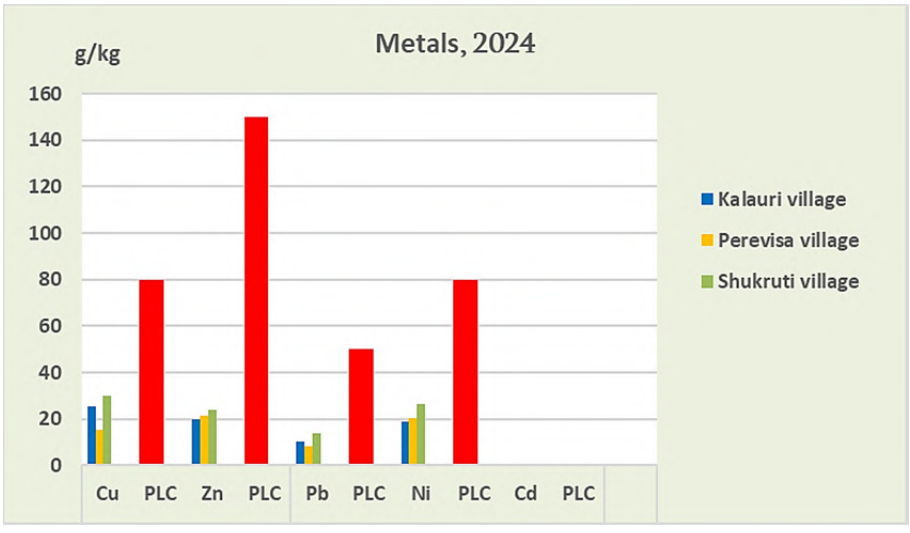
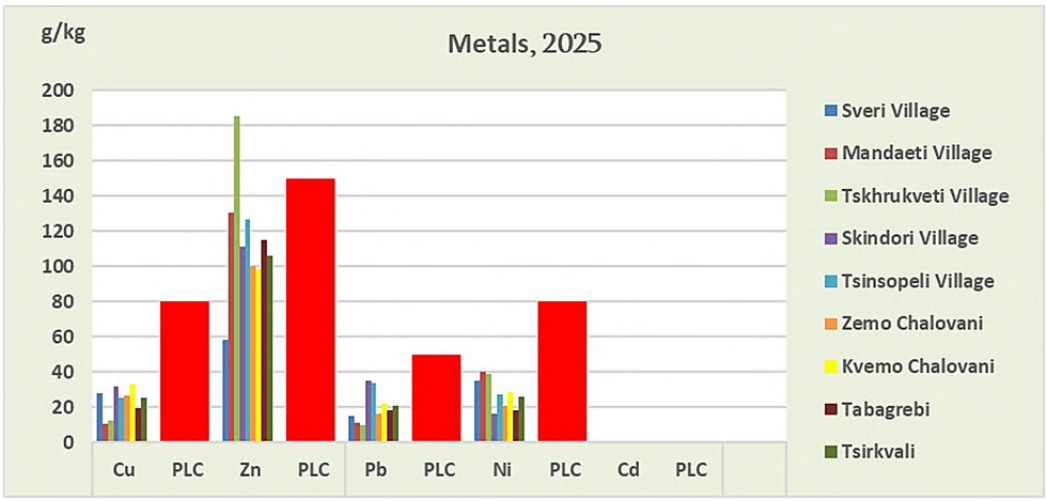



**Fig. 2.** Manganese contamination map of some villages in Chiatura Municipality.

a)



b)




c)

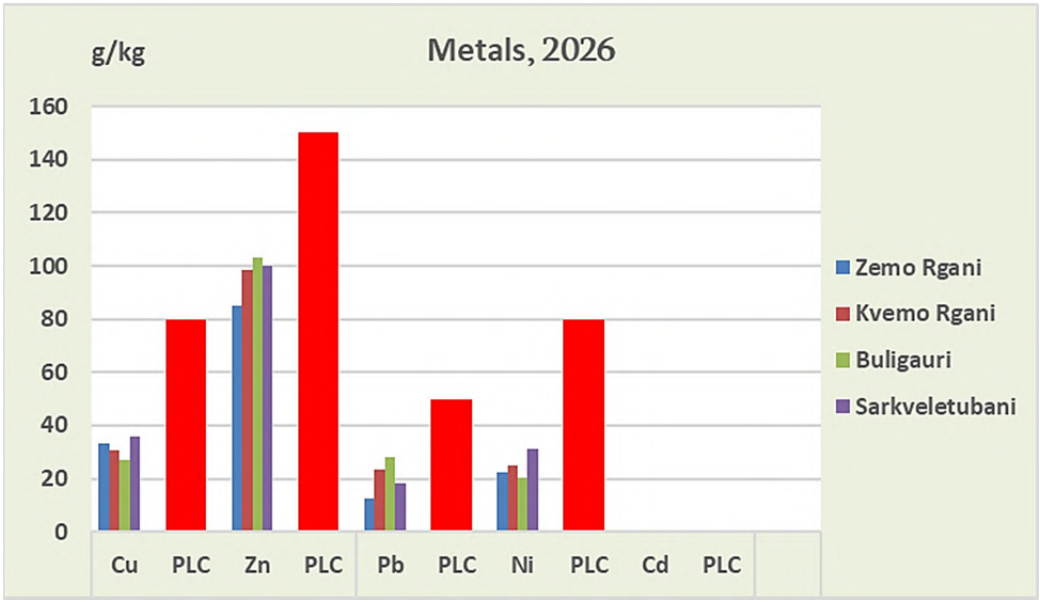



**Fig. 3.** (a), b), c)). Concentrations of heave metals in the soil of some villages of Chiatura Municipality, 2024-2026.

Fig. 2 shows of manganese pollution in the villages of Chiatura Municipality. The contours of the licensed areas are also shown. It should be noted that we assessed the manganese concentration in the study area according to the new regulations (Technical Regulations on the Degree of Soil Pollution, Resolution of the Government of Georgia N 501, 10.11.2025) [9]. According to these regulations, the maximum permissible concentrations have been increased, both for manganese (from 700 mg/kg to 3500 mg/kg), and for other heavy metals. Therefore, for other heavy metals (Cu, Zn, Pb, Cd, Ni, Co), we used Preventive Limit Concentration (PLC), which represents the upper limit values of heavy metal content, which can cause a negative impact on the healthy of soils used for agricultural purposes. Such concentrations represent a potentially acceptable risk when these preventive limits are not exceeded. As can be seen from the obtained graph (Fig. 3), in our case, of the heavy metals studied, only zinc and cadmium slightly exceeded the PLC in individual cases, while the remaining metals are within the norm.

Currently, none of the enrichment plants of the Chiatura Mining Enrichment Plant of Georgian Manganese Ltd has a functioning treatment plant, most of the hoppers and drums in the factories are out of order, and the sludge pipeline no longer exists at all, and the wastewater from the enrichment plants flows into the Kvirila River without treatment, which causes pollution of the river water with suspended particles and manganese compounds. It is also worth noting that the Kvirila River and its tributaries are significantly polluted by small manganese ore enrichment plants operating in the areas surrounding the city of Chiatura, which belong to other legal entities. None of them has more or less acceptable wastewater treatment plants.

An additional source of pollution of the Kvirila River is the aglomerat dump, where aglomerat obtained after processing intermediate products of various factories is deposited. This is an intermediate waste, which contains an average of 15.4% manganese and, if enrichment technologies are improved, it will be possible to obtain manganese concentrate from it. The dump is located on the left bank of the Kvirila River, where thousands of tons of aglomerat are stored [10]. The territory is not fenced and does not have drainage channels, which is why the aglomerat is washed into the Kvirila River along with atmospheric waters, which causes additional pollution of the Kvirila River.

Fig. 4 and Fig. 5 show the Mn content in the suspended solids and sediments of the Kvirila River. As can be seen from the results, their content in the river is high and in all cases exceeds the MPC.

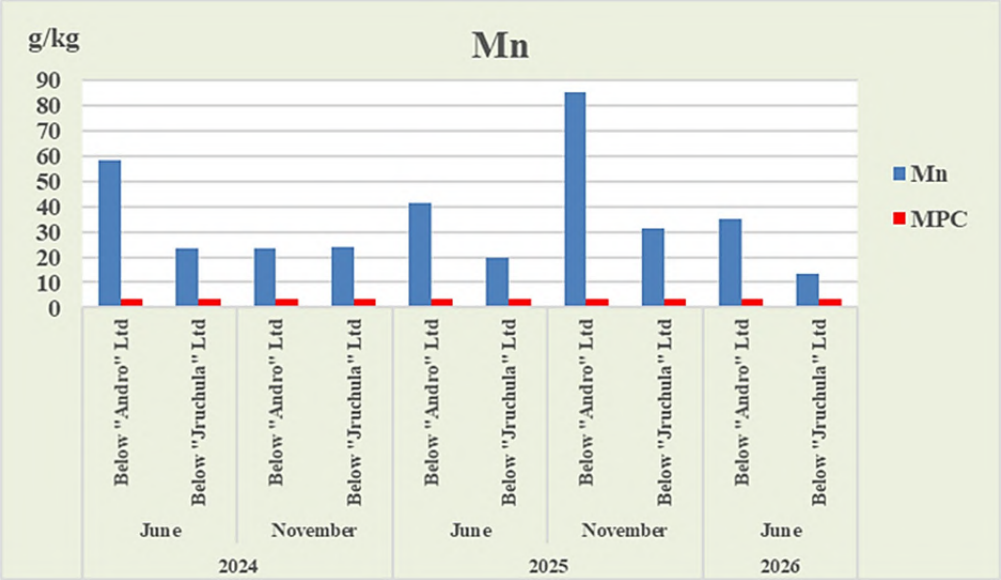



**Fig. 4.** Mn content in the suspended solids of the Kvirila River, 2024-2026.

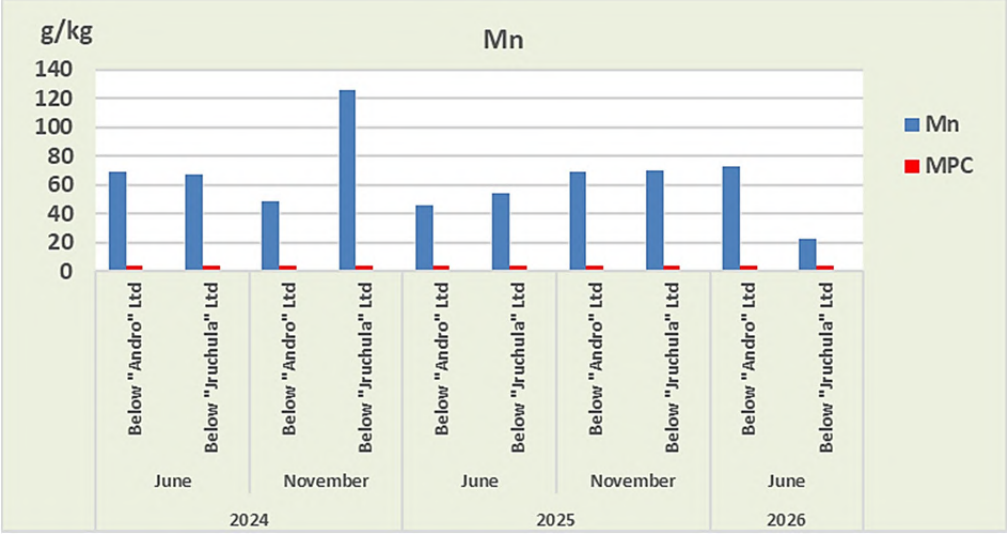



**Fig. 5.** Mn content in the sediments of the Kvirila River, 2024-2026.

## Conclusion

- High, medium and low levels of manganese contamination in the soil of some villages of Chiatura Municipality have been identified;
- In villages with high contamination, the manganese content ranges from 11.09 to 147.43; in medium – 4.65 – 9.09 and in low – 0.12 – 1.64 g/kg;

- A map of manganese contamination in the soil of some villages of Chiatura Municipality has been compiled;
- The content of heavy metals in the soil is less than the PLC, only in some cases the concentration of zinc and cadmium exceeds the permissible norm;
- The concentration of manganese in the suspended solids and sediments of the Kvirila River in all cases exceeds the MPC, which once again indicates the pollution of the Kvirila River.

**Acknowledgement:** The research was performed with the support of the Shota Rustaveli National Science Foundation of Georgia, Grant No. FR-23-6375.

## Reference

1. Tsereteli E., Gobejishvili R., Bolashvili N., Gaphrindashvili G., Nanobashvili T. //Condition of natural exodinamic catastrophe and The risk of anthropogenic load in Georgia, their management Optimizing actions// V. Bagrationi Institute of Geography Institute Collection, N 4 (83). Tbilisi, 2012, pp. 50-63. http://pdf.wri.org/mining_critical_ecosystems_full.pdf
2. "The impact of the extractive industry in developing countries", the Earth's Friends – Europe, 2007. http://www.foeeurope.org/corporates/Extractives/social.pdf
3. Avqopashvili Guranda, Ghoghoberidze Avtandil //Heavy Metal Content in Soils of Some Industrial Regions of Georgia – Publishing House "Samshoblo"//2022, 232 p.
4. Gugushvili Tamar, Tsiklauri Nino //Handbook for the Population Affected by Manganese Mining, Association Green Alternative// Tbilisi, 2010, 26 p.
5. Polluted air and water – Discussion on ecological problems of Chiatura: 2018. http://liberali.ge/news/view/15643/dabindzurebuli-haerida-tsyali--diskusia-chiaturis-ekologiur-problemebze-
6. Order of the Minister of Labor, Health and Social Affairs of Georgia on the approval of the norms of the quality of the environment N 297 / N, 16 August. Tbilisi, 2001.
7. Urushadze Tengiz // Agro-soil knowledge – Free and Agrarian University Publishing House// Tbilisi, 2020, 317 p.
8. Fomin G. S., Fomin A.G. //soil, quality control and environmental safety on international standards. – Moscow VNII Standard// 2001, 300 p.
9. Order of the Minister of Labor, Health and Social Protection of Georgia No. 501, on Approval of Technical Regulations on the Degree of Soil Pollution, 10.11.2025).
10. LEPL Grigol Tsulukidze Mining Institute. Scientific-Research Firm “Gama”. Ltd “Georgian Manganese”. Waste Management Plan Generated in the Process of Current Activities of the Chiatura Mining and Enrichment Plant. Chiatura, 2010.

2nd International Scientific Conference "Modern Problems in Geophysics", Proceedings,
ISBN 978-9941-36-562-1, ISSN 3088-4349, Tbilisi, Georgia, October 29-31, 2026

# ASSESSMENT OF HEAVY METAL CONTAMINATION RISKS IN THE SOILS OF CHIATURA MUNICIPALITY

***Shavliashvili L., *Kuchava G., *Shubladze E., **Rikadze Z., ***Gavardashvili G., *Mdivani S.**

** Institute of Hydrometeorology, Georgian Technical University, Tbilisi, Georgia*
*** National Environmental Agency, Ministry of Environmental Protection and Agriculture of Georgia, Tbilisi, Georgia*
**** Tsotne Mirtskhulav Institute of Water Management, Georgian Technical University, Tbilisi, Georgia*
*gkuchava08@gmail.com, shavliashvililali09@gmail.com*

***Abstract.*** *One of the study's objectives is to assess the risks of soil contamination by manganese and certain heavy metals (Cu, Zn, Pb, Cd, Co, Ni) in the Chiatura Municipality, using parameters such as the contamination hazard coefficient, contamination concentration coefficient, total contamination characteristic, and contamination index. To address the set objectives, soil samples were collected from the area adjacent to the pollution source, various villages in Chiatura, and background locations at depths of 0–5 cm and 5–30 cm. The collected samples were analyzed for pH, heavy metals (Cu, Zn, Pb, Cd, Ni, Co), and total manganese content. The analyses were conducted using modern methods and equipment that meet and comply with European standards.*

*The following conclusions have been reached:*

- *The risks of heavy metal contamination in the soils of Chiatura Municipality have been assessed, including the contamination hazard coefficient, contamination concentration coefficient, aggregate contamination characteristic, and contamination index;*
- *High, medium, and low levels of manganese contamination in the soil have been identified across various villages in Chiatura Municipality: manganese content ranges from 11.09 to 147.43 g/kg in villages with high contamination, 4.65 to 9.09 g/kg in those with medium contamination, and 0.12 to 1.64 g/kg in those with low contamination;*
- *The primary criteria used to assess the risk of soil contamination by heavy metals are the Maximum Permissible Concentration (MPC) or Preventive Limit Concentration (PLC) and soil Clarke values;*
- *The contamination concentration coefficient exceeds the background level in all cases, indicating the extent to which the element's concentration is elevated relative to the background; this is particularly pronounced in the case of manganese;*
- *Based on the aggregate pollution index, the village of Kvemo Chalovani falls into the "hazardous" category, with an index value of 40.21; meanwhile, the villages of Kvemo Rgani and Buligauri fall into the "exceptionally hazardous" category, with index values of 154.05 and 1041.77, respectively;*
- *According to the soil pollution index, the soil is contaminated only with manganese and falls into the "polluted" category, while the other metals fall into the "clean" category.*

***Key words:*** *Soil contamination; heavy metals; contamination hazard; contamination coefficient; aggregate characteristic; contamination index.*

## Introduction

Chiatura Municipality is one of the ecologically vulnerable areas in Georgia; against the backdrop of climate change, its primary challenge is the intensification of natural disasters – a process exacerbated by the municipality's mining activities (specifically manganese production). Ore extraction involves numerous conflicting issues. On one hand, it serves as a source of income and creates new jobs. On the other hand, it causes significant harm to the environment and the local population. Potential consequences include large-scale deforestation and the destruction of vegetation cover; significant landscape degradation, which negatively impacts biodiversity; the contamination of ecosystems and food products; soil degradation; and substantial material losses, among others [1]. Consequently, the socio-economic condition of the population deteriorates markedly, and migration processes intensify [2,3]. This issue is significant for mountainous regions, includ-

ing the territory of the Chiatura Municipality, whose population has been enduring the extremely negative impact of ore extraction for over a century.

Manganese is one of the most abundant chemical elements. It makes up approximately 0.1% of the Earth's crust. Manganese occurs in nature in its free state. It is found in the soil. Manganese often appears in combination with iron and other minerals. Manganese is a greyish-white metal that resembles iron. In its compact form, manganese is light grey, whereas in powder form, it is greyish-black.

Manganese is widely used in metallurgy, the electrical and chemical industries, medicine, the production of paints and varnishes, ceramics, glass and leather manufacturing, and photography. Manganese is also used as a mineral fertilizer in agriculture.

Manganese does not cause acute poisoning. It is a cumulative toxin that causes the following occupational diseases: manganism, coniogenic bronchitis, bronchial asthma, manganoconiosis, eczema, and allergic dermatitis [4].

## Study Area and Methods

Carbonate-sandstones, brown, yellow-brown, and alluvial soils are the predominant soil types in the Chiatura Municipality [5, 6].

This paper presents the physicochemical characterization of soils from rural areas and locations adjacent to manganese processing plants in the Chiatura Municipality.

To address the set objectives, soil samples were collected from the area adjacent to the pollution source, as well as from various villages in Chiatura and from background locations, at depths of 0–5 cm and 5–30 cm; GPS was used during the sampling process.

The collected soil samples underwent processing – drying, loosening, and sieving – and the following parameters were determined: pH, heavy metals (Cu, Zn, Pb, Cd, Ni, Co), and the total form of manganese [7].

Chemical analyses were conducted at the accredited laboratory for atmospheric air, water, and soil analysis of the Environmental Pollution Monitoring Department (under the National Environmental Agency of the Ministry of Environmental Protection and Agriculture of Georgia) and at "Scientific Research Center Gama" LLC.

The study examines the following indicators of heavy metal contamination in agricultural and non-agricultural soils: the contamination hazard coefficient, the contamination concentration coefficient, the aggregate contamination characteristic, and the contamination index.

Soil contamination was assessed using the following methodology (Technical Regulation on Soil Contamination Levels, Decree of the Government of Georgia No. 501, 10.11.2025) [8]:

Statistical data processing was performed in accordance with the literature [9].

Analyses were conducted using modern methods and equipment that meet and comply with European standards, specifically:

1. Plasma emission spectrometer – ICP-OES; EPA Method 200.8;
2. Soil digestion system – Milestone Start D microwave system;
3. pH meter – Milwaukee Mi 150.

## Discussion of the results

It should be noted that the assessment of manganese concentration in the study area was conducted in accordance with the new regulations [8]. These regulations have raised the maximum permissible concentration limits for both manganese and other heavy metals. Therefore, for other heavy metals (Cu, Zn, Pb, Cd, Ni, Co), we utilized a preventive limit value (PLC), which represents a potentially acceptable level of risk provided that these preventive limits are not exceeded.

The primary criteria used to assess the risk of heavy metal contamination in the soil are the Maximum Permissible Concentration (MPC) [8] or the Preventive Limit Concentration (PLC) [8], as well as soil Clarke values [10].

Based on soil manganese content, the villages of Chiatura Municipality are categorized into zones of high, medium, and low contamination. Corresponding coordinates are indicated for each soil sampling point. Manganese content ranges from 11.09 to 147.43 g/kg in high-contamination villages, 4.65 to 9.09 g/kg in medium-contamination villages, and 0.12 to 1.64 g/kg in low-contamination villages.

Thus, in cases of high and moderate pollution, the manganese concentration exceeds the maximum permissible concentration (MPC), indicating a high risk of pollution in these areas; conversely, in rural soils with low pollution levels, the manganese content is below the MPC, and the risk of pollution is correspondingly lower.

Regarding other heavy metals (Cu, Zn, Pb, Cd, Ni, Co) in the soils of certain villages in the Chiatura Municipality, the pollution hazard coefficient ($K_0$) exceeds 1 only in the cases of zinc, cadmium, and manganese. For zinc, the value often approaches 1 and exceeds it in only one instance (the village of Tskhrukveti). A similar situation applies to cadmium; the $K_0$ value exceeds 1 in the villages of Shukruti and Skindori. In the case of manganese, however, there are more instances where the hazard coefficient exceeds 1; specifically, this was observed in the following villages, with the corresponding values: Perevisa – 5.21 (4.01 MPC); Shukruti – 4.65 (3.58 MPC); Kvemo Chalovani – 1.64 (1.26 MPC); Tabagrebi – 37.60 (28.92 MPC); Tsirkvali – 7.33 (5.64 MPC); Kvemo Rgani – 9.62 (7.4 MPC); Buligauri – 71.70 (55.15 MPC); and Sarkveletubani – 48.43 (37.25 MPC) mg/kg. In all other cases, the hazard coefficient ($K_0$) is less than 1.

In the soils of certain villages within the Chiatura Municipality, the coefficient of concentration relative to the Clarke value ($K_k$) is high only for zinc, lead, cadmium, and manganese. Specifically, the zinc content is highest in the village of Tskhrukveti, exceeding the Clarke value by a factor of two; lead content is highest in Skindori and Tsinsopeli, also exceeding the Clarke value by a factor of two; cadmium content exceeds the Clarke value by a factor of 1–5 across all studied villages; and manganese concentration exceeds the Clarke value by a factor of 1–71 in villages characterized by average to high manganese levels.

It is noteworthy that the risk of pollution became more apparent when comparisons were made against the Clarke value – considering both the quantity of metals and the relevant Maximum Permissible Concentrations (MPC) and Preventive Limit Concentration (PLC). Specifically, lead was identified as an additional polluting metal; furthermore, while only 2–3 villages exceeded the MPC and PLC limits, a significantly larger number exceeded the Clarke value – a discrepancy we attribute to the fact that the Clarke value reflects the actual abundance of heavy metals in the Earth's crust more accurately than the MPC and PLC standards do.

The risk of contamination is greater the higher the hazard class of the substances being monitored. Among the heavy metals we studied, cadmium, lead, and zinc fall into the first hazard class; cobalt, nickel, and copper into the second; and manganese into the third.

**The pollution concentration coefficient** indicates the extent to which the concentration of an element exceeds the background level.

To determine the background value, the total form of the chemical element in the soil is measured; the total form is likewise measured in cases of technogenic pollution.

In all instances, the pollution concentration coefficient (Kc) exceeds the background level, indicating the degree to which the element's concentration is elevated relative to that background; this is particularly pronounced in the case of manganese.

**The aggregate pollution index** is calculated based on elements with a pollution coefficient greater than 1.

Based on the data, the village of Kvemo Chalovni falls into the "hazardous" category, as its aggregate pollution index (Zc) is 40.21; meanwhile, the villages of Kvemo Rgani and Buligauri fall into the "extremely hazardous" category, with aggregate pollution indices (Zc) of 154.05 and 1041.77, respectively.

**Soil contamination index**: if $\alpha > 1.0$, the soil is "contaminated" – indicating an unfavorable sanitary-hygienic environmental condition, and soil remediation is required;

if $0.75 < \alpha < 1.0$, the soil is "problematic" – levels are close to or equal to the maximum permissible concentration; if $\alpha < 0.75$, the soil is "clean."

When hygienically assessing soil "quality" based on the total content of heavy metals, the grading scale for the soil contamination index α: here $\alpha < 0.75$ is "clean," $0.75 < \alpha < 1.0$ is "problematic," and $\alpha > 1.0$ is "contaminated" – statistically aligning with the ecological-hygienic soil condition categories defined by the Zc indicator, corresponding to the heavy metal total contamination categories of "hazardous" ($Zc > 32$) and "extremely hazardous".

Based on the data, the soil contamination index (α) exceeds 1.0 only for manganese. In this case, the α value for all heavy metals other than manganese is below 0.75.

According to the soil contamination index, the soil is contaminated only with manganese and falls into the "contaminated" category, while the other metals fall into the "clean" category.

Table 1 presents indicators of the degree of soil contamination by heavy metals.

**Table 1.** Pollution level indicators.

| # | Heavy metal | Hazard class | $C_f$, mg/kg | Clarke | Kc – Concentration coefficient | $K_0$ | Zc Total pollution characteristic | α Soil pollution index |
|---|---|---|---|---|---|---|---|---|
| | | **Village Buligauri** | | | | | | |
| **1** | **Cu,** mg,kg | II | 3.16 | 47 | 8.60 | 0.34 | | 0.05 |
| **2** | **Zn,** mg,kg | I | 19.69 | 83 | 5.23 | 0.69 | | 0.10 |
| **3** | **Pb,** mg,kg | I | 8.16 | 16 | 3.45 | 0.56 | | 0.08 |
| **4** | **Mn,** mg,kg | III | 70.0 | 1000 | 1024.29 | 55.15 | 1041.77 | 7.88 |
| **5** | **Co,** mg,kg | II | 1.27 | 18 | 3.35 | 0.14 | | 0.02 |
| **6** | **Cd,** mg,kg | I | 0.19 | 0.13 | 1.74 | 0.66 | | 0.09 |
| **7** | **Ni,** mg,kg | II | 18.21 | 58 | 1.11 | 0.25 | | 0.04 |
| | | **Village Kvemo Rgani** | | | | | | |
| **1** | **Cu,** mg,kg | II | 3.16 | 47 | 9.77 | 0.39 | | 0.06 |
| **2** | **Zn,** mg,kg | I | 19.69 | 83 | 4.99 | 0.66 | | 0.09 |
| **3** | **Pb,** mg,kg | I | 8.16 | 16 | 2.87 | 0.47 | | 0.07 |
| **4** | **Mn,** mg,kg | III | 70.0 | 1000 | 137.43 | 7.40 | 154.05 | 1.06 |
| **5** | **Co,** mg,kg | II | 1.27 | 18 | 2.78 | 0.12 | | 0.02 |
| **6** | **Cd,** mg,kg | I | 0.19 | 0.13 | 0.84 | 0.32 | | 0.05 |
| **7** | **Ni,** mg,kg | II | 18.21 | 58 | 1.37 | 0.31 | | 0.04 |
| | | **Village Chalovani** | | | | | | |
| **1** | **Cu,** mg,kg | II | 3.16 | 47 | 10.49 | 0.41 | | 0.06 |
| **2** | **Zn,** mg,kg | I | 19.69 | 83 | 4.99 | 0.66 | | 0.09 |
| **3** | **Pb,** mg,kg | I | 8.16 | 16 | 2.75 | 0.45 | | 0.06 |
| **4** | **Mn,** mg,kg | III | 70.0 | 1000 | 23.43 | 21.26 | 40.21 | 3.04 |
| **5** | **Co,** mg,kg | II | 1.27 | 18 | 1.40 | 0.06 | | 0.009 |
| **6** | **Cd,** mg,kg | I | 0.19 | 0.13 | 2.0 | 0.76 | | 0.11 |
| **7** | **Ni,** mg,kg | II | 18.21 | 58 | 1.15 | 0.35 | | 0.05 |

## Conclusion

- The risks of heavy metal contamination in the soils of Chiatura Municipality have been assessed, including the contamination hazard coefficient, contamination concentration coefficient, aggregate contamination characteristic, and contamination index;
- High, medium, and low levels of manganese contamination have been identified in the soils of certain villages in Chiatura Municipality: manganese content ranges from 11.09 to 147.43 g/kg in villages with high contamination, 4.65 to 9.09 g/kg in those with medium contamination, and 0.12 to 1.64 g/kg in those with low contamination;
- The primary criteria used to assess the risk of soil contamination by heavy metals are the Maximum Permissible Concentration (MPC) or the Preventive Limit Concentration (PLC) and soil Clarke values;
- The contamination concentration coefficient exceeds the background level in all cases, indicating the extent to which the element's concentration has increased relative to the background; this is particularly pronounced in the case of manganese;
- Based on the total pollution index (Zc), the village of Kvemo Chalovani falls into the "hazardous" category (Zc = 40.21), while the villages of Kvemo Rgani and Buligauri fall into the "extremely hazardous" category, with total pollution indices of 154.05 and 1041.77, respectively;
- According to the soil pollution index, the soil is contaminated only with manganese and falls into the "polluted" category, whereas the other metals fall into the "clean" category.

**Acknowledgement:** The research was performed with the support of the Shota Rustaveli National Science Foundation of Georgia, Grant No. FR-23-6375.

## Reference

1. "Obtaining of Minerals and Ecosystems in Critical Condition: Risk Definition", World Resources Institute, Washington, 2003. http://pdf.wri.org/mining_critical_ecosystems_full.pdf
2. "The impact of the extractive industry in developing countries", the Earth's Friends – Europe, 2007. http://www.foeeurope.org/corporates/extractives/social.pdf
3. Tsereteli E., Gobejishvili R., Bolashvili N., Gaphrindashvili G., Nanobashvili T., Condition of natural exodinamic catastrophe and The risk of anthropogenic load in Georgia, their management Optimizing actions. // V. Bagrationi Institute of Geography Institute Collection, # 4 (83). Tbilisi, 2012, pp. 50-63.
4. Order of the Minister of Labor, Health and Social Affairs of Georgia on the approval of the norms of the quality of the environment N 297 / N, 16 August. Tbilisi, 2001.
5. Urushadze T., Agro-soil knowledge. // Free and Agrarian University Publishing House, Tbilisi, 2020, 317 p.
6. Soils of Georgia (Scale 1:500,000) – (Editor-in-Chief: Academician T. Urushadze) "Kartograpi" Publishing House, Tbilisi, 2019.
7. Fomin G. S., Fomin A.G., Soil, quality control and environmental safety on international standards. // Moscow VNII Standard, 2001, 300 p.
8. Order of the Minister of Labor, Health and Social Protection of Georgia No. 501, on Approval of Technical Regulations on the Degree of Soil Pollution, 10.11.2025.
9. Sirbiladze G., Data Analysis and Statistics, TSU Faculty of Exact and Natural Sciences, Department of Computer Sciences, 2013, 152 p. https:/digitallibrary.tsu.ge
10. Clarkes of elements in the earth's crust according to different authors (Vinogradov, 1962). (in Russian)

2nd International Scientific Conference "Modern Problems in Geophysics", Proceedings,
ISBN 978-9941-36-562-1, ISSN 3088-4349, Tbilisi, Georgia, October 29-31, 2026

# DEVELOPMENT PROSPECTS OF GEORGIA'S BLACK SEA PORTS AND THE STRATEGIC IMPORTANCE OF THE ANAKLIA DEEP-SEA PORT

***,**Makalatia I.,*Darbaidze S., *Kandashvili Z., *Melia S.**

**Ivane Javakhishvili Tbilisi State University, Tbilisi, Georgia*
***M. Nodia Institute of Geophysics of the I. Javakhishvili Tbilisi State University, Tbilisi, Georgia*
*irma.makalatia@ens.tsu.edu.ge*

***Abstract.*** *Georgia's strategic geographical location plays an important role in linking the transport systems of Europe and Asia. To make full use of the country's economic development and transit potential, it is necessary to develop the existing port infrastructure, expand the capacity of the ports of Poti and Batumi, modernize the Supsa and Kulevi terminals, and attract new investment. In recent years, the growth of cargo flows in the region has increased the load on Georgia's transport infrastructure. The throughput capacity of the existing ports may prove insufficient to receive and process in full the cargo flows expected in the future. This circumstance gives rise to the need to develop additional port and transit capacities. In this regard, the Anaklia Deep Sea Port can play a significant role in expanding Georgia's port system and in increasing and strengthening the country's transit function. Based on an analysis of scientific literature and statistical data, the article examines the geographical location, functional capabilities, and existing limitations of Georgia's main ports. It also analyzes their advantages and challenges, with particular attention paid to the possible role of the Anaklia Deep Sea Port in Georgia's port system.*

***Key words:*** *Black Sea, Anaklia deep-water port, Breakwater, Safety, Cargo turnover.*

## Introduction

The Middle Corridor has become established as the shortest and most important trade and economic route between Europe and Asia, and Georgia plays a key role in it. The existing ports are growing, and the role of the Middle Corridor in connecting West and East is increasing. The ports of Poti and Batumi are cur-




**Fig. 1** Important ports of the Black Sea.

rently operating at maximum capacity. In January–April 2026, cargo turnover increased by 21% compared with the previous years, and over the past four years a cumulative growth of 46% has been recorded. The Black Sea basin has long been regarded as one of the important transport routes connecting Europe and Asia. Through Georgia's territory, the Caspian Sea region, Central Asia, the South Caucasus, and the Black Sea are linked to one another, while from the Black Sea ports cargo moves toward Europe. Accordingly, the Anaklia Deep Sea Port is becoming the main hub connecting cargo flows from east to west. The location of the Anaklia port, including its proximity to the conflict zone, further increases its economic and geopolitical significance. The development of the port may promote the economic revitalization of the region, the employment of the local population, and the improvement of socioeconomic conditions. At the same time, the creation of additional economic links and opportunities for cooperation may have a positive effect on shaping an environment conducive to the peaceful resolution of the conflict.

## Research Objective

Two seaports for maritime trade operate in Georgia, and both have great potential to become major ports and commercial centers, to take part in the network of international transport corridors, and to become involved in international transit shipping. The expansion and development of the port of Batumi are constrained by natural and geographical conditions and by the dense urban development of the city. The port of Poti urgently requires reconstruction and modernization, while the Kulevi and Supsa terminals are oriented toward petroleum products. It is worth noting that the depth of the Anaklia port is 17.5 meters, which ensures the safe movement and maneuvering of large-dimension vessels. According to official information from the Ministry of Economy of Georgia for 2026, after the completion of the dredging works the design depth will be approximately 17.5 meters, a breakwater 1,376 meters in length will be built, and the turning basin will be 271 meters in length. These parameters are designed to accommodate large container ships of the Panamax and Post-Panamax classes. The marine infrastructure works are being carried out, together with Georgian partners, by the Belgian company Jan De Nul, one of the world's leading marine construction companies. The deep sea port is being developed under the "Landlord" model, whereby the state creates and owns the main port infrastructure, while private partners ensure the development and operation of the terminals. On the basis of this model, an approach to port-sector management that corresponds to global best practice is being introduced (www.worldbank.org). The state assumes the obligation to provide, alongside the creation of the port infrastructure, the access road and railway to Anaklia, while the investments required for the construction of the container and bulk cargo terminals at the port will be made by private operators and international investors.

The construction of the port has a significant impact on the morphodynamic processes of the coastal zone and may intensify erosion. The construction of the breakwater and the approach channel alters the natural regime of coastal currents and impedes the movement of sediment. As a result, erosion processes intensify in some sections, while a large part of the solid material accumulates on the other side of the breakwater. These processes alter the stability of the coastline and increase its vulnerability [5.6]. It is essential to conduct continuous monitoring of the coastal zone adjacent to the port and to ensure the active involvement of Black Sea specialists, so that changes occurring in coastal processes can be identified in a timely manner and, where necessary, appropriate measures can be taken, which will help preserve the natural morphodynamic balance of the coast.

Several ports in the Black Sea basin stand out for their particular importance, both in terms of cargo turnover and the depth of their water areas. Among them, the ports of Constanța and Novorossiysk deserve mention. The article presents ten significant ports of the Black Sea basin and their parameters for 2029. (Fig.2 )

After the completion of the first phase, by 2030 the port will handle 600,000–790,000 containers per year and after the completion of all stages, the port will handle a total of 100 million tons of cargo per year, of which container cargo will be only one component. The commissioning of the deep sea port at Anaklia will affect our country's energy sector, in view of the planned "Black Sea submarine cable," which involves connecting Europe and Asia through an energy transit country. The massive deployment of renewable energy infrastructure is under way, and the use of solar and wind energy to power the port will reduce carbon emissions and have a positive effect on the natural environment.

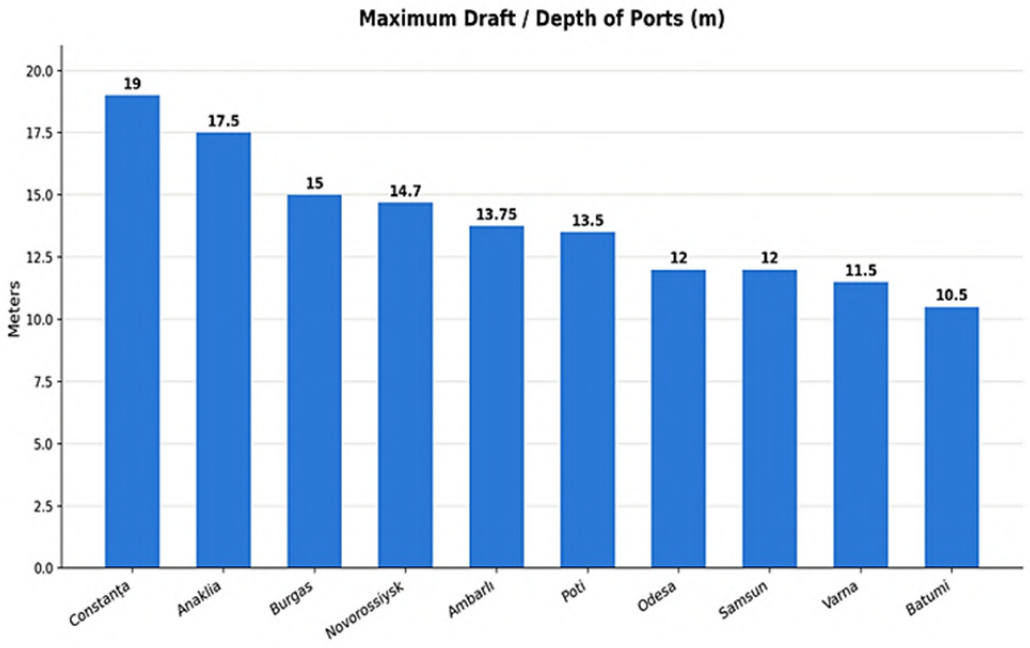



**Fig. 2.** Ten significant ports of the Black Sea basin and their parameters for 2029.

In 1986, a large group of scientists and specialists from the Georgian Coast Protection ("Saknapirdatsva") and the Georgian City Construction Project (Sakkalakmshenproekti) studied the surrounding area and concluded that Anaklia is a naturally favorable and strategic location for the construction of a deep-sea port. This was facilitated by the Enguri submarine canyon on the seabed. A canyon is a deep, steep-sided, river-valley-like depression cut into the continental slope, the head of which begins within the shelf. It absorbs a large part of the sediment and solid load carried down by rivers and also hinders the transport of material carried by the long shore current moving from the north. The site does not require extensive dredging and, importantly, there is no dense population in its vicinity, which creates favorable conditions for the expansion and development of infrastructure [7]. The ports of Poti and Batumi are located in densely built-up zones, and because of congested urban development, their potential for expansion is limited. In addition, most of the sand and sediment carried down by the Enguri River is "lost" in the canyon (it descends into deep water), so natural sediment accumulation on the coast is comparatively smaller. On the one hand, this reduces the risk of the port channel silting up; on the other hand, this process is the main cause of coastal erosion in the zone adjacent to Anaklia (Fig. 3).

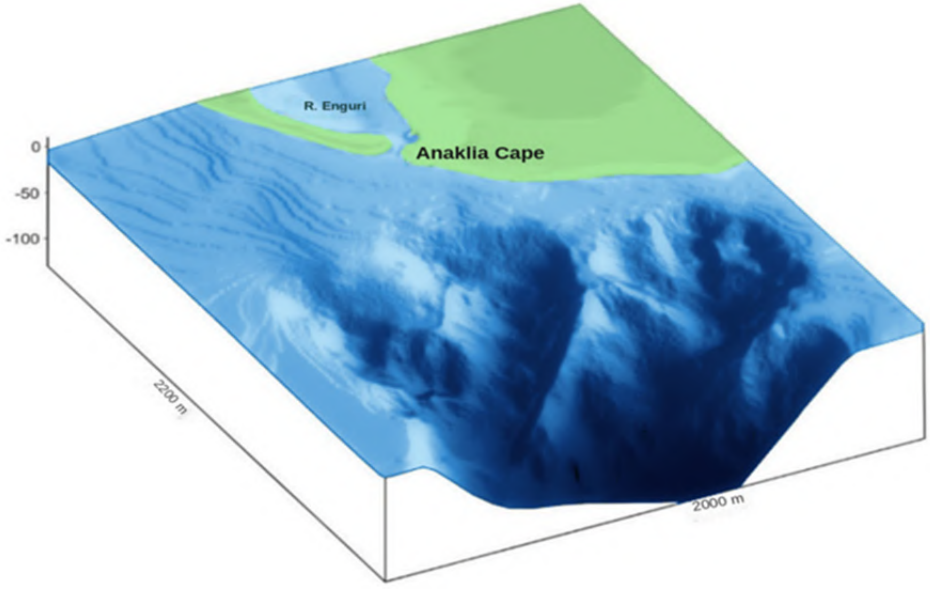



**Fig. 3** Anaklia Canyon.

## Conclusion

Georgia is part of the transit route between Europe and Asia, and the development of the Middle Corridor increases the demand placed on Georgia's transport infrastructure. Attempts to create the Anaklia port have been made more than once; the topic became particularly active in the 1970s, as evidenced by the master plans created for the port (by Zenkovich in 1974, A. Kiknadze in 1984, Eragia in 2003, and, most recently, Khazaradze in 2017), which, for a variety of reasons, were not implemented. Former Prime Minister of Georgia Mr. Otar Patsatsia invested great effort in this undertaking: to carry out the construction of the port, a 220-meter-long pier was built on the coast so that passenger ships could call at Anaklia, but, unfortunately, this idea was not fully realized [2].

The Anaklia Deep Sea Port will soon establish its place alongside the large ports of the Black Sea and become one of the key gateways of the Middle Corridor in the region. An approach to port-sector management that corresponds to global best practice is being introduced, and the port will have sufficient space for development, which will make its expansion possible over time. It will become a guarantee of our country's prosperity, especially for the population of the border area. The deep sea port will connect the transport systems of Europe and Asia and will secure its place as a connecting hub between the northern and southern corridors. It will attract international investment and increase Georgia's regional and international significance.

## References


1. Anaklia Development Consortium" Ltd., Anaklia Deep Water Harbor Environmental Impact Assessment Report (Project). 2017.
2. Adeishvili M., Georgia – A Black Sea Country. (Book) 2022.
3. Alpenidze M., Retrospective of Coastal Defense of the Seas. // Geographical Society of Georgia. Tbilisi, 2024, pp.51–69.
4. Georgia's Fifth National Communication and First Biennial Transparency Report will be submitted to the UNFCCC Secretariat by 31 December 2024. https://mepa.gov.ge/
5. Makalatia I., Bilashvili K., Kereselidze D., Morphodynamics of the Black Sea coastal zone of Adjara and Modern approaches. // Baku 2024.
6. Makalatia I., Bilashvili K., Kereselidze D., Changes caused by Chorokhi river sediment and modern approaches in Adjara coastline. // Proceedings of the Institute of Geophysics named after Mikheil Nodia of Tbilisi State University. Tbilisi, 2023, pp. 102-104.
7. Makalatia I., Tsivtsivadze N., Kereselidze D., The strategic importance and challenges of the eastern coast of the Black Sea, the way to the economic development of Georgia.Tbilisi, Georgia 2025.
8. Mirzayeva N., Anaklia Project: Strategic Importance and Challenges. // Journal of Balkan and Black Sea Studies Year, Issue 14, 2025, pp. 51–76.
9. Tsivtsivadze N., Khatiashvili E., Makalatia I., Jorbenadze N., Ivanov G., Dependencies reflecting quantitative changes in phyto-and zooplankton in the Tbilisi Reservoir. // 1st International Scientific Conference “Modern problems in Geophysics”, Proceedings, ISBN 978-9941-36-434-1, ISSN 3088-4349, Tbilisi, Georgia, November 6-8, 2025.
10. Tsivtsivadze N., Makalatia I., Khatiashvili E., Jorbenadze N., Ivanov G., Problems of Regional Water-Bodies’ Pollution. // Journals of Georgian Geophysical Society, 2025.
11. https://www.economy.ge/
12. https://www.jandenul.com/projects/building-new-deep-water-port-anaklia-georgia.
13. https://www.dpworld.com/en/ports-terminals/romania/constanta
14. https://www.worldbank.org/ext/en/home

2nd International Scientific Conference "Modern Problems in Geophysics", Proceedings,
ISBN 978-9941-36-562-1, ISSN 3088-4349, Tbilisi, Georgia, October 29-31, 2026

# ANALYSIS OF CHANGES IN THE DYNAMIC BEHAVIOR OF THE ENGURI ARCH DAM

***,**Sborshchikovi A., *Mepharidze E., *Tepnadze D., *Laliashvili L.,*Chikviladze E.**

** Mikheil Nodia Institute of Geophysics of Ivane Javakhishvili Tbilisi State University, Tbilisi, Georgia*
*** Business and Technology University, Tbilisi, Georgia*
*a.sborshchikov@gmail.com*

***Abstract.*** *This study aims to characterize the temporal and dynamical variations in the displacement behavior of the foundation of the Enguri Arch Dam and to assess their relationship with periodic changes in reservoir water level. The investigation utilizes a long-term observational dataset covering the period from 1974 to 2021, providing an extensive basis for evaluating the evolution of the dam's response over time. To identify and quantify the underlying dynamical patterns, a set of advanced nonlinear analysis techniques was employed, with particular emphasis on* ***Multifractal Detrended Fluctuation Analysis (MF-DFA)****. The obtained results demonstrate a pronounced relationship between variations in foundation displacement and the dynamic response of the dam as a whole. The analysis further suggests that fluctuations in reservoir water level constitute a significant factor affecting the observed displacement dynamics and contribute to changes in the structural behavior of the Enguri Arch Dam.*

***Key words****: Dynamical changes, nonlinear analyses, datasets.*

## Introduction

The research began with a comprehensive review of the scientific literature concerning the environmental, geophysical, and geodynamic effects associated with the construction and operation of large reservoirs. Previous investigations have demonstrated that the impoundment of substantial volumes of water can alter the natural stress state and hydrological conditions of the surrounding environment. Such changes may be associated with variations in local seismic activity, modifications of regional climatic conditions, and the development or reactivation of landslide processes. These effects reflect the complex interaction between hydrological loading, geological structures, and the mechanical response of the Earth's crust and surrounding slopes. Consequently, the investigation of large hydraulic structures requires an interdisciplinary approach that integrates geophysical observations, structural monitoring, geodynamic analysis, and advanced mathematical methods.

Within this broader context, the Enguri Arch Dam represents a particularly important case study. Located in western Georgia within the Enguri River Gorge, the dam forms the principal component of the Enguri Hydropower Plant (HPP) and, with a height of 271 m, is one of the world's largest arch dams. The exceptional dimensions of the structure, combined with its location in a tectonically active region, make continuous monitoring of its structural and geodynamic behavior particularly important.

A comprehensive geodynamical and geophysical monitoring system was established in the Enguri Dam region during the construction and early operational stages of the facility. At the time of its installation, this monitoring network represented an advanced system for recording long-term variations in the physical state of the dam and its foundation. The system has provided valuable observations of several parameters, including foundation deformation, structural tilts, temperature variations, and reservoir water-level fluctuations [1–3]. The availability of these long-term observations provides a unique opportunity to investigate how the dynamic characteristics of the dam evolve under changing environmental and operational conditions.

Of particular interest is the relationship between variations in reservoir water level and the displacement of the dam foundation. Periodic changes in the reservoir load can modify the stress and deformation state of the dam–foundation system, potentially producing measurable changes in its dynamic response. At the same time, the observed signals may contain nonlinear and long-range temporal dependencies that cannot be ade-

quately characterized using conventional statistical approaches. Identifying such features is essential for improving the understanding of the mechanisms governing the observed behavior of the structure.

In this study, we therefore investigate the long-term dynamics of foundation displacement at the Enguri Arch Dam using observations collected over the period 1974–2021. Particular attention is given to the temporal variability of the displacement signal and its relationship with reservoir water-level fluctuations. To identify persistent correlations, scaling properties, and changes in the underlying dynamics, advanced nonlinear time-series methods are employed, with **Multifractal Detrended Fluctuation Analysis (MF-DFA)** serving as one of the principal analytical techniques. The results provide additional insight into the complex dynamical behavior of the dam–foundation system and contribute to a more comprehensive assessment of the factors influencing its long-term response.

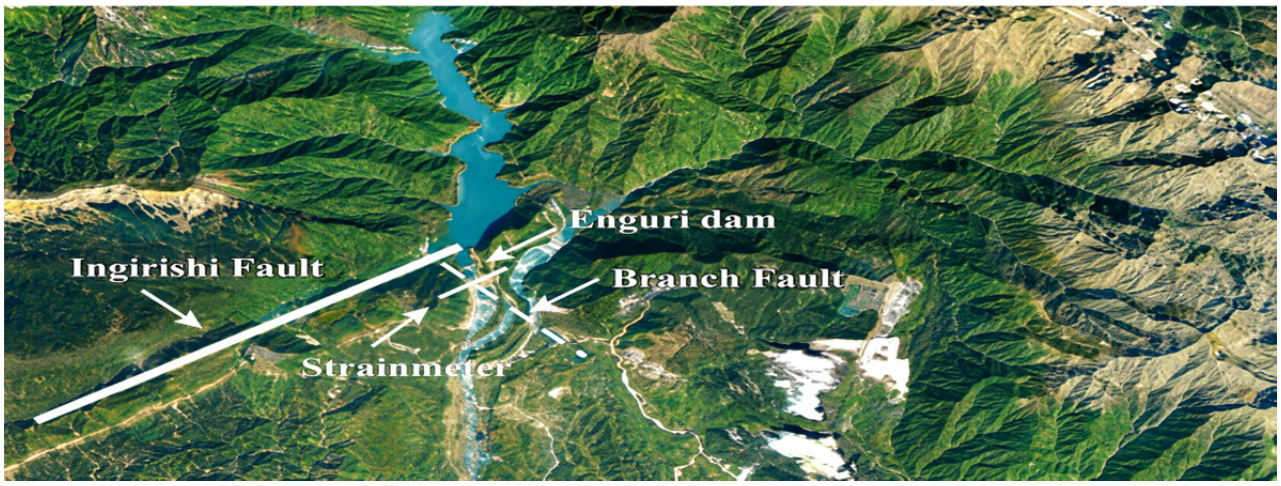



**Fig. 1.** Enguri dam and reservoir area with locations of the main Ingirishi fault and the branch fault.

Geological investigations have established that a branch of the major active **Ingirishi Fault** intersects the right abutment of the Enguri Dam foundation. The presence of an active or potentially active fault in the immediate vicinity of a large hydraulic structure constitutes an important geotechnical and structural safety concern [1,4,5]. For this reason, systematic monitoring of the fault zone was initiated prior to the construction of the dam and continued throughout the subsequent development and operation of the reservoir.

The fault branch crossing the dam foundation (Fig. 1) makes the Enguri site particularly relevant for investigating the complex interaction between tectonic deformation and anthropogenic effects. The long-term observational record available from this region provides an opportunity to regard the Enguri Dam area as a large-scale natural laboratory for studying the response of a fault–dam system to the combined influence of tectonic loading, reservoir-induced effects, and environmental variability.

Analysis of the available observations indicates the presence of two major components in the deformation behavior of the fault zone. The first is associated with **tectonic strain**, which manifests itself primarily as a piecewise-linear component of displacement and can therefore be interpreted as the underlying **trend** of the deformation process. The second component is represented by **quasiperiodic oscillations**, which are superimposed on the long-term trend. These oscillatory variations may reflect the influence of cyclic environmental conditions and operational factors, particularly changes in reservoir loading.

The dataset analyzed in the present study encompasses continuous observations collected during **1974–2021**. Its scientific value is associated not only with the extended observation period but also with the diversity of monitored parameters, including high-weir foundation and body tilt, foundation deformation, internal temperature variations within the dam body, and fluctuations in reservoir water level. Parts of these long-term observations have previously been reported in peer-reviewed publications [2–6].

In the present work, particular attention is devoted to the **foundation displacement record** covering the entire observation period (Fig. 2). Focusing on this parameter allows us to examine the long-term evolution of the deformation process and to identify changes in its dynamical characteristics. The analysis of these variations provides an important basis for assessing the relationship between tectonic processes, reservoir-induced loading, and the observed deformation response of the Enguri Dam foundation.

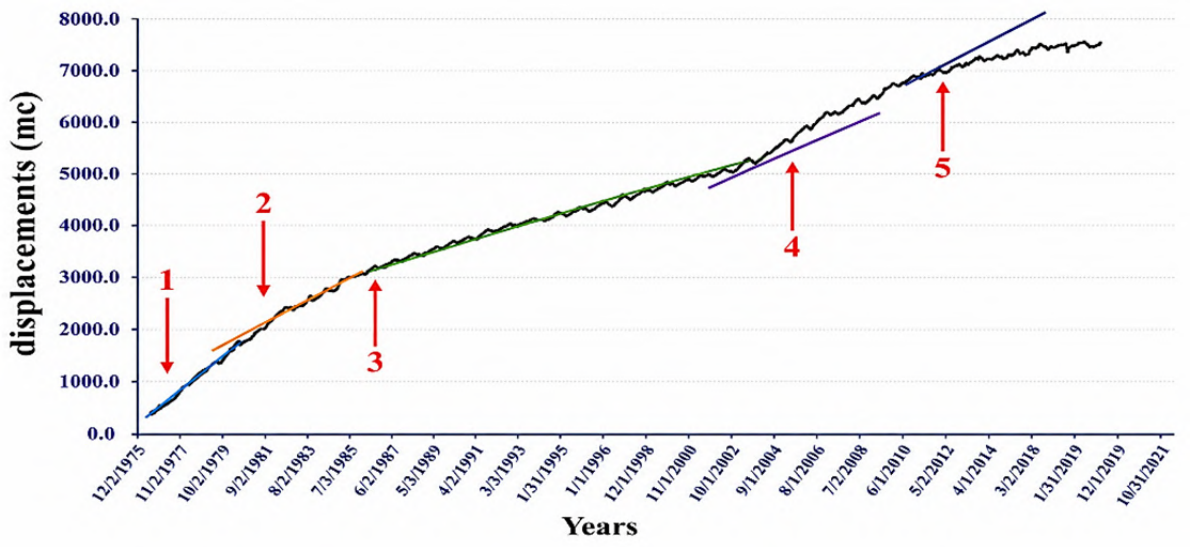



**Fig. 2.** Dam foundation displacement data sets around Enguri in period from 1974 to 2021. Arrows 1, 2, 3, correspond to the initial periods of fault zone extension.

To enable continuous monitoring of the behavior of the fault zone, a **quartz strainmeter** was installed in 1974, four years before the initial filling of the Enguri Reservoir. The instrument was positioned across the fault zone to measure the relative displacement of the rock blocks separated by the fault, which is approximately 10 m wide. Measurements are performed in the direction normal to the fault plane, allowing the strainmeter to detect both **extension and contraction** of the fault zone.

The quartz strainmeter consists of a **22.5 m long quartz tube**, with its free end equipped with a **photo-optical recording system** that currently operates in parallel with a laser-based measurement system. The fixed and free ends of the instrument are anchored on opposite sides of the fault, at distances of several meters from the fault plane. Measurements were originally recorded daily at the same time, with a system sensitivity of approximately **0.18 μm/mm**.

The **stepwise filling of the Enguri Reservoir** began on **April 15, 1978**. Since approximately **1987**, the reservoir water level has exhibited regular seasonal fluctuations. Seismic observations have been obtained from a network of monitoring stations distributed throughout the Enguri region. The local earthquake catalogue used in this study includes events with magnitudes of **M ≥ 2.2** and covers the period from **1974 to 2021**.

In the present study, **quartz strainmeter data** are used to investigate displacement processes within the foundation of the high Enguri Arch Dam. As discussed above, variations in reservoir water level may influence local seismic activity, which, in turn, can affect the deformation behavior and dynamic response of the dam foundation.

To investigate the **nonlinear and multifractal characteristics** of foundation displacement, we applied **Multifractal Detrended Fluctuation Analysis (MF-DFA)**. The analysis was performed using specialized software developed by researchers at the **M. Nodia Institute of Geophysics, Ivane Javakhishvili Tbilisi State University**. MF-DFA is an effective method for identifying **multifractal structures and long-range correlations** in non-stationary time series. It extends the conventional **Detrended Fluctuation Analysis (DFA)** and enables the characterization of scale-dependent fluctuations and correlations of different magnitudes. The methodological framework follows the approach developed by Kantelhardt et al. [7].

Our analysis focuses on the **multifractal scaling behavior** of the displacement time series. Three principal characteristics are considered:

the **generalized Hurst exponent**, (H(q));
the **multifractal spectrum dimension**, (D(q));
the **generalized fluctuation functions**, (F(q)).

The **Hurst exponent**, originally introduced by Hurst (1951), provides important information about the correlation structure and persistence of a time series. In general, values of (H(q)) greater than 0.5 indicate persistent behavior and long-range correlations, whereas values below 0.5 are associated with anti-persistent

or anti-correlated behavior. A value of (H(q)=0.5) corresponds to an approximately uncorrelated process or a process with short-range memory. Values exceeding 1 may occur in strongly non-stationary or nonstationary-like processes and should be interpreted with caution rather than being directly classified as random-walk behavior.

It should be emphasized that, although **MF-DFA provides reliable estimates of positive generalized Hurst exponents**, its accuracy may decrease in the presence of strong anti-correlations, particularly when (h(q)) approaches zero [8-10]. Despite this limitation, MF-DFA is widely regarded as an effective approach for characterizing the **multifractal properties and scale-dependent correlations of non-stationary geophysical time series**.

The displacement dataset covering the period **1974–2021** was influenced by several external factors, including **the progressive filling of the Enguri Reservoir, meteorological variability, and seismic activity**. These factors introduced pronounced trends and non-stationary components into the recorded signal, making appropriate **detrending** an essential step before performing the multifractal analysis.

To account for changes in the deformation regime over time, the complete dataset was divided into six distinct sub-periods:

**1974–1978, 1978–1985, 1985–2006, 2006–2013, 2013–2017, and 2017–2021.**

The selected intervals correspond to periods characterized by substantially different displacement patterns and loading conditions. MF-DFA was subsequently applied to each sub-period using **polynomial detrending** of different orders, including **(p=2)** and **(p=5)**. The use of different polynomial orders allows the analysis to account for both lower-order and more complex trends in the displacement series and to evaluate the robustness of the resulting multifractal characteristics (Fig. 3a, b).

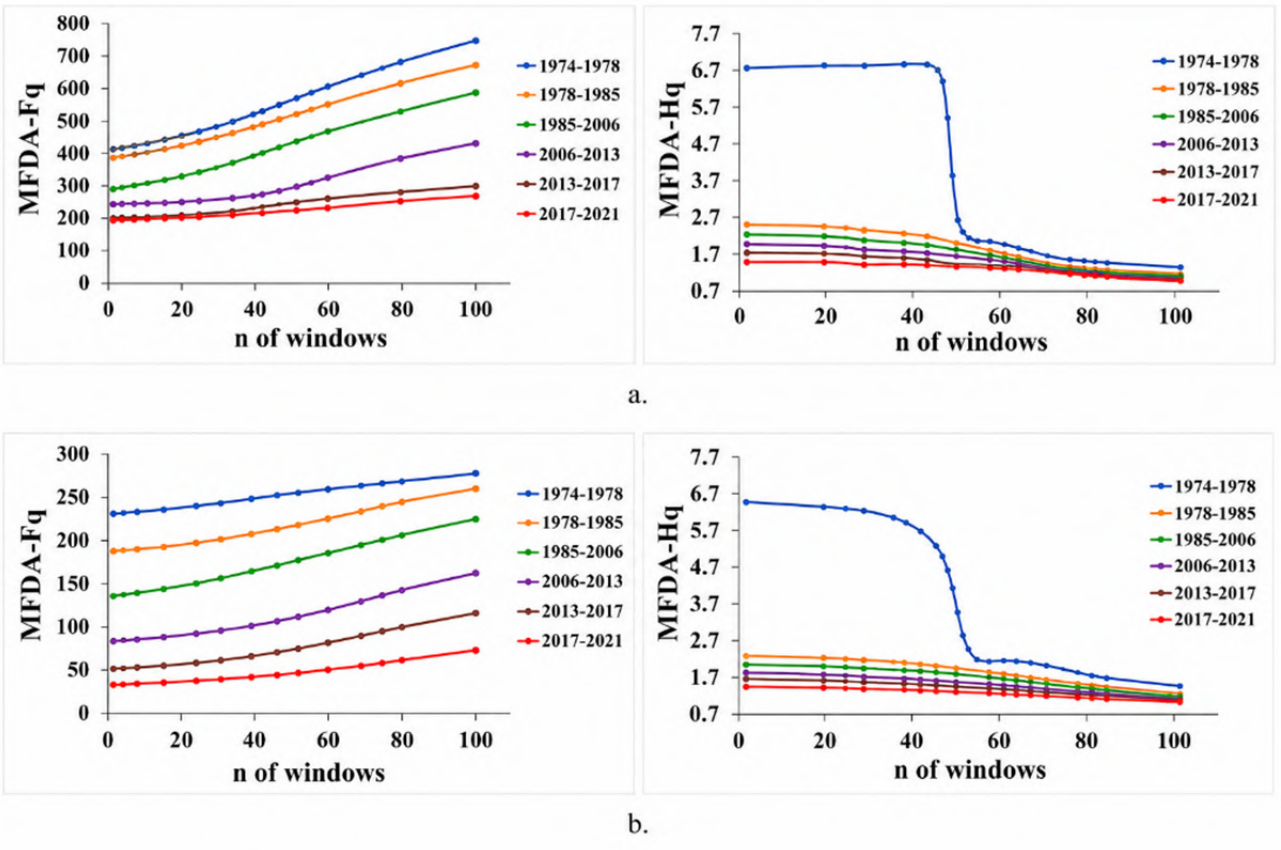



**Fig. 3.** MF-DFA (Fq, Hq) analysis of displacements of Enguri Arc Dam foundation
(a. polynomial degree =p2; b. polynomial degree =p5).

The results obtained from the MF-DFA analysis demonstrate the evolution of the principal scaling characteristics of the displacement time series, with particular changes observed during the **2017–2021** period. The analysis primarily considers the **generalized Hurst exponent, (H(q))**, and the **generalized fluctuation function, (F(q))**. The results indicate that increasing the order of the polynomial used for detrending general-

ly leads to a reduction in the magnitude of (F(q)), reflecting a decrease in the residual fluctuation amplitude after the removal of higher-order trends.

The estimated values of the **generalized Hurst exponent, (H(q))**, were predominantly within the range from approximately **0.5 to values exceeding 1**. Values of (H(q)>0.5) indicate persistent scaling behavior, suggesting the presence of positive correlations and long-range dependence over the corresponding range of scales. The occurrence of values greater than 1 should be interpreted in the context of the strong non-stationarity and trend components present in the displacement records rather than being considered direct evidence of a conventional random-walk process.

The results further indicate that increasing the **polynomial detrending degree** modifies the estimated scaling characteristics of the displacement series. Higher-order detrending removes increasingly complex components of the underlying trend and consequently reduces the magnitude of the remaining fluctuations represented by (F(q)). This effect demonstrates that the apparent multifractal structure of the displacement records is sensitive to the treatment of non-stationary trends.

The observed dependence of the MF-DFA characteristics on the detrending order, together with the differences between the analyzed time intervals, suggests that the temporal dynamics of the dam-foundation displacement are influenced by a combination of **structural, hydrological, meteorological, and seismic factors**. In particular, the pronounced changes observed during **2017–2021** may reflect a modification of the underlying deformation regime and warrant further investigation through comparison with reservoir-level variations, seismicity, and other monitoring parameters.

## Conclusion

In this study, we investigated the **dynamic characteristics of foundation displacements of the Enguri Arch Dam** using long-term monitoring data collected over the period **1974–2021**. The **Multifractal Detrended Fluctuation Analysis (MF-DFA)** method was employed to characterize the nonlinear scaling behavior, long-range correlations, and multifractal properties of the displacement time series.

The results demonstrate that the temporal dynamics of the dam foundation are influenced by several factors, with particularly important contributions from the **dam construction and reservoir-filling processes** and, subsequently, from **variations in reservoir water level**. The differences observed between the analyzed time intervals indicate changes in the scaling characteristics of foundation displacement and suggest that the deformation regime has evolved in response to changing loading and environmental conditions.

The MF-DFA approach provides a **quantitative framework for identifying changes in the dynamic structure** of the displacement records. The observed persistence and scale-dependent behavior of the time series indicate that foundation deformation cannot be adequately described solely by conventional linear or stationary models. Instead, its dynamics reflect the combined influence of **hydrological loading, structural response, seismic activity, and other geophysical and environmental factors**.

These findings contribute to a better understanding of the long-term deformation behavior of the Enguri Arch Dam foundation and demonstrate the potential of **multifractal analysis as a complementary tool for monitoring and diagnosing changes in dam-foundation dynamics**. In particular, the identification of changes in scaling behavior may provide valuable information for the development of **quantitative criteria for long-term assessment of structural stability and safety** under variable hydrological and geophysical conditions.

## Reference


1. Chelidze T., Matcharashvili T., Abashidze V., Kalabegashvili M. and Zhukova N., Real-time monitoring for analysis of dam stability: Potential of nonlinear elasticity and nonlinear dynamics approaches. // Frontiers in Structural and Civil Engineering, 7, 2013, pp. 188–205.
2. Chelidze T., Tepnadze D., Mepharidze E., Sborshchikovi A., Laliashvili L. and Matcharashvili T., Scaling features of earthquake occurrences in the equally distributed non-overlapping time windows. // Bulletin of the Georgian National Academy of Sciences 14(4), 2020, pp. 40–45.
3. Chelidze, T., Matcharashvili T., Abashidze V., Dovgal N., Mepharidze E., and Chelidze L., Time series analysis of fault strain accumulation around large dam: the case of enguri dam, greater Caucasus, building knowledge for geohazard assessment and management in the Caucasus and other orogenic regions. // In: Bonali, F. L., Mariotto, F. P,

Tsereteli, N. (eds). Building Knowledge for Geohazard Assessment and Management in the Caucasus and other Orogenic Regions. Dordrecht: Springer, 2021, pp. 185–204.
4. Matcharashvili T., Hatano T., Chelidze T. and Zhukova N., Simple statistics for complex earthquake time distributions. // Nonlinear Processes in Geophysics 25, 2018, pp. 497–510.
5. Matcharashvili,T., Chelidze T., Zhukov, N., Mepharidze E., Sborshchikovi A., Tephnadze D. and Laliashvili, L., Dynamical Changes of Foundation Displacements and Local Seismic Activity Occurred During Construction of Enguri Arch Dam. // 25th European Meeting of Environmental and Engineering Geophysics The Hague, Netherlands: European Association of Geoscientists & Engineers, vol. 1, 2019, pp. 1–5.
6. Peinke J., Matcharashvili T., Chelidze T., Gogiashvili J., Nawroth A., Lursmanashvili O. and Javakhishvili Z., Influence of periodic variations in water level on the regional seismic activity around a large reservoir: field data and laboratory model // Physics of the Earth and Planetary Interiors 156, 2006, pp. 130–142.
7. Kantelhardt J.W., Zschiegner S.A., Koscielny-Bunde E., Havlin S., Bunde A. and Stanley H.E., Multifractal detrended fluctuation analysis of nonstationary time series. // Physica A: Statistical Mechanics and its Applications 316, 2002, pp. 87–114.
8. Espen I.A.F., Introduction to multifractal detrended fluctuation analysis in Matlab. // Frontiers in Physiology 3(141), 2012, pp. 1–18.
9. Gao K., Hu J., Tung W.-W., Cao Y., Sarshar N. and Roychowdhury V. P., Assessment of long-range correlation in time series: how to avoid pitfalls .// Phys. Rev. E, Stat. Nonlin. Soft Matter Phys., 73, 2006, 016117.
10. Sborshchikovi A., Chelidze T., Mepharidze E., Tepnadze D., Zhukova N., Matcharashvili T. and LaliashviliL., The Analysis of Dynamical Changes and Local Seismic Activity of the Enguri Arch Dam. // In: Dinesh C. S. Bisht, Mangey Ram, Computational Intelligence-based Time Series Analysis, River Publishers, Denmark, 2022, pp. 53–63.

2nd International Scientific Conference "Modern Problems in Geophysics", Proceedings,
ISBN 978-9941-36-562-1, ISSN 3088-4349, Tbilisi, Georgia, October 29-31, 2026

# TEMPORAL AND DYNAMIC ANALYSIS OF ENGURI DAM MONITORING DATASETS

***,**Sborshchikovi A., *Mepharidze E. , * Chelidze T.**

** Mikheil Nodia Institute of Geophysics of Ivane Javakhishvili Tbilisi State University, Tbilisi, Georgia*
*** Business and Technology University, Tbilisi, Georgia*
*a.sborshchikov@gmail.com*

***Abstract.*** *In this study, we investigate the temporal characteristics of seismic activity in the vicinity of the Enguri Dam and the associated foundation displacement dynamics. In particular, we analyze the time intervals (waiting times) between successive seismic events in the regional seismic catalog, together with long-term foundation displacement datasets obtained from the Enguri Dam monitoring system. A statistical time-series approach is employed to characterize the temporal dynamics of these datasets and to identify underlying patterns and dependencies. To investigate their linear and nonlinear scaling properties, we apply two nonlinear time-series analysis methods: Detrended Fluctuation Analysis (DFA) and Multifractal Detrended Fluctuation Analysis (MF-DFA).The main aim of this research is to investigate the temporal dynamics and statistical characteristics of seismic activity and foundation displacement at the Enguri Dam. The analysis provides insights into the temporal organization, long-range correlations, and multifractal properties of the observed processes, thereby contributing to a better understanding of the dynamic behavior of the dam and its surrounding geophysical environment.*

***Key Words:*** *Enguri Dam, nonlinear analysis, displacement, waiting time.*

## Introduction

It is well known that the **Enguri High Arch Dam** is one of the highest arch dams in the world. Constructed in the 1970s in the canyon of the Enguri River in western Georgia, the dam is located in a seismically active region characterized by complex tectonic and geotectonic processes. Long-term observations have demonstrated that variations in reservoir water level, particularly during filling and drawdown periods, can influence the deformation processes occurring in the dam foundation. These processes make the Enguri Dam an important and valuable subject for long-term geophysical and engineering research.

Systematic monitoring of processes occurring in the dam foundation began in **1974**. During periods of reservoir filling and loading, measurable movements and deformations of the foundation were observed. The long-term monitoring data have provided evidence of complex interactions between reservoir loading, foundation deformation, and regional seismic activity. Previous studies have also indicated that changes in reservoir conditions may be associated with variations in seismic activity in the surrounding area [1–6].

In the present study, we analyze seismic and foundation-displacement data obtained from the Enguri Dam monitoring system. Particular attention is given to the **temporal characteristics of seismic activity and foundation displacement**, including the time intervals (waiting times) between successive seismic events and variations in foundation deformation.

To investigate these processes, we employ modern statistical and nonlinear methods of time-series analysis. In particular, **Detrended Fluctuation Analysis (DFA)** and **Multifractal Detrended Fluctuation Analysis (MF-DFA)** are applied to characterize long-range correlations, scaling behavior, and multifractal properties within the observed datasets. This approach allows us to examine the temporal organization and dynamic characteristics of seismic activity and foundation deformation and to improve our understanding of the response of the Enguri Dam system to natural and reservoir-induced processes.

## Methods

In the present study, we analyze the **waiting times between successive earthquakes** in the seismic catalog for the area surrounding the Enguri Dam, together with long-term foundation displacement data. The

seismic analysis is based on earthquake events occurring within a **100 km radius of the Enguri Dam** during the period **1974–2017**, while the foundation displacement dataset covers the period **1974–2020**.

To investigate the temporal dynamics and correlation properties of these datasets, we employ nonlinear time-series analysis methods, specifically **Detrended Fluctuation Analysis (DFA)** and **Multifractal Detrended Fluctuation Analysis (MF-DFA)**. These methods allow us to characterize long-range correlations, scaling behavior, and multifractal properties in the investigated time series.

**Detrended Fluctuation Analysis (DFA)** is a widely used method for quantifying long-range correlations and scaling behavior in non-stationary time series. The DFA scaling exponent provides information about the correlation structure of a time series and can be used to identify long-range dependencies that may not be detected by conventional statistical methods [7,8]. In particular, the DFA exponent characterizes the degree of persistence or anti-persistence in the fluctuations of the analyzed process.

**Multifractal Detrended Fluctuation Analysis (MF-DFA)** is an extension of the DFA method designed to identify multifractal scaling behavior in non-stationary and nonlinear time series. Unlike conventional DFA, which primarily characterizes a single scaling exponent, MF-DFA enables the investigation of a spectrum of scaling exponents and the corresponding multifractal structure of the process [9,10]. The resulting multifractal spectrum provides information about the variability of scaling behavior across different fluctuation magnitudes and, consequently, about the complexity of the underlying dynamics.

The combined application of DFA and MF-DFA provides a comprehensive framework for investigating the **temporal organization, long-range correlations, and multifractal characteristics of seismic waiting times and foundation displacement at the Enguri Dam**. This approach allows us to compare the dynamic properties of seismic activity with those observed in the dam foundation and to identify common or distinct features in their temporal behavior.

## Results and discussion

Nonlinear DFA analysis of time interval (waiting times) of seismic data area around 100 km of Enguri dam for 1974-2017 and foundation displacement data for 1974-2020 was carried out. The results of DFA analysis of seismic catalogs and displacement, show the long-range correlation of scaling features, changes in dynamical structures, and the regularity of the system. DFA analysis was carried out for polynomial fitting p=2, 3, 4 (see Fig. 1-Fig. 2).

The **DFA analysis of the Enguri Dam datasets** provides insights into changes in the correlation structure and dynamic organization of the investigated processes. The results indicate that, as the order of the polynomial detrending function increases, the identified scaling structure changes, while the strength of the correlations decreases. This behavior suggests that higher-order trends may influence the observed scaling properties and should therefore be carefully considered when interpreting the long-term dynamics of the datasets.

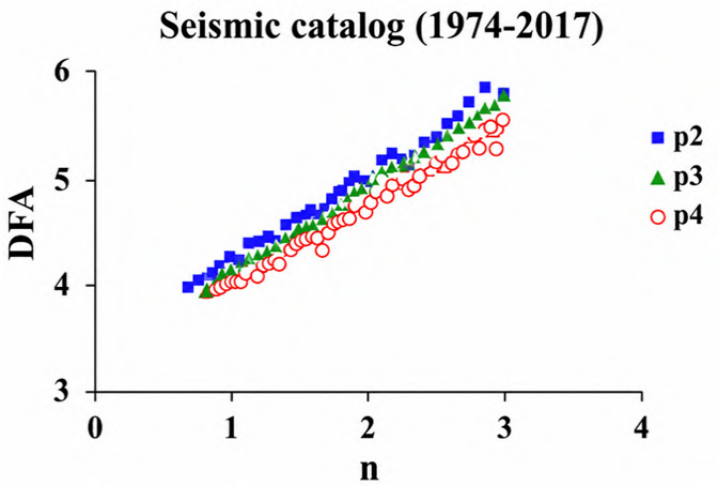



**Fig. 1.** DFA analysis of seismic data area around 100 km of Enguri dam for 1974-2017.

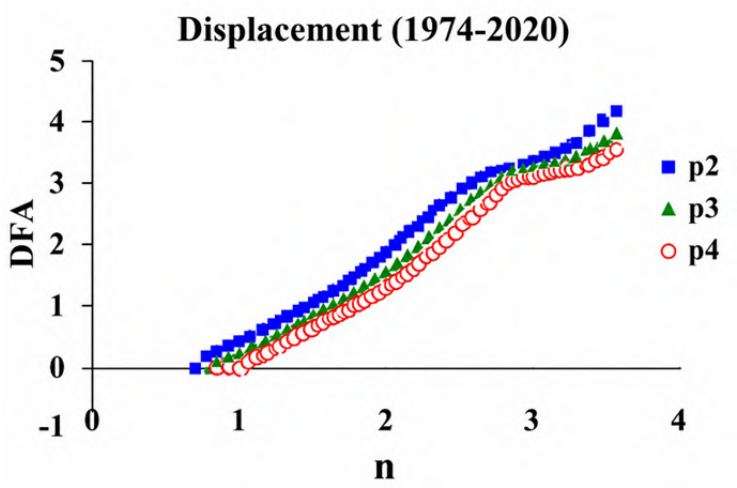



**Fig. 2.** DFA analysis of Enguri dam foundation displacement for 1974-2020.

**Multifractal Detrended Fluctuation Analysis (MF-DFA)** was subsequently applied to investigate the long-range correlations and multifractal properties of the non-stationary seismic and foundation displacement time series. The seismic dataset includes earthquake events recorded within a **100 km radius of the Enguri Dam during 1974–2017**, while the foundation displacement dataset covers the period **1974–2020**.

The multifractal spectra were obtained using a **second-order polynomial detrending function (p = 2)**. The resulting multifractal spectra characterize the variation of scaling behavior across different fluctuation magnitudes and provide information about the complexity and heterogeneity of the underlying dynamics. The corresponding results for the seismic and foundation displacement datasets are presented in **Fig. 3 and Fig. 4**, respectively.

Fig. 3 and Fig. 4 present the scaling functions (F_q(s)) and the corresponding regression slopes (h(q)) obtained from the MF-DFA analysis. The dependence of the scaling behavior on the order (q) provides important information about the correlation structure and multifractal characteristics of the investigated time series. In contrast to monofractal processes, for which the generalized Hurst exponent (h(q)) is approximately independent of (q), a significant dependence of (h(q)) on (q) indicates the presence of multifractal behavior.

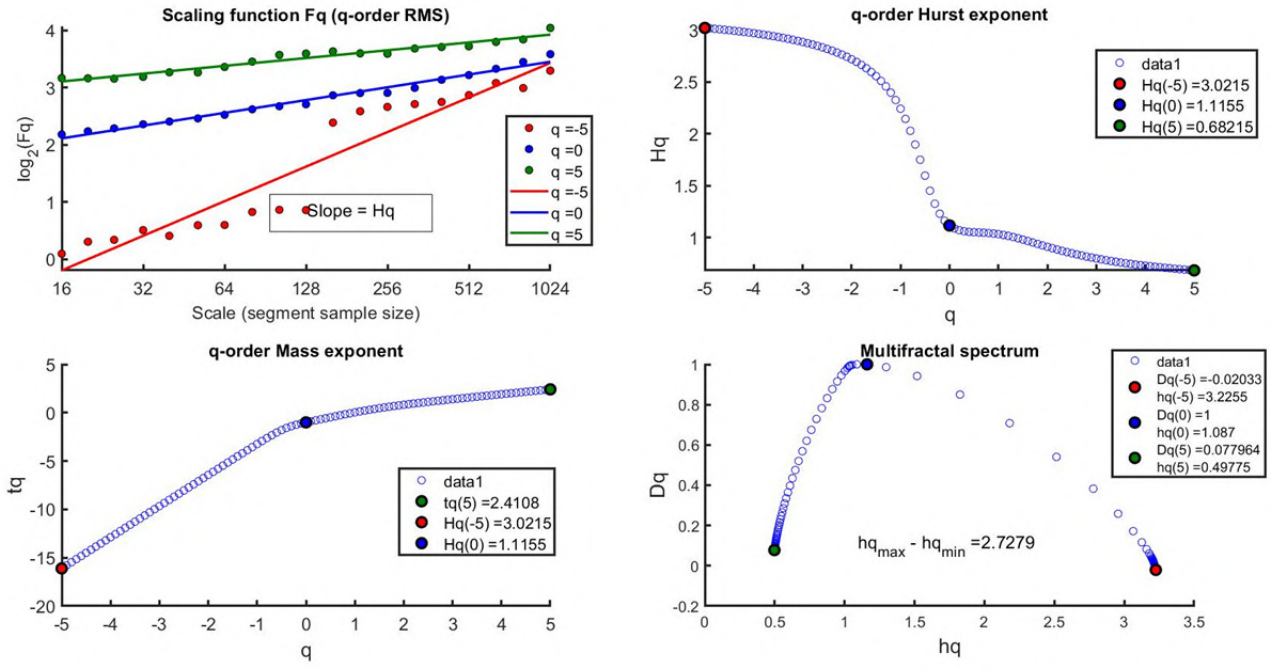



**Fig. 3.** MFDFA analysis of seismic data area around 100 km of Enguri dam for 1974-2017. % output variable: Hq: q-order Hurst exponent, Fq: q-order scaling function, tq: q-order mass exponent, Dq: q-order dimension.

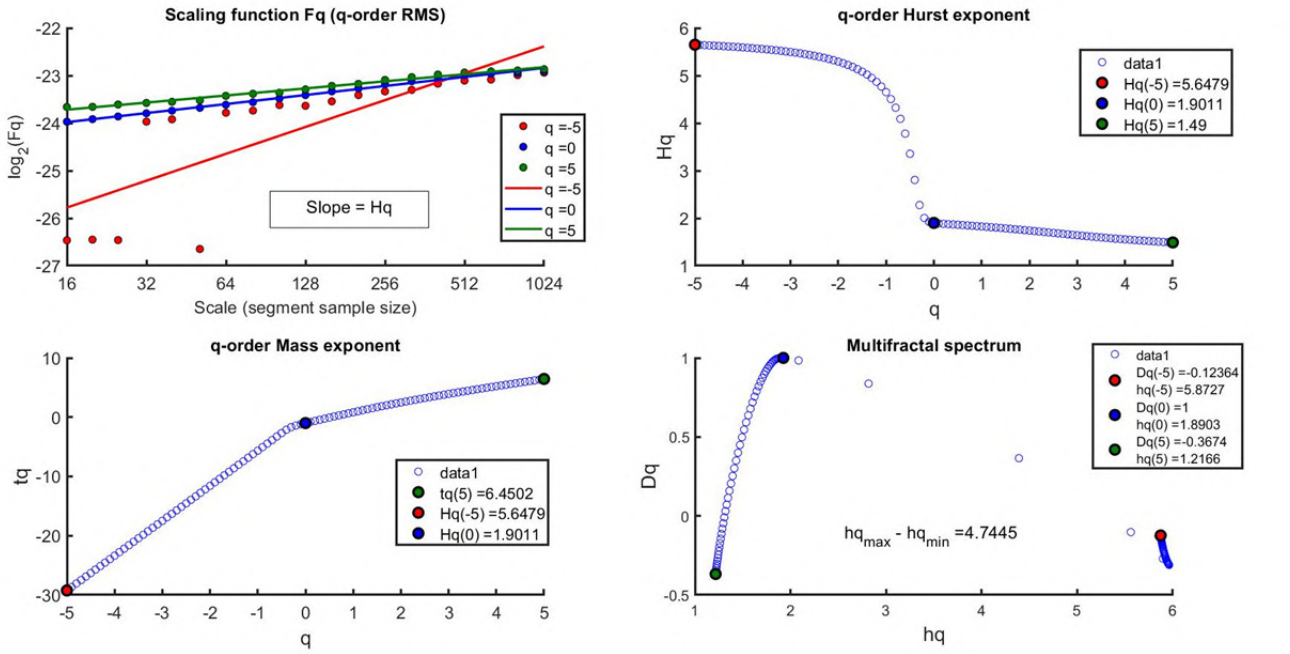



**Fig. 4.** MFDFA analysis of Enguri dam foundation displacement for 1974-2020. % output variable: Hq: q-order Hurst exponent, Fq: q-order scaling function, tq: q-order mass exponent, Dq: q-order dimension.

The MF-DFA procedure consists of several successive steps. First, the generalized Hurst exponent (h(q)) is used to determine the corresponding (q)-order mass exponent (\tau(q)). The mass exponent is then related to the singularity exponent (\alpha) and the multifractal spectrum (f(\alpha)) through the Legendre transformation. The resulting multifractal spectrum describes the distribution of scaling exponents and provides information about the complexity and heterogeneity of the underlying dynamics.

The variation of (h(q)) with (q), together with the corresponding multifractal spectrum, enables us to characterize the degree of multifractality in both the seismic waiting-time series and the foundation displacement data. The differences between the obtained spectra provide an opportunity to compare the dynamic properties of seismic activity and foundation deformation at the Enguri Dam.

## Conclusion

In this study, the temporal characteristics of seismic activity and foundation displacement at the Enguri Dam were investigated using long-term monitoring datasets. The analysis focused on the **waiting times between successive seismic events** recorded within a 100 km radius of the Enguri Dam during **1974–2017**, as well as foundation displacement data collected during **1974–2020**.

To characterize the nonlinear and long-range dependence properties of the investigated time series, **Detrended Fluctuation Analysis (DFA)** and **Multifractal Detrended Fluctuation Analysis (MF-DFA)** were applied. The DFA results provided information about the scaling behavior and long-range correlations of the datasets, while the MF-DFA analysis enabled us to identify their multifractal characteristics and variations in scaling behavior across different fluctuation magnitudes.

The obtained results demonstrate that both seismic waiting times and foundation displacement exhibit complex temporal dynamics that cannot be fully described by conventional statistical approaches. The multifractal characteristics revealed by the analysis provide additional information about the organization and variability of the investigated processes.

The analysis of seismicity and foundation displacement time series associated with the Enguri Dam provides a useful framework for characterizing the **normal dynamic regime** of the dam–foundation–seismic system. Establishing the characteristic nonlinear behavior of the system may also provide a basis for identifying significant deviations from the established regime. Such deviations could be considered as potentially important indicators for further investigation of changes in the dynamic state of the dam and its surrounding geophysical environment.

Overall, the application of DFA and MF-DFA to long-term Enguri Dam monitoring data demonstrates the potential of nonlinear time-series methods for investigating the complex interaction between seismic activity and foundation deformation and for improving the assessment of the dam's long-term dynamic behavior.

**Acknowledgement:** The research was funded and supported by Shota Rustaveli National Science Foundation of Georgia (SRNSF) Grant YS-25-2542 – "The analysis of the time distribution of the intervals between earthquakes/Using the deformation data of the Enguri Arch Dam".

## References

1. Chelidze T., Matcharashvili T., Javakhishvili Z., Zhukova N., Jorjiashvili N., Shengelia I., Mepharidze E., Chelidze Z., Sborshchikovi A., Temporal and Spatial Variations of Scaling Behavior of Seismic Process in Caucasus. // Bulletin of the Georgian National Academy of Sciences, Tbilisi, Georgia, 9(2), 2015, pp. 59-64.
2. Chelidze T., Matcharashvili T., Varamashvili N., Mepharidze E., Tephnadze D., Chelidze Z., Complexity and Synchronization Analysis in Natural and Dynamically Forced Stick-Slip: A Review. // In: Complexity of Seismic Time Series, Elsevier, Amsterdam, Netherlands, 2018, pp. 276-321.
3. Chelidze T., Matcharashvili T., Abashidze V., Dovgal N., Mepharidze E., Chelidze L., Time series analysis of fault strain accumulation around large dam: The case of enguri dam, greater caucasus. // NATO Science for Peace and Security Series C: Environmental Security, Springer, Netherlands, 2021, pp. 185–204.
4. Matcharashvili T., Hatano T., Chelidze T., Zhukova N., Simple statistics for complex Earthquake time distributions. // Nonlinear Processes in Geophysics, Göttingen Germany, 25(3), 2018, pp. 497-510.
5. Matcharashvili T., Chelidze T., Javakhishvili Z., Zhukova N., Jorjiashvili N., Shengelia I., Mepharidze E., Sborshchikovi A., Analysis of the Complexity of Seismic Data Sets: Case Study for Caucasus. // In: Complexity of Seismic Time Series, Elsevier, Amsterdam, Netherlands, 2018, pp. 3-25.
6. Matcharashvili T., Chelidze T., Zhukova N., Mepharidze E., Sborshchikovi A., Tephnadze D. and Laliashvili L., Dynamical changes of foundation displacements and local seismic activity occurred during construction of Enguri arch dam. // 25th European Meeting of Environmental and Engineering Geophysics, Held at Near Surface Geoscience Conference and Exhibition 2019, European Association of Geoscientists & Engineers, Bunnik, Utrecht, The Netherlands, 2019.
7. Lan T.-H., Gao Z.-Y., Abdalla A. N., Cheng B., Wang S., Detrended fluctuation analysis as a statistical method to study ion single channel signal. // Cell Biology International, Elsevier, Amsterdam, Netherlands, 32, 2008, pp. 247-252.
8. Hurst H. E., Long-term storage capacity of reservoirs. // Transactions of the American Society of Civil Engineers, USA, 116, 1951, pp. 770–808.
9. Kantelhardt J. W., Koscielny-Bunde E., Rego H. A. A., Havlin S., and Bunde A., Detecting long-range correlation with detrended fluctuation analysis. // Physica A, Elsevier, Amsterdam, Netherlands, 295, 2001, pp. 441–454.
10. Kantelhardt J. W., Zschiegner S. A., Koscielny-Bunde E., Havlin S., Bunde A., and Stanley H. E., Multifractal detrended fluctuation analysis of nonstationary time series. // Physica A, Elsevier, Amsterdam, Netherlands, 316, 2002, pp. 87–114.

2nd International Scientific Conference "Modern Problems in Geophysics", Proceedings,
ISBN 978-9941-36-562-1, ISSN 3088-4349, Tbilisi, Georgia, October 29-31, 2026

# INNOVATIVE PRODUCTION OF FUNCTIONAL CANDIED PRODUCTS FROM LOCAL PLANT RAW MATERIALS AND PROSPECTS FOR RATIONAL RESOURCE UTILIZATION

**Seidishvili N., **Chkhartishvili I., **Papunidze S, *, **Kiknadze N.,
**Abuladze D., *Putkaradze N.

* *Batumi Shota Rustaveli State University, Batumi, Georgia*
** *Institute Agrarian and membrane technologies, Batumi, Georgia*
*** *"Legi" Testing Laboratory, Batumi, Georgia*
*nino.seidiSshvili@bsu.edu.ge*

***Abstract.*** *The aim of the study was to develop a technology for producing candied products from a local pumpkin raw material and to evaluate the main physicochemical characteristics of the obtained product. The research object was the fruit of a local pumpkin variety cultivated in Khulo Municipality. The moisture content, soluble solids, total sugars, pH, titratable acidity, and vitamin C content of the raw material and finished product were determined. The technology for producing the candied product included raw material preparation, cutting, blanching, osmotic dehydration in multi-stage sugar syrup, and final drying at 65 °C for 8 hours. The results showed that technological processing reduced the moisture content of the raw material from 90.2% to 27.3%, while the dry matter content increased from 9.9% to 73.0%. Soluble solids increased from 5.0 to 73.0 °Brix, while total sugar content increased from 4.4% to 55.1%. The pH decreased from 6.1 to 4.0, whereas titratable acidity increased from 0.14% to 0.25%. Vitamin C content decreased from 9.8 to 3.9 mg/%. The obtained results confirm that the local pumpkin raw material can be effectively used for the production of candied products and represents a promising direction for the rational utilization and processing of local plant raw materials, contributing to efficient resource use and reduction of raw material losses.*

***Key words:*** *Pumpkin, local form, candied products, osmotic dehydration, sugars, soluble solids, vitamin C.*

## Introduction

Modern food production places particular emphasis on the rational utilization of local plant raw materials and the development of new products with high added value based on them. The growing consumer demand for natural, plant-based products with high nutritional value promotes the development of technological processes that ensure maximum preservation of the nutritional and biologically active components of raw materials while increasing the shelf life of the final product. At the same time, efficient processing of local raw materials contributes to more rational utilization of available plant resources, reduction of raw material losses, and implementation of sustainable production principles.

Pumpkin (Cucurbita spp.) is an important agricultural and food raw material. Its fruit contains carbohydrates, dietary fiber, mineral elements, vitamins, and various biologically active compounds [1,2]. The nutritional and biological value of pumpkin is largely determined by its content of carotenoids, including β-carotene, α-carotene, lutein, and zeaxanthin. The amounts of these compounds depend on the plant species and varietal characteristics, cultivation conditions, and degree of fruit maturity [1,3].

Studies of the chemical composition of different pumpkin genotypes indicate that the fruit flesh is a source not only of carotenoids but also of polyphenols, tocopherols, mineral elements, and vitamins [2,3]. Significant differences in the content of biologically active compounds among species and varieties necessitate appropriate selection of raw materials for the production of functional products with high added value [3].

In the highland conditions of Khulo Municipality, local pumpkin forms are widespread and represent interesting and promising raw materials for processing. In local practice, some pumpkin forms are known as "Khapi." Studying the technological potential of this local raw material is important for its targeted utilization and for the development of new processing directions. Local processing of plant raw materials also creates an opportunity to reduce raw material losses and increase the efficiency of utilizing existing agricultural resources.

One promising direction for pumpkin processing is the production of candied products. The quality of candied products largely depends on the physicochemical and technological properties of the raw material, including flesh density and the content of dry matter, soluble solids, sugars, and organic acids. For candied-product production, it is particularly important to select fruits with relatively firm flesh and the ability to retain their shape and structure during thermal and osmotic treatment [4,5].

The technology of producing candied products is mainly based on osmotic dehydration of fruit flesh in a sugar or other osmotic-agent solution, followed by drying. Osmotic dehydration conditions, including temperature and osmotic-agent concentration, have a significant effect on water loss, sugar uptake, dry matter content, and the textural characteristics of the final product [4]. Proper selection of the technological regime is important to ensure efficient water removal and uniform penetration of sugar into the fruit tissue without excessive hardening of the surface layer or deterioration of product structure [4,5].

Particular importance is attached to preserving biologically active compounds in pumpkin during processing. The content and stability of carotenoids depend on both the genotype of the raw material and processing and storage conditions. High temperature and prolonged exposure to oxygen and light may affect carotenoid stability, which in turn influences the color and biological value of the product [1,6].

Thus, the use of local pumpkin forms widespread in Khulo Municipality for the production of candied products is of both scientific and practical importance. Studying the physicochemical and technological properties of local raw materials and selecting appropriate processing conditions makes it possible to assess the potential of this raw material for creating a new plant-based product with high added value. In addition, rational processing of local raw materials and production of value-added products from them can be considered an approach that promotes efficient resource utilization and reduction of raw material losses.

The aim of the study was to investigate the physicochemical and technological characteristics of local pumpkin raw material widespread in Khulo Municipality, select an optimal technological regime for producing candied products, and evaluate the main quality indicators of the obtained product.

## Materials and Methods

The research objects were local pumpkin raw material widespread in Khulo Municipality and the candied products obtained from it. To evaluate the physicochemical characteristics of the raw material and the quality indicators of the obtained candied products, moisture, dry matter, soluble solids, total sugars, pH, titratable acidity, and vitamin C content were determined.

### Determination of Moisture and Dry Matter

The moisture and dry matter contents of the raw material and finished product were determined in accordance with GOST 28561-90, “Products of fruit and vegetable processing.” Dry matter content was expressed as a percentage, while moisture was determined based on the water content of the sample.

### Determination of Soluble Solids

Soluble solids content was determined by the refractometric method and expressed in °Brix. This indicator was used as one of the technological parameters characterizing the degree of sugar saturation of the raw material and finished candied products.

### Determination of Titratable Acidity

Titratable acidity of the raw material and finished candied products was determined by the titrimetric method in accordance with GOST ISO 750-2013. This standard is intended for determining titratable acidity in processed fruit and vegetable products. The method is based on neutralization of acids present in the sample with a standard sodium hydroxide solution. Results were expressed as percentages.

### Determination of pH

The pH of the raw material and finished candied products was determined by the potentiometric method using a digital pH meter.

## Determination of Vitamin C

Vitamin C (ascorbic acid) content was determined in accordance with GOST 24556-81. The method is based on titrimetric determination of ascorbic acid using 2,6-dichlorophenolindophenol. Results were expressed in mg/%.

## Determination of Total Sugars

Total sugar content was determined in accordance with GOST 8756.13-87, “Products of fruit and vegetable processing.” Results were expressed as percentages.

## Technology for Producing Candied Pumpkin Products

For the production of candied pumpkin products, fruits at technological maturity, free from mechanical damage and signs of disease, were used. The fruits were washed, and the stem, seeds, and peel were removed; damaged or undesirable parts were mechanically removed. The prepared flesh was washed again and cut into uniform segments or cubes.

The size of the segments was approximately 25 × 10 mm, while the cubes were 10–15 mm. The relatively uniform size of the pieces facilitated more uniform syrup penetration and subsequent thermal treatment conditions.

## Blanching

The prepared pumpkin pieces were blanched for 10 minutes. This operation was used to prepare the raw material for subsequent osmotic treatment and to stabilize the technological process.

## Osmotic Saturation and Multistage Thermal Treatment

Blanched pumpkin pieces were covered with pre-prepared sugar syrup at a temperature of 85–90 °C and a concentration of 50–55%. The mass ratio of fruit to syrup was 1:1.6–1.7. The syrup-covered raw material was held for 3–4 hours, which promoted sugar penetration into the fruit tissue and osmotic removal of part of the water.

Subsequently, multistage thermal treatment was carried out, during which the syrup concentration was gradually increased. The technological regime comprised four stages: at Stage I, the syrup concentration was 50%; at Stage II, 60%; at Stage III, 70%; and at Stage IV, 75%. The duration of the first three stages was at least 4 hours, while at the end of the process the dry matter content reached approximately 73%.

At the second and third stages, the syrup concentration was increased by adding syrup of a higher concentration. At the fourth stage, a 50% citric acid solution was used as necessary to adjust the sensory characteristics of the product and regulate the technological process.

## Final Drying

After completion of the fourth stage, when the dry matter content of the pumpkin pieces reached approximately 72–73%, the fruit was removed from the vessel. After removal of excess syrup remaining on the surface, the fruit pieces were placed in a drying cabinet and dried at 65 °C for 8 hours.

The purpose of final drying was to further reduce surface and internal moisture, form the characteristic consistency and structure of candied products, and ensure stability of the finished product.

## Results ans Discussion

Within the study, the main physicochemical indicators of the local pumpkin raw material and the candied products obtained from it were evaluated. The results are presented in Table 1.

**Table 1.** Main physicochemical indicators of pumpkin raw material and candied pumpkin products.

| Indicator | Pumpkin raw material* | Candied pumpkin products* |
|---|---|---|
| Moisture, % | 90.2 | 27.3 |
| Dry matter, % | 9.9 | 73.0 |
| Soluble solids, °Brix | 5.0 | 73.0 |
| Total sugars, % | 4.4 | 55.1 |
| pH | 6.1 | 4.0 |
| Titratable acidity, % | 0.14 | 0.25 |
| Vitamin C, mg/% | 9.8 | 3.9 |

* Mean values.

The study showed that technological processing substantially changed the physicochemical characteristics of the pumpkin raw material. The moisture content of the raw material was 90.2%, whereas in the obtained candied products this indicator decreased to 27.3%, corresponding to an approximately 62.9% reduction. The substantial decrease in moisture was caused by osmotic dehydration followed by thermal drying. During this process, part of the water was removed from the pumpkin tissue, while soluble substances from the sugar solution penetrated into the raw material tissue. As a result, the product acquired a denser structure and a condition more favorable for prolonged storage.

Along with the decrease in moisture, dry matter content increased markedly. Dry matter in the raw material was 9.9%, whereas in the candied products it was 73.0%, i.e., approximately 7.4 times higher. This change directly reflects intensive water removal and transfer of sugar-syrup components into the product structure. The high dry matter content is an important technological characteristic of candied products because it is associated with the formation of product structure and the achievement of the final consistency.

A similar trend was observed in the soluble solids content. In the raw material, this indicator was 5.0 °Brix, whereas in the finished candied products it reached 73.0 °Brix. Thus, the indicator increased approximately 14.6-fold. Such a substantial increase is associated with treatment using multistage sugar syrup, during which sucrose and other soluble components gradually penetrate the pumpkin tissue as a result of osmotic mass transfer. The obtained result also indicates that the applied technological regime ensures intensive mass exchange between the raw material and syrup components.

Total sugar content was 4.4% in the raw material and 55.1% in the candied products. Accordingly, it increased approximately 12.5-fold. This change was primarily caused by multistage treatment with high-concentration sugar syrup. Sugar penetration into the pumpkin tissue simultaneously provides the characteristic sweet taste and contributes to the formation of the desired consistency. The obtained data confirm that the selected technological regime is effective for processing pumpkin fruit into candied products.

Differences were also observed in acid–base status indicators. The pH decreased from 6.1 in the raw material to 4.0 in the finished product. This change indicates the formation of an acidic environment in the product. At the same time, titratable acidity increased from 0.14% to 0.25%, corresponding to an approximately 78.6% increase. This change may be associated with the use of an acidity-regulating component during the technological process, as well as with the concentration of soluble substances and organic acids. The relatively low pH and increased titratable acidity contribute to the formation of the sensory properties of candied products and create more favorable conditions for product stability.

A significant change was also observed in vitamin C content as a result of technological processing. Its amount was 9.8 mg/% in the raw material and 3.9 mg/% in the finished candied products. Accordingly, vitamin C content decreased by approximately 60.2%. This loss was probably associated with thermal exposure during processing. The pumpkin raw material undergoes blanching, treatment in hot syrup over several stages, and final drying at 65 °C for 8 hours. Vitamin C is a relatively thermolabile compound; therefore, prolonged thermal exposure caused degradation of part of it.

Overall, the obtained results show that the applied technology for producing candied pumpkin products substantially changes the physicochemical characteristics of the raw material. Particularly important are the reduction in moisture and the substantial increase in dry matter and soluble components, including sugars. These changes resulted in the formation of a denser structure and characteristic organoleptic properties of the

product. At the same time, the decrease in vitamin C indicates that, when optimizing the technological process, the duration and intensity of thermal exposure should be considered in order to maximize the preservation of biologically active components.

Thus, the production of candied products from local pumpkin raw material represents a technologically appropriate direction for its processing. The combination of osmotic dehydration, multistage treatment with sugar syrup, and subsequent drying ensures the production of a product with high dry matter and sugar content while contributing to more complete utilization of local plant raw materials.

## Conclusion

Based on the conducted study, it was established that the local pumpkin raw material widespread in Khulo Municipality is technologically suitable for the production of candied products. The obtained results confirm that this raw material can be used in the technological process of producing candied products and makes it possible to obtain a quality product with high added value.

The proposed technology can be implemented in farms, household operations, and small processing enterprises. Complex and expensive equipment is not necessary to carry out the technological process, which is particularly important for small-scale producers.

Processing local pumpkin raw material contributes to reducing crop losses, more complete utilization of raw materials, and obtaining products with high added value. At the same time, the technology can be adapted according to the production volume of the farm and the available material and technical resources.

The production of candied pumpkin products creates opportunities for processing local raw materials and increasing farm incomes. The obtained product can be used both as an independent food product and in the production of confectionery, bakery products, desserts, and other food products. It can be marketed in local markets, small retail outlets, and the tourism and agritourism sectors.

Processing local pumpkin raw material is also important from an environmental perspective, as it promotes rational utilization of local plant resources, reduction of crop losses, and maximization of the benefits obtained from available raw materials. More efficient resource utilization and local processing of raw materials represent an approach that supports sustainable production.

This direction is particularly promising in the highland regions of Adjara, where the use of local pumpkin forms can contribute to the development of agricultural-product processing, expansion of the product range, creation of additional sources of income, and more efficient utilization of local plant resources.

## References


1. Batool M., Ranjha M.M.A.N., Roobab U., Manzoor M.F., Farooq U., Nadeem H.R., Nadeem M., Kanwal R., AbdElgawad H., Al Jaouni S.K., Selim S., Ibrahim S.A., Nutritional Value, Phytochemical Potential, and Therapeutic Benefits of Pumpkin (Cucurbita sp.). // Plants, 11(11), 1394, 2022. DOI: 10.3390/plants11111394.
2. Ninčević Grassino A., Rimac Brnčić S., Badanjak Sabolović M., Šic Žlabur J., Marović R., Brnčić M., Carotenoid Content and Profiles of Pumpkin Products and By-Products. Molecules, 28(2), 858, 2023. DOI: 10.3390/molecules28020858.
3. Kulczyński B., Sidor A., Gramza-Michałowska A., Antioxidant potential of phytochemicals in pumpkin varieties belonging to Cucurbita moschata and Cucurbita pepo species. // CyTA – Journal of Food, 18(1), 2020, pp. 472–484. DOI: 10.1080/19476337.2020.1778092.
4. Abraão A.S., Lemos A.M., Vilela A., Sousa J.M., Nunes F.M., Influence of osmotic dehydration process parameters on the quality of candied pumpkins. // Food and Bioproducts Processing, 91(4), 2013, pp. 481–494. DOI: 10.1016/j.fbp.2013.04.006.
5. Katsoufi S., Lazou A.E., Giannakourou M.C., Krokida M.K., Mass transfer kinetics and quality attributes of osmodehydrated candied pumpkins using nutritious sweeteners. // Journal of Food Science and Technology, 54(10), 2017, pp. 3338–3348. DOI: 10.1007/s13197-017-2786-2.
6. Ge H., Yang L., Yao Q., Carotenes from Pumpkin Flesh and Peel: A Review on Their Physicochemical Properties, Preparation Techniques, Detection Methods and Antioxidant Potential. // ACS Food Science & Technology, 5(3), 2025. DOI: 10.1021/acsfoodscitech.4c00964.

2nd International Scientific Conference "Modern Problems in Geophysics", Proceedings,
ISBN 978-9941-36-562-1, ISSN 3088-4349, Tbilisi, Georgia, October 29-31, 2026

# LONG-TERM (1919-2023) AND EXPECTED CHANGES IN THE WATER AVAILABILITY OF GEORGIAN RIVERS

**[*]Basilashvili Ts., [**]Janelidze M., [**]Basilashvili Kh.**

[*]*Institute of Hydrometeorology of the Georgian Technical University, Tbilisi, Georgia*
[**]*Caucasus University, Tbilisi, Georgia*
*jarjinio@mail.ru*

***Abstract.*** *As a result of climate warming and anthropogenic pressure, the conditions governing the formation of water runoff in river basins have changed. Analysis of long-term data from the observation network has made it possible to identify distinct stages in changes in river water availability. In the future, high precipitation in rivers along the Black Sea coast may lead to floods, mudflows, and landslides. Further east, river water availability is expected to decrease due to reduced precipitation. In eastern Georgia, drought-induced shortages of irrigation water will lead to a decline in crop yields, negatively affecting the well-being of the population and the country's economic development. In the south-eastern region, if appropriate preventive measures are not implemented in a timely manner, desertification processes are likely to develop.*

***Key Words:*** *Drought, degradation of the coastal zone, shortage of irrigation water.*

## Introduction

The totality of water resources in Georgia's water bodies, including rivers, lakes, reservoirs, canals, ponds, groundwater, springs, glaciers, snow cover, and wetlands, amounts to 65 km³ and constitutes the State Water Fund. Among these resources, rivers are of primary importance, as their water resources, amounting to 61.45 km³, are the largest in volume. Rivers contain continuously renewable fresh water, which is easily accessible to all and is therefore widely used for the water supply of the population and enterprises, irrigation, agricultural production, electricity generation, fisheries, tourism, recreation, and sport.

Given the multifunctional importance of river water, as well as the need to design and operate roads, bridges, and all types of structures along riverbanks, it is essential to determine river water availability. Taking this indicator into account makes it possible to plan a rational water-use regime correctly. River water availability is determined by the average long-term discharge of rivers, expressed in m³/s, which is referred to as the norm of river runoff. However, this value is not constant; it varies and does not follow any fixed regularity. Therefore, it must be periodically updated on the basis of new data.

## Study Area, Materials and Methods

Water resources in Georgian rivers are distributed very unevenly. From west to east, with increasing distance from the Black Sea and decreasing precipitation, both the number of rivers and their water availability decline. There are more than 18,000 rivers in western Georgia, with water resources amounting to 48 km³, whereas eastern Georgia has approximately 8,000 rivers, with resources of only 13 km³ [1].

Georgian rivers originate in high mountains and are characterised by steep gradients, rapid flow, and substantial potential energy reserves. In terms of hydropower resources per 1 km² of area, Georgia occupies one of the leading positions in the world. At present, there are approximately 60 hydropower plants in Georgia, producing 10 billion kWh of electricity. However, the country has the potential to operate 300 hydropower plants with an output of 40 billion kWh [2].

In recent decades, climate warming and intensive anthropogenic impact have changed the conditions governing the formation of river water availability. For example, active deforestation reduces the capacity of river basins to regulate water resources and also decreases both groundwater and surface runoff. In the future,

the melting of glaciers located in river headwaters will lead to a decline in river water availability. By 2020, compared with 1970, the area of glaciers had decreased by 41% in western Georgia and by 49% in eastern Georgia. The data on glacier areas, expressed in km², in the river basins shown in Fig.1 are taken from studies [1, 4-6].

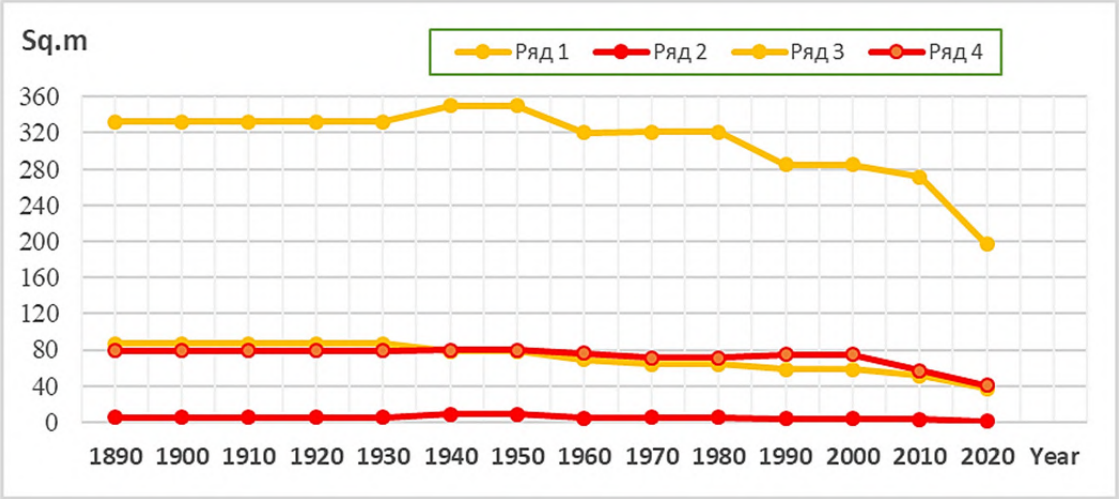



**Fig. 1.** Long-term changes in the area of glaciers located in river basins, km²:
1 – Enguri River; 2 – Rioni River; 3 – Tergi River; 4 – Greater Liakhvi River.

Although Georgia has a relatively small territory, it contains 100 types of landscapes. The landscapes of eastern Georgia are more sensitive than those of western Georgia. Droughts are recorded here annually for a period of two to three months, mainly in summer, when the risks of fires and degradation of vegetation and soil cover increase. The likelihood of such processes is particularly high on the Iori Plateau and in Kvemo Kartli.

It should be noted that the reference book published before 1981 [7] contained data from 182 hydrological gauging stations on Georgian rivers. Since the 1990s, however, only 20 gauging stations have been operating in Georgia, where water levels, rather than water discharge as before, are measured. In order to increase the number of study objects, data from previously operating gauging stations with long observation series were used. Missing observations were restored by establishing relationships between parallel observation data from analogous rivers. Through correlation analysis and graphical interpolation, water-discharge data were obtained for 21 gauging stations on rivers in western Georgia for the period 1919-2023, with observation series ranging from 36 to 86 years, and for 22 gauging stations on rivers in eastern Georgia for the period 1924-2023, with observation series ranging from 55 to 97 years.

## Results

Based on the appropriate statistical analysis of the obtained observation series, updated norms of river water availability and their main characteristics were determined [8, 9]. These constitute the principal determining parameters for all types of water-management calculations carried out by scientific, economic, and design organisations.

In order to assess long-term changes in river water availability, average long-term values of water availability were determined for individual decades [10, 11]. Their analysis revealed the trends of change: chronologically, river water availability sometimes increased and sometimes decreased. For a quantitative assessment of these changes, the differences between water availability values in consecutive decades were calculated, as shown in Table 1. Their analysis showed that, in western Georgia, river water availability until 1981, with some exceptions, was not characterised by major fluctuations. In 1981-1990, however, there was a sharp increase due to active glacier melting and high precipitation. In eastern Georgia, water availability decreased in some rivers and increased in others. In the most recent decade, 2010-2020, river water availability declined sharply, as shown in Fig. 2. This may be explained by increased evaporation under conditions of high temperatures, a decline in groundwater levels, and the drying up of springs.

In order to determine the expected future changes in river water availability, future projections of the main climatic factors governing its formation were used [12]. These projections were developed according to the global RCP4.5 scenario. It has been established that, compared with the period 1971-2000, air temperature is expected to increase during 2041-2100 by 1.8-3°C in western Georgia and by 2-3.7°C in eastern Georgia.

**Table 1.** Differences between river water discharges in individual decades.

| River | Station / Point | 1941-1950 1931-1940 | 1951-1960 1941-1950 | 1961-1970 1951-1960 | 1971-1980 1961-1970 | 1981-1990 1971-1980 | 1991-2000 1981-1990 | 2001-2010 1991-2000 | 2011-2020 2001-2010 |
|---|---|---|---|---|---|---|---|---|---|
| Enguri | Khaishi | -3,0 | 11,0 | -10,0 | 9,0 | 24,0 | -11,0 | | |
| Rioni | Chaladidi | -25,0 | 30,0 | -10,0 | -5,0 | 72,0 | 20,0 | | |
| Kvirila | Zestaponi | -3,6 | -4,3 | 0,5 | -3,6 | 11,5 | 2,4 | | |
| Tskhenistsqali | Khidi | -10,8 | -4,2 | -33,7 | 0,4 | 9,5 | -8,4 | | |
| Tekhuri | Nakalakevi | -8,5 | 2,5 | 3,4 | 3,0 | 2,3 | -2,1 | | |
| Supsa | Khidmaghala | - | 3,5 | -2,2 | 1,4 | 9,3 | -8,0 | | |
| Natanebi | Natanebi | -5,5 | 4,1 | -2,1 | -0,3 | 5,2 | - | | |
| Chorokhi | Erge | -14 | -35 | 0,6 | 1,6 | 0,5 | - | | |
| Acharistsqali | Keda | - | 2,0 | -2,1 | -1,7 | 11,3 | - | | |
| Mtkvari | Khertvisi | -5,8 | -0,6 | -1,8 | 1,7 | 0,2 | 1,5 | 0,4 | 1,8 |
| Mtkvari | Tbilisi | -26 | 6,0 | -20 | 24 | -13 | 33 | 5,0 | -24 |
| Paravani | Khertvisi | -2,6 | 1,7 | 0 | -0,9 | 1,3 | -0,8 | 1,0 | -6,6 |
| Greater Liakhvi | Kekhvi | 0,1 | -1,7 | 0,7 | 1,8 | 2,5 | -13 | 3,4 | - |
| Ksani | Korinta | 2,54 | 2,77 | -1,8 | -2,7 | 1,43 | -5,79 | 3,1 | - |
| Aragvi | Zhinvali | -8,2 | 0 | 0,6 | 3,7 | -3,3 | -4,4 | - | - |
| Iori | Lelovani | -3,3 | -1,6 | 0,2 | 2,1 | 0,2 | 2,3 | 7,7 | -7,8 |
| Alazani | Shakriani | -7,8 | 0,4 | -3,9 | 0,5 | 3,4 | -3 | 15,3 | -23,6 |
| Ktsia-Khrami | Red Bridge | -7,5 | -2,1 | -4,7 | -0,4 | 4,8 | 7,6 | 2,3 | -30,1 |

The highest annual precipitation total in western Georgia, 2,300 mm, is expected in the coastal zone of Adjara. An increase of 8-10% is expected only in Poti and Zugdidi. In the rest of the territory, with increasing distance from the Black Sea, precipitation is expected to decrease eastwards by 3-15%. In eastern Georgia, precipitation is projected to decrease by 9% in 2041-2070, while in 2071-2100 it is expected to change by only 1-6%.

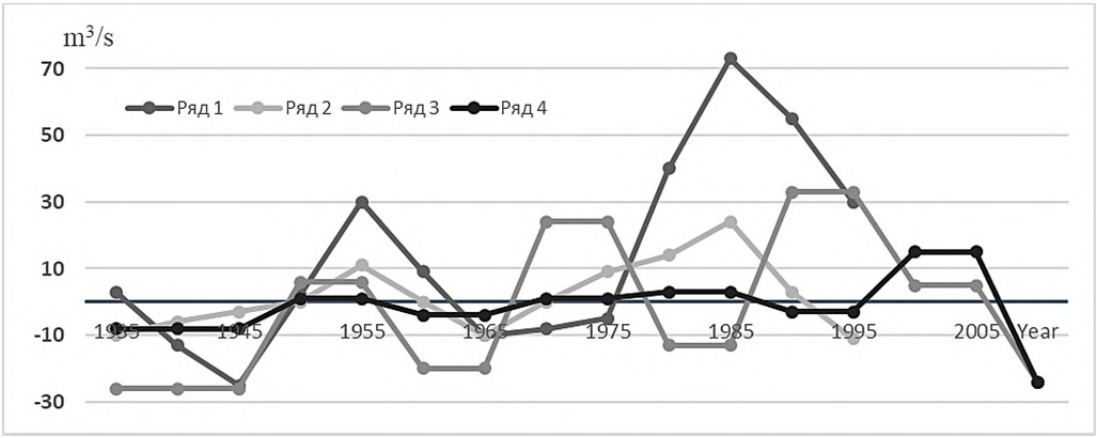



**Fig. 2.** Differences in river water availability, m³/s, between individual decades from 1921 to 2021:
1 – Rioni River, village of Chaladidi; 2 – Enguri River, village of Khaishi;
3 – Mtkvari River, Tbilisi; 4 – Alazani River, village of Shakriani.

## Conclusion

According to climate projections, intensive glacier melting is expected. However, glaciers have already decreased to such an extent that their meltwater can no longer cause a significant increase in river water availability. In the Black Sea coastal zone, however, the intensive condensation of increased evaporation in the form of heavy rainfall may cause floods, mudflows, and landslides near the mouths of individual rivers, leading to coastal degradation, destruction, and damage.

In eastern Georgia, higher temperatures, low water availability, and increased drought conditions will cause greater evaporation, drying of soils, a decline in groundwater levels, the drying up of springs, and, consequently, a sharp decrease in river water availability. The shortage of irrigation water in this region will hinder plant vegetation and crop yields, increase the risk of fires, and may initiate the development of desertification processes, especially in the south-eastern region. All of these factors will have a highly negative impact on the well-being of the population and on the country's economic development.

Under such circumstances, in order to ensure the rational use of water resources, it is necessary to implement, step by step, the relevant recommendations for their conservation and replenishment [13]. In the Black Sea coastal zone, appropriate preventive measures [14] should be carried out in order to mitigate the negative consequences of hazardous natural events.

## References


1. Water resources of Transcaucasia, Leningrad, GIMIZ, 1988, 264 p.
2. Svanidze G.G., Gagua V.P., Sukhishvili E.V., Renewable Energy Resources of Georgia. Leningrad. //GIMIZ, 1987, 175 p.
3. Basilashvili Ts., Forest cover – Main Protect from of Various in Mountainous Areas. International Scientific. // Conference "Natural Disasters in the 21 Century". Tbilisi State University, 2021, pp. 189-193.
4. Elizbarashvili E., Climate of Georgia. // Tbilisi, GTU, IHM, 2017, 360 p.
5. Catalog of Glaciers of USSR, Leningrad, // GIMIZ, Vol. 9, Issue 3, Part 1, 1975, 86 p.
6. Shengelia L., Kordzakhia G., Tvauri G., Guliashvili G., Beridze S., The Study of the Degradation of the Glacial Basin of Western Georgia against the background of ongoing climate change using satellite remote sensing data. // Transactions IHM, GTU, Vol. 135, 2024, pp. 64-68. http://doi.org/10.36073/1512-0902-2024-135-64-68
7. State Water Cadaster, Leningrad, GIMIZ, Vol. VI, Georgian SSR, 1987, 416 p
8. Basilashvili Ts., Revised Characteristics of River Runoff in Western Georgia. // Science and Technologies, Tbilisi, № 1 (750), 2026, pp. 13-18. DOI: http://doi.org/10.36073/0130-7061
9. Basilashvili Ts. Z., Updated Parameters of Average Annual River Discharge in Eastern Georgia. // Transactions IHM, GTU, Tbilisi, Vol. 136, 2025, pp. 16-22. http://doi.org/10.36073/1512-0902-2025-136-16-22
10. Basilashvili Ts. Z., Assessment of Changes in River Runoff in Western Georgia. // Transactions HIM, GTU, Tbilisi, Vol. 139, 2026, pp. 8-17. http://doi.org/10.36073/1512-0902-2026-139-8-17
11. Basilashvili Ts. Z., Changes in River Runoff in Eastern Georgia under Contemporary Climate Warming. // Science and Technologies, Tbilisi, № 2 (751), 2026, pp. 28-37. http://doi.org/10.36073/0130-7061
12. Kartvelishvili L., Tatishvili M., Amiranashvili A., Megrelidze L., Kutaladze N., Weather, Climate and their Change Regularities for the Conditions of Georgia. // Monograph, Tbilisi, Publishing House "Universal", 2023, 406 p. http://doi.org/10.52340/mng.9789941334658
13. Basilashvili Ts., Recommendations for Measures to be Implemented in Eatern Georgia under Conditions of Declining River Water Resources. // Science and Technologies, Tbilisi, №3 (752), 2026. http://doi.org/10.36073/0130-7061
14. Basilashvili Ts., Safety Issues in the Face of Increased Risk of Floods. // Science and Technologies, Tbilisi, №3 (743), 2023. http://doi.org/10.36073/0130-7061

2nd International Scientific Conference "Modern Problems in Geophysics", Proceedings,
ISBN 978-9941-36-562-1, ISSN 3088-4349, Tbilisi, Georgia, October 29-31, 2026

# MAP OF QUATERNARY LOOSE DEPOSITS OF THE REPUBLIC OF ARMENIA

**Boynagryan V., Ayriyants A.**

*Yerevan State University, Department of Cartography and Geomorphology, Yerevan, Armenia*
*vboynagryan@ysu.am, angelino@ysu.am*

***Abstract.*** *For the first time, a map of the genetic series of Quaternary surface loose deposits covering the entire territory of the Republic of Armenia has been compiled at a scale of 1:100,000. Their granulometric, mineralogical, spectral and chemical compositions, physical and mechanical properties, thickness and filtration coefficient have been determined. Alluvial deposits exceeding the permissible thickness for the Marmarik River have been identified, confirming that its valley coincides with a graben.*

***Key Words***: *Armenia, geomorphological mapping, Quaternary deposits.*

## Introduction

Quaternary loose deposits of Armenia have long remained insufficiently studied in terms of their composition and distribution. At the same time, they are of considerable scientific and practical importance and are of interest not only to geomorphologists and geologists, but also to specialists involved in the engineering-geological assessment of the territory, particularly because the foundations of various structures are often placed in these deposits and their stability under the impact of hazardous engineering-geological processes must be evaluated. Data on the composition of loose deposits can be used to determine their genesis, reconstruct the physical-geographical conditions of sediment deposition, address stratigraphic problems and for other purposes [1].

## Study area, material and methods

Based on extensive field research, including mapping of loose deposits at a scale of 1:25 000 conducted for various purposes in different parts of the republic, as well as data from numerous boreholes, laboratory analyses of approximately 3 500 soil samples, interpretation of aerial photographs and topographic maps at different scales, a map of Quaternary loose deposits at a scale of 1:100 000 was compiled on 12 sheets. An additional map at a scale of 1:25 000 was prepared for the northern regions of the republic.

Four genetic series of loose deposits are distinguished on the compiled map: the **eluvial series** (eluvium and eluvio-deluvium); the **slope series** (undifferentiated loose deposits of limited thickness over bedrock, landslide deposits and deluvio-proluvium); the **aquatic series** (*fluvial group* – flood-plain and river-terrace alluvium and proluvium of alluvial fans; *lacustrine group* – lacustrine deposits of the Leninakan and Sisian formations, lacustrine-dam deposits, silts of lake and reservoir bottoms and lacustrine clays) and the **glacial series** (moraine deposits of the Würm and Riss glaciations, fluvioglacial and glaciolacustrine deposits).

Bedrock with an exposed surface or covered only by turf is shown separately. Large landslides of seismic, exogenous and anthropogenic origin that are clearly expressed in the relief, as well as large proluvial alluvial fans, are represented by out-of-scale conventional symbols. The map indicates the age and thickness of the loose deposits and the locations of boreholes.

## Results

***In terms of granulometric composition***, the identified genetic series of Quaternary loose deposits are represented by the following varieties:

- ***Eluvial series*** – gravelly and grus accumulations with a loamy or sandy-loam matrix, locally silty sands and loams; on lavas, tuffs, volcanogenic-sedimentary and sedimentary rocks – clays, silty sands and loams with a small content of gravel and grus;

- ***Slope series*** – undifferentiated sandy loams, loams and clays with varying amounts of gravel and grus; locally, gravelly-grusy accumulations with individual boulders and a sandy-loamy matrix, forming a thin cover over bedrock; landslide grusy-gravelly accumulations with a loamy and sandy-loam matrix and individual large boulders, as well as sandy loams, loams and clays with a small content of gravel and grus;
- ***Aquatic series*** – floodplain and terrace alluvium: boulder-pebble accumulations with gravel, sand and clay; heterogeneous sands, loams and sandy loams with inclusions of gravel, pebbles and grus; proluvial deposits of alluvial fans: boulder-pebble-gravel accumulations with a sandy-loamy matrix; lacustrine deposits of the Leninakan Formation (clays, sands, etc.) and the Sisian Formation (clays, diatomites); lacustrine-dam loess-like loams, sandy loams and clays; silts of lake and reservoir bottoms; lacustrine clays;
- ***Glacial series*** – moraine deposits of the Würm and Riss glaciations; fluvioglacial and glaciolacustrine deposits. The Würmian moraines consist of boulder-gravel accumulations with a sandy-loamy-grusy matrix of a greyish-brown colour. The Rissian moraines consist of boulder-gravel accumulations with a sandy-loamy-grusy and clayey matrix of a yellowish-brown colour. Fluvioglacial deposits are represented by boulder-pebble gravels with a gravelly-grusy-sandy matrix and a small admixture of clayey material. Glaciolacustrine deposits consist of layered clays, sandy loams, loams and sands with a total thickness ranging from several metres to 35–50 m, as well as white and pale-pink porous diatomites. At the base of the glaciolacustrine deposits, there are heavy dark-brown clays that are very dense and fat, with a conchoidal fracture and a shiny bedding surface. They are highly plastic when wet; their plasticity index ranges from 17.6 to 20.1.

Deposits of the eluvial series are widespread on levelled surfaces and interfluve slopes with inclination angles of up to 5–8°. Their thickness generally does not exceed 0.1–0.5 m and rarely exceeding this value. On lavas, a sandy-loam eluvial cover with a high carbonate content, the so-called *belozems*, is formed. Their thickness ranges from 0.1–0.5 m to 3–8 m. On volcanogenic-sedimentary formations, the thickness of the eluvium is 2–8 m.

On slopes, the cover of loose deposits is generally thin (usually 0.3–0.5 m, rarely up to 1 m or more). Only in areas where ancient gullies occur in the slope relief are accumulations of loose deposits several meters thick observed, in some cases reaching 15–20 m or more. The thickness of landslide deposits varies widely, from several meters for small landslides to 100–170 m for large seismogenic landslide blocks and landslide flows.

Intermontane basins and large rivers valleys are filled with thick sequences of lacustrine, lacustrine-alluvial and alluvial deposits. On the Lori Plain (basin), the thickness of lacustrine-alluvial deposits reaches 100–114 m; in the Pambak basins – 70–157 m (near Mets Parni village); near the town of Spitak – 120–185 m; between Spitak and Vanadzor – 200–240 m; near the town of Vanadzor – 58–100 m. In the Akhuryan River basin, alluvial and lacustrine-alluvial deposits have a thickness of 25–62 m in the upper reaches of the river, 270–320 m near Gyumri, with tuff interbeds 4–10 m thick and 400 m south of Gyumri. In the Lake Sevan basin, on the Masrik Plain, the thickness of lacustrine deposits is 250–300 m near Martuni, 80–320 m near Vardenis and 190–485 m near Masrik. Lacustrine deposits of the Sisian Formation have a thickness of 20–170 m. In the Ararat Valley, the thickness of alluvial deposits reaches 100–160m and locally 193 m. In the valley of the Marmarik River, the thickness of the alluvium is 110–180 m and is approximately 20–30 times greater than the permissible normal thickness for this river, based on its maximum depths and flood heights. In our view, this is related to the fact that the Marmarik River valley represents a graben (the well-known major active Marmarik Fault passes through this area). The accumulation of alluvial material probably occurred as the structure subsided. The thickness of Würm-age moraines reaches 100 m on Mount Aragats, 10–60 m in the Gegham Range and 50 m on Mets Ishkhanasar and Tsghuk.

In the material composition of the light fraction of eluvial accumulations, clay minerals and strongly weathered grains predominate (up to 95–99%). The clay minerals are represented mainly by montmorillonite. Chlorite, hydromica and calcite occur as admixtures (the endothermic peak has a maximum at 900°C). Other minerals include quartz (1–2%), gypsum and volcanic glass are occasionally present. The chemical composition of the eluvium allows it to be classified as a calcareous type, while the presence of a large amount of $CaCO_3$ determines the alkaline reaction of the medium in which secondary minerals are formed [2].

In the light fraction of loose slope accumulations, strongly weathered feldspar grains and clay particles predominate (up to 80–95%) Gypsum and quartz occur in small amounts (1–3 and up to 6% respectively).

Geochemical coefficients indicate a greater degree of transformation of defluction, deluvial and landslide deposits, with the removal of unstable compounds, compared with deposits of the eluvial series. More readily soluble compounds have been removed from landslide deposits than from other slope accumulations.

In the northeastern part of the republic, in the basins of the Varagajur, Tavush and Khndzorut rivers, dense, microporous, light-yellow, silty and mostly free of coarse rock material, generally structureless sandy loams, loams, clays and diatomites are widespread, with a total thickness of up to 25–30 m. They occur on various landforms, overlie the alluvium of the second and third terraces, ancient alluvial fans and bedrock, can be traced high on the slopes up to absolute elevations of 1400 – 1500 m and in appearance resemble loess-like loams (Fig. 1).



**Fig. 1.** Exposure of loess-like loams in the lower reach of the river Varagajur (photo by V. Boynagryan)

These deposits are characterized by increased carbonate content (up to 8.02 – 10.58%). They contain secondary formations in the form of carbonate accumulations 2–3 to 10 cm in diameter, as well as foraminiferal shells characteristic of the limestones widespread in this area. Among the extant species is *Napaeopsis hohenackeci*, widespread throughout Transcaucasia and characteristic of arid conditions [3].

The formation of these loess-like loams apparently dates to the Middle and Late Pleistocene, since they overlie high terraces and do not occur on the floodplain or the first above-floodplain terrace. A similar age for a 25–30 m thick structureless loess-like sequence widespread in the Kura Depression was noted by M. A. Museibov [4]. Modern studies of loess-soil sequences in northeastern Armenia also indicate a Middle and Late Pleistocene age for these deposits; the chronology obtained for individual sections extends back to MIS 8 [5, 6].

There is no consensus regarding the origin of these loams. A. T. Aslanyan [7] assigned a significant role in their formation to the aeolian factor. The aeolian origin of these deposits is also considered by K. A. Kazanchyan and co-authors [8].

According to V.R.Boynagryan [9], these deposits may have formed in shallow semi-enclosed lagoons of a lacustrine basin that existed in this area. After the drainage of the basin, the accumulated deposits were exposed to arid conditions and, as a result of subsequent accumulation of calcium carbonate, changed their texture, acquiring a microporous, structureless structure. Such material could easily undergo aeolian transport. Only locally, where sandy deposits and volcanic ash accumulated, was lacustrine stratification preserved.

In the granulometric composition of these loess-like loams, fractions smaller than 0.05 mm predominate: 74.57% in loams and 75.59% in clays. Clay-sized particles smaller than 0.005 mm account for 20.71% and 29.0%, respectively, which is also reflected in their plasticity index: 13.2 for loams and 20.3 for clays [9] (Table 1).

Additional information is provided by a comparison of the silicate analysis data for the loess-like loams and the weathering crust of the underlying limestones. The weathering crust contains more relatively immobile oxides ($SiO_2$, $Al_2O_3$, $Fe_2O_3$) and less $CaCO_3$ than the loess-like loams. The higher $CaCO_3$ content of the

loess-like loams is consistent with the assumption that they were transformed under arid conditions with corresponding accumulation of calcium carbonate [9].

**Table 1.** Physico-mechanical properties of loess-like loams and clays [9]

| Rock (number of samples) | The content of granulometric fractions, % | | | | | | | Specific gravity, g/cm$^2$ | Carbonate content, % | Plasticity | | |
|---|---|---|---|---|---|---|---|---|---|---|---|---|
| | >1 mm | 1 – 0.5 mm | 0.5 – 0.25 mm | 0.25 – 0.05 mm | 0.05 – 0.01 mm | 0.01 – 0.005 mm | < 0.005 mm | | | Upper limit | Lower limit | The number of plasticity |
| Loam (9) | 4.03 | 6.04 | 0.56 | 14.8 | 38.97 | 14.9 | 20.7 | 2.55 | 8.02 | 46.1 | 32.9 | 13.2 |
| Clay (9) | 1.01 | 1.61 | 0.32 | 21.47 | 31.69 | 14.9 | 29.0 | 1.65 | 10.58 | 46.8 | 26.5 | 20.3 |

## Conclusion

Mapping of Quaternary loose clastic deposits within the Republic of Armenia made it possible to systematize their genetic and spatial distribution, characterize their composition, structure and properties, as well as establish the thicknesses of individual varieties and the features of their formation.

## References


1. Guide to the study of recent deposits. Conjugated analysis. // MSU Press, M., 1987, 238 p. (in Russian)
2. Boynagryan T. G., Boynagryan V. R., Geochemical features of loose sediments in the middle reaches of the Agstev River basin. // Izvestiya AN ArmSSR. Nauki o Zemle, v.4, 1985, pp. 31–38. (in Russian)
3. Boynagryan V. R., Boynagryan T. G., Geochemical characteristics and genesis of loose cover formations in the Agstev River basin (Armenian SSR). // Litologiya i Polezniye Iskopaemie, v.4, 1989, pp. 117–122. (in Russian)
4. Museibov M. A., Some features of the geomorphology of intermountain depressions in geosynclinal regions (on the example of Kura depression). // Uchenye Zapiski Azerbaydzhanskogo Universiteta. Geologo-Geograficheskie Nauki, v.2, 1964, pp.71–82. (in Russian)
5. Wolf D., Baumgart P., Meszner S., Fülling A., Haubold F., Sahakyan L., Meliksetian K., Faust D., Loess in Armenia – stratigraphic findings and palaeoenvironmental indications. // Proceedings of the Geologists' Association, vol. 127, no. 1, 2016, pp. 29–39. DOI: 10.1016/j.pgeola.2016.02.002.
6. Lomax J., Wolf D., Meliksetian K., Wolpert T., Sahakyan L., Hovakimyan H., Faust D., Fuchs M., Testing post-IR-IRSL dating on Armenian loess-palaeosol sections against independent age control. // Quaternary Geochronology, vol. 69. 101265, 2022. DOI: 10.1016/j.quageo.2022.101265.
7. Aslanyan A. T., Regional geology of Armenia. // Haypetrat, Yerevan, 1958, 430 p. (in Russian)
8. Kazanchyan A. A., Hayrapetyan T. A., Balyan A. S., Soil-forming rocks map. // Atlas of agriculture of the Armenian SSR, Moskva–Erevan, 1984, p. 57. (in Russian)
9. Boynagryan V. R., New data on loose formations of Varagajur, Tavush and Khndzorut river basins (Republic of Armenia). // Proceedings of the YSU C: Geological and Geographical Sciences, v.57, 3(261), 2023, pp. 106–116. (in Russian)
   DOI: 10.46991/PYSU:C/2023.57.3.106.

2nd International Scientific Conference "Modern Problems in Geophysics", Proceedings,
ISBN 978-9941-36-562-1, ISSN 3088-4349, Tbilisi, Georgia, October 29-31, 2026

# MAGNETIC FIELD REVERSALS IN MODIFIED BULLARD'S MODEL

**[*,**]Kharshiladze O., [*]Kezua L., [*,**]Tsulukidze L., [**]Zilpimiani D.**

**Ivane Javakhishvili Tbilisi State University, Tbilisi, Georgia*
***M. Nodia Institute of Geophysics of the I. Javakhishvili Tbilisi State University, Tbilisi, Georgia*
*luka.kezua913@ens.tsu.edu.ge*

***Abstract.*** *Earth's magnetic field has crucial impact on our planet. It shields the Earth from the stream of charged particles released from the Sun (solar wind). Due to its significance, physicists have been researching Earth's magnetic field and its origins for years. According to the most accepted theory, source of the Earth's magnetic field is movement of conductive fluid in planet's outer core. The geodynamo model gives us magnetohydrodynamic (MHD) equations which are complex to solve even numerically due to the extreme parameters of the outer core. Consequently, simplified models are used to study some physical mechanisms. Paleomagnetic data demonstrates that Earth's approximately dipole magnetic field has reversed its polarity multiple times. In this article, we study modified version of Bullard's 1 disk dynamo. While magnetic field reversals aren't observed in the classical model, introducing time delay arises field reversals in system. Furthermore, adding an external field effect also arises reversals and it's possible to control reversal times using external current. Our results show that when Bullard's dynamo is driven by external current which switches its sign according to real paleomagnetic data, we have synchronization between real data and model's numerical solution.*

***Key words:*** *Geomagnetic Field Reversals, Disk Dynamo Models, Bullard's Model, Delay Differential Equations.*

## Introduction

Earth's magnetic field is vitally important to our planet since acts as a protective shield against the solar wind. In first approximation, Earth's magnetic field possesses a dipolar structure, with its magnetic moment aligned along the axis of rotation [1]. Paleomagnetic observations indicate that the magnetic field has undergone polarity reversals multiple times throughout history [2]. The most recent reversal occurred 780,000 years ago (the Brunhes–Matuyama reversal). Currently, magnetohydrodynamic (MHD) dynamo theory is the most widely accepted explanation for the origin of Earth's magnetic field. Earth's core consists of a solid inner core and a liquid outer core. According to dynamo theory, the motion of the electrically conducting fluid generates circulating currents which, on the other hand, create a magnetic field. Additionally, the dynamo process requires an initial magnetic field. Numerical simulations are highly complex due to the extreme parameters of the outer core – for instance, a magnetic Prandtl number of $10^{-5}$ [1]. For this reason, it is often useful to consider simplified models to understand the mechanism. In this article we will discuss modified Bullard's 1 disk dynamo and magnetic field reversals in new system.

## Bullard's One Disk Dynamo

In 1955, Bullard [3] formulated a single-disk model (Fig. 1) consisting of a rotating conducting disk and a connected conductor. The disk moves within a magnetic field. By applying Faraday's law of induction and Kirchhoff's law, we obtain a system of equations:

$$\begin{cases} L\dfrac{dI}{dt} = -RI + MI\Omega \\ C\dfrac{d\Omega}{dt} = G - MI^2 \end{cases} \tag{1}$$

where $I$ is current in conductor, $\Omega$ – disk's angular velocity, $R$ is conductor's resistance, $L$ – self-inductance, $C$ is disk's moment of inertia, $G$ – applied torque, and $M$ is mutual inductance. To reduce parameters and simplify numerical calculations, let's use non-dimensional variables:

$$I = \sqrt{\frac{G}{M}}i, \quad \Omega = \sqrt{\frac{GL}{CM}}\omega, \quad t = \sqrt{\frac{CL}{GM}}t' \tag{2}$$

Consequently, we get the following system:

$$\begin{cases} \frac{di}{dt'} & = -\mu i + i\omega \\ \frac{d\omega}{dt'} & = 1 - i^2 \end{cases} \tag{3}$$

Where $\mu = R\sqrt{\frac{C}{LMG}}$.

According to Cook and Roberts [4], Rikitake's [5] system has two different time scales: $\tau_m = \frac{CR}{GM}$ ("Mechanical Time Scale") and $\tau_e = \frac{L}{R}$ ("Electromagnetic Diffusion Time"). Let's note that Bullard's and Rikitake's systems have similar equations. Electromagnetic diffusion time can be defined using formula: $\tau_e = \frac{L^2}{\nu_m}$ [6], where $L$ characteristic scale of the outer core $\sim 2000$ km and magnetic diffusivity: $\nu_m = 2$ m$^2$/s. $\tau_e$ will be unit of $10^4$ years. According to Cook's and Robert's estimation: $\tau_m \sim 10^4$ and $\mu = \sqrt{\frac{\tau_m}{\tau_e}}$. For our study we used: $\tau_e \sim 10^4$ years, $\tau_m \sim 10^4$ years, $t' = \sqrt{\tau_m \tau_e} = 10^4$ years.

Classical model gives us current (magnetic field) variations, but field reversals aren't observed

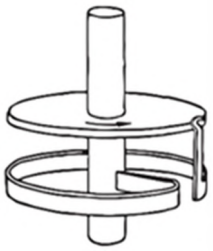


**Fig. 1.** Bullard's Dynamo.

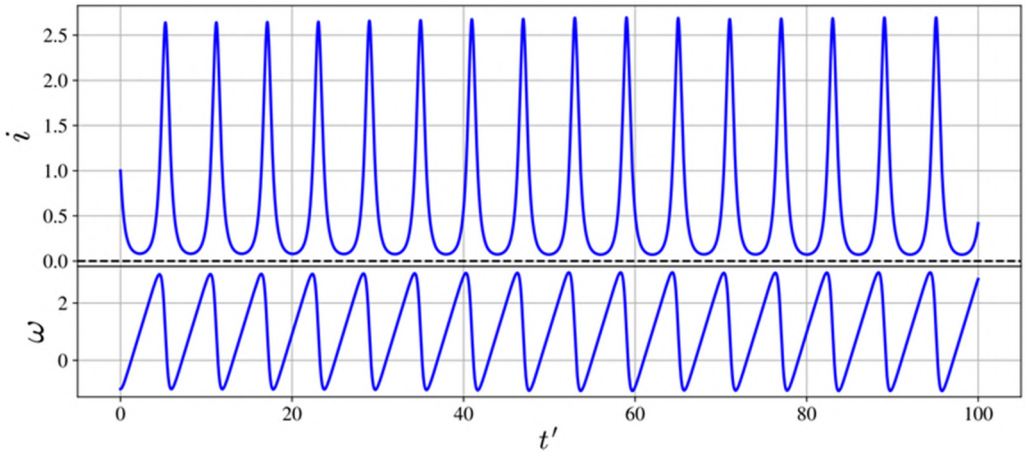



**Fig. 2.** Bullard's dynamo for the following parameters: $\mu = 1, i(0) = 1, \omega(0) = -1$ .

## Dynamo in an external field

Now similarly to Rikitake's Model [7], let's consider Bullard's dynamo in external magnetic field. According to Faraday's law, magnetic field will induce $i_0$ current and we'll get modified system:

$$\begin{cases} \frac{di}{dt'} & = -\mu i + (i + i_0)\omega \\ \frac{d\omega}{dt'} & = 1 - i(i + i_0) \end{cases} \tag{4}$$

Source of this field can be interstellar magnetic field. To estimate order of magnitude of external current, we can use Ohm's law for moving conductor:

$$\mathbf{j} = \sigma \mathbf{v} \times \mathbf{B} \tag{5}$$

In Core: $v \sim 10^{-2} - 5 \cdot 10^{-2}$ cm/s [8], $B \sim 2.5 \cdot 10$ Gauss [9], accordingly: $vB \sim 10^{-}1 - 1$In interstellar medium: $v \sim 2.5 \cdot 10^{6}$ cm/s [10] , $B \sim 10^{-7} - 10^{-5}$ Gauss, [11] , $vB \sim 10^{-1} - 10$, we get:

$$\frac{j_{external}}{j_{internal}} \sim 10^{-1} - 10^{2}$$

Currents $i$ and $i_0$ may differ by one or two orders of magnitude.

When $i_0$ is constant, current settles to a certain constant value. If we decrease $i_0$ current will need some more time to settle.

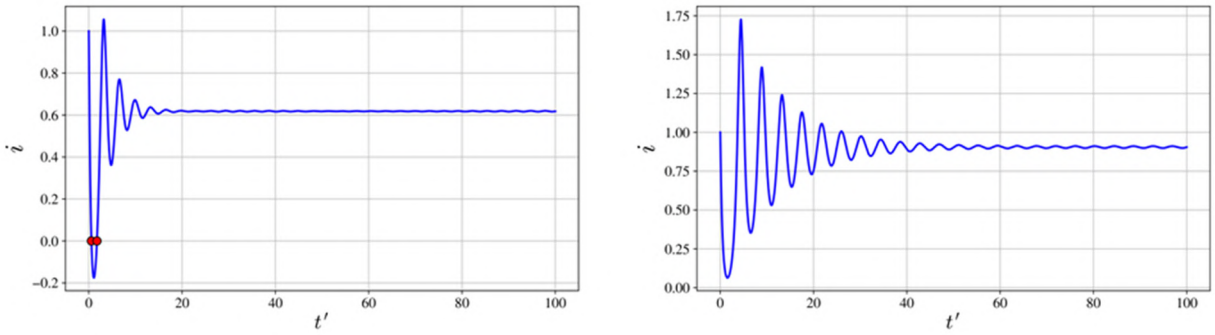



**Fig. 3.** Dynamo in external field: $\mu = 1, i_0 = const, i(0) = 1, \omega(0) = -1$.

When external current is periodic, system becomes synchronized with it: reversals occur in accordance with external current. Fig.4 shows modified Bullard's system with sinusoid (a) and rectangular wave (b) as $i_0$.

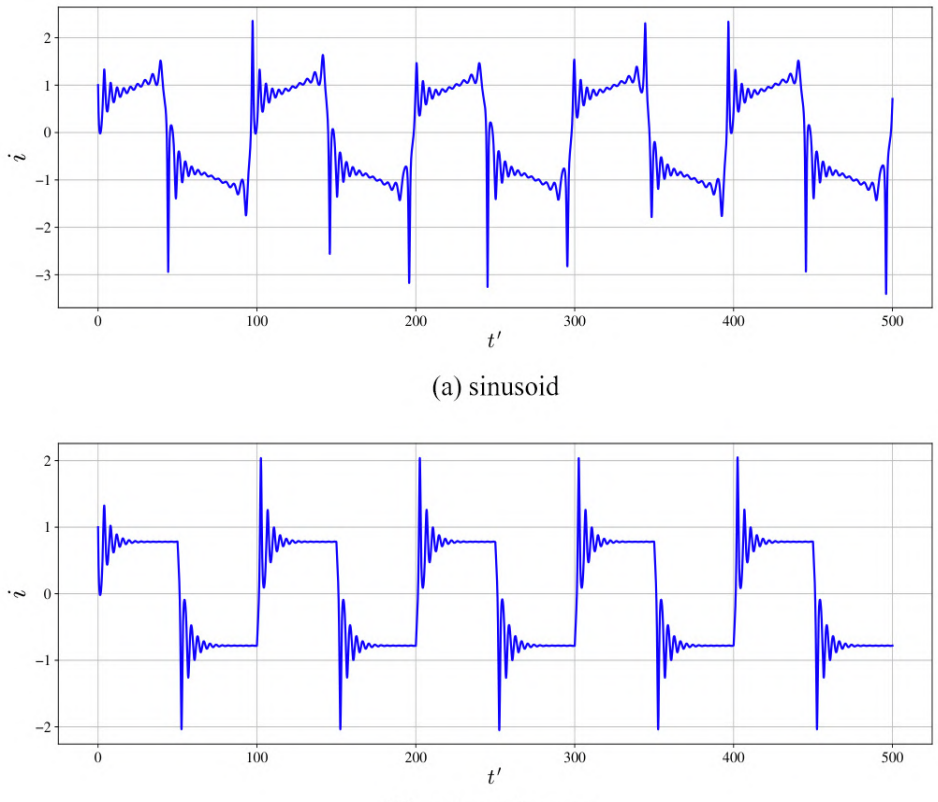



**Fig. 4.** Dynamo under periodic external current: period: 100, amplitude: 0.5.

In addition to periodic signals, we decided to utilize geomagnetic reversal data [2] and used a rectangular signal that changes polarity in accordance with that data. Figure 5 shows that, in the modified Bullard model, reversals occur at approximately the same times as the actual reversals indicated by paleomagnetic data.

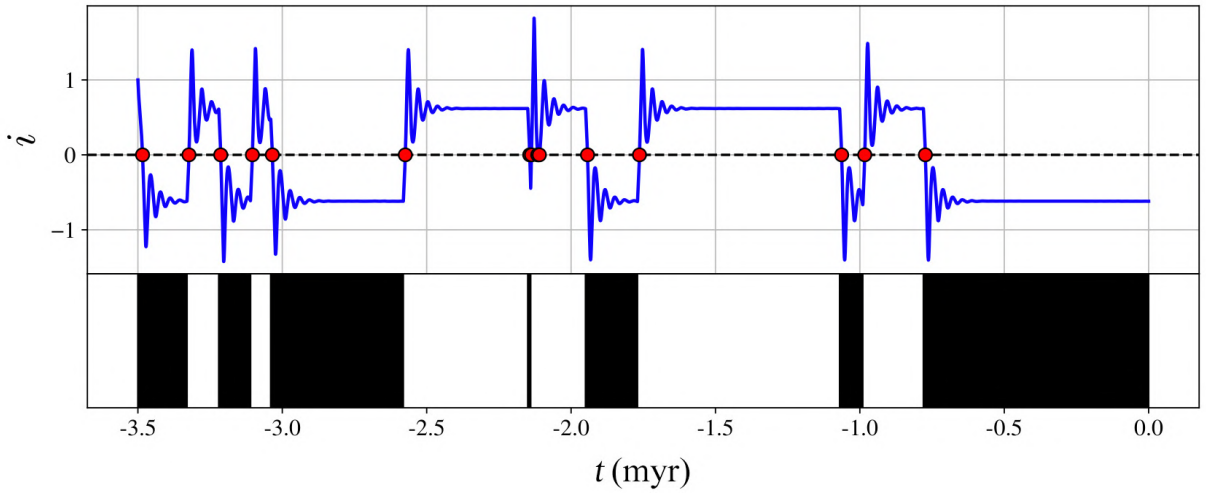



**Fig. 5.** Modified Bullard's model.

## Dynamo with time delay

(3) implies that changes in the core propagate instantaneously, whereas the transmission of changes occurring in the core through the conducting fluid must take place via Alfvén waves and electromagnetic diffusion [12]. Accounting for the time delay in the first approximation yields the following system of equations:

$$\begin{cases} \dfrac{di(t')}{dt'} = -\mu i(t') + i(t'-\tau)\omega(t') \\ \dfrac{d\omega}{dt'} = 1 - i(t'-\tau)i(t') \end{cases} \tag{6}$$

Unlike the classical Bullard dynamo, once a time delay is introduced into the system, it becomes possible to observe reversals:

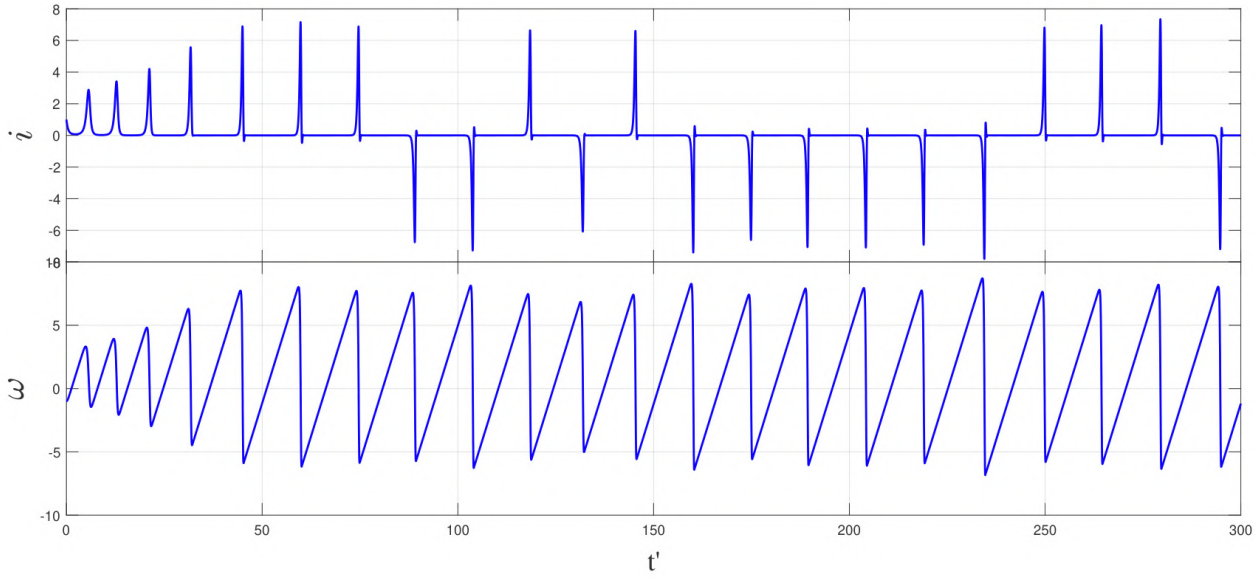



**Fig. 6.** Bullard's dynamo with time delay: $\mu = 1,\ i_0 = 1,\ \omega_0 = -1, \tau = 0.09$.

It is worth noting that reducing the delay time gives rise to inversions starting later: the shorter the delay, the later the inversions begin.

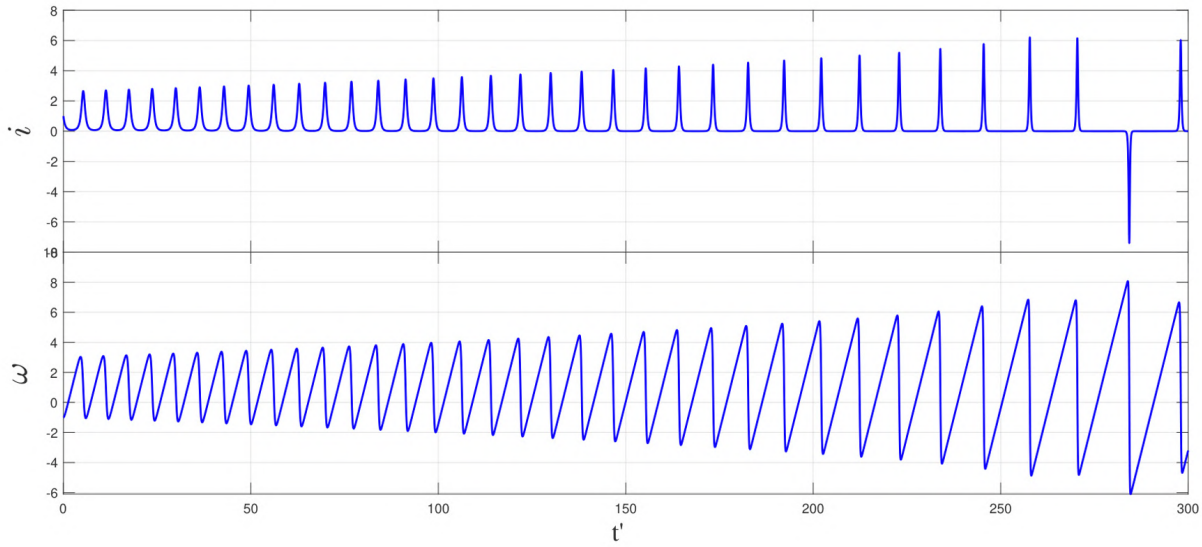



**Fig. 7.** Bullard's dynamo with time delay: $\mu = 1,\ i_0 = 1,\ \omega_0 = -1, \tau = 0.09$.

## Conclusion

In this article, we examined two different modifications of the classic Bullard model. It is well known that magnetic field reversals are not typically observed in the Bullard dynamo. First, we considered the Bullard model in the presence of an external magnetic field, the likely source of which could be the interstellar magnetic field. Applying a constant external field drove the current (and thus the magnetic field) to a steady value. Introducing a sinusoidal field synchronized the system with the external field, resulting in reversals that followed the sinusoidal pattern. Furthermore, applying a signal derived from paleomagnetic observations caused the system to undergo reversals consistent with real-world data. Additionally, based on physical considerations, we modified Bullard's dynamo by incorporating a time delay. Unlike the classic model, the model with a delayed argument allows for the observation of reversals.

## References


1. Dieter Biskamp. Magnetic reconnection. // In: Physics Reports 237, 4, 1994, pp. 179–247.
2. Cande S. C. and Kent D. V., "Revised calibration of the geomagnetic polarity timescale for the Late Cretaceous and Cenozoic". // In: Journal of Geophysical Research: Solid Earth 100.B4, 1995.
3. Bullard E.. The stability of a homopolar dynamo. // In: Mathematical Proceedings of the Cambridge Philosophical Society 51, 4, 1955, pp. 744–760. DOI: 10.1017/S0305004100030814.
4. Cook E. and Roberts P. H., The Rikitake two-disc dynamo system. // In: Mathematical Proceedings of the Cambridge Philosophical Society 68, 2, 1970, pp. 547–569.
5. Rikitake T., Oscillations of a system of disk dynamos. // In: Mathematical Proceedings of the Cambridge Philosophical Society 54, 1, 1958, pp. 89–105. DOI: 10.1017/S0305004100033223.
6. Krishan V., Astrophysical plasmas and fluids. // Springer Science & Business Media, Vol. 235, 1999.
7. Kharshiladze O. A., Tsulukidze L. K., Kezua L. B., & Zilpimiani D. O., Control of Inversions of the Earth's Magnetic Field with Rikitake's Model. // Journals of Georgian Geophysical Society, 28(2), 2025.
8. Akasofu S.I. and Chapman S., Solar-terrestrial physics. // In:Solar-terrestrial physics. by Akasofu, 1972, p. 42251.
9. Bruce A, Tidal dissipation and the strength of the Earth's internal magnetic field. // In: Nature 468.7326, 2010, pp. 952–954.
10. Opher M., Loeb A., and Peek J., A possible direct exposure of the Earth to the cold dense interstellar medium 2–3 Myr ago. // In: Nature Astronomy 8, 8, 2024, pp. 983–990.
11. Schlüter A., The Electrical Conductivity of the Interstellar Gas. // In: Gas Dynamics of Cosmic Clouds 2,1955, p. 46.
12. Cook E., Two disc dynamos with viscous friction and time delay. // In: Mathematical Proceedings of the Cambridge Philosophical Society 71, 1, 1972, pp. 135–153.

2nd International Scientific Conference "Modern Problems in Geophysics", Proceedings,
ISBN 978-9941-36-562-1, ISSN 3088-4349, Tbilisi, Georgia, October 29-31, 2026

# ANCIENT ACCOUNTS OF THE FOREST GREEN COVER OF TBILISI

***Kharebava N., **Nikolaishvili D.**

** National Agency of Public Registry, Department of Geodesy and Geoinformation, Geodesy and Cartography Service / TSU Vakhushti Bagrationi Institute of Geography, Tbilisi, Georgia*
*** Ivane Javakhishvili Tbilisi State University, Faculty of Exact and Natural Sciences, Tbilisi, Georgia*
*nino.kharebava@tsu.ge*

***Abstract****. The paper examines the dynamics of Tbilisi's historically green landscape based on written sources from different periods, legends, and cartographic materials. It shows that the city was once characterized by rich forests and gardens, as confirmed by historical accounts and descriptions by Vakhushti Bagrationi. The study also demonstrates that urbanization processes in the 19th–20th centuries significantly reduced the natural cover, although in certain stages a partial increase in green spaces can also be observed. The paper emphasizes the city's historically close connection with the natural environment and the problem of modern ecological imbalance.*
*Using various sources and GIS technologies, the dynamics of green cover change between 1867 and 2020 were determined. The study showed that over time, the urban area of the city expanded rapidly and extensively, especially from the second half of the 20th century, while green cover increased much more slowly and disproportionately. As a result, a clear imbalance between urban expansion and ecological spaces is observed.*
*Thus, both historical accounts from different authors and the present study indicate that Tbilisi was once a significantly greener city than it is today and maintained a close connection with its natural landscapes. It is particularly important that green spaces were not limited only to the outskirts of the city but also included residential areas within the old city walls. This confirms that Tbilisi's urban environment was historically closely integrated with its natural landscape.*

***Key words****: Green cover, urbanization, cartographic sources, Vakhushti Bagrationi.*

## Introduction

Tbilisi was historically considered a fairly green city, despite the fact that it is located in a climatic zone that transitions from moderately warm steppe to moderately humid. In the accounts of ancient travelers, historical documents, and works of various periods, Tbilisi is often referred to as a forested city and the "city of gardens". Obviously, the areas around Lake Kumisi and the "Tbilisi Sea" were free from forest cover even in ancient times. Here, steppe and semi-desert vegetation was naturally widespread. The legend about the hunting of Vakhtang Gorgasali also testifies to the existence of Tbilisi's green cover in ancient times, indicating that at the time of the founding of Tbilisi, this place must have been a rich, densely forested environment [1]. This is the territory of modern Abanotubani, which is currently completely treeless due to urban development. According to Niko Ketskhoveli, this forest may have represented the second-tier floodplain forest of the Mtkvari River, which was characterized by such species as oak, elm, maple, aspen, and various species of hawthorn. Ketskhoveli also notes that this forest was connected to the oak groves of the Teleti and Tabori ranges [2], which indicates the existence of a single forest ecosystem in Tbilisi. The spread of the forest is also mentioned in the legend of Saint David Garejeli. According to M. Sabinin, the supposed dwelling of David, Mtatsminda (Mama Daviti), was once covered with forests, whereas today it is covered with xerophytic shrubs, steppe, and semi-desert vegetation. Other legends also indicate a similar situation and present Tbilisi as a forested place and a hunting ground. Both the legends and the research of botanists complement each other and allow us to conclude that the city was founded in a naturally favorable environment – around the "hot spring" of the capital, against a forested backdrop. Over time, with the development of the city, this green cover was gradually destroyed.

The tradition of garden art, that is, the cultivation of decorative, specially designed gardens, has existed in Georgia since ancient times and was obviously most strongly expressed in Tbilisi. *"The development of cities was accompanied by the establishment of gardens and green spaces, which were also influenced by Eastern culture"*

[3]. Ivane Javakhishvili noted that this tradition originated in Syro-Babylonian culture and later became closely associated with the style of Arab and Persian gardens. Such gardens served not only practical purposes but also had aesthetic and cultural significance, although no old decorative gardens of this type have survived in Georgia, and they can be discussed only on the basis of historical sources and chronicles. The 10th-century Armenian historian Thomas Artsruni refers to Tbilisi as a "wooden city" rather than a "stone city" [1], which indicates the abundance of greenery in the city and its surroundings. From the 11th century onwards, historical references to Tbilisi's gardens and parks become relatively more frequent and detailed, reflecting the strengthening of the Georgian state during that period. Gardens are mentioned both within the city walls and in the surrounding areas. According to one historical document, in the 17th century, part of Avlabari was covered with forest. Today, no forest remains there [2].

Special emphasis should be placed on Vakhushti Bagrationi's works The Description of the Kingdom of Georgia [4,5] and The Plan of Tbilisi [4], which are among the most important sources for studying the natural environment and urban culture of Tbilisi in the 17th–18th centuries. Vakhushti Bagrationi notes that *"the surroundings of the city are lush and full of many trees and flowers"* [5]. At the same time, he repeatedly describes gardens within the walls of Tbilisi and in its surroundings: *"... the valley of this great mountain is covered with forests, meadows, and gardens"* [4]. According to Martali, Vakhushti did not consider Tbilisi and its surroundings to be entirely forested, but the existence of "many hunting grounds" and the abundance of wild birds clearly indicate extensive forest cover. Vakhushti Bagrationi marked 11 gardens on his plan of Tbilisi (Table 1). In addition to the gardens mentioned, the plan also depicts the residences and palaces of the kings and great nobles. Obviously, these areas were also occupied by extensive vegetation. These include the King's Palace, the Queen's Palace, the Batonishvili Palace, and others (Fig. 1).

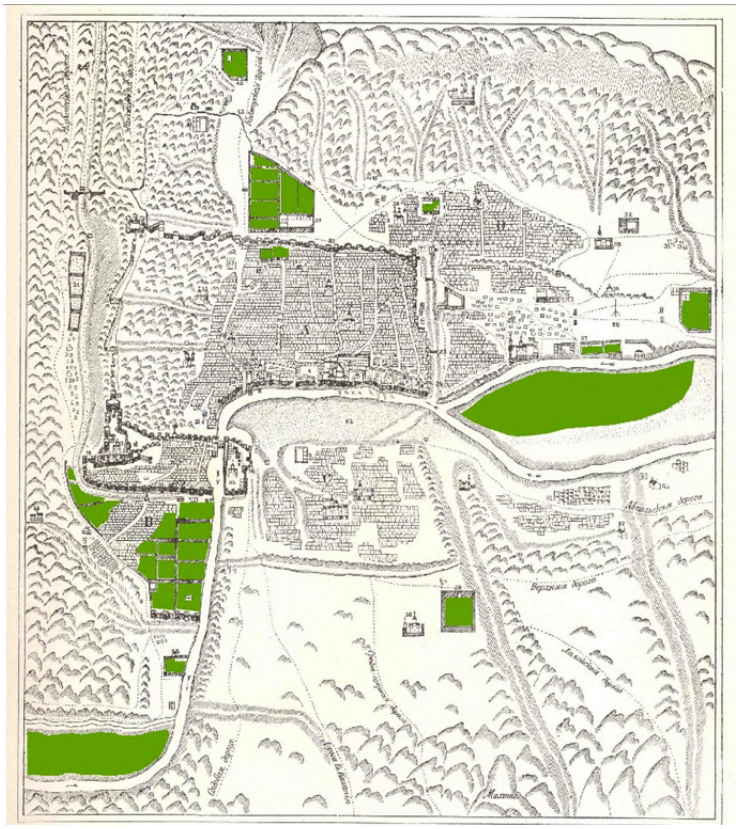


**Fig. 1.** Gardens According to Vakhushti's Map.

On the plans of Tbilisi from the 19th and early 20th centuries [1800, 1884, 1867, 1887, 1903–1904, 1907, 1913], the green cover is clearly visible not only in the suburbs but also within the inner districts. On all the plans, three large green areas are clearly distinguished: Alexander Garden, Sololaki, and Ortachala. In the outermost parts of the city, a continuous belt of gardens and orchards, or rather an agricultural landscape, is depicted instead of an urban area. With the exception of isolated rural settlements, the territory surrounding the city is almost

completely treeless. Significant changes are evident, as the intensive urban development at the expense of gardens had already begun, although the original spatial structure had not yet been lost. The city core had already become urbanized, but gardens, vineyards, and other green spaces still predominated in the surrounding areas.

**Table 1.** Tbilisi Gardens according to the plan of Vakhushti Bagrationi.

| # | Name | According to the map of Vakhushti | Modern localization |
|---|---|---|---|
| 1 | Bebuti Garden | On the left bank of the Mtkvari River, outside the city walls | Isani, Avlabari |
| 2 | Bezhanov Garden | | Isani, Avlabari |
| 3 | Queen's Garden | South of the father's garden, trapezoidal in shape | Sololaki |
| 4 | Tbileli Garden | At the corner formed by the bend of "Kozhri Road" | Sololak, at the intersection of Giorgi Leonidze and Geronti Kikodze streets |
| 5 | Krtsanisi Garden | | On the right bank of the Mtkvari River, on the southeastern outskirts of the city |
| 6 | Mamasakhlisi Garden | North of the Queen's Garden, trapezoidal in shape | Sololaki |
| 7 | New Meidani Garden | Mtkvari River Island | Isani, Avlabari |
| 8 | Great King's Garden | South of the Queen's Garden, rectangular in shape | On both sides of Giga Lortkipanidze Street |
| 9 | Tbilisi Garden – Seidabadi | In the southeastern part of Tbilisi | Between Mount Tabor and the Krtsanisi Valley |
| 10 | Kaibula Garden | Outside the city, rectangular in shape | Near the Kashveti Church |
| 11 | Castle Garden | Sololaki series | Botanical Garden |

Using various sources and GIS technologies, the dynamics of changes in green cover during 1867–2020 were determined (Fig. 2). The city boundaries remained almost unchanged between 1867 and 1913. This indicates that the city was still compact and did not undergo extensive territorial expansion [6-9]. The green cover did not undergo major changes during this period. Later, a slight but steady increase in built-up areas is observed, whereas the green cover remained relatively stable. During this period, there was no significant imbalance between urban and green spaces. Between 1924 and 1975, a sharp increase in urban development began, associated with the onset of intensive urbanization. At the same time, the total area of green spaces also increased as a result of the incorporation of natural areas into the urban fabric and the implementation of urban planning policies. This trend did not continue after 1999. Although urban development no longer increased as rapidly, the expansion of green cover lagged significantly behind the city's growth. Thus, the city's territory expanded rapidly and extensively over time, particularly since the second half of the 20th century, whereas the green cover increased much more slowly and disproportionately. As a result, a clear imbalance emerged between urban expansion and ecological spaces.

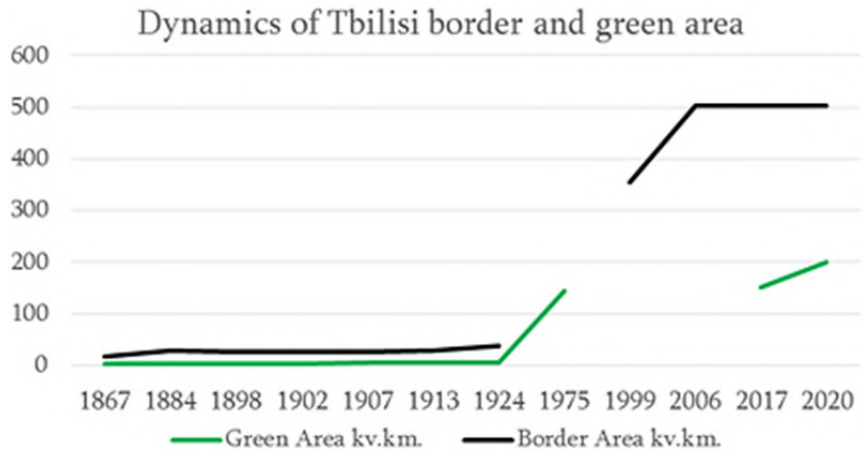



**Fig. 2.** Dynamics of Tbilisi border and green area.

Thus, the accounts of authors from different historical periods and the findings of the present study indicate that Tbilisi was a much greener city in the past than it is today and retained its natural landscapes. Of particular importance is the fact that green spaces were found not only on the outskirts of the city but also within the residential areas inside the city walls. This confirms that the urban environment of Tbilisi was historically closely connected with the natural landscape.

## References


1. Meskhia Sh., Gvritishvili D., Dumbadze, M. & Surguladze A., History of Tbilisi. // Tbilisi: Sablitgam, 1958.
2. Ketskhoveli N., Vegetation of Georgia. // Tbilisi: Publishing House of the Academy of Sciences of the Georgian SSR, 1959.
3. Kalandadze A., Ivane Javakhishvili and Georgian Archaeology. Tbilisi: Vysotsya, 1977.
4. Batonishvili V., Description of the Kingdom of Georgia. // In: Kartlis Tskhovreba, Vol. 4. Text established according to the principal manuscripts by S. Kaukhchishvili. Tbilisi: Soviet Georgia, 1973.
5. Brosset M., Description of the Kingdom of Georgia by Vakhushti Batonishvili. St. Petersburg, 1842.
6. Batonishvili V., Atlas of Georgia, 1745.
7. Bagrationi V., Atlas of Georgia. // Tbilisi: Tsvetnoy Press, 1997.
8. Nikolaishvili D., Kharebava N., Tsitsagi M., Urban green space availability and change patterns. // Journal of Environmental Biology, 45(4), 2024.
9. Plans of Tiflis: 1800, 1800, 1884, 1867, 1887, 1903-1904, 1907, 1913. (in Russian)

2nd International Scientific Conference "Modern Problems in Geophysics", Proceedings,
ISBN 978-9941-36-562-1, ISSN 3088-4349, Tbilisi, Georgia, October 29-31, 2026

# HEAVY METAL CONTENT IN THE SEASONAL SNOW COVER AT TERSKOL PEAK (ELBRUS REGION, KABARDINO-BALKARIAN REPUBLIC)

**Kurasheva O.**

*Federal State Budgetary Institution "High Mountain Geophysical Institute",*
*Nalchik, Kabardino-Balkaria, Russian Federation*
*oks.anchik@mail.ru*

***Abstract.*** *Snow samples from a snow pit at Terskol Peak were analyzed. The pit was dug at an altitude of 3100 m above sea level in 2020 to determine the content of heavy metals in the seasonal snow cover. The pit depth was 145 cm. A layer-by-layer description of the snow cover stratigraphy is provided. A total of 7 samples were taken from the seasonal snow cover. The obtained samples were analyzed using a laboratory method for the content of 9 microelements (Cr, Ni, Mo, Mn, Pb, Zn, Ag, Cd, and Co). Snow samples were analyzed using the atomic absorption method on an MGA-915 spectrometer. The maximum concentrations of heavy metals from the pit at Terskol Peak were found for Zn, Ni, Mn, and Pb.*

***Key words:*** *Terskol peak, pit, heavy metals, snow cover.*

## Introduction

The snow cover is a crucial component of mountain geosystems and glacier regimes. Snow accumulation patterns in the Caucasus are influenced by a number of factors: elevation, latitude, orographic characteristics, the duration of cold-season precipitation, air temperature, and wind-driven snow transport. The region is dominated by westerly air mass transport [7].

Peak Terskol is located on a southern spur of Mount Elbrus (in the Elbrus region). Precipitation increases with altitude up to a certain level; for the southern slope of Elbrus, this range lies between 3,100 and 3,500 meters above sea level. Maximum snow accumulation occurs at an elevation of 4,000 meters above sea level, with total precipitation reaching approximately 1,200 mm. A persistent snow cover remains year-round above the snow line (3,900 meters above sea level).

## Research methods

During fieldwork on Terskol Peak (March 23, 2020), a snow sample was collected from a snow pit at an elevation of 3,100 m a.s.l. at 10:40 Moscow Time (coordinates: N 43° 16.537', E 42° 29.974'). The research methodology involved snow sampling within the pit and statistical processing of the results. The pit reached a depth of 145 cm (down to the ground surface). A layer-by-layer description of the snowpack stratigraphy was conducted in a pit approximately 1 meter wide. The thickness of individual snow layers was measured with an accuracy of 1 cm. Snow samples were collected in 250 ml plastic containers along the vertical profile. A total of seven snow samples were collected from the seasonal snowpack. Air temperature was +5°C; snow temperature in the pit at a depth of 80 cm was -5°C.

The concentration of heavy metals in snow samples was determined at the Cloud Physics Department (CPD) – specifically, the Analytical Chemistry Laboratory of the VGI (High-Mountain Geophysical Institute). Sample analysis was performed using the atomic absorption method with an MGA-915M atomic absorption spectrometer featuring electrothermal atomization. Laboratory analysis identified the content of nine trace elements (Cr, Ni, Mo, Mn, Pb, Zn, Ag, Cd, and Co) in the samples. These elements are classified as priority anthropogenic pollutants of the natural environment.

## Discussion of results

A layer-by-layer description of the snowpack stratigraphy in the snow pit is presented in Table 1.

**Table 1.** Snowpack stratigraphy in a snow pit at Terskol Peak, 3100 m a.s.l. (March 23, 2020).

| Distance from the top of the test pit, cm | Description of the test pit |
|---|---|
| 0–13 | The snow is coarse-grained and loose. It is separated from the underlying layer by a radiation crust up to 0.5 cm thick. |
| 13–28 | The snow is fine-grained and stratified. There is a 1 cm thick ice layer in the lower part. |
| 28–48 | The snow is fine-grained and stratified. |
| 48–70 | A gray-colored snow contamination horizon. An intermittent ice layer up to 2 cm thick is visible. |
| 70–89 | The snow is fine-grained and stratified. |
| 89–110 | The snow is medium-grained. |
| 110–145 | The snow is coarse-grained and loose, extending down to the ground surface. |

Compacted firn or ice layers within the snowpack typically form on the snow surface when it remains uncovered by fresh snow for several days. Four types of crusts are distinguished: glaze ice crusts, wind crusts, radiation crusts, and ice layers.

Radiation crusts form during periods of anticyclonic weather in late winter or early spring as a result of the radiation-induced melting and recrystallization of snow. They are particularly common on sun-facing slopes. These crusts range from 0.5 to 3 cm in thickness and consist primarily of large, elongated ice crystals growing toward the sun; the crystallographic axes of these crystals are oriented parallel to the primary radiation flux. Ice layers form within the snowpack when meltwater freezes within wind or radiation crusts. Initially 0.5–1 cm thick, these layers can increase in thickness through the refreezing of meltwater. The crusts persist for a long time within the snowpack and influence recrystallization processes by impeding the vertical movement of water vapor. They form boundaries between snow layers of differing structures and play a significant role in snowpack stratigraphy [1].

A distinction is made between background and local snow contamination. Background contamination is determined by general atmospheric circulation and the interaction between the atmosphere and the Earth's surface, involving the transport and deposition of impurities over large areas; local contamination arises around ground-based pollution sources, creating zones of elevated pollutant concentrations within the snowpack. The most severe snow contamination results from dust storms, volcanic eruptions, and forest fires, as well as from human activity.

The wide range of chemical impurity concentrations in precipitation also depends on the type of atmospheric front. The highest concentrations are observed in the zone of an occluded front, where conditions favor the uplift of polluted air from the lower layers of the atmosphere to higher altitudes. Occluded fronts are frequently observed in the high-mountain regions of the Caucasus [3, 9].

According to various studies, the most intense increase in the pollution of freshly fallen snow occurs below an elevation of 3,000–3,500 m a.s.l., where the transport of local pollutants is intensified [4]. Table 2 presents the results of the analysis of snow samples collected at Terskol Peak (3,100 m a.s.l.) following autumn and spring snowfall events in 2020.

**Table 2.** Heavy metal concentrations at Terskol Peak (μg/L).

| Sample No. | Distance from the top of the test pit, cm | **Cr** | **Ni** | **Mo** | **Mn** | **Pb** | **Zn** | **Ag** | **Cd** | **Co** |
|---|---|---|---|---|---|---|---|---|---|---|
| 1. | 0–13 | – | 4,6 | 1,2 | 4 | 1,2 | 5,2 | 0,4 | 0,02 | 0,8 |
| 2. | 13–28 | 0,3 | 9,7 | – | 6 | 1,6 | 14 | 0,06 | – | 1,5 |
| 3. | 28–48 | 0,9 | 8,7 | – | 8 | 4,6 | 32 | – | 0,5 | 1 |
| 4. | 48–70 | 0,5 | 7,9 | 1,7 | 6 | 9,4 | 5,7 | – | – | 1,1 |
| 5. | 70–89 | 0,4 | 9,8 | 1,8 | 12 | 12 | 13 | – | 0,3 | 1,4 |
| 6. | 89–110 | 0,3 | 8,5 | 0,6 | 13 | 2,5 | 16 | 0,5 | 0,3 | 0,9 |
| 7. | 110–145 | 0,06 | 6 | – | 4 | 14 | 14 | 0,8 | – | 0,9 |
| Average for the test pit | | 0,3 | 7,9 | 0,7 | 7,6 | 6,5 | 14,3 | 0,2 | 0,16 | 1,08 |

(–) – indicates a content below the limit of determination for the metal.

Analysis of the obtained data showed that the highest concentrations correspond to Zn, Ni, Mn, and Pb (Fig. 1). The content of these elements in snow samples ranged as follows: Zn, 5.2–32 μg/L; Ni, 4.6–9.8 μg/L; Mn, 4–13 μg/L; and Pb, 1.2–14 μg/L. The high Zn content in the snow samples is likely of technogenic origin. The Mn content is likely attributable to local factors related to the composition of the surrounding rocks [5, 6, 10].

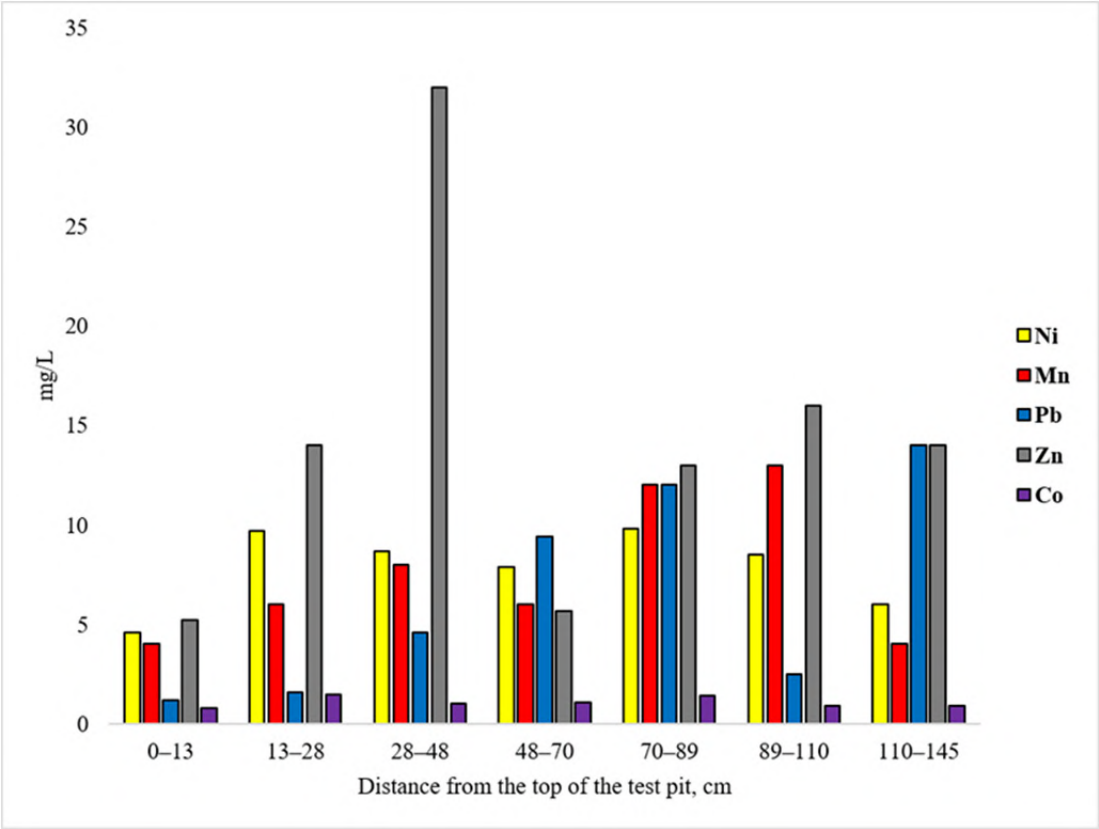



**Fig. 1.** Distribution of heavy metals in snow samples at Terskol Peak (absolute elevation 3100 m)

The Co content ranged from 0.8 to 1.5 μg/L. The total content of Cr, Mo, Ag, and Cd was low or below the metal detection limit. The authors of [7] note that at the elevation of the village of Terskol (2,150 m a.s.l.) and in the adjacent 200-meter air layer, the enrichment of precipitation with impurities due to below-cloud scavenging is at its maximum compared to higher elevations. According to data from [2], elevated Pb levels (20 μg/L) – exceeding concentrations in glacial deposits by a factor of 2–4 – were detected in atmospheric precipitation at the Terskol peak (3,100 m a.s.l.), while the Mn concentration (19 μg/L) was comparable to its content in the firn-ice layer. Such elevated concentrations of these elements in precipitation samples are likely attributable to the origin of the air masses that brought the precipitation.

It is shown in [8] that below 3,500 m, the transport of aerosols and dust particles by winds and local circulation flows from surrounding mountain slopes and valleys intensifies, leading to an increase in the Mn, Cr, and Mo content of the snow; consequently, the concentration of heavy metals increases downslope from 4,000 m a.s.l., whereas it decreases upslope from that level. Thus, snow contamination increases downslope.

## Conclusions

A layer-by-layer description of the snowpack stratigraphy in a snow pit at Terskol Peak (3,100 m a.s.l.) for 2020 is presented. Analysis of snow samples from the seasonal snowpack revealed that the highest heavy metal concentrations were found for Zn, Ni, Mn, and Pb. The content ranges were as follows: Zn, 5.2–32 μg/L; Ni, 4.6–9.8 μg/L; Mn, 4–13 μg/L; and Pb, 1.2–14 μg/L. Elevated concentrations of these elements in the snow samples are likely attributable to the origin of the air masses that brought the precipitation. The most intense increase in fresh snow contamination occurs below the 3,500–3,000 m a.s.l. level, where the transport of local pollutants is more pronounced.

## References


1. Glaciological Dictionary / Edited by Academician of the Russian Academy of Sciences V. M. Kotlyakov − L.: Gidrometeoizdat, 1984, 526 p.
2. Zhiglovskaya T. N., Makhonko E. P., Shilina A. I., Microelements in Natural Waters and the Atmosphere. // Proceedings of the IEM, Issue 2 (41), 1974, 182 p.
3. Zanina A. A., Climate of the USSR. // Caucasus. L., GIMIZ, 1961, 290 p.
4. Kampanovsky V. I., Sarkisov S. L., Stepanov G. V., Khorguani V. G., Study of Natural Aerosols in the Free Atmosphere. // In the book Dust in the Atmosphere and Near-Earth Space. M., Nauka, 1973. pp. 179−181.
5. Kerimov A.M., Kurasheva O.A., Features of the formation of the chemical composition of the glacial-fed rivers of the Caucasus during intensive degradation of glaciation. // Meteorology and Hydrology, No. 2, 2023, pp. 80 – 89. DOI: 10.52002/0130−2906−2023−1−2−80-89.
6. Kerimov A.M., Kurasheva O.A., Comparative analysis of heavy metal concentrations in the sources of the Baksan River and the Garabashi glacier (southern slope of Elbrus). // Bulletin of DSPU. Natural and exact sciences, Vol. 12 No. 1, 2018, pp. 49−56.
7. Kerimov A.M., Rototaeva O.V., Khmelevskoy I.F., Features of the formation of the chemical composition of glaciers in Kabardino-Balkaria. // MGI No. 84, 1997, pp. 66−71.
8. Kerimov A.M., Rototaeva O.V., Khmelevskoy I.F., Distribution of heavy metals in the surface layers of the snow-firn layer on the southern slope of Elbrus. // Ice and Snow No. 2(114), 2011, pp. 24−34.
9. Temnikova N.S., Some characteristics of the climate of the North Caucasus and adjacent steppes. // L., GIMIZ. 1964, 174 p.
10. Kerimov A.M., Kurasheva O.A., Peculiarities of Formation of the Chemical Composition of Caucasian Glacier-fed Rivers during Intensive Degradation of Glaciers. // Russian Meteorology and Hydrology, Vol. 48, No. 2, 2023, pp. 147–154. DOI: 10.3103/S1068373923020073.

2nd International Scientific Conference "Modern Problems in Geophysics", Proceedings,
ISBN 978-9941-36-562-1, ISSN 3088-4349, Tbilisi, Georgia, October 29-31, 2026

# SHIDA KARTLI ENVIRONMENTAL SITUATION CONDITIONED BY ANTHROPOGENIC FACTORS AND NATURAL EXODYNAMIC PROCESSES

**Salukvadze E.**

*Vakhushti Bagrationi Institute of Geography of the I. Javakhishvili Tbilisi State University,Tbilisi, Georgia*
*elene.salukvadze@tsu.ge*

***Abstract.*** *The work discusses the environment of the Shida Kartli Region as an object of intensive transformation. The main reason for environmental change is strong anthropogenic impact, which has conditioned the activation of various exodynamic processes: erosion, landslides, mudflows etc. Significant damage is caused to agricultural lands, dwelling houses, various facilities and communications. The issue of waste management is an important environmental challenge. A special problem is created by spontaneous dump sites, which are illegally located and are a significant source of environmental pollution.*

***Key words:*** *Ecological situation, anthropogenic impact, environmental pollution, Shida Kartli*

## Introduction

In contemporary conditions, the complexity of the ecological situation of the environment is becoming more and more visible, and the consequences caused by it are often large-scale. Therefore, the protection of the population and the safe operation of economic and engineering facilities have become a very important socio-economic and ecological problem.

For Shida Kartli, as well as for most regions of Georgia, such problems include unforeseeable natural processes, environmental pollution (of air, water, soil, ecosystems) caused by anthropogenic impact, soil salinization, etc.

In plain areas, significant ecological problems include swamping, riverbank washout and flooding.

## Study area, material and methods

Region Shida Kartli (Gori, Kaspi, Kareli and Khashuri Municipalityes) is located in the western part of Eastern Georgia. From a physicogeographical point of view, Shida Kartli covers the territory from the main watershed of the Caucasus to the crest of the Trialeti Range, from the Likhi Range to the Aragvi River Gorge.

The research is based on a complex physical-geographic, cartographic and field-expedition methods. The research was based also on the existing published literature and foundation material about Shida Kartli region. The important component was the field expedition research conducted in 2019- 2023.

## Results

Among the modern environmental challenges, waste management is an important problem. The main task is the disposal of industrial and household waste, which is closely related to urbanization, population growth and economic development. This issue is relevant, especially for developing countries, including Georgia. The problem is spontaneous dump sites, which are often located illegally and are not subject to environmental control. Such dump sites are a significant source of environmental pollution, causing pollution of air, soil, water and ecosystems, posing a threat to human health.

Waste management in Georgia is regulated by the "Waste Management Code" developed by the Ministry of Environmental Protection and Agriculture [1]. The purpose of this code is to promote waste reuse, prevent waste disposal in the environment and ensure environmentally safe management. The waste management system is still at its development stage and faces significant challenges, especially in the area of municipal waste control and management.

The current state of solid waste management in the regions of Georgia is not uniform and varies significantly between different municipalities and settlements.

According to existing data, the largest share falls on Tbilisi, where approximately 37% of the country's total solid waste is generated, this is due to the high concentration of population, as 34% of the total population of Georgia lives in Tbilisi [2]. After Tbilisi, a relatively high figure is recorded in the Imereti Region (approximately 13%), as well as in Kvemo Kartli and Adjara (10-10%), it is significant in Samegrelo-Zemo Svaneti (8%), while in Kakheti and Shida Kartli, waste generation is at an average level and amounts to approximately 6%.

The total volume of waste generated in the Shida Kartli Region during an year is 172,454 $m^3$. It is distributed according to municipalities as follows (Fig. 1):

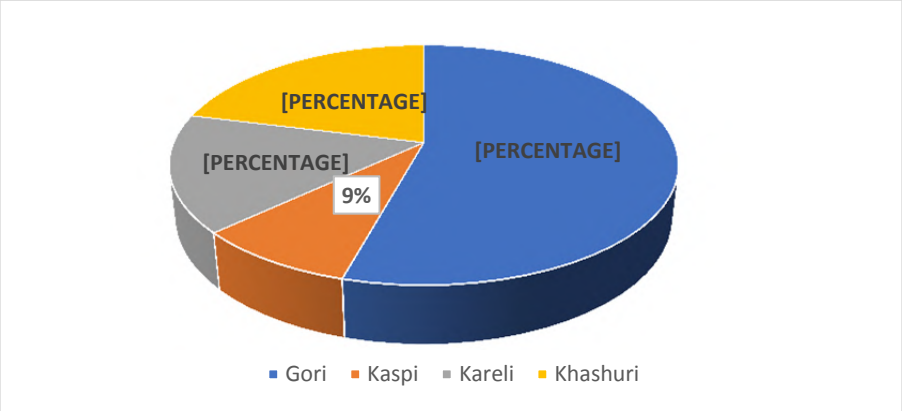



**Fig.1.** Share of municipal solid waste generation by municipalities in the Shida Kartli region.

The total volume of waste generated in Kaspi Municipality during one year is 15,132 $m^3$, which is 9% of the waste of the Shida Kartli Region, in Gori Municipality 93,660 $m^3$, 54%, in Kareli Municipality 27,266 $m^3$, 16%, in Khashuri Municipality 36,396 $m^3$, 21%.

Although the total volume of waste in some regions is relatively small, this does not mean that the problem is less urgent. On the contrary, especially in rural areas where waste services are less developed, even small volumes of waste often become the cause of the formation of spontaneous dump sites.

Spontaneous dump sites can be found along river banks, in ravines, on roadsides, in forests, river valleys, and in watersheds and these areas are characterized by active hydrological processes, which increases the risk of waste movement and the spread of pollution over a wide area.

The waste may contain dangerous harmful toxic substances: carbon monoxide (CO), dioxin, heavy metals: lead (Pb), cadmium (Cd), zinc (Zn), etc., construction waste and debris, tires, car scraps and other materials. Hazardous waste is also found at the spontaneous dump sites, which may cause a number of health problems for the population in the region in the future. The creation of spontaneous dump sites is a complex problem, it is not only a result of infrastructural and waste management system, but also related to low public awareness.

According to the 2019 study carried out in the regions of Georgia, the total amount of uncontrolled solid household waste in Shida Kartli was 4,872 tons/year in rural areas and 71 tons/year in urban areas [3]. A high degree of pollution was identified in the area surrounding spontaneous dump sites, and the hottest spot turned out to be the area of the village of Metekhi in Kaspi Municipality [4].

The quality of waste management services depends significantly on regional characteristics, such as geographical location, population density, infrastructure development and economic activity. Waste management in mountainous or remote from center areas is particularly problematic, as collection and transportation are associated with additional difficulties. Also important are the slope of the terrain, erosion processes, which contribute to both the movement of waste and the intensification of soil degradation processes. Also important are temporary floods and mudflow processes, which are characteristic of the Shida Kartli Region. Polluted surface waters enter irrigation canals and irrigate agricultural fields, inadvertently these harmful substances end up in food. This leads to the spread of various diseases, increasing the risk of ecological pollution of soil and water.

Biodegradable waste is particularly problematic, which, according to a seasonal morphological study of municipal waste conducted in three regions of Georgia (Kakheti, Shida Kartli, Adjara) in 2015-2016, accounts for 42% of municipal waste [5]. There is no infrastructure for recycling biodegradable waste, there are only a few composting enterprises (Table 1). Also, there is no possibility of recovering energy from biodegradable waste.

**Table 1.** Number of mud pools in Shida Kartli

| River basins | Number of recorded mudslides | |
|---|---|---|
| | Pool | Streams |
| Mtkvari | 277 | 642 |
| Liakhvi | 39 | 40 |
| Lekhura | 5 | 5 |
| Mejuda | 7 | 8 |
| Ksani | 17 | 18 |

Mudflows are quite frequent in the Shida Kartli Region. The activation of mudflows is associated with periods of heavy rainfall in spring and autumn, and with heavy summer rains. Mudflows are characteristic of almost all rivers, ravines and gorges on the northern slope of the Trialeti Range, as well as the foothills of the Caucasus, the Kvernaki Range. The upper reaches of the Suramula, Tiliana, Cheratkhevi, and Prone rivers, the Liakhvi River with its tributaries are characterized by mudflows [6].

Mudflow processes periodically develop in the village of Khvedureti (Kareli Municipality) on the banks of the Khvedrula River (a tributary of Dzama) and its adjacent territory, in the village of Tseronisi, in the dry ravines in the village of Knolevi (Kareli Municipality) in the Shua Prone River gorge. Mudflows cause great damage to irrigation canals (e.g., the Skra-Kareli irrigation system in the section of the villages of Khvedureti and Ghvlevi). They destroy roads and agricultural fields. In the Tana River basin particularly should be noted the left slope of the the river, witth numerous mudflow ravines from the Ateni Village to the Kirbala Village. In the territory of Surami settlement (Khashuri Municipality), the foot of the Bekami Mountain slopes, near the Suramula River terrace, it is dissected by temporarily active dry ravines, which are of a mudflow nature [7-9].

Erosion processes are quite intense in the region territory, especially on the slopes of the Caucasus and Trialeti, and on the steep slopes of the Likhi, Kvernaki, Tslevi, and Skhaltba ridges. Erosion processes have destroyed or eroded hundreds of hectares of farmland, and destructed roads and bridges.

Strong indepth and lateral erosion are observed in sections made of less stable rocks, while surface erosion is noticeable in the foothill line. The Mtkvari River causes intensive erosion in the floodplain terrace line adjacent to the Keleti Ridge. The Kura River also intensively washes out the banks near the towns of Kareli, Akhalsopeli, Kvakhvreli, etc. Banks severely damaged by lateral erosion are identified in the middle and lower reaches of the Dzama River, in the lower reaches of the Tedzami and Khveduretistskali Rivers, 12 tributaries of the latter contain mudflow danger.

The development of the agricultural sector in Georgia is significantly hampered by soil erosion processes. In eastern Georgia, more than 21% of arable land (105 thousand ha) is degraded by weathering. Soil weathering is also strongly manifested in Shida Kartli, in all four of its municipalities. Winds of especially extreme speed spread very quickly. For 2-3 days, on average once every 10 years, for example, in 2003, in January and February, very strong, extreme speed winds of 30 m/s (energy 2558 kW/m$^2$) in January, 35 m/s, (energy 3669 kW/m$^2$) in February were observed in Gori [10].

Among the industrial enterprises in the Shida Kartli Region, the Kaspi Cement Plant “Heidelberg Cement” and small cement factories are significant environmental pollutants and represent one of the main sources of emissions of the smallest solid particles, polluting the environment with specific dust, carbon dioxide and sulfur dioxide and are considered one of the largest polluting enterprises in Georgia, along with the Rustavi chemical and metallurgical plants and the Zestafoni ferroalloy plants. It should be noted that currently a continuous monitoring system for emissions into the atmospheric air has been introduced at the Kaspi cement plant.

## Conclusion

The ecological situation depends mainly on the economic impact and intensity of human activities. In Shida Kartli, the results of the impact of technogenesis were especially clearly manifested in the areas of mining and quarrying (sand, gravel, brick, tile clay – in the villages of Khovle and Metekhi, cement raw materials in the village of Kavtiskhevi), processing and some other industries, as well as in the areas of melioration, agriculture, road construction and other facilities.

Despite the progress achieved in the development of waste management policy and legislation, environmental pollution caused by waste still remains a problem, the existing old, official dump sites for municipal waste do not meet modern requirements and are a source of emissions of pollutants into the environment. In addition, there are still spontaneous, unofficial dump sites, from which waste enters the environment and water. Thus, the ecological analysis of the environment of the Shida Kartli Region showed that the impact of anthropogenic factors (along with natural ones) has currently reached a certain limit, which has led to a tension in the ecological situation.

## References


1. Georgian Law – Waste Management Code, Chapter I. (in Georgian) https://matsne.gov.ge/en/document/view/2676416?fullscreen=1&impose=parallelEn&publicati on=12
2. Georgia's 2024 population and agricultural census. National Statistics Office of Georgia, 2026. (in Georgian) World Bank, Georgia Solid Waste Sector Assessment Report, 2021. (in Georgian)
3. Buachidze N., Chikviladze Kh., Intskirveli L., Surmava Al., Tabatadze M., Affect of uncontrolled landfilills located in Georgia on the contamination processes of the surrounding areas. // Modern problems of Geography and anthropology, proceedings of international conference, dedicated to the 140th anniversary of academician Alexandre Javakhishvili, Tbilisi, Tsu Press, 2015, 277 p. (in Georgian)
4. Project "Waste Management Technologies in Georgia", Caucasus Environmental NGO Network (CENN).
5. Tsereteli E. and Tsereteli Dj. Features of the development of mudflow processes on the territory of Georgia. // In: Geological Conditions for the development of mudflows in Georgia. Monograph., Tbilisi, Publishing House "Metsniereba", 1985, pp. 9-15. (in Russian)
6. Lezhava Z., Some modern geomorphological processes in the right bank of the Mtkvari River basin (between Tashiskari and Mtskheta). // Proceedings of the Geographical Society of the Georgian SSR XVII, Tbilisi, "Metsniereba", 1988, pp. 25-27.
7. Information bulletin. The consequences of the geological disaster in Georgia and its development forecast for 2008, Tbilisi, 2008, 80 p. (in Georgian)
8. Information bulletin of the National Environmental Agency of Georgia, Results of the development of natural geological processes in Georgia in 2023 and forecast for 2024. // Tbilisi, 2024, pp. 304 – 307. (in Georgian)
9. Gogichaishvili G., Gabisonia T., Dekanoidze T., Some issues of studying the danger of wind erosion of soils in eastern Georgia. //„Caucasian Geographical Journal" № 7-8, 2007, pp. 136-140. (in Russian)

2nd International Scientific Conference "Modern Problems in Geophysics", Proceedings,
ISBN 978-9941-36-562-1, ISSN 3088-4349, Tbilisi, Georgia, October 29-31, 2026

# VALIDATION OF ERA5 REANALYSIS AIR TEMPERATURE DATA IN THE KAKHETI REGION BASED ON DATA FROM THE TELAVI UNIVERSITY METEOROLOGICAL STATION

**Samkharadze I., Tatishvili M., Zotikishvili N.**

*Institute of Hydrometeorology, Georgian Technical University, Tbilisis, Georgia*
*inga.samkharadze562@ens.tsu.edu.ge*

***Abstract.*** *The present study evaluates the accuracy and reliability of the ERA5 reanalysis 2-meter air temperature data in the Kakheti region, compared to the observation data of the Telavi Meteorological Station, using the example of June 2023 and 2024. The aim of the study is to determine the effectiveness of the model in reflecting the diurnal and synoptic variations of air temperature in the complex orographic conditions of the Alazani Valley and the surrounding foothills. The statistical analysis performed shows a strong linear relationship between the reanalysis and actual observations, where the Pearson correlation coefficient ranges from 0.83 to 0.93. It is clear that the model achieves particularly high accuracy during stable synoptic conditions, while the main errors are due to local microclimatic processes and the limitations of the model's spatial grid. The results obtained confirm the feasibility of using the ERA5 reanalysis for climatic and agro-meteorological studies in the region.*

***Key words:*** *ERA5 reanalysis, air temperature, diurnal variation, model validation, statistical analysis.*

## Introduction

High spatial-temporal resolution air temperature data play a critical role in the study of climate change, agriculture, and regional microclimate. In Georgia, and in particular in the Kakheti region, where horticulture and viticulture are leading sectors of the economy, the scarcity of a ground-based meteorological observation network often complicates detailed analysis of the temperature regime [1,3]. Global reanalysis products are increasingly used to solve this problem. The ERA5 reanalysis developed by the European Center for Medium-Range Weather Forecasts is a modern global atmospheric product, although its accuracy requires additional validation in regions with complex terrain. The interaction of the Alazani Valley and the Gombori Range creates specific mountain-valley circulation and microclimatic conditions, which often lead to errors in atmospheric models. Thus, the objective of this study is to validate the temperature data of Era 5 based on observations from the Telavi Meteorological Station during typical days of June 2023-2024 [2, 4-6].

## Study area, material and methods

The study used hourly observation data from the Telavi automatic meteorological station for the corresponding periods of 2023 (June 3, 15, 17) and 2024 (June 1, 17, 25). In parallel with the station data, hourly values of air temperature at a height of 2 meters of the ERA5 reanalysis for a spatial grid of 0.25 degrees of resolution were downloaded from the database of the European Center for Medium-Range Weather Forecasts. The comparative analysis of the data was carried out in local time (UTC+4), with precise synchronization of hourly intervals. The following statistical indicators were used to assess the accuracy and deviations of the model: Pearson's correlation coefficient (r), coefficient of determination (R2), root mean square error (RMSE), mean absolute error (MAE), mean bias (Mean Bias).

## Results

To assess the diurnal dynamics of air temperature at a height of 2 meters in the difficult geomorphological conditions of the Kakheti region (using the example of the Telavi meteorological station), a comparative analysis of hourly data from the ERA5 reanalysis and local monitoring (Telavi University Meteorological Station) was conducted for three characteristic days of June 2024 – June 1, 17 and 25 (Fig. 1).

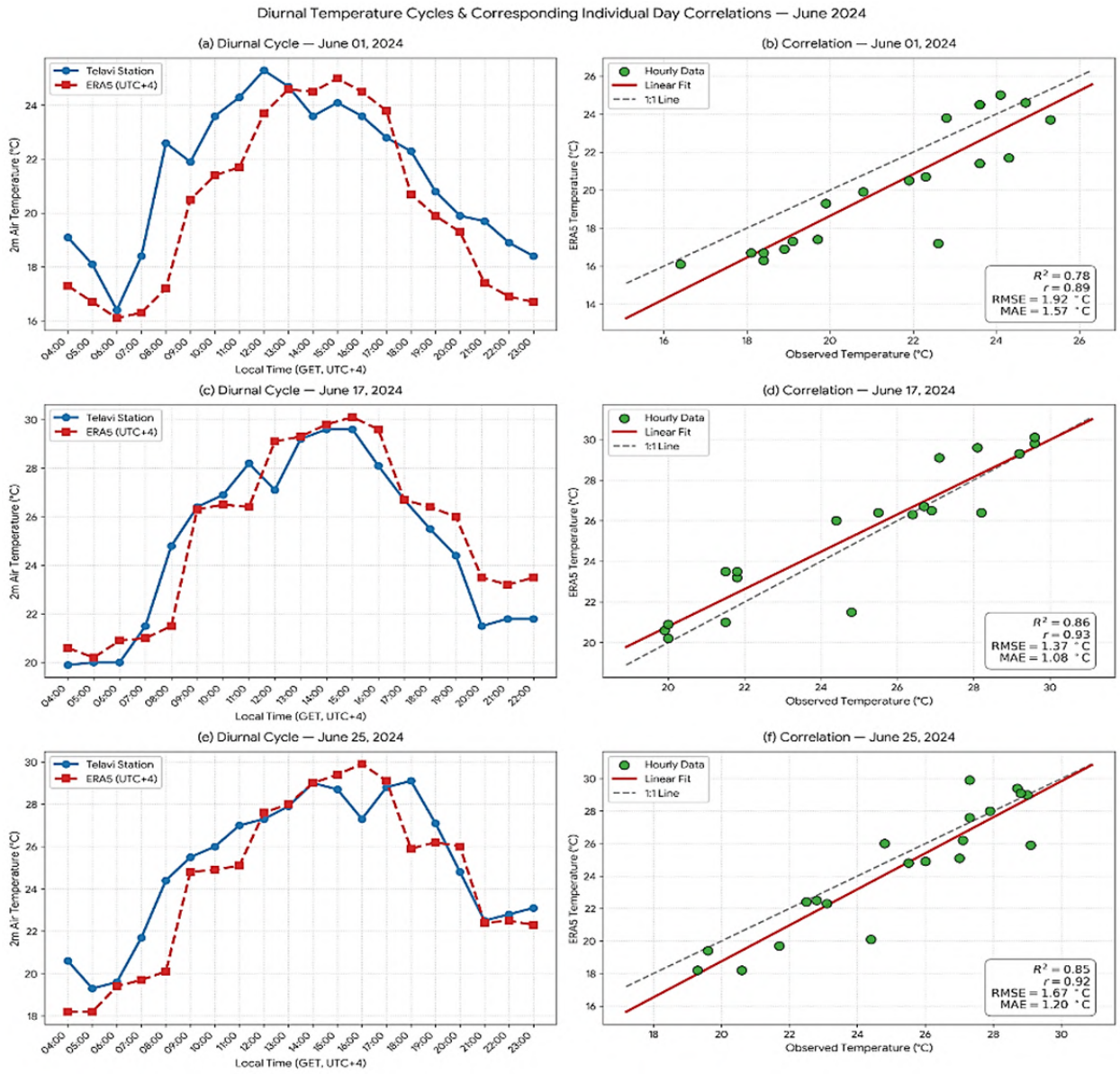



**Fig. 1.** Assessment of the diurnal variation of air temperature on individual days (June 2024).

As can be seen from Fig. 1(a), on June 1, 2024, the ERA5 model generally correctly reflects the phases of the diurnal variation, although a systematic decrease in temperature is observed in the morning (04:00–08:00) and evening-night (19:00–23:00) hours by an average of 1.5-2.5 0C. At the Telavi station, the daytime maximum was recorded at 12:00, while in ERA5 the peak shifted to 15:00. June 17, 2024 (Fig. 1c) is characterized by high agreement between the observational data and the reanalysis, especially during the daytime hours (09:00–17:00). However, during the night (20:00–22:00), the model overestimates the temperature by 1.50C compared to the station. On June 25, 2024 (Fig. 1e), the heating during the day is well modeled, although local deviations are detected – in the morning hours (04:00–08:00), ERA5 lowers the temperature by 2.0-3.0 0C. At 16:00, a sharp, short-term drop in temperature (to 27.2 0C) was observed at the Telavi station, which was likely caused by local cloudiness or micro-circulation, while ERA5 shows a daytime peak at this time (29.9 0C). At 18:00, the opposite picture is observed – the station recorded a secondary peak (29.2 0C), while ERA5 showed a rapid drop in temperature (25.9 0C).

Comparative statistical analysis showed a strong correlation between the weather station data and the ERA5 reanalysis for all three considered days (Table 1). The statistical data presented in Table 1 demonstrate the high accuracy and reliability of the ERA5 reanalysis compared to the observed data, which is confirmed by the high Pearson correlation coefficient (from 0.89 to 0.93) and the corresponding values of the coefficient of determination (0.78 to 0.86) for all three considered days. June 17, 2024, stands out with the highest agreement and minimum error, where the mean square error is 1.37 $^0$C, and the mean absolute error is 1.08 $^0$C. Relatively

high, but still quite acceptable, error rates were observed on June 1, when the root mean square error reached 1.92 $^0$C. Overall, the data show that the reanalysis model achieves particularly high accuracy on days like June 17 and 25, although the overall agreement remains solidly good and high throughout the period.

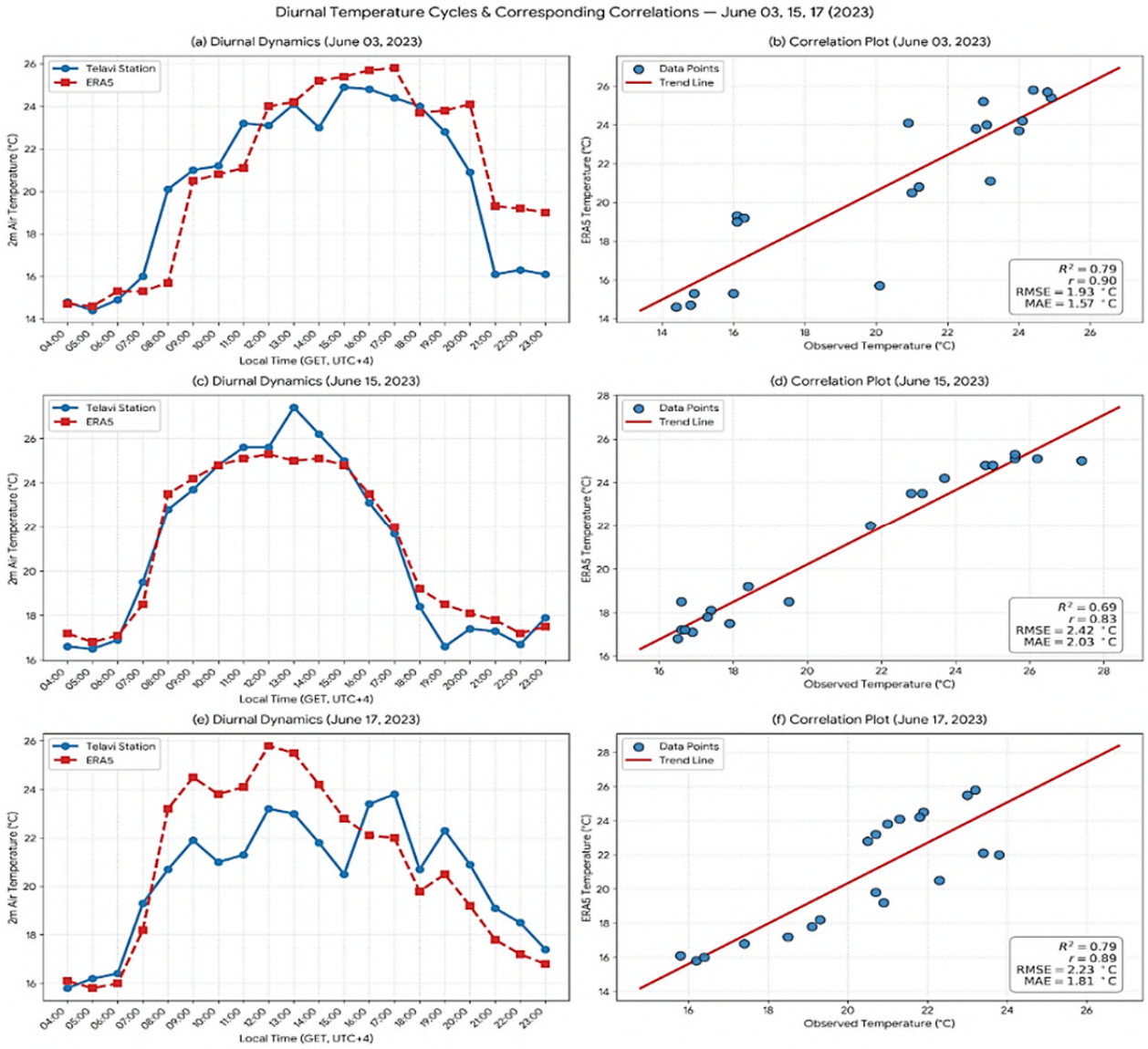



**Fig. 2** Assessment of the daily change in air temperature on individual days (June, 2023).

In the difficult geomorphological conditions of the Kakheti region, using the example of the Telavi meteorological station, a comparative analysis of the ERA5 reanalysis and local monitoring hourly data was carried out for three characteristic days of June 2023 to assess the daily change in air temperature at a height of 2 meters.

On June 3, 2023, the ERA5 model quite accurately repeats the general warming trend, although phase differences are noticeable. In the morning hours (from 07:00 to 08:00), a faster increase in temperature is observed at the Telavi station (up to 20.1 degrees at 08:00), while ERA5 delays the warming by about 1-2 hours (15.7 degrees at 08:00). During the day and evening (1:00 PM to 8:00 PM), the model overestimates temperatures by 1.0 to 3.0 degrees. After 8:00 PM, the station records a sharp cooling (dropping to 16.1 degrees by 9:00 PM), which is likely caused by the influence of cold air from the Gombori ridge and which is not reflected in the reanalysis.

June 15, 2023 is distinguished by the best phase synchronization of the diurnal movement. The model perfectly reproduces the morning heating and evening cooling. The only noticeable deviation was observed at 13:00, when a short-term peak was noted at the station (27.4 degrees), while in the reanalysis this indicator was averaged (25.0 degrees).

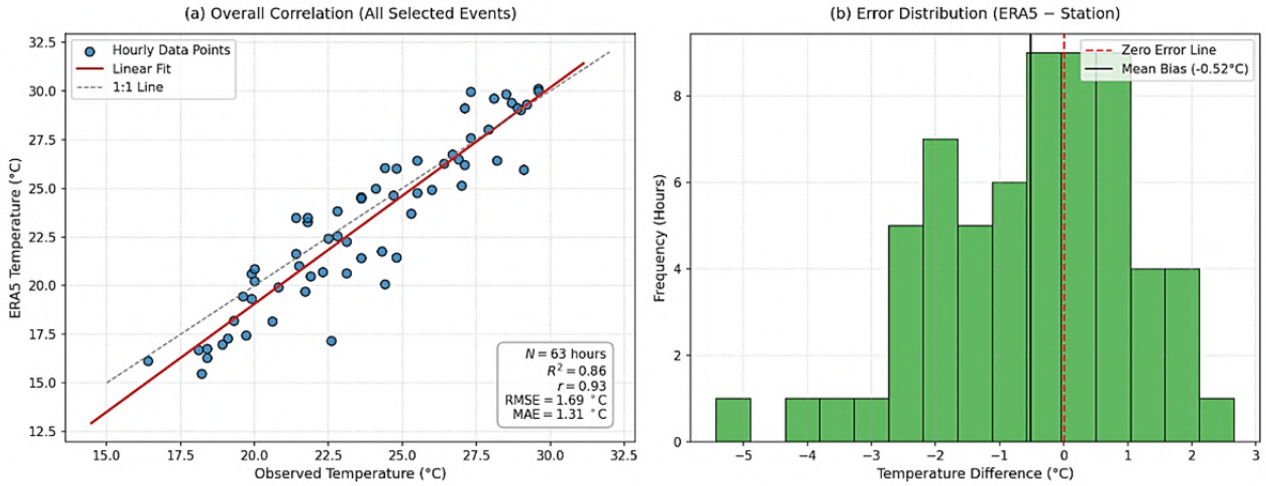
June 17, 2023, is characterized by the presence of systematic errors. During the daytime (from 08:00 to 14:00), ERA5 steadily exceeds the temperature by 2.0 to 3.0 degrees and shows a maximum of 25.8 degrees (as opposed to the station's 23.2 degrees). In the evening hours (from 16:00 to 23:00), the opposite picture is observed – the station maintains a higher temperature (23.8 degrees at 17:00), while ERA5 cools down faster. The complex nature of the observation curve (local drops at 10:00 and 15:00) is associated with local convective cloudiness and micro-precipitation, which cannot be perceived in the spatial grid of the reanalysis.

The combined analysis of the data for June 2023 and 2024 shows that the ERA5 reanalysis model is characterized by high reliability and strong synchrony with the observed data, which is confirmed by high correlation coefficients (from 0.83 to 0.93) and the corresponding values of the coefficient of determination (from 0.69 to 0.86). Comparative analysis reveals that the model accuracy in June 2024 is on average higher than in 2023. The best agreement and minimum error are observed on June 17, 2024, where the root mean square error is 1.37 degrees, and the mean absolute error is 1.08 degrees. It is followed by June 25, 2024, where the correlation reaches 0.92, and the error is 1.67 degrees. The highest errors were observed on June 15, 2023 (root mean square error 2.42 degrees) and June 17 (2.23 degrees), which is associated with local precipitation and cloudiness observed during the same period, the exact reflection of which cannot be achieved due to the limitations of the model's spatial grid. Overall, a comparison of data from both years confirms that Era5 achieves particularly high accuracy in stable and less variable weather conditions, while the increase in errors is mainly due to local microclimatic and convective processes characteristic of the Alazani Valley.

**Table 1.** Statistical performance metrics and characterization of coincidence between simulated and observed temperatures.

| Date | r (Pearson) | R2 | RMSE (°C) | MAE (°C) | Characterization of coincidence |
|---|---|---|---|---|---|
| **03.06.2023** | 0.90 | 0.79 | 1.93 | 1.57 | High |
| **15.06.2023** | 0.83 | 0.69 | 2.42 | 2.03 | Average / Good |
| **17.06.2023** | 0.89 | 0.79 | 2.23 | 1.81 | High |
| **01.06.2024** | 0.89 | 0.78 | 1.92 | 1.57 | Good |
| **17.06.2024** | 0.93 | 0.86 | 1.37 | 1.08 | High |
| **25.06.2024** | 0.92 | 0.85 | 1.67 | 1.20 | High |

Analysis of the full set of hourly data for the selected days confirms the high accuracy and statistical reliability of the Era5 reanalysis with respect to the data from the Telavi Meteorological Station. The overall correlation plot shows a strong linear relationship between the reanalysis and the observed values, where the Pearson correlation coefficient reaches 0.93, and the coefficient of determination is 0.86. The mean square error for the entire sample is 1.69 0C, and the mean absolute error is 1.31 0C. The linear trend line almost coincides with the line of perfect fit, which indicates the ability of the model to describe with high accuracy the variability of air temperature in a wide range (15 to 32 0C).



The histogram of the error distribution (difference between Era5 and the station) shows that the mean bias is -0.52 0C, which indicates a general tendency of the model to slightly decrease the temperature. The maximum error (the largest part of the hourly data) is concentrated in the interval of -2.0 and +1.0 degrees, and the frequency of observations near the zero error line is maximum. This general validation finally confirms that despite small local errors, Era5 reanalysis is a completely reliable tool for studying the air temperature regime in the Kakheti region.

## Conclusion

The present study assessed the accuracy and reliability of the ERA5 reanalysis model compared to the observation data of the Telavi Meteorological Station on characteristic days of June 2023 and 2024. The complex temporal and statistical analysis performed showed that ERA5 accurately reflects the diurnal movement of 2-meter air temperature and synoptic variability in the Kakheti region.

The analysis of the full database revealed a strong linear relationship between the reanalysis and actual observations, where the Pearson correlation coefficient ranges from 0.83 to 0.93, and the coefficient of determination reaches 0.86. The model exhibits particularly high efficiency and minimal error during stable, less cloudy synoptic conditions, such as June 17, 2024.

In addition, the study identified some limitations of the model, which are mainly related to the complex orography of the Alazani Valley and the Gombori Range. The spatial grid restriction of ERA5 (0.25 degrees) leads to the averaging of extreme daily temperature peaks, and also fails to provide a complete perception of local convective cloudiness and rapid evening cooling caused by mountain-valley circulation.

Despite the aforementioned microclimatic biases, the small average negative deviation (-0.52 degrees) confirms that the ERA5 reanalysis is a completely valid and reliable alternative tool for solving climate researchers and agro-meteorological problems in the Kakheti region, where the station observation network is limited.

## References


1. Soci C., Hersbach H., Simmons A., The ERA5 global reanalysis from 1940 to 2022. // Quarterly Journal of the Royal Meteorological Society 150(764), 2024, pp. 4014-4048. DOI: 10.1002/qj.4803, 2024.
2. Davitashvili T., Samkharadze I., Megreladze L., Kvatadze R., Using modern technology to protect vineyards from hail amid climate change", E3S Web of Conferences, 2020. www.e3sconferences.org/articles/e3sconf/abs/2021/10/e3sconf_icies2020_00034/e3sconf_icies2020_00034
3. Hersbach H., Bell B., Berrisford P., Hirahara S., The ERA5 global reanalysis. // Quarterly Journal of the Royal Meteorological Society. June 2020. 146 (730), 2020.
4. Amiranashvili A., Chikhladze V., Kekenadze E., Pipia M., Samkharadze I., Telia Sh., Varamashvili N., Meteorological conditions for the tornado formation in Kakheti (Georgia) on June 25, 2024. // International Scientific Conference "Complex Geophysical Monitoring in Georgia: History,Modern Problems, Promoting Sustainable Development of the Country", Proceedings, ISBN 978-9941-36-272-9, Tbilisi, Georgia, October 17-19, 2024.
5. Davitashvili T., Samkharadze I., Amiranashvili A., Modelling Extreme Meteorological Processes Posing a Risk to Agriculture Under Modern Climate Change. // Reliability: Theory & Applications 20 (SI 9 (87)), 2025, pp. 619-628.
6. Tatishvili M., Samkharadze I., Elbakidze K., Kapanadze N., Using of Thermodynamic Indices to Characterize Tornadoes Under Climate Change Conditions. // International Journal of Sustainability and Risk Control. 2(1), 2026, pp. 65-69.

2nd International Scientific Conference "Modern Problems in Geophysics", Proceedings,
ISBN 978-9941-36-562-1, ISSN 3088-4349, Tbilisi, Georgia, October 29-31, 2026

# STATISTICAL ESTIMATION OF QUANTILE FUNCTIONS IN THE TEMPORAL STUDY OF SEISMICITY

**Sborshchikovi A.**

*Mikheil Nodia Institute of Geophysics of Ivane Javakhishvili Tbilisi State University, Tbilisi, Georgia*
*Business and Technology University, Tbilisi, Georgia*
*a.sborshchikov@gmail.com*

***Abstract:*** *A novel method for estimating and approximating quantile and quantile density functions from statistical moment information is presented. In the proposed framework, the moments are calculated from the waiting times separating successive earthquake occurrences recorded in global seismic catalogs. Three models based on frequency moments, standard statistical moments, and transposition moments are examined to determine their efficiency in representing the underlying quantile structure. In contrast to commonly used estimation procedures, the proposed approach does not require the complete distribution of the observed data and instead utilizes moment information alone. This feature results in a simple and robust methodology for quantile function estimation in the temporal analysis of seismic activity.*

***Key Words:*** *Earthquake, waiting time, quantile function.*

## Introduction

Over the last several decades, substantial efforts have been devoted to understanding the temporal organization of seismic activity. A growing body of evidence supports the view that seismicity is closely related to the fractal properties of tectonic structures, fault networks, and the spatial distribution of earthquake hypocenters. From this perspective, earthquake occurrence can be considered a complex and evolving process rather than a stationary sequence of independent events. Temporal variations in seismicity are frequently characterized by alternating episodes of enhanced and diminished activity, reflecting the so-called switching or shifting behavior of earthquake sequences.

Despite the considerable progress achieved in the statistical investigation of seismicity, the probabilistic structure of inter-event times has received comparatively less attention. In particular, the distributional properties of the time intervals separating consecutive earthquakes are not yet completely understood, and several aspects of their statistical behavior remain open to investigation [1–3]. A more detailed characterization of these temporal intervals may therefore provide additional information about the underlying organization of seismic processes and motivates the application of alternative statistical and mathematical methods.

The moment problem is a fundamental topic in probability and statistics and has been studied extensively in various branches of mathematics and applied sciences. Its applications extend to such areas as mathematical and financial modeling, economics, and actuarial science. Although the theoretical foundations of the moment problem have been developed over several centuries, the subject continues to raise important questions and remains an active area of mathematical research [4–6].

Motivated by these considerations, the present study focuses on the estimation and approximation of the quantile function when the statistical moments of the underlying distribution are known. In particular, we investigate whether information contained in the moments can be effectively used to recover the quantile and quantile density functions associated with earthquake inter-event times [7]. This approach provides a basis for examining the temporal characteristics of seismic sequences from a moment-based perspective.

We can say that the moment problem has the only solution when the system of equations $\int x^j dF(x) = \int x^j dG(x); j = 0,1,..$, has one solution, *F=G*.

## Methods

A number of nonparametric approaches have been developed to estimate quantile functions without imposing a specific parametric form on the underlying probability distribution. Among the established methods, Harrell and Davis [8] proposed an estimator based on order statistics, whereas Bolancé et al. [9] and Brewer [10] explored the use of Bernstein polynomial approximations for quantile estimation.

The main contribution of the present study is the development of an estimation framework applicable when only partial information about the underlying probability distribution is available. More specifically, the proposed methodology assumes that the statistical moments are known, while the complete distribution itself remains unspecified. This feature makes the approach particularly suitable for data-limited situations in which conventional distribution-based estimation methods cannot be readily applied.

The study combines the temporal analysis of earthquake inter-event times with the reconstruction of their statistical characteristics through quantile functions. Computational methods are employed to support the analysis and to examine the temporal structure of seismic sequences. Both linear and nonlinear analytical techniques are considered in order to identify characteristic patterns and dependencies within waiting-time series obtained from different seismic catalogs. Particular attention is given to the temporal variability of earthquake occurrence and to the statistical information that can be extracted from the corresponding inter-event intervals.

More broadly, the proposed framework contributes to the quantitative analysis of seismic processes by integrating statistical modeling, temporal data analysis, and computational methods within a specially developed software environment. The estimation of the quantile function is performed using three alternative moment-based approaches. The first model is formulated in terms of frequency moments, the second uses conventional statistical moments, and the third employs transposition moments. Their performance is subsequently examined to determine their suitability for representing the statistical structure of earthquake waiting-time data.

## Results and discussion

To investigate the temporal characteristics of earthquake occurrence, we analyzed inter-event time series obtained from the Southern California Seismic Catalog. The analysis was based on data from the Southern California Local Earthquake Catalog, which is publicly available through the Southern California Earthquake Data Center http://www.data.scec.org/ftp/catalogs/. The selected records cover the period from 1932 to 2013.

The catalog provides a suitable basis for temporal seismicity analysis due to the extensive duration and high continuity of observations over the considered period. The original earthquake records were processed using software developed at the **M. Nodia Institute of Geophysics, Ivane Javakhishvili Tbilisi State University**. This processing procedure was used to construct a sequence of **waiting times**, defined as the temporal intervals between successive earthquake events.

The resulting waiting-time series were then used to obtain an **approximation of the quantile function** according to the first proposed model, which is based on frequency moments. To assess the performance of the proposed approximation, the obtained results were compared with those produced by the widely used **Harrell–Davis quantile estimator**.

The mathematical formulation and computational procedure employed in this analysis are presented below.

$$\widehat{Q_{HD}} = \sum_{i=1}^{n} X_{(i)} \int_{\frac{i-1}{n}}^{\frac{i}{n}} \beta(y, \lfloor \alpha x \rfloor + 1, \alpha - \lfloor \alpha x \rfloor + 1) dy$$

$$\widehat{Q_{\alpha}}(x) = \sum_{i=1}^{n+1} \Delta X_{(i)} B_{\alpha}\left(\frac{i-1}{n}, x\right) = \sum_{i=1}^{n} \Delta X_{(i)} [B_{\alpha}\left(\frac{i-1}{n}, x\right) - B_{\alpha}\left(\frac{i}{n}, x\right)]$$

The behavior for different parameters for first model will be as follows (Fig.1- Fig.3).

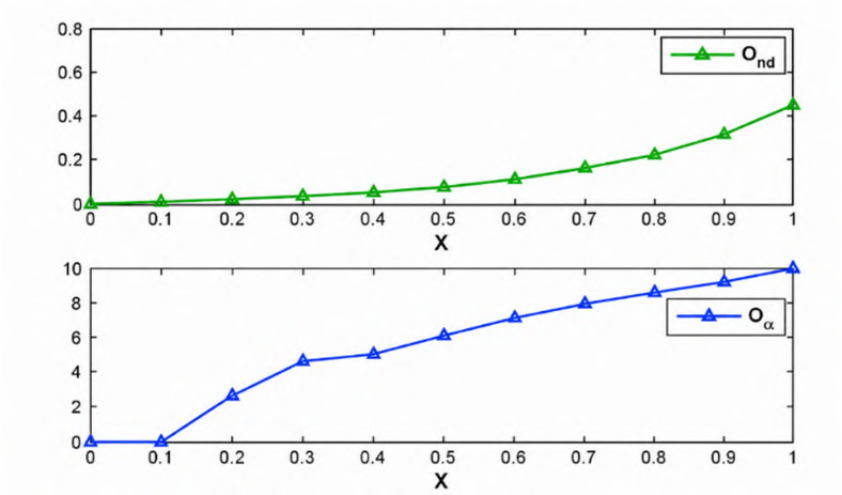



**Fig. 1.** Comparison of estimates of Harrell Davis and the first model (frequency moments) for the waiting time when.$\alpha$ =20, n=100.

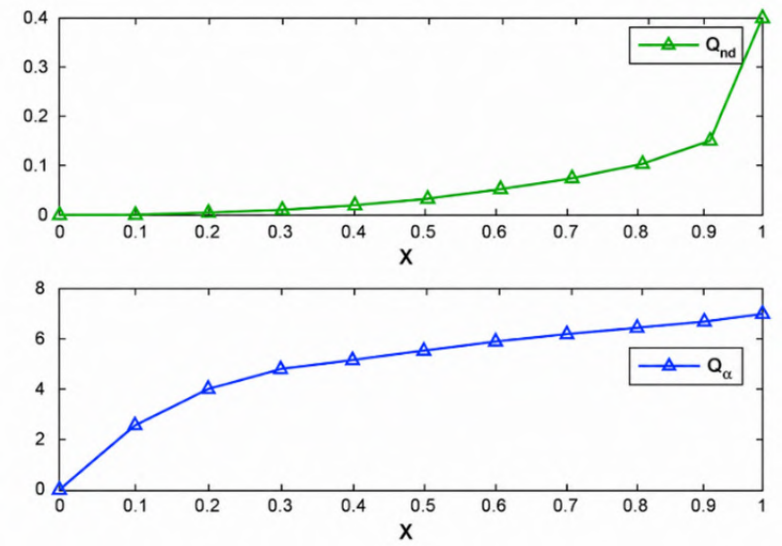



**Fig. 2.** Comparison of the estimates of Harrell Davis and the first model (frequency moments), for the waiting time when $\alpha$ =50, n=100.

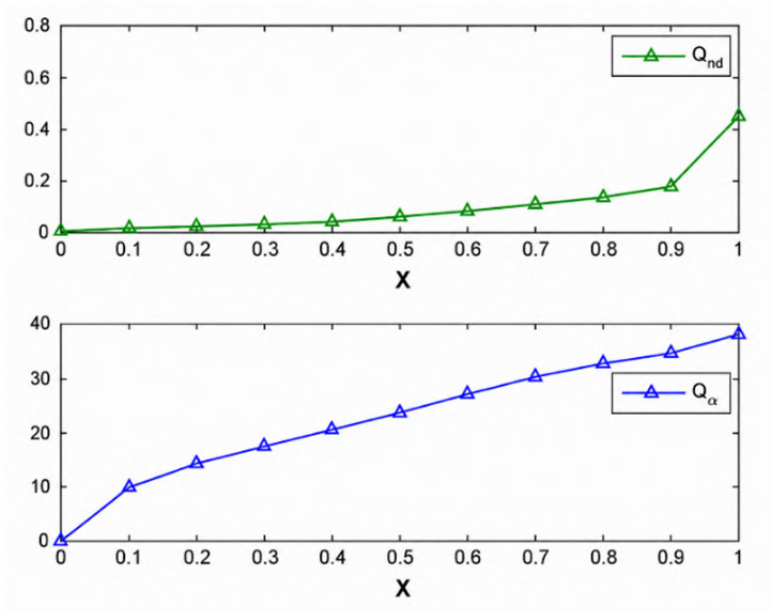



**Fig. 3.** Comparison of the estimates of Harrell Davis and the first model (frequency moments), for the waiting time when $\alpha$ =100, n=100.

The results obtained in this study provide deeper insight into the temporal characteristics of seismic activity and the underlying patterns of earthquake occurrence. In particular, the proposed approach may support further investigations into the processes governing the development of strong earthquakes and contribute to a better understanding of the mechanisms associated with major seismic events.

## Conclusion

This study focuses on the statistical analysis of the time intervals separating successive earthquake events and applies appropriate datasets to the approximation and estimation of the quantile function. The proposed methodology is not limited to seismological applications and can also be adapted to a broad range of problems in other disciplines, including financial mathematics, economics, and insurance. By addressing the problem from a global and interdisciplinary perspective, the research contributes to the solution of methodological and practical challenges relevant to several scientific fields. A detailed analysis of earthquake occurrence in time is particularly important for improving the assessment of seismic hazard and for gaining further insight into the complex processes and fundamental dynamics underlying earthquake generation.

## References


1. Telesca L., Matcharashvili T., Chelidze T., Investigation of the temporal fluctuations of the 1960–2010 seismicity of Caucasus. // Nat. Hazards Earth Syst. Sci., Göttingen Germany, 12, 2012, pp. 1905–1909.
2. Talbi A., Yamazaki F., Sensitivity analysis of the parameters of earthquake recurrence time power law scaling. // J. Seismol, Springer, Netherlands, 13, 2009, pp. 53−72.
3. Molchan G., Interevent time distribution in seismicity: a theoretical approach. // Pure Appl Geophys., Springer, Netherlands, 162, 2005, pp. 1135−1150.
4. Mnatsakanov R., Sborshchikovi A., Recovery of a Quantile Function from Moments. // Journal of Computational and Applied Mathematics, Elsevier, Netherlands, 315, 2017, pp. 354-364.
5. Mnatsakanov R., Sborshchikovi A., Recovery of quantile and quantile density function using the frequency moments. // Journal of Statistics and Probability Letters, Elsevier, Netherlands, 140, 2018, pp. 53-62.
6. Sborshchikovi A., On Nonparametric Quantile Function Estimation Using Transformed Moments. // Bulletin of the Georgian National Academy of Sciences, Tbilisi, Georgia, 11(3), 2017, pp. 22-27.
7. Cheng C., Parzen E., Unified estimators of smooth quantile and quantile density functions. // J. Statist. Plann. Inference, Elsevier, Netherlands, 59, 1997, pp. 291–307.
8. Harrell F.E., Davis C.E., A new distribution-free quantile estimator. // Biometrika, Oxford University Press, 69, 1982, pp. 635–640.
9. Bolance C., Guillen M., Nielsen J., Transformation kernel estimation of insurance claim cost distributions. // in: M. Corazza, et al. (Eds.), Mathematical and Statistical Methods for Actuarial Sciences and Finance, Springer-Verlag, Italy, 2010, pp. 43–51.
10. Brewer K.R.W., Likelihood Based Estimation of Quantiles and Density Estimation, 1986.

2nd International Scientific Conference "Modern Problems in Geophysics", Proceedings,
ISBN 978-9941-36-562-1, ISSN 3088-4349, Tbilisi, Georgia, October 29-31, 2026

# ELIMINATION OF PROBLEMS IDENTIFIED DURING THE COMPLEX STUDY OF GEORGIAN GLACIERS

***Shengelia L. D., *Kordzakhia G. I., **Tvauri G. A., ***Dzadzamia M. SH., *Shengelia M. D.**

**Hydrometeorological Institute, Georgian Technical University, Tbilisi, Georgia*
*** Andronikashvili Institute of Physics, Ivane Javakhishvili Tbilisi State University, Tbilisi, Georgia*
**** National Environmental Agency, Tbilisi, Georgia*
*larisa.shengelia@gmail.com*

***Abstract.*** *The article presents the problems identified during the complex study of the glaciers of Georgia and the ways to overcome them. For example, when using open databases available in the world, it was found that in a number of cases the preserved contours are inaccurate. The contours were refined by overlaying height isolines created on the basis of satellite images and digital terrain models. Using 3D images, watersheds were determined with high accuracy, which is crucial for the accurate determination of glacier contours. It was found that the contour of the watershed between the Gergeti and Devdoraki glaciers has changed significantly, which has consequently changed the contours of these glaciers, the areas they occupy and other characteristics of the glaciers. The results obtained served as the basis for the creation of the "Electronic Atlas of the Glaciers of Georgia" https://www.ecohydmet.ge/Glaciers-atlas-engl.html).*

***Key Words:*** *Georgian glaciers, satellite data, Satellite remote sensing (SRS).*

## Introduction

In Georgia, glaciers are located on the Caucasus Range (southern part) and are concentrated in 12 glacial basins: six in western Georgia (Bzipi, Kelasuri, Kodori, Enguri, Khobistskali, and Rioni) and six in eastern Georgia (Liakhvi, Aragvi, Tergi, Asa [Arkhotistskali], Arguni, and Pirikita Alazani). Large glaciers are found in the glacial basins of four rivers: Kodori, Enguri, Rioni, and Tergi.

The study utilizes high-resolution SRS (remote sensing) technologies, historical and open-source data, GIS technologies [1-3], and expert knowledge covering all glacial basins in Georgia.

Satellite data available through the Earth Resources Observation Systems (EROS) archive is used. This archive, which is under the jurisdiction of the US Department of the Interior, contains data obtained by Landsat satellites, as well as satellite images available from NASA.

The methods developed by the authors [4, 5] are aligned with global best practices [3, 6, 7], making it possible to define the state of glaciers simultaneously over large areas with the necessary resolution and accuracy.

## Study area, material and methods

The study area is located in the Greater Caucasus Mountains within the borders of Georgia.

Key data sources include:

- Satellite images from Landsat 5, 7, and 8 (15–30 m resolution) and commercial Azercosmos satellite SPOT 6 (1–1.5 m resolution) [8].
- Historical data from the Soviet-era glacier catalogue and 1960s topographic maps.
- Open-source databases such as NASA's and the Global Land Ice Measurements from Space (GLIMS) project.
- Google Earth's high-resolution imagery (0.5–0.8 m resolution).

The study includes historical data from the catalogue (one date) and the data determined based on SRS for three selected main dates, namely 2010, 2015 and 2020. For each SRS date, the parameters given in the catalogue , such as glacier area, morphological type, exposure, length, minimum and maximum height, firn

line height and ablation area were determined. Glaciers are divided into small (0.1–0.5 km²), medium (0.5–2.0 km²) and large (>2.0 km²) categories. The studies conducted revealed significant fragmentation and melting of glaciers over time.

Challenges such as cloud cover, inaccuracies in historical data and contouring in open databases were addressed by quality control measures, 3D visualization and manual digitization of glacier contours.

The impact of current climate change on the rapid degradation of glaciers is most clearly evident in the dynamics of retreat of large glaciers [4, 9–12] and in changes in glacial basins [13, 14], which are effective indicators of regional climate change.

## Results

During the implementation of the conducted research, a number of problems were encountered, which were successfully eliminated (Fig. 1). In particular:

- The ASTER DEM digital terrain model, the schemes given in the catalogue and the topographic maps of the USSR of the 60s of the last century (1:50000) were used to identify the glaciers to be studied. The digital terrain model was used to perform 3D visualization of the glaciers for the purpose of terrain analysis and geographical connection of the glaciers. Using 3D visualization, the location of each glacier was specified according to the river basins;
- A second method has also been used to confirm the accuracy of glacier identification. For all glaciers, their location coordinates were determined using GoogleEarth, which were compared with the coordinates given in the WGI (coordinates are not given in the catalogue). In the WGI, the identification code of each glacier is indicated near the reference glaciers, on the basis of which it is possible to determine their identification numbers and corresponding characteristics in the catalogue. The geographical coordinates of the studied glaciers turned out to be virtually identical to the data of the WGI, which confirmed the accuracy of the glacier identification;
- When using the SRS data, it turned out that inaccuracies were allowed when creating the catalogue, which could be overcome by comparing the contours of the glaciers of Georgia obtained from the SRS data and the contours of the glaciers depicted on the topographic maps of these years of the last century. In the last century, these topographic maps (1:50000) were not available, because they were compiled for the military and were classified. The conducted studies revealed that over the past 60 years, the area of all glaciers in Georgia has decreased. The area data for some individual glaciers given in the catalogue turned out to be less than that determined by the SRS, which is a mistake, because this indicates that the area of glaciers determined by the SRS has increased compared to the area of the same glacier determined in the 1960s. Comparison of the contours obtained from the SRS data with the contours of glaciers depicted on topographic maps of the 1960s allowed us to correct the unreliable data given in the catalogue;
- When using open databases available worldwide, it was found that in some cases the preserved contours are inaccurate. The contours were refined by overlaying height contours created on the basis of satellite imagery and digital terrain models, and using expert knowledge. Using 3D imagery, watersheds were determined with high accuracy, which is crucial for accurate determination of glacier contours. For example, shows the contours of the Mkinvartsvery glaciers from the GLIMS database and the contours refined using the above-mentioned methods. Discussion shows that the watershed contour between the Gergeti and Devdoraki glaciers has changed significantly, which has consequently cosiderably changed the contours of these glaciers, the areas they occupy, and other characteristics of these glaciers [10];
- In case of cloudiness, the use of satellite images is in most cases impossible. When observing glaciers, this limitation is added to the condition of the glacier surface itself. The glacier surface should be as free as possible from snow drifts, in particular, the SRS should be carried out from the end of ablation until the first snowfall. This period depends on the location of the glacier, altitude, climate and weather conditions. For Georgia, this time interval approximately covers the period from the end of June to the beginning of October . In cases where, due to these limitations, no acceptable SRS information was found for a given glacial basin for a given period, the available information for dates bordering the selected period is used.

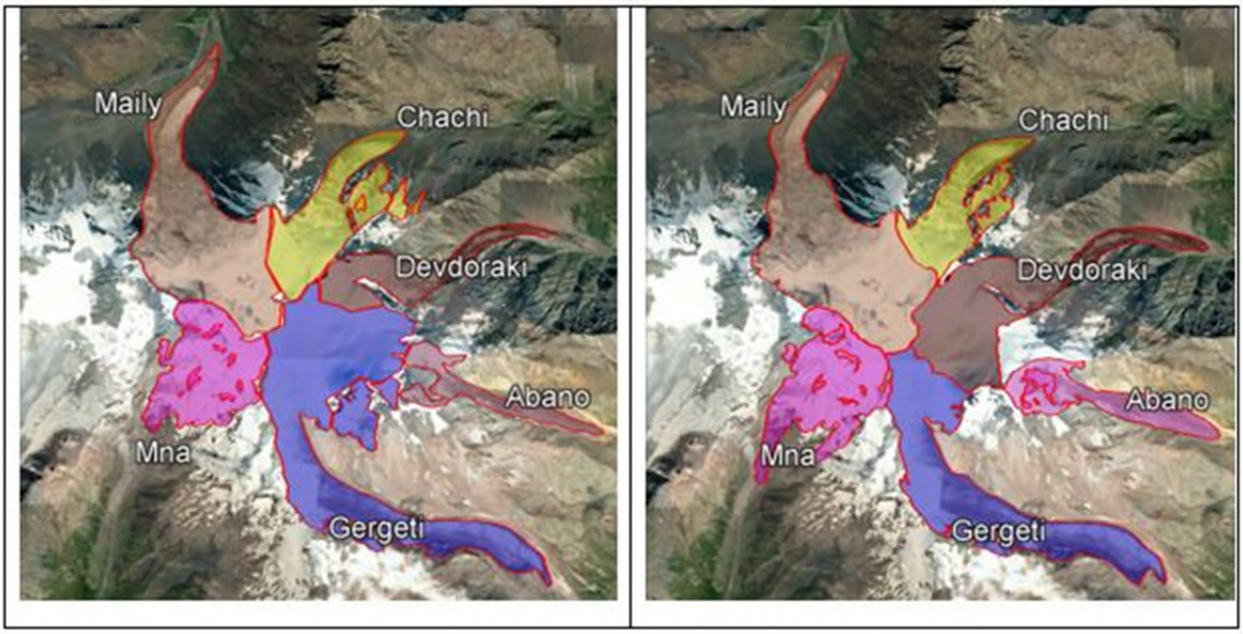



**Fig. 1.** Contours of the Mkinvarsvery glaciers: a−from the GLIMS database and b−refined using the methods used.

- Based on the conducted studies, it was determined that the degradation of glaciers is occurring much faster in eastern Georgia than in western Georgia, which is due to the large differences in the climate of these parts of the country. In particular, the climate of eastern Georgia in the subregion where glaciers are widespread is characterized by a moderately dry climate of high mountains without a real summer. The continental climate in eastern Georgia creates smaller, thinner glaciers compared to the western part of the country, although it creates spectacular landscapes (e.g. the Tergi River glacial basins). The subregion of western Georgia, where glaciers are located, is characterized by a humid highland climate with permanent snow and glaciers. In western Georgia (Enguri, Kodori, Rioni basins), humid Atlantic air masses provide abundant precipitation, which creates larger and thicker glaciers compared to the eastern part of the country. For example, the Enguri glacial basin. Taking this into account, all the planned studies were carried out separately for the eastern and western parts of the country.
- It is important that various data quality assessment and quality control (QA/QC) procedures were used at all stages of the research, as a result of which, in many cases, the reliability of the results obtained was ensured to a high degree.

## Conclusion

The elimination of problems identified during the complex study of Georgian glaciers contributed to obtaining reliable spatial resolution data, which formed the basis for the creation of the "Electronic Atlas of Georgian Glaciers" (https://www.ecohydmet.ge/Glaciers-atlas-engl.html).

## References

1. Khalsa S. J. S., Dyurgerov M. B., Khromova T., Raup B. H. and Barry R. G., Space-Based Mapping of Glacier Changes Using ASTER and GIS Tools. // IEEE Transactions on geoscience and remote sensing, vol. 42, No. 10, 2004, pp. 21-77.
2. Conrad O., Bechtel B., Bock M., Dietrich H., Fischer E., Gerlitz L., Wehberg J., Wichmann V., and Böhner J., System for Automated Geoscientific Analyses (SAGA) v. 2.1.4. // Geosci. Model Dev., 8, 2015, pp. 1991–2007. https://doi.org/10.5194/gmd-8-1991-2015
3. Gorelick N., Hancher M., Dixon M., Ilyushchenko S., Thau D. and Moore R., Google Earth Engine: Planetary-Scale Geospatial Analysis for Everyone. // Remote Sensing of Environment, 202, 2017, pp. 18-27. https://doi.org/10.1016/j.rse.2017.06.031
4. Kordzakhia G. I., Shengelia L. D., Tvauri G. A., Dzadzamia M. Sh. The climate change impact on the glaciers of Georgia. // In Journal-World Science, vol. 1, № 4(44), Warsaw, Poland, 2019, pp. 29-34.

5. Kordzakhia G., Shengelia L., Tvauri G., Dzadzamia M., Guliashvili G., Beridze S., Study of Large Glacier Retreat in Rivers Enguri and Rioni Basins. // IH SAS, Bratislava, Slovakia, E-Book, 2023, pp. 1−7.
6. Pellikka P., Gareth W., Rees – Remote Sensing of Glaciers Techniques for Topographic. // Spatial and Thematic Mapping of Glaciers 2010, 330 p.
7. Wang X, Huang Y., Liu T., Du W., Impacts of climate change on glacial retreat during 1990-2021 in the Chinese Altay Mountains. // CATENA Volume 228, July 2023, article id 107156, 2023, pp. 1-15.
8. Azercosmos Space Agency of the Republic of Azerbaijan. https://www.iafastro.org/membership/all-members/ azercosmos.html.
9. Kordzakhia G., Shengelia L., Tvauri G., Dzadzamia M., Guliashvili G., Beridze S. Comparison of Satellite Remote Sensing and Field Ground Observation Data for the Large Glaciers Retreat Study in Georgia. // Journal of the Georgian Geophysical Society, e-ISSN: 2667-9973, p-ISSN: 1512-1127; Physics of Solid Earth, Atmosphere, Ocean and Space Plasma, v. 27(1), 2024, pp. 9 – 18.
10. Kordzakhia G., Shengelia L., Tvauri G., Tsomaia V., Dzadzamia M., Satellite remote sensing outputs of the certain glaciers on the territory of East Georgia. // The Egyptian Journal of Remote Sensing and Space Sciences (2015) 18, S1−S7.
11. Kordzakhia G., Shengelia L., Tvauri G., Dzadzamia M., Guliashvili G., Beridze S., Comparison of Satellite Remote Sensing and Field Ground Observation Data for the Large Glaciers Retreat Study in Georgia. // Journal of the Georgian Geophysical Society, e-ISSN: 2667-9973, p-ISSN: 1512-1127 Physics of Solid Earth, Atmosphere, Ocean and Space Plasma, v. 27(1), 2024, pp. 9 – 18.
12. Kordzakhia G., Shengelia L., Tvauri G., Dzadzamia M., Guliashvili G., Beridze S., Georgian Large Glaciers Retreat Due to the Impact of Modern Climate Change. // Bulletin of the Georgian National Academy of Sciences, vol. 18, no. 3, 2024, pp. 77-83.
13. Kordzakhia G., Shengelia L., Tvauri G., Dzadzamia M., East Georgia Glacial Basins Degradation Dynamics Under the Impact of Current Climate Change. // Bulletin of the Georgian National Academy of Sciences, vol. 16, no. 1, Tbilisi, Georgia, 2022, pp. 32-38. (in Georgian)
14. Kordzakhia G., Shengelia L., Tvauri G., Dzadzamia M., Guliashvili G., Beridze S., Determination of the likely dates of the complete melting of the glacial basins of Georgia. // Bulletin of the Georgian National Academy of Sciences, vol. 19 (193), no. 1, 2025, pp. 57−63.

2nd International Scientific Conference "Modern Problems in Geophysics", Proceedings,
ISBN 978-9941-36-562-1, ISSN 3088-4349, Tbilisi, Georgia, October 29-31, 2026

# GEOECOLOGICAL ZONING OF THE KARMADON GORGE BASED ON A SET OF FACTORS AND EXPERT ASSESSMENTS

**Zaalishvili V., Revazov M., Melkov D., Burdzieva O.**

*Geophysical Institute of Vladikavkaz Scientific Center of the Russian Academy of Sciences,*
*Vladikavkaz, North Ossetia, Russian Federation*
*vzaal@mail.ru, cgi_ras@mail.ru*

***Abstract.*** *The objective of the study is to identify and quantify the factors that determine impact on natural systems in areas of intense anthropogenic loadings. The study's methodology is based on expert assessments of the influence of lithological, geomorphological, endogenous, exogenous, and natural-climatic factors on the geoecological state of the region. The results demonstrate endogenous activity role in activation of exogenous processes spatially associated with tectonic faults and especially fault junction zones.*

***Key words****: Geodynamic impacts, endogenous and exogenous processes, expert assessments, geoecological risks.*

## Introduction

The North Caucasus represents a unique testing ground for the study of hazardous geological processes, where their occurrence and intensity are determined by a complex interplay of endogenous and exogenous factors [1]. The formation of the modern geodynamic environment in the region is primarily due to active tectonics associated with the ongoing collision of the Eurasian and Arabian lithospheric plates. This is manifested in high seismicity (up to magnitude 8–9), a developed network of active faults, and ongoing mountain building, creating significant relief gradients and stressed rocks.

Lithological and structural prerequisites are directly superimposed on the tectonic framework. The widespread occurrence of dislocated, fractured sedimentary rocks (shales, mudstones, Cretaceous flysch strata) combined with steep slopes creates ideal conditions for the development of slope processes. The climate factor, characterized by sharp continentality in the highlands and increased precipitation on windward slopes, is the primary exogenous trigger. Intensive weathering, heavy rainfall, and seasonal snowmelt continuously supply debris, increase pore pressure, and reduce soil strength.

In recent decades, anthropogenic factors have become increasingly important in the intensification and development of geological risks. Uncontrolled development of slopes for construction, the creation of artificial reservoirs, the undercutting of slope bases during road construction, waste dump overloading, and ineffective drainage fundamentally alter the natural balance of stress and filtration. As a result, in the North Caucasus, the natural predisposition to landslides, rock falls, and mudflows is greatly enhanced by economic activity, creating a complex challenge in assessing multifactorial risks. Landslide hazard in the Republic of North Ossetia-Alania remains high, remaining one of the most destabilizing factors for the sustainable development of mountainous regions. The main hotspots are concentrated in areas with a complex combination of geological, tectonic, and climatic conditions: primarily the steep slopes of the Skalisty and Pastbishchny ridges, the sides of the gorges of the Terek, Ardon, Fiagdon, and Gizeldon rivers, as well as densely populated areas near Vladikavkaz and other populated areas.

For a comprehensive analysis of the interactions between these factors and an assessment of the effectiveness of forecasting methods, the Karmadon Gorge was selected. It represents a concentrated manifestation of virtually all the key hazardous geological processes characteristic of the North Caucasus. Its tragic history, associated with the catastrophic collapse of the Kolka Glacier in 2002, makes it a unique natural laboratory.

## Methodology of zoning

The Karmadon Gorge region is a complex geodynamic system, where the interaction of tectonic, lithological, and exogenous factors determines an exceptionally high level of hazard. The Mesozoic folded basement is intensely fragmented by a system of sublatitudinal faults (the Genaldon Anticline and the Central Graben), overlain by a mantle of Jurassic terrigenous and carbonate strata, and crowned by Quaternary volcanics of the Kazbek Center. A key factor in instability is the presence of a regional horizon of plastic, easily flooded Lower-Middle Jurassic clay shales (the Mizur and Galiat suites), which act as the main slip plane for numerous landslides. The method of zoning high-mountain areas based on geoecological loads is a comprehensive geographic and geoecological approach aimed at identifying zones with varying degrees of environmental resilience to anthropogenic impacts and natural geological processes [2–4]. A five-point scale is used to assess the impact of geodynamic and climatic factors on the environment. The role of each factor in the development of hazardous geological processes, causing changes in the geoecological situation, is considered as a rank indicator [5–6].

The methodology is based on expert assessments that determine the maximum rank of impact of individual factors [7]. Rank 1 intensity level corresponds to the minimum impact of the factor, and rank 5 to the maximum [8].

In the study area, the corresponding ranks were assessed for the following factors:

– lithological factor (rock type, their strength, susceptibility to weathering and flooding);
– geomorphological factor (slope slopes, aspect, relief dissection);
– tectonic factor (fault density, activity, intersection zones);
– seismic factor (intensity of tremors, seismic dislocations);
– climatic factor (precipitation amount, temperature regime, snowmelt);
– exogenous processes (erosion, landslides, avalanches, mudflows);
– anthropogenic factor (development, road network, man-made load).

Each factor is characterized by a specific potential $W_i$ of impact on the site. The risks $R_i$ of the impact of an individual factor with a potential $W_i$ were calculated, taking into account the geoecological vulnerability $D_i$:

$$R_i = W_i \times D_i.$$

## Geoecological load zoning results

Geoecological load zoning was performed based on the weighted contribution of each factor, which constituted four centroidal load groups: low – 30–40%; medium – 40–55%; high – 55–70% and regressive – above 70%. Calculations were performed for 2×2 km taxa using GIS technologies.

The final assessment of the geoecological state of the territory is presented in Fig. 1, which combines: an assessment of the geoecological state of individual zones, a histogram of the distribution of D values, and a zoning scheme with zone numbers.

The average value of the geoecological state D for the study area was 0.56. Zones that can be classified in this category account for a third of the territory. Extremely high values are observed for zones 5 and 8 and have identical values of D = 0.64. An above-average value is observed for zone 2, D = 0.61. Zone 3 should be considered the most favorable, D = 0.47, followed by a low level corresponding to zone 7, D = 0.51, and for three zones: 4, 6, and 9, D = 0.53. Thus, the ranking of risks of impacts on the geoecological state of the environment is implemented according to the levels of their manifestation.

Geoecological loads, according to a previously introduced classification [5] based on the use of expert assessments, are conventionally divided into weak, medium, high, and regressive. The term "regressive" was previously introduced as an indicator of instability and the hazardous state of a strata with high geoecological hazard and risk [5].

The greatest manifestation of hazardous processes occurs in the zone of the Dargavs-Karmadon highway, which determines the high risks. The greatest risk is expected in zone 2 – the developed territory of the Dargavskoye rural settlement.

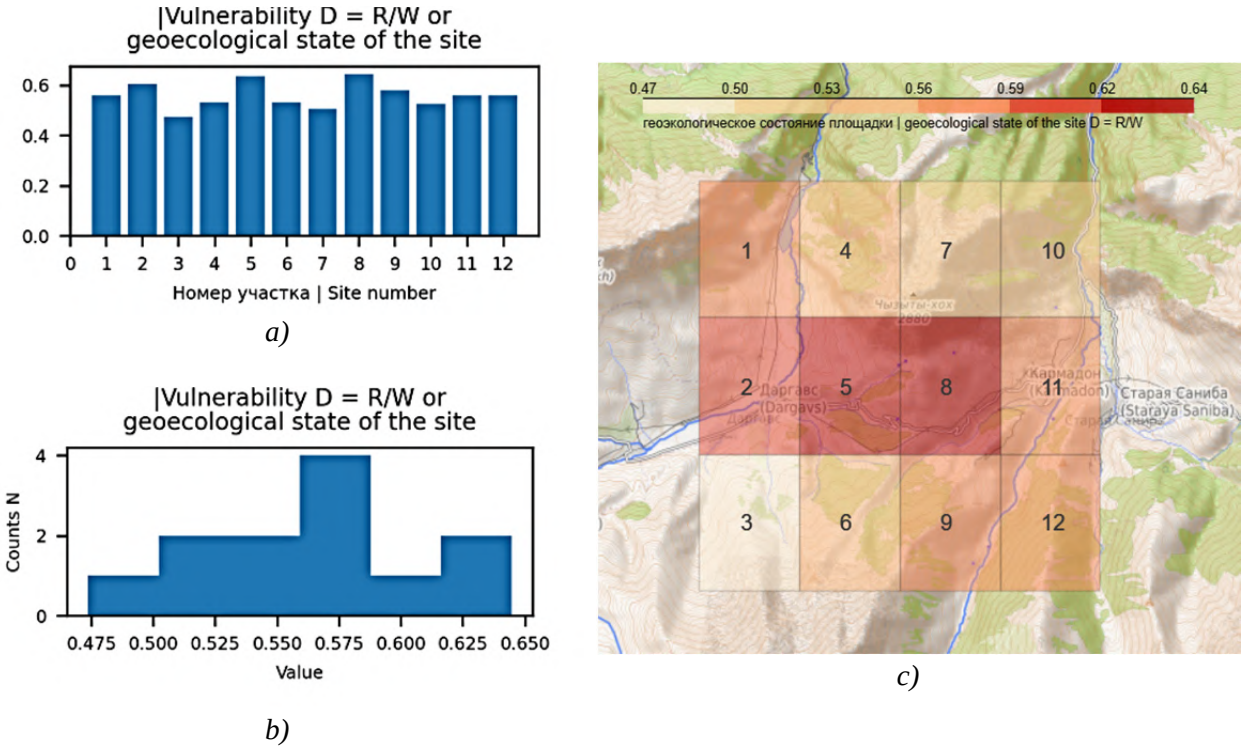



**Fig. 1.** Results of ranking the territory of the Karmadon Gorge based on a set of factors influencing geodynamic and climatic processes: (a) – assessment of the geoecological state of individual zones (bar diagram); (b) – histogram of the distribution of D values; (c) – zoning diagram with zone numbers (numbers indicate zone numbers).

Factors determining the high level of geoecological condition (zones 5 and 8):

– For zone 5: development of fracture tectonics (weight rating 5),- manifestation of seismic dislocations (weight rating 3), average terrain slope angles of 15–20 degrees (weight rating 2), active faults (weight rating 3), seismic activity (weight rating 5),- high thickness of Quaternary sediments (weight rating 3).
– For zone 8: – development of fracture tectonics (weight rating 5), manifestation of seismic dislocations (weight rating 3), average terrain slope angles of 15–20 degrees (weight rating 2), presence of intersections of sublatitudinal and submeridional faults (weight rating 4), distribution of Quaternary sediments (weight rating 4).

Thus, despite the same overall geoecological status assessment, these zones share both common and distinct factors that determine the high level of geoecological stress. For zone 2, increased erosional processes and jet erosion on slopes can be identified (rank 3).

## Discussion of Results

The results obtained allow us to draw a number of important conclusions about the nature of the geoecological load in the Karmadon Gorge.

First, the decisive role of the tectonic factor is confirmed. All zones with high and regressive loads are confined to fault intersections, crush zones, or active seismogenic structures. This is consistent with data from other researchers in the North Caucasus [1] and demonstrates the need to consider the tectonic component in any engineering-geological zoning.

Second, it is important to note that the anthropogenic factor, although not always having the highest weight rating, acts as a "trigger" for many hazardous processes. For example, slope undercutting led to a sharp increase in landslide processes in zones 2 and 5, which is confirmed by in-situ observations.

Thirdly, it has been established that Quaternary sediments, particularly their thickness and genetic type, on the one hand, smooth out uneven terrain and create flatter areas suitable for development. On the other hand, loose sediments (deluvium, colluvium, moraines) are the least resistant to erosion and landslide processes, increasing the risks for any structures.

To ensure the safe use of infrastructure, it is necessary to assess the level of impact of geodynamic activity of geotectonic and geomorphological structures in these areas using the latest software for creating 3D

models and analyzing the situation (Scoops3D, etc.) [9,10]. For practical construction in mountainous regions, detailed geophysical studies and geological engineering surveys are necessary to prevent catastrophic consequences from the possible activation of exogenous and other processes.

Thus, the results demonstrate the influence of anthropogenic load on the territory under consideration, which is increasing due to the active development of mountainous areas, and identify areas for further research. It would be appropriate to extend the developed zoning methodology to other high-mountain gorges in the North Caucasus (Fiagdon, Digorskoye, and Darialskoye) to identify common patterns and regional characteristics of geoecological load formation.

## Conclusions

1. Based on expert assessments, contributions of each factor to geoecological load formation were estimated, and corresponding zoning using the example of the mountain range between the Gizeldon and Genaldon river valleys and adjacent territories was performed. Zones of low, moderate, high, and regressive loads were identified.
2. The feasibility of predicting the impact level of natural and man-made loads is demonstrated, which provides the basis for developing appropriate measures to mitigate the severity of the consequences of hazardous processes.
3. The obtained results can serve as a basis for developing highly effective measures to reduce geoecological risks when planning the economic development of mountainous areas, and selecting priority monitoring and engineering protection areas.

## References


1. Goncharenko O.A., Zaalishvili V.B., Karaev Yu.I., Nikitin M.Yu.. Hazardous geological processes of the North Caucasus. In the collection: Hazardous natural and man-made geological processes in the mountainous and foothill territories of the North Caucasus. // Vladikavkaz: CGI VSC RAS and RNO-A, 2008, pp. 160–166.
2. Dilley M., Chen R.S., Deichmann W., Lerner-Lam A.L., Arnold M., Natural Disaster Hotspots: A Global Risk Analysis. // Washington D.C.: The World Bank, 2005.
3. Corominas J., van Westen C., Frattini P., Cascini L., Mallet J.-P., et al., Recommendations for the quantitative analysis of landslide risk. // Bulletin of Engineering Geology and Environment, Vol. 73, No. 2, 2014, pp. 209–263.
4. Jaedicke C., Van Den Eeckhaut M., Nadim F., Hervas J., Kalsnes B., et al., Identification of landslide hazard and risk 'hotspots' in Europe. // Bulletin of Engineering Geology and the Environment, Vol. 73, 2014, pp. 325–339. DOI: 10.1007/s10064-013-0541-0.
5. Chotchaev Kh.O., Burdzieva O.G., Zaalishvili V.B., Influence of geodynamic processes on the geoecological state of high-mountain territories. // Geology and Geophysics of Russian South,Vol. 10, No. 4, 2020, pp. 70–100. DOI: 10.46698/VNC.2020.87.26.005.
6. Burdzieva O.G., Revazov M.O., Kortiev A.L., Gogichev R.R., Influence of geodynamic processes on the geoecological load of a mountainous region. // Geology and Geophysics of Russian South,Vol. 14, No. 4, 2024, pp. 166–179. DOI: 10.46698/VNC.2024.50.44.01.
7. Goltsman F.M., Information content of the experiment and accounting for the correlation of non-numerical features in the recognition of geophysical objects. // Physics of the Earth, No. 10, 1980, pp. 71–85.
8. Zaalishvili V.B., Methodological aspects of seismic microzoning. // Theory of structures and seismic resistance. Zavriev ISMIS, Georgian Academy of Sciences. Tbilisi, 2000, pp. 182–188.
9. Melkov D.A., Revazov M.O., Assessment of potential landslide hazard of the Republic of North Ossetia–Alania based on geomorphological and geological data. // Procs. of the Institute of Geology, Dagestan Scientific Center, Russian Academy of Sciences, No. 2(85), 2021, pp. 48–54.
10. Burdzieva O.G., Melkov D.A., Revazov M.O., Kortiev A.L., Activation of landslide processes caused by urbanization of mountainous territories. // Geology and Geophysics of Russian South, Vol. 16, No. 4(62), 2024, pp. 1646–1658. DOI: 10.21177/1998-4502-2024-16-4-1646-1658.

2nd International Scientific Conference "Modern Problems in Geophysics", Proceedings,
ISBN 978-9941-36-562-1, ISSN 3088-4349, Tbilisi, Georgia, October 29-31, 2026

# UTILIZATION OF GEORGIA'S NATURAL RESOURCES IN THE COMPREHENSIVE TREATMENT OF DISEASES AND THE DEVELOPMENT OF MEDICAL TOURISM

**[*]Amiranashvili A., [**]Bolashvili N., [*]Chikhladze V., [***,****]Japaridze N., [*****,******]Kartvelishvili L., [*]Kereselidze Z.,[****,*******]Khazaradze K., [********]Matzarakis A., [*****,******]Megrelidze L., [*]Melikadze G., [*******]Revishvili A., [*********]Sanikidze E., [*********]Tabidze M., [**,******]Tatishvili M., [**]Tsikarishvili K.**

*[*]Mikheil Nodia Institute of Geophysics of Ivane Javakhishvili Tbilisi State University, Tbilisi, Georgia*
*[**]Vakhushti Bagrationi Institute of Geography of Ivane Javakhishvili Tbilisi State University, Tbilisi, Georgia*
*[***]Tbilisi State Medical University, Tbilisi, Georgia*
*[****]Ministry of Internally Displaced Persons from Occupied Territories, Labour, Health and Social Affair of Georgia, Tbilisi, Georgia*
*[*****]National Environment Agency, Tbilisi, Georgia*
*[******]Institute of Hydrometeorology of Georgian Technical University, Tbilisi, Georgia*
*[*******]Georgian State Teaching University of Physical Education and Sport, Tbilisi, Georgia*
*[********]Albert-Ludwigs-Universität Freiburg, Germany*
*[*********]Tbilisi Balneological Spa Resort, Tbilisi, Georgia*
*avtandilamiranashvili@gmail.com*

***Abstract.*** *Brief information is presented on research conducted in Georgia regarding the use of natural resources in the comprehensive treatment of diseases, as well as on the prospects for advancing this research to foster the development of medical tourism.*

***Key words:*** *Natural resources, bioclimate, speleotherapy, ion therapy, radon baths.*

## Introduction

Complex treatment of diseases in modern conditions requires the availability of recreational resources, capital, technology and personnel.

These resources are very diverse and include natural and anthropogenic geosystems, natural phenomena, artifacts that have comfortable properties and consumer value for recreational activities and can be used to organize recreation and health improvement for a certain contingent of people at a fixed time using existing technology and available material capabilities.

Like any other, recreational resources are not unlimited; they have a certain volume (potential reserve), time of use, operating conditions and, of course, cost [1-11]. In recent years, in order to comprehensively characterize areas suitable for the treatment of diseases, it has been customary to carry out their certification [7,11]. In Georgia, such systematic work has not been carried out, although there are many works describing the main characteristics of resort resources [1-33].

Natural resources for the complex treatment of diseases mean:

Landscape, relief, soil types, water resources, vegetation cover, territories of regulated access, hydromineral resources, therapeutic mud, unique resources (for example, speleotherapy, radon baths, etc.)

Of particular importance are bioclimatic resources (insolation regime, provision of ultraviolet radiation, equivalent effective air temperatures, precipitation regime, Tourism Climate Index, Holiday Climate Index, air ionization conditions, intense thunderstorm activity and much more).

When organizing complex treatment of diseases, one should also take into account the functional suitability of the area for organizing climatic treatment, the conditions for the improvement of the facility, anthro-

pogenic stability, the radiation background of the air basin of the territory (gamma background), the level of electromagnetic radiation of the territory, the level of pollution of the air basin, the chemical composition and bacteriological state of surface waters and etc.

Particular attention should be paid to the organization of treatment and diagnostic facilities: compliance of the equipment of treatment and diagnostic departments and offices with the recommended list depending on the profile of treatment; availability of modern medical equipment with a release date of less than 5 years and its use for the application of modern medical technologies; compliance of the areas of treatment and diagnostic rooms with the requirements of current sanitary standards; the presence of all persons working on medical equipment and equipment with appropriate permits (permits, certificates, certificates, etc.); compliance with safety requirements when working with medical equipment, confirmed by relevant documents based on the results of control and supervision.

Thus, in Georgia, in order to carry out more effective measures for the use of natural resources in the complex treatment of diseases, it is necessary to systematize the existing extensive material from past studies, as well as conduct new ones. It is also important to improve the legislative framework for the development of spa treatment. All this will help increase the interest of local and foreign consumers in this area of recreation and treatment, development of the country's economy, and improvement of the well-being of the population.

## Development prospects

**Short-term** – carrying out ongoing small-scale work in the field of recreation and treatment at specific sites in order to improve or expand services.

**Medium-term** – work on the development of recreational areas and facilities in order to use known and yet-to-be-identified bioclimatic features.

**Long-term** – full certification of spa areas and facilities taking into account climate change.

## Means of implementation

- Implementation of the results of previously conducted scientific research
- Research of territories and individual objects
- Conducting trainings, consultations, etc.
- Development of instructions, recommendations, etc.
- Creation of joint working groups to solve specific problems (advertising, booklets, banners, links, etc.)
- Publications, media

## Sources of financing

- State and local funding, national and foreign grants, sponsorships, etc.

## Form of cooperation

- Memorandum of cooperation between legal entities, agreement with individuals, personal selfless initiative, etc.

## Conclusion

Studying Georgia's bioclimatic resources is crucial for enhancing the efficiency and appeal of the country's resort, tourism, and medical tourism sectors for both residents and visitors. Preliminary studies indicate the existence of significant untapped potential in these resources, which is expected to be identified through future collaborative efforts involving various government, commercial, and scientific organizations.

## References

1. Chirakadze G.I. Mikroklimaticheskiye issledovaniya kurortnykh mestnostey. // Meteorologich. vestnik, Leningrad, 1934.
2. Gachechiladze I.E. Abastumani, klimaticheskiy ocherk. // Izd. Zak. GIZ, Tiflis, 1934.

3. Kebuladze V.V. Radioaktivnost' mineral'nykh istochnikov Skuri i Lugela, v Tsalendzhikhskom i Chkhoroykuyskom rayonakh Gruzinskoy SSR. // Tr. geofiz. in-ta Gruz. FAN SSSR, t. III, Tbilisi, 1938.
4. Nodia M.Z., Magnitnyye peski i magnitnoye pole i Chernomorskogo poberezh'ya. // Tez. sessii Gruz. FAN SSSR, 27-30 sentyabrya 1935 g., Izd. Gruz. FAN SSSR, Tbilisi, 1939.
5. Vekua L.V. Aktinometricheskiye kharakteristiki kurorta Shovi. // Tr. GGO, vyp. 1(63), Gidrometeoizdat, Leningrad, 1947.
6. Chirakadze G.I., Zadacha bioklimaticheskikh issledovaniy na kurortakh i puti ikh razresheniya. // Tez. dokl. Vsesoyuznogo soveshchaniya po klimatoterapii TSI kurortologii, Moskva, 1953.
7. Vadachkoria M.K., Ushveridze G.A., Jaliashvili V.G., Health Resorts of the Georgian SSR. // Book: "Sabchota Sakartvelo" Publishers, Tbilisi, 1987, 383 p. (in Georgia, English and Russian)
8. Kereselidze Z.A., Saakashvili N.M., Tarhan-Mouravi I.D., Tabidze M.S., Amiranashvili A.G., Chihladze V.A., Osobennosti lokal′noj magnitnoj anomalii v kurortnoj zone Ckalcminda – Ureki. // shromata k'rebuli „aramedik'ament'uri samk'urnalo pakt'orebis gamoq'enebis akt'ualuri sak'itkhebi", tbilisi, 2006, 93–99.
9. Saakashvili N., Tabidze M., Tarkhan-Mouravi I., Khelashvili E., Amiranashvili A., Kirkitadze D., Melikadze G., Nodia A., Tarkhnishvili A., Chikhladze V., Lominadze G., Tsikarishvili K., Chelidze L., Climatic, Aero – Ionizing and Radiological Characteristics of the Health Resort – Tourist Complex of Tskaltubo City. // Papers of the Int. Conference International Year of the Planet Earth "Climate, Natural Resources, Disasters in tne South Caucasus", Trans. of the Institute of Hydrometeorology, vol. 115, ISSN 1512-0902, Tbilisi, 18 – 19 November, 2008, pp. 31–40. (in Russian)
10. Amiranashvili A.G., Chelidze T.L., Melikadze G.I., Trekov I.Yu., Todadze M.Sh., Chankvetadze A.Sh., Chelidze L.T., Predvaritel'nyye rezul'taty issledovaniya soderzhaniya radona v pochve i vode v razlichnykh rayonakh Zapadnoy Gruzii. // Tr. In-ta geofiziki im. M.Z. Nodia, ISSN 1512-1135, tom. 60, Tbilisi, 2008, s. 213–218.
11. Saakashvili N.M., Tabidze M.Sh., Tarkhan-Mouravi I.D., Amiranashvili A.G., Melikadze G.I., Chikhladze V.A., To a Question About the Certification of the Health Resort and Tourist Resources of Georgia. // Modern Problems of Using of Health Resort Resources, Collection of Scientific Works of International Conference, Sairme, Georgia, June 10-13, 2010, ISBN 978-9941-0-2529-7, Tbilisi, 2010, pp. 175-180. (in Russian)
12. Saakashvili N.M., Tabidze M.Sh., Tarkhan-Mouravi I.D., Amiranashvili A.G., Melikadze G.I., Chikhladze V.A., K voprosu ob organizatsii ionoterapii na kurortakh Gruzii. // Sovremennyye problemy ispol'zovaniya kurortnykh resursov. Trudy Mezhdunarodnoy konferentsii, Tbilisi, 2010, s.168-174.
13. Amiranashvili A.G., Chikhladze V.A. Saakashvili N.M., Tabidze M.Sh., Tarkhan-Mouravi I.D., Bioclimatic Characteristics of Recreational Zones – Important Component of the Passport of the Health Resort – Tourist Potential of Georgia. // Pressing Problems in Hydrometeorology and Ecology, Papers of the Int. Conf. Dedicated to the 90th Anniversary of Academician G. Svanidze, September 27-29, Tbilisi, 2011, Trans. Of the Institute of Hydrometeorology at the Georgian Technical University, vol. 117, ISSN 1512- 0902, Tbilisi, 2011, pp. 89-92.
14. Kartvelishvili L., Matzarakis A., Amiranashvili A., Kutaladze N., Assessment of Touristical -Recreation Potential of Georgia on Background Regional Climate Change. // In the book: Proc. of IIst Int. Scientific-Practical Conference "Tourism: Economics and Business", June 4-5, Batumi, Georgia, 2011, pp. 250-252.
15. Amiranashvili A.G, Bolashvili N.R., Chikhladze V.A., Japaridze N.D., Khazaradze K.R., Khazaradze R.R., Lezhava Z.L., Tsikarishvili K.D., Some New Data about the Bioclimatic Characteristics of the Village of Mukhuri (Western Georgia). // Journal of the Georgian Geophysical Society, Issue B. Physics of Atmosphere, Ocean and Space Plasma, v.18B, Tbilisi, 2015, pp. 107-115.
16. Amiranashvili A., Chargazia Kh., Matzarakis A., Kartvelishvili L., Tourism climate index in the coastal and mountain locality of Adjara, Georgia. // Int. Sc. Conf. "Sustainable Mountain Regions: Make Them Work". Proceedings, Borovets, Bulgaria, ISBN 978-954-411-220-2, 14-16 May, 2015, pp.238-244. http://geography.bg/MountainRegions_Sofia2015
17. Bolashvili N.R., Chikhladze V.A., Khazaradze K.R., Lezhava Z.I., Tsikarishvili K.D., Some Bioclimatic Characteristics of Martvili Canyon (Western Georgia).// In the book: The Questions of Health Resort Managing, Physiotheraphy and Rehabilitation, International Collection of Scientific Articles, Vol. I, ISSN 2449-271X, Tbilisi, 2016, pp. 81-87. http://109.205.44.60/bitstream/123456789/6244/1/Bolashvili%2CChikhladze..._2016_Article.pdf
18. Amiranashvili A.G., Japaridze N.D., Kartvelishvili L.G., Khazaradze K.R., Matzarakis A., Povolotskaya N.P., Senik I.A., Tourism Climate Index of in the Some Regions of Georgia and North Caucasus. // Journal of the Georgian Geophysical Society, Issue B. Physics of Atmosphere, Ocean and Space Plasma, v. 20B, 2017, pp. 43–64.
19. Amiranashvili A.G., Japaridze N.D., Khazaradze K.R., On the Connection of Monthly Mean of Some Simple Thermal Indices and Tourism Climate Index with the Mortality of the Population of Tbilisi City Apropos of Cardiovascular Diseases. // Journal of the Georgian Geophysical Society, ISSN: 1512-1127, Physics of Solid Earth, Atmosphere, Ocean and Space Plasma, v. 21(1), Tbilisi, 2018, pp.48 -62.
20. Amiranashvili A., Bliadze T., Chikhladze V., Japaridze N. Khazaradze K., On the Influence of Landscape on the Content of Light Aeroions in Different Regions of Georgia. // Proc. Intern. Multidisciplinary Conf. "Actual Prob-

lems of Landscape Sciences: Environment, Society, Politics", September 9-13, 2019, Tbilisi, Georgia, ISBN 978-9941-13-868-3, Tbilisi, 2019, pp. 117-121.
http://dspace.gela.org.ge/bitstream/123456789/8597/1/Amiranashvili%20etc._Act_Probl_Lands_Science_2019.pdf

21. Japaridze N., Khazaradze K., Studies in the Field of the Influence of Natural and Anthropogenic Environmental Factors on Human Health in Georgia: Current Status and Planned Works. // Int. Sc. Conf. "Natural Disasters in Georgia: Monitoring, Prevention, Mitigation". Proceedings, ISBN 978-9941-13-899-7, Publish House of Iv. Javakhishvili Tbilisi State University, December 12-14, Tbilisi, 2019, pp. 201-204.
22. Kartvelishvili L., Amiranashvili A., Megrelidze L., Kurdashvili L., Turistul Rekreaciuli Resursebis Shefaseba Klimatis Cvlilebebis Fonze. Publish Hous "Mtsignobari", ISBN 978-9941-485-01-5, Tbilisi, 2019, 161 p.
http://dspace.nplg.gov.ge/bitstream/1234/293074/1/turistulRekreaciuliResursebisShefasebaKlimatisCvlilebebisFonze.pdf
23. Amiranashvili A.G., Revishvili A.A., Khazaradze K.R., Japaridze N.D., Connection of Holiday Climate Index with Public Health (on Example of Tbilisi and Kakheti Region, Georgia). // Journal of the Georgian Geophysical Society, e-*ISSN:* 2667-9973*,* p-ISSN*:* 1512-1127, Physics of Solid Earth, Atmosphere, Ocean and Space Plasma, v. 24 (1), 2021, pp. 63-76. DOI: https://doi.org/10.48614/ggs2420212884
24. Lanchava O. A., Iliashi N., Radu S., Tsikarishvili K., Lezhava Z., Amiranashvili A., Chikhladze V., Asanidze L., ts'q'alt'ubos (dasavleti sakartvelo) „tetra mghvimis" p'rakt'ik'uli sargeblianobis p'ot'entsiali. // Georgian Scientists**,** E-ISSN: 2667-9760, Vol. 3, N 1, 2021, 15 P., Retrieved from
https://journals.4science.ge/index.php/GS/article/view/285
25. Melikadze G., Vaupotič J., Kapanadze N., Tchankvetadze A., Chelidze L., Todadze M., Gogichaishvili Sh., Jimsheladze T.,Radon Concentration in Water on the Several Regions of Georgia. // Int. Sc. Conf. „Natural Disasters in the 21st Century: Monitoring, Prevention, Mitigation", Proceedings, ISBN 978-9941-491-52-8, Tbilisi, Georgia, December 20-22, 2021, pp. 127-129.
26. Amiranashvili A.G., Kartvelishvili L.G., Kutaladze N.B., Megrelidze L.D., Tatishvili M.R., Holiday Climate Index in Some Mountainous Regions of Georgia. // Journal of the Georgian Geophysical Society, e-ISSN: 2667-9973, p-ISSN: 1512-1127, Physics of Solid Earth, Atmosphere, Ocean and Space Plasma, v. 24(2), 2021, pp. 92 – 117. DOI: https://doi.org/10.48614/ggs2420213327
27. Kartvelishvili L., Tatishvili M., Amiranashvili A., Megrelidze L., Kutaladze N. ,Weather, Climate and their Change Regularities for the Conditions of Georgia. // Monograph, Publishing House "Universal", Tbilisi 2023, 406 p., https://doi.org/10.52340/mng.9789941334658
28. Amiranashvili A., Bolashvili N., Kartvelishvili L., Liparteliani G. , Tsirgvava G., Holiday Climate Index in Kvemo Kartli (Georgia). // Georgian Geographical Journal, E-ISSN: 2667-9701, 24(1), 2024, pp. 35-46.
https://doi.org/10.52340/ggj.2024.04.01.05
29. Amiranashvili A., Kartvelishvili L., Matzarakis A., Variability of the Holiday Climate Index in Tsalka (Georgia). // Journal of the Georgian Geophysical Society, e-ISSN: 2667-9973*,* p-ISSN*:* 1512-1127, Physics of Solid Earth, Atmosphere, Ocean and Space Plasma, v. 27(1), 2024, pp. 77–90.
https://ggs.openjournals.ge/index.php/GGS/article/view/7986
30. Kartvelishvili L., Amiranashvili A., Megrelidze L., Kurdashvili L., Evaluation of Tourist-recreational Resources in the Background of Climate Change in Georgia. // Georgian Geographical Journal, E-ISSN: 2667-9701, 5(2), 2025, pp. 36-40. https://doi.org/10.52340/ggj.2025.05.02.06
31. Abramishvili R., Ambokadze V., Amiranashvili A., Bolashvili N., et al. ,Geographical Atlas of Kakheti Region. // Publish House of I. Javakhishvili Tbilisi State University, ISBN 978-9941-36-316-0, Tbilisi, 2025, 214 p. (in Georgian)
32. Amiranashvili A., Bolashvili N., Gagua G., et al., Geographical Atlas of Kvemo Kartli Region. // Publish House of I. Javakhishvili Tbilisi State University, ISBN 978-9941-36-479-6, Tbilisi, 2026, 198 p. (in Georgian)
33. Khazaradze K., Giorgobiani M., Revishvili R., Garemo da janmrteloba. damkhmare sakhelmdzghvanelo st'udent'ebisa da magist'rebisatvis. // tbilisi. gamomtsemloba „dani", 2026 ts'eli, 193 gverdi ISBN 978-9941-8-8807-6.

2nd International Scientific Conference "Modern Problems in Geophysics", Proceedings,
ISBN 978-9941-36-562-1, ISSN 3088-4349, Tbilisi, Georgia, October 29-31, 2026

# EFFECT OF ENVIRONMENTAL HUMIDITY ON POST-IRRADIATION RECOVERY OF SOIL MICROORGANISMS

**Avalishvili A., Gunia N., Uchaneishvili S., Kalmakhelidze S., Ivanishvili N., Gogebashvili M.**

*Ivane Beritashvili Center of Experimental Biomedicine, Tbilisi, Georgia*
*anastasiaavalishvili1@gmail.com*

***Abstract.*** *Soil microorganisms play an important role in the functioning of biogeocenoses, nutrient cycling, and the maintenance of soil ecological conditions. Their abundance and functional characteristics are strongly influenced by the physical and chemical properties of soil and by environmental factors, including moisture. Under anthropogenic, including radiological, exposure, assessment of the resistance and recovery capacity of microorganisms is important for understanding radiation-induced damage to ecosystems and their subsequent recovery. The aim of the present study was to investigate the post-radiation recovery of soil microorganisms under different soil-moisture conditions. Brown soil, widely distributed throughout Georgia, was used in the experiments. Soil samples were exposed to gamma radiation in the dose range of 0–16 kGy using a ^137Cs gamma-radiation source at a dose rate of 1.1 Gy/min. Soil moisture was modeled according to the minimum and maximum water-holding capacity characteristic of this soil type. Radiation-induced inhibition of microbial growth and subsequent recovery were assessed based on the number of colonies formed on Sabouraud agar one week after inoculation. A dose–effect curve was constructed based on the obtained data and demonstrated a dose-dependent reduction in microbial colony formation. The $LD_{50}$ value was determined to be 4.2 kGy. Assessment of post-radiation recovery demonstrated a pronounced effect of soil moisture on microbial recovery. Under conditions of minimum soil moisture, the colony recovery coefficient relative to the control was 25%, whereas under maximum soil-moisture conditions it reached 75%. Thus, the results indicate that soil moisture is one of the important factors determining the post-radiation recovery of soil microorganisms. Reduced soil moisture substantially inhibits the recovery processes of the soil microflora and may consequently decrease the ecological stability of the microbial component of the soil ecosystem. These findings are relevant for assessing soil microbiological conditions and the recovery potential of ecosystems following radiation exposure.*

***Key words:*** *Soil microorganisms; gamma irradiation; soil moisture.*

## Introduction

Soil represents the principal reservoir and natural habitat for microorganisms that participate in soil purification and formation processes, as well as in nutrient cycling [1]. The viability of microorganisms in soil, together with their quantitative abundance and qualitative characteristics, is determined by soil conditions, including the availability of nutrients, moisture, aeration, soil reaction (pH), temperature, and other environmental factors [2]. Soil type has a substantial influence not only on the total abundance of microorganisms but also on the relative proportions of individual taxonomic groups.

Based on these considerations, it is evident that alterations or reductions in the natural balance of soil microbiological activity within different biogeocenoses may have a significant impact on the overall ecological situation. Soil microflora is particularly susceptible to changes caused by anthropogenic factors, which is why alterations in microbial communities are also used in bioindication studies. Numerous studies have demonstrated that the viability of soil microorganisms can be determined both by the intensity of the influencing factor and the degree of damage produced, as well as by the qualitative characteristics of the soil itself [3]. Because soils differ in their physical and chemical properties, they also provide different environmental conditions for microbial growth and activity. From this perspective, the territory of Georgia, characterized by considerable soil diversity, represents an interesting subject for investigation [4].

At the same time, during global catastrophes, such as the accident at the Chornobyl Nuclear Power Plant, situations may arise in which landscapes belonging to particular biogeocenoses become contaminated

regardless of their distance from the original source of contamination. A prominent example is the radioactive contamination of areas of Western Georgia associated with this technological disaster [5]. Therefore, in order to determine the damage caused by radiation exposure in a particular region, it is necessary to investigate the resistance of each individual component of the biocenosis, thereby making it possible to predict potential ecological risks.

Soil microorganisms constitute one of the important components of biocenoses. Their activity depends not only on the physical and chemical structure of the soil but also on its moisture content [6]. Accordingly, the present study was designed to investigate the post-radiation recovery of soil microorganisms under different soil-moisture conditions.

## Materials and Methods

Brown soil, which is widely distributed throughout Georgia, was used in our experiments. Soil samples were exposed to gamma radiation at doses ranging from 0 to 16 kGy.

Irradiation was performed using a gamma-irradiation facility equipped with a $^{137}Cs$ radiation source. The dose rate was 1.1 Gy/min. Soil moisture conditions were modeled according to the water-holding capacity characteristic of this soil type. With respect to dry soil weight, the minimum value of the water-holding capacity was 36.3%, whereas the maximum value was 51.8%. When recalculated relative to soil volume, the corresponding values were 39.9% and 57.0%, respectively [7].

Both non-irradiated soil samples, which served as controls, and irradiated samples were inoculated onto Sabouraud agar [8,9,10]. Radiation-induced inhibition of the growth and development of soil microorganisms was assessed according to the number of colonies developing on the culture medium one week after inoculation (Fig.1). The experimental analysis included two main components:

## Results

Based on the obtained data, a dose–effect curve was constructed (Fig. 2-I). The curve demonstrated a dose-dependent reduction in the formation of microbial colonies following gamma irradiation. An $LD_{50}$ value of 4.2 kGy was determined. Post-radiation recovery of the microorganisms was subsequently investigated under different soil-moisture conditions. As shown in Figure 2, the extent of microbial recovery differed substantially depending on soil moisture. Under conditions of minimum soil moisture, the post-radiation recovery coefficient of microbial colonies relative to the control was 52%. In contrast, under conditions of maximum soil moisture, the corresponding recovery coefficient reached 75%. These results demonstrate a pronounced dependence of microbial recovery following irradiation on the moisture conditions of the soil.

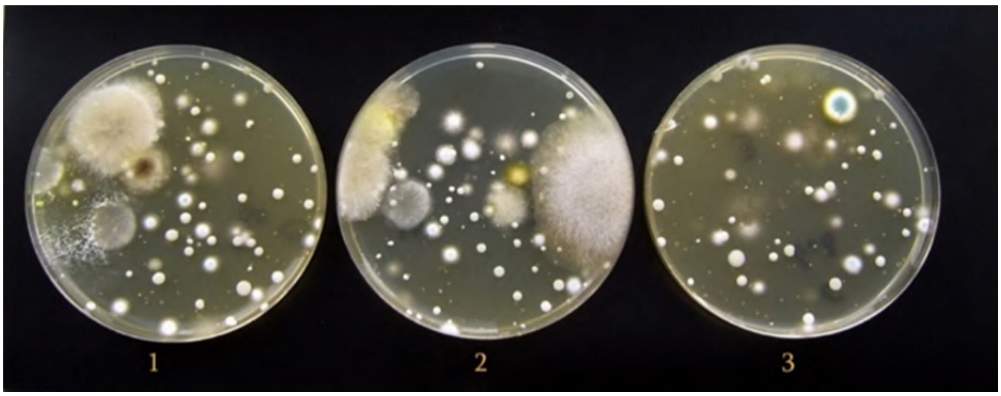



**Fig.1.** Influence of Gamma Radiation on the Recovery Dynamics of Soil Microorganisms After Irradiation: 1. Control – non-irradiated soil; 2. High-moisture group – post-radiation recovery under conditions of high soil moisture; 3. Low-moisture group -post-radiation recovery under conditions of low soil moisture.

## Discussion and Conclusion

The results of the present experiments demonstrate that soil moisture is one of the important factors influencing the post-radiation recovery of soil microorganisms. Reduction of soil moisture suppresses the reco-

very processes of the soil microflora following radiation exposure. Consequently, decreased soil moisture may reduce the resistance and recovery capacity of this component of the biogeocenosis. Since soil microorganisms represent an important functional component of terrestrial ecosystems, impairment of their recovery may potentially contribute to broader ecological disturbances and may be reflected in nonspecific changes occurring at higher levels of biological organization. The markedly greater recovery observed under conditions of maximum soil moisture, compared with minimum-moisture conditions, suggests that adequate soil moisture may contribute to the preservation of microbial viability and to the restoration of microbial populations following radiation-induced damage. From an ecological perspective, these findings emphasize the importance of maintaining the natural moisture conditions of landscapes, particularly in environments affected by radiation or other anthropogenic stressors. Preservation of natural soil-moisture regimes may help prevent alterations in the baseline microbiological structure characteristic of a particular soil type and may contribute to maintaining its capacity for recovery following environmental disturbance.

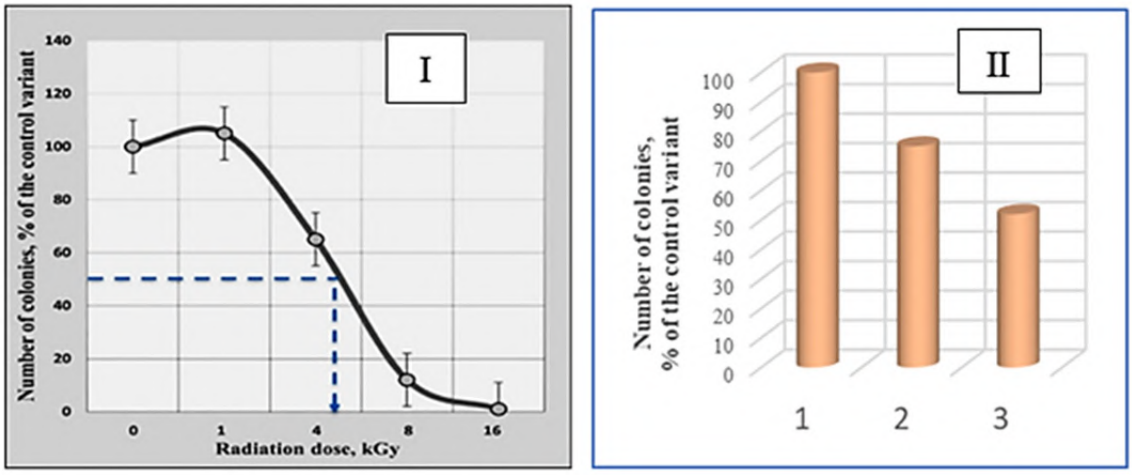



**Fig. 2.** Effect of Gamma Radiation on the Intensity of Post-Irradiation Recovery of Soil Microorganisms:
I – Effect of irradiation on the dynamics of microbial colony formation.
II – Post-radiation recovery of microbial colonies under different soil-moisture conditions.

Thus, the obtained results indicate that assessment of soil moisture should be taken into consideration when evaluating the radiological resistance and recovery potential of soil microbial communities. The interaction between radiation exposure and soil environmental conditions represents an important factor in determining the extent and persistence of microbiological disturbances within affected biogeocenoses.

## References


1. Whalen J. K., & Sampedro L., *Soil Ecology and Management.* CABI, Oxfordshire, 2010, 304 p.
2. Jansson J. K., & Hofmockel K. S., Soil Microbiomes and Climate Change. // Nature Reviews Microbiology, Vol. 18, No. 1, 2020, pp. 35–46.
3. Heger T. J., Imfeld G., & Mitchell A. D., Special Issue on 'Bioindication in Soil Ecosystems': Editorial Note. // European Journal of Soil Biology, 49, 2012, pp. 1–4.
4. Urushadze T., The Main Soils of Georgia. Tbilisi: Metsniereba, 1997.
5. Tsitskishvili M. S. et al., Main Results of Radioecological Monitoring of Transcaucasia. // Radiation Research, Tbilisi, Vol. VII, 1986, pp. 197–220.
6. McNamara N. P., Black H. I. J., Beresford N. A., & Parekh N. R., Effects of Acute Gamma Irradiation on Chemical, Physical and Biological Properties of Soils. // Applied Soil Ecology, 24(2), 2003, pp. 117–132.
7. Nakaidze E. K., Brown and Meadow-Brown Soils of Georgia. Tbilisi: Metsniereba, 1977, 304 p.
8. Daraselia G. Ya., Microbiology, Hygiene and Food Safety. Astrakhan, Russia, 2008, 504 p.
9. Larionov M. V., Smirnova E. B., Larionov N. V., & Kabanina S. V., Microbiological Studies of the Environment. // Nauka, 2010, 110 p.
10. Zvyagintsev D. G. (Ed.)., Methods of Soil Microbiology and Biochemistry. Moscow: Moscow State University Press, 1991, 304 p.

2nd International Scientific Conference "Modern Problems in Geophysics", Proceedings,
ISBN 978-9941-36-562-1, ISSN 3088-4349, Tbilisi, Georgia, October 29-31, 2026

# DISTRIBUTION THE DAILY NUMBER OF AIR EFFECTIVE TEMPERATURE ACCORDING TO MISSENARD IN BOLNISI BY MONTH

**[*,**]Japaridze N., [***,****]Kartvelishvili L., [**,*****]Khazaradze K., [******]Chkhitunidze M., [******]Nikolaishvili M., [*****]Revishvili A.**

[*]*Tbilisi State Medical University, Tbilisi, Georgia*
[**]*Ministry of Internally Displaced Persons from Occupied Territories, Labour, Health and Social Affair of Georgia, Tbilisi, Georgia*
[****]*Institute of Hydrometeorology of the Georgian Technical University*
[****]*Georgian National Environmental Agency*
[*****]*Georgian State Teaching University of Physical Education and Sport, Tbilisi, Georgia*
[******]*Mikheil Nodia Institute of Geophysics of Ivane Javakhishvili Tbilisi State University, Tbilisi, Georgia*
*n.japaridze@tsmu.edu*

***Abstract:*** *The paper presents data on distribution the number of daily mean and maximum values of air effective temperature according to Missenard in Bolnisi by month in 2018-2023. In particular, on average, for the mean daily values of effective air temperature with the category "Comfortable", the largest number of days are observed from June to September (19, 11, 13 and 15, respectively). For the maximum daily values of effective temperature – in April, May, September and October (10, 13, 10 and 15, respectively).*

***Key words:*** *Effective temperature, bioclimate, human health, ecology.*

## Introduction

Information on the bioclimatic characteristics of a territory is crucial not only for assessing their impact on human health but also for the development of the resort and tourism industry [1–7], among other applications. There is a wide range of simple and complex bioclimatic indices (combinations of temperature, relative humidity, wind speed, and other meteorological parameters) [1, 4–14]; one frequently used bioclimatic indicator is Missenard's effective air temperature (ET) [11–14].

For instance, one of our recent studies [13] presents data on the distribution of mean daily and maximum effective air temperature values (according to Missenard) in Batumi, broken down by month for the 2018–2023 period. In particular, regarding mean daily effective air temperature values falling into the "Comfortable" category, the highest number of days is observed from June to September (19, 11, 13, and 15, respectively). For maximum daily effective temperature values, this occurs in April, May, September, and October (10, 13, 10, and 15, respectively).

This study is a continuation of previous research [11–13]. Presented below are the results of an analysis of the monthly distribution of mean daily and maximum effective air temperature values (calculated according to Missenard) in Bolnisi for the period 2018–2023.

## Study area, material and methods

Study area – Bolnisi (Georgia).

The work uses data from the Georgian National Environment Agency on average daily and urgent (at 4 p.m. local time) values of temperature (T), relative humidity (RH) and wind speed (V) for the period from 2018 to 2023 [http://www.pogodaiklimat.ru/archive.php?id=ru&region=07].

The air effective temperature according to Missenard was calculated using the formula [14]:

$$ET = 37-(37-T)/(0.68-0.0014\cdot RH+1/(1.76+1.4\cdot V^{0.75})) -0.29\cdot T\cdot (1-0.01\cdot RH)$$

The categories of ET are presented in Table 1.

**Table 1.** The degree of human thermal sensation (category) depending on the values of air effective temperature.

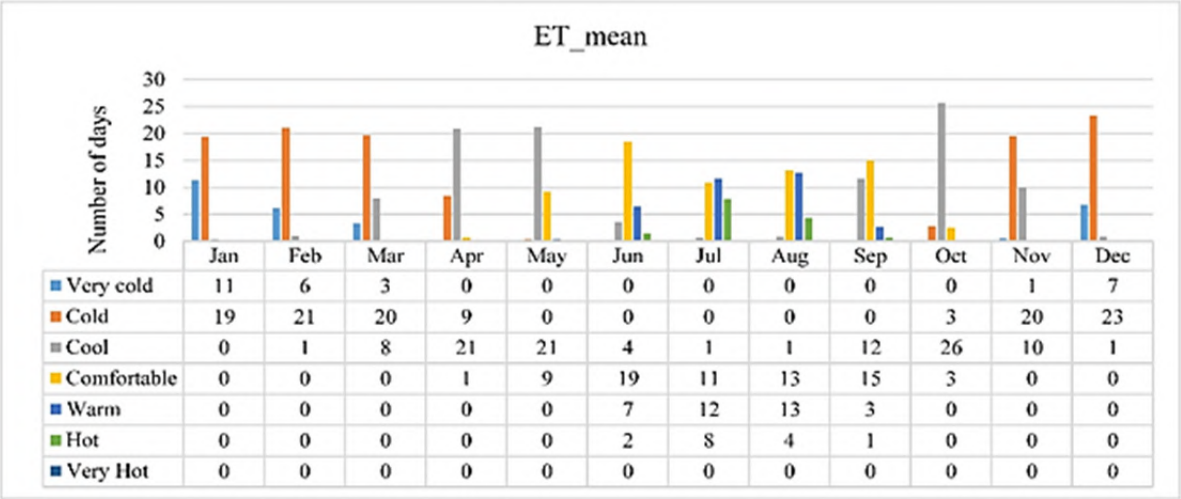
| ET | <1°C | 1-9° | 9-17° | 17-21° | 21-23° | 23-27° | >27° |
|---|---|---|---|---|---|---|---|
| ET Category | Very cold | Cold | Cool | Comfortable | Warm | Hot | Very hot |

In the proposed work the analysis of data is carried out with the use of the standard statistical analysis methods. The following designations will be used below: ET_mean – daily average air effective temperature; ET_max – daily maximum air effective temperature.

## Results and discussion

Results in Fig. 1 and 2 are presented.

In Fig. 1 data about mean number of days with different categories of ET_mean in Bolnisi from January to December are presented.



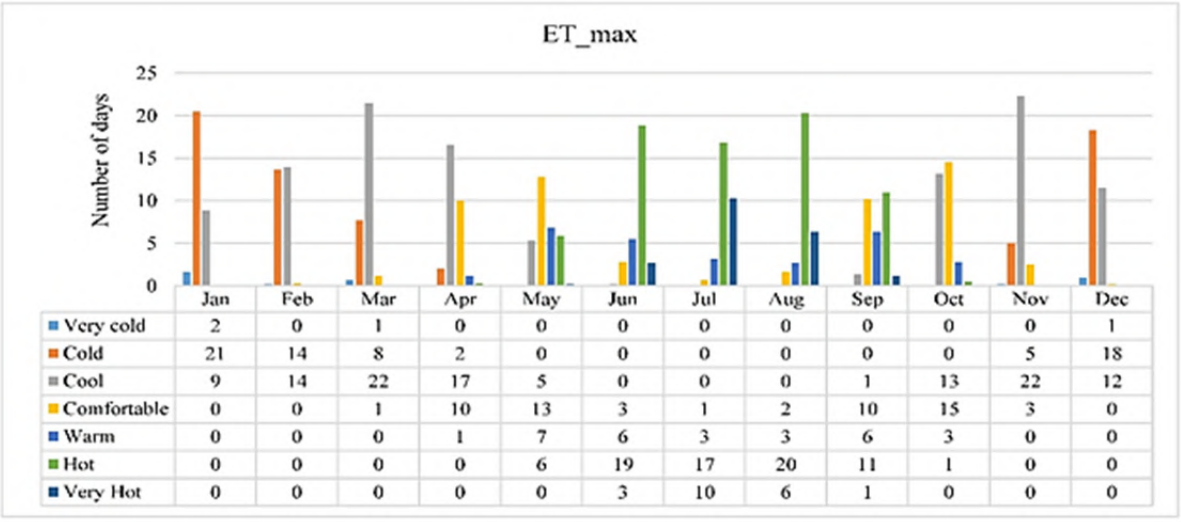

| | Jan | Feb | Mar | Apr | May | Jun | Jul | Aug | Sep | Oct | Nov | Dec |
|---|---|---|---|---|---|---|---|---|---|---|---|---|
| Very cold | 11 | 6 | 3 | 0 | 0 | 0 | 0 | 0 | 0 | 0 | 1 | 7 |
| Cold | 19 | 21 | 20 | 9 | 0 | 0 | 0 | 0 | 0 | 3 | 20 | 23 |
| Cool | 0 | 1 | 8 | 21 | 21 | 4 | 1 | 1 | 12 | 26 | 10 | 1 |
| Comfortable | 0 | 0 | 0 | 1 | 9 | 19 | 11 | 13 | 15 | 3 | 0 | 0 |
| Warm | 0 | 0 | 0 | 0 | 0 | 7 | 12 | 13 | 3 | 0 | 0 | 0 |
| Hot | 0 | 0 | 0 | 0 | 0 | 2 | 8 | 4 | 1 | 0 | 0 | 0 |
| Very Hot | 0 | 0 | 0 | 0 | 0 | 0 | 0 | 0 | 0 | 0 | 0 | 0 |

**Fig. 1.** Mean number of days with different categories of ET_mean in Bolnisi from January to December.

In particular, as follows from Fig. 1, on average during the year for mean daily values of effective air temperature with the “Comfortable” category, the greatest number of days are observed from June to September (19, 11, 13 and 15, respectively), etc.

In Fig. 2 data about mean number of days with different categories of ET_max in Bolnisi from January to December are presented.

In particular, as follows from Fig. 2, on average during the year for max daily values of effective air temperature with the “Comfortable” category, the greatest number of days are observed in April, May, September and October (10, 13, 10 and 15, respectively).




| | Jan | Feb | Mar | Apr | May | Jun | Jul | Aug | Sep | Oct | Nov | Dec |
|---|---|---|---|---|---|---|---|---|---|---|---|---|
| Very cold | 2 | 0 | 1 | 0 | 0 | 0 | 0 | 0 | 0 | 0 | 0 | 1 |
| Cold | 21 | 14 | 8 | 2 | 0 | 0 | 0 | 0 | 0 | 0 | 5 | 18 |
| Cool | 9 | 14 | 22 | 17 | 5 | 0 | 0 | 0 | 1 | 13 | 22 | 12 |
| Comfortable | 0 | 0 | 1 | 10 | 13 | 3 | 1 | 2 | 10 | 15 | 3 | 0 |
| Warm | 0 | 0 | 0 | 1 | 7 | 6 | 3 | 3 | 6 | 3 | 0 | 0 |
| Hot | 0 | 0 | 0 | 0 | 6 | 19 | 17 | 20 | 11 | 1 | 0 | 0 |
| Very Hot | 0 | 0 | 0 | 0 | 0 | 3 | 10 | 6 | 1 | 0 | 0 | 0 |

**Fig. 2.** Mean number of days with different categories of ET_max in Bolnisi from January to December.

The highest mean number of days of ET_max with the “Hot” category is observed in from June to Septmber (19, 17, 20 and 11 respectively), and with the “Very Hot” category – in July (10 days).

## Conclusion

The paper presents data on the number of days with daily mean and maximum values of air effective temperature according to Missenard in Bolnisi for each month of year, which, in addition to scientific interest, may also have practical significance for planning resort and tourist activities depending on the seasons of the year. In the future, we plan to continue similar studies for different regions of Georgia.

**Acknowledgement:** The authors are grateful to the chief of the atmospheric physics department of M. Nodia Institute of Geophysics A. Amiranashvili for assistance in the fulfillment of this work.

## References

1. Kartvelishvili L., Tatishvili M., Amiranashvili A., Megrelidze L., Kutaladze N., Weather, Climate and their Change Regularities for the Conditions of Georgia. // Monograph, Publishing House “UNIVERSAL”, Tbilisi 2023, 406 p., https://doi.org/10.52340/mng.9789941334658
2. Japaridze N., Khazaradze K., Studies in the Field of the Influence of Natural and Anthropogenic Environmental Factors on Human Health in Georgia: Current Status and Planned Works. // Int. Sc. Conf. “Natural Disasters in Georgia: Monitoring, Prevention, Mitigation”. Proc., ISBN 978-9941-13-899-7, Publish House of Iv. Javakhishvili Tbilisi State University, December 12-14, Tbilisi, 2019, pp. 201-204. http://109.205.44.60/bitstream/123456789/8671/1/47_Conf_NDG_2019.pdf
3. Japaridze N., Khazaradze K., Chkhitunidze M., Revishvili A., A Brief Overview of Research Conducted by M. Nodia Institute of Geophysics, TSU Together with Medical Organizations in the Field of “Health of the Population of Georgia and Environment” Over the Past 10 Years. // Int. Sc. Conf. "Geophysical Processes in the Earth and its Envelopes", Proceedings, Publish House of Iv. Javakhishvili Tbilisi State University, November 16-17, Tbilisi, 2023, pp. 337-343. http://dspace.gela.org.ge/handle/123456789/10469
4. Amiranashvili A., Bolashvili N., Kartvelishvili L., Liparteliani G., Tsirgvava G. Holiday Climate Index in Kvemo Kartli (Georgia). // Georgian Geographical Journal, E-ISSN: 2667-9701, 24(1), 2024, pp. 35-46. https://doi.org/10.52340/ggj.2024.04.01.05
5. Amiranashvili A., Kartvelishvili L., Matzarakis A., Variability of the Holiday Climate Index in Tsalka (Georgia). // Journal of the Georgian Geophysical Society, e-ISSN: 2667-9973, p-ISSN: 1512-1127, Physics of Solid Earth, Atmosphere, Ocean and Space Plasma, v. 27(1), 2024, pp. 77–90. https://ggs.openjournals.ge/index.php/GGS/article/view/7986
6. Aliyev V., Amiranashvili A., Bliadze T., Chikhladze V., Davitashvili M., Kartvelishvili L., Matzarakis A., Pipia M., Tatishvili M., Varamashvili N., Some Study Results of Various Meteorological Parameters Regime and Variability Based on 2005-2024 Year Data and Associated Environment Risk Factors for Baku (Azerbaijan) and Tbilisi (Georgia). // Materials of International Scientific Conference "Study and sustainable use of natural ecosystems in the conditions of modern climate change", Tbilisi, Georgia, December 11, 2025, Scientific Reviewed Proceedings of the Institute of Hydrometeorology of the GTU, ISSN 1512 – 0902, # 137, 2025, p. 35. Doi.org/10.36073/1512-0902-137, http://openlibrary.ge/bitstream/123456789/10799/1/Vol-137.pdf [37]
7. Amiranashvili A.G., Japaridze N.D., Khazaradze K.R., On the Connection of Monthly Mean of Some Simple Thermal Indices and Tourism Climate Index with the Mortality of the Population of Tbilisi City Apropos of Cardiovascular Diseases. Journal of the Georgian Geophysical Society, ISSN: 1512-1127, Physics of Solid Earth, Atmosphere, Ocean and Space Plasma, v. 21(1), Tbilisi, 2018, pp.48 -62. http://www.jl.tsu.ge/index.php/GGS/article/view/2489
8. Amiranashvili A.G., Revishvili A.A., Khazaradze K.R., Japaridze N.D., Connection of Holiday Climate Index with Public Health (on Example of Tbilisi and Kakheti Region, Georgia). Journal of the Georgian Geophysical Society, e-ISSN: 2667-9973, p-ISSN: 1512-1127, Physics of Solid Earth, Atmosphere, Ocean and Space Plasma, v. 24 (1), 2021, pp. 63-76. DOI: https://doi.org/10.48614/ggs2420212884
9. Amiranashvili A., Japaridze N., Kartvelishvili L., Khazaradze K., Revishvili A., Preliminary Results of a Study on the Impact of Some Simple Thermal Indices on the Spread of COVID-19 in Tbilisi. // Journal of the Georgian Geophysical Society, e-ISSN: 2667-9973, p-ISSN: 1512-1127, Physics of Solid Earth, Atmosphere, Ocean and Space Plasma, v. 25(2), 2022, pp. 59–68. DOI: https://doi.org/10.48614/ggs2520225961
10. Amiranashvili A., Bliadze T., Japaridze N., Khazaradze K., Revishvili A., Angstrom Fire Index as a Bioclimatic Indicator (Using the Example of the Impact on the Spread of Covid-19 in Tbilisi). // Int. Sc. Conf. "Geophysical

Processes in the Earth and its Envelopes", Proceedings, Publish House of Iv. Javakhishvili Tbilisi State University, November 16-17, Tbilisi, 2023, pp. 328-331. http://openlibrary.ge/handle/123456789/10467

11. Amiranashvili A., Japaridze N., Kartvelishvili L., Megrelidze L., Khazaradze K., Statistical characteristics of the monthly mean values of air effective temperature on Missenard in the Autonomous Republic of Adjara and Kakheti (Georgia). // Trans. of Mikheil Nodia institute of Geophysics, ISSN 1512-1135, vol. 69, Tb., 2018, pp. 118–138. (in Russian). http://dspace.gela.org.ge/bitstream/123456789/7509/1/IG_T_69_2018_Red_13.pdf
12. Japaridze N., Kartvelishvili L., Khazaradze K., Chkhitunidze M., Nikolaishvili M., Revishvili A., Statistical Characteristics of the Daily Values of Air Effective Temperature According to Missenard in Batumi. // Int. Sc. Conf. “Complex Geophysical Monitoring in Georgia: History, Modern Problems, Promoting Sustainable Development of the Country”, Proceedings, ISBN 978-9941-36-272-9, Publish House of Iv. Javakhishvili Tbilisi State University, Tbilisi, Georgia, October 17-19, 2024, pp. 133 – 136
http://dspace.gela.org.ge/bitstream/123456789/10624/1/34_MM-180.pdf
13. Japaridze N., Kartvelishvili L., Khazaradze K., Chkhitunidze M., Nikolaishvili M., Revishvili A., Distribution the Daily Number of Air Effective Temperature According to Missenard in Batumi by Month. // 1st International Scientific Conference “Modern problems in Geophysics”. Proceedings, ISBN 978-9941-36-434-1, ISSN 3088-4349, Tbilisi, Georgia, November 6-8, 2025. Publish House of Iv. Javakhishvili Tbilisi State University, Tbilisi, 2025, pp. 175-178. http://dspace.gela.org.ge/bitstream/123456789/10753/1/45_Conf_MPG_2025.pdf
14. Missenard F.A., Température effective d’une Atmosphere Généralisation Températurerés ultante d’un Milieu. // Encyclopédie in dustrielleet Commerciale, Etude physiologique et technique de la ventilation. Librerie de l’Enseignement Technique, Paris, 1933, 131-18.

2nd International Scientific Conference "Modern Problems in Geophysics", Proceedings,
ISBN 978-9941-36-562-1, ISSN 3088-4349, Tbilisi, Georgia, October 29-31, 2026

# ANTHROPOGENIC IMPACT ON ECOSYSTEM CONDITIONS: A LANDSCAPE-ECOLOGICAL APPROACH

**Burdzenidze M., Tchitchaghua E., Elizbarashvili N.**

*Ivane Javakhishvili Tbilisi State University, Tbilisi, Georgia*
*mishiko.burdzenidze033@ens.tsu.edu.ge*

***Abstract****. Modern human economic activity has become a major factor transforming the natural environment. Urbanization, infrastructure development, forest-cover reduction and intensive land use alter landscape structure and functional relationships within ecosystems. This paper examines anthropogenic impact through a landscape-ecological approach, focusing on cause-and-effect relationships and ecosystem resilience mechanisms.*

***Key words****: Anthropogenic impact, ecosystem, landscape structure, ecological sustainability.*

## Theoretical Basis and Methodology

The paper is based on a comparative analysis and synthesis of three major scientific sources [1-3]. Each source has a clearly defined functional role in the research (Table 1).

**Table 1.** Main scientific sources and their functional role in the study.

| Source | Main direction | Function in the study |
|---|---|---|
| N. Elizbarashvili – Fundamentals of Applied Geography (2016) | Landscape, structure, resilience, spatial planning | Spatial and landscape assessment of anthropogenic change |
| T. Urushadze, L. Machavariani – Fundamentals of Applied Ecology (2013) | Ecosystems, ecological processes, interaction of environmental components | Explanation of ecosystem consequences of anthropogenic impact |
| G. Kajaia – Ecology of Our Time (2022) | Contemporary ecological problems and human–environment interaction | Discussion of contemporary environmental problems in a broader context |

Methodologically, the research relies on literature review, cause-and-effect analysis and a landscape-ecological approach. The main logical chain is: anthropogenic pressure → change in a natural component → disruption of an ecological relationship → change in ecosystem function → deterioration of landscape condition.

## Anthropogenic Impact on Landscape Structure and Fragmentation

Landscape transformation is particularly evident when its spatial structure is disrupted. The construction of transport infrastructure, expansion of settlements and growth of agricultural areas divide naturally continuous territories into isolated fragments. According to N. Elizbarashvili's landscape-geographical concept, landscape components form an integrated dynamic system; therefore, a change introduced into one element inevitably affects the others (Table 2).

**Table 2.** Cause-and-effect transformation of anthropogenic changes.

| Initial condition | Anthropogenic intervention | Ecological consequence |
|---|---|---|
| Continuous natural territory | Road construction or development | Habitat fragmentation and isolation |
| Vegetated slope | Reduction of vegetation cover | Activation of erosional processes |
| Natural land surface | Asphalting and concreting | Sharp increase in surface runoff |
| Natural coastal zone | Infrastructure development | Disruption of connections between aquatic and terrestrial ecosystems |

## Soil Degradation as an Ecosystem Problem

Transformation of the soil cover is one of the most serious consequences of anthropogenic impact. Considering soil only in terms of agricultural productivity is insufficient, because soil is a basic component of ecosystem functioning.

On a slope covered by forest or natural vegetation, the root system stabilizes the soil, while vegetation reduces the direct mechanical impact of precipitation. Destruction of vegetation cover and improper land management disrupt these natural protective mechanisms. In accordance with the ecological approach of T. Urushadze and L. Machavariani, soil degradation is a chain process: reduction of vegetation cover → increased soil vulnerability → erosion → loss of fertile topsoil → reduced productivity → deterioration of ecosystem functioning.

## Urbanization and Transformation of the Natural Landscape (Case of Tbilisi)

In Georgia, urban centers, particularly the Tbilisi agglomeration, represent areas of especially intensive anthropogenic pressure. The expansion of urban development has substantially changed the natural landscapes of the Tbilisi Basin and the surrounding lower-mountain forest areas.

During urbanization, replacement of natural cover by asphalt and concrete sharply changes the hydrological regime of a territory. Water that would naturally infiltrate into the soil and replenish groundwater becomes rapid surface runoff in an urban environment. In addition, fragmentation of green spaces interrupts natural ecological corridors. Consequently, urban sustainability should be assessed not only by the volume of built infrastructure, but also by the extent to which the city preserves natural ecological functions.

## Transformation of Aquatic Ecosystems

The ecological condition of river systems is not determined solely by the chemical composition of water. According to G. Kajaia's ecological concept, a river and its floodplain form a single ecosystem in which the channel, riparian vegetation and sediment dynamics are closely interconnected.

Intensive urban or infrastructural development of riparian zones disrupts the natural buffer between terrestrial and aquatic ecosystems. Transformation of the coastal or riparian zone causes habitat loss, reduces the self-purification capacity of water and decreases biological diversity, further demonstrating the multi-component nature of anthropogenic impact.

## Ecosystem Resilience and Landscape-Ecological Modeling

Any anthropogenic intervention does not automatically mean irreversible ecosystem collapse. The decisive factors are the intensity and duration of the impact and the resilience of the landscape itself. According to N. Elizbarashvili, landscape resilience is the ability to maintain dynamic equilibrium and restore its structural and functional potential after external pressure (Table 3).

**Table 3.** Intensity of anthropogenic impact and expected ecological consequences.

| Nature of impact | Expected result and ecosystem response |
|---|---|
| Weak and short-term | Complete or partial self-restoration of the ecosystem |
| Moderate and repeated | Gradual weakening of ecological functions |
| Strong and long-term | Sharp decline in landscape resilience and resource potential |
| Cumulative (multi-component) | Disruption of ecosystem connections and irreversible degradation |

In practical environmental management, a landscape-ecological assessment model is used to prevent irreversible processes. It includes: (1) establishing the natural baseline and collecting baseline data; (2) determining anthropogenic load and identifying vulnerable components; (3) assessing direct and cumulative impacts; (4) spatial planning, zoning and defining preventive measures; and (5) monitoring and restoration of damaged ecosystems.

## Conclusion

Anthropogenic impact on ecosystem conditions is not a mechanical sum of isolated problems, but a complex, interconnected landscape-ecological process. A local change – such as clearing a small forest area, constructing a road or improperly cultivating soil – can, through a chain reaction, alter the hydrological, pedological and biological balance of an entire landscape.

Based on the theoretical concepts of N. Elizbarashvili, T. Urushadze, L. Machavariani and G. Kajaia, it is evident that ecosystem degradation often begins with the accumulation of small, initially inconspicuous spatial changes. Therefore, under Georgian conditions, the principal environmental-policy approach should not be a complete prohibition of economic activity, but landscape-based spatial planning that ensures the preservation of ecosystem functional integrity and self-restoration capacity.

## References

1. Elizbarashvili N., Fundamentals of Applied Geography. Tbilisi: Universal Publishing House, 2016.
2. Urushadze, T., & Machavariani, L., Fundamentals of Applied Ecology. Tbilisi: TSU Publishing House, 2013.
3. Kajaia G., Ecology of Our Time. Tbilisi, 2022.

2nd International Scientific Conference "Modern Problems in Geophysics", Proceedings,
ISBN 978-9941-36-562-1, ISSN 3088-4349, Tbilisi, Georgia, October 29-31, 2026

# ANALYSIS OF THE CONDITIONS OF NATURAL-TERRITORIAL COMPLEXES OF KEY SITES OF THE CARBON RANGE OF THE CHECHEN REPUBLIC "WAY CARBON"

**[**,***]Gairabekov U., [*,***]Gunya A., [***]Makhmudova L.**

*[*]Institute of Geografii RAN, Moscow, Russia*
*[**]Academy of Sciences of the Chechen Rupublic, Grozny, Chechen Rupublic, Russia*
*[***]Millionshchikov Grozny Stat Oil Technical University, Grozny, Chechen Rupublic, Russia*
*gairabekov_u@mail.ru*

***Abstract.*** *Research conducted at two key sites within the Carboniferous Polygon in the Chechen Republic revealed patterns in the spatiotemporal variability of $CO_2$ exchange parameters. Biomass reserves in the low-mountain ecosystems of Roshni-Chu are almost twice those in the lowland Chernorechye site. A strong correlation was found between the intensity of seasonal heat and moisture exchange and the conversion of phytomass to mortmass. The results provide a basis for developing regional greenhouse gas absorption strategies.*

***Key words:*** *Carbon polygon, WayCarbon, phytomass, mortmass, $CO_2$ emission.*

## Introduction

Global climate change necessitates the deployment of national and regional greenhouse gas (GHG) monitoring systems. To address these tasks, a network of specialized carbon polygons has been established across the Russian Federation. The Chechen Republic "WayCarbon" Carbon Polygon (operated jointly by the Millionshchikov Grozny State Oil Technical University – GSTOU and the Chechen State University named A.A. Kadyrov – ChSU) covers a unique transect of diverse landscape zones of the North Caucasus, stretching from lowland steppes to high-altitude mountain massifs [1, 5].

An analysis of the state of natural-territorial complexes (NTCs) in key areas of the Chechen Republic's carbon research area is based on a landscape-geophysical approach. Its primary objective is to study the relationship between the seasonal dynamics of NTCs, heat and moisture exchange processes, and the balance of greenhouse gases (carbon emissions and sequestration) [1, 2].

The study covers representative ecosystems of the region, located in different altitudinal and soil-climatic zones.

Studying the "mountain-plain" landscape ecotone is critical for understanding the migration mechanisms of chemical elements and carbon dynamics under shifting hydrothermal regimes and varying anthropogenic pressures [1, 2, 5]. The objective of this study is to provide a comparative analysis of the seasonal states of natural complexes and the structure of organic matter pools at the "Chernorechye" and "Roshni-Chu" key monitoring sites.

## Methods and Materials

Field operations and measurements were conducted at two baseline sites within the GGNTU WayCarbon Carbon Polygon:

1. **The "Chernorechye" key site** is located within the Chechen Plain (169 m above sea level). The local natural complex consists of water-protective broad-leaved forests dominated by English oak (*Quercus robur*) and European ash (*Fraxinus excelsior*). This site is subject to moderate anthropogenic pressure and influence from major transportation corridors.
2. **The "Roshni-Chu" key site** is situated in the low-mountain broad-leaved forest zone on the northern macro-slope of the Lesisty Ridge (450 m above sea level). The landscape features a more complex mesorelief and a predominance of European beech (*Fagus sylvatica*) and oak-beech stands.

**The methodological framework included:**

- **Landscape-geophysical descriptions** of vertical structures, geohorizons, and biomasses within permanent sample plots (PSPs).
- **Microclimatic monitoring** using automated logger-sensors that record air and soil temperature and moisture at 30-minute intervals.
- **Carbon pool estimation** based on tree-by-tree inventory of phytomass, as well as sampling of ground cover, litter (mortmass), and soil monoliths.
- **$CO_2$ exchange and soil respiration measurements** conducted via mobile infrared gas analyzers (e.g., Li-Cor / G4301) alongside field photosynthesis measurement systems.

## Results

### Analysis of Phytomass and Mortmass Pools

Field surveys conducted across the main vegetative seasons identified significant quantitative discrepancies in the structure of organic matter (Table 1).

**Table 1.** Comparative characteristics of organic matter stocks at the key monitoring sites

| **Parameter / Component** | **"Chernorechye" Site (Plain)** | **"Roshni-Chu" Site (Low-mountain)** |
|---|---|---|
| Altitude above sea level, m | 169 | 450 |
| Prevalent forest type | Broad-leaved (oak-ash) | Broad-leaved (oak-beech) |
| **Aboveground phytomass stocks, t/ha** | **140–165** | **270–310** |
| Mortmass stocks (litter, detritus), t/ha | 12–15 | 22–26 |
| Mean soil temperature (July), °C | 22.4 | 18.6 |

The total volume of aboveground phytomass in the low-mountain ecosystems of Roshni-Chu **is nearly twice as high** as that of the lowland Chernorechye site. This is primarily attributed to higher stand density, greater climatic stability of the low-mountain zone, and lower historical deforestation and anthropogenic disturbance in the area.

## Microclimatic Regimes and Carbon Dynamics

The seasonal succession of landscape states directly governs the intensity of regional heat-moisture exchange:

- **In Chernorechye**, the summer temperature maximum in the surface layer is reached approximately 10–14 days earlier. While this accelerates early-spring vegetation growth, moisture deficiency frequently acts as a limiting factor in mid-summer, reducing the photosynthetic intensity of the dominant tree species.
- **In Roshni-Chu**, warm-up is delayed due to the complex terrain, but the summer season (June–July) exhibits high stability and an optimal balance of heat and moisture. This configuration ensures a prolonged period of active carbon assimilation.

The decomposition rate of mortmass and its subsequent transition into either the soil pool or the gas phase ($CO_2$) are closely coupled with regional hydrothermal coefficients. In Roshni-Chu, higher humidity allows decomposition to proceed at a stable rate throughout the entire warm period.

## Discussion

The gathered data support the hypothesis that forest ecosystems within this specific landscape ecotone are highly sensitive to hydrothermal shifts. The significantly larger carbon stocks stored in the phytomass pool of the “Roshni-Chu” site position it as a vital regional carbon sink.

Conversely, the “Chernorechye” lowland site, which is exposed to traffic-induced emissions from the nearby R-217 “Kavkaz” federal highway, shows noticeable volatility in its photosynthetic parameters. An-

thropogenic stress, combined with elevated lowland temperatures, can skew the local balance toward higher greenhouse gas emissions due to accelerated soil respiration during hot, dry micro-periods [1-5].

The distinct differences in phytomass-to-mortmass conversion dynamics between the two sites underline the importance of using differentiated coefficients when performing mathematical modeling of regional carbon balances.

## Conclusion

1. A synchronized, robust ground-based monitoring system for carbon balance accounting has been successfully operationalized across the key sites of the GGNTU “WayCarbon” Polygon.
2. A two-fold superiority in aboveground phytomass accumulation was confirmed in the low-mountain landscape (“Roshni-Chu”) compared to the lowland zone (“Chernorechye”).
3. Variations in microclimatic regimes (earlier thermal peaks in Chernorechye vs. sustained humid summer conditions in Roshni-Chu) directly dictate the localized characteristics of carbon sequestration and $CO_2$ emission dynamics.

**Acknowledgements:** This work was carried out within the framework of the state assignment of the Millionshchikov Grozny State Oil Technical University (Project No. FZNU-2024-0004: “Comprehensive Study of Greenhouse Gas Fluxes in Natural and Anthropogenically Disturbed Landscapes of the Chechen Republic...”).

## References

1. Gunya A.N., Gairabekov U.T., Makhmudova L.Sh., Gagaeva Z.Sh., Seasonal states and dynamics of carbon at key sites of the Carbon Polygon in the Chechen Republic. South of Russia. // Ecology, Development., 19 (3), 2024, pp. 169-179. https://doi.org/10.18470/1992-1098-2024-3-17.
2. Gunya A.N., Gairabekov U.T., Makhmudova L.Sh., Gagaeva Z.Sh. Dynamics of the ratio of phytomass and mortmass fractions in key areas of the carbon polygon in the Chechen Republic. // Geology and Geophysics of the South of Russia, Vol. 13. No. 4, 2023, pp. 135-148.Official Website of the Carbon Polygons of the Russian Federation.
3. Pridacha V.B., Makhmudova L.Sh., Aristarkhova EA, Shamkhanov M.Ch.,Variability of photosynthesis parameters of some woody plants in key areas of the carbon polygon of the Chechen Republic. // Grozny Natural Science Bulletin. 24, Vol. 9., No. 3 (37), 2024, pp. 88-95. DOI: 10.25744/genb.2024.37.3.011.
4. Gunya A.N., Gairabekov U.T., Makhmudova L.Sh., Features of the biogeocycle and carbon dynamics in the "mountains – plains" landscape ecotone (on the example of the Carbon Polygon of the Chechen Republic). // South of Russia: Ecology and Development, Vol. 20, No. 2 (75), 2025, pp. 153-164. DOI: 10.18470/1992-1098-2025-2-12.
5. Official website of the Carbon Polygons of the Russian Federation. URL: https://carbon-polygons.ru. (Accessed: 15.09. 2026).

2nd International Scientific Conference "Modern Problems in Geophysics", Proceedings,
ISBN 978-9941-36-562-1, ISSN 3088-4349, Tbilisi, Georgia, October 29-31, 2026

# DYNAMICS OF OAK AND BEECH FOREST DEGRADATION ON THE SOUTHERN SLOPES OF THE GREATER CAUCASUS UNDER THE INFLUENCE OF CLIMATIC FACTORS: A CASE STUDY OF THE ISMAYILLI DISTRICT

**Ismayilova N.**

*Baku State University, Baku, Azerbaijan*
*naza.ismailova.7@mail.ru*

***Abstract.*** *This article presents a comprehensive study on the spatiotemporal dynamics of forest ecosystem degradation on the southern slopes of the Greater Caucasus, focusing on the Ismayilli district of Azerbaijan as the primary study area. Over the past three decades (1996-2026), these vital mountain forests, dominated by Oriental beech (Fagus orientalis) and Caucasian oak (Quercus macranthera), have experienced severe environmental pressure driven by rapid regional climate change. Meteorological data reveal a distinct aridization trend, characterized by a 1.4°C increase in average summer temperatures and an 18% reduction in precipitation. To analyze these landscape alterations, multitemporal Landsat and Sentinel-2 satellite imagery was integrated with extensive ground-truth verification conducted during field expeditions in 2025. The empirical results indicate a critical 31% reduction in the area of healthy oak stands within the lower mountain belt (800-1200 m) due to water stress and secondary pest infestations. Concurrently, high-altitude beech forests (1200-1600 m) suffer from soil desiccation, leading to premature defoliation. Predictive ecological models for the 2026-2035 period demonstrate that without immediate silvicultural adaptation measures – such as digital forest health monitoring and the introduction of drought-resistant ecotypes – these ecosystems face an irreversible transition into low-productivity shrublands, thereby threatening regional biodiversity and watershed security.*

***Key words****: Greater Caucasus, Ismayilli district, forest degradation, climate change, aridity.*

## Introduction

Mountain forest ecosystems on the southern slopes of the Greater Caucasus within Azerbaijan, specifically in the Ismayilli district, perform critical biospheric, watershed protection, anti-erosion, and climate-regulating functions [6]. These forests are primarily composed of valuable, principal canopy-forming species: Oriental beech (*Fagus orientalis*) and Caucasian/sessile oak (*Quercus macranthera*, *Quercus petraea*) [1]. Over the past three decades, these ecosystems have been subjected to the combined pressure of global climate change and localized anthropogenic stress [7].

Global warming in the Caucasus manifests as a steady increase in mean annual temperatures and a significant shift in precipitation regimes, characterized by a higher frequency of extreme summer droughts, shifts in growing seasons, and declining groundwater levels [10]. Under conditions of escalating climate aridity, beech and oak stands begin to experience profound water stress [8]. This induces physiological weakening of the tree stands, a loss of natural resilience to pathogens, and, consequently, their widespread dieback [5].

The objective of this study is to comprehensively assess the spatiotemporal dynamics of oak and beech forest degradation in the Ismayilli district over the 1996-2026 period using Earth observation remote sensing data and field expedition materials, as well as to forecast changes in these communities up to 2035.

## Methodology

The methodological approach relies on a combination of satellite-based monitoring methods (GIS technologies) and ground-based forest pathological surveys [1]. Multi-temporal satellite imagery from Landsat 5, Landsat 8, and Landsat 9/Sentinel-2 acquired during the peak of the growing season (July-August) served as the primary data source [9]. Cartographic analysis was employed to assess changes in continuous forest cover areas and to identify canopy thinning zones.

To verify the satellite data, targeted field expeditions were conducted in May and July 2025 across the forested areas of the Ismayilli district at various altitudinal zones (800-1200 m and 1200-1600 m above sea level). At key sample plots, a visual assessment of tree sanitary conditions was performed; the degree of branch dieback, top-kill, and the percentage of dead and dying trees relative to the total stand density were recorded [6].

## Results and Discussion

A retrospective analysis of long-term meteorological data for the Ismayilli district over a thirty-year period (1996-2026) reveals a steady and pronounced trend toward the general aridization of the regional climate [10]. According to the recorded data, the mean air temperature during the summer months (June-August) increased by 1.4°C. This temperature spike was accompanied by a critical reduction in summer atmospheric precipitation, averaging 18%. Such a hydrothermal imbalance leads to a sharp increase in potential evapotranspiration and a decrease in relative humidity, triggering prolonged atmospheric and soil droughts during critical vegetative phases of the forest stands (Table 1).

Cartographic analysis and the comparison of multi-temporal, high-resolution Landsat and Sentinel-2 satellite imagery confirmed a direct spatial correlation between climate shifts and the degradation of forest cover. Satellite monitoring captured a profound negative dynamic in the structure of the forest fund: once continuous, high-density, and healthy tracts are undergoing intense fragmentation. Areas of continuous, closed-canopy forests are steadily declining, breaking down into isolated patches, thinning out, and giving way to so-called "dieback gaps" and weakened vegetative assemblages [9].

**Table 1.** State dynamics of beech-oak forests in the Ismayilli district across altitudinal belts (1996-2026)

| Altitudinal belt / Dominant species | Study period | Total area of healthy forest cover (ha) | Stand sanitary condition | Key indicators of degradation |
|---|---|---|---|---|
| 800-1200 m Caucasian oak with hornbeam | 1996 | 4200 | Stable | Widespread top-kill, canopy thinning, emergence of local and continuous outbreaks of stem pests |
| | 2011 | 3850 | Weakened | |
| | 2026 | 2900 | Critical | |
| 1200-1600 m Oriental beech | 1996 | 6100 | Optimal | Premature yellowing and deformation of foliage, dieback of individual first-order skeletal branches |
| | 2011 | 5800 | Early stress | |
| | 2026 | 4950 | Severe weakening | |

The statistical and cartographic data presented in Table 1 clearly demonstrate that the oak forests of the lower and partially middle mountain belts, within the altitudinal range of 800 to 1200 meters, serve as the epicenter of degradation processes. Over the investigated thirty-year period, the area of healthy Caucasian oak stands decreased by a record 31%, representing an absolute loss of 1300 hectares.

Field expedition data collected in May and July 2025 fully verified and contextualized these alarming satellite signals. Ground-truth surveys conducted on the sample plots revealed that chronic soil moisture deficits undermine osmotic pressure and the upward transport of nutrients within oak trunks, triggering widespread top-kill.

Physiologically weakened trees lose their ability to secrete protective resins and tannins, transforming into an ideal food source for xylophagous insects. The 2025 field surveys documented the formation of extensive infestation centers by secondary stem pests, dominated by the oak bark beetle and various longhorn beetle species [5]. These insects rapidly attack the weakened stands, accelerating the process of their complete mortality.

In the higher altitudinal belt (1200-1600 m), dominated by Oriental beech, the degradation of forest communities proceeds in a more latent and protracted manner [3]. The relatively cool macroclimate of the high-altitude zones and frequent fogs partially dampen thermal stress. Nevertheless, a distinct destructive trend is observable here as well: over the 30-year period, the area of healthy beech stands decreased by nearly 19%.

The primary driver behind the degradation of beech phytocoenoses is the desiccation of the upper, most fertile horizons of brown forest soils [2]. Possessing a shallow and highly sensitive root system, Oriental beech responds instantaneously to a decline in groundwater levels. Under hydrothermal stress, the root nutrition of tree species is disrupted, triggering a protective self-regulatory mechanism – the reduction of the tran-

spiring surface area. This manifests as a pronounced deformation of leaf blades and their premature yellowing, followed by widespread defoliation as early as the first ten days of August, which severely disrupts the natural annual life cycle and reduces overall biomass increment [8].

The ecological forecasting models developed by the authors for the period up to 2035 (predicated on the scenario of sustained current rates of climate aridization) indicate severe risks of crossing a tipping point. By 2030, the degradation of oak forests at elevations below 1000 meters above sea level is projected to enter an irreversible phase [4]. The physiological depletion of parent stands will lead to a complete cessation of natural oak regeneration processes. Consequently, an irreversible ecosystem shift will commence: the gradual displacement of high-forest mesophilic oakwoods and their replacement by low-productivity xerophytic shrubby woodlands and steppe herbaceous communities, ultimately leading to the collapse of the historical landscape framework of the southern slope of the Greater Caucasus [7].

## Conclusion

The comprehensive study conducted convincingly demonstrates that the progressive climate factor - manifested in the long-term aridization of the region and rising thermal stress – acts as a key trigger and destructive catalyst for the large-scale weakening and subsequent degradation of valuable beech and oak forests on the southern slope of the Greater Caucasus (exemplified by the Ismayilli district) [1]. The identified steady trend toward forest fragmentation, the critical decline in the vital potential of edificator species in the lower and middle mountain zones, and the escalating phytopathological risks indicate that the natural homeostatic mechanisms of these ecosystems are on the verge of exhaustion. The revealed critical state of the stands demands an immediate conceptual revision of existing approaches to environmental management and the urgent implementation of a comprehensive set of preventive, protective, and adaptive forestry measures. Preserving the ecological stability, hydrological function, and biodiversity of the mountain forests of the Greater Caucasus requires the immediate execution of the following strategic steps:

1) Organization and implementation of multi-level digital monitoring: Traditional methods of visual forest health surveillance must be superseded by an operational tracking system based on the integration of high-resolution satellite imagery (Landsat 9, Sentinel-2) and regular remote sensing utilizing unmanned aerial vehicles (UAVs/drones). The deployment of UAVs will enable the automated detection of early, latent phases of degradation (such as canopy thinning and localized shifts in the spectral reflectance of foliage) at incipient stages, thereby facilitating a rapid response to the emergence of new "dieback gaps".

2) Optimization of phytosanitary measures and localization of biological threats: Under prolonged water stress, trees suffer an immune compromise, which triggers an avalanche-like proliferation of secondary xylophagous insects [5]. It is essential to establish a system for targeted biological control and the timely execution of strictly regulated sanitary logging and thinning within localized infestation centers of forest pests (such as the oak bark beetle and longhorn beetles) prior to their transition into a mass outbreak phase capable of destroying entire forestry districts.

3) Modernization of reforestation strategies in response to climate trends: The historically established practice of forest regeneration without accounting for ongoing climate shifts is no longer effective. Future artificial and combined reforestation efforts must be predicated on the selection and active deployment of the most drought-resistant ecotypes and climatic races of native species (including Caucasian oak and Oriental beech) that possess enhanced resistance to soil moisture deficits [4]. Creating such genetically adapted stands will facilitate the formation of a resilient forest framework capable of functioning successfully under the projected arid conditions of 2035, thereby minimizing the risks of irreversible ecosystem displacement.

## References:


1. Aliev A.I., Integrated monitoring of Caucasian mountain forests. // Caspian Journal of Environmental Science. Baku, No. 4, 2022, pp. 45-58.
2. Alieva F.F. Humus dynamics and ecological state of brown forest soils. // Soil Science and Agrochemistry. Baku, No. 2, 2023, pp. 89-97.
3. Gasanov S.A. Spatial structure of beech forests of Azerbaijan. // Journal of Geographical Ecology. Baku, Vol. 15, No. 1, 2019, pp. 54-62.

4. IPCC. Climate Change 2021: The Physical Science Basis. Cambridge University Press, 2021, 230 p.
5. Ismayilova N.A., Omarova U.G. Erosion processes in the forest soils of the Ismayilli region. // World Soil Day: The Soil Factor in Sustainable Agriculture, Proceedings of the Republican Scientific-Practical Conference, Ganja, 2023, pp. 247-250.
6. Mamedov R.M., Abbasova S.N. // Botanicheskiy vestnik. Baku, Vol. 36, No. 2, 2020, pp. 102-111.
7. Millennium Ecosystem Assessment. Ecosystems and Human Well-being: Forest and Land Synthesis. World Resources Institute, Washington, 2005, 134 p.
8. Smith J., Keller B., Climate-driven changes in forest ecosystems. // Global Change Biology. 2018, Vol. 24, pp. 1375-1387.
9. UNEP. Vulnerability of Mountain Ecosystems to Climate Change. United Nations Environment Programme, 2022, 114 p.
10. WMO. State of the Global Climate 2023. World Meteorological Organization, Geneva, 2024, 88 p.

2nd International Scientific Conference "Modern Problems in Geophysics", Proceedings,
ISBN 978-9941-36-562-1, ISSN 3088-4349, Tbilisi, Georgia, October 29-31, 2026

# INNOVATIVE MONITORING SYSTEM FOR THE BLACK SEA COASTAL ZONE

**Kordzakhia M., Matchavariani V., Vekua Z., Arghvliani I., Samadashvili N., Kutchava G., Bejanidze V., Pataraia G., Ketchakmadze Z., Sidamonidze E.**

*National Environmental Agency of the Ministry of Environmental Protection and Agriculture of Georgia, Tbilisi, Georgia*
*marina.kordzakhia@nea.gov.ge*

***Abstract.*** *The Black Sea is a highly sensitive, semi-enclosed marine ecosystem exposed to significant anthropogenic pressures, including pollution, climate change, and coastal development. The Black Sea Smart Marine Environmental Outcome System (BS-SEOS) [1], supported by the INTERREG NEXT Black Sea Basin Programme, an innovative framework designed to improve monitoring and management of one of the world's most sensitive marine ecosystems. The system consists of two modular catamaran-hull unmanned surface vehicle (USV) platform (max. length 125sm, width 100cm, weight up to 50kg fully equipped), propelled by two steerable electric thrusters and capable of operating autonomously for 3 to 8 hours at working speed 1-3 knots with a telemetry control range of approximately 1 km. The surface vehicles are equipped with multisensory instruments/sensors, including: Multi-GNSS receiver (GPS, GLONASS, BeiDou and Galileo) with SBAS receiver (EGNOS), with maximum positioning accuracy of 1 m; the following information is provided: date, hour, minute, second, latitude and longitude; Ultrasonic probe, with a minimum measurable depth (below the transducer) of 0.5 m and a maximum measurable depth (below the transducer) of 100 m; water depth is indicated at the measurement coordinates; Barometric pressure; Air and water temperature; pH, dissolved oxygen, and chlorophyll-a. These observations are processed through a structured data pipeline and analyzed using advanced AI models. The autonomous, multi-sensor USV fleets constitute a scalable and cost-effective IoT solution for high-frequency coastal observation, substantially increasing the capacity to capture short-term variability in coastal hydrodynamics and water quality – delivering spatially resolved environmental intelligence that fixed monitoring networks alone cannot provide. By enabling continuous, transnational data sharing and early warning capabilities, BS-SEOS supports informed decision-making and proactive environmental management. The project enhances regional cooperation, strengthens ecosystem resilience, and contributes to sustainable development and long- term protection of the Black Sea.*

***Key Words:*** *Black Sea, Climate Change, Innovative Monitoring, AI forecasting, uncrewed surface vehicles – drones.*

## Introduction

The Black Sea is one of the most unique and sensitive marine ecosystems in the world. Almost entirely enclosed, shared by six countries, and strongly influenced by human activity, it reacts faster to environmental pressure than open oceans. Key activities and pressures along the Georgian Black Sea coastal zone include shipping and port operations, Oil and fuel transportation and storage, fisheries and aquaculture, tourism and recreation, industrial and urban development, coastal construction, agricultural and riverine inputs. Monitoring such area requires flexible platforms capable of providing high-resolution spatial data and repeated measurements under variable field conditions. The innovative unmanned surface vehicles have become increasingly important for aquatic monitoring because they enable efficient, repeatable, and relatively low-cost observations for water quality assessment and coastal surveillance. Their modular structure also allows the integration of multiple sensors, telemetry systems, and autonomous navigation functions.

Recent large-scale engineering works along the Georgian coast necessitate high-frequency spatial observations that traditional methods cannot provide. These dynamics call for high-frequency, spatially distributed observations that go beyond what fixed stations or occasional vessels surveys can deliver. Within this context the BS-SEOS project, initiated under financial support of INTERREG NEXT Black Sea, will provide the institutional and technical framework for National Environmental Agency (NEA) of the Ministry of Environmental Protection and Agriculture of Georgia, targeting the monitoring of coastal sectors of Sarpi and Poti. BS-SEOS project designed to enhance the health and sustainability of the Black Sea. The Innovative

Environmental Monitoring System, by leveraging cutting-edge AI forecasting and unmanned surface vehicles – drones, will collect, analyze, and share critical environmental data across borders, ensuring a resilient and thriving marine ecosystem.

## Materials and Methods

BS-SEOS is a collaborative project aimed at enhancing the understanding of the Black Sea's ecosystem by collecting and sharing environmental data. Using innovative technologies like unmanned surface vehicles – drones (Fig. 1. USV-drone's System), the project facilitates continuous monitoring of key marine pa-rameters such as:

- Barometric pressure sensor: measured value;
- Air temperature: (at a maximum distance of 0.5 m above the water surface, using a sun-shielded sensor): measurement range from -10°C to +40°C, maximum accuracy ±0.1°C;
- Water temperature: measurement range from 5°C to +40°C, maximum accuracy ±0.5°C;
- Total pressure: measurement range 0–1 bar, maximum accuracy ±0.5%;
- Conductivity: measurement range 0–200 mS/cm, maximum accuracy ±1%;
- Dissolved oxygen (optical): measurement range 0–40.00 mg/L, maximum accuracy ±1%;
- pH (solid-state, calibration-free): measurement range 2–14 pH, maximum accuracy ±0.2 pH;
- Chlorophyll-a (optical, automatic autoscaling): measurement range 0–500 µg/L, maximum repeatability ±5%.

Calculated Parameters: Salinity, Water Resistivity, Water Density.
Data transmission: Data shall be transmitted to the ground station in near-real time over a distance of km.
Data Acquisition:

- Multi-GNSS receiver for precise positioning;
- Sampling rate: At least one measurement every 30 seconds.

The drone-mobile stations will be used along the coast and will monitor selected physical andchemical parameters via multi sensors from three vertical depths including surface, 5m, and 10m, for water quality assessment in bathing areas. It will provide immediate data acquisition in case of risk events (accidental pollution, algal blooms, etc.) regarding physical and chemical parameters.

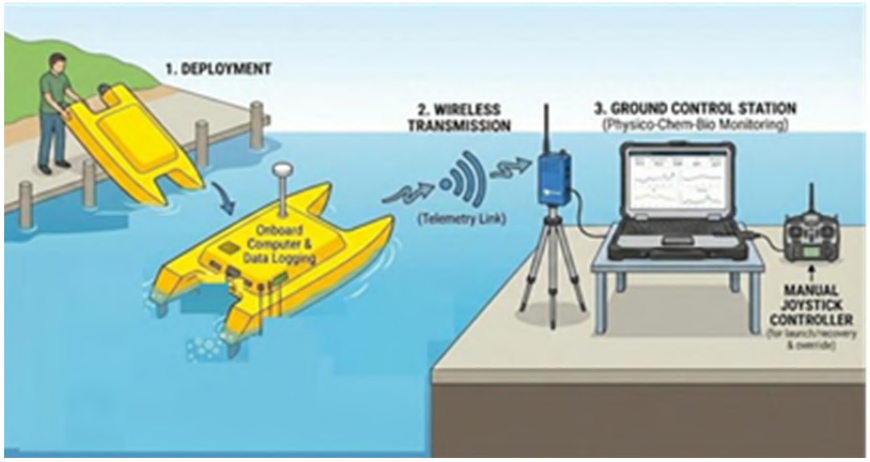



**Fig. 1.** USV-Drone's System.

In Georgia drone-mobile stations will be used along the coast in *Sarpi* and *Poti* areas is based on their strategic significance, water quality, transboundary impacts, and the need for robust water quality data to support environmental management and will monitor selected physical and chemical parameters.

- Sarpi: Located at the Georgia-Turkey border, Sarpi experiences heavy cross-border traffic, including trucks, passenger vehicles, and maritime activities;
- Poti: As a major port city, Poti has intense shipping activities, industrial operations, and energy production;

The use of a multifunctional drone to measure water and air parameters represents an innovative and efficient approach to environmental monitoring in the Black Sea. By enabling the collection of multiple envi-

ronmental parameters in a single monitoring mission, the system supports more comprehensive and efficient assessment of marine and coastal environmental conditions.

pH – Water pH directly reflects changes in marine acidity, which are linked both to increasing $CO_2$ levels (ocean acidification) and to industrial and domestic discharges;

Chlorophyll a – Chlorophyll is the main indicator of phytoplankton biomass. Its monitoring is essential for: detecting eutrophication processes; early prediction of algal blooms; and assessing marine productivity;

DO – (Dissolved Oxygen) – The level of dissolved oxygen determines the biological viability of marine ecosystems. Its depletion leads to the formation of "dead zones," posing a threat to fish and other organisms. A drone enables rapid detection of hypoxic zones and real-time monitoring of their dynamics;

Water Temperature – Water temperature affects chemical reactions, oxygen solubility, and biological processes. Detailed mapping of sea surface temperature using drones is particularly important for: monitoring climate change; identifying thermal stress zones; and predicting biological processes;

Simultaneous Measurement of Air and Water Temperature – Measuring both simultaneously allows for a better understanding of energy and heat exchange processes at the sea surface. These data are important for both meteorological and ecological modeling.

Conductivity – Combined with temperature, conductivity measurements can be used to determine seawater salinity and improve the interpretation of physical and ecological processes. Monitoring conductivity is important for: identifying changes in salinity; detecting freshwater inputs from rivers and coastal runoff; characterizing water masses and mixing processes; and supporting the assessment of changes in marine water quality.

Total Pressure – Water pressure increases with depth and provides important information about the vertical position and operating depth of the monitoring platform. When combined with other environmental parameters, pressure data can help characterize the vertical structure of the water column and support three-dimensional environmental monitoring.

## Results

BS-SEOS data flow for Mobile Multisensory Stations-drones: All sensor data will be transmitted to the ground stations, from the ground station to partner's local premises for data formatting/standardization and data quality control. Standardized and Quality Controlled datasets will be transmitted, in delayed mode, to the Joint BS-SEOS Data Center developed by Istanbul University) to be integrated into the BS-SEOS database and further on the BS-SEOS Dashboard and AI models. Standardized and Quality Controlled datasets will be submitted, by each partner, (via EMODnet Data Ingestion) to the SeaDataNet/EMODnet [2] thematic as it is illustrated in Fig. 2 below.

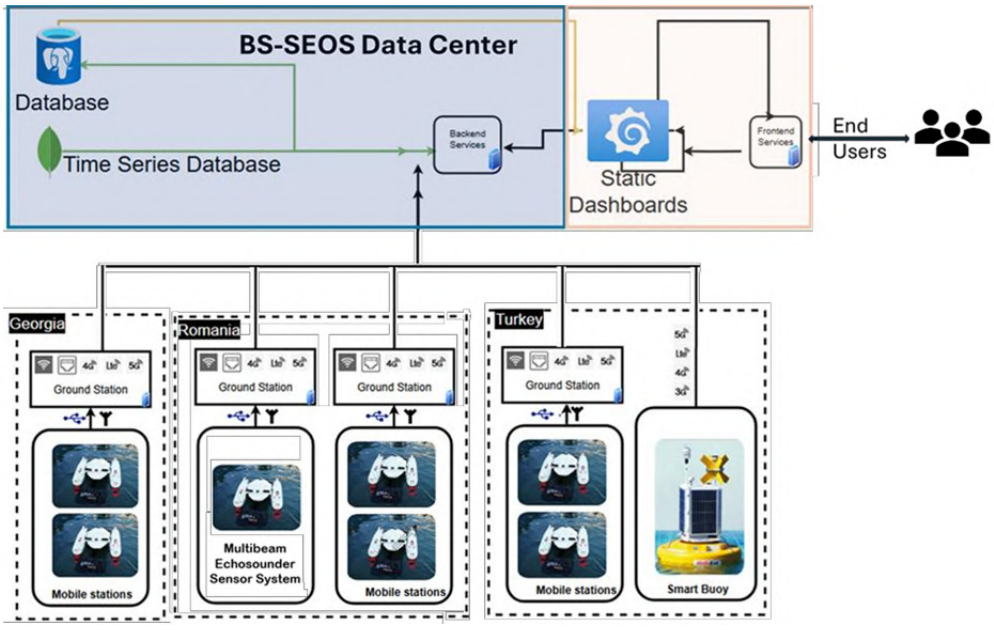



**Fig. 2.** Drone-Mobile Stations Data Flow.

The other results represent the general outcomes of Project:

- Development of a centralized platform for sharing regional environmental data;
- Enhanced collaboration among scientists, policymakers, and industries;
- Improved monitoring and assessment of marine ecosystem health;
- Informed decision-making for conservation and sustainable practices;
- Increased public awareness about the importance of marine ecosystem health;
- strengthened resilience to environmental challenges in the Black Sea region.

## Conclusion

The Black Sea stands at a critical intersection of environmental vulnerability and technological opportunity. As a semi-enclosed and highly sensitive marine basin, its health depends on the ability of surrounding nations to monitor changes continuously, respond rapidly, and cooperate effectively. The BS- SEOS project demonstrates how innovation can transform traditional environmental monitoring into a dynamic, real-time, and data-driven system. By integrating uncrewed surface vehicles, advanced multisensory measurements, and AI-based forecasting models, the project provides a comprehensive framework for understanding complex marine processes and anticipating ecological risks.

Through its structured data pipeline and cross-border collaboration, BS-SEOS not only enhances the accuracy and availability of environmental data but also supports timely decision-making and proactive management. The system's ability to detect early warning signals – such as hypoxia events, algal blooms, or temperature anomalies – represents a significant step toward preventing large-scale ecological damage.

Ultimately, the success of BS-SEOS lies in its holistic approach: combining science, technology, and regional cooperation to safeguard the Black Sea ecosystem. By strengthening resilience, promoting sustainability, and increasing public and institutional awareness, the project contributes to a more stable and thriving marine environment. Continued development and expansion of such integrated monitoring systems will be essential for ensuring the long-term health of the Black Sea in the face of growing environmental and climatic pressures.

AI-driven risk prediction in BS-SEOS directly serves the EU Marine Strategy Framework Directive (MSFD), which requires Member States to achieve and maintain Good Environmental Status (GES) in their marine waters. Early prediction of hypoxic events, harmful algal blooms, and upwelling anomalies enables pre-emptive management actions – adjusting fishing effort, issuing aquaculture alerts, triggering emergency monitoring protocols – that reactive monitoring systems cannot support. More broadly, the BS-SEOS AI framework contributes to the European Green Deal and the EU Biodiversity Strategy for 2030 by building the evidence base for ecosystem-based management of the Black Sea. The sea's ecological condition cannot be separated from the political and economic futures of the communities along its shores – and AI-powered environmental intelligence is becoming a foundational tool for navigating that connection.

**Acknowledgement:** The research is supported by the EU-funded project BSB00348, Project "Black Sea Smart Marine Environmental Outcome System" – BS-SEOS which is implemented within the framework of the Interreg NEXT Black Sea Basin Programme 2021-2027.

## References

1. https://www.bsseos.org/
2. https://www.seadatanet.org/

2nd International Scientific Conference "Modern Problems in Geophysics", Proceedings,
ISBN 978-9941-36-562-1, ISSN 3088-4349, Tbilisi, Georgia, October 29-31, 2026

# USE OF BIO-FERTILIZERS IN A TANGERINE PLANTATION AGAINST PESTS AND DISEASES

**Kutaladze N., Mikeladze Z., Gogolishvili T., Bolkvadze Ts., Kilasonia G., Gorgiladze T.**

*Batumi State University, Institute of Agrarian and Membrane Technologies, Batumi, Georgia*
*nunukutaladze@gmail.com*

***Abstract.*** *The paper describes environmentally friendly bio-fertilizers (Blackjak, Geohumate) selected on the basis of targeted and first-time field experiments in citrus plantations on the red soils of the coastal zone of Adjara, and establishes their rates and doses. The determination of the effectiveness and complex application of these biopreparations is being carried out for the first time on the soils of the coastal zone of Adjara. Through the use of the fertilizers selected as a result of the research, soil fertility was increased, and plants were protected from pests and diseases. Experimental work was carried out according to the experimental scheme in the "Unshiu" mandarin plantation, where environmentally friendly biopreparations (fertilizers) Blackjak, Geo-humate, and Cu++ were applied during the following periods: April, May, and June.*

*Based on the data obtained from the conducted experiments, it was established that:*

*The applied bio-fertilizers – Blackjak (20 ml per 3 liters of water) applied via soil watering and plant spraying, and Geohumate (15 ml per 3 liters of water) applied via soil watering and plant spraying, with Cu++ (2 ml in 10 liters of water) used as a plant-spraying background – showed the best results compared to the unfertilized variant.Following the completion of the experiment during the vegetation period, the positive effect of the applied preparations was demonstrated: plant infection caused by pests and diseases was eliminated, which was well reflected in the green parts of the plant (leaves, shoots) and in the yield, specifically on the external appearance of the tangerine fruits.*

***Key Words:*** *Citrus, mandarin, bio-fertilizers, pests and diseases.*

## Introduction

In the Adjara region, citriculture has always been and will continue to be a leading core sector. Its further development and rehabilitation serve as the primary determinants for increasing the region's export potential and the socio-economic well-being of farmers [1]. Georgian specialists conduct productive scientific work on the propagation of citrus crops and the introduction of new varieties, having developed maintenance and agrotechnical program measures for citrus plantations [2].

The solution is single-minded: to maximize the improvement of plant nutrition zones and soil fertility through both root and foliar feeding. Therefore, using bio-fertilizers via soil watering and plant spraying allows us to achieve high yields, while also yielding quite positive indicators in implementing biopreparation (insecticide) measures against plant pests and diseases, and subsequently increasing the shelf life and storage capacity of the fruits [4].

## Relevance and Objectives

On the red soils of the coastal zone of Adjara, targeted and first-time field experiments in a "Mandarin Unshiu" plantation were conducted to select new environmentally friendly preparations, and their rates and doses were determined. The study examined the effectiveness indicators of the selected preparations, their impact on soil fertility, resistance against pests and diseases, mandarin yield and quality, and storage capacity.

In recent years, worldwide and also in Georgia, bio-fertilizers obtained through natural means have been actively used. They enrich the soil with microorganisms, improve its structure, and promote a natural balance. Biological fertilizers are environmentally safe and are used to increase soil fertility, enhance nutrient content in plants, and combat plant pests and diseases [5]. Bio-organic fertilizers possess great potential in soil restoration, health preservation, and the development of green agriculture. They offer tremendous ecological and environmental benefits along with broad prospects for use. Consequently, the prospects for de-

veloping bio-organic fertilizers are very strong, and their profit potential is enormous. Bio-fertilizers promote the activity of beneficial microorganisms in the soil, enrich the soil naturally, and have a positive impact on the environment and ecosystem [7].

From an ecological perspective, bio-fertilizers are eco-friendly and fully fit into the concept of sustainable agriculture. Based on field experiments, we selected new environmentally friendly preparations: Blackjak, Geohumate, and the insecticide Cuprum.

## Research Area, Materials, and Methods

- **Blackjak** is a 100% natural product (certified in Germany). It is an innovative product that differs from other preparations by containing humic and ulmic acids – compounds that stimulate and activate the plant's roots and vegetative system, enhance the activity of beneficial microelements, and act as an agent for micro- and macro-elements, enabling them to transition into a more absorbable form and distribute evenly throughout the entire plant. It can be used both for foliar feeding and in drip irrigation systems. Additionally, it can be used either alone or in combination. **Dosage:** Foliar feeding – 10 ml dissolved in 2 liters of water, with an application interval of 10-15 days per plant. Root feeding – 10 ml dissolved in 1.5 liters of water, with an application interval of 10-15 days.
- **Geo-Humate** is an environmentally friendly humic bio-fertilizer rich in microelements, often referred to as a growth stimulant. It helps relieve plant stress, promotes green mass growth, bud formation, and prolonged, abundant flowering. It is used for the complex feeding of agricultural crops, starting from seed material treatment to subsequent plant treatment, and is effective in drip irrigation systems in both open and closed ground. The fertilizer ensures a 15-20% increase in yield and improves the absorption of nutrient elements by the plant by 10-20%. **Foliar/non-root feeding:** 800 ml is dissolved in 1000 ml of water; the plant should undergo a 4-fold foliar treatment mainly during the vegetation period (5 ml in 1 liter of water for a single plant).
- **Cu++ (Cuprum)** is essential for the functioning of the plant's immune system, acts as a catalyst for photosynthesis reactions, promotes lignin synthesis and protein metabolism, is involved in respiratory activities, and resists the activity of pests and diseases. Its deficiency causes the curling of young elongated leaves and most frequently occurs under high pH conditions, in humus-rich sandy, loose soils, as well as in cases of cold, flooding, and soil drying. **Dosage:** 10 ml in 3.5 liters of water. Cuprum is a copper-containing preparation; therefore, it is used to reduce fungal diseases, bacterial infections, and leaf spot diseases. Moreover, given that the western region experiences humid climatic conditions – which elevate the risk of disease spread in citrus crops – it is important to utilize a copper-containing preparation.

The experiments were conducted at the Chakvi collection plot and at the Laboratory of Agrochemistry and Soil Science of the Institute of Agrarian and Membrane Technologies [3].

## Experiments

Field experiments were conducted at the collection plot of LEPL Chakvi, in a mandarin "Unshiu" (broad-leaved) plantation using the generally accepted method [6], with 3 repetitions – a total of 6 model plants and 9 plants per variant. During the course of the experiment, monitoring of pest and disease spread was carried out 3 times. There are three variants in the scheme. Bio-fertilizers were applied according to the scheme four times during the vegetation period (April, May, June, July) without mineral fertilizers. Comparison was made with the unfertilized variant. The experiments were set up according to the following scheme:

1. **Blackjak** applied via plant spraying and soil watering (8 ml dissolved in 2 liters of water per plant; application interval of 10-15 days) + **Cu** (10 mg in 3.5 liters of water) applied to the plant by spraying.
2. **Geo-humate** applied via plant spraying and soil watering (5 ml dissolved in 1 liter of water per plant; application interval of 10-15 days) + **Cu** (10 mg in 3.5 liters of water) applied to the plant by spraying.
3. **Unfertilized variant.**

The damage caused by pests and diseases on citrus crops increases up to 20–50% in the absence of control measures.

The application of biopreparations on test plants was carried out according to the experimental scheme, utilizing Cu (10 mg in 3.5 liters of water) applied by plant spraying. Soil application was performed in April, May, June, and July according to the experimental scheme during the active manifestation phase of diseases and pests.

Today, bio-fertilizers are not simply an organic approach, as they deliver real results; it has been proven that they reduce the impact of pests and diseases and strengthen plant immunity. This is particularly important for plants located in soils occupied by mandarin plantations, which are frequently situated in the humid climatic conditions of Western Georgia. Moisture is one of the main prerequisites that helps plants rapidly spread fungal and other diseases, after which they gradually stop responding to preparations [8].

It is interesting to examine how bio-fertilizers combat existing diseases. For example, fungi of the *Trichoderma* type are beneficial: they hinder pathogenic fungi and prevent their spread, while also secreting antifungal substances. In many cases, they fight against *Phytophthora* and *Fusarium* fungi, which cause plant root rot (Table 1).

Therefore, bio-fertilizers are important not only as a source of nutrition, but the physiological and immune state of the plant also depends on them. They do not directly kill the pest, but the leaf becomes more durable, develops immunity, plant stress and depression are reduced, and the generation of beneficial microorganisms is promoted [9].

**Table 1.** Measures to Control Pests and Diseases of Citrus Crops. (08.07.2022–2025).

| № | Harmful Organisms | Timing of Measures | Preparation Name & Application Method | Consumption Norm (for 6 plants) |
|---|---|---|---|---|
| 1 | Scale insects, false scale insects, fungal and bacterial diseases | Late March/ Early April | 1. **Blackjak**: plant spraying and soil watering<br>2. **Geohumate**: plant spraying and soil watering<br>3. **Cu++** (+ 10 mg): plant spraying | • 60 ml / 12 L water<br>• 30 ml / 6 L water<br>• 60 ml / 21 L water |
| 2 | Citrus hairy and silver mites, false scale insects, scale insects, fungal diseases | May / Early June | 1. **Blackjak**: plant spraying and soil watering<br>2. **Geohumate**: plant spraying and soil watering<br>3. **Cu++**: soil watering | • 60 ml / 12 L water<br>• 30 ml / 6 L water<br>• 60 ml / 21 L water |
| 3 | Silver and red hairy mites, waxy false scale insects, fungal diseases | Early Jul | 1. **Blackjak**: plant spraying and soil watering<br>2. **Geohumate**: plant spraying and soil watering<br>3. **Cu++**: plant spraying | • 60 ml / 12 L water<br>• 30 ml / 6 L water<br>• 60 ml / 21 L water |

Agrotechnical and chemical measures were carried out within calendar deadlines and according to the phenophases of pest spread.

## Conclusion

Based on the data obtained from the conducted experiments, we can recommend the bio-fertilizers **Blackjak** and **Geohumate** as unique bio-fertilizers that have demonstrated the following:

**The applied bio-fertilizers** – Blackjak via soil watering and plant spraying, and Geohumate via soil watering and plant spraying, with Cu++ (2 ml in 10 liters of water) used as a plant-spraying background – **improved soil fertility**.

**During the vegetation period**, the positive effect of the applied preparations was revealed, and **plant infection caused by pests and diseases was eliminated**.

The **amount of vital nutrient elements increased** in the plant leaves.

Compared to mineral fertilizers, the use of bio-fertilizers is **economically profitable, easily accessible, and effective** for the plant.

And most importantly, **the yield, quality, and storage capacity of tangerine fruits are increased**.

## References


1. Gogolishvili T., Abuladze D., Bolkvadze Ts., Gordiladze T., Kutaladze N., Introduction of new technologies in the red soils of Adjara (without the application of mineral fertilizers). // Proceedings of the Tbilisi Conference, 2025, 199 p.
2. Kutaladze N., Mikeladze Z., Papunidze S. Introduction of high-efficiency technologies in red soils occupied by mandarin plantations in the Adjara region using environmentally safe biopreparations. // Proceedings of the Baku Conference, 2025, 48 p.
3. Margvelashvili G., Dazhamia T., Practicum in Agrochemistry. // Tbilisi, 2021. ISBN: 978-9941-8-1511-9.
4. Menagarishvili A., Agrochemistry. // Tbilisi: Ganatleba, 1966, pp. 335–336.
5. Chkhaidze G., Subtropical Crops. // Tbilisi, 1996, 531 p.
6. Chanishvili Sh., Methodology of Experimental Work. // Tbilisi: Metsniereba, 1973.
7. Fikry A. M., Radhi K. S., Abourehab M., Effect of Inorganic and Organic Nitrogen Sources and Biofertilizer on Murcott Mandarin Fruit Quality. // Life, 2022. DOI: 10.3390/life12122120.
8. Mikeladze Z., Kutaladze N., Lominadze Sh., Influence of the biopreparation “Gaupsin” on storability of mandarin fruits. // International Journal of Scientific Research and Management, India, ISSN: 2454-2008, Volume 9, Issue 1, 2021, pp. 304–312.
9. Muhammad O. H., Khan A. W., Mardan U., Hassan S., Paradigm Shift towards Beneficial Microbes Enhancing the Efficiency of Organic and Inorganic Nitrogen Sources for a Sustainable Environment. // Land, March 2023. DOI: 10.3390/land12030680.

2nd International Scientific Conference "Modern Problems in Geophysics", Proceedings,
ISBN 978-9941-36-562-1, ISSN 3088-4349, Tbilisi, Georgia, October 29-31, 2026

# EFFECT OF THE BIOREGULATOR "BIORAG" ON SEED GERMINATION AND EARLY GROWTH OF TOMATO AND BASIL

**Gakhokidze R., Beruashvili M., Markarashvili E.**

*Ivane Javakhishvili Tbilisi State University, Tbilisi, Georgia*
*eliza.markarashvili@tsu.ge*

***Abstract.*** *The present study aimed to evaluate the effect of the bioregulator "Biorag" on the germination dynamics of tomato and basil seeds. Within the experimental framework, seeds were pre-treated in a bioregulator solution and compared with untreated control samples. The obtained results demonstrated that seeds soaked in Biorag exhibited 100% germination, with emergence occurring 10 days earlier than in the control group. It was established that the bioregulator accelerates physiological and biochemical processes, thereby promoting seed growth. The study confirms the effectiveness of Biorag as an environmentally safe agro-technical agent.*

***Key words:*** *Bioregulator, Biorag, seed, germination, tomato, basil.*

Solving the problem of world hunger does not depend on a single factor. It requires the integrated development of several key areas:

1. **Modern agricultural technologies** – high-yield crop varieties, biotechnology, efficient irrigation systems, soil conservation, and sustainable agricultural practices.
2. **Reducing food losses and waste** – approximately one-third of the food produced worldwide is lost or wasted. Improving food storage, processing, and distribution could significantly reduce hunger.
3. **Fair distribution of food** – in many cases, the problem is not a lack of food but its unequal distribution. It is essential to develop infrastructure, transportation systems, and markets.
4. **Application of science and innovation** – genetic engineering, artificial intelligence, vertical farming, hydroponics, and alternative sources of protein (microorganisms, algae, and laboratory-produced foods) will play an important role in the future.
5. **Adaptation to climate change** – developing crops that are more resistant to droughts, floods, and other extreme environmental events.
6. **Poverty reduction and education** – hunger is often a consequence of economic hardship. Improving education, employment opportunities, and incomes contributes to better access to food.
7. **International cooperation and peace** – wars and conflicts are among the major causes of hunger. Peace and humanitarian cooperation are essential prerequisites for global food security.

Thus, the world can best combat hunger through a **combination of science, sustainable agriculture, economic development, and international cooperation**. In theory, the Earth currently produces enough food to feed its entire population; the main challenges are ensuring access to food, its equitable distribution, and sustainable food production. Bioregulators (growth stimulants) play an important role in increasing crop yield. They regulate physiological processes in plants and promote better growth and development[1-7].

Their role can be summarized as follows:

- They accelerate seed germination and plant growth.
- They improve root system development.
- They increase plant resistance to stress factors (drought, cold, and diseases).
- They improve the uptake of nutrients.
- They promote flowering and fruit formation.

As a result, the use of bioregulators contributes to higher-quality and higher-yield crops.

The regulation of plant growth and development represents one of the key directions in modern agrobiotechnology. In the context of climate change, soil degradation, and increasing stress factors in agroecosystems, the use of agents that improve early plant ontogenesis is of particular importance.

Bioregulators are natural or synthetic compounds that, even at low concentrations, exert significant effects on plant metabolism. Pre-sowing seed treatment is a widely used method that enhances germination energy, uniformity, and resistance to environmental stress.

Tomato (*Solanum lycopersicum L.*) and basil (*Ocimum basilicum L.*) are widely cultivated agricultural crops, and their successful germination is essential for obtaining high-quality yields. The present study aims to assess the effect of the bioregulator "Biorag" on the germination of these crops.

The results revealed significant differences between the experimental and control groups:

- Seeds treated with Biorag showed **100% germination**
- Germination started and completed **10 days earlier**
- Germination was **uniform and intensive**
- The control group exhibited **slower and less uniform germination**

**Table 1.** Seed Germination Parameters.

| Crop | Treatment | Germination Time (days) | Germination (%) | Uniformity |
|---|---|---|---|---|
| Tomato | Biorag-treated | 5–7 | 100% | High |
| Tomato | Control | 15–17 | 70–80% | Medium |
| Basil | Biorag-treated | 4–6 | 100% | High |
| Basil | Control | 14–16 | 65–75% | Medium |

**Table 2.** Germination Acceleration Effect.

| Crop | Control (days) | Biorag (days) | Difference (days) |
|---|---|---|---|
| Tomato | 16 | 6 | −10 |
| Basil | 15 | 5 | −10 |

**Table 3.** Comparison of Bioregulators.

| Bioregulator | Mechanism of Action | Benefits for Tomato | Benefits for Basil | Application Method | Recommended Dose |
|---|---|---|---|---|---|
| Biorag | Contains natural hormones; accelerates germination | Rapid seedling growth, strong roots | Faster germination, improved leaf development | Seed soaking | 10–12 h, dilution 1:1000 |
| Gibberellin (GA3) | Growth hormone; stimulates cell division | Rapid elongation growth | Faster leaf development, stronger roots | Seed soaking or foliar spray | 50–100 mg/L, 12–24 h |
| Cytokinins | Promote cell division and leaf growth | Enhanced vegetative growth | Improved leaf formation | Foliar application | 1–5 mg/L, 1–2 times/week |

**Table 4.** Seedling Height Growth (after ~2 weeks).

| Bioregulator | Average Height (cm) | Growth Characteristics |
|---|---|---|
| Control | 8–10 | Normal but relatively slow |
| Biorag | 15–18 | Rapid, uniform, vigorous |
| GA3 | 17–20 | Very rapid, but stems may be weak |
| Cytokinins | 12–14 | Moderate growth, good leaf development |

The results indicate that the bioregulator significantly increases seed viability and reduces the germination phase. These findings are consistent with modern studies demonstrating the positive effects of bioregulators on seed physiological processes.

The effect of Biorag can be explained by several key mechanisms:

1. **Increased enzymatic activity** – stimulation of hydrolytic enzymes accelerates the breakdown of reserve substances
2. **Enhanced water uptake capacity**, essential for germination
3. **Regulation of hormonal balance**, possibly increasing gibberellin and auxin activity
4. **Stress reduction** – decreased oxidative stress and increased antioxidant activity

Importantly, seeds treated with Biorag not only germinated earlier but also exhibited more uniform development, which is of practical significance in agronomy.

Based on the study, the following conclusions can be drawn:

- The bioregulator "Biorag" effectively accelerates germination of tomato and basil seeds
- It ensures high-quality and uniform germination
- It reduces germination onset time by approximately **10 days**
- It increases early plant vigor
- The use of Biorag represents a promising and environmentally safe method in agriculture

## References


1. Davies P. J. (Ed.), Plant Hormones: // Biosynthesis, Signal Transduction, Action! Springer, 2010.
2. Taiz L., Zeiger E., Møller I. M., & Murphy A., Plant Physiology and Development (6th ed.). // Sinauer Associates. 2015.
3. Rademacher W., Growth retardants: Effects on gibberellin biosynthesis and other metabolic pathways. // Annual Review of Plant Physiology and Plant Molecular Biology, 51, 2000, pp. 501–531.
4. Basra, A. S. (Ed.), Plant Growth Regulators in Agriculture and Horticulture: Their Role and Commercial Uses. // CRC Press, 2000.
5. Srivastava L. M., Plant Growth and Development: Hormones and Environment. // Academic Press, 2002.
6. Arteca R. N., Plant Growth Substances: Principles and Applications. // Chapman & Hall, 1996.
7. Kumar N., & Reddy M. P., Plant growth regulators and their role in crop production. // Journal of Plant Sciences, 2010.

2nd International Scientific Conference "Modern Problems in Geophysics", Proceedings,
ISBN 978-9941-36-562-1, ISSN 3088-4349, Tbilisi, Georgia, October 29-31, 2026

# ASSESSMENT OF MAIZE CULTIVATION POTENTIAL AND HARVEST FORECAST IN THE AGROCLIMATIC CONDITIONS OF TSALKA-DMANISI

**[*]Meladze M., [*]Meladze G., [**]Japiashvili N.**

[*]*Institute of Hydrometeorology of the Georgian Technical University, Tbilisi, Georgia*

[**]*Georgian Technical University, Tbilisi, Georgia*

*m.meladze@gtu.ge*

***Abstract.*** *The aim of the study is to assess the potential of maize cultivation in the Tsalka-Dmanisi geobotanical region, based on the analysis of the region's agroclimatic and soil resources. The study is based on literary sources and agroclimatic data, which allows to theoretically determine the favorable and limiting factors for the growth and development of maize, as well as the development of practical recommendations in the direction of hybrid selection and cultivation technology. The work structurally includes a comparative analysis of the geobotanical characteristics of the region, soil and temperature resources, the biological requirements of maize, an assessment of agroclimatic risks and relevant conclusions and recommendations, which gives it practical value from an agronomic point of view.*

***Key Words:*** *Maize, air temperature, atmospheric precipitation.*

## Introduction

Maize (Zea mays L.) is one of the most important crops in the world, both for human and animal nutrition. Its high productivity, wide range of uses and good adaptability have led to the spread of the crop in various agro-climatic zones. Its effective cultivation is closely related to the agro-climatic and soil resources of a particular region, which is especially important for mountainous regions. In the conditions of Georgia, maize cultivation is traditionally concentrated in the lowland and steppe zones.

The development of modern agricultural technologies and hybrid material has made it possible to expand the area of cultivation to relatively high altitudes. In this context, the Tsalka-Dmanisi geobotanical region is of particular interest, which is distinguished by its specific relief, wide altitude range, high soil fertility and peculiarities of agroclimatic conditions.

The Tsalka-Dmanisi region is a poorly studied zone in terms of agricultural production, especially in terms of targeted cultivation of annual grain crops, including corn. The available data are mainly generalized and do not provide a complete picture of the extent to which the soil-climatic resources of the region correspond to the biological requirements of maize. Accordingly, there is a need for a complex assessment that includes temperature regime, precipitation distribution, soil properties and agro-climatic risks [1].

## Study area, material and methods

The Tsalka-Dmanisi geobotanical region includes the Tsalka Basin and the high plateaus of the Khrami (Ktsia) River basin (Gomareti, Trialeti, Dmanisi, etc.). The surface of the plateaus (Chochiani Plateau – up to 1400-1600 m above sea level; Gomareti Plateau – 1250-1450 m; Dmanisi Plateau – 900-1700 m, etc.) is dissected by deep (from 70-80 m to 500 m) erosional canyons. The hydrographic network of the region is represented by the Khrami (Ktsia) River and its tributaries – the Chochiani, Karabulakhi, Mashavera, etc.

For the study areas, multi-year (70-year) meteorological observation data were processed and analyzed using the method of mathematical statistics. The meteorological and agrometeorological databases of the Institute of Hydrometeorology of the Georgian Technical University were used; the multi-year (1948-2017) baseline (current) meteorological observation data of the National Environmental Agency of Georgia for the vegetation period were used. Classical methods of agrometeorological research were used. The agrometeorological observation data were processed using the method of mathematical statistics.

## Results

The agroclimatic resources of the Tsalka-Dmanisi geobotanical region allow for the cultivation of maize. Since the growth and development of corn depends mainly on temperature and is not controlled by the length of the day, we do not consider the duration of physiologically active solar radiation (PAR) and the main emphasis is placed on soil and air temperature. During the study, the agroclimatic resources of the given region were analyzed – soil type, air and soil temperature, frost risks, the sum of active temperatures, etc., in order to determine the possibility of normal growth and development of maize culture in a given territory, as well as to identify which corn variety or hybrid can be optimally used. It is known that within the Tsalka-Dmanisi mountain "meadow-valley" zone, mountain black soils and meadow black earthy soils are mainly found, which are replaced by mountain-meadow soils higher up.

The soil analysis (0-30 cm) conducted by us in Gomareti in 2021 showed 4.44% humus, which is close to the above-mentioned indications for Gomareti, therefore the rest of the data is also more reliable. According to the same analysis, we obtained: light loam, pH 7.4 (within the total Ca norm of 8543 mg/kg), and in terms of mineral balance, P – low (1.3 mg/kg) and K, Mg – very high 256.5 and 383.7 mg/kg. The balance of Mn, Cu, Fe, B is also normal, while Zn is low.

The soil requirements of maize, soil pH affects the availability of nutrients to plant roots. The preferred soil pH for maize ranges from 5.8 to 7.0. In our case, the pH is slightly higher, however, the use of mineral fertilizers, especially ammonium and sulfur-containing fertilizers, reduces the soil pH over time, while in other regions where the pH can be up to 7.5 – 8, a normal corn harvest is obtained (in the Tirifona Valley, in the Shida Kartli Plain). Therefore, the soil composition can be considered satisfactory.

When considering the timing of maize sowing, the calendar date is not as important as the soil and air temperature. Good germination is expected when the soil temperature at a depth of 13 cm at 9:00 am is 13°C for three days. Table 1 presents the average air temperatures for the study region [2].

**Table 1.** Average air temperature.

| Meteo-station | M o n t h | | | | | | | | |
|---|---|---|---|---|---|---|---|---|---|
| | III | IV | V | VI | VII | VIII | IX | X | XI |
| Dmanisi | 1.8 | 6.9 | 11.9 | 15.1 | 18.2 | 18.1 | 14.0 | 9.4 | 3.6 |
| Tsalka | -0.5 | 5.5 | 10.3 | 13.6 | 16.4 | 16.0 | 12.3 | 7.4 | 2.3 |

The table shows that the average air temperature in May for Dmanisi is 11.9°C, and for Tsalka – 10.3°C.

Corn seedlings are easily damaged at temperatures of -30°C, therefore, it is necessary to know the end of spring frosts at a given location. This indicator for Tsalka and Dmanisi up to 1500 meters in altitude is from April 15 to May 2, and the first frosts can begin in the second decade of October. As for the sum of active temperatures, in Dmanisi it is 247°C, and in Tsalka – 192°C. Corn does not grow when the temperature is below 10°C, and at temperatures above 30°C, the intensity of plant growth decreases. Since maize germination occurs at a temperature of 10-15°C, it seems logical to wait until the temperature reaches this level, but here the presence of atmospheric precipitation must be taken into account, since the highest precipitation during the year falls in May, both in Dmanisi and Tsalka municipalities (Table 2). Accordingly, corn should be sown before the May rains begin, although it is important to ensure that the plot is not prone to waterlogging in order to eliminate the possibility of rotting of the sown seeds [2].

**Table 2.** Atmospheric precipitation (mm).

| Meteo-station | M o n t h | | | | | | | | |
|---|---|---|---|---|---|---|---|---|---|
| | III | IV | V | VI | VII | VIII | IX | X | XI |
| Dmanisi | 70 | 92 | 118 | 114 | 54 | 46 | 62 | 66 | 62 |
| Tsalka | 50 | 72 | 130 | 100 | 70 | 58 | 71 | 49 | 42 |

Based on the above, maize should already have sprouted in the third decade of May, so we will have 128 days for the vegetation period until October 1. Therefore, from October the temperature begins to drop below 10°C. Therefore, a variety/hybrid should be selected whose vegetation period will be no more than 128-130 days (for example: Pioneer P9241, Fao 627, Fao 757, etc.). maize requires a total of approximately 508–762 mm of precipitation during the vegetation period, depending on weather conditions, plant sowing density (feeding area), soil fertility, soil type, etc. In most years, corn's water requirement is approximately 508–610 mm of precipitation [3].

The extent of yield loss depends on the stage of maize development when the moisture deficit occurs, especially during the grain filling phase of the ears. The daily water requirement of maize is relatively low during the first 3-4 weeks of vegetative growth, and available rainfall is usually sufficient to meet water requirements during this period. When maize has about 8 fully developed leaves, its growth rate increases significantly. At this time, the number of grain rows per ear is determined, so drought stress for the plant should be avoided during this period. If the plant receives sufficient water and nutrients dissolved in it, rapid growth is guaranteed. The number of grains in the ear and the size of the ear begin to form when the plant has 12 leaves. The final number of grains is determined at the 17-leaf stage, so this period should be provided with water. Table 3 shows the range of daily water consumption at different stages of maize development [4].

**Table 3.** Daily water consumption range in maize development phases.

| Days since maize sowing | Water, mm per day |
|---|---|
| 0-30 (early growth) | 1.3-2.5 |
| 30-60 (rapid growth) | 2.5-5 |
| 60-100 (reproductive stage) | 5-7.5 |
| 100-120 (grain maturity) | 6.5-2.5 |

As Table 3 shows, for 0-30 days the crop will be provided with water, moreover, the precipitation received is 3 times higher than that consumed by the plant, since in 0-30 cm of soil we have 4.44% humus, and humus can retain 3-5 times more water, we can calculate how much reserves we will have in the form of water retained in the soil: accordingly, in a 30 cm layer of 1 hectare of soil we have 4500 tons of dry soil, which means approximately 200 tons of humus calculated at 4.44%. Accordingly, from 600 to 1000 tons of water will be accumulated in such soil.

0.3*10 000 *1.5=4500 tons, 4500*4.44%=199.8~200 tons, 200*3=600, 200*5=1000 tons

1 mm of precipitation per 1 hectare is equal to 10 cubic meters of water, respectively 600-1000 t = 60-100 mm of water. Therefore, after the precipitation and water consumption, the soil will still store at least 60 mm of precipitation as a reserve, and for the next accounting period of 30-60 days, i.e. during the rapid growth phase, in our case it will coincide with the third decade of June and July, respectively, in July we will need 116 mm of precipitation, while 54 mm is expected for Dmanisi and 70 mm for Tsalka in the form of rain. Accordingly, this period will be provided by rain and water in the soil, since 54+60=114 mm, this is a minimum calculation that exceeds the limit of demand. The reproductive period of 60-100 days will coincide with the month of August, where a more difficult situation is created, since the productive moisture reserves in the soil cannot provide plants for a long time. Therefore, it will be necessary to carry out irrigation in August. During this period, the plant consumes 180 mm of precipitation, while in Dmanisi and Tsalka we have 46 and 58 mm of precipitation.

Wind is a significant meteorological hazard. Moderate wind is considered in terms of plant pollination, strong wind belongs to abiotic stresses, and wind increases the transpiration coefficient (evaporation rate) from both the plant and soil surface. Accordingly, strong and constant winds have a negative impact on plant growth and development. Fig. 1 shows the number of windy days during the growing season.

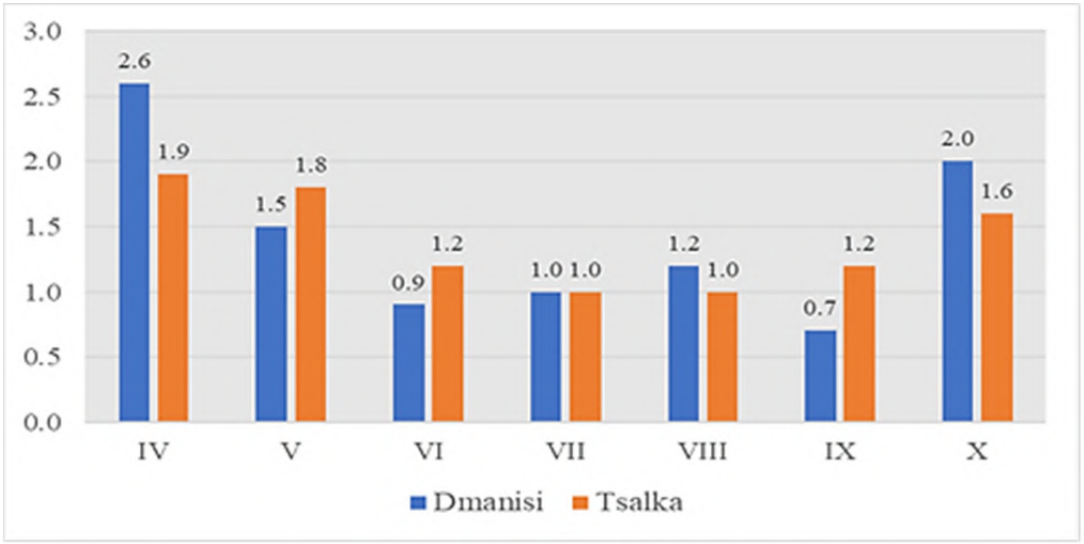



**Fig. 1** Number of days with strong winds (≥15 m/s) during the growing season

Fig.1 shows that Dmanisi and Tsalka are much less windy municipalities than the plain regions, where maize are traditionally always present. In the Tsalka-Dmanisi zone, the frequency of strong winds is low and does not represent a limiting factor for corn cultivation, although its occurrence during the critical phase of pollination can be a reason for yield reduction.

Hail is one of the most dangerous meteorological phenomena for agricultural crops. Fig. 2 shows the number of hail days during the warm period.

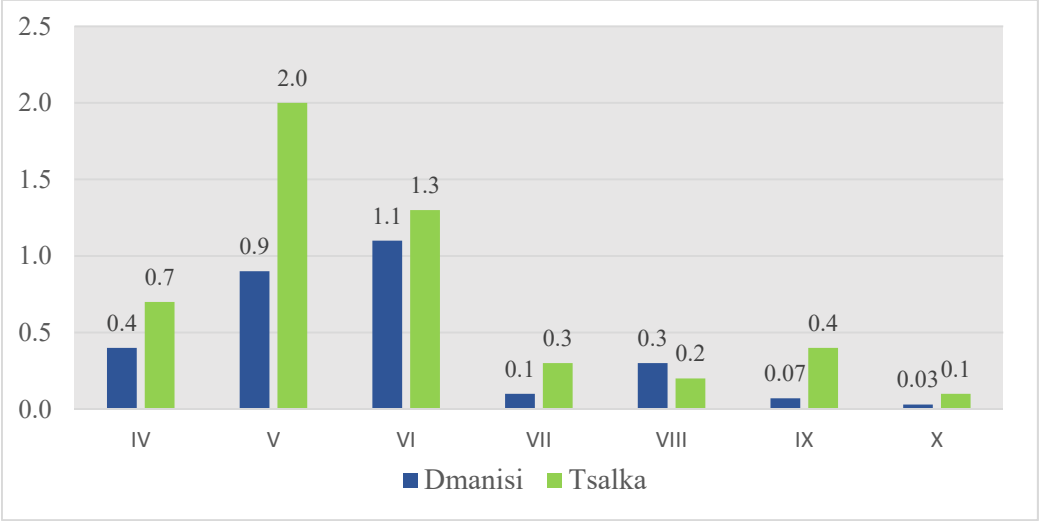



**Fig. 2** Number of hail days in the warm season

Fig. 2 shows that the main risk of hail occurs in May and June. At this time, the plant is still in the early growth phase and therefore hail does not pose a significant threat until the 5-leaf stage.

The data of observations at the meteorological and agrometeorological stations of the Hydrometeorology Department of the National Environmental Agency, along with the harvest, have been analyzed and processed. Correlations have been identified and a regression equation for the forecast of maize harvest (t/ha) for the Kvemo Kartli region has been compiled:

$$U=4.438x-0.626y-5.052z+158.532$$

In the equation, U is the forecast harvest (t/ha), x is the total atmospheric precipitation (mm), in VI-VII months, y is the number of days with ≥5 mm precipitation (in VI-VII months), z is the total productive moisture at a depth of 20 cm of soil (mm), in VI-VII months.

## Conclusion

The plateaus of the Tsalka-Dmanisi geobotanical region, due to their soil and climatic resources, are suitable for maize cultivation; corn should be sown in April, before the onset of intense precipitation; the vegetation period of the selected corn hybrid should not exceed 120-130 days; hybrids can be Pioneer P9241, Fao 627, Fao 757, etc.; sowing in May and June is provided by atmospheric precipitation, in July it is provided by water present in the soil, and in August it requires additional irrigation; abiotic stresses (wind, hail) are not a systemic limiting factor, although in individual years they may have a local impact on yield.

## References


1. Kvachakidze R., Saqartvelos Geobotanikuri Raionebi. // Tbilisi, gamomc. "Ganatleba", 2010, pp. 162-166. (in Georgian)
2. Meladze G., Meladze M., Saqartvelos Agmosavlet Regionebis Agroklimatiri Resurse. // Tbilisi, gamomc. "Universali", 2010, 293 p. (in Georgian)
3. Schneider M., Wasserspeicher Humus. // Groß-Umstadt, "DLG-Deutsche Landwirtschafts-Gesellschaf", 2019, pp. 2-4.
4. Corn production handbook. University of Arkansas, United States Department of Agriculture and County Governments Cooperating, Fayetteville, 2001, pp. 5-22.

2nd International Scientific Conference "Modern Problems in Geophysics", Proceedings,
ISBN 978-9941-36-562-1, ISSN 3088-4349, Tbilisi, Georgia, October 29-31, 2026

# ECOLOGICAL ASSESSMENT OF "GREEN INFRASTRUCTURE" AND THE ANTHROPOGENIC LOAD OF SUSTAINABLE TOURISM IN THE COASTAL ZONES OF THE CASPIAN SEA

**Osmanova S.**

*Baku State University, Baku, Azerbaijan*
*osmanova-sona@mail.ru*

***Abstract.*** *This article provides a comprehensive investigation into the impacts of rapidly expanding tourism infrastructure on coastal "green infrastructure" systems – including coastal forests, sand dunes, and natural buffer zones – within the Azerbaijani sector of the Caspian Sea. Spanning a 30-year period from 1995 to 2025, the study subjects landscape alterations, anthropogenic loading, and ecosystem adaptation capacities to rigorous scientific analysis. To achieve an accurate quantitative assessment of the ecological load, remote sensing technologies (Sentinel-2, Landsat 8/9) integrated with coastal zone management models were utilized. The empirical findings reveal that intensive construction activities along the coastline over the past three decades have led to a significant reduction in natural green zones, threatening local biodiversity with severe degradation. Specifically, restoring cross-sectoral ecological balance is paramount to mitigating the degradation inflicted on the ecosystem by tourism facilities. Furthermore, this study demonstrates that the implementation of sustainable and ecosystem-based tourism management models can enhance the resilience of coastal ecosystems by up to 30% in the coming decades. To foster economic development without environmental compromise, the author recommends the preservation of green corridors and the mandatory enforcement of "zero-waste" principles across tourism establishments. Ultimately, this research establishes a novel management framework for the future ecological protection and sustainable development of the Caspian Sea coastlines.*

***Key words****: Caspian Sea, green infrastructure, sustainable tourism, ecological load, biodiversity.*

## Introduction

The Azerbaijani sector of the Caspian Sea is considered one of the most dynamic and vulnerable components of regional ecosystems, owing to its unique hydrological and landscape characteristics. Coastal zones are noteworthy not only for their high biodiversity but also for the strategic role they play in the socio-economic development of the country, particularly within tourism and recreational activities [8]. However, the rapid expansion of tourism infrastructure in the region in recent years has led to fundamental alterations in the landscape structure of coastal areas and a sharp increase in anthropogenic pressure on natural resources.

In this context, the concept of "green infrastructure" – encompassing wetlands, coastal forest belts, sand dunes, and other natural buffer zones – plays a critical role in preserving the self-regulation capacity of the ecosystem and adapting to global climate change [2]. However, against the backdrop of global warming, sharp fluctuations in sea levels and intensive construction activities lead to the fragmentation of this natural "green framework" [10]. The general findings of ongoing research indicate that the fragmentation of coastal ecosystems results in a reduction of habitats for biodiversity (both fauna and flora), as well as a decline in the coastline's resilience to erosion [4].

The primary objective of this article is to evaluate the current state of the tourism-ecosystem balance in the coastal areas of the Azerbaijani sector of the Caspian Sea, to analyze the impact of anthropogenic loading on the functionality of "green infrastructure," and to propose scientifically grounded management mechanisms for the implementation of sustainable tourism models. The study is based on an integrated approach that incorporates the principles of environmental preservation and restoration for the sake of sustainable economic development.

## Method

The methodological foundation of this study comprises a multi-level monitoring and analytical approach spanning the period from 1995 to 2025. To ensure the reliability of the data obtained during the research pro-

cess, contemporary geo-ecological methods were employed. *Landsat 8* and *Landsat 9* satellite imagery were processed to evaluate land-use/land-cover (LULC) changes occurring within the coastal zones. The imagery was analyzed using specialized software within a Geographic Information Systems (GIS) environment to determine the spatial distribution and temporal dynamics of "green infrastructure" (vegetation, wetlands, and sand dunes) over the 30-year period. The Ecological Load (EL) index was applied to measure the anthropogenic pressure exerted on the coastal zones. This index reflects the balance between the recreational capacity of the area and its actual utilization:

$$EL=\frac{T \times F}{R}$$

Where: T (number of tourists): The average annual number of tourists visiting the coastal zone during the respective year; F (activity coefficient): The degree of impact inflicted upon the ecosystem, varying according to the type of tourist activity (e.g., active beach tourism, ecotourism, or mass recreation); R (recreational capacity of the ecosystem): The maximum number of individuals that the area can accommodate under natural conditions without causing degradation to biodiversity. To validate the results obtained from satellite data and conduct ground-truth verification, field surveys were carried out in selected pilot coastal zones in May 2025. During these field investigations, soil salinity levels, vegetation density and diversity, as well as the volume of solid waste along the coastline were assessed in situ. This methodological combination allows the study to accurately determine not only the visual landscape alterations but also the underlying anthropogenic driving forces behind these changes.

## Analysis and Discussion

The results of comprehensive 30-year (1995-2025) monitoring and satellite remote sensing conducted in the coastal areas of the Azerbaijani sector of the Caspian Sea confirm a functional, direct negative correlation between the unplanned and extensive expansion of tourism infrastructure and the degradation of "green infrastructure". Throughout the analyzed period, the stark discrepancy between the natural recreational carrying capacity of the area and the actual influx of tourists has driven a progressive and perilous increase in the regional Ecological Load (EL) index (Table 1).

**Table 1.** Dynamics of tourism load and landscape alterations in coastal zones (1995-2025).

| Period | Number of tourists (thousands/year) | Green infrastructure area (ha) | Built-up area (ha) | Ecological load index (EL) |
|---|---|---|---|---|
| 1995-2005 | 120 | 1200 | 150 | 0,45 (stable) |
| 2006-2015 | 350 | 1050 | 420 | 0,68 (moderate risk) |
| 2016-2025 | 800 | 850 | 790 | 0,92 (critical crisis) |

Statistical indicators clearly demonstrate that since 1995, an approximate 6.6-fold increase in the regional tourist influx has led to a sharp 29.1% decline in the "green infrastructure" areas (natural buffer zones, coastal forests, phytocoenoses) that protect the coastline. In parallel, urbanization and mass construction areas surged from 150 hectares to 790 hectares. The Ecological Load index reaching 0.92 during the final decade spanning 2016-2025 provides scientific evidence of the complete depletion of the ecosystem's homeostasis (self-regulation) and biological self-purification potential [3].

The intensification of construction activities for recreational facilities, hotels, and paved roads in coastal zones has led to the mechanical compaction of the soil-ground layer. This physical transformation drastically impairs the aeration and infiltration (water absorption) capacity of the soil. Consequently, the natural mechanisms through which atmospheric precipitation and seawater percolate into the groundwater are severely disrupted.

Analysis of spectral reflectance coefficients derived from Landsat satellites within a GIS environment indicates that soil compaction has driven an increase in surface runoff, leading to internal stagnation and the formation of secondary salinization hotspots within internal buffer zones. This process directly triggers the degradation of the root systems of coastal phytocoenoses and accelerates soil erosion.

The fragmentation of green buffer zones by construction and beach development areas isolates the habitats of native flora species. This ecological crisis results in the displacement of dominant species within the

structure of phytocoenoses. Field investigations recorded an expansion of xerophytic and halophytic plants that are resilient to anthropogenic pressure, whereas the functionality and prevalence of moisture-loving and endemic species have significantly declined.

**Table 2.** Structural dynamics and area variations of coastal plant communities under anthropogenic pressure (1995-2025).

| Plant community / Species | Initial distribution area (1995, %) | Current distribution area (2025, %) | Change trend / Ecological status |
|---|---|---|---|
| *Phragmites australis* (Common reed beds) | 45 | 28 | -17% (sharp decline) |
| *Salicornia europaea* (Common glasswort) | 20 | 14 | -6% (fragmentation) |
| *Ambrosia artemisiifolia* (Invasive species) | <2 | 18 | +16% (aggressive expansion) |
| Native coastal sand dune vegetation | 33 | 12 | -21% (anthropogenic degradation) |

As evidenced by table 2, the reed bed distribution areas that constitute the backbone of the native ecosystem have experienced a sharp decline, allowing the aggressive invasive species *Ambrosia artemisiifolia* (common ragweed) to establish dominance within the vacant ecological niches. By gaining a competitive advantage over native flora for nutrients and water resources, this plant severely weakens the gene pool of the natural biodiversity.

The mass movement of tourists along the coastline, vehicular noise, and nocturnal artificial lighting (light pollution) exert a direct negative impact on the vital activities of migratory and sedentary waterfowl and wading birds [9]. These impacts can become lethal, particularly during the breeding, egg-laying, and migratory stopover periods of the avifauna [5]. The loss of the buffering function of green infrastructure destroys avian concealment habitats. This phenomenon ultimately leads to a reduction in individual population counts and a decline in nesting success at the regional level.

The unsatisfactory operation of local wastewater treatment plants (local aeration stations) in the majority of modern tourism complexes results in a massive influx of biogenic elements (Nitrogen (N) and Phosphorus (P)) into the coastal ecosystems. In this regard, gaps in transboundary and coastal management mechanisms further exacerbate the process [1]. This regional hydrochemical pressure initiates an acute eutrophication (water blooming) process in the coastal waters.

As a result of eutrophication, the amount of dissolved oxygen in the water decreases sharply, which leads to mass mortality of benthic organisms and coastal fish species. As noted in the literature [7], this chain-reaction ecological crisis fundamentally undermines the resilience and trophic stability of biodiversity along global migratory routes (Eurasian Flyways).

Mathematical-ecological forecasting models implemented for the 2026-2035 period indicate that if the current extensive tourism trends and unregulated exploitation of coastal zones persist in this manner, it will be inevitable for coastal ecosystems to transition into an irreversible degradation phase after 2030. Within the framework of Integrated Coastal Zone Management (ICZM) models, the immediate transformation of tourism zones through "green and ecosystem-based" technologies stands as an absolute necessity for ensuring regional ecological security.

## Conclusion

The conducted research and analytical assessments demonstrate that the preservation of "green infrastructure" in the coastal areas of the Caspian Sea is not merely an environmental protection measure, but a fundamental cornerstone for the development of sustainable tourism [6]. The critical level reached by the current ecological load necessitates a paradigm shift in the management of coastal zones. In this context, integrated management models recommended for implementation through public-private partnerships should encompass the following strategic directions.

Strengthening the legal status of specific "green buffer zones" for coastal areas: These zones must be classified as construction-free areas utilized exclusively for ecosystem restoration purposes. Research indicates that the expansion of green buffers allows for a 25-30% reduction in coastal erosion driven by sea-level fluctuations.

Ensuring continuous biodiversity monitoring along ecotourism routes: Implementing robust monitoring frameworks [7] that transcend mere visual surveillance to incorporate digital ecological monitoring. This includes satellite and drone-based tracking of avian populations during migration, as well as dynamic spectral analysis of coastal flora conditions. The resulting monitoring datasets must be published annually as open scientific reports by the relevant authorities.

Mandating the implementation of "zero-waste" technologies for efficient waste and resource management at tourism facilities: Management models must be structured around ecosystem-based approaches that fully account for the natural self-purification potential of marine coastlines, minimize anthropogenic load, and foster development in harmony with nature.

The resilience of coastal ecosystems must be measured not by the damage inflicted upon nature by economic growth, but by the investments allocated toward environmental restoration. This integrated approach stands as the only effective and scientifically grounded pathway toward achieving the Sustainable Development Goals (SDGs) in the Caspian Sea region by 2030.

## References


1. Aliev A. I., & Mammadov K. H., Integrated management of coastal zones in the South Caspian region: Challenges and opportunities. // Caspian Journal of Environmental Science, 20(1), 2022, pp. 45-58. https://doi.org/10.22124/cjes.2022.5643
2. IPCC. Climate Change 2021: The Physical Science Basis. Cambridge University Press, 2021.
3. Mamedov R. M., Abbasova S. N. & Akhundov V. G., Izmeneniya v rastitelnosti solonchakov Gyzylagacha pod vozdeystviyem klimaticheskikh faktorov. // Botanicheskiy vestnik, 36(2), 2020, pp. 102-111.
4. Millennium Ecosystem Assessment. Ecosystems and Human Well-being: Wetlands and Water Synthesis. World Resources Institute, 2005.
5. Ornithological Society of Azerbaijan. Ornithological Reports of Azerbaijan. State Ornithological Institute, 2023.
6. Ramsar Convention Secretariat. An Introduction to the Ramsar Convention on Wetlands. Ramsar Secretariat, 2016.
7. Smith J., Thompson L. & Keller B., Climate-driven changes in migration timing and population decline of waterbirds in Eurasian flyways. Global Change Biology, 24(3), 2018, pp. 1375-1387. https://doi.org/10.1111/gcb.13985
8. UNEP. Caspian Sea Environment Programme: Vulnerability of Coastal Wetlands to Climate Change. United Nations Environment Programme, 2022.
9. Wetlands International. Waterbird Population Estimates (5th ed.). Wetlands International, 2020.
10. WMO. State of the Global Climate 2023. World Meteorological Organization, 2024.

2nd International Scientific Conference "Modern Problems in Geophysics", Proceedings,
ISBN 978-9941-36-562-1, ISSN 3088-4349, Tbilisi, Georgia, October 29-31, 2026

# REDUCING ANTHROPOGENIC IMPACT BY UTILIZING MANDARIN PROCESSING WASTE AS A RESOURCE

**Papunidze G., Chkhartishvili I., Papunidze S., Seidishvili N., Mikeladze Z., Abuladze D.**

*Shota Rustaveli State University, Institute of Agrarian and Membrane Technologies, Batumi, Georgia*
*sofiapapunidze@gmail.com*

***Abstract.*** *Along with scientific and technological progress, population growth, and the development of industry, agriculture, and urbanization, the human impact on the environment has increased significantly. During the industrial processing of mandarin fruit, a significant amount of organic waste is generated, the irrational management of which increases anthropogenic impact on the environment. This article discusses the global problem arising from the linear economy model, using the industrial processing of mandarin (Citrus unshiu Marc.) fruit as an example. Waste generated after product manufacturing is dumped in landfills, polluting the environment. This paper demonstrates the return of mandarin processing waste – rich in biologically active substances – back into production for the manufacturing of new products using a circular economy model.*

***Key words:*** *Mandarin waste, waste management, functional product.*

## Introduction

Global citrus production reached 173.8 million tons in 2026, with an average annual growth rate of 1.2% compared to 158.5 million tons in 2020 [1]. Worldwide, approximately 15 million tons of organic waste are generated annually during the industrial processing of citrus fruits. Under a linear economy model, waste is dumped in landfills after product manufacturing. In an anaerobic environment, fermentation occurs rapidly, causing oxidation, releasing methane and other toxic compounds into the atmosphere, losing valuable components, having an extremely negative impact on ecology, polluting the environment (soil, atmosphere, water), and adversely affecting human health [2]. The approach to managing "bio-waste" – the accompanying waste of industrial fruit and vegetable processing – has shifted from traditional linear economy practices to a more sustainable circular economy, which is an important result of circular economy principles. Applying a circular economy model allows us to return inexpensive waste with high biological value back into production [3, 4].

Due to its health-beneficial phytochemical composition and growing awareness of healthy nutrition, citrus is considered an essential component of the human diet [5, 6, 7]. Mandarin fruit (*Citrus unshiu* M.) peel is a rich source of pectic substances, amino acids, minerals, carotenoids, dietary fibers, essential oils, and vitamins P, C, and B [8]. With its polyphenolic content, polymethoxyflavones such as nobiletin, tangeretin, and narirutin, as well as pectin, exhibit antioxidant properties, slow down cellular aging, and possess antimicrobial, antitumor, anti-inflammatory, and anti-diabetic properties. Nobiletin prevents obesity, hinders fat accumulation in the liver, protects brain cells from damage, reduces the risk of neurodegenerative diseases (e.g., Alzheimer's), and shows potential in slowing cancer cell growth, particularly in lung, liver, and breast tissues. Oncologists at the Michigan Cancer Foundation discovered through research that cancer cells form strong, solid complexes with pectin, which prevents the spread of tumor metastases [9–13]. According to recent studies, pectin hydrolysate obtained from citrus peel via acid hydrolysis features good solubility and is successfully used as a prebiotic fiber in the production of liquid food products, especially functional beverages [14].

The novelty of this study lies in obtaining a stable mandarin beverage following zero-waste theory, which involves processing the peel, obtaining pectin hydrolysate, and reintroducing it into the mandarin pulp mass. According to a technology previously developed by us (GE P 2004 3284 B), during the production of mandarin nectar from peeled mandarin fruit, the waste peel constitutes 27–28%, which was previously discarded into the environment and exerted an anthropogenic impact. The chemical compositions of mandarin peel and mandarin pulp are presented in Table 1.

**Table 1.** Chemical composition of mandarin peel and mandarin pulp.

| № | Subject of Study | Dry Matter (by drying) % | Total Sugars % | Acidity % | Essential Oil % | Vitamin C % | Total Carotenes % | Total Pectin % | Soluble Pectin % | Insoluble Pectin % | Flavonoids % | Crude Fiber % | Cellulose % | Hemicellulose % |
|---|---|---|---|---|---|---|---|---|---|---|---|---|---|---|
| 1 | Mandarin Peel | 26.8 | 7.5 | 0.2 | 2.1 | 0.125 | 6.5 | 4.8 | 0.6 | 4.2 | 2.8 | 4.5 | 3.4 | 1.8 |
| 2 | Mandarin Pulp | 20,2 | 7,0 | 0,8 | - | 0,036 | 2,4 | 0,5 | 0,2 | 0,3 | 0,8 | 1.1 | 0,4 | 0,1 |

This paper describes obtaining a stable, pectin-rich beverage from mandarin (*Citrus unshiu* Marc.) fruit according to zero-waste theory, which involves obtaining a functional bio-additive through physical and chemical processing of the mandarin peel and adding it back to the pulp by optimizing technological parameters.

## Materials and Methods

The subjects of study are mandarin fruit peel and pulp. During the experiments, the following physico-chemical analysis methods were used:

- Dry matter determination – HI 96801 digital refractometer.
- Acidity determination – GOST 2555.0-82.
- pH determination – HANNA HI2213 pH/ORP Meter.
- Pectin content – Calcium pectate method.

## Technological Processing Scheme

The technological process involves sorting, washing, separating peel and pulp, and processing the mandarin fruit:

1. Crushing the pulp and transferring it to a collector.
2. Peel preparation for hydrolysis: Crushing the peel into 1–2 mm particles and multiple washings with water at temperatures up to 30°C at a 1:3 ratio to maximize the removal of essential oils and simple sugars.
3. Hydrolysis process: Adding 2 L of water per 1 kg of wet mass, introducing citric acid to maintain pH within 2.0–2.3, and hydrolyzing at 90°C for 60–90 minutes. Blending or passing through a colloid mill yields a homogeneous puree – a "natural stabilizer" – rich in soluble and soft insoluble fibers, minerals, amino acids, and vitamin P (hesperidin).
4. Combining the "natural stabilizer" with the pulp in the collector.
5. Acidity adjustment for stabilization: To achieve beverage stability, an optimal pH of 3.2–3.6 is maintained in the combined mass.
6. Homogenization of the combined mass through a colloid mill to reduce particle size to 40–50 μm.
7. Blending (Coupage) – Adding the required amount of sugar syrup to the combined mass according to the recipe, achieving a total dry matter content of 12–13% in the final product.
8. Deaeration and thermal processing: The mass is transferred to a vacuum vessel. Vacuuming ensures complete air (oxygen) removal, with deaeration occurring at approximately 50–60°C.
9. Packaging: Hot filling of the finished product at 90°C (pasteurizer, 30–60 seconds).

## Results

Waste valorization is an important step toward a "green economy". The developed technology offers several advantages: the peel returns to production as a functional additive; production costs are reduced as stabilizer (pectin) purchasing costs are eliminated; citric acid usage adheres to Green Chemistry principles without aggressive mineral acids (hydrochloric, nitric, sulfuric), making the product safe and eco-friendly.

Hydrolyzed natural soluble pectin returned to the beverage renders it self-stabilizing and rich in soluble fiber. The process is energy-efficient, skipping fiber drying and grinding steps. Valorizing mandarin peel enriches the beverage with bioactive compounds and supports import substitution by creating a local alternative to imported pectin and stabilizers in Georgia. The ecological footprint of production is minimized, putting circular economy principles into practice. Equipment was selected based on energy efficiency (e.g., thermally insulated tanks), reducing carbon dioxide emissions.

## Conclusion

Reintroducing secondary, low-cost, high-biological-value resources into circulation expands the raw material base and significantly protects the environment from negative waste impacts.

This research was funded by the Shota Rustaveli National Science Foundation of Georgia (Grant No. FR 23-1945) – " Multifunctional bio supplements for functional products from waste remaining after processing subtropical raw material following the model of circular economy."

## References

1. Inca A., Ladux J. L., Castro N., Silva A., Introductory Chapter: World Citrus Production and Research. // Citrus – Modern Uses and Processing, 2023. DOI: 10.5772/intechopen.110519.
2. Raveendran S., Edgard G., Sharrel R., Parameswaran B., Sunita V., Thakur Indu S., Ramkumar B. N., Pandey A., Conversion of food and kitchen waste to value-added products. // Journal of Environmental Management, Vol. 241, 2019, pp. 619–630. 10.1016/j.jenvman.2019.02.053
3. Campos D. A., Gomez-Garcia R., Vilas-Boas A. A., Madureira A. R., Pintado M. M., Management of Fruit Industrial By-Products-A Case Study on Circular Economy Approach. // *Molecules*. Vol. 25, 2020. https://doi.org/10.3390/molecules25020320
4. Elisha O. D., Moving Beyond Take-Make-Dispose to Take-Make-Use for Sustainable Economy. // International Journal of Sciences and Research Education. Vol. 13, 2020, pp. 497–516.
5. Panwar D., Panesar P. S., Chopra H. K.,Recent trends on the valorization strategies for the management of citrus by-products. // Food Reviews International. Vol. 37, 2021, pp. 91–120. https://doi.org/10.1080/87559129.2019.1695834
6. Andrade M. A., Barbosa C. H., Shah M. A., Ahmad N., Vilarinho F., Khwaldia K., Silva A. S., Ramos F.; Citrus By-Products: Valuable Source of Bioactive Compounds for Food Applications. // Molecules. Vol. 26, 2021, 5991. https://doi.org/10.3390/antiox12010038
7. Rafiq R., Kaul R., Sofi S. A., Bashir N., Nazir F., Nayik G. A., Citrus peel as a source of functional ingredient: A review. // Journal of the Saudi Society of Agricultural Sciences, Vol. 17 (4), 2018, pp. 351–358. http://dx.doi.org/10.1016/j.jssas.2016.07.006
8. Papunidze G. R., Lazishvili L. A., Romanenko E. V., Nakaidze Z. M., Chkhartishvili I. N., Rekhviashvili N. Sh., Kalandadze V. L., Method for Obtaining Vitamin P. // USSR Author's Certificate No. 1686730; 1991. (in Russian)
9. Li S., Pan M.-H., Lo C.-Y., Tan D., Wang Y., Shahidi F., Ho C.-T., Chemistry and health effects of polymethoxyflavones and hydroxylated polymethoxyflavones. // Journal of Functional Foods, Vol. 1, 2009, pp. 62–75. 10.1016/j.jff.2008.09.003
10. Urgancı Ü., Işık F., A review: The protective effects of dietary polyphenols on Alzheimer's disease. // *Analecta* Technica Szegedinensia. Vol. 16, No. 01, 2022, pp. 14–26. https://doi.org/10.14232/analecta.2022.1.14-26
11. Cirmi S., Navarra M., Woodside J. V., Cantwell M. M., Citrus fruits intake and oral cancer risk: A systematic review and meta-analysis. // Pharmacological Research. Vol. 133, 2018, pp. 187–194. https://doi.org/10.1016/j.phrs.2018.05.008
12. Cirmi S., Maugeri A., Ferlazzo N., Gangemi S., Calapai G., Schumacher U., Navarra M., Anticancer Potential of Citrus Juices and Their Extracts: A Systematic Review of Both Preclinical and Clinical Studies, // Frontiers in Pharmacology. 2017; Vol. 8, 420. 10.3389/fphar.2017.00420
13. Yu Z., Wu Y., Ma Y., Cheng Y., Song G., Zhang F., Systematic analysis of the mechanism of aged citrus peel (Chenpi) in oral squamous cell carcinoma treatment via network pharmacology, molecular docking and experimental validation. // Journal of Functional Foods. Vol. 91, 2022, 105012. 10.1016/j.jff.2022.105012
14. Dangi N., Yadav B. S., Characterization of partial acid hydrolysates of citrus pectin for their pasting, rheological and thermal properties. // Journal of Food Science and Technology. Vol. 57 (7), 2020, pp. 2681–2692. 10.1007/s13197-020-04304-w.

2nd International Scientific Conference "Modern Problems in Geophysics", Proceedings,
ISBN 978-9941-36-562-1, ISSN 3088-4349, Tbilisi, Georgia, October 29-31, 2026

# EXSPERIMENTAL STUDIES OF THE STRUCTURAL STRENGTH EFFECT ON THE SWELLING OF CLAY SOILS

**Gabibov F.**

*Azerbaijan Research Institute of Construction and Architecture, Baku, Azerbaijan*
*farchad@yandex.ru*

***Abstract.*** *The paper notes that the influence on the increase in the clay soil swelling disturbs both intra-aggregate and inter-aggregate bonds. A new technique and device for studying the "sensitivity" of swollen clay soils have been developed, which make it possible to study more accurately the swelling of clay soils in the natural state and also in the structurally disturbed one on the same sample. Studies of the swollen clay soils "sensitivity" selected from various regions of Azerbaijan have shown that with an increase in the depth of clay soils, their coefficient of structural strength influence on swelling, i.e., "sensitivity" increases significantly.*

***Key Words:*** *Exsperimental studies, structural strength, swelling, clay, soil, water, indicator.*

## Introduction

Swelling is usually understood as the process of increasing the volume of clay soil when it interacts with water.

The increase in the scale of construction has shown that the swollen clay soils have a much greater development on the earth's surface than previously supposed. As noted by (Cromko [1]; Sorochan [2]) and others, ignoring the negative properties of swollen clay soils leads to significant material damage.

The works of (Fityuş, Smith and Allman [3]; Peredalskiy and Ananjev [4]; Mustafayev [5]; Kulchitskiy and Usiyarov [6]; Al-Homond, Bagma, Husein Malkavi and Al Bashabsheh [7]; Gabibov [8]; Day [9. 10, 11]; Noamooz, Jahangir and Masrouri [12]; Cui, Yahia-aissa and Delage [13]; Alonso, Romero, Hoffmann and Escudero [14]; Sun and Sun [15]) and others are devoted to the study of swollen clay soil stress-strain state regularities

It is well-known that as a rule, violation of natural structural bonds in clay soil leads to an increase in swelling, and often to a very significant one.

## State of knowledge of the problem under study

In natural conditions, structural bonds are disrupted by weathering, increased pressure, recent tectonic movements, anthropogenic impact, etc. (Schmetmann [16]) proposed the term "sensitivity" of clays to denote the phenomenon of increased swelling of clays due to the repeated repetition of significant shear deformations during mechanical grinding of clay soils. The value of this "sensitivity" is expressed by the ratio of the clay swelling indicators with disturbed( $\delta_{s_{dis.}}$ )and undisturbed ( $\delta_{s_{unddis.}}$ ) texture, i.e.

$$K_C = \frac{\delta_{s_{dis.}}}{\delta_{s_{unddis.}}}$$

In this formula, $K_c$ is the value of "sensitivity" or the coefficient of clay soil structural strength influence on soil swelling. This formula shows that when the coefficient $K_c$ is equal to or close to unit, the structural bonds do not affect the clay soil swelling. In the work of (Snezhkin and Ziangirov [17]), it is noted that in some clays with a high strength of interaggregate bonds, the violation of the structure leads to an increase in swelling by 3-20 times. It should be noted that according to our research, the violation of interaggregate bonds also has a noticeable effect on the increase in the swelling of clay soils.

## Development of a new technique for studying the structural strength effect on clay soil swelling

Under laboratory conditions, the change in the coefficient of clay soil structural strength ("sensitivity") influence on swelling of various swollen clay soils in Azerbaijan was studied by a refined method on an improved device (see Fig.1). Unfortunately, none of the published works on the study of clays " sensitivity " mentions how the equality of the samples density in the natural and disturbed state was achieved in comparative studies.

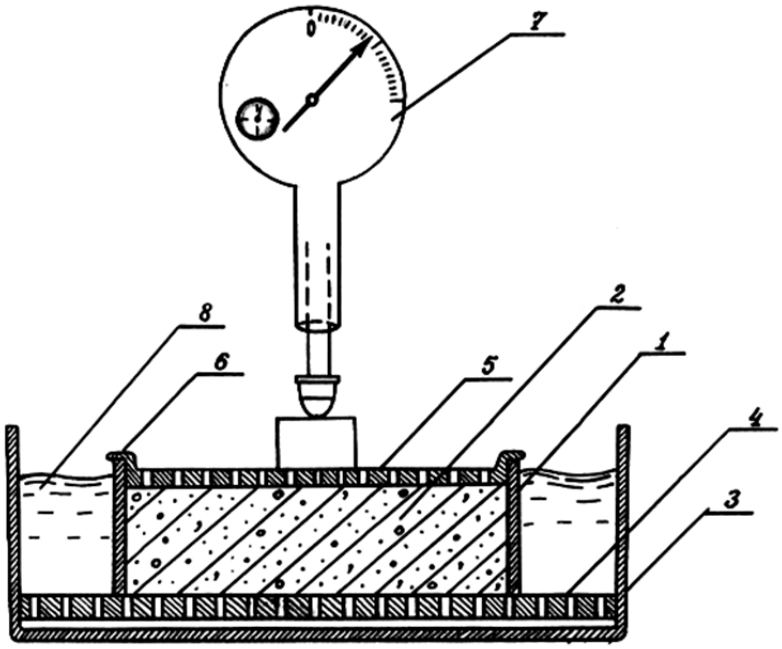



Fig. 1. Device for studying the "sensitivity" of swellen clay soils: 1 is composite ring; 2 is soil sample; 3 is cup; 4 is tray; 5 is stamp-piston; 6 is collar; 7 is clock-type indicator; 8 is water.

The improved device includes composite ring 1 with soil sample 2, cup 3, at the bottom of which permeable tray 4 is installed, stamp-piston 5 with collar 6 protruding beyond the upper edge of the ring, and clock-type indicator 7. During the test, water 8 is poured into cup 3.

As it is known, when selecting a structurally undisturbed sample into a ring, the sample receives a strictly specified cylindrical shape, defined by the selected ring size. After testing of the structurally undisturbed sample, the water is drained, the indicator and the piston are removed. Then, with the help of a special spoke, the sample is loosened in the ring, then piston 5 is again placed under pressure on the sample until its collar 6 stops at the upper edge of ring 1. Again, indicator 7 is set to zero and the soil is tested for swelling by pouring water into the cup, but in a structurally disturbed state. As can be seen on the described device, the initial density of the soil is achieved in the simplest way. The tests in both disturbed and undisturbed states are performed on the same soil sample. This allows you to increase the reliability of the "sensitivity"test results.

## Experimental study of the structural strength influence on clay soil swelling in certain regions of Azerbaijan

The samples of swollen clay soils from the Vilyashchay hydroelectric complex facilities (south of Azerbaijan) and the village of Shirvan (near the city of Sumgait, Azerbaijan) were examined for structural strength ("sensitivity"). Table 1

As can be seen from table 1, the" sensitivity " of Vilyashchay clays to swelling varies from 1.025 to 2.252 increasing with depth. Apparently, this is due to an increase in the degree of weathering from the depth to the mass surface.

Fig. 2 shows a curve of changes in the value of the Vilyashchay clays sensitivity to swelling with the depth of occurrence. This dependence has the pattern of a broken line, although it can be averaged as a linear function.

Table 2 shows the results of testing clay soils in the village of Shirvan on "sensitivity" to swelling.

Table 2 shows that the sensitivity of clay soils in the village of Shirvan to swelling ranges from 1.033 to 2.207 (Fig. 3). In general, the increase in sensitivity in depth is visible, but it is not as clearly expressed as in the Vilyashchay clays.

**Table 1.** Results of testing clay soils in the village of Vilyashchaisky for "sensitivity" to swelling.

| Sampling depth, m | Free swelling in an undisturbed state, $\delta_{s_{unddis.}}$, % | Free swelling in a disturbed state, $\delta_{s_{dis.}}$, % | Sensitivity of clay soils to swelling $K_c$ |
|---|---|---|---|
| 0.5 | 8.0 | 8.2 | 1.025 |
| 1.0 | 10.3 | 12.1 | 1.175 |
| 1.5 | 10.8 | 13.2 | 1.222 |
| 2.0 | 22.3 | 30.1 | 1.350 |
| 2.5 | 24.5 | 43.6 | 1.780 |
| 3.0 | 23.0 | 51.8 | 2.252 |

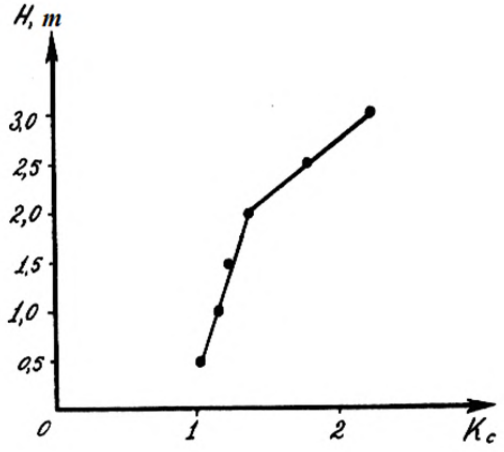



**Fig. 2.** Curve of changes in the value of the Vilyashchay clays sensitivity to swelling with the depth of occurrence.

**Table 2.** Results of testing clay soils in the village of Shirvan for "sensitivity" to swelling.

| Sampling depth, m | Free swelling in an undisturbed state, $\delta_{s_{unddis.}}$, % | Free swelling in a disturbed state, $\delta_{s_{dis.}}$, % | Sensitivity of clay soils to swelling $K_c$ |
|---|---|---|---|
| 1.0 | 3.0 | 3.1 | 1.033 |
| 2.0 | 10.8 | 12.5 | 1.157 |
| 3.0 | 12.4 | 18.2 | 1.469 |
| 4.0 | 12.1 | 22.5 | 1.860 |
| 5.0 | 16.7 | 24.1 | 1.443 |
| 6.0 | 21.0 | 31.8 | 1.515 |
| 7.0 | 20.4 | 43.2 | 2.112 |
| 8.0 | 28.1 | 48.1 | 1.715 |
| 9.0 | 24.1 | 53.2 | 2.207 |
| 10.0 | 26.9 | 55.8 | 2.075 |

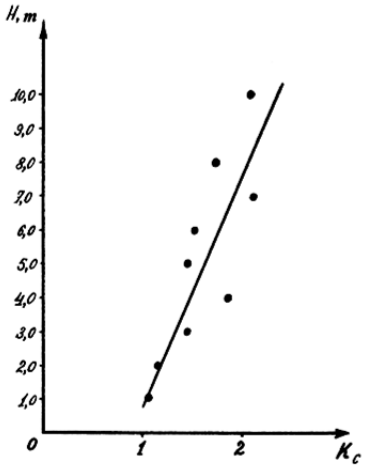



**Fig. 3.** Graph of changes in the "sensitivity" of the Shirvan village clay soils to swelling with depth.

## Conclusion

1. According to our research, the increase in the swelling of clay soils was greatly influenced by the disturbance of not only intra-aggregate bonds, but inter-aggregate bonds, as well.
2. A new technique and device for studying the "sensitivity" of swollen clay soils were developed, which made it possible to study more accurately the swelling of clay soil both in a natural and structurally disturbed state on the same sample, thus helping to increase the accuracy of the test results obtained.
3. Studies of the "sensitivity" of swollen clay soils selected from various regions of Azerbaijan showed that with an increase in the depth of clay soils, their coefficient of influence of structural strength on swelling, i.e., "sensitivity" significantly increased.

## References


1. Gromko G. J., Overview of expansive soils Journal of the Geotechnical Engineering Division (ASCE) 100 (6), 1974, pp. 667–687.
2. Sorochan E. A., Construction of structures on swelling soils. // Moskow, Stroyizdat, 1989.
3. Fityus S. G., Smith D. W. and Allman M. A., Expansive soil test site near Newcastle. // Journal of Geotechnical and Geoenvironmental Engineering (ASCE), 130 (7), 2004, pp. 686–695.
4. Peredelskiy L. V. and Ananiev V. P., Swelling clay soils of the North Caucasus. // Rostov-on-Don: Rostov University Publishing House, 1987.
5. Mustafayev A. A. Foundations on subsiding and swelling soils. // Moskow, High School, 1989.
6. Kulchitskiy L. I. and Usiyarov O. G., Physical and chemical basics of clay soil properties formation. // Moskow, Nedra, 1981.
7. Al-Homond A. S., Basma A. A., Hudein Malkavi A. I. and Al Bashabsheh M. A. Cyclic swelling behavior of clays. // Journal of Geotechnical Engineering (ASCE). 121 (7), 1995, 562 p.
8. Gabibov F. G., Theory and practice of improving properties of structurally unstable clay soils in solving geotechnical and engineering – and – geoecological problems, Baku, Elm, 2011.
9. Day R. W., Expansion potential according to Uniform Building Code. // Journal of Geotechnical Engineering (ASCE), 119 (6), 1993, pp. 1067–1071.
10. Day R. W., Stady of capillary rise and thermal osmosis. // Environmental and Engineering Geoscience, 2 (2), 1996, pp. 249–254.
11. Day R. W., Foundation engineering handbook: Design and construction with the 2009 International Building Code. // New York, McGrav Hill, 2010.
12. Novamooz H., Jahangir E. and Masrouri F., Volume change in behavior of swelling soils compacted at different initial states. // Engineering Geology 153, 2013, pp. 25–34.
13. Cui Y. J., Yahia-aissa M. and Delage P., A model for the volume change behavior of heavily compacted swelling clays. // Engineering Geology 64, 2002, pp. 233–50.
14. Alonso E. E., Romero E., Hoffmann C. and Escudero E. G., Expansive bentonite/sand mixture in cyclic controlled suction drying and wetting. // Engineering Geology, 81, 2005, pp. 213-226.
15. Sun W. J. and Sun D. A., Coupted modeling of hydro-mechanical behavior of unsaturated expansive soils International. // Journal for Numerical and Analytical Methods in Geomechanics 36, 2011, pp. 1002–1022.
16. Schmetmann J. H. 1969 Swell sensitivity. // Geotechnics 19, 4, 1969.
17. Snezhkin B. A. and Ziangirov R. S., Assessment of the structural relationships of clay soils. // Engineering and geological characteristics of soils and processes in them, Moscow, Stroyizdat, 1985, pp. 3–11.

2nd International Scientific Conference "Modern Problems in Geophysics", Proceedings,
ISBN 978-9941-36-562-1, ISSN 3088-4349, Tbilisi, Georgia, October 29-31, 2026

# BIOMASS AND CARBON STOCKS OF ALDER FORESTS IN WESTERN GEORGIA BY TREE FRACTIONS AND GEOPHYSICAL MONITORING PERSPECTIVES WITH AI INTEGRATION

***Tsereteli G., **Aftsiauri B., ***Tiginashvili Z., ****Merabishvili M., *Kakhadze R.**

**Mikheil Sabashvili Institute of Soil Science, Agrochemistry and Reclamation, Agricultural University of Georgia, Tbilisi, Georgia*
***Vasil Gulisashvili Forest Institute, Agricultural University of Georgia, Tbilisi, Georgia*
****Georgian Academy of Agricultural Sciences, Tbilisi, Georgia*
*****Institute of Farming, Agricultural University of Georgia, Tbilisi, Georgia*
*g.tsereteli@agruni.edu.ge*

***Abstract.*** *Forest ecosystems represent one of the most vital components of Georgia's natural environment. According to the First National Forest Inventory, approximately 44.5% of the country's territory is covered by forests. These ecosystems perform numerous ecological functions: regulating water balance, protecting soil from erosion, sequestering atmospheric carbon dioxide, providing habitats for biodiversity, and playing a crucial role in climate regulation. Forests serve as the largest natural carbon reservoir for Georgia.*

*Studies revealed that in the alder forests (Alnus spp.) of Western Georgia, biomass and carbon stocks partitioned by tree fractions are highest in the stem (59.3% and 59.5%, respectively) and lowest in the foliage (1.9% and 1.7%, respectively). Based on the analysis of field and laboratory work conducted in alder forests, conversion factors transforming growing stock volume into biomass of individual stand fractions were established across five age groups. These factors are independent of inventory source materials and remain constant; thus, their application in determining forest biomass and deposited carbon stocks is fully justified.This article discusses the future integration of these data with information obtained through remote sensing and geophysical methods. This integration will enable spatial assessment, modeling, and operational monitoring of biomass and carbon stock dynamics in forest ecosystems under climate change using Artificial Intelligence (AI).*

***Key words:*** *Stem, Branch, Conversion Factor, Remote Sensing, AI.*

## Introduction and Methodology

Today, the global community faces critical tasks: the rational use of natural resources, assessing economic impacts on the environment and pollution, evaluating anthropogenic footprints, and maintaining biological equilibrium [1]. Consequently, the rational management of forest resources is an essential objective.

One of the key indicators of forest productivity is the dynamics of biomass accumulation over time. Individual trees or stands accumulate varying amounts of biomass (stem, branches, leaves, roots) across developmental stages due to environmental factors and species-specific biological growth potential [2].

In forest communities, biomass and carbon stocks are evaluated using the conversion-volume method [3, 4]. The biomass expansion factor (conversion-volume ratio) represents the ratio of biomass (B-t/ha) of an individual forest fraction (stem, branch, leaf, root) to the stem wood volume with bark (M-$m^3$/ha). This method relies directly on forest inventory data.

Because a comprehensive database of biomass fractions for individual tree species in Georgia is currently lacking, stem and crown biomass (branches and foliage) were calculated using volumetric/merchantable assessment tables [5], which provide percentage proportions of branch and foliage volume relative to stem volume. This methodology aligns with modern international standards, basing biomass estimation on forest inventory (taxation) metrics and allometric relationships. Belowground (root) biomass was calculated in accordance with the guidelines for greenhouse gas inventories [6] and recommendations on the state of the world's forests [7].

Currently, Artificial Intelligence (AI) is transforming forestry by enabling more efficient and precise resource management. AI-driven tools, such as remote sensing technologies and Geographic Information Sys-

tems (GIS), allow real-time monitoring and analysis of forest health, biodiversity, and biomass. The integration of 3D data in forestry revolutionizes forest management through enhanced visualization, improved data accuracy, and better communication among stakeholders.

Because 3D data are frequently paired with AI algorithms, this combination enhances processing precision across various applications, including tree species identification, forest mapping, and biomass estimation. Research evaluating data collection methods and digital 3D data highlights a growing trend in their application within forestry, underscoring significant potential to improve stakeholder communication [8].

## Results and Discussion

The total area of alder forests in Western Georgia is 112,530 ha, with a total standing volume of 8,671.1 thousand $m^3$. To investigate these ecosystems, 27 sample plots were selected in pure alder stands of Western Georgia (covering a total area of 17,545 ha, with a wood volume of 1,001.4 thousand $m^3$).

The study was conducted using height-class volume tables for tree species [5]. In the absence of local standing volume data, applying recommendations from greenhouse gas inventory handbooks [9] and general guidelines [6] is deemed appropriate.

The total biomass and stored carbon within individual forest fractions depend on stand age, timber volume, and crown canopy closure. Biomass and carbon stocks of Western Georgia's alder forests were evaluated by age groups and tree fractions (Table 1).

**Table 1.** Biomass and carbon stocks of alder forests in Western Georgia by age groups and tree fractions in (B/C, thousand tons).

| **Age Group, Duration (years)** | **Total Area (ha) / Volume (thousand $m^3$)** | **Fractions**, B/C | | | | |
|---|---|---|---|---|---|---|
| | | Stem | Branch | Leaf | Root | Total |
| Young, 1-20 | 28 973 | 461.07 | 128.66 | 22.76 | 253.62 | 866.11 |
| | 1 030.1 | 230.54 | 64.33 | 10.24 | 126.81 | 431.92 |
| Biomass (%) | | 53.2 | 14.9 | 2.6 | 29.3 | 100.0 |
| Middle-aged, 21-30 | 34 181 | 966.31 | 266.72 | 27.40 | 406.76 | 1 667.19 |
| | 2 157.9 | 483.15 | 133.36 | 12.33 | 203.38 | 832.22 |
| Biomass (%) | | 58.0 | 16.0 | 1.6 | 24.4 | 100.0 |
| Ripening, 31-40 | 22 897 | 895.76 | 241.79 | 35.80 | 318.58 | 1 491.93 |
| | 1 999.9 | 447.88 | 120.89 | 16.11 | 159.29 | 744.17 |
| Biomass (%) | | 60.0 | 16.2 | 2.4 | 21.4 | 100.0 |
| Mature, 41-60 | 19 606 | 1 092.02 | 289.52 | 26.08 | 359.21 | 1 766.83 |
| | 2 437.0 | 546.01 | 144.76 | 11.73 | 179.61 | 882.11 |
| Biomass (%) | | 61.8 | 16.4 | 1.5 | 20.3 | 100.0 |
| Older than mature, 61 and > | 6 873 | 469.12 | 120.10 | 11.19 | 153.16 | 753.57 |
| | 1 046.2 | 234.56 | 60.05 | 5.04 | 76.58 | 376.23 |
| Biomass (%) | | 62.3 | 15.9 | 1.5 | 20.3 | 100.0 |
| **Total for Western Georgia** | **112 530** | **3 884.28** | **1 046.79** | **123.23** | **1 491.33** | **6 545.63** |
| | **8 671.1** | **1 942.14** | **523.39** | **55.45** | **745.67** | **3 266.65** |
| Biomass **B (%)** | | **59.3** | **16.0** | **1.9** | **22.8** | **100** |
| Carbon **C (%)** | | **59.5** | **16.0** | **1.7** | **22.8** | **100** |

In young alder stands of Western Georgia, stem biomass constitutes 53.2% of the total biomass. In middle-aged stands, this share increases by approximately 5% compared to young stands. In subsequent age classes, stem biomass proportion increases by around 2%. The proportion of branch biomass relative to total biomass also increases, from 14.9% in young stands to 15.9% in overmature stands. Conversely, the relative proportions of foliage and root biomass/carbon are highest in young stands (2.6% for foliage, 29.3% for

roots) and drop noticeably in older age classes (down to 1.5% for foliage and 20.3% for roots). The percentage distribution of carbon stocks follows a nearly identical pattern to that of biomass.

In evaluating carbon stocks within forest biocenoses, the primary aim was to establish a practical and reliable approach. We adopted the conversion factors developed by D. Zamolodchikov, A. Utkin, and O. Chestnykh [10], which convert standing timber volume into biomass (conversion-volume ratios).

Based on extensive field and laboratory analyses conducted across alder forests in Western Georgia, age-specific biomass conversion factors were derived for all five age groups of *Alnus* spp. (Table 2).

These conversion factors allow for the determination of total forest biomass and accumulated carbon stocks across age categories directly during forest inventory processes. Because these ratios are independent of changing inventory raw materials, they remain constant, providing a fully justified framework for biomass and carbon accounting.

**Table 2.** Conversion coefficients for Alder Forests in Georgia B/M ($t.m^3$).

| **Age Group** | **Total Ratio** | Fractions, Biomass/Timber stock, $t/m^3$ | | | |
|---|---|---|---|---|---|
| | | Stem | Branch | Leaf | Root |
| Young | 0.8408 | 0.4476 | 0.1249 | 0.0221 | 0.2462 |
| Middle-Aged | 0.7726 | 0.4478 | 0.1236 | 0.0127 | 0.1885 |
| Ripening | 0.7460 | 0.4479 | 0.1209 | 0.0179 | 0.1593 |
| Mature | 0.7250 | 0.4481 | 0.1188 | 0.0107 | 0.1474 |
| Older than mature | 0.7203 | 0.4484 | 0.1148 | 0.0107 | 0.1464 |

To convert biomass stocks into carbon stocks, guidelines from the Intergovernmental Panel on Climate Change (IPCC) [6] recommend multiplying the derived stand biomass estimates by a carbon conversion factor of 0.48.

## Conclusion and Future Perspectives

The empirical data on biomass, sequestered carbon, and conversion factors established in this study provide essential baseline metrics for long-term monitoring of Georgian forests. Future work should prioritize integrating these ground-based datasets with remote sensing and geophysical data. Such integration will facilitate spatial modeling, precise mapping of biomass and carbon stocks, and prompt monitoring of forest ecosystem dynamics under climate change scenarios using Artificial Intelligence (AI).

Traditional forest taxation (inventory) and modern geophysical methods are inherently complementary. Inventory data ensure high local accuracy and calibration capability for predictive models, while geophysical and remote sensing methods enable broad spatial extrapolation and periodic monitoring. This synergy forms the core foundation upon which future spatial monitoring architectures should be constructed, ultimately increasing the precision of carbon accounting across Georgia's forest ecosystems.

## References


1. Babunashvili G., & Khutashvili M., General Ecology and Environmental Protection. // TSU, Tbilisi, 2003, 235 p. (In Georgian)
2. Gigauri G., Forest Biodiversity of Georgia. // Tbilisi, 2000, 159 p. (In Georgian)
3. Zamolodchikov D. G., Utkin A. I., & Korovin G. N., Determination of carbon stocks by age-dependent conversion//volume coefficients. // Lesovedenie, 3, 1998, pp. 84–93. (In Russian)
4. Utkin A. I., Zamolodchikov D. G. & Pryazhnikov A. A., Methods for determining carbon sequestration in phytomass and net primary productivity of forests//(on the example of the Republic of Belarus). // Lesovedenie, 1, 2003, pp. 48–57. (In Russian)
5. Gigauri G. N. & Dzebisasvili G. S., Handbook: Assortment and Commodity Tables for Main Forest-Forming Species of Mountain Forests of the USSR. // Agropromizdat, Moscow, 1990, 312 p. (In Russian)
6. Guidelines of National Inventorying of Greenhouse Gases, IPCC, Chapter 4, forest areas, 4, 89, 2006, pp. 1-4.
7. Global Forest Resources Assessment 2010: Main Report. FAO Forestry Paper 163, Rome, 2011, 340 pp. (In Russian)
8. Kuzmenko M., AI for Forests*:* Monitoring & 3D Data. // LinkedIn Pulse. 2024. https://www.linkedin.com/pulse/ai-forestry-log-detection-tracking-maryna-kuzmenko-ph-d-jefme.
9. Good Practice Guidance for Land Use, Land-Use Change and Forestry (GPG-LULUCF). IPCC, Chapter 3, 3, 199, 2003, pp. 1–3.
10. Zamolodchikov D. G., Utkin A. I., & Chestnykh O. V., Conversion factors of stand volume to phytomass for major forest-forming species of Russia. //Siberian State Technological University, 2003, pp. 119–127. (In Russian)

2nd International Scientific Conference "Modern Problems in Geophysics", Proceedings,
ISBN 978-9941-36-562-1, ISSN 3088-4349, Tbilisi, Georgia, October 29-31, 2026

# FROM SOIL VARIABILITY TO FOOD-CHAIN ASSESSMENT: A FRAMEWORK FOR $^{137}$CS RESEARCH IN GEORGIA

***, ****Uchaneishvili S., **Gunia N., **Avalishvili A., **, ****Kalmakhelidze S., **Ivanishvili N., **Gogebashvili M.**

** Ivane Beritashvili Center of Experimental Biomedicine, Laboratory of Biophysics, Tbilisi, Georgia*
*** Ivane Beritashvili Center of Experimental Biomedicine, Laboratory of Radiation safety Problems, Tbilisi, Georgia*
****Tbilisi State Medical University, Tbilisi, Georgia*
*****International Black Sea University, Tbilisi, Georgia*
*sofiauchaneishvili@gmail.com*

***Abstract.*** *Radiological contamination may affect agriculture far beyond the release site. This study integrates Georgian radioecological, soil, agrochemical and agricultural evidence to identify contrasting agroecosystems for future $^{137}$Cs soil-to-plant-to-food transfer research. The study considers contrasting radioecological environments representative of Georgia. The framework links spatial prioritization with local validation in edible products and subsequent dietary-exposure, dose and preparedness assessment.*

***Key words****: $^{137}$Cs; soil–plant transfer; agroecosystems; exchangeable potassium.*

## Introduction

Growing energy demand and the continuing role of nuclear power reinforce the importance of radiological preparedness as an environmental and public-health responsibility. Importantly, this responsibility extends beyond countries operating nuclear facilities, because the consequences of a radiological release are not necessarily confined by national borders. Atmospheric transport and deposition are inherently transboundary processes, as demonstrated by the widespread distribution of radionuclides following the Chernobyl accident. The European Atlas of Caesium. Deposition after the Chornobyl Accident subsequently integrated monitoring data from across Europe to provide a coherent spatial representation of $^{137}$Cs deposition [1]. This experience demonstrated both the geographic scale of transboundary contamination and the importance of harmonised environmental monitoring and spatial evidence integration. For Georgia, situated within the South Caucasus–Black Sea region, the capacity to assess the possible consequences of transboundary radiological contamination is therefore relevant to environmental, agricultural and public-health preparedness.

For terrestrial contamination, deposition represents only the beginning of a longer pathway: deposition → soil retention and availability → plant uptake → edible agricultural product → food exposure→ human dose. $^{137}$Cs is particularly informative as a model radionuclide because of its approximately 30-year half-life, persistence in terrestrial environments and potential involvement in soil–plant–food-chain transfer. Exchangeable potassium is important because of the chemical relationship between K and Cs, but K alone cannot predict plant uptake. Soil mineralogy and fixation capacity, pH, competing ions, management and crop biology may also influence radiocaesium availability and transfer [2].

Georgia has an important but still limited radioecological evidence base. Earlier national studies demonstrated substantial differences in $^{137}$Cs behaviour among major Georgian soil types, including distinctive behaviour in western yellow podzolic soils associated with their mineralogical characteristics and comparatively lower non-exchangeable fixation [3]. Subsequent experimental work investigated radionuclide migration in soil and the potential influence of soil amendments on its movement [4]. Importantly, radionuclide transfer in grapevine has also been studied: radiocaesium uptake into vegetative organs of Vitis vinifera was examined in relation to its distribution within the soil profile, providing direct Georgian evidence connecting soil

contamination conditions with transfer into the vine [5]. Together, these studies establish a valuable national foundation spanning soil behaviour, migration and plant uptake. The next step is to link contrasting Georgian soil and agrochemical environments with $^{137}Cs$ transfer into edible crop components and subsequently with potential dietary exposure.

International experience provides an indispensable methodological reference, but not a ready-made Georgian solution. Evidence from Chornobyl-affected countries demonstrated that agricultural consequences depend not only on deposition, but also on radionuclide transfer through soil–plant–food pathways and agricultural countermeasures [6]. Post-Fukushima studies further developed this approach. In eastern Japan, Takata et al. integrated radioactive Cs measurements from 3,461 agricultural fields with soil group, land use, field characteristics and cultivated crops to support spatial interpretation of agricultural contamination [7]. Japanese crop-oriented studies subsequently demonstrated substantial variability in soil-to-crop transfer. In soybean fields, exchangeable K and radiocaesium interception potential were important determinants of $^{137}Cs$ transfer [8], while studies of Fukushima soils with contrasting parent materials further demonstrated the influence of mineralogical characteristics, K status and Cs-fixation capacity on phytoavailability [9]. These findings show why spatial information should be connected with locally measured soil properties and crop-specific transfer. International evidence should therefore inform, rather than substitute for, Georgian validation.

Accordingly, this study integrates Georgian radioecological, soil, agrochemical and agricultural evidence to identify contrasting agroecosystems for locally validated $^{137}Cs$ soil-to-food transfer research and subsequent exposure and preparedness assessment.

## Materials and Methods

An integrative, hypothesis-generating approach was used to combine four evidence domains: published Georgian radioecological research; information on Georgian soil types; spatial information on exchangeable K and soil reaction (pH); and agricultural evidence, including wine-growing geography. International post-accident evidence was used to identify variables relevant to soil-to-plant $^{137}Cs$ transfer and to inform the conceptual design of subsequent Georgian studies.

The spatial component was designed for exploratory research prioritisation rather than reconstruction of current contamination. Soil type, exchangeable K and pH were cross-compared with agricultural context to identify environmentally contrasting systems in which future transfer measurements could be most informative (Fig. 1). The framework was restricted to $^{137}Cs$ because spatially interpretable exchangeable-K information was available, whereas a comparable spatial dataset for exchangeable Ca, relevant to soil-to-plant $^{90}Sr$ transfer, was not available; $CaCO_3$ was not treated as a substitute for exchangeable Ca.

Because the available maps differ in scale, spatial resolution and source characteristics, candidate areas represent broad research-prioritisation environments requiring field verification rather than exact sampling polygons or radiological-risk zones.

## Results and Discussion

### *From soil variability to contrasting research environments*

Integration of the available evidence demonstrates pronounced spatial heterogeneity in soil and agrochemical conditions relevant to future $^{137}Cs$ transfer research. The purpose is not to designate presumed contamination, but to identify contrasting soil–crop environments in which the influence of local soil characteristics on transfer can subsequently be tested.

Grapevine provides a particularly useful first comparative system because the same perennial crop occurs across markedly different Georgian agroecological environments. Kakheti, Imereti and Samegrelo provide broad eastern, intermediate-western and humid-western environments for field verification of contrasting soil type, exchangeable K and pH. These three environments were selected by visual cross-comparison of the soil-type, exchangeable-K, pH, and wine-growing maps, identifying areas where the same crop occurs under contrasting combinations of the mapped soil and agrochemical conditions. Their value therefore lies in the contrast created by overlaying independent lines of spatial evidence, rather than in any indication of present radiological contamination. Existing Georgian evidence of radiocaesium uptake in

grapevine [5] strengthens this choice. The next scientific question is therefore not simply whether radiocaesium can enter the vine, but how transfer varies among contrasting Georgian soil environments and how this behaviour relates to the edible fruit.

The broader framework may subsequently be extended to additional agriculturally relevant soil–crop combinations, including maize in western yellow-podzolic settings, potato in highland environments and wheat in eastern agricultural landscapes. These systems provide annual/perennial and grain/fruit/tuber contrasts and represent contrast-based research design rather than a ranking of radiological risk.

### *From spatial prioritisation to food-chain assessment*

Soil type, exchangeable K, pH and agricultural distribution can guide selection of representative environments, but cannot predict $^{137}$Cs concentrations in edible products. The critical missing link is locally validated transfer from soil to the consumed plant component – fruit, grain or tuber. For grapevine, this means extending existing Georgian evidence on vegetative uptake toward comparative assessment of transfer into edible fruit under contrasting, locally verified soil conditions.

Thus, the research sequence is: existing Georgian radioecological evidence → spatial integration of soil and agricultural context → contrasting soil–crop–edible-part systems → locally validated transfer → agricultural production and food-consumption data → dietary exposure → dose assessment.

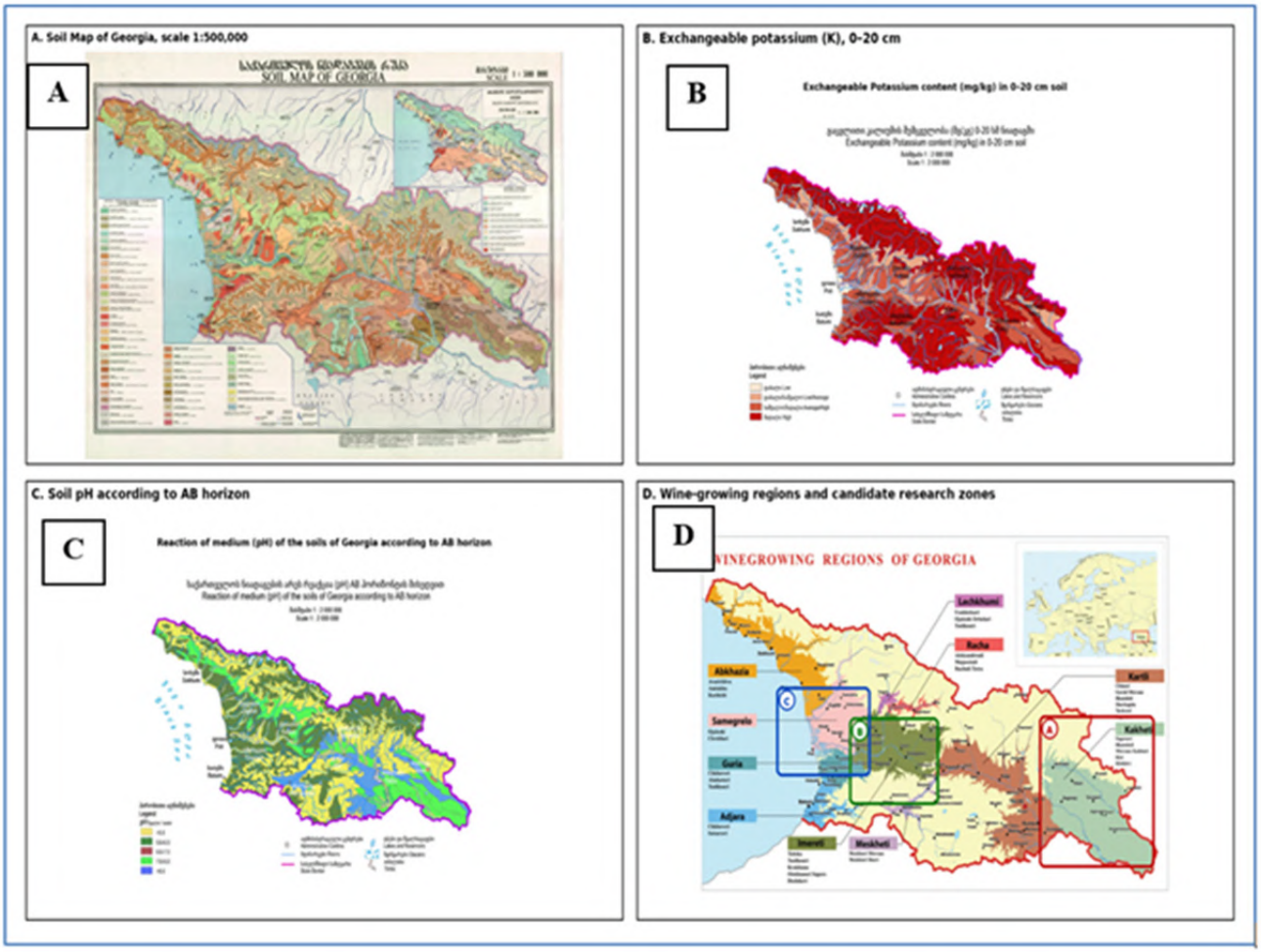



**Fig. 1.** Spatial evidence and contrasting wine-growing environments for future $^{137}$Cs transfer research in Georgia.

Spatial evidence used for exploratory identification of contrasting Georgian agroecosystems for future $^{137}$Cs soil-to-food transfer research. (A) Soil Map of Georgia, 1:500,000; (B) exchangeable K, 0–20 cm; (C) soil pH according to the AB horizon; (D) wine-growing regions and broad candidate environments. Candidate areas are research-prioritisation environments, not current contamination or radiological-risk zones.

Sources: Panel A – Soil Map of Georgia, 1:500,000, T. Urushadze, Joint-Stock Company "Cartography", European Soil Data Centre (ESDAC/JRC), https://esdac.jrc.ec.europa.eu/content/soil-map-georgia. Panels B-C – National Soil Atlas of Georgia; [10]. Panel D – Wines of Georgia, Regions & Appellations, https://www.winesgeorgia.com/appellations/.

This sequence is inherently interdisciplinary: soil science characterises retention and availability; agronomy defines crop and management context; radioecology quantifies transfer; production and consumption data establish potential intake; and dose assessment translates environmental and food-chain measurements into information relevant to human protection. Future integrated modelling should follow, rather than precede, local validation. Once representative Georgian transfer, production and consumption parameters are available, modelling environments such as ARAMS/FRAMES may be evaluated for integrating contaminant fate, food-chain exposure and dose-assessment components.

## Conclusions

Georgia has a valuable but still insufficient radioecological evidence base for comprehensive assessment of radionuclide behaviour across its diverse agroecosystems. Existing national research provides important evidence on $^{137}$Cs behaviour in soils, radionuclide migration and uptake into plants, including grapevine. The principal unresolved step is systematic connection of these environmental observations with locally validated transfer into edible agricultural products.

The present framework converts this evidence gap into a defined research strategy. Integration of soil type, exchangeable K, pH and agricultural context can identify contrasting Georgian soil–crop systems for field verification without interpreting them as currently contaminated or at elevated radiological risk. The immediate scientific priority is local validation of $^{137}$Cs transfer from contrasting Georgian soils to edible crop components.

Connecting these measurements with agricultural production and food-consumption data would provide the evidence required for subsequent dietary-exposure and dose assessment and, ultimately, support evidence-based agricultural monitoring and radiological preparedness focused on protection of population health.

## References


1. De Cort M., Dubois G., Fridman Sh.D., et al., Atlas of Caesium Deposition on Europe after the Chernobyl Accident. Luxembourg: Office for Official Publications of the European Communities, 1998. 130 p.
2. International Atomic Energy Agency. Handbook of Parameter Values for the Prediction of Radionuclide Transfer in Terrestrial and Freshwater Environments. Technical Reports Series No. 472. Vienna: International Atomic Energy Agency, 2010. 194 p.
3. Urushadze T.F., Manakhov D.V., Radioactive contamination of the soils of Georgia, // Annals of Agrarian Science. Tbilisi, 15(3), 2017, pp. 375–379.
4. Gogebashvili M.E., Gongadze A.D., Tulashvili E.V., Ivanishvili N.I., Osidze I.G., Kiparoidze S.A. Reducing the Depth Migration of Radionuclides by Incorporation Organic and Inorganic Components into the Soil // Annals of Agrarian Science. Tbilisi; 2020; 18(2): pp. 201–205.
5. Ivanishvili N., Gongadze A., Kalmakhelidze S., Tulashvili E., Gogebashvili M., Study of the radionuclide absorption into the vegetative organs of grapes to increase the efficiency of soil mechanical decontamination. // Radiobiology and Radiation Safety. Tbilisi, 4(5), 2024, pp. 73–78.
6. Fesenko S.V., Alexakhin R.M., Balonov M.I., et al., An extended critical review of twenty years of countermeasures used in agriculture after the Chernobyl accident. // Science of the Total Environment. Amsterdam, 383(1–3), 2007, pp. 1–24.
7. Takata Y., Kohyama K., Obara H., Maejima Y., Ishitsuka N., Saito T., Taniyama I. Spatial prediction of radioactive Cs concentration in agricultural soil in eastern Japan. // Soil Science and Plant Nutrition. 60(3), 2014, pp. 393–403.
8. Takeda A., Tsukada H., Yamaguchi N., Takeuchi M., Sato M., Nakao A., Hisamatsu S., Relationship between the radiocesium interception potential and the transfer of radiocesium from soil to soybean cultivated in 2011 in Fukushima Prefecture, Japan. // Journal of Environmental Radioactivity, 137, 2014, pp. 119–124.
9. Ogasawara S., Eguchi T., Nakao A., Fujimura S., Takahashi Y., Matsunami H., Tsukada H., Yanai J., Shinano T., Phytoavailability of $^{137}$Cs and stable Cs in soils from different parent materials in Fukushima, Japan. // Journal of Environmental Radioactivity, 198, 2019, pp. 117–125.
10. Urushadze T., Kvesitadze G. (Eds.), National Soil Atlas of Georgia. Tbilisi, 2019, 216 p.

2nd International Scientific Conference "Modern Problems in Geophysics", Proceedings,
ISBN 978-9941-36-562-1, ISSN 3088-4349, Tbilisi, Georgia, October 29-31, 2026

# DEVELOPMENT OF AN ATMOSPHERIC AIR POLLUTION MAP FOR VLADIKAVKAZ USING GIS TECHNOLOGIES

**Burdzieva O. G., Kanukov A. S., Korbesova K. V., Arkhireeva I. G., Dadteeva E. V.**

*Geophysical Institute of the Vladikavkaz Scientific Center, Russian Academy of Sciences,*
*Vladikavkaz, North Ossetia, Russian Federation*
*vzaal@mail.ru, cgi_ras@mail.ru*

***Abstract.*** *The article discusses spatial interpolation methods used for mapping atmospheric air and soil pollution, including inverse distance weighting (IDW), kriging, and radial basis functions (RBF). A comparative analysis of the accuracy and limitations of these methods is carried out, with special attention paid to their smoothing effect, which leads to underestimation of local maxima and overestimation of minima, thereby significantly affecting the identification of contaminated areas. A new integral indicator of atmospheric air pollution, $Z_{atm}$, is proposed, which takes into account the exceedance of pollutant concentrations over maximum permissible concentrations. Based on the integral indicator $Z_{atm}$, a map of the spatial distribution of air pollution in Vladikavkaz was constructed for the first time, which made it possible to identify the most unfavorable zones.*

***Key words:*** *Geoecology, spatial interpolation, atmospheric air pollution, integral pollution indicator, mapping.*

In recent years, there has been a significant increase in the population, which corresponds to the accelerated rates of industrialization. This is accompanied by more and more significant environmental pollution, which poses a serious threat to public health [1]. Factors affecting the state of the natural environment in high-altitude conditions are of a priority importance due to special features of the landscape, territorial and geographical plan. Mining and processing waste disposed in cramped conditions creates an environmentally tense situation in the regions and contributes to the degradation of the natural environment [2]. The geoecological capacity of the mountain system biospheres is limited in comparison with flat areas, so technogenic intervention in the mountain landscape system requires a balanced approach.

The most important part of modern life is transportation. The economic development of all regions is based on people's access to goods and services provided by modern transport infrastructure. Road transport is the main method of transportation of goods and population. At the same time, the positive aspects of transport use are closely related to environmental pollution.

Studies conducted in recent decades indicate that air pollution has a significant negative impact on health, and transport is one of the most important sources of pollution [3]. Road traffic is the largest source of emissions of many harmful air pollutants, such as carbon monoxide, nitrogen oxides, benzene and primary PM10 (particles of various substances with a diameter of 10 microns or less).

The accuracy of maps of the spatial distribution of pollutants is crucial for risk management [4]. Pollutants always exhibit considerable spatial variability in distribution.

The classical statistical methods typically require that data satisfy a number of assumptions: the independence of observations from each other, the exact or approximate normality of observations, and a large and repeated sample. Given the cost of sampling and analyzing soil and atmospheric air samples, dense and repeated sampling is usually impractical. Mapping the spatial distribution of soil contamination requires spatial interpolation techniques. Consequently, interpolation methods such as Inverse Distance Weighting (IDW), kriging, and spline are widely used in pollution mapping [5].

The accuracy of the interpolation is related to the precise determination of the contaminated territory and its boundaries. Therefore, this directly affects the accuracy of the pollution assessment. There are many studies of the effectiveness of the spatial interpolation methods mentioned above, but the results are not unambiguous [6].

Research on heavy metal contamination, for example, focuses on identifying areas with high pollution risk. Samples from areas with a high risk of pollution are usually local spatial outliers [7]. All interpolation methods have a smoothing effect that underestimates local high values and overestimates local low values. It is important to minimize the systematic error in the estimation of pollution caused by interpolation methods, and to understand the uncertainty in the estimation of pollution caused by interpolation error and the differences in the estimation of pollution between different interpolation methods.

One of the interpolation methods, kriging, is based on the assumption that the interpolated parameter can be considered as a regionalized variable. As with IDW, the kriging estimate is given by a linear combination of observed values with weights. Depending on the stochastic properties of random fields, different types of kriging are applied. The kriging type determines the linear constraint on the weights implied by the unbiased condition. Kriging weights are derived from the kriging equations using the semivariance function. The parameters of the semivariance function can be estimated using the empirical semivariance function [8]. The unbiased estimate of the semivariance function is equal to half the mean squared difference between the values of the paired data:

$$\gamma(p) = \frac{1}{2N(h)} \sum_{i=1}^{N(h)} [z(x_i) - z(x_i + h)]^2 \tag{1}$$

where $\gamma(h)$ is the semivariance value over the distance interval $h$, and $N(h)$ is the number of pairs of samples in the distance interval $h$, $z(x_i + h)$ and $z(x_i)$ are the sample values at two points separated by the distance interval $h$.

The next type of interpolator – radial basis functions (RBFs) – is the name given to a large family of exact interpolators that use a basic equation that depends on the distance between the interpolated point and the sample points [8]. The value of the RBF forecast can be expressed as the sum of two components:

$$Z(x) = \sum_{i=1}^{m} a_i f_i(x) + \sum_{j=1}^{n} b_j \psi(d_j) \tag{2}$$

where $\psi(d_j)$ shows the radial basis functions, and $d_j$ is the distance from the sampling location to the prediction point $x$, and $f_i(x)$ is the trend function, a basis term for the space of polynomials of degree $<m$. The coefficients $a_i$ and $b_j$ are calculated by solving the following system *of* $n + m$ linear equations; $n$ is the total number of known points used in the interpolation.

Polynomial interpolation is the process of finding a formula (often a polynomial) whose graph will pass through a given set of points. The global polynomial interpolation corresponds to the entire surface polynomial, while the local polynomial interpolation can be considered as a combination of the global polynomial methods and the moving average procedure. Instead of fitting the polynomial to the entire data set, it is fitted to a local subset defined by the window, as in the moving average model. This window should be large enough to include a reasonable number of data points in the process.

Given that the interpolation methods discussed in this article lead to almost identical results, we used the inverse distance weighting method (IDW) as an interpolation method, which is based on the assumption that the forecasts are a linear combination of available data. Interpolating function:

$$\begin{aligned} Z(x) &= \sum_{i=1}^{n} w_i z_i \Big/ \sum_{i=1}^{n} w_i, \\ w_i &= d_i^{-u} \end{aligned} \tag{3}$$

where $Z(x)$ is the predicted value at the interpolated point, $Z_i$ is the value at the known point, $n$ is the total number of known points used in the interpolation, $d_i$ is the distance between point $i$ and the prediction point, and $w_i$ is the weight assigned to point $i$. A higher weight value is assigned to values close to an interpolated point. As the distance increases, the weight decreases [9], and $u$ is the weighting power, which determines how the weight decreases with increasing distance.

Interpolation methods determine how discrete sample data is transformed into a continuous map. The accuracy of the interpolation depends on how well this interpolation method reflects the spatial variation and

correlation of soil characteristics [9]. Kriging quantifies the spatial autocorrelation between measured points and takes into account the spatial configuration of sample points around the predicted location. Hence, ordinary kriging provides the best linear unbiased estimate. In practice, it is very difficult to obtain an ideal variogram with a small sample size [9]. Kriging is a low-pass filter that smooths out local detailed information (extreme values). In the region of high variability, which has a weak spatial correlation, the smoothing effect of kriging is much stronger [5]. As a result, local maxima are usually underestimated, and the area of contamination is probably underestimated.

The polynomial is not usually used as an interpolator, but is used to determine trends and patterns in data. The interpolated surface is very smooth, which gives detailed information that exists in the smoothed local area. IDW and RBF are exact interpolators that predict a value that is identical to the measured value at the selected location. Local peaks (maxima) or troughs are reserved on the outer surface. While IDW creates a surface from the measured samples based on the degree of similarity, RBF is based on the degree of smoothing [8]. RBFs can predict values above the maximum and below the minimum measured values. However, the maximum and minimum values on an interpolated surface using IDW can only occur at sample points. IDW is very sensitive to the power of the weighting factors, which controls their decrease as the distance from the prediction site increases. The higher the power, the smaller the impact of samples that are far from the prediction location during interpolation. As the weighting power increases, the forecast value approaches the value of the nearest sample.

IDW and RBF are convenient to use because they use fewer input parameters, while kriging is harder to use. Typically, kriging interpolation involves the following steps: statistical test, data transformation and inverse transformation, spatial structure analysis, fitting the semivariance function, and so on. The selection of the semivariance function is subjective, and different researchers may get different results.

The accuracy of interpolation is a relative concept, and the criteria change for the purpose of interpolation. The main two goals of soil pollution mapping are to analyze the spatial pattern of soil pollution and identify contaminated areas. In order to analyze the spatial structure of pollution, the result of predicting the overall spatial trend of pollutants in the atmospheric air should be as accurate as possible. There is no doubt that kriging has the best ability to predict the overall trend of atmospheric pollution. However, in order to identify contaminated areas, interpolation methods are necessary for more accurate prediction of local features of atmospheric pollution, especially local foci of pollution. Local maxima are likely to be smoothed out by kriging.

Obviously, all the interpolation results contain errors. Identification of a region as contaminated should not be based solely on the results of interpolation. It is suggested to consider the natural background and human activity before making a decision [10]. To get a more reliable pollution estimate, you can add more samples from the area of uncertainty of the pollution estimate. The uncertainty of the pollution assessment is mainly in the region of high local variations, so additional sampling in the area of uncertainty is recommended.

To assess atmospheric air pollution, we proposed to introduce the integral indicator $Z_{atm}$, calculated as the sum of the ratios of the concentration of individual pollutants to the MPC values, minus the number of indicators used minus one:

$$Z_{atm} = \sum_{i=1}^{n} \frac{C_i}{C_{MPIi}} - (n-1), \tag{4}$$

where $C_i$ is the concentration of the i-th pollutant in the atmosphere, and $C_{MPIi}$ is the value of the MPC of the i-th pollutant.

For the introduced integral indicator $Z_{atm}$, we developed a new assessment scale for the categories of atmospheric air pollution. Let the concentration of each indicator taken into account be equal to the maximum permissible concentration (MPC), then, according to the definition of the developed integral indicator, the hazard level will be 1. Exceedance of one of the indicators will increase this value even more. Accordingly, the value of one unit must be determined as acceptable. In this case, by analogy with the Zc indicator, the levels of exposure to the human body will be determined as follows: acceptable – less than 1; moderately dangerous-1-2; dangerous-2-8; extremely dangerous-more than 8.

Fig. 1 shows a map of the spatial distribution of the values of the developed indicator of atmospheric air pollution for the territory of Vladikavkaz.

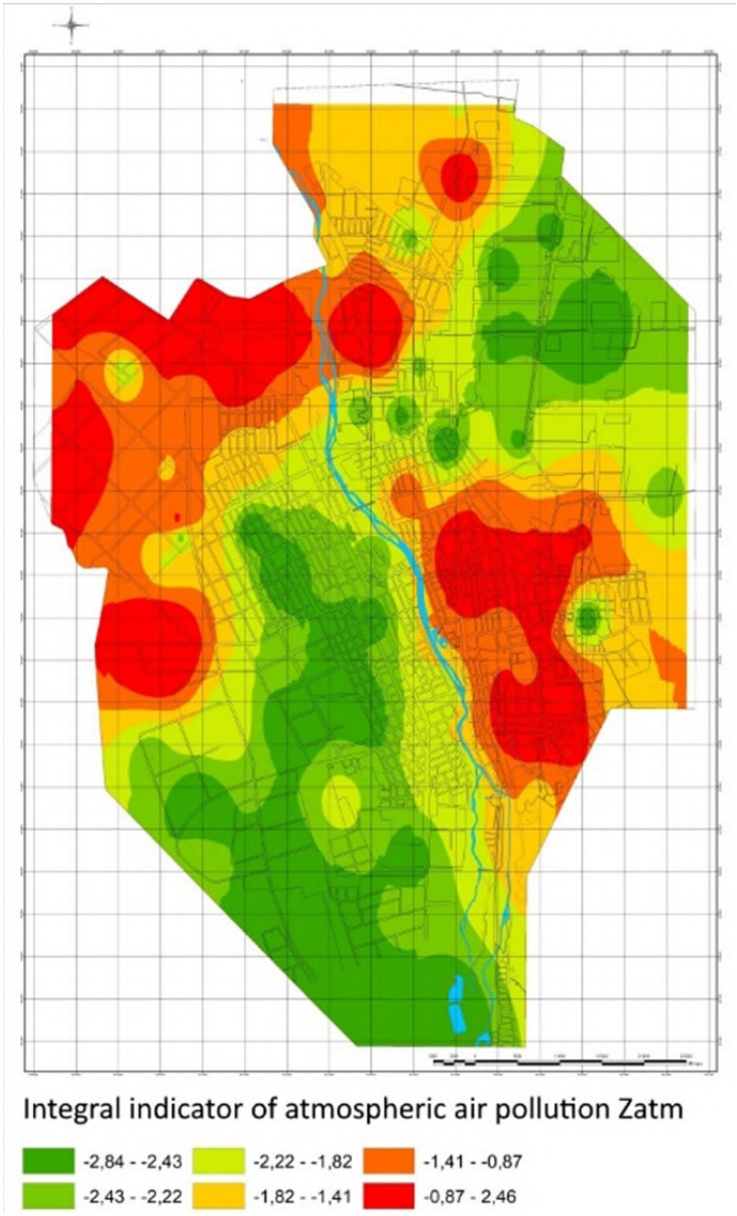



**Fig. 1.** Map of values of the integral indicator of atmospheric air pollution $Z_{atm}$ for Vladikavkaz.

Although most zones are considered acceptable in terms of the level of human exposure, this approach allowed nevertheless made it possible to identify the most unfavorable places. To refine the values of the integral indicator, it is necessary to conduct additional studies on the content of other pollutants in the atmospheric air. The following road sections that are most polluted are highlighted on the map: the main entrances and exits from the city from the Arkhonskaya station, Gizel village, Chermenskiy Krug, as well as the central (historical) part of the city. The pollution of the central part is evidently associated with the narrow width of the roadways in the historical part, poor ventilation and high traffic level on the roads.

## Conclusions

Mapping the spatial distribution of soil pollution requires spatial interpolation techniques.

Interpolation methods such as Inverse Distance Weighting (IDW), kriging (OK), and spline are widely used in soil studies and pollution mapping.

All interpolation methods have a smoothing effect that underestimates local high values and overestimates local low values. Interpolation accuracy is a relative concept, and the criteria vary with the purpose of interpolation.

The main two goals of soil pollution mapping are to analyze the spatial pattern of soil pollution and identify contaminated areas. Identification of a region as contaminated should not be based solely on the re-

sults of interpolation. It is suggested to consider the natural background and human activity before making a decision.

For the first time, maps of atmospheric air pollution by road transport have been constructed for the territory of Vladikavkaz using the proposed $Z_{atm}$ indicator, with the identification of the most unfavorable zones.

**Acknowledgements:** The work was carried in the framework of the state assignment of the Geophysical Institute of the VNC RAS, reg. No. 125022802998-8.

## References:

1. Zaalishvili V.B., Beriev O.G., Burdzieva O.G., Zaks T.V., Kanukov A.S., Cancer incidence in the population of Vladikavkaz and its relationship with various factors. // Geology and Geophysics of the South of Russia, No. 3. 2013, pp. 29-38.
2. Burdzieva O.G., Zaks T.V., Kanukov A.S., Korbesova K.V., Analysis of the Relationship between Population Morbidity and Pollution in an Urbanized Area Using GIS Technologies. // Transactions of the Institute of Geology, Dagestan Scientific Center of the Russian Academy of Sciences, No. 4 (79), 2019, pp. 115-123.
3. Burdzieva O.G., Kanukov A.S., Korbesova K.V., Development of a Methodology for Experimental Research to Determine the Level of Air Pollution by Mobile Sources. // Transactions of the Institute of Geology, Dagestan Scientific Center of the Russian Academy of Sciences, No. 4 (103), 2025, pp. 77-88.
4. Senesil G.S., Baldassarre G., Senesi N., Radina B., Trace element inputs into soils by anthropogenic activities and implications for human health. // Chemosphere 39, 1999, pp. 343–377.
5. Lee C.S.-l., Li X., Shi W., Cheung S.C.-N., Thornton I., Metal contamination in urban, suburban, and country park soils of Hong Kong: a study based on GIS and multivariate statistics. // Sci. Total. Environ., 356, 2006, pp. 45–61.
6. Shi W., Liu J., Du Z., Song Y., Chen C., Yue, T., Surface modelling of soil pH. // Geoderma 150, 2009, pp. 113–119.
7. Zhang C., Tang Y., Luo L., Xu W., Outlier identification and visualization for Pb concentrations in urban soils and its implications for identification of potential contaminated land. // Environ. Pollut. 157, 2009, pp. 3083–3090.
8. Aguilar F.J., Aguera F., Aguilar M.A., Carvajal F., Effects of terrain morphology, sampling density, and interpolation methods on grid DEM accuracy. // Photogramm. Eng. Rem. S. 71, 2005, pp. 805–816.
9. Webster R., Is soil variation random? // Geoderma. 2000. 97, 149–163Li Q. Multifractal-Krige interpolation method. // Adv. Earth Sci. 20, 2005, pp. 218–256
10. Zaalishvili V.B., Burdzieva O.G., Kanukov A.S., Dzobelova L.V., Development of maps of the carcinogenic risk index for the territory of Vladikavkaz. // Geology and Geophysics of the South of Russia, Vol. 11, No. 4, 2021, pp. 147-160. DOI 10.46698/VNC.2021.98.22.012.

2nd International Scientific Conference "Modern Problems in Geophysics", Proceedings,
ISBN 978-9941-36-562-1, ISSN 3088-4349, Tbilisi, Georgia, October 29-31, 2026

# COMPARATIVE ANALYSIS OF THE VARIABILITY OF MEAN MAX ANNUAL AND SEMI-ANNUAL AIR TEMPERATURE AND PRECIPITATION SUMS IN TBILISI AND PASANAURI IN 1980-2025

**[*]Aliyev V., [**]Amiranashvili A., [***]Davitashvili T., [****]Matchavariani L., [*****]Samkharadze I., [*****]Zotikishvili N.**

*[*]CEO & Founder, International Event Organizer Company AMIR Technical Services Azerbaijan, Baku, Azerbaijan*
*[**]Mikheil Nodia Institute of Geophysics of Ivane Javakhishvili Tbilisi State University, Tbilisi, Georgia*
*[***]I. Vekua Institute of Applied Mathematics of I. Javakhishvili Tbilisi State University, Tbilisi, Georgia*
*[****]Tbilisi State University, Tbilisi, Georgia*
*[*****]Institute of Hydrometeorology of Georgian Technical University, Tbilisi, Georgia*
*prof.vugar.aliyev@gmail.com; avtandilamiranashvili@gmail.com*

***Abstract.*** *A statistical analysis of time series of observations of annual and seasonal (year, cold and warm seasons) values of mean maximum annual and seasonal air temperature and precipitation sums in Tbilisi and Pasanauri in 1980 – 2025 was carried out. Trends of mean maximum air temperature in Tbilisi and Pasanauri in 1980-2025 are linear, while trends of mean precipitation sum in Tbilisi are linear and in Pasanauri have the form of a third-degree polynomial. Difference between mean maximum air temperature in 2011-2025 and in 1980-1994 for Tbilisi and Pasanauri are significant for three periods of the year and change from 1.38 °C (Pasanauri, warm period) to 1.61 °C (Tbilisi, warm period). A significant difference between mean precipitation sum in 2011-2025 and in 1980-1994 for Tbilisi was observed in the cold period only (-19.4 mm) and for Pasanauri are significant for three periods of the year and change from -87.0 mm (warm period) to -174.6 mm (annual data). This is a cause for concern regarding the water supply for the Zhinvali Hydroelectric Power Plant reservoir, which is fed by tributaries of the Aragvi River; the discharge of these tributaries is largely linked to both intense glacial melting (driven by rising air temperatures) and changes in precipitation patterns.*

***Key Words:*** *Mean max air temperature, atmospheric precipitation, climate change, statistical analysis.*

## Introduction

Georgia, with its wide variety of climatic zones, is highly sensitive to global climate change [1]. Despite the country's small size, regional variations in climate change patterns are frequently observed. Consequently, climate research has always been a priority in Georgia. Air temperature and precipitation are key climatic components, and numerous studies have focused on them [1, 2].

For instance, it has been established that long-term air temperature variability in Tbilisi closely mirrors fluctuations in the average global air temperature within the 24°–64° N latitudinal belt [3]. This allows Tbilisi's air temperature data to serve as a benchmark for assessing the impact of global climate change on temperature regimes across various regions of Georgia.

Data from 1844 to 2023 show no significant changes in annual or semi-annual precipitation sums for Tbilisi [4], whereas data from 1936 to 2023 reveal highly varied precipitation trends across six locations in Kakheti [5]. For example, comparing the 1984–2023 period to 1936–1975, the average annual precipitation in Lagodekhi increased by 90.6 mm, while in Sagarejo, it decreased by 106.1 mm [5] – despite the two locations being only 80 km apart.

Studies have shown that, generally, the impact of global climate change on air temperature intensifies with increasing elevation [6]. For example, in Shovi (1507 m a.s.l.), compared to Tbilisi, during the 2011–2020 period (according to annual data), the rates of increase in average maximum air temperatures were higher: 2.9 times higher overall, 2.7 times higher during the cold half of the year, and 3 times higher during the warm half of the year [6].

This is corroborated by the intensification of glacier melting [7, 8]. The disaster in Shovi on August 3, 2023 – which claimed the lives of over 30 people due to a mudflow triggered by glacier melt – serves as an example of the negative environmental impact of this process.

This event has reaffirmed the need for further research into climate change, particularly in mountainous regions (encompassing the measurement and analysis of climatic parameters, as well as short- and long-term forecasting).

This article presents the results of a comparative analysis regarding the variability of average maximum annual and semi-annual air temperatures and precipitation totals in Tbilisi and Pasanauri against the backdrop of global warming during the 1980–2025 period. Pasanauri is located in the vicinity of the Zhinvali Hydroelectric Power Plant, the reservoir of which is fed by tributaries of the Aragvi River [8]. Water discharge in these rivers is largely linked to both intense glacier melting (driven by rising air temperatures) and changes in precipitation patterns.

## Study area, material and methods

Study area – Tbilisi and Pasanauri. Data of the Georgian National Environment Agency about monthly mean maximum air temperature and sum of precipitation in Tbilisi (Tb) and Pasanauri (Pas) in the period from 1980 to 2025 are used. The standard statistical methods are used [10,11]. The following designations will be used below: Mean – average values; Min – minimal values; Max – maximal values; St Dev – standard deviation; $R^2$ – coefficient of determination; R – coefficient of linear correlation; R' – index of correlation for nonlinear relationships; α – level of significance; annual period (year), cold season (October-March, cold), warm season (April-September, warm). Missing observational data were recovered using standard methods [12]. Comparison of mean values of precipitation in two fifteen-year periods of time (2011-2025 and 1980-1994) was produced with the use of Student's criterion with the level of significance α not worse than 0.25.

The trend curve is the regression equation of the connection of the investigated parameter with time at the significant value of the coefficient of determination and such values of $K_{DW}$, where the residual values are accidental. If the residual values are not accidental the connection of the investigated parameter with time will be considered as simply regression. The statistical program Data Fit 7 was used for calculations.

The degree of correlation was determined in accordance with [10]: very high correlation ($0.9 \leq R \leq 1.0$); high correlation ($0.7 \leq R < 0.9$); moderate correlation ($0.5 \leq R < 0.7$); low correlation ($0.3 \leq R < 0.5$); negligible correlation ($0 \leq R < 0.3$).

## Results

Results in Figs. 1,2 and Tables 1-6 are presented.

**Table 1.** Statistical characteristics of mean maximum air temperature in Tbilisi and Pasanauri in 1980-2025.

| Variable | Tb_Year | Tb_Cold | Tb_Warm | Pas_Year | Pas_Cold | Pas_Warm |
|---|---|---|---|---|---|---|
| Max | 21.0 | 13.9 | 29.2 | 17.2 | 10.4 | 24.0 |
| Min | 17.3 | 9.3 | 24.9 | 12.7 | 5.4 | 20.0 |
| Average | 19.3 | 11.7 | 27.0 | 15.1 | 7.9 | 22.3 |
| St Dev | 0.94 | 1.13 | 1.10 | 0.97 | 1.23 | 1.05 |
| | Correlation Matrix | | | | | |
| Tb_Year | 1 | 0.85 | 0.83 | 0.92 | 0.82 | 0.77 |
| Tb_Cold | 0.85 | 1 | 0.42 | 0.78 | 0.90 | 0.38 |
| Tb_Warm | 0.83 | 0.42 | 1 | 0.76 | 0.46 | 0.93 |
| Pas_Year | 0.92 | 0.78 | 0.76 | 1 | 0.88 | 0.79 |
| Pas_Cold | 0.82 | 0.90 | 0.46 | 0.88 | 1 | 0.45 |
| Pas_Warm | 0.77 | 0.38 | 0.93 | 0.79 | 0.45 | 1 |

Linear correlations between mean maximum air temperature in Tbilisi and Pasanauri in 1980-2025 in three periods of the year (Table 1) change from 0.38 (pair: Pas_Warm – Tb_Cold, low correlation) to 0.92 (pair: Pas_Year – Tb_Year, very high correlation). Trends of mean maximum air temperature in Tbilisi and Pasanauri in 1980-2025 are linear (Table 2, Fig. 1).

**Table 2.** Coefficients of the time trend equation of mean maximum air temperature in Tbilisi and Pasanauri in 1980-2025. X – number of years: 1 – 1980, …., 46 – 2025.

| Variable | Tb_Year | Tb_Cold | Tb_Warm | Pas_Year | Pas_Cold | Pas_Warm |
|---|---|---|---|---|---|---|
| Regression | $Y = a \cdot x + b$ | | | | | |
| $R^2$ | 0.49 | 0.339 | 0.352 | 0.411 | 0.314 | 0.279 |
| R | 0.70 | 0.58 | 0.59 | 0.64 | 0.56 | 0.53 |
| $K_{DW}$ | 1.755 | 1.82 | 2.08 | 1.99 | 1.58 | 2.33 |
| a | 0.048973 | 0.049146 | 0.04848 | 0.046537 | 0.051366 | 0.041159 |
| b | 18.19043 | 10.57333 | 25.81072 | 14.02812 | 6.716812 | 21.29797 |

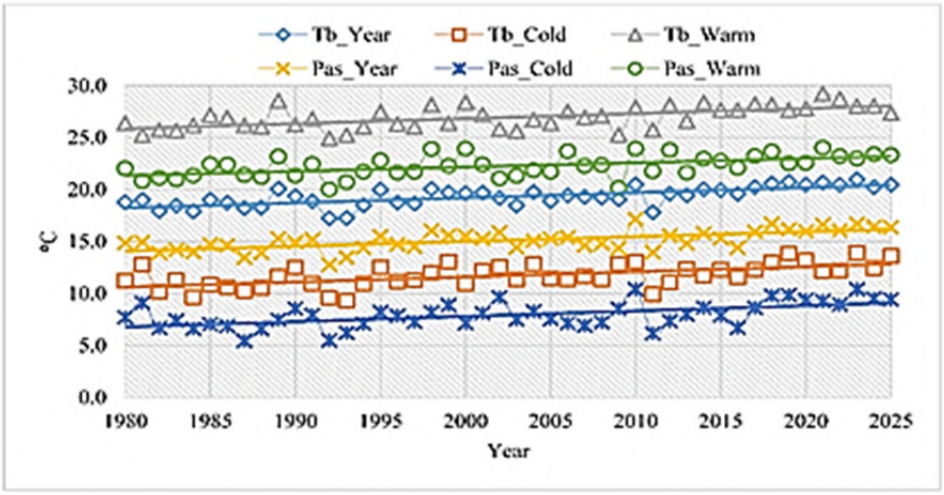



**Fig. 1.** Trend of mean maximum air temperature in Tbilisi and Pasanauri in 1980-2025.

**Table 3.** Difference between mean maximum air temperature in 2011-2025 (II per) and in 1980-1994 (I per) for Tbilisi and Pasanauri ($\alpha<0.01$).

| Variable | Tb_Year | Tb_Cold | Tb_Warm | Pas_Year | Pas_Cold | Pas_Warm |
|---|---|---|---|---|---|---|
| II per – I per | 1.58 | 1.54 | 1.61 | 1.48 | 1.59 | 1.38 |

Difference between mean maximum air temperature in 2011-2025 (II per) and in 1980-1994 (I per) for Tbilisi and Pasanauri are significant for three periods of the year (Table 3) and change from 1.38 °C (Pas_Warm) to 1.61 °C (Tb_Warm).

**Table 4.** Statistical characteristics of precipitation sum in Tbilisi and Pasanauri in 1980-2025.

| Variable | Tb_Year | Tb_Cold | Tb_Warm | Pas_Year | Pas_Cold | Pas_Warm |
|---|---|---|---|---|---|---|
| Max | 724 | 301 | 565 | 1446 | 801 | 922 |
| Min | 355 | 47 | 195 | 437 | 125 | 231 |
| Average | 502 | 164 | 338 | 942 | 333 | 609 |
| St Dev | 96.2 | 47.4 | 90.0 | 202.0 | 128.9 | 135.5 |
| | Correlation Matrix | | | | | |
| Tb_Year | 1 | 0.37 | 0.87 | 0.33 | 0.19 | 0.32 |
| Tb_Cold | 0.37 | 1 | -0.13 | 0.30 | 0.46 | 0.01 |
| Tb_Warm | 0.87 | -0.13 | 1 | 0.20 | -0.05 | 0.34 |
| Pas_Year | 0.33 | 0.30 | 0.20 | 1 | 0.75 | 0.78 |
| Pas_Cold | 0.19 | 0.46 | -0.05 | 0.75 | 1 | 0.17 |
| Pas_Warm | 0.32 | 0.01 | 0.34 | 0.78 | 0.17 | 1 |

Linear correlations between mean precipitation sum in Tbilisi and Pasanauri in 1980-2025 in three periods of the year (Table 4) change from -0.05 (pair: Pas_Cold – Tb_Warm, negligible correlation) to 0.87 (pair: Tb_Warm – Tb_Year, high correlation). Trends of mean precipitation sum in 1980-2025 in Tbilisi are linear and in Pasanauri have the form of a third-degree polynomial (Table 5, Fig. 2).

**Table 5.** Coefficients of the time trend equation of precipitation sum in Tbilisi and Pasanauri in 1980-2025.

| Variable | Tb_Year | Tb_Cold | Tb_Warm | Pas_Year | Pas_Cold | Pas_Warm |
|---|---|---|---|---|---|---|
| Regression | $Y = a \cdot x + b$ | | | $Y = a \cdot x^3 + b \cdot x^2 + c \cdot x + d$ | | |
| $R^2$ | 0.0069 | 0.0290 | 0.0138 | 0.290 | 0.216 | 0.164 |
| R, R' | 0.08 | 0.17 | 0.12 | 0.54 | 0.46 | 0.40 |
| $K_{DW}$ | 1.59 | 1.79 | 1.47 | 1.52 | 1.49 | 1.87 |
| a | 0.59537 | -0.18964 | 0.78723 | -0.02116 | -0.00742 | -0.01376 |
| b | 488.26957 | 168.69565 | 319.52174 | 1.09989 | 0.22556 | 0.87615 |
| c | | | | -15.9062 | 1.522244 | -17.4594 |
| d | | | | 1052.438 | 321.7767 | 730.6257 |

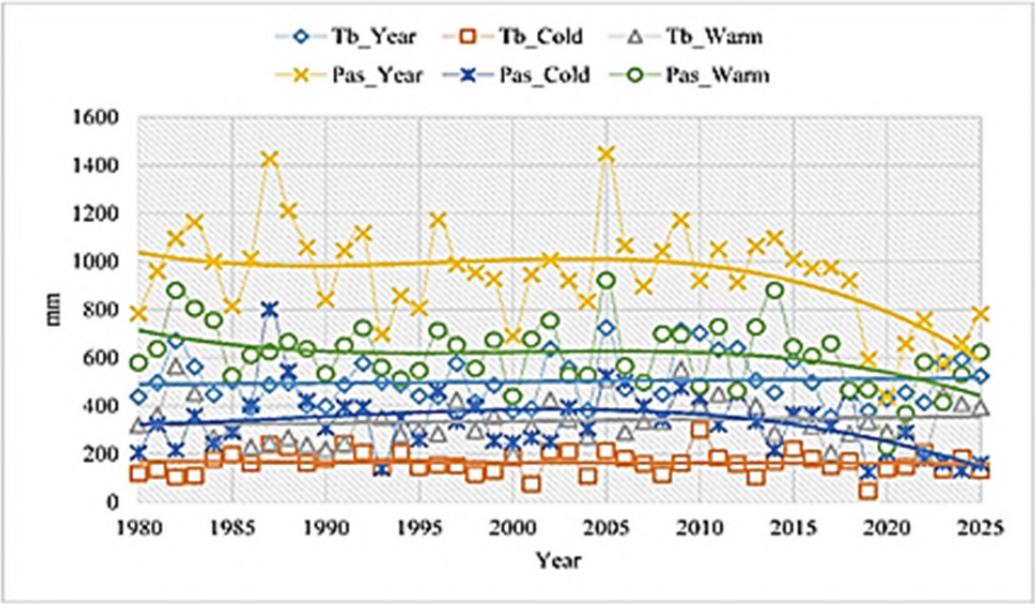



**Fig. 2.** Trend of precipitation sum in Tbilisi and Pasanauri in 1980-2025.

**Table 6.** Difference between mean sum of precipitation in 2011-2025 (II per) and in 1980-1994 (I per) for Tbilisi and Pasanauri.

| Variable | Tb_Year | Tb_Cold | Tb_Warm | Pas_Year | Pas_Cold | Pas_Warm |
|---|---|---|---|---|---|---|
| II per – I per | 11.2 | -19.4 | 30.6 | -174.6 | -87.5 | -87.0 |
| α | No sigh | 0.25 | No sigh | 0.04 | 0.1 | 0.1 |

Significant difference between mean precipitation sum in 2011-2025 (II per) and in 1980-1994 (I per) for Tbilisi observed in cold period only (-19.4 mm) and for Pasanauri are significant for three periods of the year (Table 6) and change from -87.0 mm (Pas_Warm) to -174.6 mm (Pas_Year).

## Conclusion

Climate change has led to a linear rise in air temperatures in both Tbilisi and Pasanauri. At the same time, the rate of increase in the average maximum air temperature (Table 2) in Tbilisi is higher than in Pasanauri based on annual data (0.049°C/year and 0.0465°C/year, respectively), lower based on data for the cold period (0.049°C/year and 0.051°C/year, respectively), and higher based on data for the warm half-year (0.0485°C/year and 0.0412°C/year, respectively).

In Tbilisi, climate change has had little impact on precipitation variability, whereas in Pasanauri, precipitation decreased significantly during the 2011–2025 period compared to 1980–1994: by 174.6 mm annually, 87.5 mm during the cold half-year, and 87.0 mm during the warm half-year.

This is a cause for concern regarding the water supply for the Zhinvali Hydroelectric Power Plant reservoir, which is fed by tributaries of the Aragvi River; the discharge of these tributaries is largely linked to both intense glacial melting (driven by rising air temperatures) and changes in precipitation patterns.

In the near future, we intend to examine in greater detail the variability of the flow regime of the rivers feeding the Zhinvali Hydroelectric Power Plant reservoir, taking into account new data.

## References


1. Kartvelishvili L., Tatishvili M., Amiranashvili A., Megrelidze L., Kutaladze N., Weather, Climate and their Change Regularities for the Conditions of Georgia. // Monograph: Publishing House "Universal", Tbilisi, 2023, 406 p., https://doi.org/10.52340/mng.9789941334658
2. Alibegova D., Elizbarashvili E. Statisticheskaia struqtura atmospernikh osadkov v gornikh raionakh. // Leningrad, 1980, 136 p. (in Russian)
3. Amiranashvili A., Analysis of Variability of Mean Annual Air Temperature in Tbilisi in 1844-2023 Against the Background of Climate Change. // Int. Sc. Conf. "Complex Geophysical Monitoring in Georgia: History, Modern Problems, Promoting Sustainable Development of the Country". // Proceedings, ISBN 978-9941-36-272-9, Publish House of Iv. Javakhishvili Tbilisi State University, Tbilisi, Georgia, October 17-19, 2024, pp. 145–149. http://dspace.gela.org.ge/bitstream/123456789/10621/1/37_MM-180.pdf
4. Bolashvili N., Chikhladze V., Kartvelishvili L., Tatishvili M., Variability of Atmospheric Precipitation in Tbilisi in 1844-2023. // Int. Sc. Conf. "Complex Geophysical Monitoring in Georgia: History, Modern Problems, Promoting Sustainable Development of the Country". // Proceedings, ISBN 978-9941-36-272-9, Publish House of Iv. Javakhishvili Tbilisi State University, Tbilisi, Georgia, October 17-19, 2024, pp. 150 – 154. http://dspace.gela.org.ge/bitstream/123456789/10620/1/38_MM-180.pdf
5. Amiranashvili A., Bliadze T., Davitashvili M., Kirkitadze D., Zuroshvili L., Sukhitashvili G., Changeability of Atmospheric Precipitation in Kakheti (Georgia) in 1936-2023 Against the Backdrop of Climate Change. // 2nd Int Sc. Conf. „Modern problems in Geophysics", Proceedings, Tbilisi, Georgia, October 29 – 31, 2026.
6. Amiranashvili A., Kartvelishvili L., Kutaladze N., Megrelidze L., Tatishvili M. Comparison of the Mean Max Annual, Seasonal and Monthly Air Temperature Variability in Tbilisi and Shovi in 1956-2022. // Int. Sc. Conf. "Geophysical Processes in the Earth and its Envelopes". Proceedings, ISBN 978-9941-36-147-0, Publish House of Iv. Javakhishvili Tbilisi State University, November 16-17, 2023, pp. 127-132. http://www.openlibrary.ge/bitstream/123456789/10418/1/32_IG_90.pdf
7. Tielidze L., The Glacio-Geomorphological Study of the Glaciers of the Caucasus on the background of Modern Climate Change and evolution of the Late Pleistocene and Holocene Glaciation. // PhD thesis, 2016, 129 p. (in Georgian) https://www.tsu.ge/assets/media/files/48/disertaciebi/Levan_Tielidze.pdf
8. Kordzakhia, G., Shengelia, L.,Tvauri, G., Dzadzamia, M. Current Climate Change Impact on the Mtkvari (Kura) River Basin Glaciers Degradation. // Bulletin of the Georgian National Academy of Sciences, Vol. 14, №1, 2020, pp. 56-63. ISSN – 0132 – 1447
9. Zhinvali Hydro Power Plant. (2012). Archived from the original on February 29, 2012. https://www.gem.wiki/Zhinvali_hydroelectric_plant
10. Hinkle D. E., Wiersma W., Jurs S. G., Applied Statistics for the Behavioral Sciences. // Boston, MA, Houghton Mifflin Company, 2003.
11. Kendall M. G. Time-series. // Moscow, 1981, 200 p. (in Russian)
12. Kobisheva N., Narovlianski G. Climatological processing of the meteorological information. // Leningrad, Gidrometeoizdat, 1978, 294 p. (in Russian)

2nd International Scientific Conference "Modern Problems in Geophysics", Proceedings,
ISBN 978-9941-36-562-1, ISSN 3088-4349, Tbilisi, Georgia, October 29-31, 2026

# CHANGEABILITY OF ATMOSPHERIC PRECIPITATION IN KAKHETI (GEORGIA) IN 1936-2023 AGAINST THE BACKDROP OF CLIMATE CHANGE

**[*]Amiranashvili A., [*]Bliadze T., [**]Davitashvili M., [*]Kirkitadze D., [**]Zuroshvili L., [**]Sukhitashvili G.**

*[*]M. Nodia Institute of Geophysics of the I. Javakhishvili Tbilisi State University, Tbilisi, Georgia*
*[**]Iakob Gogebashvili Telavi State University, Telavi, Georgia*
*avtandilamiranashvili@gmail.com, magda.davitashvili@tesau.edu.ge*

***Abstract.*** *The results of statistical analysis of data on monthly precipitation for six points of Kakheti – Dedoplistskaro, Gurjaani, Kvareli, Lagodekhi, Sagarejo, and Telavi are presented. The study period is from 1936 to 2023. In particular, it was established that during the specified period, precipitation variability across various locations in Kakheti – and across different months of the year – was characterized by significant heterogeneity. For instance, comparing the 1984–2023 period to 1936–1975, the mean annual precipitation in Dedoplistskaro remained virtually unchanged; it increased by 18.2 mm during the cold season (November–February) but decreased by 16 mm during the warm season (March–October). In Gurjaani, mean annual precipitation decreased by 25 mm; changes were negligible during the cold season (-2 mm), while a 22 mm decrease occurred during the warm season. In Kvareli, mean annual precipitation decreased by 25 mm; changes were negligible during the cold season (-2 mm), while a 22 mm decrease occurred during the warm season. In Lagodekhi, mean annual precipitation increased by 90.6 mm, with increases of 25.4 mm and 65.2 mm in the cold and warm seasons, respectively. In Sagarejo, mean annual precipitation decreased by 106.1 mm, with decreases of 23.2 mm and 82.9 mm in the cold and warm seasons, respectively. In Telavi, mean annual precipitation decreased by 37.8 mm; changes were negligible during the cold season (-7 mm), while a 30 mm decrease occurred during the warm season. Despite spatially heterogeneous changes in precipitation during individual months, the general trend for the region is a decrease in precipitation (except in Lagodekhi) during the warm season, particularly in June.*

***Key Words:*** *Regional climate change, atmospheric precipitation.*

## Introduction

In recent years, the issue of observed and anticipated climate change on our planet has become particularly pressing. Given the diversity of climatic zones within Georgia, this matter is of special significance there [1]. Consequently, the study of precipitation in Georgia has consistently received close attention [1–4]. In particular, recent years have seen a number of studies focusing on the climatic characteristics of daily, monthly, seasonal, and annual precipitation sums [3–7] and the role of precipitation in shaping bioclimatic conditions [3], as well as the impact of precipitation deficits or surpluses on the occurrence of droughts [8, 9], floods [10], landslides [10, 11], and other adverse phenomena. As new information has accumulated, data regarding precipitation variability across various regions of Georgia have been continuously updated [6, 7].

Study [12] presents the results of a statistical analysis of monthly precipitation totals for six locations in Kakheti: Telavi, Sagarejo, Kvareli, Gurjaani, Dedoplistskaro, and Lagodekhi. The research covered the period from 1956 to 2015. Specifically, it was found that precipitation variability across different locations in Kakheti – and across different months of the year – was characterized by significant heterogeneity during this period. For instance, a comparison of the 1986–2015 and 1956–1985 periods revealed a downward trend in summer precipitation in Kakheti, a shift that negatively affects the condition of agricultural crops.

The present study extends and refines the results obtained in [12] by incorporating a longer series of precipitation observations (1936–2023).

## Study area, material and methods

The study area is the Kakheti region of Georgia. Data of the Hydrometeorological department of Georgia about monthly sum of precipitation in six locations of Kakheti – Dedoplistskaro (Ded), Gurjaani (Gur),

Kvareli (Kvar), Lagodekhi (Lag), Sagarejo (Sag) and Telavi (Tel) – are used. Period of observation from 1936 to 2023. Location of meteorological stations in Kakheti in Fig.1 is presented.

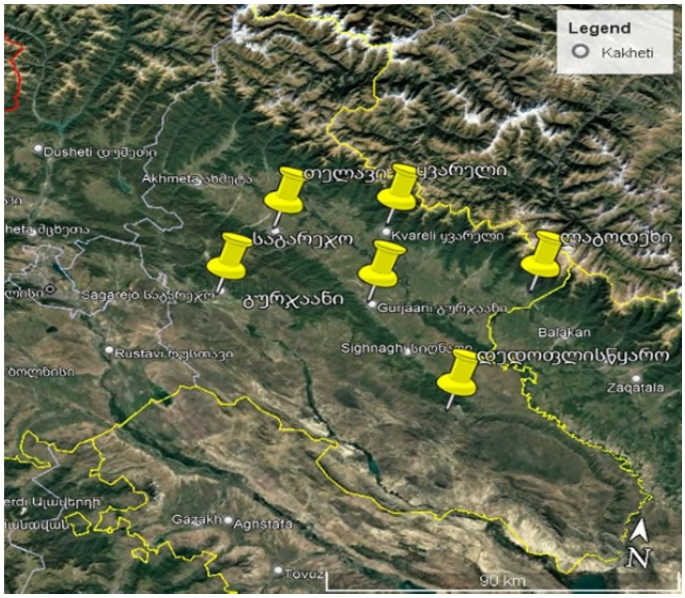



**Fig. 1.** Location of meteorological stations in Kakheti.

The standard statistical methods are used. The following designations will be used below: Mean – average value of precipitations for 1936-2023; I – average value for 1936-1975 (first period of time); II – average value for 1984-2023 (second period of time); November ÷ February – cold period (season); March ÷ October – warm period (season). Missing observational data using standard methods were recovered. Comparison of mean values of precipitations in two periods of time was produced with the use of Student's criterion with the level of significance $\alpha \leq 0.25$.

## Results

Results in Figures 2 and 3 are presented.

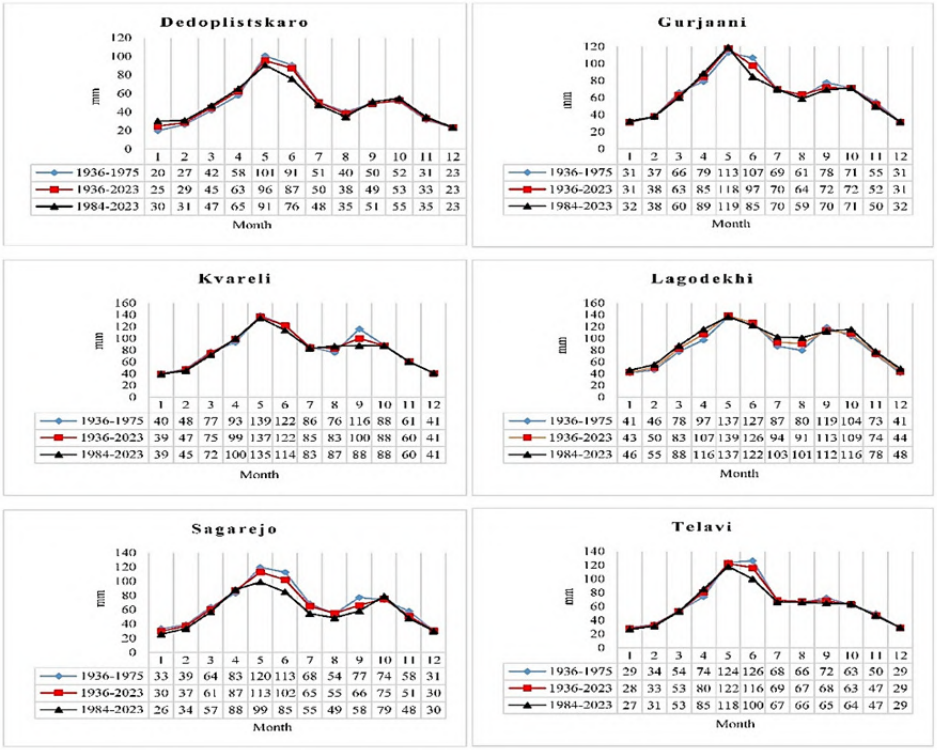


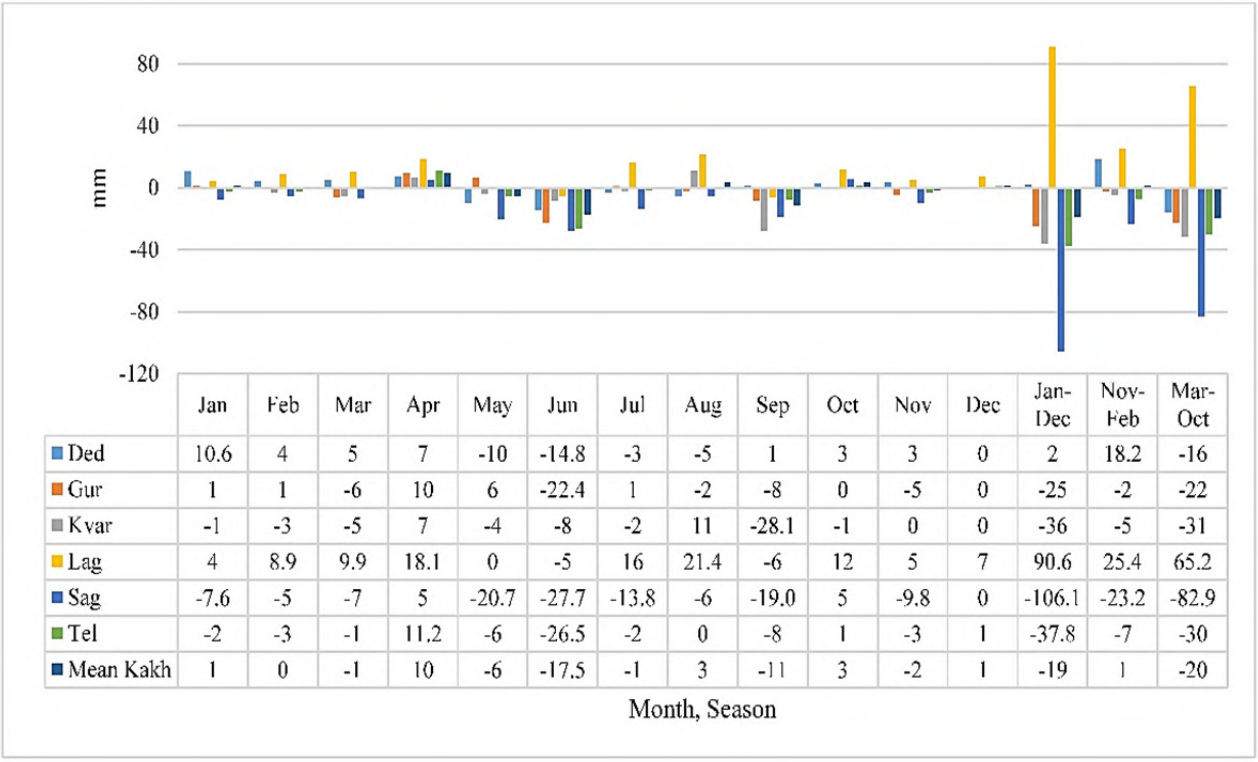

**Fig. 2.** Intra annual distribution of monthly average sums of atmospheric precipitation in six locations of Kakheti in 1936-1975, 1936-2023 and 1984-2023.

Between 1936 and 2023, average monthly precipitation at the meteorological stations ranged from 23 mm (Dedoplistskaro, December) to 139 mm (Lagodekhi, May). Consequently, the monthly precipitation distribution in the study area is characterized by marked seasonality. Peak precipitation at all stations is typically recorded in May and June, while minimum values occur during the winter months, primarily January and December. This distribution is characteristic of Kakheti and reflects the region's primary annual precipitation pattern (Fig. 2).

A comparison of the two study periods (1936–1975 and 1984–2023) revealed that changes in average monthly precipitation varied by station (Fig. 3).

Dedoplistskaro. In the second period, an increasing tendency in precipitation was observed from January to April and from September to November, while a decreasing tendency was noted from May to August. The most significant increase occurred in January (+10.6 mm), and the greatest decrease in June (−14.8 mm). Precipitation patterns remained unchanged in December. The total annual precipitation sum in the second period showed virtually no change compared to the first (a difference of 2 mm). An increase in precipitation was observed during the cold season (18.2 mm), whereas a decrease occurred during the warm season (−16 mm).

Gurjaani. An increasing tendency in precipitation was observed in January, February, April, May, and July, with the greatest increase occurring in April (+10.0 mm). A decrease was observed in March, June, August, September, and November, with the largest drop recorded in June (−22.4 mm). Precipitation patterns remained unchanged in December. The mean annual precipitation decreased by 25 mm; changes were negligible during the cold season (−2 mm), while a decrease of 22 mm occurred during the warm season.




| | Jan | Feb | Mar | Apr | May | Jun | Jul | Aug | Sep | Oct | Nov | Dec | Jan-Dec | Nov-Feb | Mar-Oct |
|---|---|---|---|---|---|---|---|---|---|---|---|---|---|---|---|
| Ded | 10.6 | 4 | 5 | 7 | -10 | -14.8 | -3 | -5 | 1 | 3 | 3 | 0 | 2 | 18.2 | -16 |
| Gur | 1 | 1 | -6 | 10 | 6 | -22.4 | 1 | -2 | -8 | 0 | -5 | 0 | -25 | -2 | -22 |
| Kvar | -1 | -3 | -5 | 7 | -4 | -8 | -2 | 11 | -28.1 | -1 | 0 | 0 | -36 | -5 | -31 |
| Lag | 4 | 8.9 | 9.9 | 18.1 | 0 | -5 | 16 | 21.4 | -6 | 12 | 5 | 7 | 90.6 | 25.4 | 65.2 |
| Sag | -7.6 | -5 | -7 | 5 | -20.7 | -27.7 | -13.8 | -6 | -19.0 | 5 | -9.8 | 0 | -106.1 | -23.2 | -82.9 |
| Tel | -2 | -3 | -1 | 11.2 | -6 | -26.5 | -2 | 0 | -8 | 1 | -3 | 1 | -37.8 | -7 | -30 |
| Mean Kakh | 1 | 0 | -1 | 10 | -6 | -17.5 | -1 | 3 | -11 | 3 | -2 | 1 | -19 | 1 | -20 |

**Fig. 3.** The difference in precipitation sums for six meteorological stations in the Kakheti region and their average values for the periods 1984–2023 and 1936–1975 (insignificant differences are presented as rounded whole numbers; $\alpha > 0.25$).

Kvareli. A tendency toward increased precipitation is observed only in April and August, with the highest value in August (+11.0 mm). Precipitation patterns remained unchanged in November and December. A decrease in precipitation was recorded in the remaining months, particularly in September (−28.1 mm). The mean annual precipitation decreased by 36 mm; changes were negligible during the cold season (−5 mm), while a decrease of 31 mm occurred during the warm season.

Lagodekhi. In the second period, a tendency toward increased precipitation is observed from January to April, in July and August, and from October to December. The largest increase was recorded in August

(+21.4 mm). A decrease was recorded only in June and September, with a relatively significant drop observed in September (−6.0 mm). Precipitation patterns remained unchanged in May. The mean annual precipitation increased by 90.6 mm, rising by 25.4 mm and 65.2 mm during the cold and warm seasons, respectively.

Sagarejo. Precipitation patterns remained unchanged in December. An increase in precipitation is observed only in April and October (approximately +5 mm), whereas a downward tendency is noted in the other months, particularly from May to September. The largest decrease was recorded in June (−27.7 mm). Mean annual precipitation decreased by 106.1 mm; decreases of 23.2 mm and 82.9 mm were observed for the cold and warm seasons, respectively.

Telavi. Precipitation patterns remained unchanged in August. Increases in precipitation were observed in April, October, and December – peaking in April (+11.2 mm) – while decreases occurred in the remaining months, particularly in June (−26.5 mm). Mean annual precipitation decreased by 37.8 mm; the change was negligible during the cold season (−7 mm), whereas a 30 mm decrease occurred during the warm season.

Kakheti average (Mean Kakh). Regional averages show increased precipitation in January, April, August, October, and December, and decreases in March, the May–July period, September, and November. The largest negative difference was noted in June (−17.5 mm). Mean annual precipitation decreased by 19 mm in the second period compared to the first, with a 20 mm decrease during the warm season. No significant change occurred during the cold season (1 mm).

It is worth noting that the most significant decrease in precipitation was recorded in June at the majority of meteorological stations, indicating a general regional trend in shifting precipitation patterns at the start of summer.

Thus, changes in monthly precipitation patterns in Kakheti are characterized by non-uniformity. In the second period (1984–2023), compared to the first (1936–1975), an increase in precipitation is observed primarily in late winter and early spring (especially in April), as well as at specific stations in August and October, whereas a decrease is mainly evident in June and September. The most significant regional-average decrease was recorded in June (-17.5 mm), indicating a trend toward reduced precipitation during the warm season. Thus, the monthly precipitation distribution in Kakheti retains a distinct seasonal character, with peaks in May–June.

## Conclusion

Future plans include extending this research to other regions of Georgia, including an examination of the role of precipitation in the formation of various processes that impact the environment.

## References


1. Alibegova D., Elizbarashvili E. Statisticheskaia struqtura atmospernikh osadkov v gornikh raionakh. // Leningrad, 1980, 136 p. (in Russian)
2. Tavartkiladze K., Begalishvili N., Kharchilava J., Mumladze D., Amiranashvili A., Vachnadze J., Shengelia I., Amiranashvili V., Contemporary Climate Change in Georgia. Regime of Some Climate Parameters and Their Variability. // Monograph, ISBN 99928-885-4-7, Tbilisi, 2006, 177 p. (in Georgian)
3. Kartvelishvili L., Tatishvili M., Amiranashvili A., Megrelidze L., Kutaladze N., Weather, Climate and their Change Regularities for the Conditions of Georgia. // Monograph – Tbilisi, 2023, 406 p., Publishing House "Universal". https://doi.org/10.52340/mng.9789941334658
4. Amiranashvili A., Chelidze T., Kiria T., Tsamalashvili T., Varamashvili N., Statistical Analysis of Annual Precipitation Sum with Different Provision in Georgia. // 2nd International Scientific Conference „Modern problems in Geophysics". // Proceedings, Tbilisi, Georgia, October 29–31, 2026.
5. Amiranashvili A.G. Special Features of Changeability of Daily Sum of Precipitation in Tbilisi in 1957-2006. // Journal of the Georgian Geophysical Society, Issue B. Physics of Atmosphere, Ocean and Space Plasma, v.18B, Tbilisi, 2015, pp. 81-91.
6. Pipia M., Meladze M., Davitashvili M., Beglarashvili N., Jamrishvili N., Pipia G. Statistical Analysis of Atmospheric Precipitation in the Racha-Lechkhumi and Kvemo Svaneti Region of Georgia in 1936-2023. // Reliability: Theory and Applications, ISSN 1932-2321, Volume 20, Special Issue No. 9 (87), November 2025, pp. 92-101. https://doi.org/10.24412/1932-2321-2025-987-92-101

7. Bolashvili N., Chikhladze V., Kartvelishvili L., Tatishvili M., Variability of Atmospheric Precipitation in Tbilisi in 1844-2023. // Proceedings – Int. Sc. Conf. "Complex Geophysical Monitoring in Georgia: History, Modern Problems, Promoting Sustainable Development of the Country", ISBN 978-9941-36-272-9, Tbilisi, Georgia, October 17-19, 2024, pp. 150 – 154, Publish House of Iv. Javakhishvili Tbilisi State University. http://dspace.gela.org.ge/bitstream/123456789/10620/1/38_MM-180.pdf.
8. Meladze M., Meladze G., Kapanadze N., Pipia M., Impact of Droughts on the Agricultural Sector of the Eastern Georgia Regions. Proceedings // Int. Sc. Conf. "Complex Geophysical Monitoring in Georgia: History, Modern Problems, Promoting Sustainable Development of the Country", Proceedings, ISBN 978-9941-36-272-9, Tbilisi, Georgia, October 17-19, 2024, pp. 72 – 75, Publish House of Iv. Javakhishvili Tbilisi State University. (in Georgian)
9. Amiranashvili A., Davitashvili T., Kharshiladze O., Samkharadze I., Amilakhvari D. Statistical Analysis of the Total Number of Dry Months in Eastern Georgia in 1936-2023 Using the SPI-3 Index ≤ 0 and an Assessment of the Variability of this Number until 2045. // Journal of the Georgian Geophysical Society, e-ISSN: 2667-9973, p-ISSN: 1512-1127, v.28(2), 2025, pp. 44-56.
10. Amiranashvili A., Chelidze T., Kiria T., Svanadze D., Tsamalashvili T., Varamashvili N. Retrospective Analysis of Landslides Processes in Akhaldaba (A Suburb of Tbilisi, Georgia) on June 13-14, 2015. // Journal of the Georgian Geophysical Society, e-ISSN: 2667-9973, p-ISSN: 1512-1127, Physics of Solid Earth, Atmosphere, Ocean and Space Plasma, v.29(1), 2026, pp. 50-59. https://ggs.openjournals.ge/index.php/GGS/article/view/12084
11. Chelidze T., Kiria T., Amiranashvili A., Svanadze D., Tsamalashvili T., Varamashvili N. Landslide Hazard Maps of Georgia Using Machine Learning Approach. // Bulletin of the National Academy of Sciences of Georgia, ISSN: 0132 – 1447, vol. 20(194), no. 2, 2026, pp. 23-29. http://science.org.ge/bnas/t20-n2/03_Chelidze_Geophysics.pdf
12. Bliadze T., Gvasalia G., Kirkitadze D., Mekoshkishvili N. Changeability of the Atmospheric Precipitations Regime in Kakheti in 1956-2015. // Proceedings – Int. Sc. Conf. "Natural Disasters in Georgia: Monitoring, Prevention, Mitigation". ISBN 978-9941-13-899-7, December 12-14, Tbilisi, 2019, pp. 74-77, Publish House of Iv. Javakhishvili Tbilisi State University.

2nd International Scientific Conference "Modern Problems in Geophysics", Proceedings,
ISBN 978-9941-36-562-1, ISSN 3088-4349, Tbilisi, Georgia, October 29-31, 2026

# 90 YEARS OF SCIENTIFIC RESEARCH IN THE FIELDS OF ATMOSPHERIC PHYSICS AND CLIMATOLOGY AT THE M. NODIA INSTITUTE OF GEOPHYSICS OF I. JAVAKHISHVILI TBILISI STATE UNIVERSITY

**Amiranashvili A., Bliadze T., Chikhladze V., Kereselidze Z.**

*Mikheil Nodia Institute of Geophysics of Ivane Javakhishvili Tbilisi State University, Tbilisi, Georgia*
*avtandilamiranashvili@gmail.com*

***Abstract.*** *This paper presents a brief overview of scientific research in the fields of atmospheric physics and climatology conducted over the past 90 years at the Mikheil Nodia Institute of Geophysics of Ivane Javakhishvili Tbilisi State University.*

***Key Words:*** *Atmospheric physics, climatology, weather modification, ecology, comprehensive geophysical surveys.*

Research in atmospheric physics and climatology has been conducted at the Institute of Geophysics since 1936.

During this period, work has been carried out in the following areas traditional to the field: cloud physics and active modification of atmospheric processes (hail, thunderstorms, fog, ozone, etc.); atmospheric and thunderstorm electricity; radar observations of clouds; physico-statistical modeling of the radar structure of convective clouds and cloud systems; physics of atmospheric aerosols and ozone, and atmospheric chemistry (ground-based and airborne studies); a 1989 study – conducted jointly with the Central Aerological Observatory – of ozone concentrations over the Pacific Ocean and its vertical distribution (during the 46th expedition of the research vessel "Akademik Shirshov"); interaction between clouds and minor atmospheric constituents; experimental laboratory modeling of atmospheric processes and active modification techniques; contemporary climate change in Georgia; environmental aspects of various natural and anthropogenic meteo-geophysical factors; comprehensive risk assessment of meteo-geophysical disasters for the territory of Georgia; identification of links between various atmospheric parameters (atmospheric and thunderstorm electricity, cloud cover, air ionization, radon, ozone, aerosols, etc.) and geodynamic processes; study of geomagnetic field variations as a factor affecting human health and as a potential earthquake precursor; investigation of MHD effects associated with the finite electrical conductivity of the solar wind near Earth's magnetosphere; study of turbulence in neutral and conducting atmospheric layers; modeling of Earth's magnetic boundary layer; investigation of the kinetics of water phase transitions in the turbulent atmosphere; study of the dynamics of Earth's ionospheric-magnetospheric plasma; regionalization of Georgian territory based on bioclimatic characteristics to foster the development of resorts and medical tourism; space weather.

For instance:

A theoretical model of heterogeneous nucleation on modified aerosol particles has been developed. This model employs a generalized heterogeneous nucleation equation that accounts for the dependence of specific interfacial surface energy on water vapor supersaturation. Issues regarding the formation of secondary ice crystals and the influence of particle size on the ice-forming activity of aerosols were examined.

A flowchart illustrating the interaction between atmospheric aerosols and convective clouds – as well as the atmospheric and in-cloud formation of condensation nuclei, crystallization nuclei, and ice crystals – was proposed, taking into account atmospheric ionization and electrification processes. It was demonstrated that intense convective and thunderstorm clouds can make a significant contribution to direct and indirect radiative effects.

The influence of ionizing radiation (radon, gamma radiation, cosmic rays) on the formation of secondary atmospheric aerosols via the gas-to-particle pathway was investigated. It was found that all the aforementioned types of ionizing radiation act as catalysts for the formation of submicron aerosols from gases.

The impact of atmospheric aerosol pollution (including radioactive pollution) on the variability of atmospheric electricity parameters in Eastern Georgia was studied.

A study was conducted on long-term changes in precipitation, thunderstorm activity, and hailstorm processes in Eastern Georgia, as well as their links to anthropogenic atmospheric pollution. Statistical models were developed to relate thunderstorm and hailstorm activity to atmospheric aerosol pollution. Specifically, it was found that the intensity of thunderstorm and hailstorm processes depends significantly on atmospheric aerosol pollution (including radioactive pollution), although this relationship is quite complex. Overall, the increase in non-radioactive atmospheric aerosol pollution led to greater hailstorm intensity and, consequently, reduced the effectiveness of hail suppression operations.

A large-scale monitoring program for radon in soil, drinking water, and indoor air was carried out in Western Georgia; maps showing radon distribution in these media were produced; links between radon levels and the incidence of lung cancer were identified; and recommendations were issued for protecting the population against hazardous radon levels. Concurrently, the chemical composition of drinking water was analyzed, and measurements were taken of gamma radiation from soil and room walls, light ion concentrations, meteorological parameters, and other factors.

Data from 1984–2010 indicate that elevated concentrations of ground-level ozone (and associated smog components harmful to human health) increase the average annual mortality rate in Tbilisi by an average of 1,680 deaths. This figure represents 14.1% of the city's average annual mortality – approximately three times higher than the rate observed in developed countries under similar conditions. It has been established that, compared to the 1980s, Tbilisi's population has become more sensitive to air pollution in recent years; adverse health effects and fatalities now occur at lower concentrations of ground-level ozone. Overall, on smog days – in addition to pollution from ozone, ozone-forming gases, and aerosols – human health in Tbilisi (particularly among those with cardiovascular diseases) is significantly affected by fluctuations in factors such as air temperature, atmospheric pressure, and cosmic rays (the latter serving primarily as an indicator of geomagnetic conditions).

A "Tbilisi-type smog" has been identified – a specific meteorological and environmental phenomenon characterized by an unusual feedback relationship between atmospheric ionizing radiation and the concentration of light ions under conditions of heavy pollution.

For outstanding scientific and practical achievements in the field of cloud physics, A. Kartsivadze was awarded the USSR State Prize in 1969 and the USSR Council of Ministers Prize in Science and Technology in 1985.

In 1999, a group of scientists (A.I. Kartsivadze, V.V. Patrikeev, A.D. Malkina) received Diploma No. 192 for Discovery No. A-220 from the Russian Academy of Natural Sciences, recognizing their work on the properties of organic inner-complex (chelate) compounds to induce active crystallization in supercooled atmospheric aqueous systems.

In 2009, a group of leading scientists from the institutes of Geography (K. Tavartkiladze), Geophysics (A. Amiranashvili), and Hydrometeorology (N. Begalishvili) received the National Prize of Georgia for a series of studies on climate change in Georgia.

In recent years, research has continued on the natural and anthropogenic characteristics of the atmosphere and related phenomena in Georgia, the assessment of their environmental impact in the context of climate change, and protective measures against such impacts, all aimed at creating safe ecosystems and fostering the country's sustainable economic development.

With the participation of specialists from the Institute of Geophysics, work was carried out in 2015 to restore the operations of the anti-hail service in Kakheti – a service that had previously existed from 1967 to 1989.

A detailed zoning of the Kakheti region was conducted based on the extent of hail damage to vineyards, utilizing radar data on hailstone sizes. For the first time in Georgia, studies have been conducted on bioclimatic indices such as the Tourism Climate Index and the Holiday Tourism Climate Index, as well as the forest fire danger index (Angstrom Fire Index).

Expeditionary studies on the air-ionization state were conducted in various regions of Georgia and in karst caves. The overall impact of specific meteorological parameters, their combinations, and cosmic radiation on human health was also assessed. The influence of certain thermal indices and ground-level ozone concentrations on the spread of COVID-19 was investigated.

The first database of parameterized data on hazardous natural phenomena (landslides, mudflows, gale-force and hurricane-force winds, floods, and hail) for Georgia (GeNHs) was created. An assessment of the long-term risk of severe hurricanes in Georgia was conducted based on data from 1961 to 2022. A statistical analysis of parameterized landslide data for Georgia covering the period from 1900 to 2022 was carried out.

Modeling was performed for extreme meteorological processes that pose a threat to agriculture under current climate change conditions.

Research was initiated on the patterns and variability of various meteorological parameters – and their combinations – as well as associated environmental risk factors for Baku (Azerbaijan) and Tbilisi (Georgia).

Links were established between landslide activation processes and precipitation events of varying durations, ranging from minutes and hours to several days, months, and years.

Developed stationary susceptibility and dynamic landslide hazard forecasting system for Georgia using ERA5, Fuzzy Logic and Hybrid Machine Learning; and much more.

More than 1000 scientific works have been published, including 23 major scientific publications (books, monographs, a catalog, and geographic atlases) [1–23]. Intellectual property rights have been obtained for over 25 inventions. Specialists from the Institute of Geophysics regularly participate in local and international scientific conferences as both speakers and organizers; serve as reviewers and editors for various publications and provide expertise on issues such as ecology, natural disasters, and active modification of atmospheric processes; engage in teaching activities; and actively participate in the implementation of international and local grant projects as well as joint research with domestic and foreign organizations.

**Acknowledgement:** The authors thank all the staff of the M. Nodia Institute of Geophysics and other local and foreign organizations for their fruitful cooperation in conducting joint scientific research.

## References

1. Gzirishvili T.G., Kartsivadze A.I., Okudzhava A.M., Geterogennaya nukleatsiya l'da. // ”Metsniyereba”,1984, 140 c. (in Russian)
2. D'yakonova I.N., Imyanitov I.M., Kartsivadze A.I., Klimin N.N., Mordovina L.S., Morozov V.N., Faber O.A., Chubarina Ye.V. Laboratornoye modelirovaniye protsessov kontaktnoy elektrizatsii oblachnykh chastits. // Pod redaktsiyey Imyanitova I.M., Chubarinoy Ye.V., Leningrad, Gidrometeoizdat, 1985, 88 s. (in Russian)
3. Kereselidze Z.A., MGD effekty konechnoy elektricheskoy provodimosti solnechnogo vetra vblizi magnitosfery Zemli. // Tbilisi : Izd-vo Tbil. un-ta, 1986, 122 s. (in Russian)
4. Kharchilava D.F., Amiranashvili A.G., Studies of Atmospheric Ozone Variations in Soviet Georgia. // Monograph, Academy of Sciences of the USSR Soviet Geophysical Committee, Moscow, 1988, 114 p. (in Russian) https://openlibrary.ge/handle/123456789/540
5. Amiranashvili A.G., Gzirishvili T.G., Aerosols and ice crystals in the Atmosphere. // Monograph, Metsniereba, Tbilisi, 1991,1 13 p. (in Russian) https://openlibrary.ge/bitstream/123456789/631/1/Aerosols%20and%20ice%20crystals.pdf
6. Amiranashvili A.G., Jishkariani J.M., Nodia A.G., Sepiashvili R.I., Tatashidze Z.K., Natural Air Radioactivity and Aeroions in Tskaltubo Cave. // Tbilisi, 1994, 54 p. (in Russian) https://openlibrary.ge/bitstream/123456789/537/4/Амиранашвили%2CДжишкариани%2CНодия%2CСепиашвили%2CТаташидзе_Содержан.pdf
7. Aivazishvili I., Amiranashvili A., Kapanadze E., Kirkitadze D., Napetvaridze R., Salukvadze T., Tatishvili M., Khelaia E., Atmospero da atmosperuli movlenebi. // Metsniereba, Tbilisi, 1995, 101 gv. (in Georgian)
8. Gvelesiani A. I., Jandieri G.V., Diasamidze Zh. M., Turbulence in Neutral and Conductive Atmospheric Layers. // Monograph, BSU, Tbilisi-Batumi, 1998, 278 p. (in Russian)
9. Saluqvadze T., Xvedelidze Z., Xelaia E. konveqciuri Rrublebis radiolokacia. // saqarTvelos mecnierebata akademiis m. nodias sax. geofizikis institutis Sromebi, ISSN 1512 – 1135, t. LVII, (monografia), Tbilisi, 2002, 258 gv. (in Georgian)
10. Amiranashvili A.G., Amiranashvili V.A., Gzirishvili T.G., Kharchilava J.F., Tavartkiladze K.A. Modern Climate Change in Georgia. Radiatively Active Small Atmospheric Admixtures. // Institute of Geophysics, Monograph, Trans. of M. Nodia Institute of Geophysics of Georgian Acad. of Sci., ISSN 1512-1135, vol. LIX, 2005, 128 p.
11. Tavartkiladze K., Begalishvili N., Kharchilava J., Mumladze D., Amiranashvili A., Vachnadze J., Shengelia I., Amiranashvili V. Contemporary climate change in Georgia. Regime of some climate parameters and their variability.

// Monograph, Georgian Academy of sciences, Vakhushti Bagrationi institute of geography, M. Nodia institute of geophisics, Institute of hydrometeorology. ISBN 99928–885–4.7, Tbilisi, 2006, 177 p. (in Georgian)
https://openlibrary.ge/handle/123456789/535
12. Kereselidze Z., Gabisonia I. Modeling of Earth's Magnetic Boundary Layer. // Monograph, "Meridian", Tbilisi, 2011, 175 p. (in Georgian)
13. Amiranashvili A., Bliadze T., Chikhladze V., Photochemical Smog in Tbilisi. // Monograph, Transaction of Mikheil Nodia institute of Geophysics of Ivane Javakhishvili Tbilisi State University, vol. LXIII, ISSN: 1512-1135, Tbilisi, 2012, 160 p. (in Georgian)
14. Amiranashvili A.G., History of Active Effects on Atmospheric Processes in Georgia.// In the book: Essays of the History of Weather Modification in the USSR and the Post-Soviet Territory, ISBN 978-5-86813-450-0, St. Petersburg, RSHMU, 2017, 352 pp., ill., pp. 234-254. (in Russian)
http://mig-journal.ru/toauthor?id=4644.
15. Varamashvili N., Chelidze T., Devidze M., Chikhladze V., Laboratory and Mathematical Modeling of Landslides Triggered by External Factors. Field Research. // Monograph, Trans. of M. Nodia Institute of Geophysics, TSU, vol. LXVIII, ISSN 1512-1135, Tbilisi, 2017, 138 p. (in Georgian)
https://openlibrary.ge/handle/123456789/6359
16. Kartvelishvili L., Amiranashvili A., Megrelidze L., Kurdashvili L., Turistul rekreaciuli resursebis shefaseba klimatis cvlilebebis fonze. // Publishing House "Mtsignobari", ISBN 978-9941-485-01-5, Tbilisi, 2019, 161 p. (in Georgian)
17. Gvelesiani A.I., Kinetika fazovykh perekhodov vody v turbulentnoy atmosfere. // Monografiya, izdatel'stvo Tbilisskogo gosudarstvennogo universiteta imeni Ivane Dzhavakhishvili, ISBN 978-9941-13-957-4, Tbilisi, 2020, 140 s. (in Russian)
https://openlibrary.ge/bitstream/123456789/8866/1/2_Gvelesiani_Monografiya_2020.pdf
18. Gvelesiani A.I., K voprosu o dinamike ionosferno- magnitosfernoy plazmy Zemli. // Monografiya, izdatel'stvo Tbilisskogo gosudarstvennogo universiteta imeni Ivane Dzhavakhishvili, ISBN 978-9941-13-958-1, Tbilisi, 2020, 112 p. (in Russian)
https://openlibrary.ge/bitstream/123456789/8865/1/1_Gvelesiani_Monografiya_2020.pdf
19. Kartvelishvili L., Tatishvili M., Amiranashvili A., Megrelidze L., Kutaladze N. Weather, Climate and their Change Regularities for the Conditions of Georgia. // Monograph, Publishing House “UNIVERSAL”, ISBN: 978-9941-33-465-8, Tbilisi 2023, 406 p. (in Georgian)
https://doi.org/10.52340/mng.9789941334658
20. Varazanashvili O., Gaprindashvili G., Elizbarashvili E., Basilashvili, Ts., Amiranashvili A., Fuchs S., The First Natural Hazard Event Database for the Republic of Georgia (GeNHs). // Catalog, 2023, 270 p.
http://dspace.gela.org.ge/handle/123456789/10369; DOI: 10.13140/RG.2.2.12474.57286
21. Chikhladze V., Set’q’vis sats’inaaghmdego rak’et’ebi. // monograpia, ivane javakhishvilis sakhelobis tbilisis sakhelmts’ipo universit’et’is gamomtsemloba, ISBN 978-9941-36-400-6, tbilisi, 2025 ts’., 128 p. (in Georgian)
22. Abramishvili R., Ambokadze V., Amiranashvili A., Bolashvili N., et al. Geographical Atlas of Kakheti Region. // Publish House Ivane Javakhishvili Tbilisi State University, ISBN 978-9941-36-316-0, Tbilisi, 2025, 214 p. (in Georgian)
23. Amiranashvili A., Bolashvili N., Gagua G., et al. Georgia: Geographical Atlas of Kvemo Kartli Region. // Publish House of Ivane Javakhishvili Tbilisi State University, ISBN 978-9941-36-479-6, Tbilisi, 2026, 198 p. (in Georgian)

2nd International Scientific Conference "Modern Problems in Geophysics", Proceedings,
ISBN 978-9941-36-562-1, ISSN 3088-4349, Tbilisi, Georgia, October 29-31, 2026

# VARIABILITY OF TEMPERATURE AND PRECIPITATION IN TBILISI AND BAKU IN 2005-2024

**[*]Aliyev V., [**]Amiranashvili A., [***,****]Kartvelishvili L., [*****]Matzarakis A., [****,******]Tatishvili M, ****Kapanadze N.**

*[*]CEO & Founder, International Event Organizer Company AMIR Technical Services Azerbaijan, Baku, Azerbaijan*
*[**]Mikheil Nodia Institute of Geophysics of Ivane Javakhishvili Tbilisi State University, Tbilisi, Georgia*
*[***,****]National Environmental Agency, Tbilisi, Georgia*
*[*****]Albert-Ludwigs-Universität Freiburg, Germany*
*[****]Institute of Hydrometeorology of Georgian Technical University, Tbilisi, Georgia*
*[******]Vakhushti Bagrationi Institute of Geography of Ivane Javakhishvili Tbilisi State University, Tbilisi, Georgia*
*avtandilamiranashvili@gmail.com*
*marika.tatishvili@yahoo.com, m.tatishvili@gtu.ge*

***Abstract.*** *The variability of main climatic parameters: temperature and precipitation for two capitals Tbilisi (Georgia) and Baku (Azerbaijan)has been investigated using climatic indices according IPCC recommendations. To conduct the analysis, meteorological observation data of National Environmental Agency and Azerbaijan Meteo Service were used for the 2005- 2024 period. The results show that climate change has a different character in those two locations.*

***Key Words:*** *Climate change, atmospheric precipitation, statistical analysis.*

## Introduction

The problem of observed and expected climate changes on our planet has become especially relevant in recent years. This problem is of great importance in Georgia, due to the diversity of climatic regions on its territory [1]. Atmospheric precipitation is one of the most important components of the climate and special attention has always been paid to its research in Georgia [1-4]. In particular, a large number of studies have been conducted on the climatology of seasonal, monthly and daily precipitation amounts [1-4]; the role of precipitation in the formation of bioclimatic conditions of areas [1]; the impact of precipitation deficiency and excess on the provocation of droughts [5], floods [6], landslides [7] and other negative phenomena, etc. As new information accumulated, data on the variability of the precipitation regime in various regions of Georgia were constantly updated [8-12].

## Study area, material and methods

Study area – Baku (the capital of the Republic of Azerbaijan, 40.45° N, 50.0667° E, -4 m above sea level) and Tbilisi (the capital of the Republic of Georgia, 41.75785° N, 44.7552° E, 427 m above sea level). Distance – 470 km.

For the analysis, data of the National Environment Agency of Georgia and [http://www.pogodaiklimat.ru/] for Baku and Tbilisi in 2005-2024 are used.

To characterize extreme deviations in climate events, the Intergovernmental Panel on Climate Change (IPCC) [13] has developed climate change indices, some of most applicable are: $T_{25}$, $T_{28}$, $T_{30}$, $T_{35}$ day numbers when $T_{max}$ > 25, 28, 30, 35, 38 °C; $T_{min}$ >:< 0, -5; Frost days ($T_{min}$ < °C). For precipitation the indices are as following: day numbers when P=0; P>0; P>15; P>10 mm.

## Results

The precipitation in Tbilisi according calculated indices is reduced, but in last years it is slightly increased. Maximal precipitation amounts 113 mm. It is expected that intensity of catastrophic rainfalls would inc-

rease and small rains decrease due to global climate change (Fig.1., Table 1). The Fig.1. represents precipitation day number changes when P=0; P>0; P>15; P>10. It is expected that due to rain redistribution number of dry days will increase and at the same time number of showers will also increase at the outflow of small rain. the escape

Baku is characterized by small amount of precipitation and this regime remains unchained due to influence of Caspian Sea and atmospheric stratification.

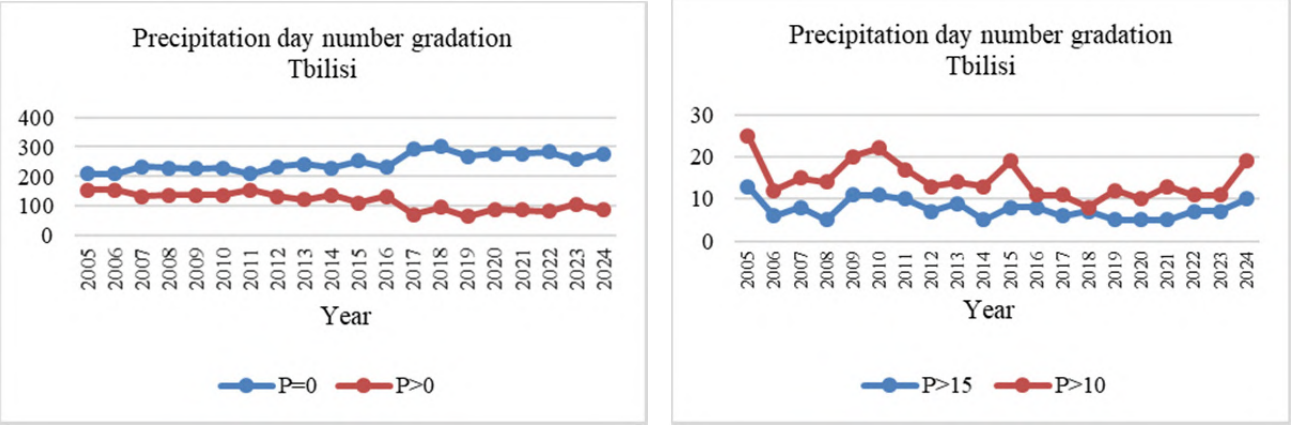


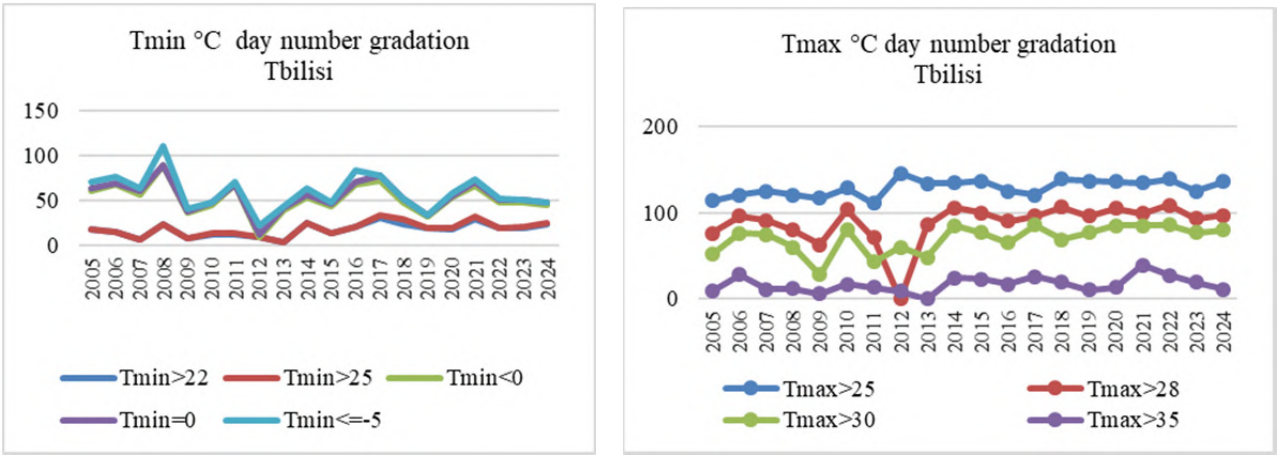

**Fig. 1.** Precipitation day number gradation in Tbilisi (2005-2024)

The $T_{max}$ reaches its highest value 40.6 °C; minimal value is -4.8 °C; Minimal value of $T_{min}$ is -13.9 and maximal 27 in Tbilisi. The $T_{max}$ reaches its highest value 42.76 °C; minimal value is –5.5 °C; Minimal value of $T_{min}$ is -9.6 and maximal 31.1 in Baku.

Table 1. Maximal, minimal values of $T_{max}$, Maximal, minimal values of $T_{min}$ and Maximal precipitation in Tbilisi and Baku for 2005-2024 period.

| Temperature,°C<br>Precipitation, mm | Max $T_{max}$ | Min$T_{max}$ | Max$T_{min}$ | Min$T_{min}$ | MaxP |
|---|---|---|---|---|---|
| Tbilisi | 40.6 | -4.8 | 27.0 | -13.9 | 113 |
| Baku | 42.7 | -5.5 | 31.1 | -9.6 | 76 |

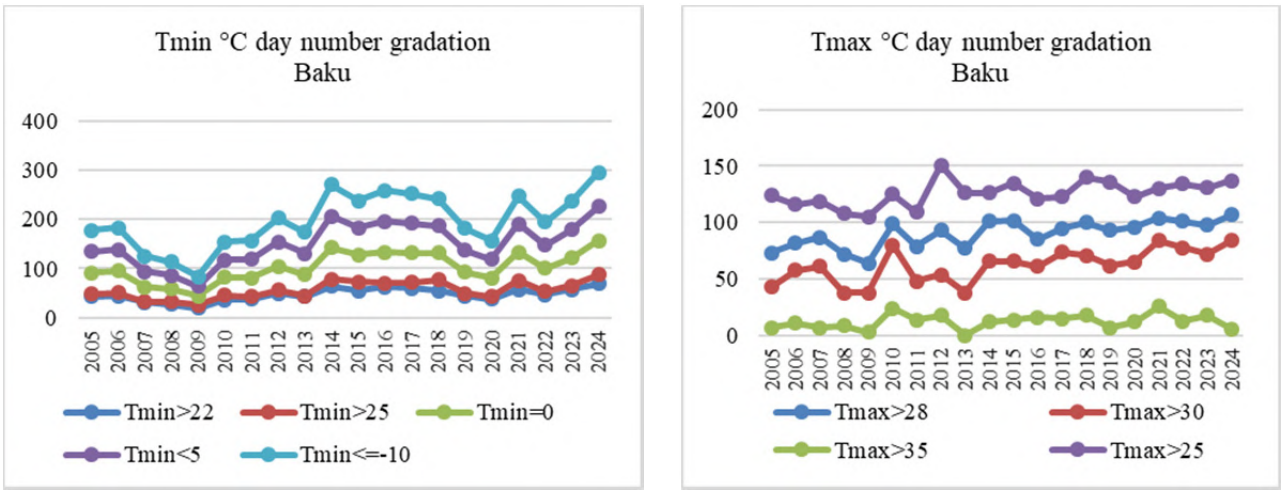
$T_{min}$ day number has reduction character only extreme $T_{min}$>25 °C increases in last year. $T_{max}$ day number also decrease according indices, only for 25 and 28 °C days will increase. This indicates that temperature rise isn't too acute in Tbilisi. This may be explained by its location- so called Tbilisi Hollow.




(a) (b)

**Fig. 2.** $T_{min}$ (a) and $T_{max}$ (b) day number gradation in Tbilisi for 2005-2024 period.

$T_{min}$ day number increases for all 5 gradations. This increase is especially notable in last years 2021-2024. $T_{max}$ also increases not so sharply but slightly except extreme 35 °C- day numbers for this gradation decreased for last year.




(a) (b)

**Fig. 3.** $T_{min}$ (a) and $T_{max}$ (b) day number gradation in Baku for 2005-2024 period.

The climate state remains as it is established for this region: hotter with small irregular amount of precipitations. The results for both places clearly show that their location and character atmospheric circulation play essential role in formation of local climate.

## Conclusion

Based on the obtained results the climate change is strict in Baku than in Tbilisi. Temperature rises sharply in Baku than in Tbilisi. Accordingly, it is expected that tropical day number will increase, that isn't pleasant phenomenon especially for cardiovascular diseases. In the future, it is planned to continue these studies using more indices and longer period.

## References


1. Kartvelishvili L., Tatishvili M., Amiranashvili A., Megrelidze L., Kutaladze N., Weather, Climate and their Change Regularities for the Conditions of Georgia. // Monograph: Publishing House "Universal", Tbilisi, 2023, 406 p., https://doi.org/10.52340/mng.9789941334658
2. Kartvelishvili L., Amiranashvili A., Megrelidze L., Kurdashvili L., Evaluation of Tourist-recreational Resources in the Background of Climate Change in Georgia. // Georgian Geographical Journal, E-ISSN: 2667-9701, 5(2), 2025, pp. 36-40. https://doi.org/10.52340/ggj.2025.05.02.06
3. Aliyev V., Amiranashvili A., Kartvelishvili L., Matzarakis A., Tatishvili M., Comparative Analysis of the Variability of Daily Minimum, Maximum and Mean Air Temperature in Baku and Tbilisi in 2005-2024. // Int. Journal of Sustainability and Rick Control, e-ISSN: 3104-8358, p-ISSN: 3104-834X, Baku, Azerbaijan, Vol. 1, No. 2 (2), September 2025, pp. 63-70. DOI: https://doi.org/10.64599/GDOF7452
4. Aliyev V., Amiranashvili A., Kartvelishvili L., Matzarakis A., Tatishvili M., Changeability of Average Values of Daily Absolute Minimum, Maximum and Mean Air Temperature for Each Month of the Year in Baku and Tbilisi in 2005-2024. // 1st International Scientific Conference "Modern problems in Geophysics". Proceedings, ISBN 978-9941-36-434-1, ISSN 3088-4349, Tbilisi, Georgia, November 6-8, 2025. Publish House of Iv. Javakhishvili Tbilisi State University, Tbilisi, 2025, pp. 117-120. http://dspace.gela.org.ge/bitstream/123456789/10768/1/30_Conf_MPG_2025.pdf
5. Tatishvili M., Amiranashvili A., Tsitsagi M., Palavandishvili A., Zotikishvili N., Microcirculation and Heat Uniqueness of Tbilisi. // 1st International Scientific Conference "Modern problems in Geophysics". Proceedings, ISBN 978-9941-36-434-1, ISSN 3088-4349, Tbilisi, Georgia, November 6-8, 2025. Publish House of Iv. Javakhishvili Tbilisi State University, Tbilisi, 2025, pp. 167-170. http://dspace.gela.org.ge/bitstream/123456789/10755/1/43_Conf_MPG_2025.pdf

6. Aliyev V., Amiranashvili A., Bliadze T., Chikhladze V., Davitashvili M., Kartvelishvili L., Matzarakis A., Pipia M., Tatishvili M., Varamashvili N., Some Study Results of Various Meteorological Parameters Regime and Variability Based on 2005-2024 Year Data and Associated Environment Risk Factors for Baku (Azerbaijan) and Tbilisi (Georgia). // Materials of International Scientific Conference "Study and sustainable use of natural ecosystems in the conditions of modern climate change", Tbilisi, Georgia, December 11, 2025, Scientific Reviewed Proceedings of the Institute of Hydrometeorology of the GTU, ISSN 1512 – 0902, # 137, 2025, p. 35. Doi.org/10.36073/1512-0902-137. http://openlibrary.ge/bitstream/123456789/10799/1/Vol-137.pdf
7. Aliyev V., Bliadze T., Chikhladze V., Davitashvili M., Tatishvili M., Comparison of Angstrom Fire Index for Baku (Azerbaijan) and Tbilisi (Georgia). // 1st International Scientific Conference “Modern problems in Geophysics”. Proceedings, ISBN 978-9941-36-434-1, ISSN 3088-4349, Tbilisi, Georgia, November 6-8, 2025. Publish House of Iv. Javakhishvili Tbilisi State University, Tbilisi, 2025, pp. 171-174. http://dspace.gela.org.ge/bitstream/123456789/10754/1/44_Conf_MPG_2025.pdf
8. Aliyev V., Amiranashvili A., Pipia M., Varamashvili N., Wind Conditions at the Heydar Aliyev Baku and Shota Rustaveli Tbilisi International Airports in 2015–2024. // Theory and Applications, ISSN 1932-2321, Volume 20, Special Issue No. 9 (87), November 2025, pp. 651-659. https://doi.org/10.24412/1932-2321-2025-987-651-659
9. Matzarakis A., Biometeorologie einfach erklärt: Wetter, Klima und der Mensch. // Auflage, Selbstverlag, Bad Krozingen, ISBN: 978-3-00-088241-8, 82 s.
10. Matzarakis A., Human Biometeorology. How Weather and Climate Shape Our Health and Well-being. // First edition, Author and publisher (self-published), ISBN: 978-3-00-088330-9, Rösslegarten 3, D-79189 Bad Krozingen, Germany, 2026, 259 p. https://matzarakis.4lima.de/humanbiometeorology.pdf
11. Bolashvili N., Elbakidze K., Palavandishvili A., Tatishvili M, Tsitsagi M., Modern Methods and Big Data to Study Dangerous Hydrometeorological Events. // Reliability: Theory and Applications, ISSN 1932-2321, Volume 20, Special Issue No. 9 (87), November 2025, pp. 472-477. https://doi.org/10.24412/1932-2321-2025-987-472-477
12. Hinkle D. E., Wiersma W., Jurs S. G., Applied Statistics for the Behavioral Sciences. // Boston, MA, Houghton Mifflin Company, 2003.
13. The 5th assessment report of the IPCC (2013), https://www.ipcc.ch/assessment-report/ar5/

2nd International Scientific Conference "Modern Problems in Geophysics", Proceedings,
ISBN 978-9941-36-562-1, ISSN 3088-4349, Tbilisi, Georgia, October 29-31, 2026

# SPATIAL PATTERNS OF LONG-TERM CLIMATE CHANGE: A GIS-BASED AND GEOSTATISTICAL ANALYSIS

***Bolashvili N., *Chichinadze T. , *,**Gulashvili Z. , *Suknidze N. , *Tatishvii M.**

** Vakhushti Bagrationi Institute of Geography at Ivane Javakhishvili Tbilisi State University, Tbilisi, Georgia*
***Institute of Hydrometeorology, Georgian Technical University, Tbilisi, Georgia*
*nana.bolashvili@tsu.ge*

***Abstract.*** *This paper examines climate-change trends in the study area. The study aims to assess the long-term dynamics of air temperature, identify its spatial distribution, and present climate data in map form. Particular attention is given to areas where instrumental observation records are incomplete and can be supplemented with gridded data. The study combines statistical analysis with geostatistical interpolation to better understand the spatial characteristics of climate change.*

***Key words****: Air Temperature, Climate change, Gridded Data.*

## Introduction

Mountain regions are particularly sensitive to climate change because variations in temperature can affect snow cover, runoff, vegetation, and slope stability. These effects are influenced by complex terrain, which creates substantial climatic differences over relatively short distances. Consequently, climate change in mountainous areas should be assessed not only through average values but also through its spatial distribution [1, 2, 3].

Long-term climate observations are essential for identifying temperature trends. However, in regions where meteorological records are incomplete or interrupted, gridded datasets can provide valuable supplementary information. Their use requires comparison with available station observations to assess their reliability.

GIS and geostatistical methods make it possible to combine climatic data with topographic information and produce maps showing spatial patterns of change. This approach is especially useful in areas with pronounced relief and limited instrumental observations.

The present study evaluates temporal trends, compares different periods, and maps the spatial distribution of temperature changes using gridded data and GIS-based geostatistical methods. The results are intended to support further climate monitoring and the assessment of environmental and climate-related risks.

## Data and Methods

The study uses daily mean, minimum, and maximum air-temperature data for 1950–2023. The main data source is the Copernicus E-OBS gridded dataset (https://cds.climate.copernicus.eu), which covers the study area. Daily climate information was extracted for 108 grid points. The data were converted from NetCDF-4 into an Excel format before analysis.

Climate indices and time series were analysed using the R-based ClimPact2 software package. Spatial maps were produced in a GIS environment. The maps were generated using co-kriging, with climate data as the primary variable and elevation derived from a digital elevation model as the secondary variable. To assess data reliability, the gridded data were compared with historical meteorological observations [4]. The comparison showed close agreement in the temporal behavior of temperature and precipitation.

Correlation coefficients between individual points were high: 0.99 for temperature and 0.95 for precipitation. The differences are mainly explained by elevation differences between the meteorological stations and the corresponding grid points.

The non-parametric Mann-Kendall test [5] was used to identify trends in the time series. This test detects upward or downward tendencies and does not require the data to follow a normal distribution. Taylor

diagrams [6] were also used to evaluate the similarity between modelled and observed data in terms of correlation, standard deviation, and root mean square error.

## Discussion

The analysis showed an increasing trend in mean annual air temperature across almost all climate types in the study area (Fig. 1). The change is particularly pronounced in the northern mountainous part, where the increase in mean annual temperature reaches approximately 1.5°C. In the relatively low-lying southern part, the increase is about 0.7°C, while the average increase across the study area is 1.1°C [7].

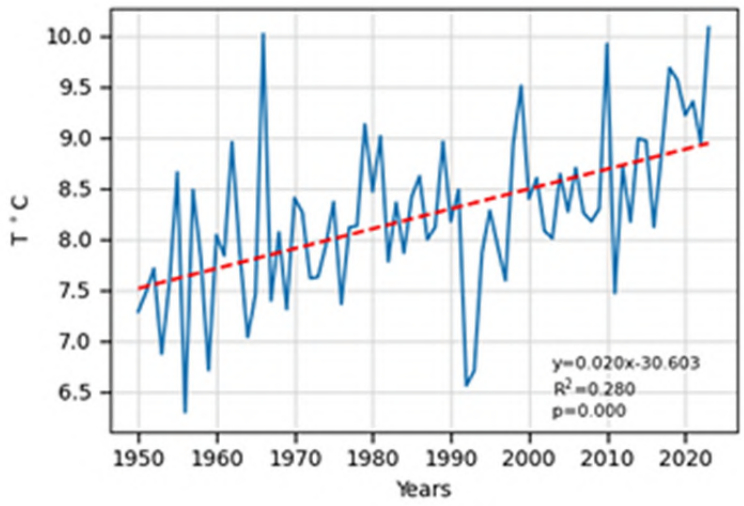



**Fig. 1.** Example of changes in mean annual air temperature, 1950–2023 (Grid point 41).

Time series for individual grid points show that the increase in temperature is not uniform. Although some years are marked by substantial fluctuations, the long-term trend is upward. At a grid point 41, near the city of Tskhinvali, mean annual temperature increased by approximately 0.5°C during 1957-2023, which is close to the 0.45°C change obtained from the reconstructed observation series.

Seasonal analysis indicates that temperatures have increased, to varying degrees, in all seasons, although the clearest warming is observed in summer (Fig. 2). This is important for natural ecosystems, agriculture, water resources, and human health, because a longer warm season can increase evaporation and intensify moisture deficits.

The spatial distribution of the data also indicates a shift in climatic zones. A comparison of the periods 1961-1980, 1981-2000, and 2001-2023 shows that the area affected by colder temperatures is shrinking in the northern part, while warmer conditions are expanding (Fig. 3). According to the study, the average northward shift of natural zones is approximately 0.04 degrees [7].

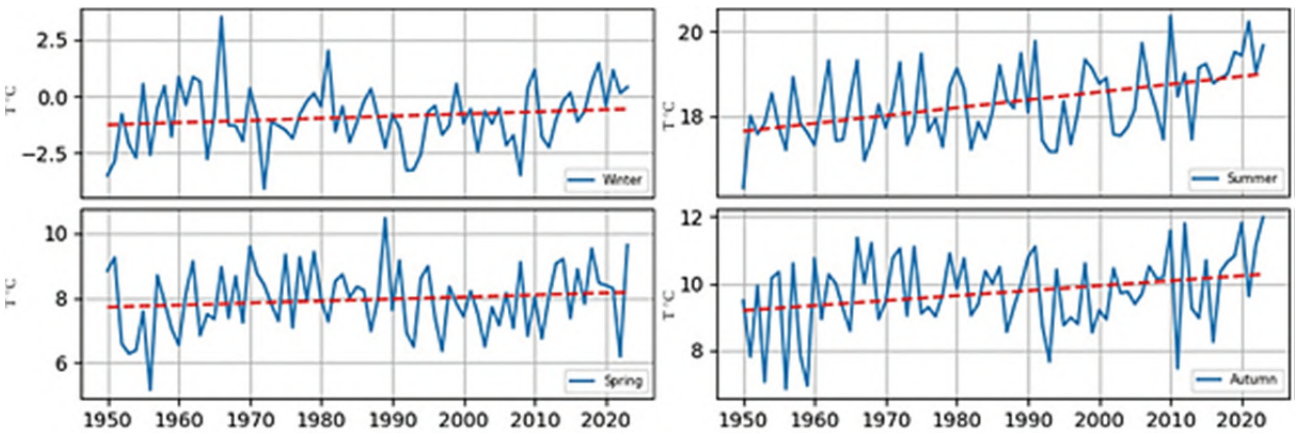



**Fig. 2.** Seasonal changes in average air temperature from 1950 to 2023 (Grid point 41).

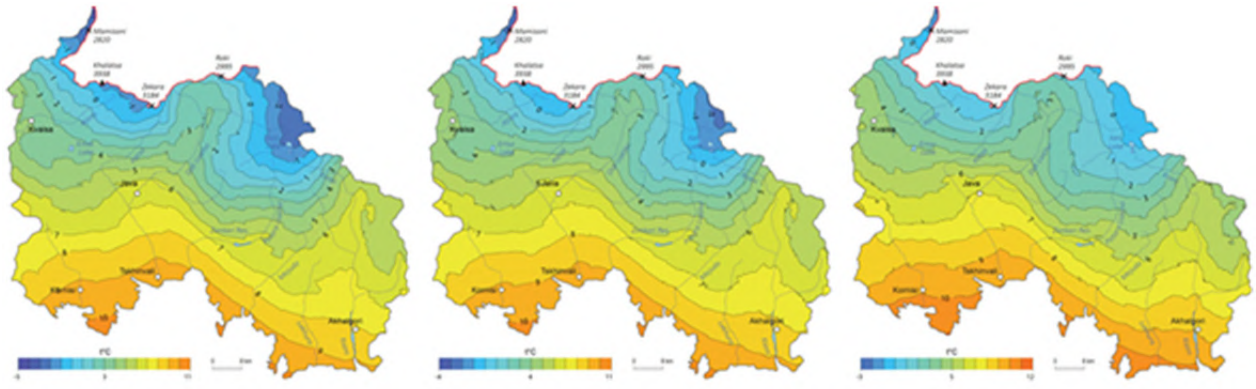


**Fig. 3.** Mean air temperature: a) 1960-1980, b) 1981-2000, c) 2001-2023.

## Conclusions

The maps clearly show that the increase in temperature is not spatially uniform. The change is more pronounced in the high mountainous north, while the increase is smaller in the low-lying foothill areas. Nevertheless, a persistent upward trend is also evident in these areas.

The results confirm that assessing climate change requires the combined use of historical station observations and modern gridded data. Validation showed that E-OBS data can be used for periods when instrumental observations at the local level are limited or unavailable. This approach makes it possible to reconstruct climate time series and generalise them spatially.

Rising temperatures have important environmental and social consequences. These may include a shorter duration of snow cover, seasonal redistribution of water resources, increased risks of drought and wildfire, and more active landslide and debris-flow processes. The results can therefore support climate-risk assessment, adaptation planning, and improved environmental management.

In conclusion, a clear increase in mean annual air temperature was identified in the study area during 1950–2023. The most substantial changes occur in the mountainous part, while seasonal warming is most pronounced in summer. The use of a GIS database and statistical methods provides a basis for continued climate-change monitoring and the preparation of updated maps.

### Acknowledgements

The research was carried out with the financial support of the Shota Rustaveli National Science Foundation of Georgia. Grant # OTG-I-24-456.

The authors gratefully acknowledge the National Environment Agency of Georgia for providing historical meteorological station data for the period 1960–1990 used in this study.

## References

1. Tavartkiladze K., Bolashvili N., & Suknidze N., Determining Parameters of Tbilisi's Winter Regime under Conditions of Climate Change and the Accuracy of their Determination. //Georgian Geographical Journal, 5(3), 2025, pp. 43–49. https://doi.org/10.52340/ggj.2025.05.03.06
2. Tavartkiladze K., Bolashvili N., & Suknidze N., Changes in the Atmospheric Precipitation Regime in Georgia// TSU. // Proceedings of the 1st International Scientific Conference "Modern Problems of Geophysics", 2025, pp. 143-146.
3. Tatishvili M., Bolashvili N., & Palavandishvili A., Impact of short-term geomagnetic activity on the variability of meteorological parameters. // Georgian Geographical Journal, 2(1), 2022. https://doi.org/10.52340/ggj.2022.756
4. National Environment Agency of Georgia (NEA), Historical meteorological station data, 1960–1990. Tbilisi, Georgia, 2026.
5. Mann-Kendall Test, https://real-statistics.com/time-series-analysis/time-series-miscellaneous/mann-kendall-test/Taylor, K.E.: Summarizing multiple aspects of model performance in a single diagram. // J. Geophysics. Res., 106, 2001, pp. 7183-7192.
6. Taylor K.E., Summarizing multiple aspects of model performance in a single diagram. // J. Geophysics. Res., 106, 2001, pp. 7183-7192.
7. Bolashvili N., Gulashvili Z., Suknidze N., Tatishvili M., Chichinadze T., Development of Climate Databases and Risk Assessment of Climate Change Impacts in the Occupied Territories of the Tskhinvali Region Using Modern Methods, Tbilisi, Universali, 2025, 194 p.

2nd International Scientific Conference "Modern Problems in Geophysics", Proceedings,
ISBN 978-9941-36-562-1, ISSN 3088-4349, Tbilisi, Georgia, October 29-31, 2026

# LABORATORY STUDIES OF ICE-FORMING PROPERTIES OF PYROTECHNIC COMPOSITION BASED ON SILVER IODIDE AND ZINC

**Budaev A.**

*High-Mountain Geophysical Institute, Nalchik, Kabardino-Balkaria, Russian Federation*
*budayalim@yandex.ru*

***Abstract.*** *The article presents the results of laboratory experiments investigating the ice-forming properties of the standard pyrotechnic composition AD-1, modified with the addition of zinc (Zn). Silver iodide (AgI) serves as the active component of this pyrotechnic composition. The aim of the experiments was to determine the effect of specific additives on the yield of ice-forming nuclei per gram of reagent. The results yielded specific ice-forming nuclei output values for the modified silver iodide- and zinc-based pyrotechnic composition. The ice-forming efficiency of the zinc-modified composition is an order of magnitude higher than that of the standard AD-1 composition. Utilizing this composition in anti-hail devices would reduce reagent consumption and operational costs associated with active cloud modification.*

***Key Words:*** *Pyrotechnic composition, silver iodide, zinc, zinc oxide, ice-forming nuclei.*

## Introduction

Silver iodide remains one of the most widely used ice-nucleating agents in cloud seeding operations. The high ice-nucleating activity of AgI is attributed to the minimal difference between its crystal lattice and that of ice [1]. In its solid state, water possesses a hexagonal crystal structure in which each water molecule is surrounded by four nearest neighbors. The intermolecular distance is 2,76 angstroms, and the molecules are arranged at the vertices of a regular tetrahedron. Silver iodide has a similar crystal structure.

However, at air temperatures above -6°C, the efficiency of the AgI-based pyrotechnic composition AD-1 drops sharply. One method for enhancing the efficiency of pyrotechnic compositions involves the use of additives that promote the formation of particles with a crystal lattice similar to that of ice [2]. Consequently, the development of new agents or the improvement of existing compositions is a matter of current importance.

## Study area, material and methods

Zinc was selected as an additive to the standard AD-1 pyrotechnic composition because its crystal structure resembles that of AgI. This facilitates the adsorption of $H_2O$ molecules onto the zinc surface and the formation of multiple water-molecule layers (Fig.1). Consequently, a surface water film forms; upon reaching a critical thickness, this film freezes under supercooled conditions. Within this water film, micro-regions containing oriented H2O molecules emerge, acquiring an ice-like structure as supercooling progresses.

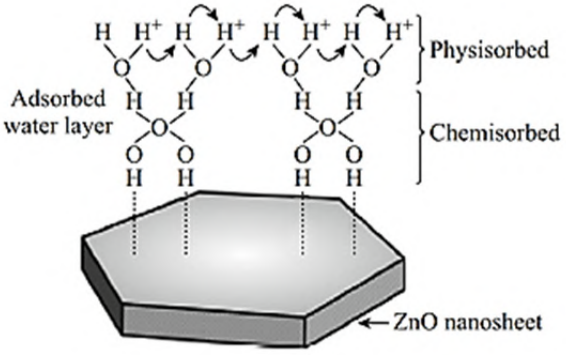



**Fig.1. Schematic** of the interaction between water molecules and a zinc oxide nanoparticle [3].

It should be noted that rapidly heating zinc powder to temperatures exceeding its boiling point promotes the formation of zinc oxide nanotubes. Such nanotubes can serve as ice nucleation sites [4]. Importantly, the boiling point of zinc falls within the combustion temperature range of the AD-1 pyrotechnic composition. When seeding clouds with an ice-nucleating agent via rocket, the combustion of the rocket propellant charge and the subsequent formation of the aerosol occur at temperatures ranging from 700 to 1400°C [5].

Laboratory studies of this composition were conducted using the standard methodology for evaluating the ice-nucleating properties of reagents, as described in the relevant regulatory document [6]. The full experimental cycle utilized a 6 m³ cloud chamber, a cloud-generating device, an electronic balance, a reagent sublimation unit, and a microscope for counting crystals. The temperature within the large cloud chamber was maintained in the range of 0 to -13,4°C.

In these experiments, zinc powder with a particle size of 0,01–0,05 mm was used as an additive to the standard AD-1 pyrotechnic composition. This particle size range was selected because fine particles mix thoroughly with the other composition components during the manufacture of propellant charges for hail-suppression rockets. The zinc powder was incorporated into the AD-1 pyrotechnic composition at levels of 3%, 6%, and 9% of the total mass.

The reagent's effectiveness was assessed based on the number of ice crystals formed when the pyrotechnic composition sample was introduced as an aerosol into the supercooled fog within the cloud chamber. The specific yield of crystallization nuclei for each sample was calculated using the method described in [7]. The number of crystals in the chamber was determined based on the number of crystals deposited on the substrate.

## Results

The results of the experimental studies are presented in Table 1 and Figure 2. Curve 1 represents the yield of ice-forming particles from one gram of the AD-1 composition without zinc; curve 2, with 3% zinc; curve 3, with 9% zinc; and curve 4, with 6% zinc.

**Table 1.** Specific yield of ice-forming nuclei of pyrotechnic composition of AD-1 particles and modified composition with addition of zinc.

| Specific yield, $\times 10^{13}$ $g^{-1}$ | | | | | | | |
|---|---|---|---|---|---|---|---|
| AD-1 | | AD-1, Zn (3%) | | AD-1, Zn (6%) | | AD-1, Zn (9%) | |
| t, °C | | t, °C | | t, °C | | t, °C | |
| -13,4 | 0,44 | -12,5 | 1,70 | -13,3 | 10,0 | -12,7 | 3,50 |
| -11,9 | 0,57 | -12,3 | 1,70 | -12,2 | 14,0 | -12,1 | 3,20 |
| -10,6 | 0,12 | -11,5 | 0,90 | -11,7 | 9,00 | -11,3 | 1,90 |
| -10,2 | 0,12 | -10,6 | 1,50 | -10,8 | 7,00 | -10,7 | 1,40 |
| -9,8 | 0,23 | -10,5 | 1,10 | -10,4 | 10,0 | -10,0 | 2,10 |
| -9,7 | 0,64 | -9,2 | 2,00 | -10,2 | 5,50 | -9,5 | 1,60 |
| -9,6 | 0,27 | -9,1 | 1,70 | -10,2 | 6,30 | -7,2 | 1,30 |
| -9,5 | 0,50 | -9,1 | 0,74 | -10,0 | 6,00 | -7,0 | 0,72 |
| -9,4 | 0,16 | -9,0 | 1,10 | -9,6 | 5,20 | -5,9 | 1,30 |
| -9,1 | 0,62 | -8,7 | 0,86 | -7,5 | 5,40 | -5,2 | 0,51 |
| -8,7 | 0,13 | -8,5 | 1,90 | -5,0 | 1,80 | -4,5 | 0,39 |
| -8,2 | 0,33 | -7,5 | 0,99 | -4,2 | 1,20 | -4,4 | 0,27 |
| -7,5 | 0,32 | -5,5 | 0,90 | -3,8 | 1,80 | -4,3 | 0,62 |
| -7,3 | 0,21 | -4,4 | 1,10 | -3,4 | 1,00 | | |
| -7,2 | 0,53 | -2,2 | 0,82 | -2,2 | 1,30 | | |
| -7,0 | 0,53 | | | -2,0 | 0,40 | | |
| -6,8 | 0,07 | | | -1,6 | 0,47 | | |
| | | | | -1,1 | 0,90 | | |
| | | | | -1,0 | 0,66 | | |

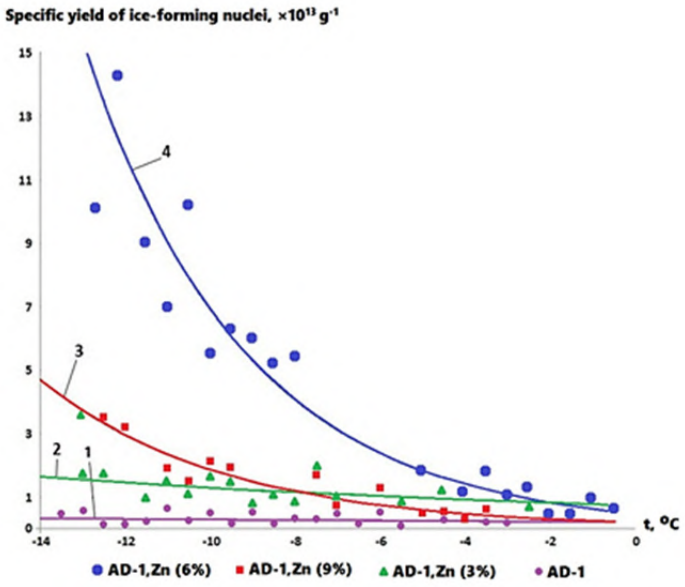



**Fig. 2.** Specific yield of active AD-1 pyrotechnic nuclei with different zinc content.

To clarify and confirm these experiments, studies were conducted with the addition of other mass concentrations of zinc in the range from 1 to 9%. Then the reference values of the air temperature in the cloud chamber were selected. The research results are shown in Figure 3.

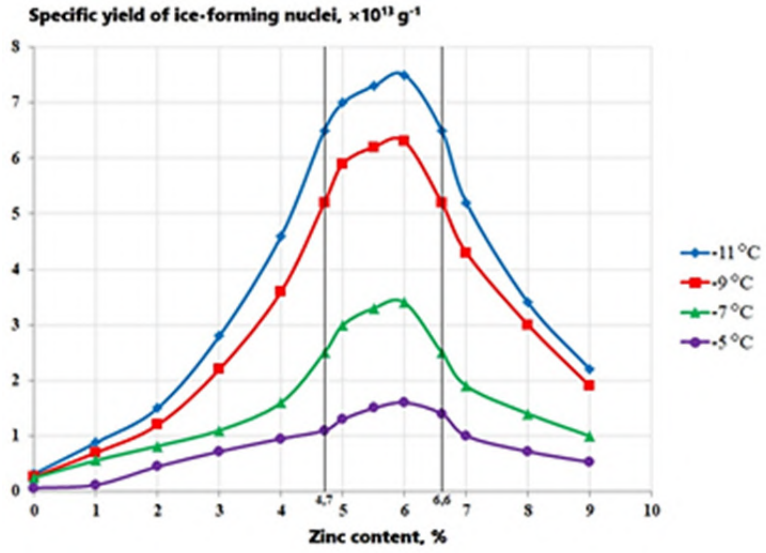



**Fig. 3.** Dependence of the specific yield of ice-forming cores of the AD-1 pyrotechnic compound on the zinc concentration at various temperatures.

According to the data presented in Table 1, Figure 2 and Figure 3 the specific yield of ice-forming nuclei from the AD-1 pyrotechnic composition with a 6% zinc additive increases by an order of magnitude compared to that of the standard AD-1 composition. This increase in the yield of active ice-forming particles is attributed to the formation of zinc oxide nanotubes of various sizes and shapes. These form during the combustion of pyrotechnic compositions through the oxidation of zinc at high temperatures and subsequently interact with supercooled water vapor.

The cloud layer situated between the -6°C and -10°C isotherms is favorable for crystal growth and aggregation and corresponds to the crystallization efficiency threshold of the reagents used [8].

The effectiveness of hail suppression measures depends on numerous factors, including the selection of the optimal reagent consumption rate [9]. The dosage of hail suppression agents for seeding the target area is determined based on the requirement that the concentration of ice-forming nuclei within the seeded volume reaches at least $10^7$ $m^{-3}$ after 3 minutes – and ideally $10^8$ $m^{-3}$ – thereby ensuring a dramatic improvement in

seeding efficiency. The use of the modified AD-1 reagent with added zinc allows for a several-fold reduction in the consumption of hail suppression agents.

## Conclusion

Experimental studies were conducted to evaluate the ice-forming efficiency of the AD-1 reagent, which is based on silver and zinc iodides. The experiments were performed in a cloud chamber at 100% relative humidity and temperatures ranging from 0 to -13,4°C. Analysis of the results showed that incorporating finely dispersed zinc powder into the standard pyrotechnic composition at a level of 6% of the total mass significantly increases the yield of ice-forming particles across the entire temperature range studied (0 to -13,4°C).

The increase in the specific yield of ice-forming nuclei is attributed to the formation of zinc oxide nanotubes of various shapes and sizes during the combustion of the pyrotechnic compositions. These nanotubes actively interact with the cloud environment. The yield of ice-forming nuclei increases by nearly an order of magnitude at -12°C and almost doubles in the -2 to -4°C range, enabling modification of warmer supercooled cloud regions.

Based on the standard AD-1 composition, methods have been developed to produce a modified, highly effective pyrotechnic composition for use in meteorological rockets designed for cloud modification [10]. The new composition can also be used in ground-based generators to treat supercooled fogs in order to create favorable meteorological conditions..

## References


1. Vonnegut B., Experiments with silver-iodide smokes in the natural atmosphere. // Bull. Amer. Meteor. Soc., 1950, Vol. 31.
2. Koloskov B.P., Korneev V.P., Shchukin G.G., Methods and means of modification of clouds, precipitation and fog. St. Petersburg. // RSHMU., 2012, pp. 36-38. (in Russian)
3. Tsai F.-S., Wang S.-J. Enhanced sensing performance of relative humidity sensors using laterally grown ZnO nanosheets. // Sens. Actuators B: Chem. 193, 2014, pp. 280–287.
4. Zakinyan R.G., Kinetics of ice growth on surfaces of objects of various shapes placed in a supercooled aerosol stream. // Materials of the V Scientific and Technical Conference of the SC Technical University, 2001. 20 p. (in Russian)
5. Abshaev A.M., Abshaev M.T., Barekova M.V., Malkarova A.M., Guidelines for the organization and conduct of anti-hail operations. // Nalchik, 2014. pp. 219-237. (in Russian)
6. Khuchunaev B.M., Gekkieva S.O., Baysiev H.M.H., Budaev A.H., Ivanov V.N., Savchenko A.V., Shilin A., Puzov Yu.A., Danelyan B.G., Sosnikova E.V., Methods for determining the ice-forming efficiency of anti-hail products in wind tunnels and laboratory installations. // RD 52.37.914-2021, Nalchik, 2021. (in Russian)
7. Khuchunaev B.M., Stepanova S.I., Khuchunaev A.B., Panaetov V.P., Investigation of the ice-forming properties of zinc oxide crystallohydrates and nanotubes. // In collection: Reports of the All-Russian Conference on Cloud Physics and Active Effects on Hydrometeorological Processes. Nalchik, 2011, pp. 396-402. (in Russian)
8. Ivlev L.S., Dovgalyuk Yu.A. Physics of atmospheric aerosol systems. // St. Petersburg: NIIH St. Petersburg State University, 1999, 76 p.
9. Issues of cloud physics. Collection of selected articles by the MGO. Asterion, // St. Petersburg, 2008, pp. 98-106. (in Russian)
10. Khuchunaev B.M., Baysiev Kh.-M.Kh., Gekkieva S.O., Budaev A.Kh., IOP Conference Series: Materials Science and Engineering PAPER OPEN ACCESS Researches of ice-forming efficiency of products of sublimation of pyrotechnic compositions consisting of silver iodide AgI particles and zinc oxide. 2021 IOP Conf. Ser.: Mater. Sci. Eng.1083 012097.

2nd International Scientific Conference "Modern Problems in Geophysics", Proceedings,
ISBN 978-9941-36-562-1, ISSN 3088-4349, Tbilisi, Georgia, October 29-31, 2026

# EXPERIMENTAL DATA ANALYSIS OF SHORTWAVE-INFRARED RADIANCE USING MACHINE LEARNING METHODS

**Elbakidze Kh.**

*M. Nodia Institute of Applied Mathematics, Tbiisi, Georgia;*
*Institute of Hydrometeorology, Tbilisi, Georgia*
*khatunachargazia@gmail.com*

***Abstract****. This study examines 2025 shortwave-infrared (SWIR) sky-radiance observations from the SKYNET sun–sky radiometer network at Aosta, Italy, and Takayama, Japan. Radiances at 1627 and 2200 nm were evaluated against AOD500, solar zenith angle, time and instrument temperature. The analysis emphasizes one-to-one temporal synchronization and representative scan-level sampling. The results show strong coherence between the two SWIR channels, while AOD500 alone explains only a limited part of radiance variability. Solar geometry is important and temperature effects are comparatively weak.*

***Key words****: SKYNET; shortwave infrared; AOD500; solar zenith angle; radiance; Takayama; Aosta.*

## Introduction

SKYNET sun–sky radiometers provide measurements of direct and diffuse solar radiation at multiple wavelengths and are widely used for monitoring aerosol optical properties. Shortwave-infrared (SWIR) observations at 1627 and 2200 nm are of particular interest because their atmospheric responses differ from those of conventional visible wavelengths and may provide complementary information on aerosol, atmospheric absorption, surface contribution and instrument behaviour. The interpretation of SWIR radiance is nevertheless complex because the measured signal is influenced simultaneously by aerosol loading, solar illumination geometry, viewing geometry, atmospheric transmission, surface reflectance and instrument conditions.

The present analysis considers 2025 observations from two geographically and environmentally different SKYNET stations: Aosta, Italy, representing an Alpine environment, and Takayama, Japan, representing an East Asian environment. The principal objectives are to characterize the two SWIR radiances, investigate their relationships with aerosol optical depth at 500 nm (AOD500) and solar zenith angle (SZA), evaluate possible temperature dependence, examine temporal behaviour and compare the 1627- and 2200-nm channels. Particular attention is given to synchronization because DT4 files contain multiple angular radiance samples within an individual scan, whereas AOD, solar geometry and auxiliary temperature measurements are primarily scan-level observations. Reusing one atmospheric observation for multiple angular samples can artificially increase the apparent sample size and distort relationships.

The processing strategy therefore uses one representative radiance observation per scan and one-to-one nearest-time matching between radiance, AOD and auxiliary records. This produces independent scan-level associations and provides a more appropriate basis for interpreting the observed SWIR variability.

## Data and Methods

Three principal data products were used. DT4 angular-scan files provide sky-radiance measurements and scan geometry, from which the 1627- and 2200-nm radiances were extracted. SUN/DAT auxiliary files provide solar-angle information and instrument-temperature measurements. Level-2 NetCDF files provide AOD at 500 nm. The final analysis therefore includes observation time, station, radiance at both SWIR wavelengths, AOD500, SZA, DT4 scan angular position and normalized radiance.

At Aosta, the source inventory contained 85 DT4 files, 96 SUN files, 87 DAT files and 65 Level-2 NetCDF files. The raw DT4 record included 78,391 angular radiance samples representing 4,053 unique scans. After validity screening and representative scan selection, 3,938 observations remained after radiance

quality control. One-to-one temporal matching yielded 1,685 DT4–AOD matches. The final combined database covers 1 January to 12 April 2025 because the available Level-2 AOD record ends earlier than the DT4 record, which continues into late April.

For Takayama, the processing window was defined as the full calendar year 2025. The working inventory contained 536,287 DT4 rows representing 10,011 unique scan times, together with 5,173 AOD records and 256,939 DAT observations. After initial screening, representative-angle selection produced 2,760 scan-level observations. Fourteen were removed by radiance quality control, leaving 2,746 clean scan-level observations. One-to-one synchronization produced 1,947 unique DT4–AOD matches and 2,264 unique DT4–DAT matches. The actual overlapping observations used in the graphical analysis are concentrated mainly between January and April, with Level-2 AOD availability extending into May; no extrapolation beyond the available overlap was performed.

Temporal synchronization was performed using nearest-time matching with a one-to-one constraint, so a single AOD or auxiliary record could not be assigned repeatedly to multiple radiance scans. At Aosta, the median DT4–AOD time difference was approximately 3.08 min and the mean difference approximately 3.42 min, while DT4–auxiliary observations were effectively simultaneous. At Takayama, most DT4–AOD matches were within several minutes, with a concentration around approximately 2–5 min; DT4–auxiliary matches were much tighter and concentrated close to zero.

The solar-angle definition was independently checked. At Aosta, treating the auxiliary value directly as SZA produced a median absolute discrepancy of approximately 36.27° relative to DT4 geometry. Interpreting the value as solar elevation and converting it using SZA = 90° − solar elevation reduced the median absolute discrepancy to approximately 0.10°, with an RMSE of approximately 0.157°. At Takayama, the adopted auxiliary SZA closely followed the DT4 SZA. The distinction between SZA and DT4 scan angular position was also maintained: SZA describes the Sun's position relative to the local vertical, whereas the DT4 angular position describes where the instrument points during a sky scan. For time-series comparisons, a representative radiance was selected near $|\varphi| \approx 30°$.

Radiance quality control required finite and positive values at both wavelengths, valid AOD where applicable, physically meaningful solar geometry and a non-zero DT4 angular position. Because radiances span several orders of magnitude, logarithmic radiance axes were used. This representation retains the main low-radiance population while allowing higher-radiance observations to remain visible.

## Results

### 1 Aosta

The final Aosta database contains 1,685 synchronized observations. AOD500 has a mean of approximately 0.080, a median of 0.066 and an interquartile range of approximately 0.048–0.094; the maximum observed value is approximately 0.449 [1]. The dataset is therefore dominated by relatively low aerosol optical depth, although several higher-AOD cases are present. SZA ranges from approximately 37.3° to 82.7°, with a mean near 60.0° and median near 61.9°.

Both SWIR channels show substantial scatter when radiance is compared with AOD500. The relationship is positive but weak: for 1627 nm, the correlation between log-transformed radiance and AOD500 is $r = 0.249$, while for 2200 nm it is $r = 0.155$. These values indicate that AOD500 alone accounts for only a limited part of the observed SWIR radiance variability.

The association with SZA is stronger. For 1627 nm the correlation is $r = −0.460$, and for 2200 nm it is $r = −0.370$. Thus, radiance generally decreases as SZA increases in the synchronized Aosta observations. This identifies solar geometry as an important first-order correlate of the measured SWIR signal in this dataset.

Temperature relationships are comparatively weak. For Temperature 1, correlations with log radiance are approximately 0.083 at 1627 nm and 0.077 at 2200 nm. For Temperature 2, they increase to approximately 0.184 and 0.151, respectively. These results do not indicate a dominant direct thermal control, although temperature remains relevant as a secondary instrumental or environmental factor [1,2].

The two SWIR channels show a much stronger common response. The correlation between 1627- and 2200-nm radiance is $r = 0.865$ with $p < 0.001$. The temporal series also shows simultaneous enhancements in both channels. This coherence suggests that a substantial component of the measured variability is shared

between the wavelengths and may reflect common changes in illumination, viewing geometry, atmospheric transmission and aerosol or cloud conditions [3].

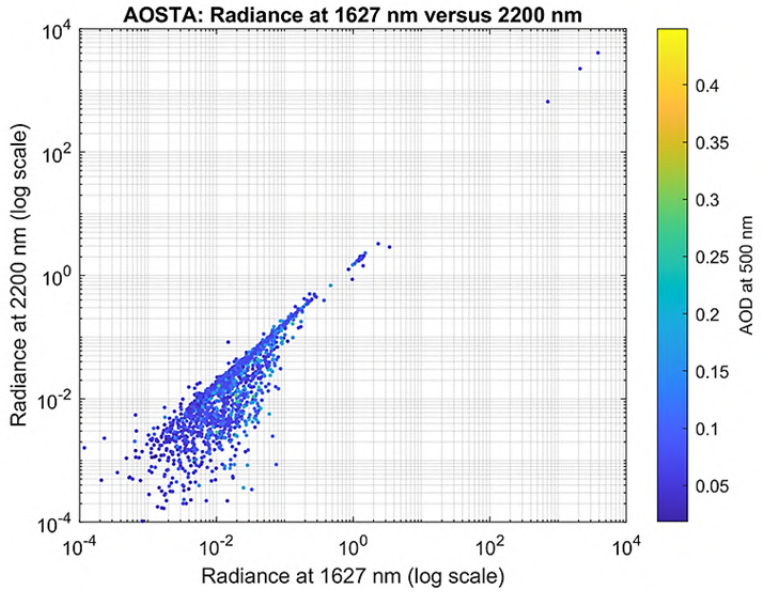



**Fig. 1.** Relationship between 1627- and 2200-nm SWIR radiance at Aosta (2025).

## 2 Takayama

Takayama radiances span several orders of magnitude in both channels, with the dominant population approximately between $10^{-3}$ and $10^{-1}$ in the plotted radiance units and a smaller number of observations extending through $10^{0}$, $10^{2}$ and occasionally above $10^{3}$. The occurrence of high-radiance observations in both wavelengths and in several diagnostic plots supports treating them as part of the observed distribution rather than automatically classifying them as isolated channel failures[1-3].

The 1627-nm radiance–AOD500 relationship is dominated by relatively low aerosol loading, generally below AOD500 = 0.2. Nevertheless, observations at similar AOD values span several orders of magnitude in radiance. The 2200-nm relationship shows the same broad behaviour. In the reported statistical test, the 2200-nm radiance versus AOD500 correlation is r = −0.001, p = 0.803, for N = 58,385. These results reinforce the conclusion that AOD500 cannot be treated as a single-variable proxy for SWIR radiance at Takayama [1-3].

The SZA distribution is concentrated roughly between 10° and 50°, with additional observations at higher angles. The central radiance distribution generally increases from the lowest SZA range toward intermediate values, although the relationship is not adequately described by a simple monotonic function over the full angular range. The reported linear correlations are very small: r = −0.023 for 1627 nm and r = −0.047 for 2200 nm, despite the reported p-values being below 0.001. The plots therefore indicate that SZA contributes to the structure of the radiance distribution, but neither SZA nor aerosol loading alone explains the observed variability.

Instrument-temperature relationships are also weak. For 1627 nm, Pearson correlations are r = 0.032 for Temperature 1 and r = 0.043 for Temperature 2. For 2200 nm, the corresponding values are r = 0.025 and r = 0.040. The temperature plots also show systematic changes in SZA across parts of the temperature range, demonstrating that temperature and observation geometry covary. Consequently, the results support monitoring temperature without attributing the dominant SWIR variability exclusively to detector or instrument temperature.

The Takayama time series shows intermittent observations from January through April 2025, with greater density during late March and April. Higher-radiance periods generally occur simultaneously at both wavelengths. The direct 1627–2200 nm comparison produces a pronounced approximately diagonal relationship in log–log space across several orders of magnitude. This indicates strong common-mode behaviour and provides an important internal consistency check for the two channels.

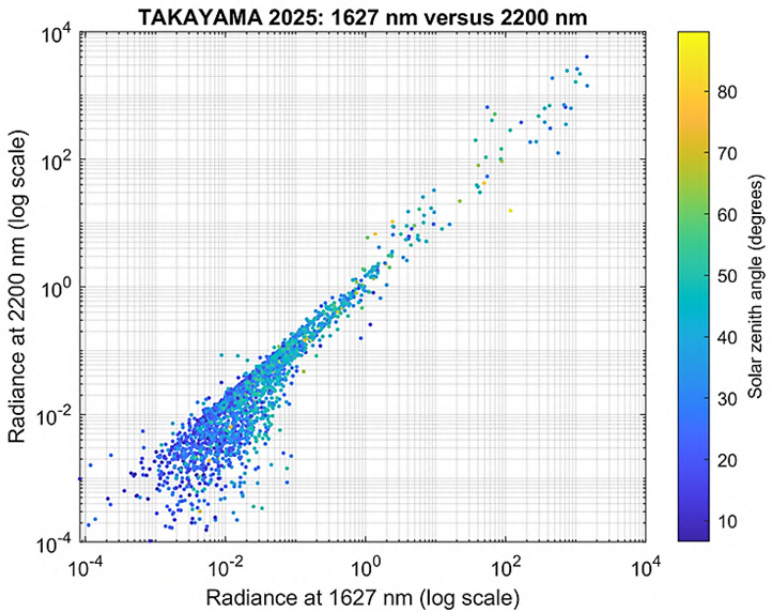



**Fig. 2.** Relationship between 1627- and 2200-nm SWIR radiance at Takayama (2025).

## Discussion

The comparison of Aosta and Takayama demonstrates that SWIR radiance is a multifactor measurement. At both stations, the two wavelengths behave coherently, while AOD500 alone leaves substantial unexplained dispersion. At Aosta, the stronger statistical association with SZA indicates a clear geometrical component. At Takayama, the linear SZA correlations are weak, but the distribution still changes across the SZA domain, illustrating that station-specific relationships can differ even when the same measurement strategy is applied.

The contrast also highlights the importance of controlling measurement geometry before interpreting aerosol–radiance relationships. DT4 scans contain multiple angular samples for a single scan time, whereas atmospheric and auxiliary variables are not independent for each angle. Using all angular samples would repeatedly assign the same AOD, SZA or temperature to different radiances and could create artificial patterns [1-3]. The representative scan-level approach reduces this problem and makes temporal comparisons more physically interpretable.

The synchronization diagnostics are therefore an analytical result in their own right. The close temporal correspondence between DT4 and auxiliary observations, together with the one-to-one treatment of AOD and auxiliary records, provides evidence that the variables used in the final relationships are temporally representative of the corresponding radiance measurements. The explicit verification of solar-angle definitions is equally important because solar elevation and solar zenith angle are complementary quantities rather than interchangeable variables.

Taken together, the results support interpreting the measured SWIR signal as the combined response of atmospheric state, solar and viewing geometry, and instrumental conditions. The strong 1627–2200 nm coherence at both stations indicates that much of the variability is common to the two channels, while the remaining dispersion suggests wavelength-specific effects and measurement variability, especially at the extremes of the radiance distribution.

## Conclusions

The 2025 SKYNET analysis at Aosta and Takayama provides a consistent characterization of SWIR sky radiance at 1627 and 2200 nm. At Aosta, the final synchronized dataset contains 1,685 observations covering 1 January–12 April 2025. At Takayama, representative scan selection and quality control produce 2,746 clean scan-level observations, including 1,947 unique AOD matches and 2,264 unique DAT matches.

The principal result is that AOD500 alone does not determine SWIR radiance. At Aosta, its correlations with logarithmic radiance are weak compared with the stronger SZA relationships, while at Takayama substan-

tial radiance dispersion remains at similar AOD values and the 2200-nm AOD correlation is effectively zero in the reported test. Temperature effects are weaker and are partly confounded with observation geometry.

A second major result is the strong coherence of the 1627- and 2200-nm channels. At Aosta, their correlation is $r = 0.865$ with $p < 0.001$, and Takayama shows a similarly pronounced common response in log–log space. This coherence provides an internal consistency check and indicates that shared atmospheric and geometrical influences account for a substantial component of the observed variability [3].

Finally, the study demonstrates that methodological control is essential for SWIR interpretation. Verified solar-angle definitions, representative scan-level selection, one-to-one temporal synchronization, explicit scan geometry, and logarithmic radiance representation reduce the risk of artificial relationships. The resulting dataset provides a sound basis for subsequent multi-station analysis, calibration assessment, and more detailed multivariate or radiative-transfer modelling.

**Acknowledges:** The study was conducted by financial support of Cost Project CA21119 and Shota Rustaveli Science Foundation Grants #FR 25-1725 and 25-16-929.

## References

1. Diémoz H., Campanelli M., & Estellés V., One year of measurements with a POM-02 sky radiometer at an Alpine EuroSkyRad station. // Journal of the Meteorological Society of Japan, 92A, 2014, pp. 1–16. https://doi.org/10.2151/jmsj.2014-A01
2. Campanelli M., Nakajima T., Khatri P., Takamura T., Uchiyama A., Estellés V., Liberti G. L., & Malvestuto V., Retrieval of characteristic parameters for water vapour transmittance in the development of ground-based sun–sky radiometric measurements of columnar water vapour. // Atmospheric Measurement Techniques, 7, 2014, pp. 1075–1087. https://doi.org/10.5194/amt-7-1075-2014
3. Campanelli M., Nakajima T., & Olivieri B. Determination of the solar calibration constant for a sun-sky radiometer: Proposal of an in-situ procedure. // Applied Optics, 43(3), 2004, pp. 651–659. https://doi.org/10.1364/AO.43.000651

2nd International Scientific Conference "Modern Problems in Geophysics", Proceedings,
ISBN 978-9941-36-562-1, ISSN 3088-4349, Tbilisi, Georgia, October 29-31, 2026

# CLIMATE AND METEOROLOGICAL HAZARDS OF THE KINTRISHI RIVER BASIN

***Elizbarashvili M., **Elizbarashvili E., ***Chikhradze N.**

**Faculty of Exact and Natural Sciences, Ivane Javakhishvili Tbilisi State University,Tbilisi, Georgia*
*** Institute of Hydrometeorology at Georgian Technical University, Tbilisi, Georgia*
****LEPL National Environmental Agency, Tbilisi, Georgia*
*mariam.elizbarashvili@tsu.ge*

***Abstract.*** *The article discusses the climatic conditions of the Kintrishi River basin and its characteristic meteorological hazards. The research used databases of the National Environmental Agency of Georgia and the Institute of Hydrometeorology of the Georgian Technical University, climate directories, atlases and the Catalog of Natural Disasters created at the M. Nodia Institute of Geophysics. The main characteristics of air temperature, atmospheric precipitation, relative humidity, snow cover and wind regime are studied.*

***Key words:*** *Climate change, natural hazards, early warning, adaptation.*

## Introduction

The study of climate and meteorological hazards is particularly relevant in the context of modern climate change, when the frequency and intensity of extreme weather events are increasing in many regions of the world. Western Georgia, including the Kintrishi River basin, is distinguished by its complex terrain, the interaction of sea and mountain climatic factors, and high humidity, which contribute to the formation of such dangerous meteorological events as whirlwinds, hail, heavy precipitation, fog, and blizzards. These events have a significant impact on the safety of the population, agriculture, transport infrastructure, and tourism activities.

## Study object

The Kintrishi River catchment basin is located in the humid subtropical climatic zone of Western Georgia, on the territory of the Autonomous Republic of Adjara. The river originates on the northwestern slope of the Meskheti Range, at an altitude of 2,599 m above sea level, and flows into the Black Sea near Kobuleti. Its length is 60 km, and the basin area is 291 km². Thus, the large difference in elevation between the river's headwaters and its confluence acts as the main climate-forming factor, and the distribution of climatic parameters in the basin area, despite its small size, is characterized by significant variability.

## Method and material

To analyze the climatic background and expected meteorological hazards of the Kintrishi Basin, long-term observation data from the Kobuleti, Chakvi, Chakvistavi, and Bakhmaro meteorological stations were used, starting from the date of organization of the observations and ending in 2022. The Bakhmaro data characterize the mountainous zone of the basin.

Observation data from the National Environmental Agency and climate references were used [1,2]. Databases of the Institute of Hydrometeorology of the Georgian Technical University, climatic researches of Georgia and Adjara conducted at the same institute – monographs and atlases [3,4,5], Catalogue of Natural Disasters created at the M. Nodia Institute of Geophysics of Tbilisi Ivane Javakhishvili State University [6] and other literary sources [7,8]. The study used statistical and comparative analysis methods.

## Results and discussion

According to the maps of the "Climatic and Agroclimatic Atlas of Georgia" [4], the average annual air temperature in the mouth of the Kintrishi River basin and the Kolkheti Lowland exceeds 14°C, while in the

headwaters of the river it is approximately 6-8°C. The average maximum temperature in most of the basin is 36-38°C, dropping to 30°C at the headwaters. The average absolute minimum temperature is minus 4 to minus 8°C, and in the mountains it drops to minus 10 to minus 16°C. The relative air humidity is high throughout the year, averaging 75-80% in January and 75-85% in July.

The annual total precipitation in the basin area is also included in the "Climatic and Agroclimatic Atlas of Georgia" [4]. According to maps, it averages 2,000-2,800 mm. Precipitation in the cold season of the year exceeds precipitation in the warm season. The annual duration of precipitation is approximately 1,400-1,600 hours. The daily maximum precipitation within the basin is 150-300 mm. There are more than 160 rainy days on average in the basin during the year.

On the Meskheti range, a stable snow cover forms from November 10, which is broken in late March or early April. The snow cover lasts for about 100-150 days. Its average decadal maximum height in the mountains reaches 200 cm. There is a medium and strong avalanche danger here.

The duration of sunlight in the basin area is less than 2,000 hours per year. Breeze and monsoon circulation prevail, which determines the daily circulation of winds and the dominance of sea winds during the warm period of the year, and the predominance of land winds during the cold period of the year. The average annual wind speed in the basin area is 4 m/s or less. The number of days with strong winds, when the speed is greater than or equal to 15 m/s, is 10-24 days per year [5].

Table 1 presents the number of days with special atmospheric events characteristic of the basin.

**Table 1.** Characteristics of the Kintrishi River basin special atmospheric phenomena [2, 6, 9].

| Stations | Atmospheric event, number of days | | | | | |
|---|---|---|---|---|---|---|
| | Lightning | Hail | Fog | Blizzard | Strong wind | Whirlwind |
| Kobuleti | 35 | 2.4 | 8 | - | 24 | 0.02 |
| Chakvi | 39 | 1.1 | 5 | - | 20 | - |
| Chakvistavi | 28 | 0.8 | 16 | - | - | - |
| Bakhmaro | 41 | 2.8 | 102 | 30 | 11 | 0.6 |

As can be seen from Table 1, among the special atmospheric phenomena, thunderstorms are more common in the lowlands, while fog is increasing in the mountains.

The number of days with **thunderstorms** exceeds 25 days in most of the territory, although in some years it may be 45-65 days. Throughout the basin, thunderstorms are most frequent in the summer months, while a secondary maximum of days with thunderstorms is observed in the lowland zone at the beginning of autumn, and in the mountainous zone at the end of spring. The main maximum of thunderstorms in the summer months is explained by the fact that during this period, solar radiation is the highest and the Earth's surface is intensively heated. As a result, strong vertical convection develops – warm and humid air quickly rises, cools and forms powerful cumulus and cumulonimbus clouds, which cause lightning, thunderstorms, and heavy rains. The high humidity characteristic of western Georgia further enhances these processes. The secondary maximum of thunderstorm days in the lowland zone in early autumn is explained by the thermal influence of the Black Sea. After summer, the sea retains accumulated heat for a long time and intensively evaporates moisture. When relatively cold air masses begin to invade the region, their interaction with warm and humid air increases the instability of the atmosphere and leads to the reactivation of thunderstorm processes. In mountainous areas, a secondary maximum occurs in late spring, when melting snow, rapid surface warming, and orographic uplift of moist air promote strong convection.

The number of **foggy** days per year in Kobuleti and Chakvi is 5-8 days, and in Chakvistavi it is already 16, although there are years when it reaches 40 days, and the most frequent is 16-20 days, when the frequency is 24%. In the mountains, the number of foggy days exceeds 100, in Bakhmaro it sometimes reaches 140 days, and in 50% of cases it is 90-110 days. In the annual course, the lowland zone is characterized by a spring maximum, mainly in April, while in the mountains the maximum corresponds to the summer months. For example, according to Bakhmaro data, the number of foggy days in the summer months is 14, 19 and 17 days, respectively in June, July and August. The spring maximum in the annual number of foggy days on the coastal plain is mainly explained by high humidity, the influence of the sea, and

the features of the mountain-valley relief. In spring, evaporation from the surface of the Black Sea intensifies, as a result of which the amount of water vapor in the atmosphere increases. Moist air masses move from the sea towards the basin and accumulate in the valleys. When this air touches the relatively cold mountain slopes and the land surface cooled at night, water vapor condenses and fog forms. In the high-mountainous zone, for example, in the vicinity of Bakhmaro, the increase in fog in summer is facilitated by convective processes developed due to the orographic factor – the forced rise of moist air on the slopes, its cooling, and the intensive development of cloudiness and fog.

**Hail** is not a frequent occurrence for the region. In the coastal zone, the number of hail days per year is on average 1-2, in Chakvistavi it decreases, and in the mountains it increases again to 3 days.

The hail frequency in the Kintrishi River basin can be discussed in more detail in Table 2, which presents the average and maximum number of hail days per year, as well as the period of the annual maximum in the Kintrishi basin and Bakhmaro, which can be indirectly used to characterize the mountainous zone of the basin.

**Table 2.** Characteristics of hail days during the year

| Station | Average number | Annual maximum, month | The largest number |
|---|---|---|---|
| Kobuleti | 2.4 | October | 5 |
| Chakvi | 1.1 | October-November-December | 5 |
| Chakvistavi | 0.8 | October-November | 4 |
| Bakhmaro | 2.8 | June | 14 |

The table shows that in the lowland zone of the Kintrishi River basin and on the sea coast, the number of days with hail per year does not exceed 2 on average, in Kobuleti it is 2.4, but in some years hail may occur for 4-5 days. Considering the data from Bakhmaro, hail is relatively frequent in the mountainous zone of the basin and occurs on average 3 days per year, although it can occur for 14 days. In the annual course, hail is most frequent in lowland areas in October-December, because during this period the Black Sea is still warm, and relatively cold air masses are already penetrating the upper layers of the atmosphere.

**Blizzards are** common in mountainous areas. According to Bakhmaro data, the number of blizzard days per year is 30, and in some years it reaches 50. The most frequent are 21-35 days, which account for almost 50% of cases.

The basin area experiences **strong winds** on average 10-24 days per year, when their speed is greater than or equal to 15 m/s. Sometimes it reaches 30-40 days. Such winds are most frequent during the cold period of the year. For example, the number of days with strong winds in February in Kobuleti is 3.2, in Chakvi – 2.6, and in Bakhmaro – 1.7. The increase in the frequency of strong winds in the cold period of the year, especially in winter, is associated with the seasonal intensification of atmospheric circulation and the increase in sea-land thermal contrasts.

A dangerous weather phenomenon is a **whirlwind** when its speed exceeds 32 m/s. Its recurrence, as can be seen from Table 3, is not expressed in large numbers, but it can bring catastrophic results. According to Bakhmaro, the recurrence of whirlwind in the mountains is 0.6, that is, 6 cases of gale are expected every 10 years, while on the coast it is observed once every 50 years.

Table 3 presents some characteristics of the whirlwind in the Kintrishi River basin and its neighboring areas for the period 1961-2022.

**Table 3.** Some characteristics of the whirlwind, 1961-2022

| Station | Whirlwind characteristic | | | | |
|---|---|---|---|---|---|
| | N | Nmax | Year | Vmax | Year |
| Kobuleti | 0.22 | 5 | 2010 | 34 | - |
| Batumi | 0.24 | 2 | 2002 | 35 | 2002 |
| Chakvi | 0.03 | 1 | - | 36 | 1978 |
| Bakhmaro | 0.37 | 5 | 1984 | 40 | 1976 |

In Table 3, a dash (-) indicates that the recurrence of the whirlwind of the corresponding magnitude has been recorded several times, N–is the average recurrence rate of the whirlwind per year (number of cases), Nmax–is the greatest recurrence of the whirlwind per year (number of cases), and Vmax–is the highest speed of the whirlwind.

It follows that the cyclone does not develop annually in the study area. Its recurrence on the coast and in the lowland zone of the basin is 0.03-0.25 days per year, which means that the periodicity of the cyclone here varies from 4 to 30 and more years, its maximum speed is expected to be 34-36 m/s. If we extend the Bakhmaro data to the mountainous zone of the basin, then the cyclone recurrence in the mountains is 0.37 days per year, that is, its periodicity will be on average 2.5 years, which means that the cyclone is expected once every 2.5 years and its maximum speed will be 40 m/s. Such a cyclone may cause medium and strong effects. It is possible to protect yourself from such a cyclone by warning the population in advance, which is successfully done by the National Environmental Agency of Georgia in case of worsening weather conditions.

**Drought** is not observed in the basin area. This is facilitated by the significant amount of precipitation and high relative humidity, as well as the large reserves of productive moisture in the soil. Strong, moderate and weakly drained soils are common here, with a 1 m-thick layer containing more than 200 mm of productive moisture [10].

## Conclusion

The Kintrishi River catchment basin is located in the humid subtropical climatic zone of Western Georgia. The length of the river is 60 km, the basin area is 291 km², and the height difference between the river source and the confluence is about 2,600 m. The distribution of climatic parameters in the basin area, despite its small size, is characterized by significant variability. The average annual air temperature in the Kintrishi River basin mouth and on the Colchis plain exceeds 14 degrees, and in the river source, it is approximately 6-8 degrees. The annual total atmospheric precipitation in the basin area averages 2,000-2,800 mm.

Of the special atmospheric phenomena, thunderstorms are frequent in the plains, and fog increases in the mountains. The number of foggy days per year in Chakvistavi already exceeds 60, and in the mountains it exceeds 100. The number of days with thunderstorms exceeds 25 days in most of the territory. Hail is not a frequent occurrence; the number of hail days per year in the basin is on average 1-3. Blizzards are frequent in mountainous areas. According to Bakhmaro, the number of blizzard days per year is 30.

A dangerous weather phenomenon is a whirlwind. The recurrence rate of a whirlwind in the mountains is 0.6, that is, 6 cases of a whirlwind are expected every 10 years, while on the coast, it is observed once every 50 years.

In the lowland zone of the Kintrishi River basin and on the sea coast, the number of days with hail does not exceed 2 on average per year, in Kobuleti it is 2.4, but in some years hail may occur for 4-5 days. If we take into account the data from Bakhmaro, hail is relatively frequent in the mountainous zone of the basin and occurs on average 3 times per year, although there may be much more cases.

## References


1. Scientific and Applied Climatic Handbook of Georgia. Tbilisi, 2020. (in Georgian)
2. Handbook of the USSR Climate. Issue 14, Parts 1-5, Leningrad, 1960-1971. (in Russian)
3. Georgian resorts and resort resources. Atlas, Moscow: USSR Ministerial With the Council Existing Geodesy And Cartography Home Department, Tbilisi: Kartfabrik, 1989. (in Russian, Georgian and English) https://dspace.nplg.gov.ge/handle/1234/440483
4. Climatic and Agroclimatic Atlas of Georgia. Tbilisi, 2011. (in Georgian)
5. Elizbarashvili E., Samukashvili R., Vachnadze J., Climate of Georgia., Vol. 1, Adjara. (Edited by ). // Proceedings of the Institute of Hydrometeorology, Vol. 110, 2003. (in Georgian)
6. Varazanashvili O., Gaprindashvili G., Elizbarashvili E., Basilashvili Ts., Amiranashvili A., Fuchs S., First Natural Hazard Event Database for the Republic of Georgia. // (GeNHs). Catalog, 2023. The http://dspace.gela.org.ge/handle/123456789/10369; 270 p. DOI: 10.13140/RG.2.2.12474.57286
7. Blanutsa S., Elizbarashvili E., Kartsivadze N., Resort Ureki. Tbilisi, 1982. (in Georgian)

8. Varazanashvili O., Tsereteli N., Amiranashvili A., Tsereteli E., Elizbarashvili E., Dolidze J., Qaldani L, Saluqvadze M., Adamia S., Arevadze N., Gventcadze A., Vulnerability, hazards and multiple risk assessment for Georgia. // Natural Hazards Journal of the International Society for the Prevention and Mitigation of Natural Hazards. volume 64, 2012, pp. 2021–2056. DOI 10.1007/s11069-012-0374-3
9. Elizbarashvili E. Sh., Varazanashvili O. Sh., Tsereteli N. S., Elizbarashvili M. E., Hurricane winds in the territory of Georgia. // Russian Meteorology and Hydrology volume 38, Issue 3, 2013, pp. 168–170. DOI: 10.3103/S1068373911060069
10. Elizbarashvili E. Sh., Chavchanidze Z. B, Elizbarashvili M. E, Maglakelidze R. V., Sulkhanishvili N. G., Elizbarashvili Sh.E., Soil-climatic zoning of Georgia. // Eurasian Soil Science, Volume 39, Issue 10, 2006, pp. 1062-1065, Issue 10, 2006, pp. 1062-1065.

2nd International Scientific Conference "Modern Problems in Geophysics", Proceedings,
ISBN 978-9941-36-562-1, ISSN 3088-4349, Tbilisi, Georgia, October 29-31, 2026

# CHANGES IN PRECIPITATION AMOUNT AND INTENSITY IN GEORGIA UNDER GLOBAL WARMING

**Tavartkiladze K., Karalashvili T.**

*Vakhushti Bagrationi Institute of Geography of the I. Javakhishvili Tbilisi State University, Tbilisi, Georgia*
*tamaz.karalashvili@tsu.ge*

***Abstract.*** *The increase in Earth's energy potential due to global warming significantly impacts atmospheric processes, including the water cycle. Global warming intensifies the hydrological cycle and contributes to changes in the precipitation regime, including variations in precipitation amount, intensity, and spatio-temporal distribution. The amount of atmospheric precipitation is determined by many natural and anthropogenic factors, though the hydrological cycle was relatively stable prior to the industrial era. The Caucasus region is particularly sensitive to climate change, but long-term observational data are still limited. Consequently, the results obtained using Georgia as an example are important both for a better understanding of regional climatic processes and for adaptation measures, water resource management, and natural hazard assessment. The aim of this research is to evaluate long-term changes in the amount and intensity of atmospheric precipitation in Georgia based on data from 1961–2020, with particular emphasis on regional differences and trends in precipitation patterns under contemporary global warming.*

***Key words:*** *Climate, global warming, precipitation.*

## Introduction

Due to the exceptional diversity of climatic conditions across the territory of Georgia, the amount of atmospheric precipitation and its long-term changes differ substantially between regions, as noted by several researchers [1,2,3].

Modern studies indicate that the hydrological cycle intensifies under global warming conditions, manifesting in changes to precipitation amounts, their spatio-temporal distribution, and the frequency of extreme events [6,7,8,9].

According to studies conducted in Georgia, the long-term dynamics of atmospheric precipitation are closely linked to changes in air temperature. An assessment of the relationship between climate change and desertification showed that in the initial stage of global warming, a slight decrease in precipitation in Georgia contributed to the development of arid processes [4]. In the mid-20th century, average annual precipitation decreased by approximately 5–9%, especially during the cold season. Results published in recent years indicate that long-term changes in precipitation in Georgia align with global trends, though their intensity and direction vary by region [5].

## Methods/Materials and Methods




**Fig. 1.** Layout diagram of selected weather stations

The study aims to evaluate long-term changes in the amount and intensity of atmospheric precipitation in Georgia based on data from 1961–2020, with particular emphasis on regional differences and trends in precipitation patterns in the context of contemporary global warming. Data from 14 meteorological stations (Fig. 1) were used and processed using Obukhov's method [10] to ensure uniformity and completeness.

The territory is conditionally divided into four parts – North, East, South, and West – with corresponding analysis of station data (Table 1).

**Table 1.** Mean annual precipitation and long-term changes in Georgia during 1961–2020 based on the dynamic norm

| Observation Point | Mean Annual Precipitation (mm/year) | Change (Dyn. Norm mm/year) | Change (%/year) | Observation Point | Mean Annual Precipitation (mm/year) | Change (Dyn. Norm mm/year) | Change (%/year) |
|---|---|---|---|---|---|---|---|
| Ambrolauri | 1092.4 | 2.37 | 0.22 | Tsalka | 676.8 | -1.34 | -0.2 |
| Pasanauri | 971.7 | 0.21 | 0.02 | Akhaltsikhe | 536.5 | 0.2 | 0.04 |
| Tianeti | 746.1 | -5.81 | -0.78 | Bolnisi | 511.5 | -0.2 | -0.04 |
| **North** | 936.7 | 1.62 | 0.17 | **South** | 574.9 | -0.45 | -0.08 |
| Sagarejo | 773.3 | 3.2 | 0.41 | Kobuleti | 2398.6 | 6.53 | 0.27 |
| Telavi | 758.2 | -0.58 | -0.08 | Poti | 1963.1 | 6.21 | 0.32 |
| Gori | 518.2 | 0.06 | 0.01 | Zugdidi | 1829.1 | 0.85 | 0.05 |
| Tbilisi | 502.2 | 0.88 | 0.18 | Kutaisi | 1385.7 | -0.28 | -0.03 |
| **East** | 638 | 0.89 | 0.14 | **West** | 1894.1 | 3.33 | 0.18 |

## Results

The table presents the average annual precipitation for each meteorological station determined on the basis of observational data from 1961–2020, as well as their long-term changes evaluated by the dynamic norm method. Unlike the "difference method," which only compares the mean values of the first and third periods, the dynamic norm considers the entire multi-year period as a whole and linearly describes the average trend of the process, thereby providing a more comprehensive picture.

Thus, long-term changes in precipitation in Georgia are not characterized by a single uniform pattern: a sharp increase in the west, a relatively weak increase in the north and east, and a slight decrease in the south. This confirms that under global warming conditions, precipitation changes, along with climatic factors, are significantly determined by the country's complex terrain and physical-geographical diversity.

The total amount of annual precipitation provides only a general idea, as it combines precipitation of varying intensities. Therefore, to evaluate the impact of global warming, daily precipitation totals were divided into four categories: light (0.1–5.0 mm), moderate (5.1–20.0 mm), heavy (20.1–50.0 mm), and very heavy (>50 mm). Data from each meteorological station were grouped according to this classification, regional data were combined, and dynamic norms were calculated.

Figs. 2 – Figs.5 present the obtained results, where the dynamic norms are plotted along with approximation curves obtained by 6th and 7th-order polynomials. Polynomials allow for a more detailed evaluation of temporal variability and long-term fluctuations. The analysis showed that 6th and 7th-order polynomials describe the actual course of precipitation most satisfactorily, which is why their curves are presented alongside the dynamic norm in all figures.

The obtained results show that light precipitation across almost the entire territory of Georgia exhibits a decreasing trend. Regional analysis indicates that the intensity of decline in northern, eastern, and western Georgia is close to each other, while the rate in the south is relatively low. This difference is due to the fact that the temperature rise in southern Georgia started earlier and more intensely, which led to a different mode of change in the light precipitation regime.

The curves presented in the figures confirm that against the background of climate change, the share of light precipitation is gradually decreasing, which can be considered one of the manifestations of water cycle intensification.

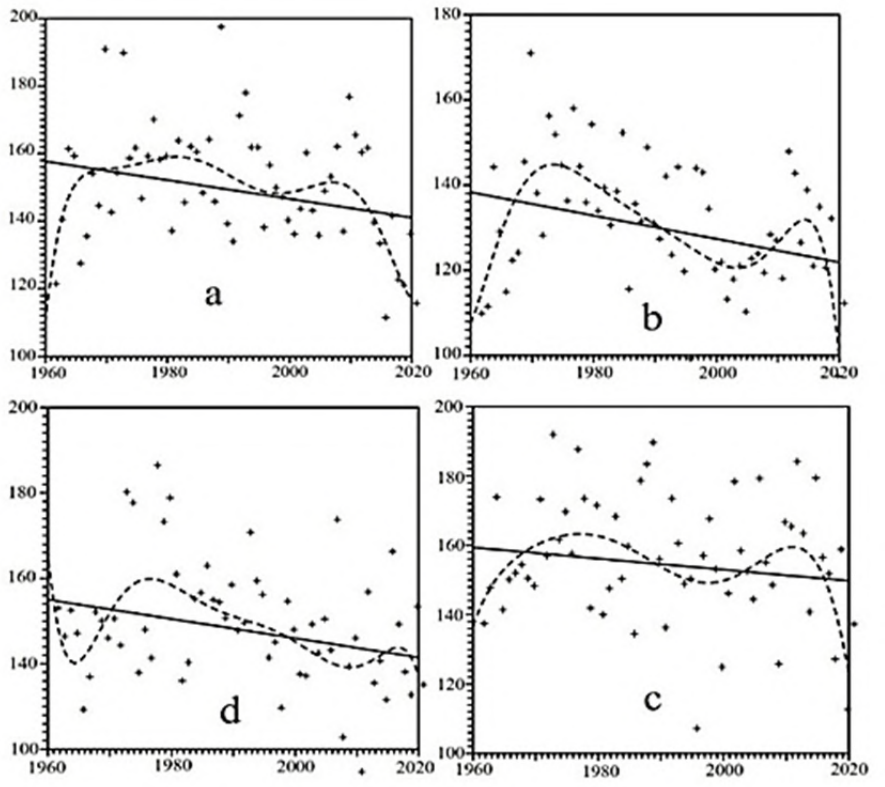



**Fig. 2.** Long-term changes in light precipitation in Georgia during 1961-2020, changes by dynamic norms (straight line) and 7th-order polynomial (curve) in the North (a), East (b), South (c), and West (d).

Thus, the reduction of light precipitation indicates that under global warming conditions, the precipitation regime becomes more contrasted, and the intensification of the water cycle changes the ratio of precipitation of different intensities.

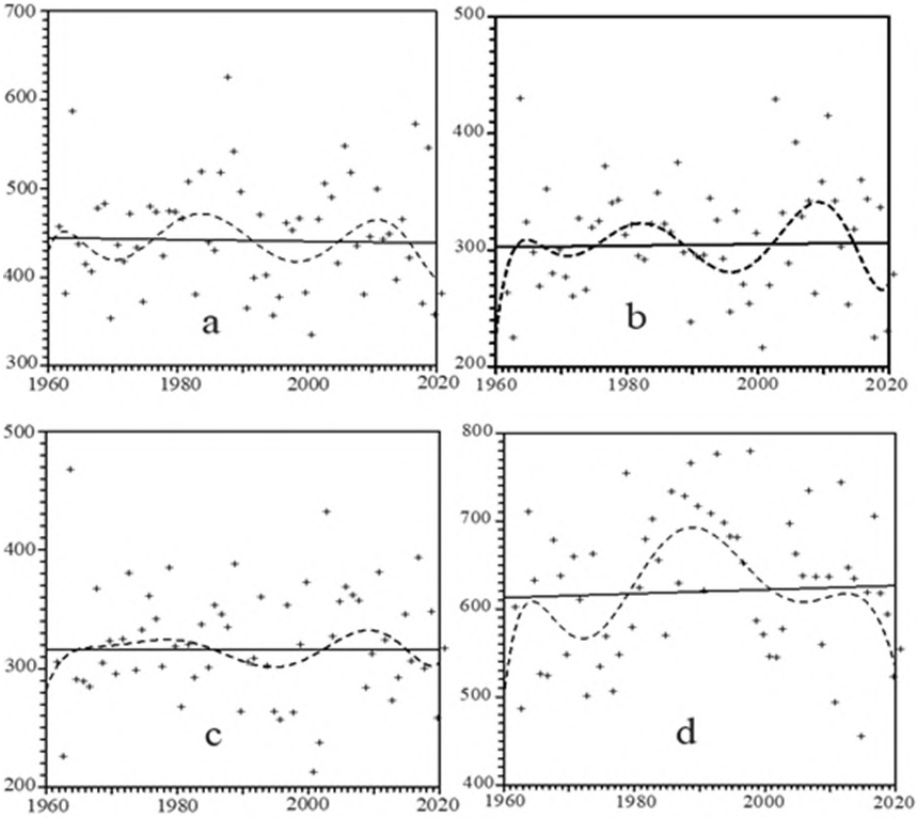



**Fig. 3.** Long-term changes in moderate precipitation in Georgia (for notations, see Fig. 1).

Long-term changes in moderate-intensity precipitation (Figure 3) show that in most regions of Georgia, their amount remains practically stable, though variations are observed in individual regions. In southern Georgia, a slight increase is recorded, which differs from the trend in the rest of the country and is likely related to a more intense temperature increase in the region, causing a portion of light precipitation to shift into the moderate category.

The curves indicate cyclic fluctuations, but they do not alter the overall trend – the moderate precipitation regime is much more stable than that of light precipitation.

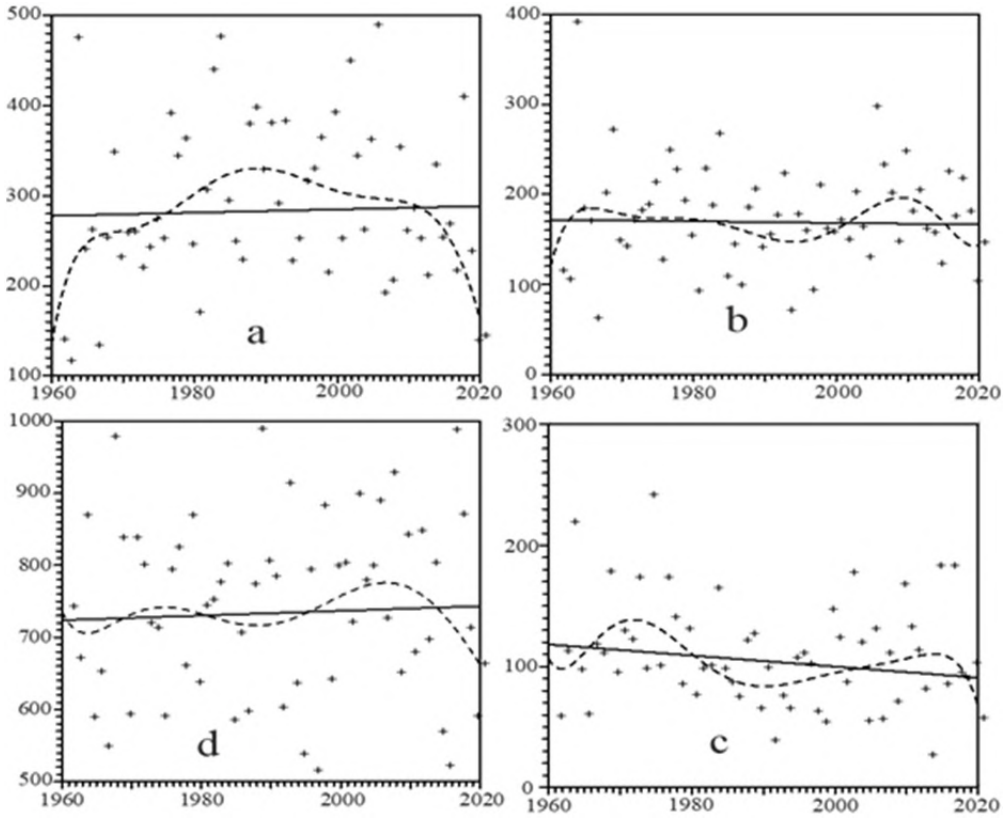



Fig. 4. Long-term changes in heavy precipitation in Georgia (for notations, see Fig. 1).

Long-term changes in heavy intensity (20.1–50.0 mm) precipitation (Figure 4) are of particular importance, as they play a decisive role in the formation of surface runoff and the development of hydrometeorological processes such as flash floods, mudflows, and others. Consequently, the evaluation of their changes has not only theoretical but also significant practical value.

Graph analysis shows that the regional nature of changes in heavy precipitation basically repeats the regularities of light and moderate precipitation, though the intensity varies by region. In northern, eastern, and western Georgia, long-term changes are relatively small, and the average trend remains practically unchanged despite fluctuations in individual years.

In southern Georgia, a decreasing trend is observed, which corresponds to the changes in the total annual precipitation in the same region. This peculiarity is related to the specific local climatic regime and atmospheric circulation, which react differently against the background of global warming.

Long-term changes in very heavy (>50 mm) precipitation (Fig. 5) are a subject of special attention, since dangerous hydrometeorological events are most frequently associated with this specific category.

Changes in very heavy (>50 mm) precipitation in Georgia vary sharply by region. A decrease is recorded on the southern slopes of the Caucasus and the plains of eastern Georgia (27.8 mm and 10.7 mm/100 years), a more intensive decrease on the Meskheti-Javakheti plateau (-73.4 mm/100 years), while a sharp increase is observed in the Kolkheti lowland and the Black Sea coast (+982 mm/100 years).

Analysis of dynamic norms shows that the growth is most evident in western Georgia, which is associated with the strengthening of humid circulation under the influence of the Black Sea. In the northern and eastern regions, the changes are moderate, while in the south, they remain stable with minor fluctuations.

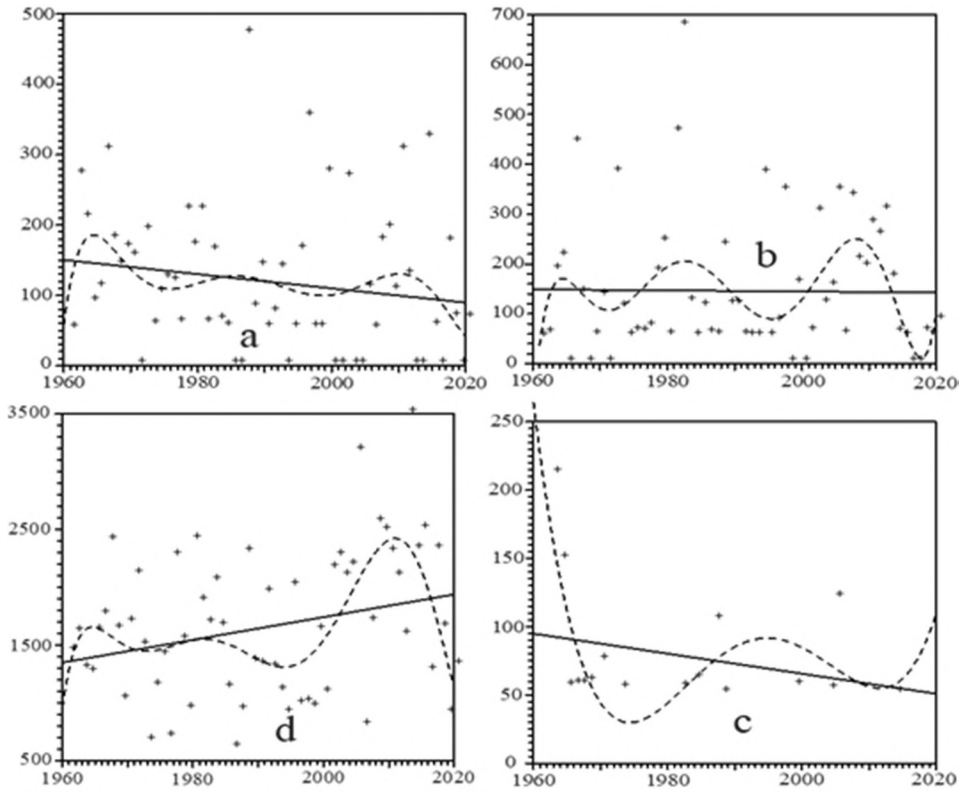



**Fig. 5.** Long-term changes in very heavy precipitation in Georgia (for notations, see Fig. 1).

The multi-year dynamics are non-uniform: phases of increase and decrease alternate, but the overall trend in the west is clearly positive. This indicates that under global warming conditions, the probability of high-intensity precipitation formation increases, especially in regions under the influence of the Black Sea.

Thus, against the background of a decrease in light precipitation, the increase in very heavy precipitation, especially in western Georgia, makes the precipitation regime more contrasted and increases the probability of extreme hydrometeorological events, which requires further monitoring and detailed research.

## Conclusion

The obtained results indicate that under contemporary global warming conditions, the change in atmospheric precipitation is manifested not only by a change in their total amount but also by the transformation of the ratio of precipitation of different intensities. The scale and intensity of this process vary across different regions of Georgia, which once again emphasizes the important role of relief and local climatic conditions in shaping the precipitation regime.

Therefore, the impact of global warming in Georgia does not manifest itself unambiguously: changes depend both on precipitation intensity and physical-geographical conditions. The decrease in light precipitation and regionally differing changes in heavy precipitation indicate that not only the total amount of precipitation is transforming, but also its regime, which can be considered one of the manifestations of water cycle intensification.

## References

1. Elizbarashvili E., Tatishvili M., Elizbarashvili M., Meskhia R., Elizbarashvili Sh., Climate Change in Georgia under Global Warming Conditions. Tbilisi, 2013.
2. Kordzakhia M., The Climate of Georgia. Tbilisi. // Metsniereba, 1961.
3. Tavartkiladze K., Begalishvili N., Tsintsadze T., et al., The Impact of Global Warming on the Atmospheric Precipitation Field in Georgia. // Meteorology, Climatology, No. 121, Tbilisi, 2015.
4. Tavartkiladze K. & Bolashvili N. Influence of Temperature and Precipitation Changes on Desertification. // In Proceedings of the 18th International Conference of the World Academy of Science, Engineering and Technology (WASET), London, United Kingdom, November 24–25, 2016, pp. 1808–1812.

5. Tavartkiladze K., Bolashvili N., Sukhnidze N., Changes in the Atmospheric Precipitation Regime in Georgia (1960–2019). // Proceedings of the 1st International Scientific Conference “Modern Problems in Geophysics”. Tbilisi: Ivane Javakhishvili Tbilisi State University Publishing House, 2025, pp. 143–146.
6. Douville H., Raghavan K., Renwick J., et al., Water Cycle Changes. In: Climate Change 2021: The Physical Science Basis. Contribution of Working Group I to the Sixth Assessment Report of the Intergovernmental Panel on Climate Change. Cambridge University Press, Cambridge, 2021.
7. Hirabayashi Y., Mahendran R., Koirala S., et al., Global Flood Risk under Climate Change. // Nature Climate Change, 3(9), 2013, pp. 816–821.
8. Kundzewicz Z. W., Kanae S., Seneviratne S. I., et al., Flood Risk and Climate Change: Global and Regional Perspectives. // Hydrological Sciences Journal, 59(1), 2014, pp. 1–28.
9. Trenberth K. E., Changes in Precipitation with Climate Change. Climate Research, 47, 2011, pp. 123–138.
10. Obukhov A.M., On statistical orthogonal expansions of empirical functions. // Izv. AN SSSR, Ser. Geofiz., 3, 1960, pp. 432-439.

2nd International Scientific Conference "Modern Problems in Geophysics", Proceedings,
ISBN 978-9941-36-562-1, ISSN 3088-4349, Tbilisi, Georgia, October 29-31, 2026

# REVIEW OF ICE-FORMING REAGENTS FOR PRECIPITATION MANAGEMENT FROM CONVECTIVE CLOUDS

**Gekkieva S.**

*High-Mountain Geophysical Institute, Nalchik, Kabardino-Balkaria, Russian Federation*
*sgekkieva@list.ru*

***Abstract.*** *This review systematizes current data on active modification of convective clouds for precipitation management and hail suppression. The physicochemical properties of modern pyrotechnic compositions and the mechanisms of ice-forming aerosol formation are analyzed. Particular attention is paid to the formation of various zinc oxide nanostructures during high-temperature combustion and their kinetic interaction with the supercooled cloud environment. Factors determining the yield of active particles within the studied temperature ranges are examined. Promising directions for the development of nanotechnology for cloud process modification are outlined.*

***Key Words:*** *Convective clouds, active modification, pyrotechnic compositions, ice-forming aerosols, zinc oxide nanostructures.*

## Introduction

Implementing projects to actively modify atmospheric processes – aimed at preventing hail damage and artificially regulating precipitation – is of strategic importance for the development of the Russian Federation's agro-industrial complex and national economy. Current data indicate that Russia possesses 155.8 million hectares of fertile land (accounting for 8.3% of the global total), ranking fourth in the world. However, more than half of the country's agricultural land is classified as a zone of high-risk farming. These areas are regularly exposed to destructive climatic phenomena, including droughts, hail, flash floods, tornadoes, and squalls. Hailstorms cause multifaceted environmental and economic damage: they damage or completely destroy crops, devastate forests and orchards, and injure or kill local wildlife. Weather modification is a highly relevant and sought-after objective. However, to ensure the economic viability of such projects, technologies and reagents must undergo continuous improvement. This is essential for significantly cutting operational expenses and reducing the cost of these activities.

## Study area, material and methods

### Ice-forming nuclei

The existence of atmospheric ice-forming nuclei (IFN) is currently a well-established scientific fact. Their physicochemical and structural characteristics – including spatiotemporal concentration variability, temperature dependence, size distribution, morphology, and properties – have been studied in detail. Furthermore, the kinetics and heterogeneous mechanisms of ice nucleation on the surfaces of these aerosol particles have been extensively investigated [1–4]. Atmospheric IFN concentration Detecting IFN in the atmosphere is a long and laborious process due to their extremely low concentration relative to the total mass of aerosol particles. Cloud condensation nuclei (CCN): their concentration in marine air masses is on the order of $10^8$ $m^{-3}$, whereas in continental air masses it ranges from $10^9$ to $10^{10}$ $m^{-3}$. Ice-forming nuclei (IFN): the characteristic concentration at a temperature of -20°C reaches only $10^3$ $m^{-3}$ [5–7]. Thus, the IFN concentration is several orders of magnitude (millions to tens of millions of times) lower than that of CCN, a fact that long hindered their experimental isolation and identification.

### Genesis and material composition

The difficulty of detecting ice-nucleating particles (INPs) has given rise to numerous hypotheses regarding their genesis, ranging from terrestrial origins to suggestions of extraterrestrial provenance (e.g., resulting

from the combustion and ablation products of meteors and meteorites). Current understanding holds that the sources of INPs are identical to the processes and mechanisms that form atmospheric aerosols in general, including cloud condensation nuclei (CCN). The classical distinction between them is based on the fact that CCN are predominantly hydrophilic and water-soluble, whereas INPs are traditionally viewed as hydrophobic and insoluble substances. However, in the actual atmosphere, aerosol particles are rarely homogeneous. More often, they are heterogeneous conglomerates formed through the coagulation of soluble and insoluble components. Consequently, INPs can exhibit hygroscopic properties, which complicates their differentiation and activates mixed ice-formation mechanisms. The most common natural INPs are particles of finely dispersed minerals eroded from the soil during weathering (desert and agricultural dust). Typical representatives of this group include:

Kaolinite – $Al_4Si_4O_{10}(OH)_8$;
Montmorillonite – $Na(Mg, Al)_2Si_4O_{10}(OH)_2 \cdot 4H_2O$;
Quartz – $SiO_2$.

Many metal salts and oxides – of both natural and anthropogenic origin – also exhibit varying degrees of ice-nucleating activity. A significant portion of these substances enters the atmosphere through emissions from metallurgical plants (steel and aluminum production), thermal power stations, and internal combustion engines in motor vehicles. A certain proportion of the atmospheric organic aerosol structure consists of fine particles of organic origin formed by forest fires or the destructive combustion of organic fuels. A distinct group is formed by certain types of viable and inactivated bacteria (e.g., *Pseudomonas syringae*) that develop in leaf litter and seawater; these are classified as biogenic organic aerosols [8].

## Mechanisms of action of ice-forming nuclei

Currently, there is no universal theory of ice nucleation on aerosol particles, nor is there a unified mechanism of action for ice-forming nuclei (IFN). Cloud physics classifies four distinct mechanisms of ice embryo formation, each corresponding to a specific type of nucleus: Deposition nuclei. Crystallization on the surface of heterogeneous particles occurs directly from the gas phase (desublimation). This mechanism operates in the air when the relative humidity is below water saturation but above ice saturation:

$$E_i < e < E_w.$$

It is assumed that under these thermodynamic conditions, water vapor does not condense on non-hygroscopic substrates, thereby ensuring a direct "vapor-to-ice" phase transition (in this context, Ostwald's rule of stages does not apply to heterogeneous processes).

Condensation-freezing nuclei. When the water vapor pressure exceeds saturation over water, condensation is initiated on the surface of an insoluble aerosol particle of critical size. Consequently, hydrophilic surface areas become covered with a water film, and ice embryos form at the water-nucleus interface. Once an embryo reaches a critical radius, the entire volume of the liquid phase rapidly crystallizes. The resulting active ice particle continues to grow through vapor diffusion. Immersion nuclei. This type of nucleus is located within cloud droplets. Particles enter the liquid phase either through coagulational capture from the atmosphere or during the droplet formation stage on mixed (soluble and insoluble) cloud condensation nuclei. Formation of the ice phase occurs at the water-nucleus interface. Similar to the condensation-freezing mechanism, the fluctuation of a supercritical-sized ice embryo leads to the instantaneous crystallization of the droplet and its transition to the frozen state. Contact nuclei. This mechanism is driven by the kinetic collision of supercooled droplets with ice-forming nuclei. Ice nucleation is induced precisely at the moment the nucleus surface contacts the liquid-gas interface, after which the crystallization front propagates throughout the entire volume of the droplet. Kinetic differences between the mechanisms Despite the apparent similarity between the immersion and condensation-freezing mechanisms, they exhibit fundamental kinetic differences: Immersion nuclei can remain within the liquid phase in a metastable state for an extended period without triggering a phase transition. The action of condensation-freezing nuclei is governed by the rapid growth of a water film in supersaturated vapor and the virtually simultaneous formation of ice embryos within that film. Due to this specific characteristic, the second mechanism is kinetically similar to the contact mechanism and is often interpreted in the literature as "self-contact nucleation" [2, 5, 8, 9].

## Results

Artificial ice-nucleating agents. The physicochemical mechanism by which artificial ice-nucleating agents act within a cloud is identical to the process of natural ice formation. While aerosols of numerous inorganic and organic substances possess this property, silver iodide (AgI) and lead iodide (PbI2) aerosols exhibit the greatest crystallizing capacity. Currently, the use of PbI2 has been completely discontinued due to its high toxicity, relatively low activity, and higher temperature threshold for crystallization. Notably, particles of virtually any substance (such as quartz sand or dust) can acquire the ability to initiate crystallization if they are artificially subjected to deep cooling. AgI aerosol is the most widely used agent for cloud seeding. Silver iodide is a compound that is virtually insoluble in water. According to various studies, the high ice-nucleating activity of AgI is attributed to the structural similarity between its crystal lattice and that of ice. Under Earth's atmospheric conditions, ice exists in a hexagonal modification (Ih) in which each H2O molecule is surrounded by four nearest-neighbor molecules located at the vertices of a regular tetrahedron, all at an equal distance of 2.76 Å. A similar geometry characterizes the crystal structure of AgI. The ice-like structure of AgI particles facilitates the adsorption of water molecules onto their surfaces, leading to the formation of polymolecular layers and a surface water film. Upon reaching a critical thickness – and as supercooling progresses – micro-regions containing oriented water molecules form within this film, with a structure approaching that of ice. Upon reaching a sufficient size, these micro-volumes transform into stable ice crystal embryos. At the same time, a broad class of organic compounds – specifically plant pollen components found in resins, steroids, and essential oils – exhibits high ice-nucleating activity despite lacking any pronounced structural resemblance to ice.

Analysis of existing solutions. Pyrotechnic compositions containing an active reagent (AgI, $PbI_2$, CuS) and iodinating components (KI, $NH_4I$, $NH_4IO_3$, $C_7H_5IO_2$) are traditionally used to generate ice-forming aerosols for active cloud modification. These components are incorporated into the formulation to intensify the nucleation process and enhance overall ice-forming efficiency. Modern pyrotechnic generators typically employ compositions based on silver oxide and ammonium perchlorate or ammonium nitrate, with an AgI mass fraction ranging from 2% to 40% [4, 5, 10].

Physicochemical Generation Mechanism

The process of generating the ice-forming aerosol is based on the high-temperature sublimation (in the 700–1400°C range) of AgI into an atomic state. Subsequent condensation of $Ag^+$ and $I^-$ ions occurs on a substrate formed by the combustion products of the pyrotechnic base, under conditions of rapid decompression expansion and adiabatic cooling of the reaction volume. As a result of this mechanism, the dispersed product formed is a thermocondensation aerosol.

Research Results and Composition Modification with Zinc Powder

Experimental Parameters and ALCP Yield Kinetics Comprehensive theoretical and experimental studies were conducted on the simultaneous thermal sublimation of the AD-1 grade ice-nucleating composition, modified by the addition of 6% finely dispersed zinc oxide (ZnO) powder. Data from numerical modeling and chamber tests revealed a sharp increase in the specific yield of active ice-nucleating particles (ALCPs) across the entire sub-zero temperature range. The maximum kinetic effect was observed in the temperature range of −20 to −40°C, where the numerical yield of ice-nucleating nuclei increased by a factor of 1.9–2.0.

## Conclusion

The increased yield of active ice-forming particles within the studied temperature range is attributed to the formation of zinc oxide nanostructures of various modifications and sizes under the high-temperature combustion conditions of the pyrotechnic composition. These dispersed phases facilitate intense interaction with the supercooled cloud medium. Additionally, ZnO nanoparticles and nanoclusters act as spatial "buffers" between AgI nuclei, effectively preventing the kinetic coagulation and polydisperse agglomeration of the ultrafine phase; this stabilizes and preserves the high specific surface area of the active reagent (AgI).

## References


1. Nikandrov V. Ya., Artificial modification of clouds and fog. Leningrad. // Gidrometeoizdat., 1959, 191 p. (in Russian)
2. Plaude N. O., On the mechanism of supercooled fog crystallization using silver iodide aerosol. // Proceedings of the Main Geophysical Observatory (GGO), Issue 186, 1966, pp. 10–17. (in Russian)

3. Koloskov B. P., Korneev V. P., Shchukin G. G. Methods and means for modifying clouds, precipitation, and fog. Monograph. // St. Petersburg: RSHU (Russian State Hydrometeorological University), 2012, pp. 36–38. (in Russian)
4. Abshaev M. T., Abshaev A. M., Barekova M. V., Malkarova A. M. Guidelines for organizing and conducting hail suppression operations. // Nalchik: Pechatny Dvor., 2014, 508 p. (in Russian)
5. Bekryaev V. I., Selected issues in cloud physics and cloud modification. // St. Petersburg: RSHU, 2007, 337 p. (in Russian)
6. Pruppacher H. R., Klett J. D., Microphysics of Clouds and Precipitation. – A fundamental international reference work on the thermodynamics and kinetics of phase transitions in the atmosphere.
7. Mason B. J., The Physics of Clouds.- A classic work detailing early experiments regarding the search for, concentration of, and extraterrestrial origin hypotheses concerning Ice-Forming Nuclei (IFN).
8. Khrgian A. Kh., Physics of the Atmosphere. – Moscow: Moscow State University Press. – A standard Russian academic textbook covering macro- and microphysical processes in cloud systems. (in Russian)
9. Mazin I. P., Shmeter S. M., Clouds: Structure and Physics of Formation. – Leningrad: Gidrometeoizdat. – A monograph providing a detailed analysis of the relationships between cloud-active nuclei (CAN) and ice-nucleating particles (INP), aerosol coagulation processes, and the temperature-dependent activity spectrum of nuclei. (in Russian)
10. Burrows S. M., et al., Ice-Nucleating Particles That Impact Clouds and Climate: Observational and Modeling Research Needs // Reviews of Geophysics. – A review of current understanding regarding mineral and anthropogenic sources of ice-nucleating particles (INP).

2nd International Scientific Conference "Modern Problems in Geophysics", Proceedings,
ISBN 978-9941-36-562-1, ISSN 3088-4349, Tbilisi, Georgia, October 29-31, 2026

# LABORATORY MODELING OF THE EFFECT OF CLOUD ELECTRICAL CHARACTERISTICS ON WATER VAPOR CRYSTALLIZATION PROCESSES ON ZINC OXIDE PARTICLES

**Gekkieva S., Budaev A.**

*High-Mountain Geophysical Institute, Nalchik, Kabardino-Balkaria, Russian Federation*
*sgekkieva@list.ru*

***Abstract.*** *Research into weather modification is a core area of activity for the High-Mountain Geophysical Institute. Within this field, the study of the ice-forming properties of various substances – such as silver iodide-based pyrotechnic compositions and zinc oxide nanotubes – stands out as a key focus. Alongside investigations into the ice-forming activity of these substances, laboratory experiments are being conducted to examine how cloud electrical characteristics influence the formation of the ice phase on zinc oxide particles. This article presents the results of a study on the effects of electric field strength (E) and the electric charge (q) of zinc oxide particles on their ice-forming properties.*

***Key Words:*** *Electric charge, electric field strength, reagent, ice-forming particles.*

## Introduction

The influence of electric forces on the phase and microstructural characteristics of clouds and fogs is a subject of interest to many researchers. These issues have been investigated both theoretically and experimentally. As a result, the understanding of the mechanism by which charge polarity affects droplet condensational growth has been refined and theoretically substantiated; the influence of droplet surface charge on the rate of ice nucleation has been studied, and a physical concept of this phenomenon has been formulated; furthermore, empirical data have been obtained regarding the effects of medium ionization and a constant external electric field on the freezing of supercooled water droplets [1].

In operations involving the active modification of hail processes, reagents are introduced into intense cumulonimbus clouds characterized by strong electric fields and high concentrations of charged hydrometeors. The presence of an electric field and charges on reagent particles in the atmosphere can influence the specific yield of ice-forming nuclei during weather modification activities [2, 3].

Therefore, investigating the impact of electric field strength $E$ and specific charge $q/m$ on the ice-forming efficiency of reagents and pyrotechnic compositions is a matter of current importance.

## Study area, material and methods

Research conducted in recent years in this area indicates that the growth of embryonic precipitate particles from the vapor phase depends on electric field strength, the charge of the nucleating core, and the specific growth mechanism involved [4]. When a particle is situated in an electric field, ionic charging occurs. Ions moving through the air collide with the particle and deposit on its surface. They cannot return to the surrounding medium because they require a specific amount of energy to overcome the potential barrier at the interface. Consequently, ions accumulate on the particle [5].

Under the influence of electric forces, the particle enlargement process effectively becomes one of coagulation. In cloud conditions, the diffusion mechanism of particle charging predominates; however, contact charging is the dominant mechanism for particles larger than 0,1 μm [6, 7]. Since the reagent particle size ranges from 0,02 to 10 μm, the charging of these particles will occur via both contact and diffusion mechanisms [8].

Methodology for studying the effect of electric field strength on the ice-forming efficiency of zinc oxide. A specific quantity of zinc powder is first weighed on an electronic balance. It is then loaded onto the graphite substrate of the reagent sublimation device. Thermostated substrates placed at the bottom of the cloud

chamber. An artificial cloud environment is generated within the chamber using an ultrasonic steam generator. Subsequently, high voltage from a high-voltage rectifier is applied to the capacitor plates. Current is supplied to the sublimation device, causing the zinc to evaporate and form zinc oxide nanoparticles. After sublimation, the air in the chamber is mixed by a fan; as the first small crystals appear in the field of view, the substrates are opened one by one, and the crystals are deposited onto them. Each substrate is examined under an optical microscope, the number of crystals in the field of view is counted, and the specific yield is then calculated using a computer [9].

## Results

A series of experiments was conducted to investigate how the specific yield of ice-forming nuclei from charged zinc oxide particles depends on temperature. The experiments were carried out in the temperature range of –5 to –14°C, using capacitor plate polarities of "0", "+" and "0", "–". The results of the study are presented in Table 1 and Fig. 1.

**Table 1.** Dependence of the specific yield of ice-forming nuclei temperature.

| Without electric field | | Negatively charged particles | | Positively charged particles | |
|---|---|---|---|---|---|
| t, °C | Specific yield, $\times 10^{12}$ $g^{-1}$ | t, °C | Specific yield, $\times 10^{12}$ $g^{-1}$ | t, °C | Specific yield, $\times 10^{12}$ $g^{-1}$ |
| -13,9 | 2,8 | -13,6 | 0,6 | -11 | 6,4 |
| -12,9 | 1,8 | -12,5 | 0,8 | -10,8 | 4,2 |
| -11,3 | 2,0 | -12,5 | 1,0 | -9,5 | 5,6 |
| -11,1 | 0,9 | -12,5 | 0,6 | -8,9 | 0,9 |
| -10,5 | 2,8 | -12,2 | 0,7 | -8,5 | 1,1 |
| -10,1 | 5,4 | -11,2 | 0,8 | -7,9 | 4,1 |
| -8,9 | 1,0 | -11,2 | 2,3 | -7,8 | 3,2 |
| -8,2 | 1,5 | -10 | 5,5 | -6,4 | 2,3 |
| -7,1 | 1,1 | -8,5 | 1,4 | -6,1 | 2,6 |
| -6,9 | 2,9 | -8 | 2,2 | -5,7 | 1,9 |
| -6,8 | 1,3 | -7,9 | 2,4 | - | - |
| -5,4 | 2,3 | -7 | 0,8 | - | - |

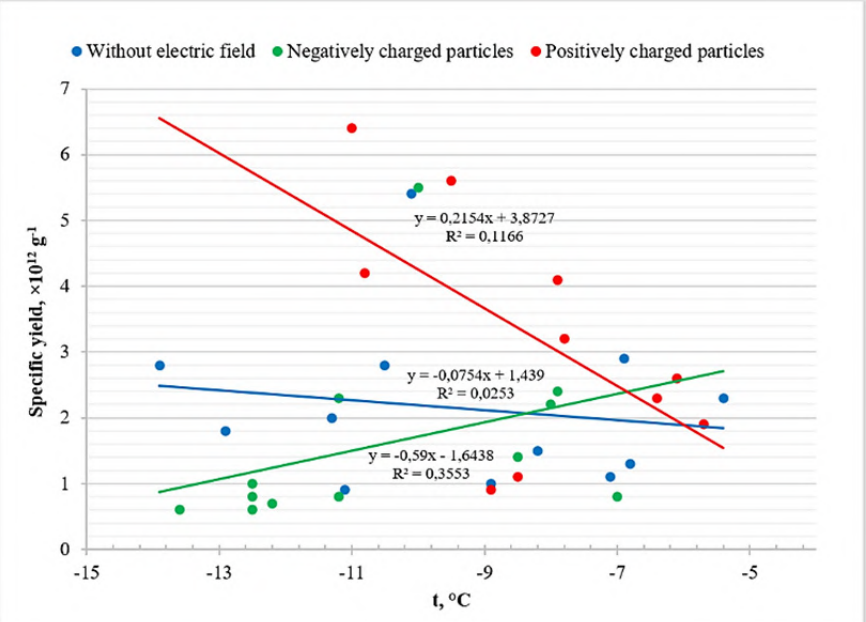



**Fig. 1.** Dependence of the specific yield of ice-forming nuclei from charged zinc oxide particles on temperature.

Table 1 and Fig.1 show that ice crystal growth on positively charged zinc oxide particles occurs more actively than on negatively charged particles. The differences are particularly noticeable in the temperature range of –10 to –13°C. However, at temperatures above –7°C, negatively charged zinc oxide particles exhibit higher ice-forming activity than positively charged particles.

In the temperature range of –8 to –14°C, the specific yield of negatively charged zinc oxide particles is lower than that of uncharged particles. In the range of –5 to –8°C, the specific yield of negatively charged zinc oxide particles is higher than that of uncharged particles. In the range of –5 to –14°C, the specific yield of positively charged zinc oxide particles is higher than that of uncharged particles.

Series of experiments investigating the effect of electric field strength on the ice-forming efficiency of zinc oxide were conducted at an electric field strength of $2250\times10^3$ V/cm and in the temperature range of –5 to –11°C.

Table 2 and Fig.2 present the dependence of the specific yield of zinc oxide particles on electric field strength.

**Table 2.** Dependence of the specific yield of zinc oxide particles on electric field.

| $E$ = 0 V/cm | | $E = 2250\times10^3$ V/cm | |
|---|---|---|---|
| t, °C | Specific yield, $\times10^{13}$ $g^{-1}$ | t, °C | Specific yield, $\times10^{13}$ $g^{-1}$ |
| -11,1 | 0,1 | -8,9 | 0,5 |
| -10,5 | 0,3 | -8,7 | 1,2 |
| -10,1 | 0,5 | -7,8 | 0,7 |
| -8,9 | 0,1 | -7,7 | 1,1 |
| -8,2 | 0,2 | -7,7 | 0,5 |
| -7,1 | 0,1 | -7,6 | 1,1 |
| -7,1 | 0,3 | -7,4 | 1,4 |
| -6,8 | 0,1 | -5,8 | 1,0 |
| -5,4 | 0,2 | -5,7 | 1,5 |
| - | - | -5,4 | 0,9 |

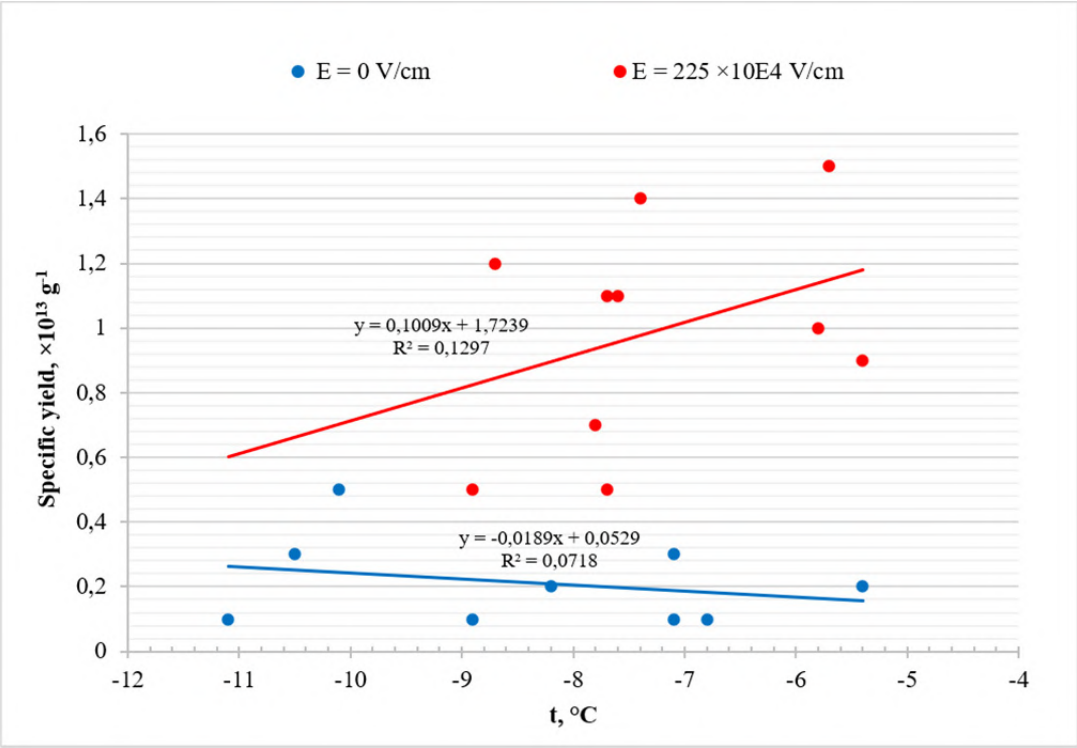



**Fig. 2.** Dependence of the specific yield of ice-forming nuclei from charged zinc oxide particles on temperature.

As shown in the Table 2 and Figure 2, the lowest specific yield values are observed in experiments conducted without an electric field. A significant increase in the ice-nucleating activity of zinc oxide is observed; specifically, the specific yield values are 3–5 times higher than those obtained in experiments without an electric field across the entire temperature range.

Electron microscopy revealed that zinc oxide sublimation particles form nanoparticle complexes in the presence of an electric field. These complexes act as ice-nucleating particles; the larger the complex, the higher the crystal formation temperature. These complexes undergo mutual coagulation, which is the primary reason for the reduction in the number of ice-nucleating particles [10].

## Conclusion

A study on the influence of the charge on zinc oxide particles and an electric field on the specific yield of ice-forming nuclei revealed that ice crystal growth proceeds more actively on positively charged particles than on negatively charged ones. These differences are particularly pronounced in the temperature range of –10 to –13°C. However, at temperatures above –7°C, negatively charged zinc oxide particles exhibit higher ice-forming activity than positively charged particles. The lowest specific yield values are observed in experiments conducted without an electric field; in the presence of an electric field, the specific yield increases by a factor of 3 to 5.

## References


1. Ivlev L.S., Physics of atmospheric aerosol systems. // L.S. Ivlev, Yu.A. Dovgalyuk – SPb.: NIIX SPbGU, 1999, 76 p. (in Russian)
2. Krasnogorskaya N.V., Experimental study of the efficiency of collision and merging of charged droplets of equal size / N.V. Krasnogorskaya, A.I. Neizvestny. // Bulletin of the Academy of Sciences of the Soviet Union. Physics of the atmosphere and ocean – M.: Nauka, 1973, vol. 9. (in Russian)
3. Kalov R.K., Study of the influence of electric charges and electric fields on the efficiency of ice-forming reagents, dis....of PhD in Natural sciences: 25.00.30 : defense of the thesis 2001-03-16: approved 2001-10-24. // Kalov R.K. – Nalchik, 2001, 128 p. (in Russian)
4. Adzhiev A.K., Data analysis of long-term atmospheric-electrical observations on the territory of the North Caucasus region / A.K. Adzhiev, Z.M. Kerefova, A.G. Klovo et al. // Proceedings of the Military Space Academy named after A.F. Mozhaisky, 674, 2020, pp. 75-79. (in Russian)
5. Sinkevich A.A., Problems of the physics of clouds. // Collection of selected articles of the MGO / A.A. Sinkevich, V.D. Stepanenko, Yu.A. Dovgalyuk – SPb.: Asterion, 2008, 513 p. (in Russian)
6. Stepanenko V.D., Investigation of the influence of electric discharges on phase and microstructural transformations of water in clouds. // Meteorology and Hydrology, № 3, 2002, pp. 39-50. (in Russian)
7. Vereshchagin O.A., High-voltage electrical technologies (textbook). // O.A. Vereshchagin, A.A. Anoshin – M.: MEI, 1999, 204 p. (in Russian)
8. Emelyanov V.N., Results of the development of new pyrotechnic compositions of ice-forming aerosol for means of active influence on clouds / V.N. Emelyanov, P.A. Nesmeyanov, N.Yu. Erlandtz et al. // Proceedings of the jubilee conference, dedicated to the 40th anniversary of the beginning of production works on protection from hail; Nalchik: Pechatny dvor, 2011, pp. 259-260. (in Russian)
9. Khuchunaev B.M., Gekkieva S.O., Budaev A.K., Methods for determining the ice-forming efficiency of anti-hail products on laboratory installations. // Science. Innovations. Technologies, № 3, 2021, pp. 105-119. (in Russian)
10. Khuchunaev B.M. Gekkieva S.O., Budaev A.K., Apparatus, methodology and preliminary results of measuring the specific charge on reagent particles formed during the sublimation of pyrotechnic compositions. // Proceedings of the MGO, № 599, 2020, pp. 128-139. (in Russian)

2nd International Scientific Conference "Modern Problems in Geophysics", Proceedings,
ISBN 978-9941-36-562-1, ISSN 3088-4349, Tbilisi, Georgia, October 29-31, 2026

# PM10 SPATIAL DISTRIBUTION IN THE ATMOSPHERE OF BATUMI CITY IN SUMMER DURING BACKGROUND LIGHT AIR

***, **Surmava A., **Kukhalashvili V., *Gigauri N., *Intskirveli L., ***Dumbadze G.**

** Institute of Hydrometeorology of the Georgian Technical University, Tbilisi, Georgia*
*** M. Nodia Institute of Geophysics of the I. Javakhishvili Tbilisi State University, Tbilisi, Georgia*
**** Batumi Shota Rustaveli State University, Batumi, Georgia*
*intskirveliliana@gmail.com, aasurmava@yahoo.com*

***Abstract.*** *Spatial distribution and time change features of PM10 concentration in summer season of 2025 in the atmospheric air of Batumi and its adjacent territories have been analysed via operating supervision, experimental measurements and computer modeling. It has been obtained that the atmospheric air pollution level is mainly within the norms. Patterns of PM10 concentration spatial distribution discharged resulting from motor transport traffic have been obtained, and areas of high and low pollution have been established. It has been shown that in the lower part of surface layer of the atmosphere, the PM10 concentration field is a unity of,, thermal" -like pollution clouds.*

***Key Words:*** *Light breeze, PM10 concentration, Batumi atmosphere pollution, numerical modelling.*

## Introduction

Socioeconomic purpose of Batumi and strategy of sustainable regional development [1] puts on the agenda the necessity of provision of regional ecological security. In this aspect, protection of Batumi atmospheric air from contamination and maintenance of high air quality of its purity is of great importance. Over the last 5-8 years, a series of important practical air-protecting measures have been conducted in Georgia. Among them it's worth noting the implementation of monitoring over PM2.5 and PM10 pollution of atmospheric air of cities of Georgia [2-4, 6].

PM10 microparticles are very hazardous for human health. Due to small sizes, they easily penetrate human's visceral organs and cause multiple types of diseases, even a lethal outcome [5]. That is why, protection of urban areas from microaerosol pollution is a very important environmental issue.

## Research goal and method

Research goal is the assessment of PM10 contamination of Batumi atmospheric air based on available operation data and experimental measurements, as well as the determination of time change and spatial distribution of concentration via computer modeling.

Operating observations over PM10 concentration in Batumi has been made since 2018 in two observation points. These points are located at densely urbanized territories: T. Abuseridze Street (TAS) and Central Park (CP) of the city. They are distant from each other by 1,8 km. Operational observations in these locations is carried-out by the Batumi branch of National Environmental Agency of Georgia using internationally recognized physical-chemical methods of standard analysis and via statistical data processing (APDA-372 PM10&PM2.5-HORIBA; StatSoft STATISTIKA 10.0 portable, Microsoft ®Exel219). As for the experimental measurements, they were conducted in 65 observation points located in city of Batumi and its adjusted territories in the summer season of 2025 using mobile measuring device Aeroqual S500. For investigation of microaerosols' spatial distribution and time change the computer modeling technique was used. For this purpose, 3D nonlinear nonstationary quasistatic equation of passive ingredients' transfer-diffusion in the atmosphere and an equation system describing evolution of β-mesoscale atmospheric processes at the territory of complex terrain using respective initial and boundary conditions have been numerically integrated [4, 6, 7].

**Research results and analysis. Operating supervision data.** Diagram of PM10 average daily concentration (ADC) value, plotted in Jule in summer of 2025 according to data of operating observation points located in TAS and CP are shown in Fig. 1. It seen from Fig. 1 and analogic graphs for June and August, that ADC

values are less than maximum permissible average daily concentration (MPADC = 50 μg/m$^3$). In observation points located in TAS and CP, ADC is changed synchronically. There is a small quantitative difference between concentrations. ADC values in TAS are mainly 1.1-1.3 times higher than those obtained in CP. Calculations showed that there is very high correlation dependence between ADC data of points located in TAS and CP. Linear correlation coefficient values in June, July and August are equal to 0.96, 0.95 and 0.91 respectively.

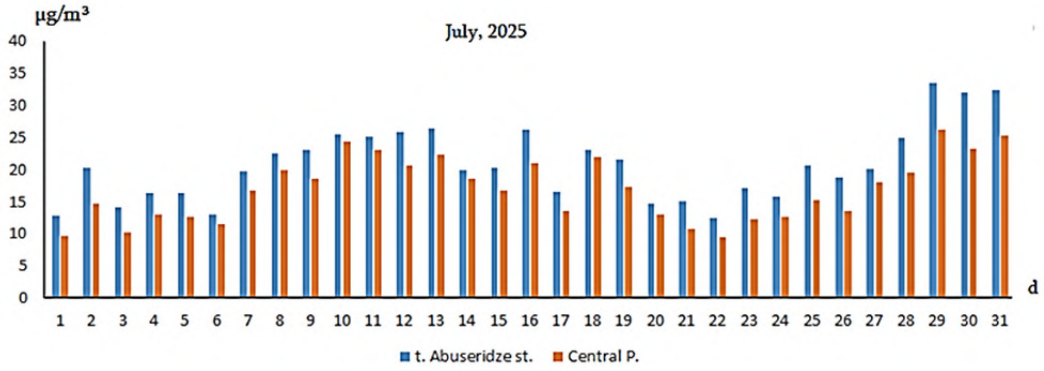



**Fig. 1.** Column diagrams of PM10 average daily concentration changes in summer of 2025.

**Experimental measurement data.** Fig. 2 shows concentrations' column diagrams obtained via 20-minute averaging of experimental measurements conducted on 11-14 July, 2025 in the central part of Batumi. Measurements were performed in dry sunny weather under conditions of the surface light air. It is seen from the Figure that PM10 concentration exceeds MPADC in three observation points only. In two points, concentration is equal to 54 μg/m$^3$ and this value is associated with railway and automobile transportations. Extremely severe contamination (82 μg/m$^3$) takes place in the vicinity of the Batumi Sea Port, in the surroundings of crossroads of Z. Gorgiladze and N. Baratashvili streets. Visual observation of this territory showed that a high pollution level is caused by road maintenance works. In the major part of the Black Sea coastal zone, concentration is mainly within the limits of 20-45 μg/m$^3$ and its increased value is associated with ingrown stream of people and dense vehicular traffic. At some distance from the central part of the city, in its eastern intensely verdure d hilly part, concentration is mainly ≤ 20 μg/m$^3$.

**Numerical modeling results.** Spatial distribution of PM10 concentration in city of Batumi and its adjacent territories with area of 13.4*13.4 km$^2$ has been numerically simulated. It has been assumed that the atmospheric pollution is caused by propagation process of microparticles hitting the air due to vehicular traffic in dry weather of summer season. Hypothetic synoptic situation has been considered, when there is a background western light air (velocity ≈ 1 m/sec) at the upper limit of surface layer of the free atmosphere. Fig. 3 shows the PM10 concentration field at 2 m height from the earth surface, obtained via modeling, when t = 3, 9, 15 and 21 h. It is seen from Fig. 3 that PM10 particles discharged by motor transport within a day, are spread over quite wide land territory. High concentrations are obtained, when t = 9 and 21h in the surroundings of avenues located in the central part of the city, and their crossroads. 40-50 μg/m$^3$ concentration is obtained in several parts of the city: Batumi by-pass highway, F. Khalvashi, P. Bagrationi, I. Chavchavadze avenues, "Boni Gorodoki".




**Fig. 2.** Spatial distribution of PM10 concentration (mkg/m$^3$) obtained via experimental measurements on 11-14 of July, 2025.

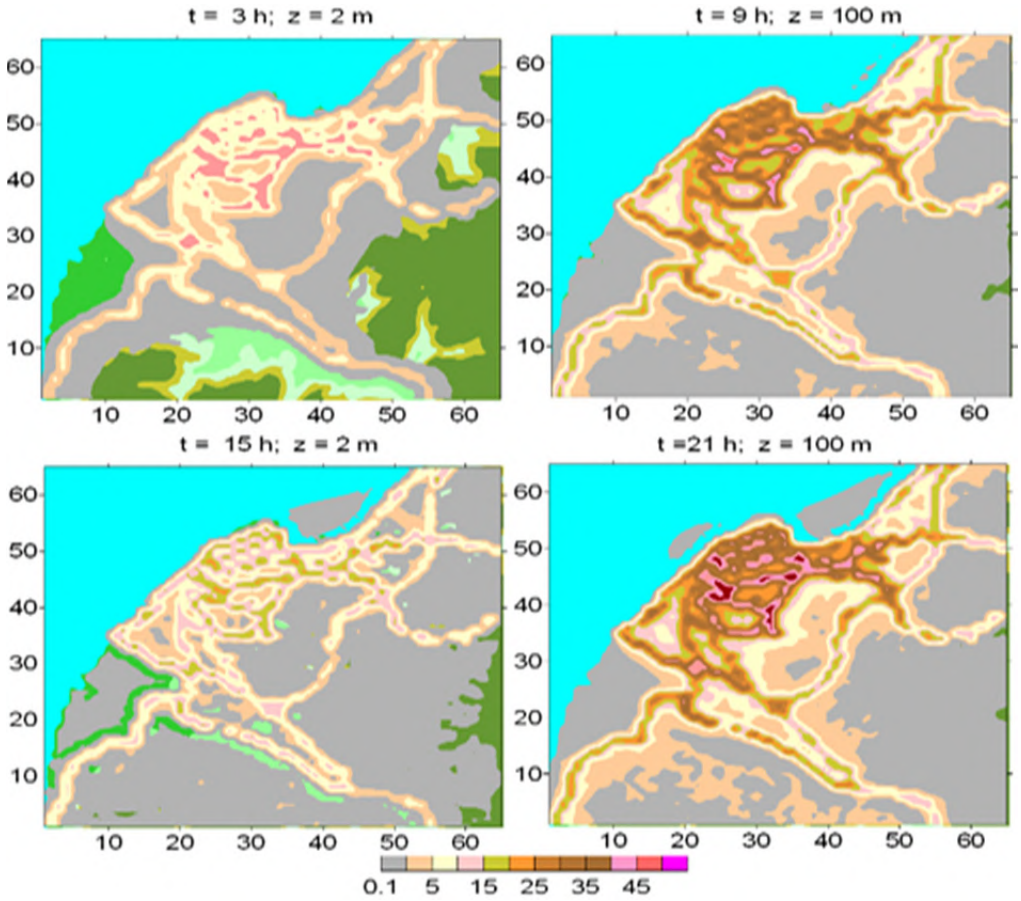



**Fig. 3.** PM10 concentration field obtained by modeling during background western light air, at 2 m height from the earth surface, when t = 3, 9, 15 and 21 h.

In severe contamination zones, maximum values of concentration obtained at 9h are 5-10 μg/m$^3$ less than those registered by t = 21 h. Despite the fact, that there is a constant intensity of aerosol emission in the atmosphere, air pollution at t = 15h is less than values obtained at 9 and 21 h. The mentioned effect is caused by time change of atmosphere thermal stability. In daylight hours, the earth surface warming promotes development of vertical turbulent diffusion and convective transfer processes, and respectively, admixtures' withdrawal from the modeling area (Fig. 4). In Fig. 4, there is shown microaerosol concentration distribution in zonal vertical cross section passing through meridian coordinate y = 45.

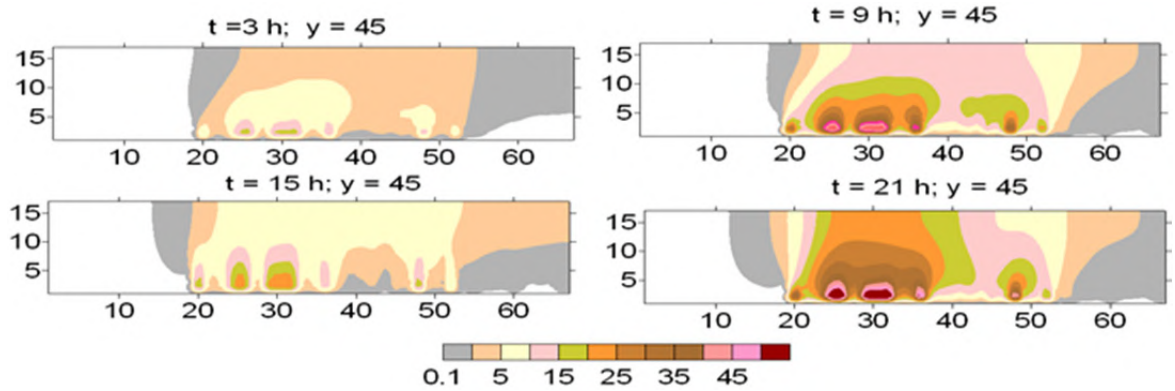



**Fig. 4.** Microaerosol concentration distribution in zonal vertical cross section passing through meridian coordinate y = 45.

It is seen from Fig. 4, that particles discharged in the atmosphere nearby the earth surface generate "thermal"-like pollution clouds. With distance from the underlying surface, "thermals" are growing in height, going wider and form a united pollution cloud in the upper part of surface layer of the atmosphere, which spreads in the local wind direction.

## Conclusions

Atmospheric air pollution of Batumi and its adjacent territories with PM10 particles in summer season of 2025 and namely on $11^{th}$-$14^{th}$ of July has been assessed. Column diagrams of PM10 concentration values in two points of operating and in 65 experimental observation points located within a city have been plotted. It has been shown that the level of atmospheric air pollution with the mentioned microparticles is mainly within allowable limits. At that, there are cases of concentration excess over maximum permissible concentration in separate observation points, which is associated with ongoing local municipal works. A pattern of PM10 spatial distribution has been obtained using numerical modeling, high and low concentration areas have been established. It has been that shown that motor transport emissions generate severe pollution in the vicinity of central highways and their crossroads. Effect of the surface thermal field on pollution distribution dynamics has been shown.

**Acknowledgment:** The scientific research has been funded and performed within the frameworks of the Grant project FR-24-223 of the Shota Rustaveli National Scientific Foundation.

## References

1. Regional Development Strategy of the Autonomous Republic of Adjara. (in Georgian) https://faolex.fao.org/docs/pdf/geo212892.pdf
2. Environmental pollution, 2021. https://air.gov.ge/reports_page
3. Surmava A., Intskirveli L., Gigauri N., PM2.5 and PM10 Microaerosols in the atmosphere of Tbilisi. // Tbilisi, Publishing House of the Institute of Hydrometeorology, 2021, 94 p.
4. Gigauri N., Intskirveli L., Surmava A., Kukhalashvili V., The Results of Kutaisi City Atmospheric Air Pollution with PM Particles. // Bulletin of the Georgian National Academy of Sciences, vol. 18, no. 3, 2024, pp. 90-96.
5. Integrated Science for Particulate MatterEPA. United States Environmental Protector Agency, 2019, 1967 p. EPA/600/R-19/188. www.epa.gov.isa.
6. Surmava A., Intskirveli L., Kukhalashvili V., Numerical Modeling of the Transborder, Regional and Local Diffusion of the Dust in Georgian Atmosphere. // Publishing House, Technical University", Tbilisi, Georgia. ISBN 978-9941-28-810-42021, p.139. http//www.gtu.ge (in Georgian)
7. Kazakov A., Lazriev G., On the parametrization of the surface layer of the atmosphere and the active soil layer. Izvestiya AN USSR. // Physics of the Atmosphere and Ocean, 14, 3, 1978, pp. 257–265. (in Russian)

2nd International Scientific Conference "Modern Problems in Geophysics", Proceedings,
ISBN 978-9941-36-562-1, ISSN 3088-4349, Tbilisi, Georgia, October 29-31, 2026

# APPLICATION OF THE MOS CONCEPT FOR STATISTICAL FORECASTING OF SEVERE CONVECTIVE HAZARDS AND FLASH FLOODS IN THE SOUTHERN REGION OF RUSSIA

**Kagermazov A.**

*Federal State Budgetary Institution "High-Mountain Geophysical Institute" (FSBI "HGI"),*
*Nalchik,Kabardino-Balkaria, Russian Federation*
*ka5408@mail.ru*

***Abstract.*** *This paper addresses the methodology of short-term forecasting for severe convective weather events and associated hydrological hazards (severe winds, torrential rainfall, and flash floods) across the North Caucasus and Southern Federal Districts. The approach is based on the Model Output Statistics (MOS) concept, which links large-scale prognostic fields from the GFS NCEP global numerical weather prediction model with localized historical observations. Multivariate linear regression equations are developed and verified. The quality of the resulting predictive schemes is comprehensively evaluated using the Durbin-Watson autocorrelation test, the Chaddock scale, and Variance Inflation Factors (VIF) to ensure resilience against multicollinearity. The developed models demonstrate statistical significance and can be integrated into operational regional early-warning pipelines.*

***Key Words:*** *MOS concept, GFS model, severe convective hazards, linear regression, multicollinearity, flash floods, heavy rainfall.*

## Introduction

Timely and accurate forecasting of severe convective hazards (SCH) and associated emergencies – such as flash floods, windstorms, and torrential downpours – remains a critical task for regional synoptic meteorology [3-7]. While high-resolution hydro-thermodynamic mesoscale atmospheric models are widely used, they require extensive computational resources and often fail to accurately resolve sub-grid convective processes in complex mountainous terrains.

An elegant and computationally efficient alternative is the **Model Output Statistics (MOS) concept** [1,5]. The MOS approach establishes mathematical and statistical relationships between the direct output of numerical weather prediction (NWP) models (predictors) and local weather variables observed at the surface (predictands) [8], thereby correcting systematic model biases. This study implements the MOS concept using prognostic fields from the **Global Forecast System (GFS NCEP, USA)** (www.noaa.gov) and the historical database compiled by the Hydrometeorological Center of the Kabardino-Balkarian Republic (KBR).

## Materials and Software Framework

The predictive schemes were derived using observational data from cases of severe weather hazards across the multi-regional domain of the South of Russia, including the Stavropol and Krasnodar Krais, Kabardino-Balkaria, North Ossetia, Chechnya, Ingushetia, Karachay-Cherkessia, and Adygea. Because the application of the MOS framework in this region is relatively recent, the available observational time series are short. This limitation necessitates rigorous statistical control to avoid over-fitting and to guarantee the stability of the equations.

Thermodynamic parameters of the atmosphere were calculated using an advanced software suite designed similarly to radio-sounding processing codes. The architecture relies on three primary software components:

**SUBROUTINE INPUT:** Manages data entry, formatting, and quality control. It processes data chunks equivalent to a single radiosonde profile, ensuring flexible run-time data allocation.

**SUBROUTINE TCOND:** Manages data entry, formatting, and quality control. It processes data chunks equivalent to a single radiosonde profile, ensuring flexible run-time data allocation.

**SUBROUTINE TCLOUD:** Models the cloud-air state curve (moist adiabat) originating from the condensation point. It is uniquely capable of projecting the curve both upward and downward on an emagram blank from any point with known temperature and dew point values.

This structural setup enables the derivation of the wet-bulb temperature profile and the determination of pseudo-potential temperatures. The final regression schemes were generated using the **SPSS** analytical framework.

To ensure the mathematical validity of the regression equations, the following diagnostic metrics were utilized: Coefficient of Determination ($R^2$ and $Radj^2$), evaluated qualitatively using the **Chaddock scale**; **Durbin-Watson (DW) Test** for the presence of first-order autocorrelation among the residuals (values near 2.0 confirm independent errors); and **Variance Inflation Factors** ($VIF = 1/(1-Rj^2)$ to monitor multicollinearity. The strict acceptance thresholds were set to **Tolerance > 0.1** and **VIF < 10**.

## Results

The multi-factor linear regression equations were derived for three main types of severe convective hazards.

*1. Severe Wind Speed Forecasting ($V_1$):*

The model was compiled for the republics of the North Caucasus and the Stavropol Krai using the following GFS-derived predictors: DTM (maximum cloud-to-environment temperature difference), VM (maximum updraft velocity), DJ (generalized instability index), and TTMI (Miller index). The resulting linear regression equation for wind speed ($V_1$, m/s) is:

$$V_1 = 0.514DTM - 0.251VM + 0.294\,DJ + 0.143TTMI - 71.953$$

The model achieved an ($R^2 = 0.377$), indicating a moderate correlation according to the Chaddock scale. The Durbin-Watson statistic is ($DW = 2.229$), proving the absence of residual autocorrelation. The maximum VIF was observed for the DTM predictor (6.064), satisfying the safety threshold (<10). The standardized Beta coefficient (-0.391) shows that VM yields the highest relative impact on the target wind speed.

*2. Torrential Rainfall Amount Forecasting ($QL_1$):*

Two distinct regional models were established for predicting heavy rainfall ($QL_1$), mm) using variables such as $V_{700}$ (ordered vertical velocity at 700 hPa), SQZ5 (total specific humidity in the surface–500 hPa layer), DSS (energy characteristic of the sub-cloud layer), TDSR5 (average moisture deficit in the $H_k$+5 km layer), and TTMI.

**Model A (Krasnodar Krai and Adygea):**

$$QL_1 = 0.09DSS - 2.542\,TTMI - 1.039\,TDSR5 - 0.55\,SQZ5 - 0.521\,V_{700} + 192.036$$

Metrics: $R^2 = 0.437$; $DW = 2.048$; all VIF values remain below 2.54.

**Model B (North Caucasus republics and Stavropol Krai):**

$$QL_1 = 1.403TTMI - 1.741TDSR5 - 0.0058\,DSS - 0.297\,SQZ5 - 0.16\,V_{700} - 11.193$$

Metrics: $R^2 = 0.445$; $DW = 2.021$; VIF values remain below 1.14., indicating negligible multicollinearity.

*3. Flash Flood Height Forecasting($H_1$):*

The dependent variable $H_1$ represents the water level rise above the datum line (cm). Predictors included $Q_3$ (accumulated rainfall over the 3 days prior to the event) and $Q_П$ (rainfall recorded on the day of the flood).

**Equation for Krasnodar Krai and Adygea:**

$$H_1 = 10.518\,Q_3 - 6.981\,Q_P + 273.330$$

Metrics: $R^2 = 0.423$; $DW = 1.863$; $VIF = 1.87$.

**Equation for the North Caucasus republics and Stavropol Krai:**

$H_1 = 2.027\ Q_3 - 6.214\ Q_P + 405.25$
Metrics: $R^2 = 0.401$; $DW = 1.545$; $VIF = 1.507$.

## Discussion

A direct comparison between the values estimated by the regression models and the actual historical measurements reveals an acceptable level of prognostic capability. The $R^2$ values ranging from 0.377 to 0.445 correspond to a moderate but statistically meaningful connection on the Chaddock scale. Given the short observational baselines typical for localized extreme hazards, these results are highly representative and mathematically sound ($Sig.F_{Change} < 0.05$ for the baseline configurations).

The negative coefficient for $Q_P$ reflects the specific hydro-geomorphic traits of the local mountain rivers: the peak discharge and maximum gauge heights are temporally shifted relative to the onset of the current day's precipitation. Instead, the antecedent soil moisture condition ($Q_3$) acts as the primary driver, showing a high positive standardized Beta coefficient (0.530). Normal probability (P-P) plots of the standardized residuals confirmed their adherence to a normal distribution line. Furthermore, the Durbin-Watson indicators and controlled VIF ranges guarantee that the models are free from spurious regressions and computational inaccuracies triggered by multicollinearity.

## Conclusion

A comprehensive short-term forecasting methodology for dangerous convective weather phenomena and subsequent environmental emergencies on the territory of the South of Russia was successfully designed and validated based on the GFS NCEP output data and the MOS concept. The derived statistical equations demonstrate structural resilience and offer actionable diagnostic value. This operational technology can be integrated into the workflow of local weather services (www. meteorf.gov.ru) to improve disaster risk reduction and protect regional infrastructure. In the future, it is planned to continue these studies, including forecasting changes across adjacent regional domains for several decades.

## References


1. Glahn H. R., Lowry D. A., The use of Model Output Statistics (MOS) in objective weather forecasting. // Journal of Applied Meteorology, 11(8), 1972, pp. 1203–1211.
2. Kagermazov A. Kh., et al., Automated methods for upper-air data processing and thermodynamic modeling. // FSBI HGI Publishing, Nalchik, 2018.
3. Kagermazov A. Kh., Hail forecasting based on the output data of the global atmospheric model (T254 NCEP). *Meteorologiya i Gidrologiya*, (3), 2012, pp. 28–34. (In Russian)
4. Kagermazov A. Kh., Fedchenko L. M., Using the concept of the "Perfect Prognosis" (PP) statistical analysis method for hail forecasting. // Izvestiya KBRC RAN, Nalchik, (2), 2012, pp. 75–80. (In Russian)
5. Kagermazov A. Kh., Kesheva L. A., Khuchunaeva S. B., Forecasting heavy rainfall and floods based on the MOS (Model Output Statistics) concept of output statistical models. // Proceedings of the International Symposium "Sustainable Development: Problems, Concepts, Models" dedicated to the 20th anniversary of KBRC RAN, Nalchik, Vol. II, 2013, pp. 126–128. (In Russian)
6. Kagermazov A. Kh., Fedchenko L. M., The use of statistical methods for forecasting hail processes and their characteristics. *Meteorologiya i Gidrologiya*, (4), 1988, pp. 41–50. (In Russian)
7. Kagermazov A. Kh., Sirotenko L. A., Results of testing software modules for calculating meteorological parameters and computer forecasting of hail based on aerological sounding data in the North Caucasus. // Izvestiya Vuzov. Severo-Kavkazskii Region. Fizika Atmosfery, Special Issue, 2010, pp. 49–53. (In Russian)
8. Kagermazov A. Kh., Validation of the Global Forecast System (GFS) output data with the results of aerological sounding. // Izvestiya KBRC RAN, Nalchik, 3(59), 2014, pp. 32–36. (In Russian)

2nd International Scientific Conference “Modern Problems in Geophysics”, Proceedings,
ISBN 978-9941-36-562-1, ISSN 3088-4349, Tbilisi, Georgia, October 29-31, 2026

# SEASONAL VARIATIONS IN THE DIURNAL COURSE OF THE EARTH'S ATMOSPHERIC ELECTRIC FIELD STRENGTH

**Kazakova S.**

*Federal State Budgetary Institution “High Mountain Geophysical Institute”,*
*Nalchik, Kabardino-Balkaria, Russian Federation*
*saniya_07@mail.ru*

***Abstract.*** *Variations in the electric field strength in the surface layer of the atmosphere during the day are caused by both global and local factors [1, 2]. The global component is manifested in the existence of a unitary daily variation of the atmospheric electric field over the oceans and polar regions of the Earth (Carnegie curve) [1]. Local factors influencing the intensity of the electric field of the atmosphere are natural phenomena (cloudiness, precipitation, wind, thunderstorms, etc.) and anthropogenic impact. In this work, we conducted studies of daily and seasonal variations in the strength of the atmospheric electric field, obtained using an EFM550 flux meter installed on the building of the Federal State Budgetary Institution "VGI" in the city of Nalchik.*

***Key words:*** *Electric field, atmospheric electric field, EFM550, unitary daily variation, daily and seasonal variations.*

## Equipment and Methodology

A vertical electric field is always present in the atmosphere. In fair weather, this field is weak, ranging approximately from 0 to +200 volts per meter (V/m). During stormy weather, the field is much stronger due to the presence of electric charges in thunderclouds. As a thunderstorm develops, the electric field typically reverses polarity and steadily intensifies. By the time the electric field reaches ±2000 V/m, the probability of lightning occurrence increases significantly.

Although lightning cannot be predicted, an electric field meter provides a means to measure the ambient conditions necessary for lightning formation.

The operation and underlying theory of the electric field meter are based on fundamental laws of electromagnetism. If a conductive plate is placed in an electric field, a charge proportional to the field strength and the plate's area accumulates on it. The atmosphere's normal resistivity is too high for a simple direct measurement of the electric field; consequently, it does not induce a detectable current in the meter's conductors. To facilitate measurement, the electric field meter generates an alternating electric field using a motor-driven rotor and a stator.

A hardware setup consisting of a Vaisala (Finland) EFM550 electric field meter and a personal computer running specialized software was used to measure and record atmospheric electric field strength values. The EFM550 continuously measures atmospheric electric field strength at a rate of two readings per second, with a measurement range of ±10,000 V/m. The specialized software saves the values measured by the EFM550 to files on the hard drive. The EFM550 meter is installed at a location with the coordinates: latitude 43.4694° and longitude 43.5861°.

Peripheral devices connected to an electric field meter display electric field strength and/or signal a hazard when the electric field reaches dangerous levels. Monitoring and interpreting the local electric field is one of the best ways to provide early warning of thunderstorm conditions and to determine when those conditions have stabilized and the danger has passed. The use of an electric field meter alongside other sources of meteorological information – such as radar, satellite data, and thunderstorm display systems – is common practice today.

Diurnal and seasonal variations in atmospheric electric field strength were analyzed separately for "fair-weather" days (cloudless days) and for the dataset as a whole, without distinguishing between "fair-weather" and "disturbed-weather" days (days with cloud cover, precipitation, etc.).

## Results

Based on atmospheric electric field strength values recorded over the entire period – without distinguishing between days with "fair" and "disturbed" weather – diurnal variations in field strength were obtained for the four seasons: winter, spring, summer, and autumn. The data were averaged over hourly intervals across all days within each respective season.

Figure 1 presents plots of the diurnal variations in atmospheric electric field strength for the four seasons: winter, spring, summer, and autumn.

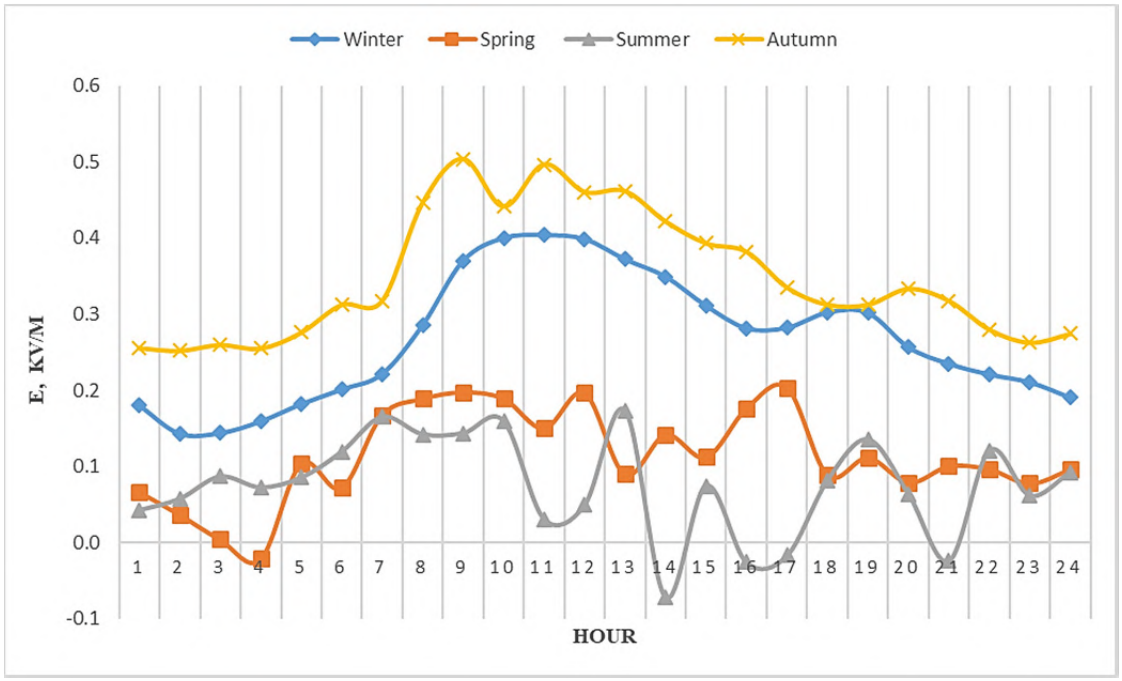



**Fig. 1.** Plots of diurnal variations in atmospheric electric field strength across all seasons.

The plots show that maximum values occur during the autumn period, with lower values in winter, and even lower values in spring and summer.

More distinct patterns emerge when the year is divided into two half-years based on the spring and autumn equinoxes: the warm half-year (March 22 to September 21) and the cold half-year (September 22 to March 21). Table 1 presents statistical parameters for the field strength values by season and half-year. The data were averaged over hourly intervals across all days of the respective periods.

**Table 1.** Statistical parameters of atmospheric electric field strength values by season and half-year.

| Periods | Mean value, V/m | Maximum value, V/m | Minimum value, V/m | Standard deviation, V/m |
|---|---|---|---|---|
| Winter | 289 | 404 | 143 | 84 |
| Spring | 123 | 204 | -21 | 61 |
| Summer | 82 | 173 | -71 | 65 |
| Autumn | 378 | 503 | 252 | 84 |
| Cold half-year | 314 | 454 | 194 | 84 |
| Warm half-year | 122 | 210 | 51 | 44 |

It is well known that the magnitudes of the field maxima and minima, as well as the mean field value, differ from station to station [1, 3]. For instance, the mean field strength is 171 V/m in Slutsk (Leningrad), 70 V/m in Uppsala (Sweden), 304 V/m in Kew (England), 86 V/m in Java, and 88 V/m in Antarctica [2]. For our location, the mean value is 218 V/m. This value is calculated as the average over two half-years or as the average over four seasons.

Diurnal variations for "fair-weather" days were also calculated separately for the two half-years. Figure 2 shows plots of the diurnal variations in field strength for these cases.

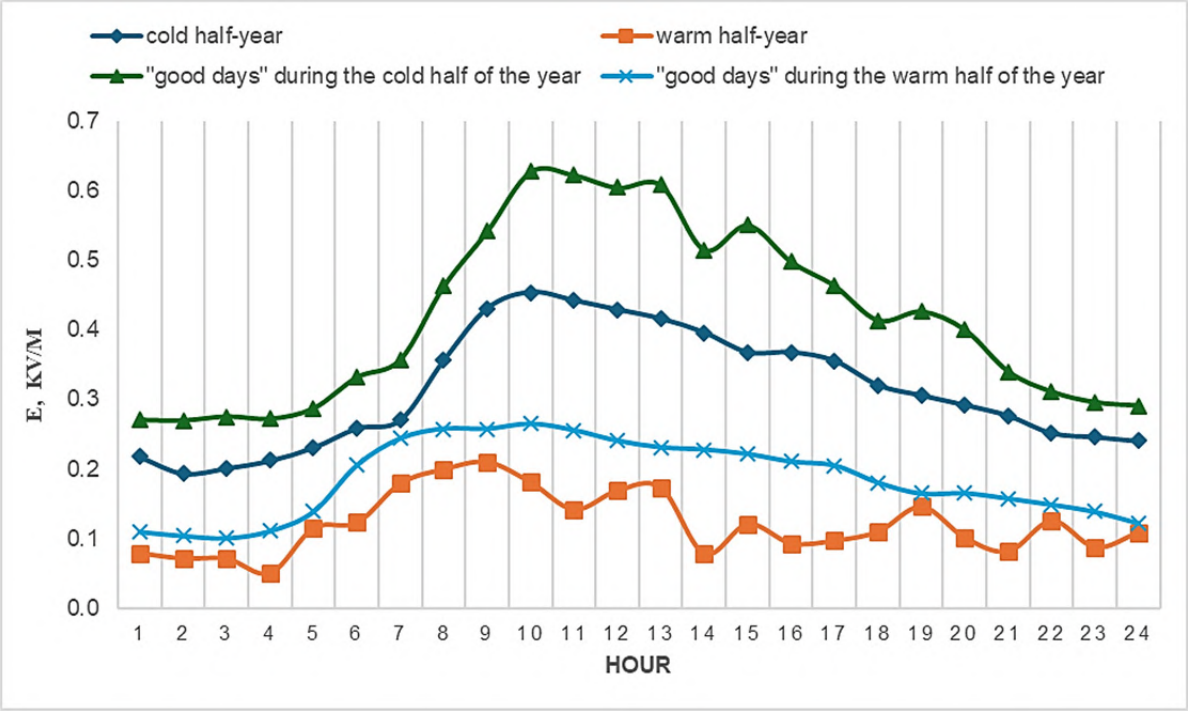



**Fig. 2.** Diurnal variations in atmospheric electric field strength for the warm and cold half-years, considering all days and "fair-weather" days

This figure clearly shows that days with "disturbed" conditions, regardless of the season, exert a lowering effect on the diurnal variation of atmospheric electric field strength.

## Conclusion

The data obtained clearly demonstrate that the averaged values of atmospheric electric field strength are higher during the "cold" season than during the "warm" season. Mean field strength values peak in autumn, are lower in winter, decrease further in spring, and reach their minimum in summer.

The results indicate that atmospheric phenomena such as cloud cover, precipitation, thunderstorms, etc. – that is, days with "disturbed" conditions – exert a depressing effect on the diurnal variation of atmospheric electric field strength.

## References

1. Imyanitov I.M., Shifrin K.S. // UFN [Physics-Uspekhi], Vol. 76, No. 4,1962, pp. 593–642.
2. Tverskoy P.N., Atmospheric Electricity. // Leningrad, Gidrometeoizdat, 1949.
3. Adzhiev A.Kh., Kupovykh G.V., Variations of the atmospheric electric field at high-altitude observation sites. // Doklady Akademii Nauk [Doklady Earth Sciences], Vol. 462, No. 2, 2015, pp. 213–216.

2nd International Scientific Conference "Modern Problems in Geophysics", Proceedings,
ISBN 978-9941-36-562-1, ISSN 3088-4349, Tbilisi, Georgia, October 29-31, 2026

# APPLICATION OF MODERN TECHNOLOGIES FOR STUDYING THUNDERSTORM ACTIVITY

**[*]Kerefova Z., [**]Dakhova O.**

*[*]Federal State Budgetary Institution "High Mountain Geophysical Institute", Nalchik, Kabardino-Balkaria, Russian Federation*
*[**]Kabardino-Balkarian State University, Nalchik, Kabardino-Balkaria, Russian Federation*
*zknyaz-kbsu@mail.ru*

**Abstract.** *The article presents the results of a comparative analysis of modern methods and means of monitoring thunderstorm activity on the territory of Russia.The lightning direction detection network of Roshydromet includes 87 sensors located in the European part, in the Urals and the Far East of the Russian Federation. Of these, 30 lightning direction finding sensors are manufactured by Vaisala (Finland) and 57 sensors are manufactured by Alwes (Russia).*
*The Federal State Budgetary Institution "VGI" carried out comparative tests of various lightning direction finding sensors. Good agreement was obtained between the output data of the compared lightning direction finding systems when recording ground-based lightning discharges.*

**Key words:** *Lightning, lightning direction network, lightning registration, atmospheric electricity, sensors.*

## Introduction

Lightning direction-finding systems (GPS) determine in real time a large number of lightning activity characteristics that are impossible to obtain through observations at meteorological stations, route measurements by weather radars (every 10 minutes), or meteorological satellites. These characteristics include coordinates and time, as well as the type (some GPS systems can separately record both cloud-to-ground and cloud-to-cloud lightning discharges) and current characteristics.

As a result, the advantage of GPS systems is their greater range (compared to weather radars and observations at meteorological stations) and low operating costs.

## Purpose of the Study

The purpose of this study is to improve the reliability of protection against lightning events. To achieve this, it is crucial to have up-to-date and continuous information on thunderstorm characteristics for specific geographic areas, as well as reliable and convenient methods for obtaining this information. This article examines lightning direction-finding systems currently in operation in Russia.

## Research Materials and Methods

This study provides a comparative analysis of modern methods and means for monitoring thunderstorm activity in Russia. Currently, five main GPS systems are in operation: three foreign-made and two domestically produced. This study provides a comparative analysis of these systems.

Domestic and foreign GPS systems:

– LS8000 GPS system by Vaisala (Finland) [1, 2];
– EN Lightning System GPS system by Earth Networks (USA) [3];
– LPS-200 GPS system by TOA Systems Inc (USA) [4];
– Alves GPS system [5]; – Vereya GPS [6,7].

All of the above GPS systems consist of geographically distributed sensors and a central point for receiving, processing, storing, and transmitting information to consumers. The sensors record radio frequency signals emitted by lightning. Two possible recording methods are time-of-arrival (TOA) and magnetic bearing distance (MDF) of the direction of the emitter (lightning).

## EARTH NETWORKS Lightning Sensor Network

The ENTLS system is one of the most technologically advanced lightning detection sensor networks, capable of detecting both cloud-to-cloud lightning and ground-to-ground lightning discharges.

The Total Lightning Network is used worldwide to detect severe weather events and generate timely warnings. Compared to traditional radar and other conventional technologies, ENTLS has the ability to significantly improve warning times for approaching extreme weather conditions. With its built-in early forecasting capabilities, ENTLS not only improves the time from warning to the onset of severe storms but also supports weather management planning. This makes ENTLS invaluable for mobile alerting and is used by governments and meteorological services, aviation, and sports and recreation organizations worldwide.

The ENTLS system operates using a unique sensor technology – Earth Networks Lightning Sensors (ENLS). Compared to lightning detection sensors from other companies, which are only capable of detecting intra-cloud lightning, ENLS has a wide frequency range from 1 Hz to 12 MHz, which allows it to detect both intra-cloud and ground lightning.

## Lightning detection network of sensors LS8000 (LS7002)

Roshydromet has deployed a lightning detection network across the Russian Federation using LS sensors from Vaisala, Finland.

Roshydromet's lightning detection system currently covers the entire European part of Russia, the Far East (Khabarovsk Krai, Amur Oblast, Jewish Autonomous Oblast), and Sakhalin Island.

The lightning detection network consists of 30 LS8000 and LS7002 sensors. The European segment includes 14 sensors connected into a single network. There are six sensors in the North Caucasus (four LS8000 and two LS7002 sensors), and a network of eight sensors in the Moscow Oblast (Fig.1).




**Fig. 1.** Field of view of LF sensors of the VGI and Planeta GPS systems.

The LS8000 lightning direction finder consists of two sensors – LF and VHF. The VHF sensor detects only cloud-to-cloud lightning discharges, while the LF sensor primarily detects cloud-to-ground lightning discharges.

The LS7002 lightning direction finder has only one sensor, but thanks to improved hardware and software, this sensor detects both ground- and cloud-to-ground lightning discharges. The LS7002 is also much more compact, making it easier to install and maintain.

## Lightning detector TOA

The TOA Systems Inc. lightning detector, equipped with LPS-200 sensors, is also an effective lightning direction-finding system for intra-cloud and cloud-to-ground lightning, classifying them into positive and negative [4]. The network consists of three segments in the Northwestern, Central, Volga, and Ural Federal Districts, with a total of 28 TOA LPS-200 lightning direction-finders. The general layout of the sensors is shown in Fig. 2.



**Fig. 2.** Layout of the "Groza" lightning direction finders.

The author also conducted comparative evaluations of the effectiveness of the TOA GPS and the LS8000 GPS. The TOA GPS, like the LS8000 and ENTLN GPS discussed above, is an effective means of monitoring thunderstorm days. Moreover, the TOA GPS is more sensitive than the LS8000 GPS and records a greater number of lightning strikes across the entire frequency range.

The most significant differences in favor of the LS8000, and possibly significant for operating the GPS in hard-to-reach areas, are:

a) The LS has a detection range of electromagnetic radiation from 1 Hz to 120 MHz, while the EN has a detection range from 1 Hz to 12 MHz. This means that the LS has a higher-frequency detection range (120 MHz) that is 10 times higher. Consequently, it will detect weak cloud lightning more effectively than the EN and TOA.

b) The LS has a higher detection threshold for positive ground lightning than the other GPS systems, approximately 10 times higher. c) The LS system's coverage area with the minimum number of sensors is 100 km² larger than that of the other systems.

d) LS has 14 years of operational experience in European Russia, while the other systems have just over three years.

d) The minimum number of sensors required for the LS system is two, while EN requires five and TOA requires three.

This characteristic is particularly relevant for Siberian conditions with their rugged terrain. The systems are identical in all other respects.

## Alves 7.04 Lightning Recorders

Fifty-seven Alves sensors are installed across the Russian Federation. To obtain information on the location of lightning strikes, the Alves GPS records the electromagnetic radiation (EMR) of lightning strikes at geographically dispersed locations.

The lightning recording system from Alves LLC allows lightning strike coordinates and electromagnetic radiation parameters to be determined. It also allows lightning activity maps to be created and combined with meteorological data from weather radars and satellites.

## VEREYA-MR Lightning Recorders

The Vereya-MR lightning detection system is deployed across Russia by the Federal State Institution "Avialesookhrana." The system operates as follows: each station records the time of signal reception, its direction, and the amplitude characteristics of the received signal, and transmits the data to a processing center. The existing lightning detection network consists of 26 lightning detection stations.

These zones cover an area of 11 million square kilometers with a discharge location error of 3 km. The hardware module records pulsed electromagnetic radiation signals, processes them, generates operational messages containing signal parameters, and transmits the information to the processing center. It also receives and displays lightning detection data. A distinctive feature of this system is its remote antenna unit, which has higher sensitivity and is significantly smaller in size than similar foreign products. High sensitivity provides a 2-3-fold advantage in range and at least a 4-9-fold reduction in specific costs per unit of monitored area (with the same cost of stations). Thanks to these characteristics, the system records lightning discharges at a range of up to 1,500 km.

## Research Results and Discussion

Federal State Budgetary Institution "VGI" conducted comparative tests of various lightning detection systems. Specifically, it compared the LS8000 and Earth Networks systems.

The comparative tests showed that the Earth Networks GPS and LS8000 GPS are effective tools for monitoring thunderstorms. During the comparative tests, covering the survey area from July 11 to November 24, 2019, the Earth Networks GPS recorded 59,605 cloud-to-ground lightning discharges, including 5,427 of positive polarity, 51,237 of negative polarity, and 2,941 of undetermined polarity.

Over the same area and period, the LS8000 system recorded 106,090 cloud-to-ground lightning discharges, including 39,330 of positive polarity and 66,760 of negative polarity.

The data obtained shows that, for the selected area, the Earth Networks GPS recorded 46,485 fewer cloud-to-ground lightning discharges than the LS8000 GPS, which is approximately 43%.

In our opinion, the main reason for the large difference in the ratio between the numbers of lightning discharges of different polarities is the different approach to defining positive-polarity ground lightning in the compared GPS systems. Specifically, when classifying positive-polarity lightning discharges, the Earth Networks GPS assumes, in accordance with published scientific research, that positive-polarity lightning discharges with a current of less than +15 kA are considered cloud discharges. The LS8000 GPS has no such current limitations for ground-based positive discharges.

The differences are particularly pronounced in such important parameters as the average and median current for positive lightning discharges, and the minimum and maximum values for negative lightning discharges. For positive discharges, the average and median current values according to Earth Networks GPS are +38.1 kA and +29.4 kA, while according to LS8000 GPS, they are +13.7 kA and +9.1 kA. This means that these values for Earth Networks GPS are three times greater than those for LS8000 GPS.

## Conclusion

1. Roshydromet's GPS system includes 87 lightning direction-finding sensors/indicators located in the European part of the Russian Federation, the Urals, and the Far East. Of these, 30 are manufactured by Vaisala (Finland) and 57 are manufactured by Alwes (Russia).

   In the European part, 14 Vaisala-manufactured GPS systems are located, connected into a single network (VGI and the European Center of the Planeta Research Center).

   Currently, the current GPS density at the Planeta Research Center is insufficient. The number of GPS systems in the central European part of the Russian Federation needs to be increased to improve the accuracy of lightning activity recording in this area.

2. In addition to the Roshydromet GPS, a limited number of sensors such as ENTLS (USA) and TOA LPS-200 (USA) are deployed across the Russian Federation. However, a significant portion of the Russian Federation is still not covered by a lightning direction-finding sensor network.
3. Comparative testing of various lightning direction-finding sensors was conducted at the Federal State Budgetary Institution "VGI." Good agreement was found between the output data of the compared lightning direction-finding systems when recording ground-level lightning discharges.

   Combining lightning direction-finding data from both Earth Networks and LS8000 GPS systems with cloud echo data obtained by weather radars demonstrated good agreement between the output data for both GPS systems. Approximately 90% of lightning discharges are concentrated in the cloud and precipitation echo zones.

   The data obtained allow us to conclude that the use of a lightning detection system based on Earth Networks sensors will improve the accuracy and effectiveness of warnings of hazardous weather events, as well as the lead time of their forecasts.
4. There is overlap between the lightning activity monitoring areas of Roshydromet, TOA LPS-200, and ENTLS systems, and there is also a portion of the Russian Federation covered by Roshydromet lightning detection sensors. Therefore, until a lightning detection network covering the entire Russian Federation is created, it is recommended to use TOA LPS-200 data for monitoring lightning activity.

**Acknowledgement:** The work was supported by a grant from the Russian Science Foundation (Agreement No. 26-17-20002).

## References

1. Adzhiev A.Kh., Stasenko V.N., Tapaskhanov V.O., Lightning Direction Finding System in the North Caucasus. // Meteorology and Hydrology, No. 1, 2013, pp. 5-11.
2. Thompson K.B., Bateman M.G., Carey L.D., A Comparison of Two Ground-Based Lightning Detection Networks against the Satellite-Based Lightning Imaging Sensor (LIS). // Journal of Atmospheric and Oceanic Technology. Vol. 31, No. 10, 2014, pp. 2191-2205, DOI:10.1175/JTECH-D-13-00186.1
3. Goodman S.J., et al., The GOES-R Geostationary Lightning Mapper (GLM). // Atmos. Res. 125–126, 2013, pp. 34–49. doi:10.1016/j.atmosres.2013.01.006.
4. Gubenko I. M., Rubinstein K. G. An example of data assimilation from several lightning direction-finding networks in numerical weather forecasting. // Atmospheric and Oceanic Optics, Vol. 34. No. 10, 2021, pp. 803–807. DOI: 10.15372/AOO20211007.
5. Lay E. H., Investigating lightning-to-ionosphere energy coupling based on VLF lightning propagation characterization, // University of Washington, Seattle, Washington State, USA, 2008, pp. 20–46.
6. Snegurov A.V., Snegurov V.S., Experimental lightning direction-finding system. // Proceedings of the Main Geophysical Observatory, Issue 567, 2012, pp. 188-200.
7. Snegurov A.V., Snegurov V.S., Shapovalov A.V., Shchukin G.G., Experience of joint observations of thunderstorms using a lightning direction-finder-rangefinder and a weather radar, // Proceedings of the Scientific Center for Defense and Aviation Safety (Branch of the Main Geophysical Observatory), Issue 7(555), 2006, pp. 139-148.

2nd International Scientific Conference "Modern Problems in Geophysics", Proceedings,
ISBN 978-9941-36-562-1, ISSN 3088-4349, Tbilisi, Georgia, October 29-31, 2026

# SPATIOTEMPORAL DYNAMICS OF CLOUD LIGHTNING DISCHARGES

**Kerefova Z., Adzhiev A.**

*Federal State Budgetary Institution "High Mountain Geophysical Institute",*
*Nalchik, Kabardino-Balkaria, Russian Federation*
*zknyaz-kbsu@mail.ru*

***Abstract.*** *The article presents the results of an instrumental study of the spatiotemporal dynamics of cloud lightning discharges in the North Caucasus. The study utilizes the Earth Networks Total Lightning Network (TLN) lightning location data collection system, which allows for determining the formation altitude of cloud lightning discharges. The TLN lightning direction-finding system was developed by Earth Networks (USA). In 2023, the lightning direction-finding system recorded 2,265,613 cloud-borne lightning events, accounting for approximately 80% of the total number of lightning events of all types.*

*More than half of cloud-borne lightning events occur in clouds at depths between 3 and 5 km (on isotherms from 0°C to -10°C), where, according to current understanding, most of the cloud's negative electric charge is concentrated.*

***Key words:*** *Thunderstorm, lightning, lightning direction-finding, thunderstorm processes, cloud reflectivity, wind.*

## Introduction

Unlike ground lightning, cloud lightning has not been fully studied. Data on neutralized lightning currents, discharge durations, and other parameters are lacking. However, cloud lightning, like ground lightning, can negatively impact radio equipment, particularly aircraft. Cloud lightning accounts for approximately 88% of all discharges [1, 2], with data for the North Caucasus region.

This paper examines the statistical and spatial-temporal distributions of cloud lightning.

### Research Methodology

Cloud discharges and cloud-to-ground discharges emit radio waves over a wide frequency range. Streamers – elements of ground lightning that create conductive channels in the atmosphere – generate strong emissions in the VHF (Very High Frequency) range. During the passage of high currents through previously created channels (return strokes), the strongest emissions occur in the LF (Low Frequency) and VLF (Very Low Frequency) ranges. In the LF and VLF ranges, cloud-to-ground lightning discharge radiation is most intense [3-5]. Based on the patterns of these electromagnetic radiations from lightning discharges, methods and tools have been developed for measuring lightning discharge characteristics, including lightning strike time, its coordinates, discharge duration, ground-to-ground lightning polarity, current strength, and others.

Currently, lightning direction-finding networks (LDNs) are widely used in Russia and abroad to monitor lightning discharges and measure lightning parameters [6].

Their use has made it possible to obtain a wide range of ground-to-ground lightning discharge characteristics. Specifically, the following data have been obtained for the North Caucasus [7]:

- Seasonal thunderstorm activity dynamics are characterized by a summer peak of up to 22 days in June and a minimum of 2-3 days in December.
- The ratio between the number of cloud, ground, ground positive, and ground negative lightning strikes is characterized by the following values:
  - The shares of ground and cloud lightning strikes in the total number of all discharges are 12% and 88%, respectively.
  - The shares of positive and negative lightning strikes in the total number of ground discharges are 23% and 77%, respectively.
- The average current of positive lightning strikes is +10.6 kA. The median value is +7.6 kA.
- The average current of negative lightning strikes is –13.5 kA. The median value is –9.8 kA.

Unlike ground-based lightning, the characteristics of cloud lightning discharges have not been studied as well. This is due to the lack of technical capabilities to determine a number of cloud discharge parameters, such as polarity, current strength, and others. Earth Networks (USA) has developed a global lightning location data collection system, the Earth Networks Total Lightning Network (TLN), which allows for the determination of the formation altitude of cloud discharges [8].

Other widely used GPS systems [9] lack this capability. This study utilizes the Earth Networks Total Lightning Network to study the spatiotemporal dynamics of cloud lightning. An example of such a sensor, installed in Cherkessk, is shown in Figure 1.



**Fig. 1.** Earth Networks Total Lightning Network lightning detector sensor installed in Cherkessk.

Over the course of the year, the study area experiences more than 30 days with hail. According to the regulatory document "SP Construction Climatology," the daily maximum precipitation exceeds 100 mm.

Based on these factors, it can be concluded that there was a good opportunity to study thunderstorm processes.

## Results and discussions

An analysis of the spatiotemporal dynamics of cloud lightning discharges in the North Caucasus for 2023 was conducted using data from the aforementioned lightning direction-finding network of Earth Networks. During 2023, 117 days with thunderstorms were observed in the study area. More than 80% of thunderstorms were associated with frontal air mass intrusions, while the remainder were caused by the development of intra-mass processes. Thunderstorm forecasts noted that the zero isotherm height ranged from 1 km to 1.5 km in autumn and spring. In summer, the zero isotherm height ranged from 3 km to 3.5 km. According to data from the MRL5 (VGI) and DMRL-S (Mineralnye Vody) radar stations, the vertical boundaries of convective thunderclouds ranged from 1 km to 8 km in spring and autumn. The vertical boundaries of convective thunderclouds during the summer ranged from 2 km to 12 km.

Fig. 2 shows the distribution of cloud-borne lightning at various altitudes by month in 2023. As the table shows, the lightning detection system recorded 2,265,613 cloud-borne lightning events. A total of 2,832,016 lightning events were recorded, of which 566,403 were classified as ground-borne lightning. Analysis of the obtained data allows us to draw the following conclusions:

1. In terms of cloud height, the highest cloud-borne lightning density occurs at an altitude of 3 km – from 70 lightning/km to 1,993 lightning/km in winter, from 179 lightning/km to 123,720 lightning/km in spring and autumn, and from 104,703 lightning/km to 217,106 lightning/km in summer.

2. The highest number of cloud-borne lightning strikes during the year was observed in June – 720,879. The seasonal distribution of cloud-borne lightning discharges is shown in Figure 4. As Figure 4 shows, even in winter, low-intensity thunderstorms are observed in the North Caucasus.

3. More than half of cloud-borne lightning strikes occur in clouds at levels between 3 and 5 km, where, according to modern concepts, the majority of the negative electric charge is concentrated.

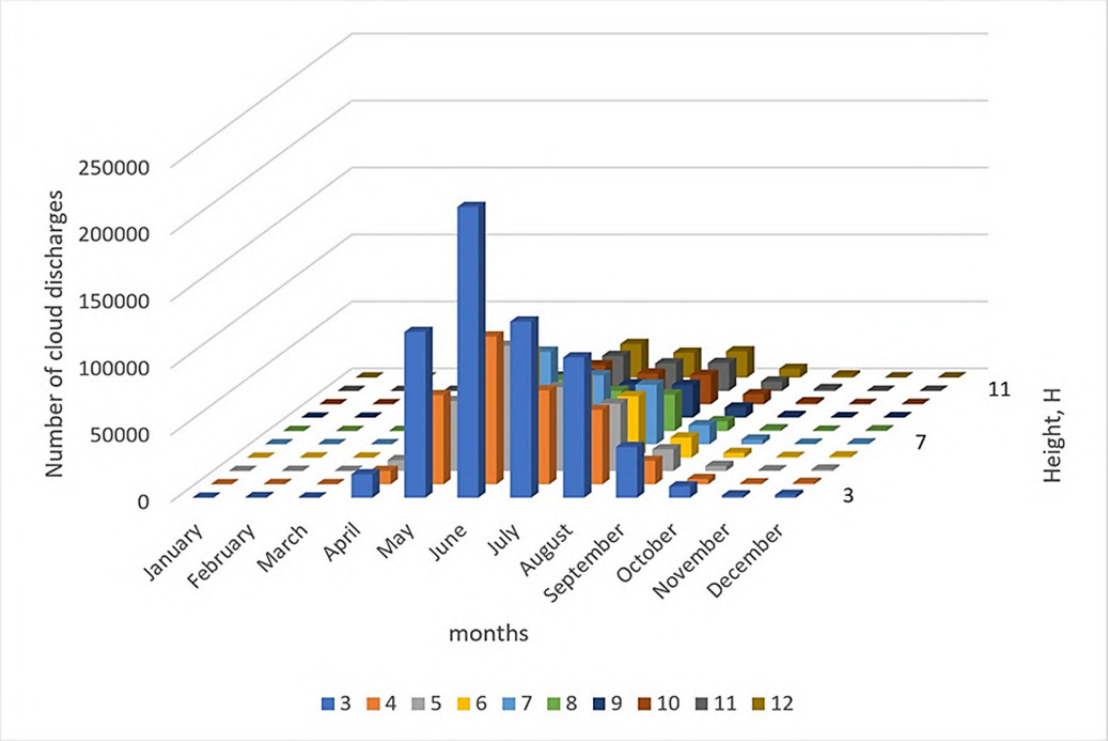



**Fig. 2.** Distribution of the number of cloud lightning discharges depending on the altitude (km) and season of the year.

## Conclusion

Analysis of experimental data showed that intracloud lightning discharges in convective clouds in the North Caucasus begin after radar reflectivity reaches approximately 40 dBZ. As the cloud develops further and precipitation and hail formation intensifies, the frequency of intracloud discharges decreases to VHF. This is explained by the fact that the processes of raindrop growth, their splashing, crystal formation and division, and hail formation and growth lead to the electrification of cloud particles, the spatial dispersion of both small and large particles with opposite charges by vertical currents, and an increase in electric field strength to breakdown levels.

The proportions of ground- and cloud-based discharges in the total number of all discharges are 12% and 88%, respectively. Most cloud-to-cloud lightning discharges occur in clouds at altitudes of 3 to 5 km, with temperatures ranging from 0°C to -10°C. This is where the primary negative electric charge is generated by microphysical and dynamic processes. It can be assumed that the rise of light crystals and small particles to the upper part of the cloud, where they are caught in a strong horizontal flow and carried to the leeward flank, where high microphysical and dynamic inhomogeneities and increased turbulence are observed, contributes to the formation of positively charged zones. The more intense the microphysical and dynamic processes, the greater the frequency of lightning discharges between oppositely charged cloud regions.

The seasonal distribution of cloud-to-cloud lightning discharges in the North Caucasus indicates that the highest monthly number occurs in June. Even in winter, low-intensity thunderstorms are observed.

**Acknowledgement:** The work was supported by a grant from the Russian Science Foundation (Agreement No. 26-27-20025).

## References


1. Adzhiev A.Kh., Kuliev D.D., Characteristics of thunderstorm activity and parameters of lightning discharges in the south of the European part of Russia. // Izvestiya RAS. Physics of the Atmosphere and Ocean, Vol. 54, No. 4, 2018, pp. 437–445.
2. Adzhiev A.Kh., Kuliev D.D., Stasenko V.N., Evaluation of the performance parameters of the LS8000 and ENTLS lightning detection systems in the North Caucasus region. Meteorology and Hydrology, No. 4, 2022, pp. 117–126.
3. Cummins K.L., Krider E.PH., Malone M.D. The U.S., National Lightning Detection Network and Applications of Cloud-to-Ground Lightning Data by Electric Power Utilities. // IEEE Transactions on Electromagnetic Compatibility, V. 40, No. 4, 1998, pp. 465–480.
4. Poelman D. R., Schulz W., Vergeiner C., Performance characteristics of three distinct lightning detection networks covering Belgium // 22nd International Lightning Detection Conference. 2–3 April 2012, Broomfield, Colorado, USA.
5. Schulz W., Saba M., First results of correlated lightning video images and electric field measurements in Austria // 10th International Symposium on Lightning Protection, Curitiba, Brazil, 2009.
6. Adzhiev A.Kh., Stasenko V.N., Tapaskhanov V.O., Lightning direction finding system in the North Caucasus. // "Meteorology and Hydrology", No. 1, 2013, pp. 5–11.
7. Adzhiev A.Kh., Bogachenko E.M., Thunderstorms of the North Caucasus. // Nalchik: LLC “Poligrafservice and T”, 2011. 151 p.
8. Boccippio D.J., Cummins K.L., Christian H.J., Goodman S.J., Combined Satellite- and Surface-Based Estimation of the Intracloud-Cloud-to-Ground Lightning Ratio over the Continental United States. // Mon. Weather Rev. V. 129, 2001, pp. 108–122.
9. Liu, C. and Heckman, S., January. The application of total lightning detection and cell tracking for severe weather prediction. // In 91st American Meteorological Society Annual Meeting, 2011, pp. 1-10.

2nd International Scientific Conference "Modern Problems in Geophysics", Proceedings,
ISBN 978-9941-36-562-1, ISSN 3088-4349, Tbilisi, Georgia, October 29-31, 2026

# THE IMPACT OF CLIMATE CHANGE ON THE DYNAMICS OF CLOUDINESS IN TBILISI

**Khomasuridze G., Lagidze L.**

*Ivane Javakhishvili Tbilisi State University, Tbilisi, Georgia*
*khomagio@gmail.com*

***Abstract.*** *Climate change and its adverse effects have become particularly evident since the mid-20th century, both in Georgia and worldwide. The negative effects of climate change have been especially pronounced in megacities, where air pollution from motor vehicle and industrial emissions is substantial, while green cover has been critically reduced. Recent studies have revealed significant changes in meteorological parameters. The study examines two meteorological parameters of Tbilisi: total number of clouds and the number of low-level clouds. The study is based on observational data for the period 1972–2021 collected at the Dighomi (Vashlijvari) meteorological station of the National Environmental Agency. The dynamics of changes in the total number of clouds and number of low-level clouds were assessed by month, season, year, five-year and ten-year periods, and over the entire 50-year period. A comparison of the ten-year periods produced the following results: over the 50-year period from 1972 to 2021, the total number of clouds decreased by 0.41 points, while number of low-level clouds increased by 0.11 points. Cloud cover also decreased according to the linear approximation trend. This contributed to an increase in air temperature and, consequently, to increased evaporation. According to the linear approximation trend, over the 50-year period, the total number of clouds decreased by 0.36 points, while the number of low-level clouds decreased by 0.01 points. This is presumably attributable to the reduction in natural green cover in the capital, the extensive area occupied by paved roads, and the dense and uncontrolled development of residential buildings.*

***Key words:*** *Climate Change, Tbilisi Cloudiness.*

## Introduction

Climate change and its adverse effects have become particularly evident since the mid-20th century, both in Georgia and worldwide. The negative effects of climate change have been especially pronounced in megacities, where air pollution from motor vehicle and industrial emissions is substantial, while green cover has been critically reduced. Recent studies have revealed significant changes in meteorological parameters. For example: average, minimal and maximal air temperatures, average precipitation, relative humidity, average wind speed and number of cloudy days has changed [2-4].

Cities are the preferred locations for cloud development. The urban effect on clouds is due to the combined influence of urban heat island, surface roughness and aerosols. During the summer season when instability and convective uplift dominate in light regional airflow increased cloudiness is found in cities. In many cases urban effects enhance or suppress pre-existing clouds rather than initiate new events [1, 6].

Due to the urban heat island effect, cloud cover in cities is increasing rather than decreasing, although specific conditions can lead to a decrease in cloud cover: 1. Dry air – cities have less vegetation and widely developed drainage systems, which leads to a decrease in water evaporation, and dry air prevents water vapor from condensing into clouds, 2. Compact arrangement of buildings – Compact arrangement of buildings can limit air circulation and vertical mixing, which will prevent the transport of heat and moisture necessary for cloud development to the upper layers of the air [4, 6, 7].

## Materials and Methods

The study aimed to study the impact of global climate change on cloud cover in the city of Tbilisi. Data on the total number of clouds and the number of low-level clouds (in points) from the Dighomi meteorological station of the National Environment Agency for the years 1972-2021 were used for the study. In the study, the numerical values of the two meteorological parameters mentioned were divided into five ten-year

periods (the data for July 1990 were missing from the data). The study assessed the change in the two parameters according to months, seasons, year, 5 ten-year and total 50-year periods. In addition, the air temperature data of the Dighomi (Vashlijvari) meteorological station for 1972-2021 were used to assess the influence of cloudiness on the average air temperature. The correlation coefficient between the total number of clouds and the average air temperature was calculated according 50-year annual data. Tables and graphs were compiled based on the data on the total number of clouds and the number of low-level clouds. (Table 1, Table 2, Fig. 1- Fig. 3) [5].

## Main results and discussion

The study revealed that during the years 1972-2021, the total number of clouds in Tbilisi by month was the highest in April at 6.68 points, and the lowest in August at 4.95 points. By season, the highest was in spring at 6.54 points, and the lowest was in summer at 5.18 points. By year, the highest cloudiness was recorded in 2018 at 6.48 points, and the lowest was in 1997 at 5.22 points. A decrease in the total number of clouds is observed in all seasons according to ten-year periods. The total number of clouds decreased by 0.41 points over 10-year periods. Over the entire period of 1972-2021, the total number of clouds changes from 6.12 points to 5.76 points with a linear approximation trend, i.e. over 50 years it decreased by 0.36 points. (Table 1, Fig. 1) [5].

The data for the second parameter, the number of clouds on the low level, are as follows: by month, the highest is 5.5 points in March, the lowest is 4.1 points in August. By season, the highest is 5.34 points in spring, the lowest is 4.24 points in summer. By year, the highest is 5.8 points in 2018, the lowest is 3.09 points in 1999. According to 10-year periods, we have an increase in all seasons except summer. The number of clouds on the low level increased by 0.11 points over 10-year periods. Over the entire period of 1972-2021, the number of clouds on the low level changes from 4.93 points to 4.92 points with a linear approximation trend, i.e. Over 50 years, the number of clouds on the low level decreased by 0.01 points (Table 2, Fig. 2) [5].

**Table 1.** Tbilisi. Total number of clouds by 10-year periods and months in 1972-2021.

| | I | II | III | IV | V | VI | VII | VIII | IX | X | XI | XII | Average |
|---|---|---|---|---|---|---|---|---|---|---|---|---|---|
| 1972-1981 | 6.82 | 6.96 | 7.11 | 6.87 | 6.98 | 5.98 | 5.46 | 5.18 | 5.56 | 6.06 | 6.15 | 6.22 | 6.28 |
| 1982-1991 | 5.91 | 6.67 | 6.56 | 6.31 | 6.23 | 5.50 | 5.28 | 5.18 | 4.75 | 5.66 | 6.77 | 5.73 | 5.88 |
| 1992-2001 | 6.15 | 5.76 | 6.08 | 6.46 | 5.99 | 5.04 | 5.06 | 4.97 | 5.06 | 5.59 | 5.75 | 6.17 | 5.67 |
| 2002-2011 | 6.33 | 6.71 | 6.70 | 7.16 | 6.07 | 5.40 | 5.16 | 4.88 | 5.59 | 6.12 | 5.81 | 5.94 | 5.99 |
| 2012-2021 | 6.23 | 6.47 | 6.83 | 6.62 | 6.14 | 5.03 | 5.09 | 4.56 | 5.29 | 5.92 | 6.33 | 5.90 | 5.87 |
| Average | 6.29 | 6.51 | 6.66 | 6.68 | 6.28 | 5.39 | 5.21 | 4.95 | 5.25 | 5.87 | 6.16 | 5.99 | 5.94 |

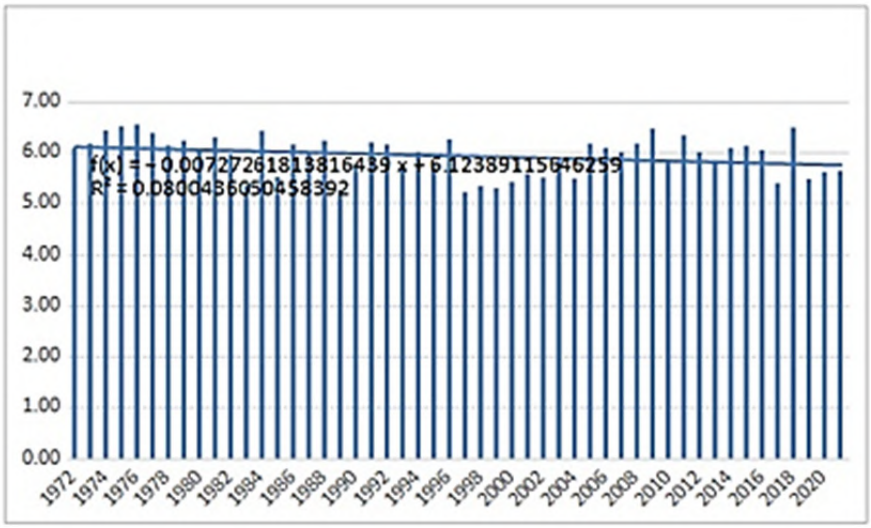



**Fig. 1.** Tbilisi. Total number of clouds by years in 1972-2021.

**Table 2.** Tbilisi. Number of low-level clouds by 10-year periods and months in 1972-2021.

| | I | II | III | IV | V | VI | VII | VIII | IX | X | XI | XII | Average |
|---|---|---|---|---|---|---|---|---|---|---|---|---|---|
| 1972-1981 | 5.25 | 5.68 | 5.87 | 5.25 | 5.31 | 4.71 | 4.20 | 4.22 | 4.75 | 4.94 | 4.85 | 5.02 | 5.00 |
| 1982-1991 | 5.02 | 5.95 | 5.87 | 5.28 | 5.31 | 4.48 | 4.56 | 4.59 | 4.17 | 5.25 | 6.02 | 5.08 | 5.13 |
| 1992-2001 | 4.61 | 4.52 | 4.60 | 4.81 | 4.44 | 3.82 | 3.74 | 3.97 | 4.04 | 4.58 | 4.66 | 5.01 | 4.40 |
| 2002-2011 | 5.09 | 5.52 | 5.39 | 5.99 | 5.17 | 4.50 | 4.14 | 3.95 | 4.90 | 5.24 | 4.83 | 4.70 | 4.95 |
| 2012-2021 | 5.37 | 5.57 | 5.86 | 5.54 | 5.35 | 4.28 | 4.59 | 3.91 | 4.58 | 5.35 | 5.59 | 5.43 | 5.12 |
| Average | 5.07 | 5.45 | 5.52 | 5.37 | 5.12 | 4.36 | 4.25 | 4.13 | 4.49 | 5.07 | 5.19 | 5.05 | 4.92 |

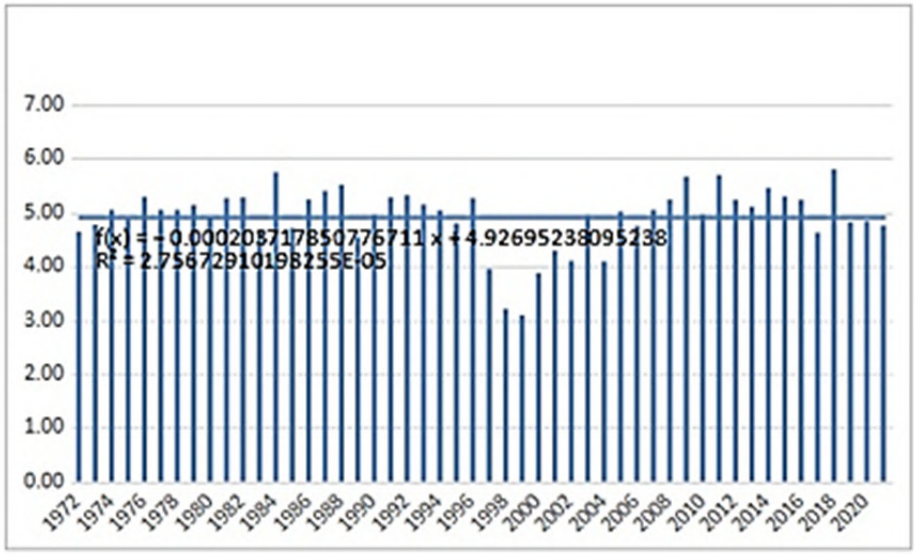



**Fig 2.** Tbilisi. Number of low-level clouds by years in 1972-2021.

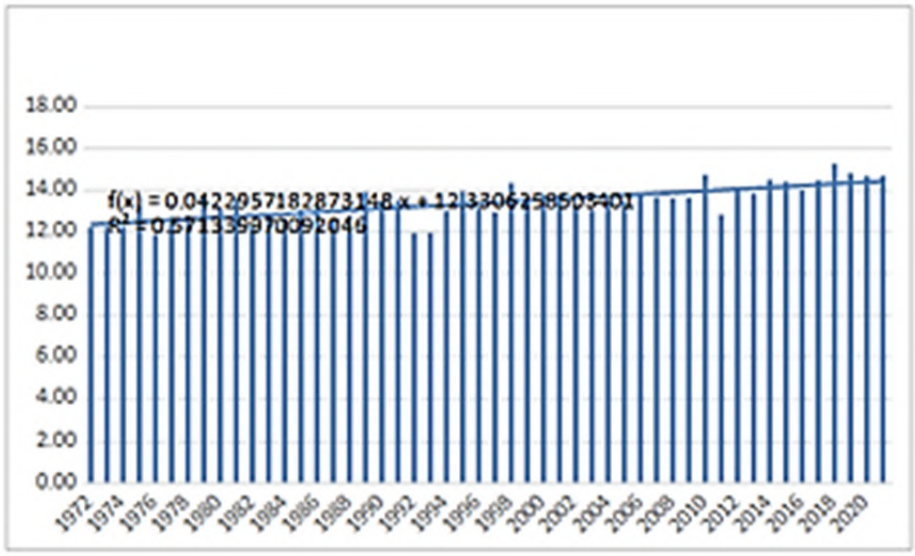



**Fig. 3.** Tbilisi. Annual air temperatures in 1972-2021.

The correlation coefficient between two Tbilisi meteorological parameters: the total number of clouds and the average air temperature (1972-2021) is -0.29. (Fig. 1, Fig. 3) [5].

The study revealed that in the city of Tbilisi in 1972-2021, i.e. Over the 50-year period, the total amount of clouds with a linear approximation trend decreased by 0.36 points, and the amount of clouds in the low level decreased by 0.01 points. Both cloudiness parameters have decreased. This is likely due to the critical reduction of green cover in the capital, the abundance of paved roads, and the dense and chaotic development of residential buildings. (Fig. 1, Fig. 2) [5].

## Conclusion

According to the linear approximation trend, over the 50-year period, total cloud cover decreased by 0.36 points, while cloud cover in the low level decreased by 0.01 points. [5] This is presumably attributable to the reduction in natural green cover in the capital, the extensive area occupied by paved roads, and the dense and uncontrolled development of residential buildings [6, 7].

## References


1. Carter T.R., Benzie M., Campiglio E., Carlsen H., Fronzek S., Hildén,, M., Reyer C.P.O., West C., A Conceptual Framework for Cross-Border Impacts of Climate Change. // Glob. Environ. Chang., 69, 2021, 102307. https://doi.org/10.1016/j.gloenvcha.2021.102307
2. Coombes M.A., Viles H.A., Integrating Nature-Based Solutions and the Conservation of Urban Built Heritage: Challenges, Opportunities, and Prospects. // Urban For. Urban Green., 63, 2021, 127192. https://doi.org/10.1016/j.ufug.2021.127192
3. Liu, Y.; Xu, Y.; Weng, F.; Zhang, F.; Shu, W., 2021: Impacts of Urban Spatial Layout and Scale on Local Climate: A Case Study in Beijing. *Sustain. Cities Soc.*, *68*, 102767. https://doi.org/10.1016/j.scs.2021.102767
4. Martínez I., Climate of Madrid City, 2023. Available online: http://imartinez.etsiae.upm.es/Env/Climate-Madrid/Climate.pdf (accessed on 10 March 2025).
5. Meteorological data of National Environmental Agency (Tbilisi, Dighomi meteorological station).
6. Oke T.R., Mills G., Christen A., Voogt J.A., // Urban Climate, Cambridge University Press., 2017, 548 p. https://doi.org/10.1017/9781139016476
7. Su Y., Li Z., Wang C., Meng Q., Gong A., Wu Z., Zhao Q., Summer Outdoor Thermal Comfort Assessment in City Squares – A Case Study of Cold Dry Winter, Hot Summer Climate Zone. // Sustain. Cities Soc., 101, 2024, 105062. https://doi.org/10.1016/j.scs.2023.105062

2nd International Scientific Conference "Modern Problems in Geophysics", Proceedings,
ISBN 978-9941-36-562-1, ISSN 3088-4349, Tbilisi, Georgia, October 29-31, 2026

# PROSPECTS FOR THE USE OF SUNFLOWER (HELIANTHUS ANNUUS L.) IN THE PHYTOREMEDIATION OF MINING-IMPACTED SOILS IN GEORGIA: A REVIEW AND PRACTICAL RECOMMENDATIONS

**Matiashvili S.**

*M. Nodia Institute of Geophysics of the I. Javakhishvili Tbilisi State University, Tbilisi, Georgia*
*matiashvilisophiko@gmail.com, sophiko.matiashvili@tsu.ge*

***Abstract.*** *The restoration of soils affected by mining and industrial activities is particularly important in Georgia, especially in the Kvemo Kartli, Chiatura, and Zestafoni areas, where potentially toxic elements (PTEs) have been detected in soils. Phytoremediation is a relatively low-cost and environmentally compatible approach, while sunflower (Helianthus annuus L.) is characterized by high biomass production, rapid growth, and the capacity to absorb different contaminants. This paper presents a literature review and a conceptual framework for a sunflower-based pilot phytomanagement approach under Georgian mining-industrial conditions. The mechanisms of phytoextraction and phytostabilization are considered, together with the roles of soil pH, organic matter, texture, moisture, and cation exchange capacity (CEC), as well as the distribution of elements among different plant organs. Particular attention is given to the bioconcentration factor (BCF) and translocation factor (TF). For Georgia, GIS-based zoning, controlled experiments, and safe biomass management are proposed. Final effectiveness should be established experimentally for the specific site, cultivar, and contaminant.*

***Key words:*** *Sunflower; phytoremediation; radionuclides; mining soils.*

## Introduction

Mining, ore processing, metallurgical production, and the accumulation of industrial waste can cause long-term soil contamination. Under such conditions, some contaminants may remain in the soil for extended periods, while their solubility, migration, and bioavailability may change. [1-6] Particular attention should be given to Cu, Zn, Cd, Pb, Ni, Cr, Co, As, Hg, and Mn because their environmental risk depends not only on total concentrations but also on soil properties and chemical forms. Studies conducted in Georgia's mining-industrial regions have demonstrated spatial heterogeneity in heavy-metal contamination. In Kvemo Kartli, including the Bolnisi–Kazreti and Rustavi areas, elevated concentrations of different PTEs have been identified. Local studies also indicate that contamination assessment should be based on repeated monitoring, GIS mapping, and characterization of the physical and chemical properties of soils (Gventsadze et al., 2024; Matiashvili et al., 2025a, 2025b). Phytoremediation involves the use of plants to restore contaminated soils and reduce environmental risks. Sunflower is an interesting crop because it produces substantial aboveground biomass and exhibits different uptake capacities for various metals.[7-9] At the same time, its effectiveness depends on cultivar, soil type, metal, contaminant dose, duration, and agronomic conditions (Rizwan et al., 2016).

The principal approaches to phytoremediation are phytoextraction and phytostabilization; other mechanisms include rhizofiltration, phytodegradation, and phytovolatilization. In PTE-contaminated soils, phytoextraction occurs when plants take up elements from the soil and accumulate them in aboveground tissues, after which removal of the biomass reduces the contaminant stock in the soil. During phytostabilization, vegetation reduces erosion, dust dispersion, and contaminant mobility, while the element remains mainly within the root zone (Ali et al., 2013; Vangronsveld et al., 2009). When sunflower is used, it is essential to distinguish a high concentration of an element in plant tissue from the actual removal of a significant mass of that element from the soil. Assessment should therefore consider tissue concentration, dry biomass, and the total mass removed during a growing season simultaneously. Soil properties strongly control PTE bioavailability. pH, organic matter, clay fraction, moisture, and CEC influence metal solubility and retention (Alloway, 2013; Kabata-Pendias, 2011).

## Sunflower as a Phytoremediation Crop

The principal advantages of sunflower are its capacity for high biomass production and its rapid growth. Rizwan et al. (2016) show that the outcomes of sunflower phytomanagement vary considerably with cultivar, soil, and metal. Therefore, cultivar selection is an important stage of a pilot experiment. For quantitative assessment of phytoremediation performance, calculation of BCF and TF is recommended. BCF can be defined as the ratio between the concentration of an element in plant tissue and its corresponding concentration in soil. TF describes the translocation of an element from roots to aboveground plant parts. High BCF and TF values may indicate phytoextraction potential; however, final assessment should be based on biomass production and the actual mass of the element removed.

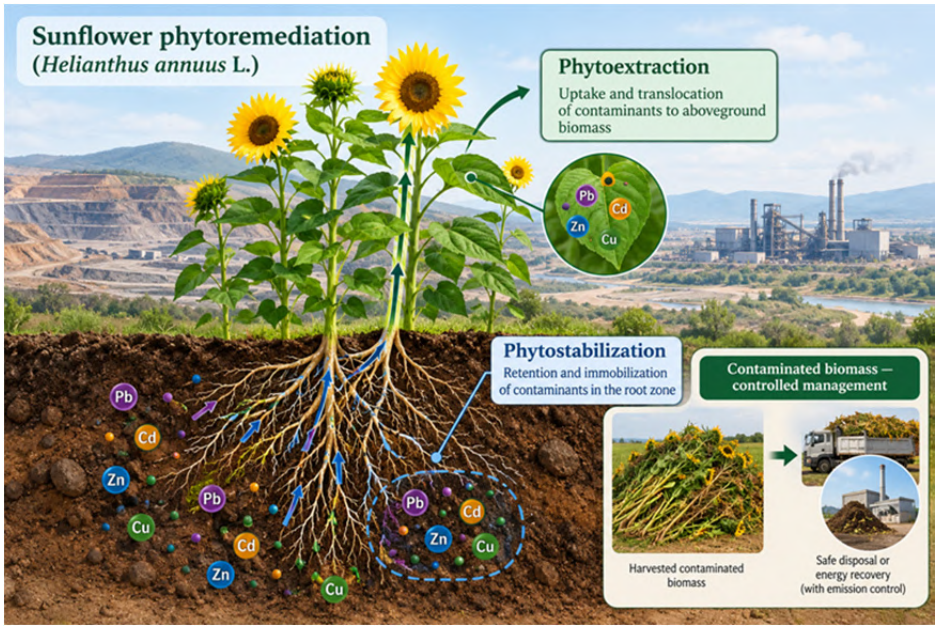



**Fig. 1.** Conceptual scheme of sunflower use for phytoremediation of contaminated soil.

Studies confirm the potential use of sunflower in soils contaminated with Pb, Cu, Zn, Cd, and other elements. Additional approaches, including biodegradable chelating agents and plant-growth-promoting bacteria, have also been investigated (Chen et al., 2020; Mohammadzadeh et al., 2017). However, chelating agents may increase contaminant mobility; therefore, their application should be carefully controlled.

## Context of Mining-Industrial Soils in Georgia

In the Kazreti–Bolnisi zone, accumulation of PTEs associated with mining activities is related to ore extraction and processing. Gventsadze et al. (2024) investigated the distribution of Fe, Cu, Mn, Ni, Zn, Cd, and Pb in soils of Kvemo Kartli and examined land-use characteristics. High values of Cd, Zn, Mn, and Ni were recorded in specific Kazreti samples. For example, in one sample Cd was approximately 298.5 mg/kg, Mn approximately 1159 mg/kg, and Ni approximately 140 mg/kg; in another sample, Mn reached approximately 1743 mg/kg. These are data from specific samples and should not be interpreted as regional mean values. In the Rustavi industrial area, important contamination sources include industrial emissions, dust, and historically accumulated waste. High values of Pb and Fe have also been identified in the Gardabani area. Under such conditions, sunflower may be considered an additional risk-management tool; however, preliminary zoning is essential. In the Chiatura and Zestafoni areas, assessment of Mn, Zn, Pb, Ni, and other elements is important. The use of sunflower in these regions should be tested separately under experimental conditions [10-15].

## International Experience and Comparative Analysis

Nehnevajova et al. (2005), through screening of different sunflower cultivars, demonstrated that metal-extraction capacity varies among genotypes. Mench et al. (2018) investigated phytomanagement of Cu-contaminated soils using high-yielding crops. Liduino et al. (2018) examined the use of sunflower, assisted

by biosurfactants, for remediation of multi-contaminated industrial soil. Dhiman et al. (2017) focused on metal accumulation and subsequent use of sunflower biomass. Biomass safety is particularly important. Sunflower seeds, oil, meal, or other products obtained from plants grown on contaminated soil should not automatically be considered suitable for food or feed use. Zehra et al. (2020) specifically addressed seed and oil safety in relation to sunflower grown on Pb-contaminated soils. In a pilot study, contaminated biomass should be treated as potentially contaminated non-food material until laboratory analysis and applicable requirements confirm its safety. The modern approach increasingly considers phytoremediation as phytomanagement, whose objective is not always complete contaminant removal, but rather risk reduction, erosion control, management of bioavailability, and preparation of land for safe use.

## Proposed Pilot Methodological Framework for Georgia

The first stage should include GIS-based zoning, integration of historical and current data, and selection of study sites. Initial soil samples should be collected according to a standardized scheme, preferably from the 0–30 or 0–40 cm layer, with geographic coordinates recorded. At the second stage, pH, humus/organic matter, texture, moisture, and CEC should be determined for each site. In parallel, the contaminant profile of the specific area should be established. At the third stage, a controlled field or micro-field experiment should be established with control and contaminated treatments. Comparison of several cultivars is recommended. Roots, stems, leaves, and seeds should be analyzed separately. Heavy metals may be determined using AAS, ICP-OES, or ICP-MS, while radionuclides should be analyzed using appropriate gamma-spectrometric and/or radiochemical methods. BCF and TF should be calculated for each target element. The mass removed by the plant during a season may be estimated using the formula $M = C_{biomass} \times M_{dry\ biomass}$. Repeated soil analysis at the end of the growing season is essential. A separate protocol is required for biomass management. In cases of high contaminant concentrations, biomass should not enter the food or feed chain, and its subsequent management should be determined according to the type of contaminant.

## Discussion

The main advantage of using sunflower in Georgia's mining-industrial soils is the possibility of studying soil chemical status, plant physiological response, element translocation, and GIS-based changes within an integrated system.

In the Kazreti–Bolnisi area, the phytoextraction potential for Cd, Zn, Cu, Pb, and Ni should be investigated as a priority. In Rustavi, a combined approach is appropriate, in which phytostabilization and phytoextraction are considered together. In Chiatura and Zestafoni, particular attention should be given to Mn and associated elements. A high total concentration does not automatically mean high plant uptake. Therefore, total soil chemical analysis should be complemented by assessment of bioavailable fractions and plant-tissue concentrations. High BCF or TF values alone are also insufficient to demonstrate practical remediation; the total biomass produced and the total mass of the element removed must be calculated.Thus, in the Georgian context, sunflower should more appropriately be considered a high-biomass phytomanagement crop that can be used to reduce contamination risk, protect the soil surface, and achieve partial extraction of certain elements [16].

## Conclusions

The high biomass production of sunflower and its capacity to accumulate different PTEs make it a promising candidate for phytomanagement of mining-industrial soils in Georgia. International literature confirms that outcomes depend on cultivar, contaminant, soil properties, and agronomic condi

Under Georgian conditions, gradual investigation of contaminated sites in Kazreti–Bolnisi, Rustavi, Chiatura, and Zestafoni is particularly relevant. Research should be based on GIS zoning, a standardized sampling scheme, determination of key soil properties, separate analysis of plant organs, and calculation of BCF/TF. The present paper does not report the results of a completed field phytoremediation experiment. Rather, it provides a basis for a pilot study through which the actual effectiveness of sunflower can be established for a specific cultivar, site, and contaminant. Plant biomass obtained from contaminated soil should be regarded as potentially contaminated material, and its use as food or animal feed should be decided only on the basis of an appropriate safety assessment.

## Research and Work

Further research requires comparative screening of several cultivars, assessment of plant growth and element accumulation at different contamination levels, comparison of roots and aboveground organs, and multi-season monitoring. Determination of bioavailable PTE fractions and their relationships with pH, organic matter, texture, and CEC is particularly important. For radionuclides, additional assessment of plant uptake and translocation is required. Future results may be used to develop a decision-support model for phytomanagement of mining-industrial soils in Georgia.

**Table 1.** Proposed phytomanagement directions for mining-industrial areas in Georgia.

| Region | Main PTEs | Potential approach | Priority |
|---|---|---|---|
| Kazreti–Bolnisi | Cu, Zn, Cd, Pb, Ni | Phytoextraction / phytostabilization | High |
| Rustavi | Cd, Zn, Mn, Ni, Pb, Cr | Combined phytomanagement | High |
| Chiatura | Mn and associated elements | Phytostabilization / phytoextraction research | High |
| Zestafoni | Mn, Zn, Pb, Ni | Research on phytoextraction and stabilization | High |

## References


1. Khan H., & Sajad M. A., Phytoremediation of heavy metals – Concepts and applications. // Chemosphere, 91(7), 2013, pp. 869–881. https://doi.org/10.1016/j.chemosphere.2013.01.075
2. Alloway B. J., Heavy Metals in Soils: Trace Metals and Metalloids in Soils and their Bioavailability (3rd ed.). // Springer, 2013.
3. Chen Y., Yang L., & Wang Q., Phytoremediation of uranium and cadmium contaminated soils by sunflower enhanced with biodegradable chelating agents. // Journal of Cleaner Production, 2020. https://doi.org/10.1016/j.jclepro.2020.121491
4. Dhiman S., et al., Metal accumulation by sunflower and efficacy of biomass in enzymatic saccharification. // PLOS ONE, 12(4), 2017, e0175845. https://doi.org/10.1371/journal.pone.0175845
5. Gventsadze G., Ghambashidze G., Chankseliani Z., Sarjveladze I., & Blum W. E. H., Impacts of Crop-Specific Agricultural Practices on the Accumulation of Heavy Metals in Soil in Kvemo Kartli Region (Georgia). // A Preliminary Assessment. Sustainability, 16(10), 2024, 4244 p. https://doi.org/10.3390/su16104244
6. IAEA, Handbook of Parameter Values for the Prediction of Radionuclide Transfer in Terrestrial and Freshwater Environments. // Technical Reports Series No. 472, 2010.
7. Kabata-Pendias A., Trace Elements in Soils and Plants (4th ed.). // CRC Press, 2011.
8. Liduino V. S., et al., Biosurfactant-assisted phytoremediation of multi-contaminated industrial soil using sunflower. // Journal of Environmental Science and Health, Part A, 53(7), 2018 pp. 609–616. https://doi.org/10.1080/10934529.2018.1429726
9. Mench M., et al., Phytomanagement and remediation of Cu-contaminated soils by high yielding crops at a former wood preservation site: Sunflower biomass and ionome. // Frontiers in Ecology and Evolution, 6, 123, 2018. https://doi.org/10.3389/fevo.2018.00123
10. Matiashvili S., Chankseliani Z., & Mepharidze E. Comparison of radionuclides and heavy metals distribution in Georgian soils. // Journal of the Georgian Geophysical Society, 25(1), 2022, pp. 95–102.
11. Matiashvili S., Matchavariani L., Chankcseliani Z., Khvedelidze I., & Makalatia I., Risk of soil and water contamination by industrial toxic waste in the Kazreti and Zestafoni regions of Georgia. Reliability: Theory & Applications, 20(Special Issue 9(87)), 2025, pp. 594–602. https://doi.org/10.24412/1932-2321-2025-987-594-602
12. Matiashvili S., Matchavariani L., & Chankcseliani Z., Radioecological monitoring of soils in Kvemo Kartli, Georgia. // Proceedings of the 25th International Multidisciplinary Scientific GeoConference SGEM 2025, 25(3.1), 2025, pp. 351–360. https://doi.org/10.5593/sgem2025/3.1/s12.41
13. MohammadzadehA., et al. Effects of plant growth-promoting bacteria on the phytoremediation of cadmium-contaminated soil by sunflower. // Archives of Agronomy and Soil Science, 63(6), 2017, pp. 807–816. https://doi.org/10.1080/03650340.2016.1235781
14. Nehnevajova E., et al., Screening of sunflower cultivars for metal phytoextraction in a contaminated field prior to mutagenesis. // International Journal of Phytoremediation, 7(4), 2005, pp. 337–349. https://doi.org/10.1080/16226510500327210
15. Rizwan M., Ali S., Rizvi H., Rinklebe J., Tsang D. C. W., Meers E., Ok Y. S., & Ishaque W., Phytomanagement of heavy metals in contaminated soils using sunflower: A review. // Critical Reviews in Environmental Science and Technology, 46(18), 2016, pp.1498–1528. https://doi.org/10.1080/10643389.2016.1248199
16. From Phytoremediation to Safe Land Reuse: A PRISMA-ScR Review and Decision-Support Framework for Non-Food Crops on Metal-Contaminated Mining Soils. // Agronomy, 16(14), 2026, 1346 p.

2nd International Scientific Conference "Modern Problems in Geophysics", Proceedings,
ISBN 978-9941-36-562-1, ISSN 3088-4349, Tbilisi, Georgia, October 29-31, 2026

# APPROBATION OF AN AUTOMATED METHOD FOR HAIL FORECASTING BASED ON THE OUTPUT PRODUCT OF THE GFS NCEP MODEL

**Sozaeva L., Kagermazov A.**

*High-Mountain Geophysical Institute, Nalchik, Kabardino-Balkaria, Russian Federation*
*ljk_62@rambler.ru*

***Abstract.*** *This paper presents a scheme for forecasting hail using data from the GFS NCEP global model with a 30-hour lead time, which was approved and tested within the area of responsibility of the North Caucasian Paramilitary Service. In the course of this study, it was found that the overall forecast accuracy is 87.2%, the detection rate for the presence of the phenomenon is 76.5%, the accuracy of the forecast for the presence of the phenomenon is 81.3%, the accuracy for the absence of the phenomenon is 89.6%, and the detection rate for the absence of the phenomenon is 92.0%. The high forecast quality criteria allowed concluding that the proposed approach can be introduced into the operational practice of hail suppression services.*

***Key words:*** *Global atmospheric model, hail forecast, atmospheric parameters, aerological sounding of the atmosphere.*

## Introduction

Short-range forecasting of hazardous convective processes, particularly hail, represents one of the most labor-intensive and critically important tasks in modern meteorology. Despite the continuous improvement of numerical weather prediction (NWP) methods, operational assessment of hail probability is still predominantly based on physico-statistical algorithms analyzing the thermohydrodynamic state of air masses.

Traditional calculation methods, including algorithms from the Hydrometeorological Research Center of Russia (www.method.meteorf.ru), are characterized by high computational complexity, which significantly hinders their operational implementation into the daily practice of regional paramilitary services for active influence on meteorological processes. An additional destabilizing factor is the heavy dependence of traditional approaches on atmospheric radiosonde data. The current aerological network in many regions is characterized by insufficient spatial density, and standard balloon launch times often do not coincide with periods of maximum development of convective activity.

To minimize the subjective factor in decision-making, specialists from the High-Mountain Geophysical Institute have been actively developing automated forecasting methods based on global hydrodynamic models in recent years. The representativeness and high promise of the output data from the GFS NCEP global atmospheric model (www.emc.ncep.noaa.gov) for prognostic purposes has been confirmed by its high degree of correlation with the results of direct aerological sounding in the North Caucasus region [3, 4].

This is fully consistent with global practice, where global model predictors are successfully applied to compensate for the shortage of local aerological sounding data [5, 6].

The main objective of this study is the approbation of a hail forecasting technique based on data from a global atmospheric model within the area of responsibility of the North Caucasian Paramilitary Service. To achieve this, the following tasks were solved:

- calculation of atmospheric parameters based on model data and subsequent hail forecasting;
- comparison of prognostic data with actual observations;
- evaluation of forecast quality using various criteria.

## Materials and Methods of Research

Approbation of the developed prognostic methodology was carried out during the hail-hazardous season of 2023 in the territories of the Republic of Kabardino-Balkaria, North Ossetia–Alania, and Karachay-

Cherkessia. The total sample size consisted of 109 synoptic situations, in 34 of which the fall of hail was recorded based on actual observations of the North Caucasian Paramilitary Service for Active Influence on Meteorological Processes.

To compensate for the shortage of direct aerological sounding data, the prognostic output of the GFS NCEP global atmospheric model was used (gridded fields of air temperature, dew point temperature, as well as wind speed and direction). Model profiles were extracted for geographic coordinates corresponding to the geometric center of the studied region (43°40′ N, 44°05′ E).

## Research Results and Discussion

The calculation of thermodynamic predictors of convection and subsequent automated hail forecasting are implemented within a single computational algorithm functioning in several stages (Fig. 1).

At the first stage, a set of specialized physical parameters (Atmosphere Parameters) is calculated from the input high-altitude profiles of the atmospheric model: atmospheric instability indices (George's index and Miller's total index); moisture content of the air mass (total specific humidity in the layer from the earth's surface to a height of 5 km, as well as the average moisture deficit in the five-kilometer layer above the convection level); altitude and temperature characteristics (convection level and temperature at its boundary, maximum cloud overheating level relative to the environment); dynamic and energetic indicators (energy characteristic of the sub-cloud layer and the velocity of updrafts in the developing cloud).

At the forecasting stage, the calculated parameters are transferred to the alternative hail damage probability assessment block (Hail Forecast), which combines a group of independent physical-statistical approaches:

1. **The authors' prognostic model based on discriminant analysis (Discriminant Function)** – an alternative classification of atmospheric states using a linear discriminant function developed by the authors, which takes into account a combination of the obtained instability, moisture content, and kinetic energy indices [1].
2. **Reshetov's method** – assessment of hail probability taking into account the predicted height of the upper boundary of the convective cloud and its corresponding temperature (www.method.meteorf.ru).
3. **Glushkova's Method** – forecasting based on a joint analysis of the calculated maximum updraft velocity and the height of the zero-isotherm level (www.method.meteorf.ru).

The final prognostic decision is formed according to the "majority voting" principle: the hail forecast is considered positive if at least two of the three methods used indicate a high probability of the phenomenon developing.

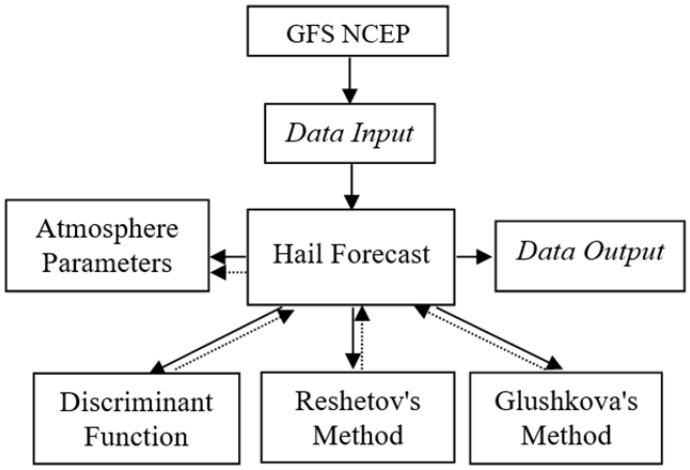



**Fig. 1.** Block diagram of the hail forecasting algorithm.

To verify the proposed approach, the modeling results were compared with actual ground observation data from the paramilitary service, and a complex of quality criteria was calculated based on «forecast» – «fact» contingency tables.

- Overall forecast accuracy (87.2%): A high result for a 30-hour lead time, confirming that the vast majority of issued forecasts (both for the presence and absence of the phenomenon) proved correct.
- Detection rate of the presence of the phenomenon (76.5%): The model successfully captured 76.5% of actual hail cases, which minimizes dangerous missed alerts for the hazardous event.
- Accuracy of the forecast for the presence of the phenomenon (81.3%): A high accuracy index. The false alarm rate was only 18.7%, minimizing unjustified economic costs for the hail suppression service.
- Accuracy for the absence of the phenomenon (89.6%): Demonstrates the high reliability of negative forecasts: when the absence of hail is predicted, the model turns out to be right in almost 90% of situations.
- Detection rate of the absence of the phenomenon (92.0%): Confirms the algorithm's capability to effectively differentiate between hail-hazardous situations and stable atmospheric states.

The model is perfectly balanced – it does not overestimate the number of false alarms while efficiently identifying the conditions for actual hail formation with a 30-hour lead time. The obtained result exceeds similar forecast performance metrics based on actual aerological sounding data (76.5% and 68.0%, respectively) [2].

## Conclusion

The developed hail forecasting method with a 30-hour lead time possesses high prognostic value and practical efficiency: it successfully identifies most cases of hazardous phenomenon initiation while keeping the number of false alarms at a minimal level. High reliability in confirming both the presence and absence of hail allows minimizing economic risks, eliminating expenditures on unjustified false deployments, and effectively utilizing this algorithm in the operations of hail suppression services and the agricultural sector.

## References


1. Kagermazov A. Kh., Digital atmosphere. Modern methods and methodology for the study of dangerous meteorological processes and phenomena. Nalchik: Pechatny Dvor, 2015, 215 p. (In Russian)
2. Kagermazov A. Kh. & Sirotenko L. A., Results of approbation of software modules for calculating meteorological parameters and computer forecasting of hail based on aerological sounding data in the North Caucasus. // Izvestiya Vuzov. Severo-Kavkazskii Region. Natural Sciences. Atmospheric Physics, (Special Issue), 2010, pp. 49–53. (In Russian)
3. Kagermazov A. Kh. & Sozaeva L. T., Validation of global atmospheric model output data against aerological sounding data with increasing lead time. // Science. Innovations. Technologies, (4), 2020, pp. 137–148. (In Russian)
4. Kagermazov A. Kh. & Sozaeva L. T., Hail forecast with a lead time of up to three days based on the output data of a global atmospheric model. // Proceedings of the Main Geophysical Observatory [Trudy GGO], (598), 2020, pp. 204–214. (In Russian)
5. Adams-Selin R. D. & Ziegler C. L., Forecasting hail using a one-dimensional hail growth model within WRF. // Monthly Weather Review, 144(12), 2016, pp. 4919–4939.
6. Giaiotti D. B. & Stel F., The difficulty of forecasting hail: aerological networks vs. remote sensing. // Atmospheric Research, 203, 2018, pp. 88–99.

2nd International Scientific Conference "Modern Problems in Geophysics", Proceedings,
ISBN 978-9941-36-562-1, ISSN 3088-4349, Tbilisi, Georgia, October 29-31, 2026

# MODELING OF C-BAND RADAR BACKSCATTERING CHARACTERISTICS BY DEFORMABLE DROPLETS IN STRONG ELECTRIC FIELDS

**Sozaeva L.**

*High-Mountain Geophysical Institute, Nalchik, Kabardino-Balkaria, Russian Federation*
*ljk_62@rambler.ru*

***Abstract.*** *A method for calculating backscattering cross-sections for droplets growing in an electromagnetic field has been developed based on the separation of variables method (SVM). The calculations account for particle deformation both under the influence of a horizontal electric field and in its absence at* $\lambda = 5.5\ cm$. *It was found that the increase in droplet asphericity in strong fields causes a critical deviation of backscattering values from the classical spherical model. A growing discrepancy between the horizontally* $(TE)$ *and vertically* $(TM)$ *polarized signal components was revealed, reaching its maximum at the pre-breakup stage of the droplet. The results are applicable for upgrading the algorithms of DMRL – C weather radars.*

***Key words:*** *Backscattering, droplet deformation, thunderstorms, electric field, separation of variables method, DMRL – C.*

## Introduction

The development of modern methods for radar sounding of cumulonimbus clouds requires accounting for the electrical activity of the environment, which significantly affects the geometry of hydrometeors. In highly electrified convective environments, the localized electrostatic forces can equal or even exceed aerodynamic drag, radically altering the microphysical properties of precipitation. This is essential for the correct interpretation of dual-polarization weather radar signals, as standard hydrometeor classification and quantitative precipitation estimation (QPE) algorithms traditionally assume purely aerodynamic equilibrium shapes. The evolution and growth of large droplets in an electromagnetic field are accompanied by severe deformation, the detailed theoretical analysis of which is challenging due to the highly non-linear nature of fluid dynamics coupled with strong electrohydrodynamic interactions.

To bridge this gap between theoretical assumptions and complex physical realities, laboratory experiments provide irreplaceable empirical insights. Unique data from high-resolution photographic registration of droplets in vertical wind tunnels under specified field characteristics allow for an accurate estimation of their size, shape, and orientation. These experimental setups recreate the terminal velocity conditions and intense electric fields typical of mature convective cells. Within this microphysical cycle, the most critical stage is the deformation of the droplet immediately prior to final breakup, when its geometric dimensions peak far beyond the values observed in the absence of a field, making a defining contribution to the total reflectivity of the cloud volume. During this pre-rupture phase, extreme horizontal stretching introduces a severe polarimetric bias that can disrupt automated operational radar systems.

The objective of this work is to quantitatively evaluate the impact of a strong horizontal electric field on the polarimetric scattering properties of large raindrops at the stage of reaching their maximum size before breakup. By utilizing rigorous electromagnetic scattering frameworks on these experimentally captured extreme profiles, this study aims to establish a precise mathematical link between microscale electrohydrodynamic deformations and macroscale dual-polarization radar observables.

## Materials and Calculation Methods

Traditional interpretation of weather radar data relies on the assumption of a strictly spherical particle shape, calculated using the classical Mie algorithm [1]. However, large droplets deform during fall, and the spherical model leads to systemic meteorological errors.

To calculate scattering by aspherical droplets, this study utilizes the rigorous separation of variables method ($SVM$) on a spheroidal basis, the algorithmic foundations of which were established in foundational works [2]. The use of a spheroidal coordinate system ensures high stability under conditions of strong shape anisotropy [3]. The origin of the coordinate system coincides with the center of the spheroid; the major semi-axis is denoted by $a$, and the minor semi-axis by $b$. An incident plane wave at an angle $\alpha$ is represented as a superposition of a vertically polarized wave ($TM - mode$) and a horizontally polarized wave ($TE - mode$). The backscattering cross-sections $\sigma\_TM(\alpha)$ and $\sigma\_TE(\alpha)$ are computed via expansion coefficients in terms of prolate or oblate spheroidal functions without loss of computational convergence.

In the absence of an external electric field, the droplet shape is approximated as an oblate spheroid, where the axis ratio as a function of the equivalent diameter $D_e$ (in cm) is given by the well-known Edsager empirical expression [4]:

$$\frac{a}{b} = 1.0048 + 0.0057D_e \ - 2.628D_e^2 + 3.682D_e^3 - 1.677D_e^4.$$

## Calculation Results and Discussion

Numerical calculations were performed for a wavelength of $\lambda = 5.5\ cm$ ($C$-band $DMRL - C$) at a temperature of $10\ °C$, typical for the lower part of a convective cloud where large liquid hydrometeors are concentrated.

In the absence of an electric field, droplets with a radius of $r < 0.12$ cm lie within the Rayleigh region, where the influence of shape is negligible. At $r > 0.12$ cm, anisotropy manifests: cross-sections for horizontal polarization ($TE$-mode) monotonically exceed the values for equivalent spheres, while the vertical component ($TM$-mode) shifts into the region of lower values.

In thunderstorm clouds, droplets deform under the action of a strong horizontal electric field with an intensity of $E = 500\ kV/m$, experiencing extreme stretching along the field lines in the horizontal plane, as recorded experimentally in wind tunnels [5]. Based on photographic registration data, a geometric approximation of the semi-axes $a$ and $b$ (halves of the total linear dimensions of the deformed particle) was carried out. The calculation results for normalized backscattering cross-sections (in $dB$) are presented in Table 1.

**Table 1.** Normalized droplet backscattering cross-sections under deformation in a horizontal electric field ($E = 500\ kV/m$).

| Equivalent radius $r\_v$, mm | Major semi-axis $a$, mm | Minor semi-axis $b$, mm | Shape factor, $a/b$ | Spheroid, $TM$ (vert.), dB | Spheroid, $TE$ (horiz.), dB | Sphere (classical), dB |
|---|---|---|---|---|---|---|
| **Moderate deformation** | | | | | | |
| **3.30** | 7.49 | 2.20 | 3.41 | -20.82 | -1.37 | -7.39 |
| **3.50** | 7.90 | 2.34 | 3.38 | -19.58 | -0.50 | -6.04 |
| **3.63** | 8.54 | 2.37 | 3.61 | -19.30 | 0.27 | -5.40 |
| **Maximum deformation** | | | | | | |
| **3.30** | 8.85 | 2.02 | 4.38 | -21.46 | 0.06 | -7.39 |
| **3.50** | 9.53 | 2.13 | 4.48 | -20.96 | 1.08 | -6.04 |
| **3.63** | 10.04 | 2.18 | 4.60 | -20.68 | 1.63 | -5.40 |
| **Extreme deformation** | | | | | | |
| **3.50** | 14.50 | 1.72 | 8.43 | -21.70 | 4.81 | -6.04 |
| **3.63** | 21.00 | 1.51 | 13.95 | -22.50 | 7.68 | -5.40 |

To validate the developed methodology, the obtained relationships were compared with independent meteorological studies of single scattering by large droplets in the C-band [6]. The nature of the divergence of the $TE$ and $TM$ mode curves relative to the sphere demonstrates full qualitative and quantitative agreement with reference profiles. The high computational stability of the SVM algorithm under extreme asphericity (shape factor $a/b = 13.95$) confirms the rigor of the spheroidal basis of the St. Petersburg scientific

school [2], which completely eliminates the loss of convergence characteristic of standard T-matrix methods during critical particle deformations.

Analysis of Table 1 shows that as droplet deformation increases up to the pre-breakup stage, when its horizontal semi-axis reaches extreme values of 14.5 and 21.0 mm, the difference between horizontal and vertical polarizations reaches a maximum (about 30 dB). Under natural conditions without a field, the existence of liquid particles of such dimensions is impossible. In thunderstorm clouds, the appearance of such extremely elongated droplets can drastically overestimate the measured differential reflectivity ($Z\_DR$), leading to severe errors in automated precipitation intensity retrieval using standard spherical algorithms [6].

## Conclusion

In the course of this work, the following main objectives were achieved and key results were obtained:

Mathematical modeling was performed for the processes of electromagnetic wave scattering in the C-band by highly elongated liquid spheroidal hydrometeors under thunderstorm cloud conditions.

The high efficiency and stability of the Separation of Variables Method ($SVM$) algorithm was proven, maintaining strict convergence under an extreme particle shape factor ($a/b \approx 14$), which surpasses the capabilities of the standard $T$-matrix method.

A physical effect was revealed involving an ultra-high polarization contrast (up to 30 dB) between the $TE$ and $TM$ modes during pre-breakup droplet deformations induced by an electric field of $E = 500\ kV/m$.

The scientific novelty of the work lies in the quantitative description of the anisotropy of radar characteristics for critically deformed droplets using a rigorous spheroidal basis, as well as in the physical justification of the nature of anomalous jumps in differential reflectivity ($Z\_DR$) within thunderstorm cells.

The practical significance of the results consists in the possibility of integrating the obtained correction factors into the current software of modern dual-polarization meteorological radars (in particular, *DMRL – C*). This will significantly increase the accuracy of measuring heavy rainfall intensity and improve the quality of automated detection of severe weather hazards.

Prospects for further research are related to expanding the developed approach to multi-particle ensembles with a specified droplet size distribution.

## References


1. Mie G., Beiträge zur Optik trüber Medien, speziell kolloidaler Metallösungen. // Annalen der Physik, vol. 330, no. 3, 1908, pp. 377–445. https://doi.org/10.1002/andp.19083300302
2. Voshchinnikov N., Farafonov V., Optical properties of spheroidal particles. // Astrophysics and Space Science, vol. 204, no. 2, 1993, pp. 19–86. https://doi.org/10.1007/BF00658095
3. Farafonov V., Il'in V., Prokopjeva M., On the Spheroidal Model of Light Scattering by Nonspherical Particles. // Optics and Spectroscopy, vol. 126, no. 4, 2019, pp. 443–449. (in Russian)
4. Andsager K., Beard K., Laird N., Laboratory measurements of axis ratios for large raindrops. // J. Atmos. Sci., vol. 56, 1999, pp. 2673–2683. https://doi.org/10.1175/1520-0469(1999)056<2673:LMOARF>2.0.CO;2
5. Bhalwankar R., Deshpande C., Kamra A., Breakup modes of the drops suspended in a vertical wind tunnel in presence of the horizontal electric field. // Journal of Geophysical Research: Atmospheres, vol. 121, no. 4, 2016, pp. 1838–1849.
6. Thurai M., Bringi V., et al., Drop Shapes, Model Comparisons, and Calculations of Single Scattering Properties at C- and X-Band. // Journal of Atmospheric and Oceanic Technology, vol. 24, no. 6, 2007, pp. 1019-1032.

2nd International Scientific Conference "Modern Problems in Geophysics", Proceedings,
ISBN 978-9941-36-562-1, ISSN 3088-4349, Tbilisi, Georgia, October 29-31, 2026

# WIND FIELD VARIABILITY FOR SELECTED LOCATIONS OF GEORGIA

***,***Tatishvili M., *Kapanadze N., *,****Megrelidze L., *,***Palavandishvili A., *Mkurnalidze I.**

**Institute of Hydrometeorology of Georgian technical University, Tbilisi, Georgia*
** *Vakhushti Bagrationi Institute of Geography of Ivane Javakhishvili Tbilisi State University, Tbilisi, Georgia*
**** National Environmental Agency, Tbilisi, Georgia*
*m.tatishvili@gtu.ge*

***Abstract.*** *Wind is one of the important components of atmospheric circulation. Wind changes are related to both large-scale circulation processes and local physical and geographical conditions. The study of strong winds is especially important, as they have a negative impact on the country's infrastructure, agriculture, transport systems, energy facilities, and population safety. To assess the multi-year variability of strong wind days, observation data from four meteorological stations in Eastern Georgia – Tbilisi, Bolnisi, Akhaltsikhe, and Mta-Sabuti – received from the Georgian National Environment Agency were used. All data were analyzed using a statistical approach.*

***Key words****: Wind field, Climate change, Observation Data.*

## Introduction

Wind is one of the important components of atmospheric circulation. Wind changes are related to both large-scale circulation processes and local physical and geographical conditions. The study of strong winds is especially important, as they have a negative impact on the country's infrastructure, agriculture, transport systems, energy facilities, and population safety. According to the National Environmental Agency, in 1995-2010, according to data recorded at the weather station, 20 people died in Georgia due to strong winds, and the damage reached 99 million GEL [1]. The most severe consequences were caused by strong winds in March 2018, and in December 2023, the disaster raged throughout the country. Therefore, the study of strong wind problems is very relevant, to which many works have been devoted in Georgia [2-5]. The aim of the study is to assess the recurrence and multi-year variability of strong winds in the territory of Eastern Georgia during the period 1970-2025, both in annual and seasonal terms.

## Data and Methods

To assess the multi-year variability of strong wind days, observation data from four meteorological stations in Eastern Georgia – Tbilisi, Bolnisi, Akhaltsikhe, and Mta-Sabueti – received from the Georgian National Environment Agency were used. The number of days when the wind speed reached or exceeded 15 m/s ($V \geq 15$ m/s) was selected as the research criterion. To assess the multi-year variability of strong wind days, the observation period 1970–2025 was divided into two equal, 28-year intervals: the first 1970–1997, the second – 1998–2025. Such a division allows comparing time periods of equal duration and assessing the change in the number of strong wind days both in annual and seasonal terms.

## Discussion

To assess the multi-year change in strong wind days, time series of annual values were used, based on which the annual distribution of days with $V \geq 15$ m/s winds recorded at selected stations was constructed for the period 1970-2025 (Fig. 1). The multi-year average values of strong winds at the mentioned stations, maximum and minimum annual quantities and their corresponding years were also determined (Table 1).

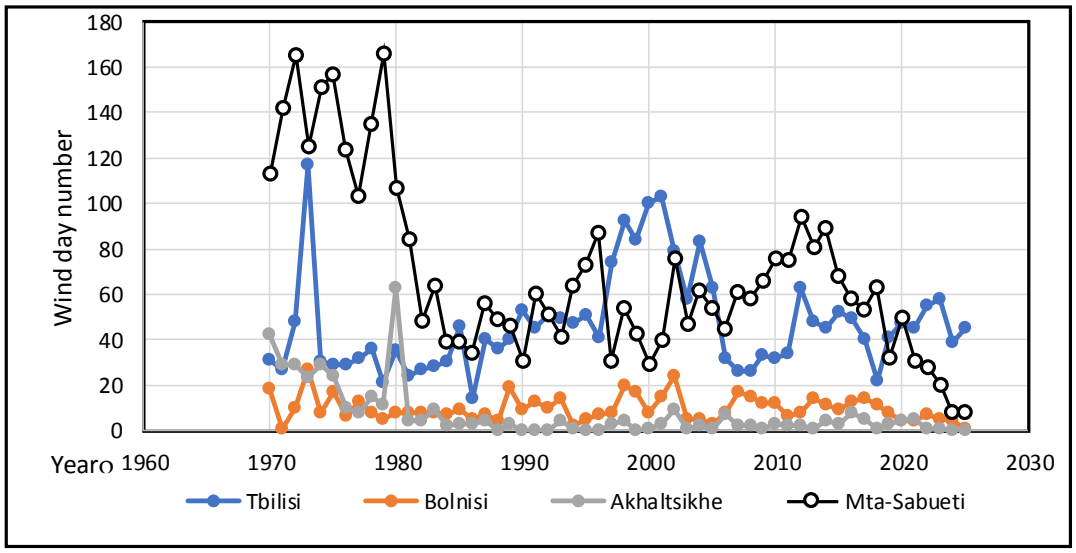



**Fig.1.** Annual distribution of days with wind speed V≥15m/s at selected meteorological stations in Eastern Georgia (Tbilisi, Bolnisi, Akhaltsikhe, Mta-Sabueti) during the period 1970-2025.

As it is evident from Fig. 1, the recurrence of strong wind days and their multi-year variability are not uniform in space and time. The number of strong wind days at the four selected meteorological stations is characterized by alternating periods of both relatively high and low values from year to year. The highest value of windy days – 3854 days – during the 56-year period under consideration was recorded in Mta-Sabuti, followed by Tbilisi with 2625 days, Bolnisi – 544 and finally Akhaltsikhe, with 369 days (Table 1).

**Table 1.** Statistical characteristics of strong winds in the period 1970-2025.

| Station | Elev.(m) | Day number in 1970-2025period | Annual av, number | Min | Max |
|---|---|---|---|---|---|
| Tbilisi | 403 | 2625 | 46.9 | 14 (1986 ) | 117 (1973 ). |
| Bolnisi | 534 | 544 | 9.7 | 1 (1971 ). | 27 (1973) |
| Akhaltsikhe | 982 | 399 | 7.1 | 0 (1990-1993) | 63 (1980) |
| Mta-Sabueti | 1250 | 3854 | 68.8 | 8 (2024-25.) | 166 (1979) |

Differences in the frequency of strong wind days and the characteristics of the annual course of the wind may be related to the relief location of the stations, altitude, orientation of valleys and ridges, and local aerodynamic conditions [ 5,6,7]. Thus, when assessing the change in the regime of strong winds, it is necessary to consider geographical conditions in addition to regional or large-scale atmospheric circulation factors.

To assess the multi-year variability of strong wind days at the study stations, the entire period was divided into two equal periods (1970- 1997 and 1998- 2025), and for each period, both annual and seasonal distributions were studied (Table 2).

**Table 2.** Annual and seasonal changes in windy days with a speed of V≥15m/s at Tbilisi, Bolnisi, Akhaltsikhe and Mta-Sabueti meteorological stations by periods.

| **Station** | Period | Spring | Summer | Fall | Winter | Day (%) |
|---|---|---|---|---|---|---|
| | 1970-1997 | 339 | 280 | 246 | 266 | 1131 |
| Tbilisi | 1998-2025 | 528 | 357 | 265 | 344 | 1494 |
| | Dev | 189 | 75 | 19 | 78 | +363 (32.2) |
| | 1970-1997 | 95 | 40 | 38 | 91 | 264 |
| Bolnisi | 1998-2025 | 88 | 51 | 46 | 95 | 280 |
| | Dev | -7 | 11 | 8 | 4 | +16 (6.4) |
| | 1970-1997 | 158 | 80 | 48 | 38 | 324 |

| | | | | | | |
|---|---|---|---|---|---|---|
| Akhaltsikhe | 1998-2025 | 33 | 21 | 7 | 16 | -77 (-76,2%) |
| | Dev | -125 | -59 | -41 | -22 | -247 |
| | 1970-1997 | 666 | 535 | 648 | 536 | 2385 |
| Mta-Sabueti | 1998-2025 | 435 | 272 | 399 | 363 | 1469 |
| | Dev | -231 | -263 | -249 | -173 | -916(-(38.4%) |

As it can be seen from Table 2, according to the data of the Tbilisi Meteorological Station, in 1970–1997 the total number of days with wind speed V≥15 m/s was 1131, while in 1998–2025 their number increased to 1494. Accordingly, in the second 28-year period, 363 more days with strong winds were recorded, which corresponds to an increase in the annual average number from approximately 40.4 to 53.4 days, and in percentage terms to 32.2%.

This change manifests itself differently seasonally (Table 2, Fig. 2). The most significant increase was noted in spring: in the first period, 339 strong winds were recorded during this season, and in the second period – 528, i.e. the increase amounted to 189 days. In summer, the number of strong winds increased from 280 to 357 days, and in winter from 266 to 344 days. A relatively small change of only 19 days was noted in the fall.

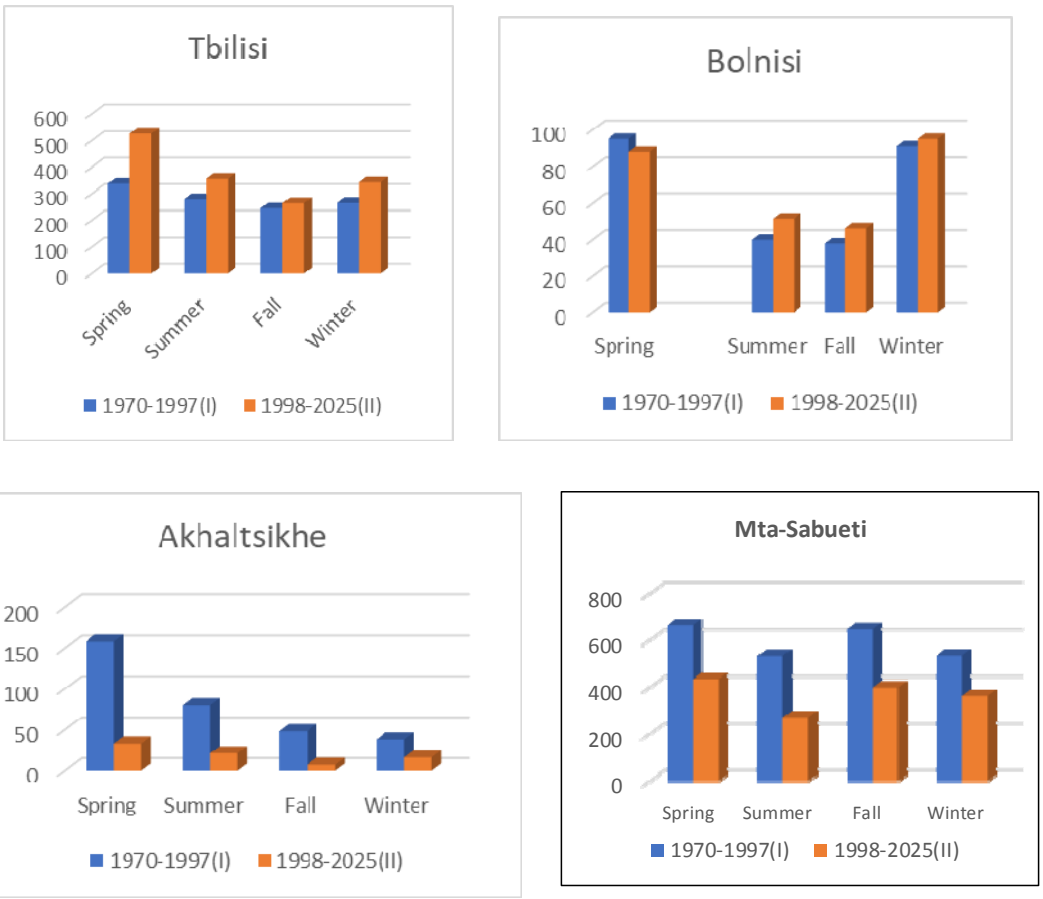



**Fig. 2.** Seasonal distribution of windy days with a speed of V≥15m/s at Tbilisi, Bolnisi, Akhaltsikhe and Mta-Sabueti meteorological stations by periods

At the Bolnisi meteorological station, the increase in the second period was 16 days, and the annual average increased from 9.4 to 10.0 days (6%).

In the case of Bolnisi, the number of days with strong winds in spring decreased from 95 to 88 days, while in summer it increased from 40 to 51 days, in autumn from 38 to 46 days, and in winter from 91 to 95 days.

At the Akhaltsikhe station. In 1970–1997, the average annual number of days with winds V≥15 m/s was 324 days, while in 1998–2025 it is only 77 days. Accordingly, the total average annual number decreased by 247 days, or 76.2%. The average annual change for Mta- Sabueti by periods is as follows: in the first period – 2385 days were recorded, in the second period – 1469, and in the total number of days with strong winds decreased by 916 days, which corresponds to 38.4%.

In Akhaltsikhe, the seasonal maximum of strong winds is maintained in both periods in spring (158 and 33 days), but in the second period, against the background of a sharp decrease in the total number of days with strong winds, the seasonal contrast partially changes. The decrease is especially noticeable in autumn.

In Mta-Sabueti, in 1970–1997, the number of days with strong winds was highest in spring – 666 days, followed by autumn – 648 days, winter – 536 and summer – 535 days, i.e., Mta- Sabueti is characterized by a significant share of strong winds not only in spring, but also in autumn, which sharply distinguishes it from Akhaltsikhe.

## Conclusion

The obtained results show a pronounced spatial heterogeneity of the regime of strong windy days at different stations in Eastern Georgia. An increasing trend was observed in Tbilisi and Bolnisi, while a decreasing trend was observed in Akhaltsikhe and Mta- Sabueti. However, the scale of the change is different between the stations. This difference provides the basis for further analysis of data from other stations and assessment of the sustainability of the identified spatial differences across Eastern Georgia.

**Acknowledgement:** The research was carried out with the financial support of the Shota Rustaveli National Science Foundation of Georgia. Grant # FR 25-16-929.

## References

1. Atlas of Natural Hazards & Risks of Georgia. Prepared by CENN/ITC Tbilisi, Georgia. April, 2012.
2. Beritashvili B., Kapanadze N., Chogovadze I. High easterly winds at the Kolkhida Lowland as an indicator of the impact of Siberian High on the South Caucasus. // Transactions of the Institute of Hydrometeorology of Georgian Technical University, ISSN 1512-0902, Tbilisi, v.116, 2011, pp. 9-12.
3. Kapanadze N., Beritashvili B., Khvedelidze Z., Zotikishvili N. Variability of HighWinds Regime in the R. Mtkvari (Kura) Gorge. // International Scientific Conference „Geography in Global Context: Achievements and Challenges "Proceedings, ISBN 978-9941-9043-2-5 /Kutaisi, Georgia, June 3-4 , 2017, pp. 135-143
4. Marika R., Khvedelidze Z., Samkharadze I., Palavandishili A., Study of Local Wind Field in Georgiaatishvili, // Journals of Georgian Geophysical Society; Physics of Solid Earth, Atmosphere, Ocean and Space Plasma, Vol. 22 No. 1, 2019.
5. Weather, climate and their change regularities for the conditions of GeorgiaL Kartvelishvili, M Tatishvili, A Amiranashvili, L Megrelidze, N Kutaladze. // Monograph, Publishing House "UNIVERSAL", Tbilisi. 2023.
6. Kapanadze N., Khvedelidze Z., Zotikishvili N., The Statistical Distribution of Strong Wind in the Imereti Region and its Role in the Evolution of Ecological Processes. // International Scientific Conference „Modern Problems of Ecology"Proceedings, ISSN 1512-1977, Kutaisi, Georgia, 21-22 September, v., 2018, pp. 139-143.
7. Tatishvili M., Khvedelidze Z., Samkharadze I., & Zotikishvili N., Atmosphere processes and climate parameter variation in the Mtkvari River basin. // In Proceedings of the International Scientific Conference "Natural Disasters in Georgia: Monitoring, Prevention, Mitigation", Tbilisi, 2019, pp. 117–121. http://dspace.gela.org.ge/handle/123456789/8648

2nd International Scientific Conference "Modern Problems in Geophysics", Proceedings,
ISBN 978-9941-36-562-1, ISSN 3088-4349, Tbilisi, Georgia, October 29-31, 2026

# INFORMATIVENESS OF CONVECTIVE CLOUD AND ATMOSPHERIC PARAMETERS IN HAIL FORECASTING BASED ON OPTIMIZED ENSEMBLES OF THE GFS NCEP MODEL

**Zhaboeva M.**

*High-Mountain Geophysical Institute, Nalchik, Kabardino-Balkaria, Russian Federation*
*jaboevam@mail.ru*

***Abstract****. The article investigates the informativeness of convective cloud and atmospheric parameters for hail forecasting based on the GFS NCEP model in the North Caucasus. To address this problem, two ensembles of hail events were compiled, comprising 72 and 32 cases with lead times of 24 and 72 hours, respectively. Based on ROC analysis, a predictor evaluation was performed, which confirmed the synoptic invariance of the total Totals index (Miller), and also revealed a local increase in the predictive value of the temperature difference between the cloud and the ambient air at the minimum forecast lead time.*

***Key words****: Hail, global atmospheric model GFS NCEP, convective parameters, multicollinearity, ROC analysis, area under the curve (AUC).*

## Introduction

At present, there is a trend toward an increase in the number and intensity of hazardous meteorological phenomena, among which hail occupies a special place. The zone of maximum hail hazard in the Russian Federation is traditionally localized in the south of the Krasnodar Krai and in the Kabardino-Balkarian Republic, which is associated with the complex mountainous terrain [1]. Hailstorms cause significant economic damage, which requires forecasting such events with high lead times. Since the frequency of aerological sounding in the region is insufficient, an actual alternative is the use of output products from the global numerical model GFS NCEP, which includes data on the vertical stratification of temperature, humidity, and wind [4]. However, when constructing regional forecasting schemes, the problem of feature space redundancy arises. The inclusion of strongly correlated variables (multicollinearity) leads to biased statistical estimates.

The aim of the study is to optimize the feature space of convective atmospheric parameters and to assess their predictive power based on ROC (Receiver Operating Characteristic) analysis as the forecast lead time changes from 24 to 72 hours.

Statistical analysis was conducted using IBM SPSS Statistics [2, 5].

## Materials and Methods

The research material consisted of observational data on hail processes during the 2005–2019 seasons within a radius of 150–200 km from the «Mineralnye Vody» weather station. The first ensemble ($N_1 = 72\ cases$) includes situations with hail and a GFS NCEP forecast at 24 hours. The second ensemble ($N_2 = 32\ cases$) was compiled for situations with a forecast lead time of 72 hours. For all cases, based on the output of the Global Atmospheric Model (ambient air temperature and dew point, wind speed and direction), 10 atmospheric parameters responsible for the formation of hazardous convective phenomena were calculated [3]:

$DTM$ – maximum temperature difference between the cloud and the ambient air, °C;

$HM$ – the level at which the temperature difference between the cloud and the ambient air is maximum, m;

$DTK$ – vertical temperature gradient in the layer above the condensation level by 4–4.5 km, °C;

$SQZ5$ – total specific humidity in the layer from the surface to 5 km (hereinafter – total specific humidity), g/kg;

$TDSR5$ – mean humidity deficit in the layer above the condensation level by 5 km (hereinafter – mean humidity deficit), °C;

$PH1$ – convection level, hPa;

$TH1$ – temperature at the convection level, °C;

$DJ$ – George's instability index, K;

$TTMI$ – Miller Total Totals index, °C;

$DSS$ – energy characteristic of the sub-cloud layer, J/kg.

At the first stage, the matrix of Pearson pairwise correlation coefficients ($r$) was calculated for the ensemble $N_1 = 72$. Atmospheric parameters with $r \geq 0.75$ were excluded from further analysis. At the second stage, ROC analysis was performed on the combined dataset ($N = 104$). The binary state variable was the forecast lead time ($1 - 24\ h,\ 0 - 72\ h$). The main criterion for informativeness was the area under the ROC curve (AUC − Area Under Curve) [6].

## Results and Discussion

**Optimization of the feature space.** Analysis of the correlation matrix revealed three nodes of multicollinearity at r ≥ 0.73. A linear relationship was established between the parameters $DTM$ and $HM$ ($r = 0.807$), $HM$ and $PH1$ ($r = 0.805$), as well as $TH1$ and $PH1$ ($r = -0.775$), $TH1$ and $TTMI$ ($r = -0.738$). High collinearity was noted between the gradient $DTK$ and the $TTMI$ index ($r = 0.748$). To eliminate redundancy, 3 parameters were completely excluded from the baseline set: $HM$, $DTK$ and $TH1$. The remaining 7 parameters ($DTM$, $SQZ5$, $TDSR5$, $PH1$, $DJ$, $TTMI$, $DSS$) represent independent physical components and serve as an optimal basis for hail forecasting.

**Quantitative assessment of predictor informativeness.** To comparatively evaluate the forecasting efficiency and diagnostic value of the studied parameters ($DTM$, $SQZ5$, $TDSR5$, $PH1$, $DJ$, $TTMI$, $DSS$), ROC analysis was performed. Based on empirical data, areas under the curves ($AUC$) were calculated and statistical significance levels were determined. The results of the ROC analysis for the optimized parameter set are presented in Table 1.

**Table 1.** Results of ROC analysis of atmospheric parameters.

| **Atmospheric parameters** | **AUC** | **Significance ($p$)** |
|---|---|---|
| $DTM$ (Maximum temperature difference), °C | 0.626 | 0.048 |
| $SQZ5$ (Total specific humidity), g/kg | 0.405 | 0.137 |
| $TDSR5$ (Mean humidity deficit), °C | 0.522 | 0.727 |
| $PH1$ (Convection level), hPa | 0.578 | 0.224 |
| $DJ$ (George's instability index), K | 0.616 | 0.070 |
| $TTMI$ (Miller Total Totals index), °C | 0.675 | 0.006 |
| $DSS$ (Energy characteristic of the sub-cloud layer), J/kg | 0.502 | 0.976 |

Based on the calculated areas under the ROC curves, the heterogeneity of the response of the studied parameters was established. It was found that the dynamics of the system state can be described by a limited set of physical variables: of the seven tested indicators, only two ($TTMI$ and $DTM$) demonstrate a stable and statistically significant association with physical changes in the object, standing out against the background fluctuations of the environment.

1. The $TTMI$ parameter (Miller Total Totals index) was identified as the principal physical vector of the dynamics of the studied process, showing the highest discriminatory ability ($AUC = 0.675$, $p = 0.006$). The high statistical significance and the distance of the confidence interval ($0.567 - 0.784$) from the zone of random noise prove that $TTMI$ fluctuations are associated with changes in the physical states of the atmosphere. The Miller Total Totals index is characterized by the highest informativeness and the minimal loss of predictive properties with an increase in the time horizon.

2. The maximum temperature difference between the cloud and the ambient air ($DTM$) was identified as a parameter at the boundary of the statistical significance region ($AUC = 0.626, p = 0.048$). It reflects accompanying or less pronounced trends of the process.

3. An inverted relationship was detected for the parameter $SQZ5$ ($AUC = 0.405, p = 0.137$). The physical meaning of this indicator's value indicates the presence of an inverse relationship: when meteorological conditions characteristic of the conditionally positive comparison group is formed, the numerical values of the $SQZ5$ parameter naturally decrease. This justifies the expediency of changing the sign (mathematical inversion) of this feature to utilize its potential predictive power at the level of $AUC = 0.595$.

4. The group of variables $DJ$, $PH1$, $TDSR5$ and $DSS$ (AUC in the range of $0.502 - 0.616, p > 0.05$ **)** does not have a statistically significant association with the studied changes in the atmospheric state. The dynamics of these parameters are predominantly determined by accompanying background fluctuations of the environment and do not reflect the main physical processes in the system. In this regard, the inclusion of these indicators in the final forecasting model is impractical, as it does not lead to an increase in the accuracy of calculations and may introduce additional uncertainty into the system.

## Conclusion

In this work, the effectiveness of the calculated atmospheric parameters was verified for two comparison groups with lead times of 24 and 72 hours. The obtained data allowed separating the significant signals of the air environment dynamics from the background fluctuations of the meteorological system.

The selective sensitivity of the atmospheric model to a limited number of factors with increasing time horizon was established. The Miller index $TTMI$ ($AUC = 0.675$) was verified as the main stable predictor, possessing a time-stable discriminatory ability. The parameter $DTM$ ($AUC = 0.626$) − the maximum temperature difference between the cloud and the ambient air − was recognized as an auxiliary marker retaining informativeness predominantly at a lead time of 24 hours. The discriminatory ability of the remaining parameters ($DJ$, $PH1$, $TDSR5$, $DSS$, $SQZ5$) was determined to be insufficient or inverted.

## References


1. Abshaev M.T., Abshaev A.M., Malkarova A.Kh., Guidelines for the organization and conduct of hail suppression operations. // Nalchik: Pechatny Dvor, 2014, 500 p. (In Russian)
2. Bühl, A., & Zöfel, P., // SPSS: Art of Information Processing. Statistical Data Analysis and Recovery of Hidden Patterns (V. E. Momot, Ed.). // Moscow: DiaSoftUP, 2005. (In Russian)
3. Kagermazov A.Kh., Digital Atmosphere. Modern methods and methodology for the study of hazardous meteorological processes and phenomena. // Nalchik: Pechatny Dvor, 2015, 215 p. (In Russian)
4. Kagermazov A.Kh., Sozaeva L.T., Hail forecast with a lead time of up to three days based on the output data of the global atmospheric model. // Trudy GGO, No. 598, 2020, pp. 204–214. (In Russian)
5. Nasledov A. D., IBM SPSS Statistics 20 and AMOS: professional statistical data analysis. // St. Petersburg, Piter Publ., 2013, 416 p. (In Russian)
6. Marzban C., The ROC curve and the area under it as performance measures. // Weather and Forecasting, Vol. 19, No. 6, 2004, pp. 1106–1114.

2nd International Scientific Conference "Modern Problems in Geophysics", Proceedings,
ISBN 978-9941-36-562-1, ISSN 3088-4349, Tbilisi, Georgia, October 29-31, 2026

# MULTI-YEAR TEMPORAL AND SPECTRAL ANALYSIS OF GEOMAGNETIC VARIATIONS AT DUSHETI OBSERVATORY

**Kiria T., Nikolaishvili M., Chkhaidze T.**

*Ivane Javakhishvili Tbilisi State University, Mikheil Nodia Institute of Geophysics, Tbilisi, Georgia*
*kiria8@gmail.com, manananikola@gmail.com*

***Abstract.*** *This study analyzes 3,016,664 quality-controlled one-minute X, Y, and Z geomagnetic measurements from Dusheti Observatory for 11 January 2020-26 August 2026. Welch spectra and wavelet analysis resolve 24-, 12-, and 8-hour variations and power near the solar-rotation band. External Kp validation confirms 17 disturbed days among 59 candidates. The strongest complete response occurred during the G5 storm of 10-11 May 2024, when the X daily range exceeded 600 nT.*

***Key words:*** *Dusheti Observatory; geomagnetic variations; Kp index; spectral analysis.*

## Introduction

Ground magnetic observatories provide direct measurements of the time-dependent magnetic field at Earth's surface. Their records integrate contributions from magnetospheric and ionospheric currents, induction in the conducting Earth, local baseline behaviour, and instrumental effects. One-minute data are particularly valuable because they retain storm-time changes and short-period variability while remaining suitable for multi-year analysis. International observatory practice emphasizes stable timing, calibration, documented baselines, and explicit data-quality control [1, 2].

The Dusheti Observatory is positioned to characterize mid-latitude geomagnetic variability in the Caucasus, a region that is less frequently represented in published event studies than Western Europe or North America. A continuous regional record is useful both for basic geomagnetism and for assessing space-weather exposure of technological systems. The present study analyses relative X, Y, and Z variations in nanotesla. Because absolute baselines were not supplied, component means are treated as instrument-relative levels and are not interpreted as secular variation.

The study has three objectives. First, it establishes a reproducible quality-control description of the 2020–2026 archive. Second, it quantifies dominant temporal scales using diurnal composites, Welch spectra, and wavelet power. Third, it identifies disturbed days from the local record and validates them independently using the planetary Kp index. Particular attention is given to the extreme storm of 10–11 May 2024, for which global studies reported Kp=9 and a Dst minimum near −412 nT [4].

## Scientific contribution

The main contribution is the first unified quantitative assessment of this multi-year Dusheti minute record, including transparent handling of mixed date conventions and overlapping yearly exports. The analysis also demonstrates why local threshold detection alone is insufficient: an external activity index and multi-component coherence are required to prevent isolated sensor excursions from entering a storm catalogue.

## Data and quality control

| Year | Records | Coverage % | X SD | Y SD | Z SD |
|---|---|---|---|---|---|
| 2020 | 508,906 | 96.6 | 23.3 | 33.7 | 50.9 |
| 2021 | 481,706 | 91.6 | 23.7 | 27.4 | 87.7 |
| 2022 | 311,582 | 59.3 | 22.4 | 25.9 | 130.1 |
| 2023 | 346,472 | 65.9 | 23.5 | 19.2 | 17.1 |
| 2024 | 511,077 | 97.0 | 27.3 | 21.5 | 21.7 |
| 2025 | 521,926 | 99.3 | 23.7 | 20.6 | 22.0 |
| 2026 | 334,995 | 63.7 | 24.4 | 19.7 | 11.7 |

The source files contain UTC time and three columns labelled MagnitX, MagnitY, and MagnitZ. Values are expressed in nT and represent variations rather than absolute field elements. Export conventions changed within the archive: files from 2020–2024 use month/day/year, whereas 2025–2026 use day/month/year. Both alternatives were parsed for each file, and the convention yielding the largest number of valid monotonically ordered times was selected. The 2026 export also contained the complete 2025 record; 521,926 duplicate timestamps were removed while retaining the earlier yearly source.

Coverage is high for 2020, 2021, 2024, and 2025. The lower calendar percentages in 2022 and 2023 represent substantial gaps. The 2026 calendar percentage is not a missing-data rate because the record ends on 26 August; coverage between its first and last 2026 timestamps is approximately 98.8%. No missing numeric X, Y, or Z values remained in valid timestamp rows (Fig. 1).

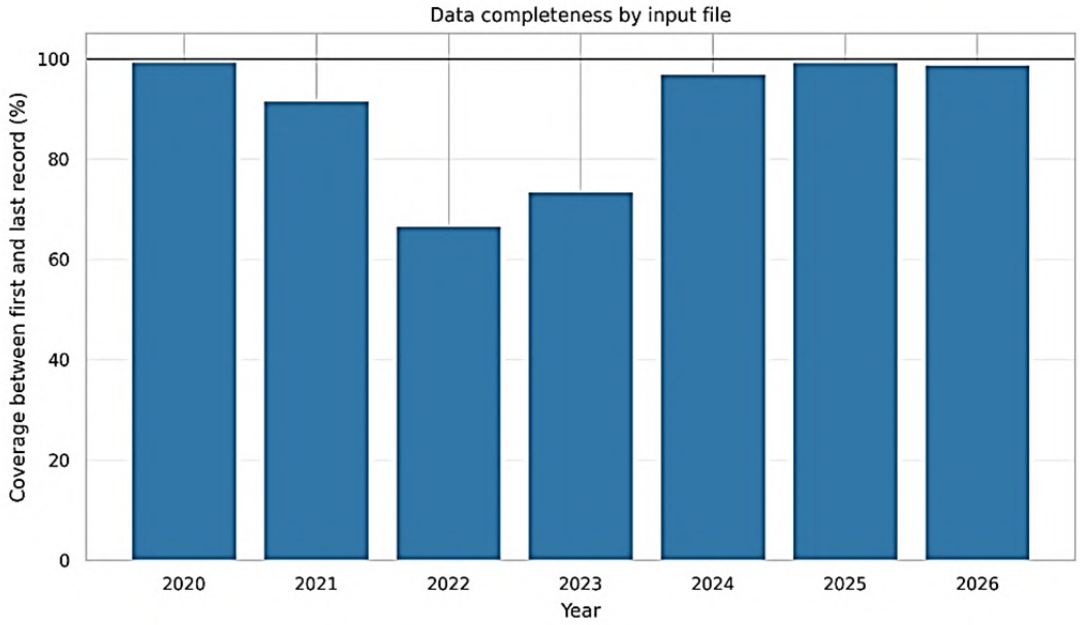



**Fig. 1.** Coverage by source file between its first and last valid timestamp.

## 1. Methods

### *1.1 Aggregation and robust activity metrics*

Daily and monthly count, mean, median, standard deviation, minimum, maximum, and range were calculated separately for X, Y, and Z. Minute-to-minute activity was summarized as the daily root mean square of first differences. Robust z-scores were calculated from the median and median absolute deviation. Abrupt changes were flagged rather than automatically deleted, because rapid physical disturbances can resemble spikes.

### *1.2 Diurnal and spectral analysis*

Hourly UTC profiles were computed for each year and month. Monthly medians were removed before heat-map visualization so that daily morphology was not obscured by baseline offsets. Power spectral density was estimated from hourly medians with Welch's method after linear detrending. The main resolved periods were ranked by spectral power. Continuous complex Morlet wavelet analysis was applied to daily medians to display the time dependence of power between approximately 2 and 256 days.

### *1.3 Event detection and external validation*

Initial candidate days were identified when the robust z score of daily RMS first-difference activity exceeded 6 in at least one component. Candidate days were then merged with three-hour Kp values from the official GFZ service [3, 7]. A strict article event required $Kp \geq 5$, at least 75% local daily coverage, and robust daily-range enhancement in at least two components. This joint rule separates globally disturbed, locally coherent intervals from isolated component excursions.

### *1.4 Reproducibility*

All stages were implemented in Python using pandas, NumPy, SciPy, Matplotlib, Seaborn, and PyWavelets. Outputs include quality-control tables, daily and monthly statistics, spectral peaks, event classifications, and 300-dpi figures. Timestamps remain in UTC throughout the workflow.

## Temporal and spectral results

The Welch spectra show a clear daily line near 24 hours in X, Y, and Z, accompanied by harmonics near 12 and 8 hours. The Y component has the strongest daily and semidiurnal spectral power. These periodicities are consistent with recurring ionospheric current systems and their harmonics, although a formal separation of quiet-time Sq variation from disturbed days requires selection by geomagnetic activity and season.

Broader peaks occur near 682.7 hours in X and Y and near 585 hours in Z. The X/Y value corresponds to approximately 28.4 days and is close to the solar-rotation recurrence band. Because long gaps and component baseline changes can redistribute low-frequency power, this feature should be described as a near-solar-rotation periodicity rather than assigned uniquely to a physical driver (Fig.2).

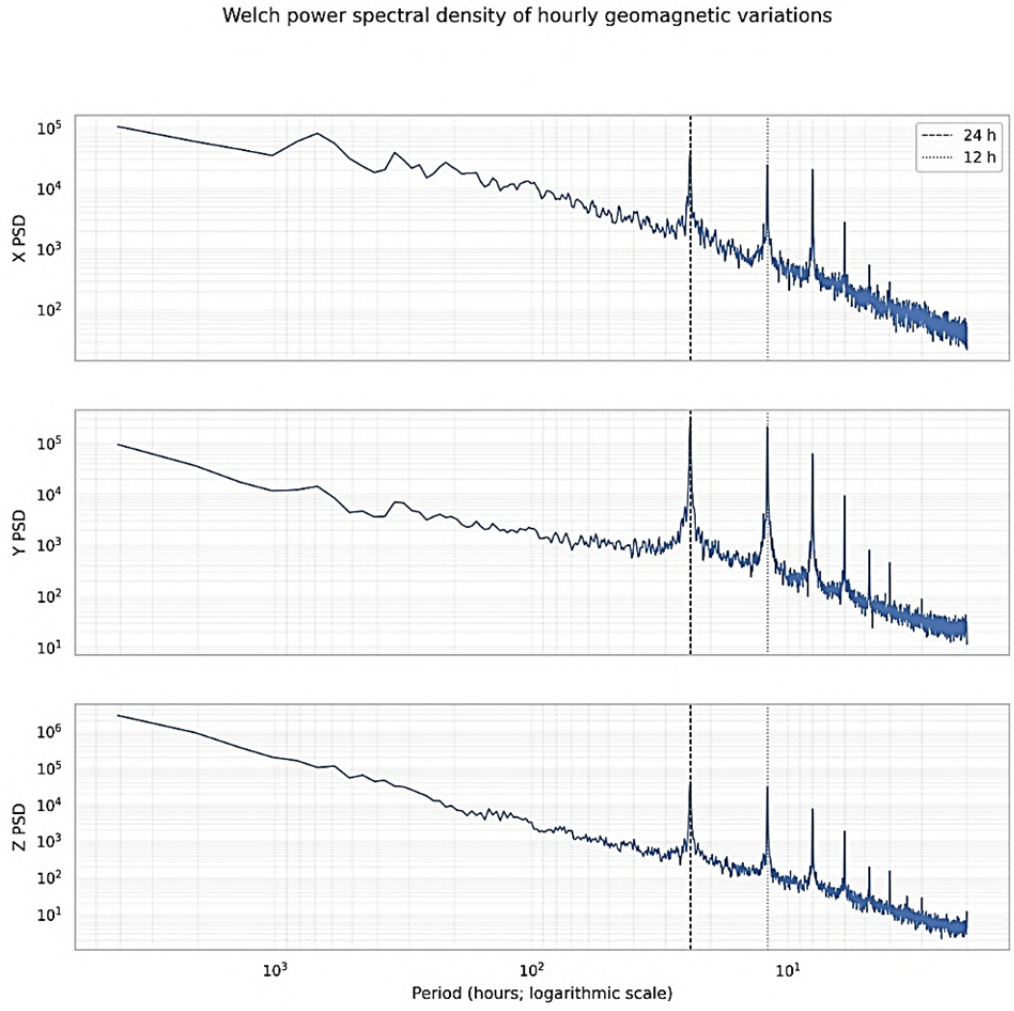



**Fig. 2.** Welch power spectral density of hourly X, Y, and Z variations.
Dashed markers identify the 24-hour and 12-hour periods.

## Validated disturbed days

The local detector produced 59 candidate days. External and coherence screening retained 17 article-ready days. Thirteen additional days had Kp ≥ 5 but did not reach the strict two-component range criterion, six were likely instrumental or local spikes, six remained ambiguous, and seventeen lacked sufficient local coverage for classification. The strict catalogue therefore prioritizes specificity over completeness.

| UTC date | Kp max | X range | Y range | Z range |
|---|---|---|---|---|
| 2024-05-11 | 9 | 407.0 | 290.6 | 177.7 |
| 2024-05-10 | 8.67 | 606.7 | 317.6 | 94.5 |
| 2024-10-10 | 8.67 | 537.8 | 285.0 | 88.1 |
| 2025-11-12 | 8.67 | 415.8 | 325.1 | 80.2 |
| 2026-01-19 | 8.67 | 634.4 | 414.0 | 83.8 |
| 2023-04-23 | 8.33 | 261.9 | 189.3 | 52.8 |
| 2024-03-24 | 8.33 | 268.5 | 138.6 | 67.1 |
| 2024-10-11 | 8.33 | 238.7 | 200.8 | 53.6 |
| 2024-08-12 | 8 | 295.2 | 145.8 | 86.4 |
| 2025-01-01 | 8 | 416.3 | 305.2 | 94.9 |
| 2024-06-28 | 7.67 | 190.0 | 144.9 | 69.2 |
| 2025-04-16 | 7.67 | 222.8 | 144.0 | 79.5 |
| 2026-01-20 | 7.67 | 284.2 | 192.7 | 71.4 |
| 2023-11-05 | 7.33 | 251.0 | 209.1 | 91.0 |
| 2021-05-12 | 7 | 405.0 | 243.1 | 123.2 |
| 2026-07-04 | 7 | 204.0 | 186.8 | 46.5 |
| 2025-03-21 | 5.33 | 143.1 | 107.9 | 66.1 |

Ranges are daily maximum minus minimum in nT. The concentration of seven validated days in 2024 reflects the enhanced activity around the maximum of Solar Cycle 25, but comparisons of annual event counts must account for incomplete coverage in 2022 and 2023 and the partial 2026 interval.

## The May 2024 superstorm at Dusheti

The largest complete and independently validated response occurred during 10–12 May 2024. On 10 May, the X range reached 606.7 nT and the Y range 317.6 nT. On 11 May, when the daily maximum Kp reached 9 and the mean of the eight three-hour Kp intervals was 8.375, the X, Y, and Z ranges were 407.0, 290.6, and 177.7 nT, respectively. Elevated activity continued on 12 May, although that day did not meet the strict range-coherence rule.

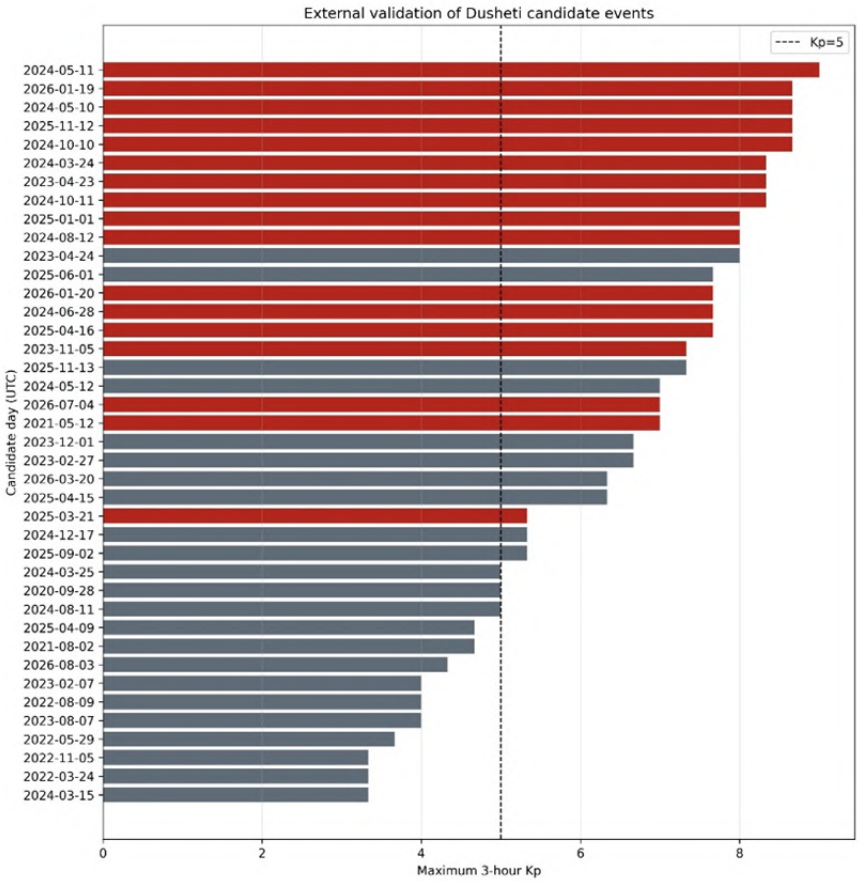



**Fig. 3.** Maximum Kp for the leading Dusheti candidate days. Red bars satisfy the strict external and local-coherence rule.

The timing agrees with the global storm sequence. NOAA reported G5 conditions on 10 May 2024 [8], and recent studies [4-6] associated the storm with interacting Earth-directed coronal mass ejections from active region 13664. Their reported Dst minimum of −412 nT at 02 UT on 11 May places the event among the strongest storms of the modern index era. The large Dusheti X and Y ranges demonstrate a strong mid-latitude ground response in the Caucasus sector (Fig. 3).

## Discussion

The combined results show that the Dusheti record captures both regular solar-controlled variability and episodic storm-time disturbances. The daily and subdaily harmonics provide a stable basis for future Sq studies, while the Kp-validated catalogue supplies a defensible set of event intervals for case analysis. The strong May and October 2024 responses indicate that the station resolves major mid-latitude disturbances with amplitudes of several hundred nanotesla.

The analysis also exposes essential data-management issues. Mixed date conventions would have removed more than 800,000 valid rows if a fixed parser had been used. The overlapping 2025 content in the 2026 export would have duplicated an entire year. These are not minor technical details: both errors would bias seasonal profiles, spectral power, coverage estimates, and event counts.

## Instrumental and baseline effects

Several initial candidates had very high Z first-difference scores while X and Y remained quiet and Kp was low. Such intervals are more consistent with component-specific instrumental behaviour or local interference than with large-scale geomagnetic storms. They were not used as confirmed events. Likewise, year-to-year changes in component means, particularly in Z, are not interpreted geophysically without absolute observations, baseline corrections, and instrument logs.

## Limitations

The archive contains major gaps in 2022 and 2023, and 2026 is incomplete. Kp is a planetary three-hour index and does not represent all regional disturbances. A complete storm analysis should add hourly Dst or one-minute SYM-H, solar-wind speed and IMF Bz, and at least one neighbouring observatory. Quiet-day diurnal analysis should use internationally quiet days or a Kp-based exclusion rule. These additions would strengthen causal interpretation but do not change the observed local amplitudes.

## Conclusions

1. The corrected archive contains 3,016,664 unique one-minute X, Y, and Z records from January 2020 through August 2026.
2. Automatic per-file date detection and cross-file duplicate removal are necessary for this archive.
3. The spectra resolve dominant 24-, 12-, and 8-hour variations and broader power near the solar-rotation band.
4. Seventeen disturbed days meet the strict joint Kp and local-coherence criterion.
5. The 10–11 May 2024 G5 storm produced the strongest complete validated response, including an X daily range above 600 nT on 10 May.
6. Component means cannot be interpreted as secular variation without absolute baselines and calibration information.

## Data and code availability

The analysis workflow produces machine-readable quality, aggregation, spectral, and event-validation tables together with publication-resolution figures. The observatory data remain under the control of the data owner. GFZ Kp values are obtained from the official web service [7].

## References

1. Love J. J., Chulliat A., An international network of magnetic observatories. // Eos., 94(42), 2013, pp. 373-374. https://doi.org/10.1002/2013EO420001

2. Bracke S., et al., INTERMAGNET Technical Reference Manual. Version 5.3.2. // GFZ Data Services, 2025, 2025.001. https://doi.org/10.48440/INTERMAGNET
3. Matzka J., et al., The geomagnetic Kp index and derived indices of geomagnetic activity. // Space Weather. 2021, 19:e2020SW002641. https://doi.org/10.1029/2020SW002641
4. Hayakawa H., et al., The solar and geomagnetic storms in May 2024: A flash data report. // Astrophysical Journal, 979, 49, 2025. https://doi.org/10.3847/1538-4357/ad9335
5. Tulasi Ram S., et al., Super-intense geomagnetic storm on 10-11 May 2024. // Space Weather. 2024. https://doi.org/10.1029/2024SW004126
6. Weiler E., et al., First observations of a geomagnetic superstorm with a sub-L1 monitor. // Space Weather. 2025, 23:e2024SW004260. https://doi.org/10.1029/2024SW004260
7. GFZ Helmholtz Centre for Geosciences. Kp index data service. https://kp.gfz.de/en/data
8. NOAA Space Weather Prediction Center. G5 Conditions Observed. 10 May, 2024. https://www.spaceweather.gov/news/g5-conditions-observed

2nd International Scientific Conference "Modern Problems in Geophysics", Proceedings,
ISBN 978-9941-36-562-1, ISSN 3088-4349, Tbilisi, Georgia, October 29-31, 2026

# THREE-DIMENSIONAL REPRESENTATION OF THE GEORADIOLOCATION STUDY OF THE INTERNAL SPACE OF THE GEORGIAN CATHEDRAL SVETITSKHOVELI AND THE NEARBY TERRITORY

**Odilavadze D., Chelidze T., Yavolovskaya O.**

*Ivane Javakhishvili Tbilisi State University, Mikheil Nodia Institute of Geophysics, Tbilisi, Georgia*
*odildavit@gmail.com*

**Abstract.** *Since 2010, the Georadiolocation study of the internal and external surrounding territory of the Georgian Cathedral Svetitskhoveli has been carried out by the Institute of Geophysics, Applied and Experimental Geophysics Sector, Archaeogeoradiolocation Laboratory. At different times, the collection of georadar data for the corresponding profiles with the 2GHz, 500MHz, 150MHz, 75MHz antennas of the Zond 12-e georadar was carried out and their processing/interpretation was carried out with the Prizm 2.6 software. This time, a three-dimensional representation of the results obtained with the 150MHz antennas of the inner territory of the temple and the 500MHz antennas of the surrounding territory of the temple is presented.*

***Key words*:** *Archaeogeoradiolocation survey, georadar works, radio image.*

## Instruments and methodology/software used

Based on the results collected by the Zond 12-e georadar and processed and interpreted with the Prizm 2.6 software [1, 2, 3, 4, 5, 6], their presentation in a three-dimensional form was carried out using the Voxler 4 software.

Four georadiolocation profiles were conducted in the inner territory of the Svetitskhoveli temple using a 150MHz receiving-transmitting antenna. Georadiolocation profiles were conducted along the outer perimeter of the Svetitskhoveli temple with a 500MHz receiving-transmitting antenna.

Here we present a visualization of three-dimensional subsurface objects created by radio images of both internal and perimeter radar profiles.

## Results and discussion

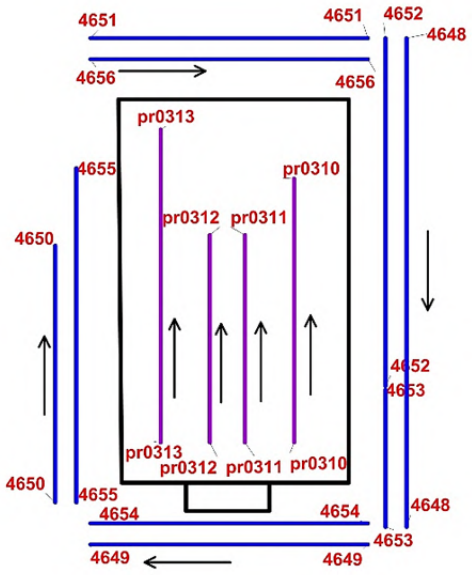



**Fig. 1.** Prof.310-313 – 150MHz, Prof.4648-4656 – 500MHz

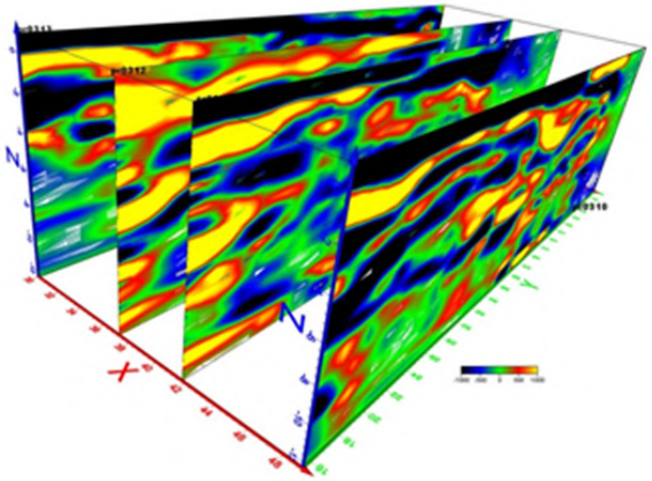


**Fig. 2.** Prof. 310, 311, 312, 313.

Fig. 1 and Fig. 2 presents a radio image of the subsurface objects of the Svetitskhoveli Cathedral, collected with a 150MHz GPR antenna and processed with Prizm 2.6, composed of parallel profiles. The beginning of the profiles coincides with the central entrance of the Svetitskhoveli Cathedral, X-axis.

Radargrams of parallel profiles obtained with a 150MHz antenna in the internal area of Svetitskhoveli Cathedral create radio images of subsurface objects, some of which extend to neighboring profiles, indicating the existence of their continuous form. The radio-spectrum axes of the objects clearly reflect their parallel placement and their geometric shapes. On the first profile, a continuous cavity is visible, with overlap and filling, which extends along the remaining profiles at the same level and with the same shapes. Also, at a depth of 7m, the appearance of anthropogenic origin layer-type material is clearly visible on profiles 1, 2, 3 and on profile 4 at a depth of approximately 6m in the profiles Fig.2.

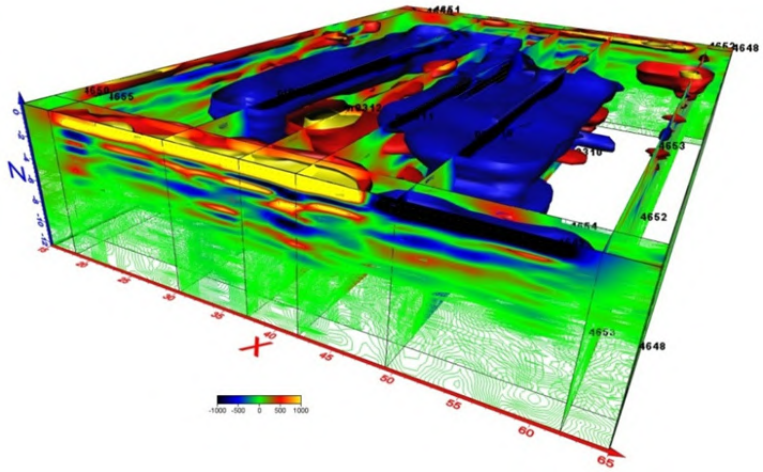


**Fig. 3.** Approximately 6m in the profiles.

Fig. 3 presents a complex radio image of the subsurface objects of the Svetitskhoveli Cathedral, collected with a 150MHz and 500MHz GPR antenna and processed with Prizm 2.6 and composed with parallel profiles. The beginning of the profiles coincides with the central entrance of the Svetitskhoveli Cathedral, X-axis 65m. Radargrams around the perimeter were created with a 500MHz shielded receiving-transmitting antenna. The results were processed with Voxler 4 software.

At the entrance to the Svetitskhoveli Cathedral, the embedded heterogeneity observed in Fig. 1 along the entire length of the initial coordinates of the profiles was clearly delineated and the radio image of an archaeological architectural object formed from a material of strong reflectivity was distinguished. Along the X-axis, from a distance of 45m to a distance of 60m and to a depth of 6m, a radio image of an object containing a cavity of a different composition from the surrounding material is visible. There are also radio images of a smaller object at distances of 30m and 40m, their depth is up to 5m. The overlap of the profiles

carried out in the inner territory of the temple with a material of different reflectivity was clearly identified; the contouring indicates the area of their distribution.

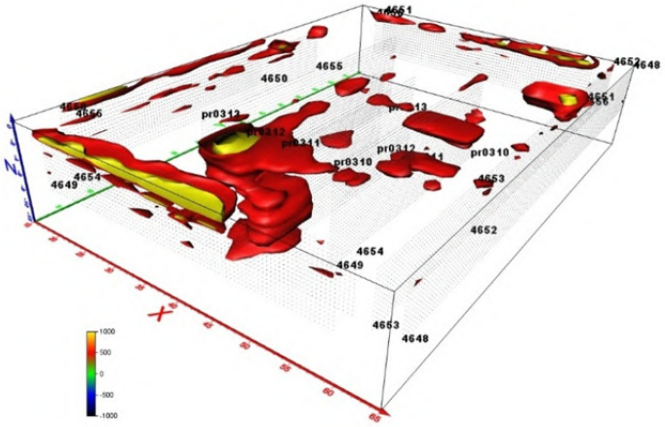



**Fig. 4.** Complex radio image.

Fig. 4 presents a complex radio image created with antennas of the internal territory (150MHz) and external perimeter (500MHz) of the Svetitskhoveli Cathedral.

During the digital processing of the complex radio image of the Svetitskhoveli Cathedral (Fig. 3), a number of objects were identified by removing the covering material that were not visible on the other radio images. In particular, a deep and volumetric object at a distance of 40m, a coiled object up to 8m deep, approximately 2-3m wide (Prof. 311, 312, 150MHz). Also important is to note, that at a distance of 45m are two parallelepiped-like objects, presumably at depths of 4m and 6m (Prof. 310, 311, 312, 150MHz). Also, a parallelepiped-shaped object with a yellow filling at the end of the external perimeter (Prof. 4649, 4654, 500MHz).

## Conclusion

Radargrams of parallel profiles obtained with 150MHz and 500MHz antennas on the inner territory of the Svetitskhoveli Cathedral create radio images of subsurface objects, some of which extend to neighboring profiles, indicating the existence of their continuous form. The axes of the radio profiles of the objects clearly reflect their parallel placement with their geometric shapes [7, 8, 9, 10]. The first profile on Fig. 1 shows a continuous cavity, with overlap and filling, which extends along the rest of the profiles at the same level and with the same shapes. Fig. 2 as in Fig. 1, shows the radio profile of an object containing a cavity of a different composition from the surrounding material. The same, but smaller, object has radio profiles at distances of 30m and 40m, their depth is down to 5m. The overlap of the profiles taken in the inner territory of the temple with materials of different reflectivity was clearly identified, the contours indicate their area of extension. There is a deep and volumetric object at a distance of 40m (See Fig. 3), an object curled up to 8m deep, approximately 2-3m wide (Prof. 0311, 0312, 150MHz). Also important are two parallele piped-like objects at a distance of 45m, approximately at 4m and 6m depths (Prof. 0310, 0311, 0312, 150MHz). Also, interesting is a parallelepiped-shaped object with a yellow filling at the end of the outer perimeter (Prof. 4649, 4654, 500MHz).

## References

1. Odilavadze D., Chelidze T., Yavolovskaya O., Archaeogeoradiolocation nearsurface survey of the area surrounding Svetitskhoveli Cathedral. // Journal of the Georgian Geophysical Society, e-ISSN: 2667-9973, p-ISSN: 1512-1127. Physics of Solid Earth, Atmosphere, Ocean and Space Plasma, v.29 (1), 2026.
2. Kudava B., The burial place of the Georgian king: personal choice, tradition or political decision? // “Historian” (a scientific collection dedicated to the 80th anniversary of the birth of RoinMetreveli), Tbilisi, 2019, pp. 139-167.
3. Odilavadze D., Goguadze N., Jakhutashvili M., Vepkhvadze S., Kachakhidze M., Kachakhidze N. Results of primary georadiolocation searching of Svetitskhoveli Temple. // (1 – Iv. Javakhishvili State University, M. Nodia Institute of Geophysics. 2 – Saint Andrews Georgian University). GESJ: Physics, ISSN 1512-1461, No.1(9), 2013, 31 p.

4. Odilavadze D., Kiria J., Ghlonti N., Yavolovskaya O., The Results of archaeogeoradiolocation investigations of the territory inside the rampart of St. Sophia Church of Khobi. // „Moambe", Bulletin of the Georgian National Academy of Sciences, V.14, n.4, 2020, pp. 51-56.
5. Chelidze T., Odilavadze D., Pitskhelauri K., Archaeogeophysics in Georgia-New Results, New Prospects. // Proceedings of the Georgian National Academy of Sciences.Series of History, Archeology, Ethnology and Art History, №.15, 2013, pp. 24-34.
6. Kofman L., Ronen A., Frydman S., Detection of model voids by identifying reverberation phenomena in GPR records. // Journal of Applied Geophysics. (59), 2006, pp. 284-299.
7. Odilavadze D., Chelidze T., Yavolovskaya O., Some georadiolocation images of cylindrical bodies built with different dielectric fillers, placed in a dielectric environment. // International Scientific Conference "Geophysical Processes in the Earth and its Envelopes". Proceedings, ISBN 978-9941-36-147-0, Tbilisi, Georgia, November 16-17, 2023, pp. 217-220.
8. Odilavadze D., Chelidze T., Yavolovskaya O., The radio image of an object with an elongated, face-fragmented, dielectrically complex structure was studied using the method of georadar physical modeling. // Journal of the Georgian Geophysical Society, e-ISSN: 2667-9973, p-ISSN: 1512-1127, Physics of Solid Earth, Atmosphere, Ocean and Space Plasma, v. 27(2), 2024, pp. 15-28.
9. Odilavadze D., Chelidze T., Yavolovskaya O., Preliminary archaeogeophysical survey of the construction site in the vicinity of the Narikala Citadel. // Journal of the Georgian Geophysical Society, e-ISSN: 2667-9973, p-11.ISSN: 1512-1127. Physics of Solid Earth, Atmosphere, Ocean and Space Plasma, v. 28(1), 2025, pp. 27-35.
10. Odilavadze D., Chelidze T., Glonti N., Kiria J., Yavolovskaya O., Archaeogeoradiolocation Research of the Territory of the Ninotsminda Monastery Complex. // Transactions of Mikheil Nodia Institute of Geophysics, ISSN 1512-1135, vol.LXXVIII, 2025, pp. 20-34.

2nd International Scientific Conference "Modern Problems in Geophysics", Proceedings,
ISBN 978-9941-36-562-1, ISSN 3088-4349, Tbilisi, Georgia, October 29-31, 2026

# LOW-ORDER MODELS OF THE GEODYNAMO

**[*,**]Kharshiladze O., [**]Tsulukidze L., [***,****]Sorriso-Valvo L.,
[*]Kezua L., [**]Elbakidze Kh., [**]Zilpimiani D.**

**Ivane Javakhishvili Tbilisi State University, Tbilisi, Georgia*
***M. Nodia Institute of Geophysics of the I. Javakhishvili Tbilisi State University, Tbilisi, Georgia*
****Department of Electromagnetics and Plasma Physics, School of Electrical Engineering and Computer Science, KTH Royal Institute of Technology, Stockholm, Sweden*
*****Institute for Plasma Science and Technology (ISTP), National Research Council (CNR), Rende, Italy*
*luka.tsulukidze617@ens.tsu.edu.ge*

***Abstract.*** *The long-term evolution of the Earth's magnetic field, particularly the phenomenon of irregular polarity reversals, presents a significant modeling challenge. Spatially resolved global geodynamo models are computationally prohibitive for generating the massive statistical ensembles required to study reversals over geological timescales. To overcome this limitation, low-dimensional phenomenological systems, such as the classic two-disk Rikitake dynamo, are utilized because they successfully capture the fundamental nonlinear and chaotic dynamics of polarity inversions while allowing for rapid, long-term temporal integration. This paper investigates the dynamics of a modified Rikitake system forced by an external current ($i_{ext}$ ), which represents potential macroscopic external magnetic influences. We present a parameter sensitivity and robustness analysis, evaluating the system's dynamic response under varying mechanical-to- electromagnetic damping ratios ($\mu$=1 and $\mu$=2) and forcing amplitudes ($a_{ext}$= 0.5 and $a_{ext}$ = 1). Our analysis reveals that while variations in these fundamental parameters alter the amplitude and frequency of the chaotic internal oscillations during stable polarity epochs, the macroscopic synchronization of polarity reversals to the external signal remains remarkably robust. These findings confirm the structural stability of externally triggered inversions in low-order geodynamo models, suggesting that external pacing can reliably override internal chaotic variability across divergent physical regimes.*

***Key words:*** *Geodynamo, Reversals, Low-order models, Rikitake disk dynamo, External forcing.*

## Introduction

The long-term dynamics of the geodynamo, particularly its irregular polarity reversals, present a profound theoretical challenge [1, 2]. Because direct numerical integration of the core's magnetohydrodynamic equations over geological timescales is computationally expensive, researchers frequently rely on low- dimensional phenomenological models. A cornerstone of this approach is the classic two-disk Rikitake dynamo [3], which inherently produces chaotic polarity inversions mimicking paleomagnetic data and new studies showcase that it also exhibits metastable states like "rare-reversal chaos" [4].

While these low-order models successfully generate spontaneous reversals, Earth is not an isolated system. A recent modification introduced an external forcing current ($i_{ext}$) to represent the effect of weak interstellar magnetic fields [5]. This study demonstrated that an external signal can effectively pace the system's chaotic reversals, aligning them with empirical paleomagnetic records [5].

Building directly upon this framework [5], we present a parameter sensitivity and robustness analysis of the externally forced dynamo. By systematically varying the mechanical-to-electromagnetic damping ratio and the external forcing amplitude, we aim to determine whether this macroscopic synchronization remains structurally robust across different physical regimes.

## Mathematical model

To investigate the influence of external macroscopic magnetic fields, we adopt the modified dimensionless Rikitake framework introduced by Kharshiladze et al. [5]. This framework integrates an external current, $i_{ext}$, into the governing equations. The dynamic evolution of this forced system is described by four coupled nonlinear ordinary differential equations [5]:

$$\frac{di_1}{d\tau} = -\mu i_1 + \omega_1(i_2 + i_{ext}), \quad (1)$$

$$\frac{di_2}{d\tau} = -\mu i_2 + \omega_2(i_1 + i_{ext}), \quad (2)$$

$$\frac{d\omega_1}{d\tau} = 1 - i_1(i_2 + i_{ext}), \quad (3)$$

$$\frac{d\omega_2}{d\tau} = 1 - i_2(i_1 + i_{ext}), \quad (4)$$

Here, $i_1$ and $i_2$ represent the dimensionless currents flowing through the respective disks, while $\omega_1$ and $\omega_2$ are their angular velocities [5]. The system's behavior is dictated by two primary control parameters. The first is $\mu$, the fundamental damping ratio ($\mu = \sqrt{\tau_m/\tau_e}$) established by Cook and Roberts [6], which balances the mechanical time scale against the electromagnetic diffusion time [6]. The second is the external forcing amplitude $a_{ext}$, where the external current is defined as $i_{ext}(\tau) = a_{ext} \times S(\tau)$[5]. In this study, $S(\tau)$ acts as a normalized rectangular signal mirroring the empirical paleomagnetic reversal record [5].

## Results and Discussion

To evaluate the robustness of the externally paced inversions, we conducted numerical integration of the modified Rikitake equations across four distinct parameter regimes. The external signal, $S(\tau)$, was configured as a rectangular wave whose polarity strictly mirrors the empirical paleomagnetic reversal record for the last 3.5 million years, established by Cande and Kent [7]. The extraction and processing of this reversal data were performed utilizing the PmagPy Python package [8]. We analyzed the temporal evolution of the dimensionless current $i_1$ under varying mechanical-to-electromagnetic damping ratios, μ, and forcing amplitudes, $a_{ext}$,

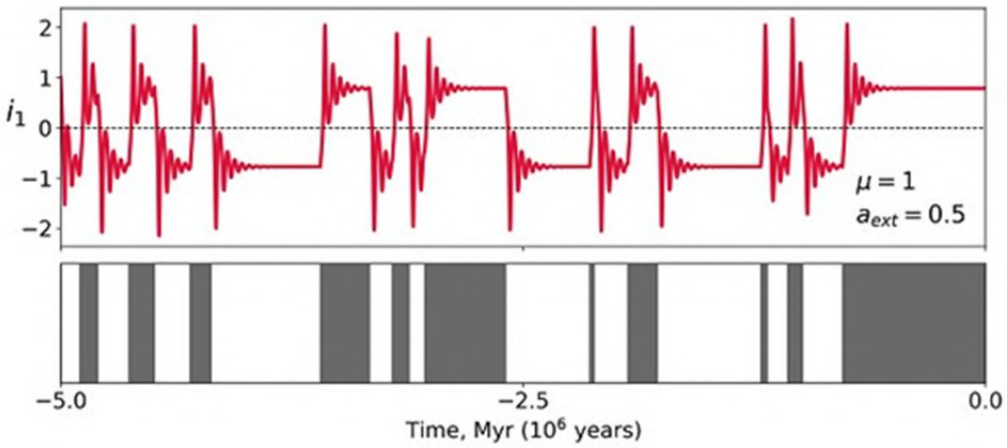



**Fig. 1.** Time evolution for $i_1$, for $\mu = 1$, $\alpha_{ext} = 0.5$.

Fig. 1 and Fig. 2 present the system's dynamics for a baseline damping ratio of $\mu = 1$. In both scenarios, the chaotic inversions are entirely suppressed by the external driver; the system's polarity (the sign of $i_1$) flips almost instantaneously in response to the polarity changes of the external current [5] Notably, the system retains its fundamental chaotic properties during the stable epochs (chrons). Between reversals, the amplitude of $i_1$ exhibits the chaotic, growing oscillations characteristic of the standard Rikitake model. Comparing Fig. 1 and Fig. 2 demonstrates that halving the relative strength of the external forcing does not break the macroscopic synchronization.

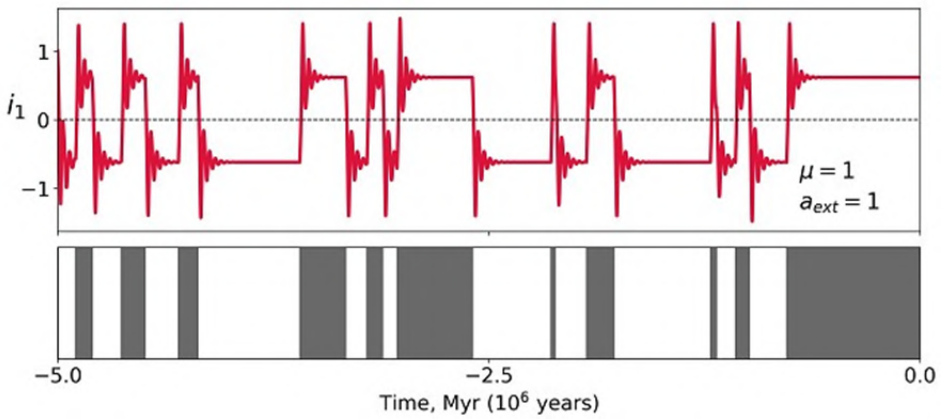



**Fig. 2.** Time evolution for $i_1$, for $\mu = 1$, $a_{ext} = 1$.

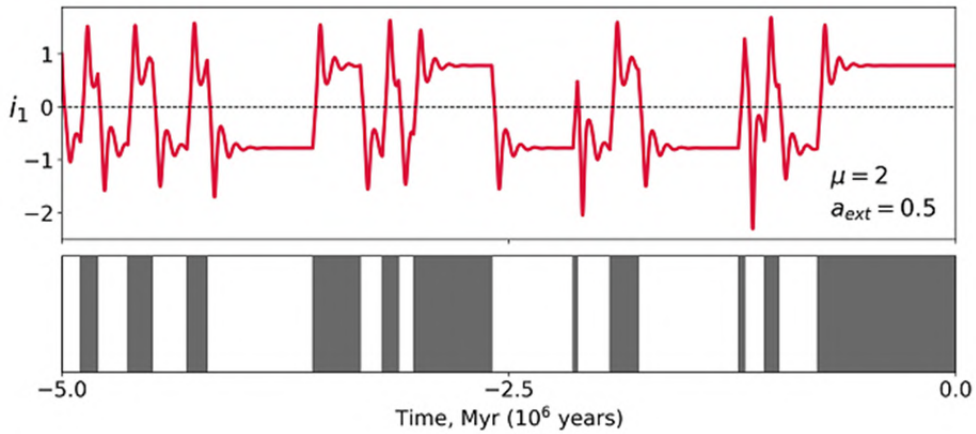



**Fig. 3.** Time evolution for $i_1$, for $\mu = 2$, $a_{ext} = 0.5$.

Fig. 3 and Fig. 4 illustrate the system's response when the mechanical-to-electromagnetic damping ratio is doubled to $\mu = 2$. Increasing this ratio fundamentally alters the internal chaotic micro-dynamics of the dynamo. The specific waveform, frequency, and growth rate of the amplitude oscillations within the stable polarity epochs change noticeably compared to the $\mu = 1$ regime [5]. However, despite these internal dynamic shifts, the macroscopic synchronization to the paleomagnetic barcode remains perfectly intact. The timing of the reversals is strictly paced by the external signal across both $a_{ext} = 0.5$ and $a_{ext} = 1$.

This parameter sweep reveals a distinct decoupling between micro-dynamics and macro-dynamics. The chaotic intra-chron oscillations are highly sensitive to variations in μ, confirming that the system is not locked into a trivial stationary state [5]. Yet, the inter-chron reversals exhibit profound structural robustness, proving that external pacing can reliably override internal chaotic variability across divergent physical regimes.

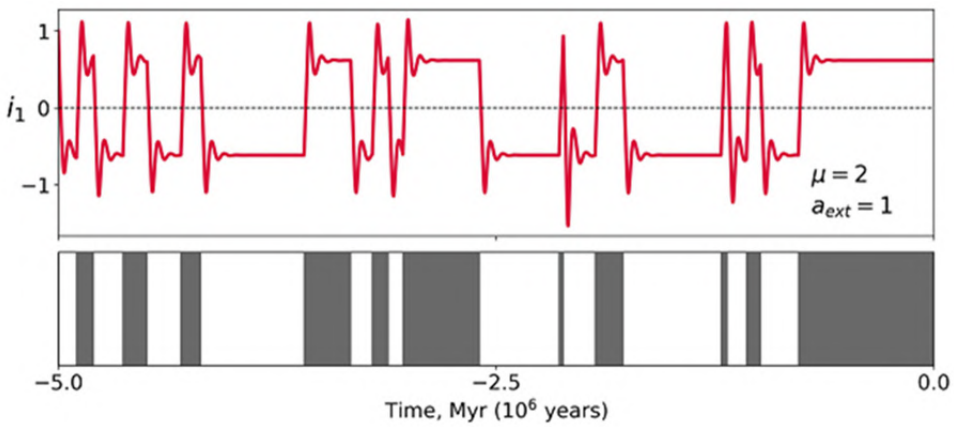



**Fig. 4.** Time evolution for $i_1$, for $\mu = 2$, $a_{ext} = 1$.

## Conclusion

This study investigated the structural stability of externally forced geomagnetic reversals using a modified low-dimensional Rikitake dynamo model. By conducting a systematic parameter sensitivity analysis, we demonstrated that the synchronization of chaotic polarity inversions to a macroscopic external magnetic signal is not an artifact of a highly tuned parameter set. Even when the mechanical-to-electromagnetic damping ratio is altered – which significantly modifies the internal chaotic oscillations – the timing of the macroscopic reversals remains robustly locked to the external driver. Furthermore, this forced synchronization persists even when the external forcing amplitude is halved. These findings confirm that low-order phenomenological models provide a robust and highly efficient framework for investigating the deterministic external pacing of chaotic geodynamo cycles over geological timescales.

**Acknowledgments:** Research was supported by Shota Rustaveli National Science Foundation of Georgia Grant FR-25-1725.

## References

1. Moffatt H. K., Magnetic Field Generation in Electrically Conducting Fluids. Cambridge University Press, 1978.
2. Stefani F., et al. Reversals in nature and the nature of reversals. „arXiv preprint physics/0701026“.
3. Rikitake T., Oscillations of a system of disk dynamos. // Mathematical Proceedings of the Cambridge Philosophical Society, 54(1), 1958, pp. 89-105.
4. Frick P., & Pleshkov R., Rare-reversal chaos in two-disk dynamo models. // Physical Review E, 110(6), 064203, 2024.
5. Kharshiladze O. A., Tsulukidze L. K., Kezua L. B., & Zilpimiani D. O. // Control of Inversions of the Earth's Magnetic Field with Rikitake's Model. „Journal of the Georgian Geophysical Society“, 28(2), 2025, pp. 94-101.
6. Cook A. E. & Roberts P. H., The Rikitake two-disc dynamo system. // Mathematical Proceedings of the Cambridge Philosophical Society, 68(2), 1970, pp. 547-569.
7. Cande S. C., & Kent, D. V., Revised calibration of the geomagnetic polarity timescale for the Late Cretaceous and Cenozoic. // Journal of Geophysical Research: Solid Earth, 100(B4), 1995, pp. 6093-6095.
8. Tauxe L., et al., PmagPy: Software package for paleomagnetic data analysis and a bridge to the Magnetics Information Consortium (MagIC) Database. // Geochemistry, Geophysics, Geosystems, 17(6), 2016, pp. 2450-2463.

2nd International Scientific Conference "Modern Problems in Geophysics", Proceedings,
ISBN 978-9941-36-562-1, ISSN 3088-4349, Tbilisi, Georgia, October 29-31, 2026

# TEMPERATURE VARIABILITY AND GEO-STORMS

***,**Tatishvili M., *Elbakidze-Chargazia Kh, *,**Palavandishvili A., *Khutsishvili E., *Chelidze N.**

**Institute of Hydrometeorology of Georgian technical University, Tbilisi, Georgia*
***Vakhushti Bagrationi Institute of Geography of Ivane Javakhishvili Tbilisi State University, Tbilisi, Georgia*
*m.tatishvili@gtu.ge*

***Abstract.*** *A geomagnetic storm is a major disturbance of Earth's magnetosphere that occurs when there is a very efficient exchange of energy from the solar wind into the space environment surrounding Earth. These storms result from variations in the solar wind that produce major changes in the currents, plasmas, and fields in Earth's magnetosphere. The correlation between geomagnetic storms and meteorological elements (Tmax, Tmin) for Tbilisi city using meteorological observation and NASA's Solar Dynamics Observatory and NOAA Space Weather Prediction Center data has been conducted. The results show that there exists dependence between weather parameters and income radiation. Especially important is wind parameter variability investigation. Such research hasn't been carried out yet in Georgia and is important for space weather researches.*

***Key words****: Earth magnetic field, Geomagnetic storm, geomagnetic indices Temperature.*

## Introduction

The sun plays a role in our climate in direct and indirect ways. The sun changes in its activity on time scales that vary from 27 days to 11, 22, 80, 180 years and more. A more active sun is brighter due to the dominance of faculae over cooler sunspots with the result that the irradiance emitted by the sun and received by the earth is higher during active solar periods than during quiet solar periods. The amount of change of the solar irradiance based on satellite measurements since 1978 during the course of the 11 year cycle just 0.1% [1] has caused many to conclude that the solar effect is negligible especially in recent years. Over the ultra long cycles (since the Maunder minimum), irradiance changes are estimated to be as high as 0.4%.

However, this does not consider the Sun's eruptive activity (flares, solar wind bursts from coronal mass ejections and solar wind bursts from coronal holes) which may have a much greater effect. This eruptional activity may enhance warming through ultraviolet induced ozone chemical reactions in the high atmosphere or ionization in higher latitudes during solar induced geomagnetic storms., Solar variance is a much more important driver for climate change than currently assumed. Because, it is more easily measured and generally we find eruptional activity tracking well with the solar irradiance, we may utilize solar irradiance measurements as a surrogate or proxy for the total solar effect [2]. Correlations with Total Solar Irradiance studies vary on the importance of direct solar irradiance especially in recent decades.

Approximately every 11 years, the Sun undergoes a complete personality change from quiet and calm to violently active [3]. The height of the sun's activity, known as solar maximum, is a time of numerous sunspots, with profound eruptions that send radiation and solar particles out into the far reaches of space. However, the timing of the solar cycle is far from precise. Now Solar cycle 25 is acting.

## Data and Methods

To evaluate influence of geo-activity on meteorological parameters (Tmax., Tmin) in 2025 for the Tbilisi meteorological station, satellite-derived magnetic field tension data ( NASA/GEO, Sun Watch, SOHO, Aurora Alerts, NOAA) [4, 5, 6, 7] were used. Correlation analysis is most applicable for this reason.

## Discussion

When an intense surge of solar wind reaches Earth, there are many changes which occur in the magnetosphere. The day side of the magnetosphere is compressed closer to the surface of Earth and the geomagnetic

field fluctuates wildly. This type of event is generally called a geomagnetic storm. During a geomagnetic storm the high-latitude currents which occur in the ionosphere change rapidly, in response to changes in the solar wind. These currents produce their own magnetic fields which combine with Earth's magnetic field. At ground level, the result is a changing magnetic field which induces currents in any conductors that are present.

When a mass of plasma is ejected from the Sun, the plasma travels outward in the solar wind. These plasma bursts have their own magnetic fields which are carried along with the plasma. How these fields are oriented when they arrive at Earth determines whether magnetic reconnection will occur. When the direction of the solar wind field is opposite the direction of Earth's field, magnetic reconnection occurs, and the geomagnetosphere essentially becomes a part of the solar magnetic field. In this condition, Earth is much more prone to the effects of the solar wind. Solar wind particles can enter the magnetosphere more easily, and those already within the magnetosphere are energized. Changes in solar wind magnetic fields cause wild fluctuations in the magnetospheric fields. In response to these fluctuations, in accordance with Lenz's Law, massive currents flow throughout the magnetosphere. It is these high-altitude currents that induce voltages at ground level. If the magnetic field of the solar wind is in the same direction as the Earth's field, then magnetic reconnection does not occur and the magnetosphere is much more separated and protected from the solar wind [6]. The Sun-Earth environment has variables, which are changing on regular basis due to starbursts. These variables are the Kp, proton flux and E-flux. Sudden changes in these parameters may abruptly influence the environment of the Earth. If an E-flux hike is responsible for global warming, then an E flux lowering may lead to snowfall, thunderstorms and erratic rainfall. The effect of earth directed CME would not only trigger the earthquake, but affect the whole environment of the Earth, including the destruction of ozone layers leading to climate change.

The effect of Earth directed Coronal Mass Ejections (CME) from the Sun reveals a sensational impact on the atmosphere and geosphere. It has been observed that there is a close relationship between Kp values (Planetary Indices) and particle flux (Electron flux and Proton Flux) with the CME. The response of the magnetosphere to interplanetary shocks or pressure pulses can result in sudden injections of energetic particles into the inner magnetosphere. Solar active regions usually reach kilogauss values in their magnetic field. When the Earth-directed CME glances along the magnetic shield, local disturbances in the atmosphere of the Earth have been noticed. Cyclic changes of the general atmosphere circulation are of prime interest as are the transformation and recurrence of circulation forms, which characterize planetary wave dynamics. The changes of the atmospheric pressure in geomagnetically and electronically excited cases (including the solar activity effect) in comparison to the variations in geomagnetically and electronically quiet cases.

**Solar cycle 25** is the current solar cycle, the 25th since 1755, when extensive recording of solar sunspot activity began. It began in December 2019 with a minimum smoothed sunspot number of 1.8. It is expected to continue until about 2030.[ While it was initially predicted by most scientists that cycle 25 would be relatively weak, solar activity has been much stronger than the predictions.

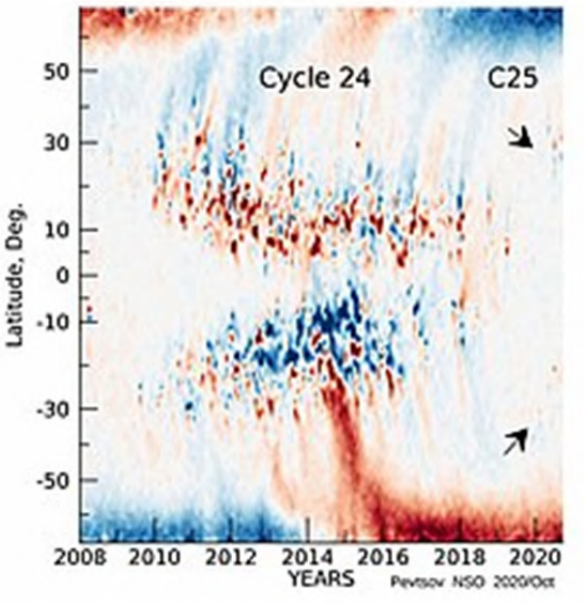



**Fig.1.** Time vs. solar latitude diagram of the radial component of the solar magnetic field (supersynoptic map or "butterfly" diagram) for cycle 24 based on the (zero-point corrected) integer rotation synoptic maps from GONG. Blue/red show negative/positive polarity fields scaled between ±5 Gauss. Two black arrows mark approximate location of two latitudinal bands of cycle 25. Data are acquired by GONG instruments operated by NISP/NSO/AURA/NSF.

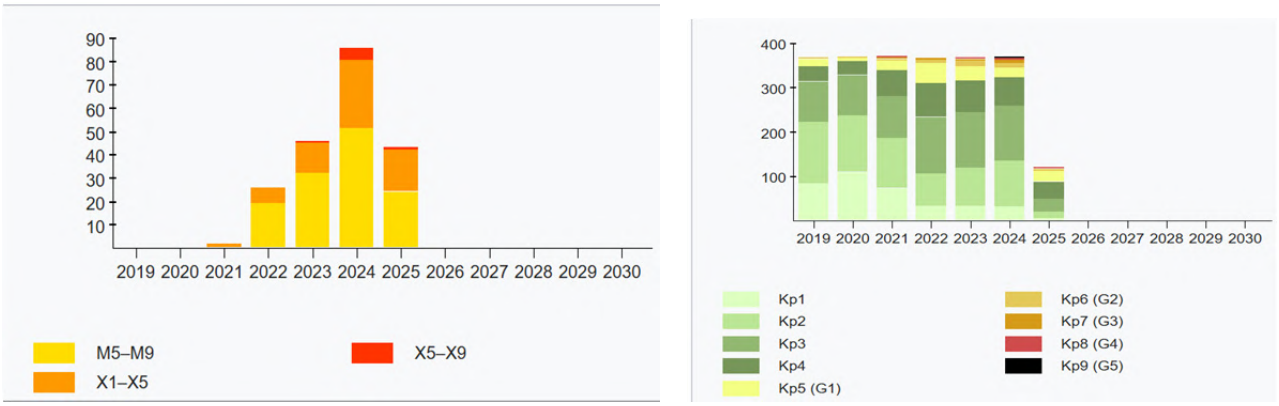



**Fig. 2.** (a)Solar flares by year (b) Days Number with geo-magnetic activity

The dependence of Temperature parameters on Solar induced geo-storms is shown on Fig.3 as case study for Tbilisi during 2025 January-February. Similar to previous studies (9, 12, 13, 14) in this case this dependence is also evident

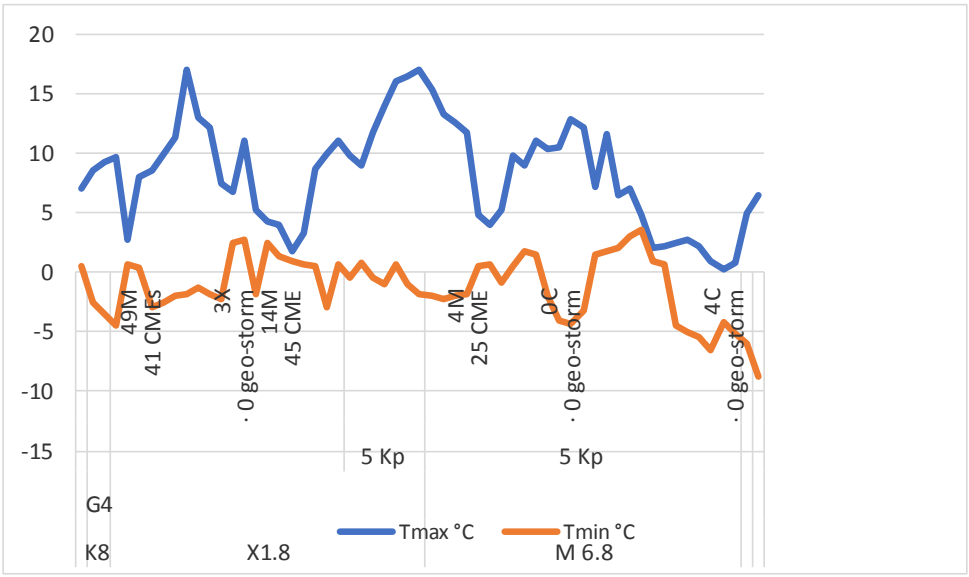



**Fig. 3.** Case study: Tmax and Tmin parameters variation in 2025 January-February in Tbilisi depending on geo-storms expressed in geo0indices.

## Conclusions

In most cases, the ability to predict the behavior of nature comes from a mathematical model. For example, the motion of an object falling in a gravitational field can be modeled using the mathematical expression $v = g \_ t$. Earth weather forecasters have been trying for the last 30 years to construct a mathematical model of the global weather using the very complex equations of fluid dynamics to describe the circulation of the oceans and atmosphere. Even with the best supercomputers to run these models, it has proven impossible to precisely model Earth weather. Modeling the solar-terrestrial environment is vastly more complex. The physics necessary to do this includes not only fluid dynamics but also Maxwell's equations. This combination is known as magnetohydrodynamics (MHD), and at the present time the equations of MHD cannot be completely solved analytically. Numerical solutions exist which involve the use of a computer in a "trial and error" fashion. Numerical solutions, however, can give incorrect results and at best are an approximation. There is some suspicion that we have not yet developed the physics necessary to fully understand the Sun, where strong magnetic fields are erupting and plasmas swirl at ultra-high temperatures. The issue needs further investigation applying quantum filed theory that is more suitable for description of photon-photon or photon-charged particle interaction [8-14]. It may be assumed that for weather forecasting the only existed

numerical weather models aren't sufficient and they have to be enhanced by electromagnetic models to make forecasting more precise.

**Acknowledgement:** The research was carried out with the financial support of the Shota Rustaveli National Science Foundation of Georgia. Grant # FR 25-16-929.

## References

1. Mlynczak M.G., Hunt L.A., Marshall B.T., Russell J.M. III, Mertens C.J., Thompson R.E., Gordley L.L., A Combined Solar and Geomagnetic Index for Thermospheric Climate. // Geophys. Res. Lett., 42, 2015, pp. 3677–3682. doi: 10.1002/2015GL064038.
2. Mlynczak M.G., Hunt L.A., Russell M.J. III, Marshall B.T., Thermosphere Climate Indexes: Percentile Ranges and Adjectival Descriptors. // Journal of Atmospheric and Solar-Terrestrial Physics, 2018. https://doi.org/10.1016/j.jastp.2018.04.004
3. Mlynczak M.G., Hunt L.A., Russell J. M. III, Marshall B.T., Mertens C.J., Thompson R.E., The Global Infrared Energy Budget of the Thermosphere from 1947 to 2016 and Implications for Solar Variability. // Geophys. Res. Lett., 43, 11, 2016, pp. 11934–11940. doi: 10.1002/2016GL070965
4. NASA Science Mission Directorate. https://science.nasa.gov
5. NOAA. Office of Satellite and Product Information. National Environmental Satellite, Data and Information Service.
6. NOAA/SWPC, Boulder, Co, USA. spaceweatherlive.com https://www.spaceweatherlive.com/en/archive/2022/01.html.
7. Tatishvili M., Developing Weather Forecasting System in Georgia. // Ecology & Environmental Sciences 2 (7), 2017. DOI:10.15406/mojes. 2017.02.00046.
8. Tatishvili M., Bolashvili N., Karalashvili T., & Suknidze N., Impact of Atmosphere Perturbation and Microcirculation on Tbilisi Thermal Regime. // Georgian Geographical Journal, 5(3), 2025, pp. 34–42. https://doi.org/10.52340/ggj.2025.05.03.05
9. Tatishvili M. Energy Transformation in Clouds According Quantum Principles. // International Scientific Journal. Journal of Environmental Science. vol 3. ISBN- 13: 978-1499721980; ISBN -10: 1499721986, Vienna, Austria 2014. pp. 7-9.
10. Tatishvili M., On Some Considerations of Cloud Particles and Photons Interaction. // Journal of the Georgian Geophysical Society, e-ISSN: 2667-9973, p-ISSN: 1512-1127 Physics of Solid Earth, Atmosphere, Ocean and Space Plasma, v. 24(2), 2022. DOI: https://doi.org/10.48614/ggs2420213324
11. Tatishvili M., Bolashvili N., Palavandishvili A. Impact of Short-Term Geomagnetic Activity on Meteorological Parameters Variability on The Middle Latituge Region. // Georgian Geographical Journal, Vol. 2, 2022. https://doi.org/10.52340/ggj.2022.756 2022
12. Tatishvili M., Mkurnalidze I., Samkharadze I., Tsintsadze N., Impact of Solar Coronal Mass Ejections (CME) on Formation of Earth Climate and Weather Pattern. // International Scientific Journal. Journal of Environmental Science. Vol.7, Iss 1, ISBN -13:978-1721539185, 2018, pp. 1-5.
13. Tatishvili M.R., Palavandishvili A.M., Impact of Short-Term Geomagnetic Activity on Weather and Climate Formation in Georgian Region. // Journal of the Georgian Geophysical Society, Physics of Solid Earth, Atmosphere, Ocean and Space Plasma, ISSN: 1512-1127, v. 23(2), 2020.
14. The US/UK World Magnetic Model for 2015-2020: Technical Report, National Geophysical Data Center, NOAA National Centers for Environmental Information. NOAA. 2017.

2nd International Scientific Conference "Modern Problems in Geophysics", Proceedings,
ISBN 978-9941-36-562-1, ISSN 3088-4349, Tbilisi, Georgia, October 29-31, 2026

# SOLAR ACTIVITY AND COSMIC RAYS: FROM THE MAY 2024 STORM TO CENTURIES OF SOLAR CYCLES

[*,**]Kharshiladze O., [*,**]Aslamazishvili M.

[*]*M. Nodia Institute of Geophysics of the I. Javakhishvili Tbilisi State University, Tbilisi, Georgia*
[**]*Ivane Javakhishvili Tbilisi State University, Tbilisi, Georgia*
*mariam.aslamazishvili722@ens.tsu.edu.ge*

***Abstract.*** *We study how solar activity controls the flux of galactic cosmic rays reaching the Earth on time scales from hours to centuries. During the extreme G5 geomagnetic storm of 10–11 May 2024, the neutron monitor of the Cosmophysical Observatory in Tbilisi recorded a Forbush decrease of about 7.5 %. Wavelet coherence between the interplanetary magnetic field (OMNI) and the Tbilisi cosmic-ray intensity is high ($R^2 > 0.8$) and significant from 8 to 20 May at periods of 10 hours to 4 days, directly linking the decrease to the magnetic structure of the coronal mass ejection. On decadal scales, Oulu neutron-monitor data (1964–2020) mirror the sunspot number over five solar cycles ($r = -0.87$) and show the alternating peaked and flat-topped maxima of the 22-year solar magnetic cycle. No significant relation is found with global temperature or low cloud cover over Tbilisi. Finally, a harmonic model built from the 11-, 22-, 88- and 208-year solar cycles reproduces three centuries of sunspot observations and points to the late 2040s as the next period of strongly enhanced solar activity.*

***Key words:*** *Cosmic rays, solar activity, Forbush decrease, wavelet coherence, solar cycle, climate.*

## Introduction

Galactic cosmic rays are high-energy charged particles that arrive at the Earth from outside the solar system. Before reaching the Earth, they must cross the heliosphere, where the solar wind and the magnetic field it carries partly shield the inner solar system. As a result, the cosmic-ray flux measured by ground-based neutron monitors follows solar activity in the opposite sense: it is lowest at solar maximum and highest at solar minimum, an effect known as solar modulation . On short time scales, coronal mass ejections (CMEs) sweep cosmic rays away from the Earth and cause sudden drops of several percent, called Forbush decreases.

Solar activity itself is not a single cycle. Besides the 11-year Schwabe cycle, the Sun shows the 22-year Hale cycle of magnetic polarity reversal, the ~88-year Gleissberg cycle and the ~208-year Suess–de Vries cycle. Because cosmic rays also ionize the lower atmosphere, it has been proposed that they could influence cloud formation and, through clouds, the climate. This idea is still debated and needs testing with long, independent data sets [1-7].

In this work we examine the connection between the Sun and cosmic rays on three-time scales. First, we model three centuries of solar activity as a superposition of four solar cycles. Second, we use wavelet coherence to link the May 2024 Forbush decrease, recorded by the Tbilisi neutron monitor, to the interplanetary magnetic field measured by spacecraft (OMNI). Third, we compare six decades of Oulu neutron-monitor data with the sunspot number, global temperature and low cloud cover over Tbilisi from the ERA5 reanalysis.

## Results and discussion

Representing solar activity as the sum of four known solar cycles (Fig. 1) (Schwabe, Hale, Gleissberg and Suess–de Vries) reproduces the rhythm of more than three centuries of sunspot observations, including the timing of the current maximum of cycle 25. The model has real predictive skill: built only from 1700–1899 data, it reproduces the 1900–2024 record ($r = 0.58$). Projected forward, it shows the strongest future maximum in 2047 (SSN ≈ 139), when the crests of the 11- and 22-year cycles coincide with the high phase of the 88-year Gleissberg cycle. This is a clear case of constructive interference of solar cycles. Because real cycle lengths vary, the exact year carries some uncertainty, but the model points to the late 2040s as a period of enhanced solar activity and, consequently, reduced cosmic-ray flux at Earth.

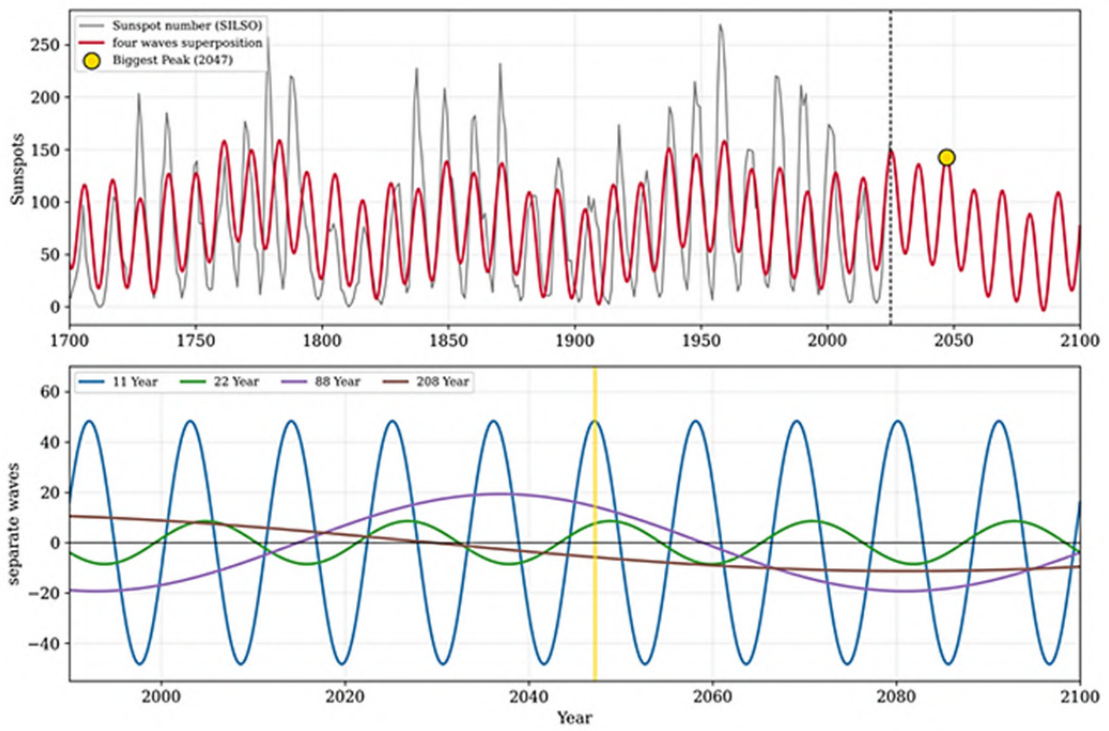



**Fig. 1.** Solar cycle superposition.

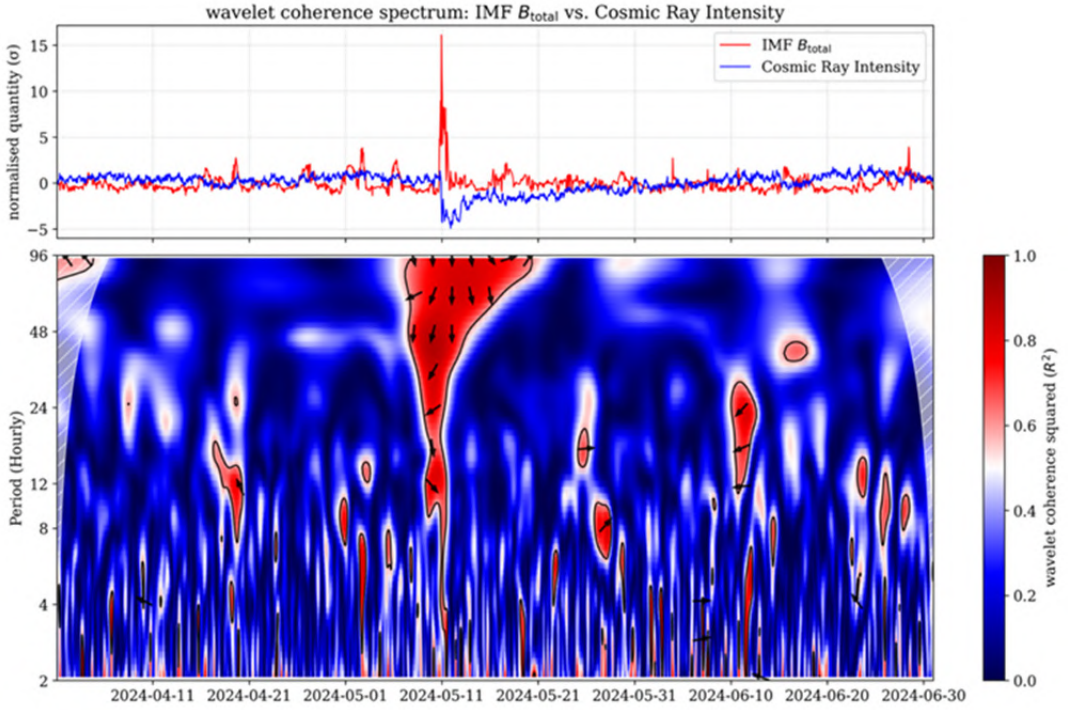



**Fig. 2.** Wavelet coherence of IMF B and cosmic ray intensity.

The wavelet coherence directly links the cosmic-ray decrease observed in Tbilisi to its cause in interplanetary space (Fig. 2). When the coronal mass ejection reached Earth on 10 May 2024, the magnetic field jumped to about 16σ above its mean, and at the same moment the cosmic-ray intensity fell by about 5σ. The two signals become strongly coherent ($R^2 > 0.8$) from 8 to 20 May across periods from about 10 hours to 4 days (Fig. 3). This shows that the magnetic structure of the CME controlled the cosmic-ray flux throughout the storm. The arrows point downward to down-left, meaning the two signals move in opposite directions with the cosmic rays lagging behind: the field enhancement passes within a day or two, while the cosmic-ray depression persists much longer. Smaller coherent areas around 19–21 April and 10–12 June coincide with weaker cosmic-ray decreases, so the method also picks out moderate disturbances.

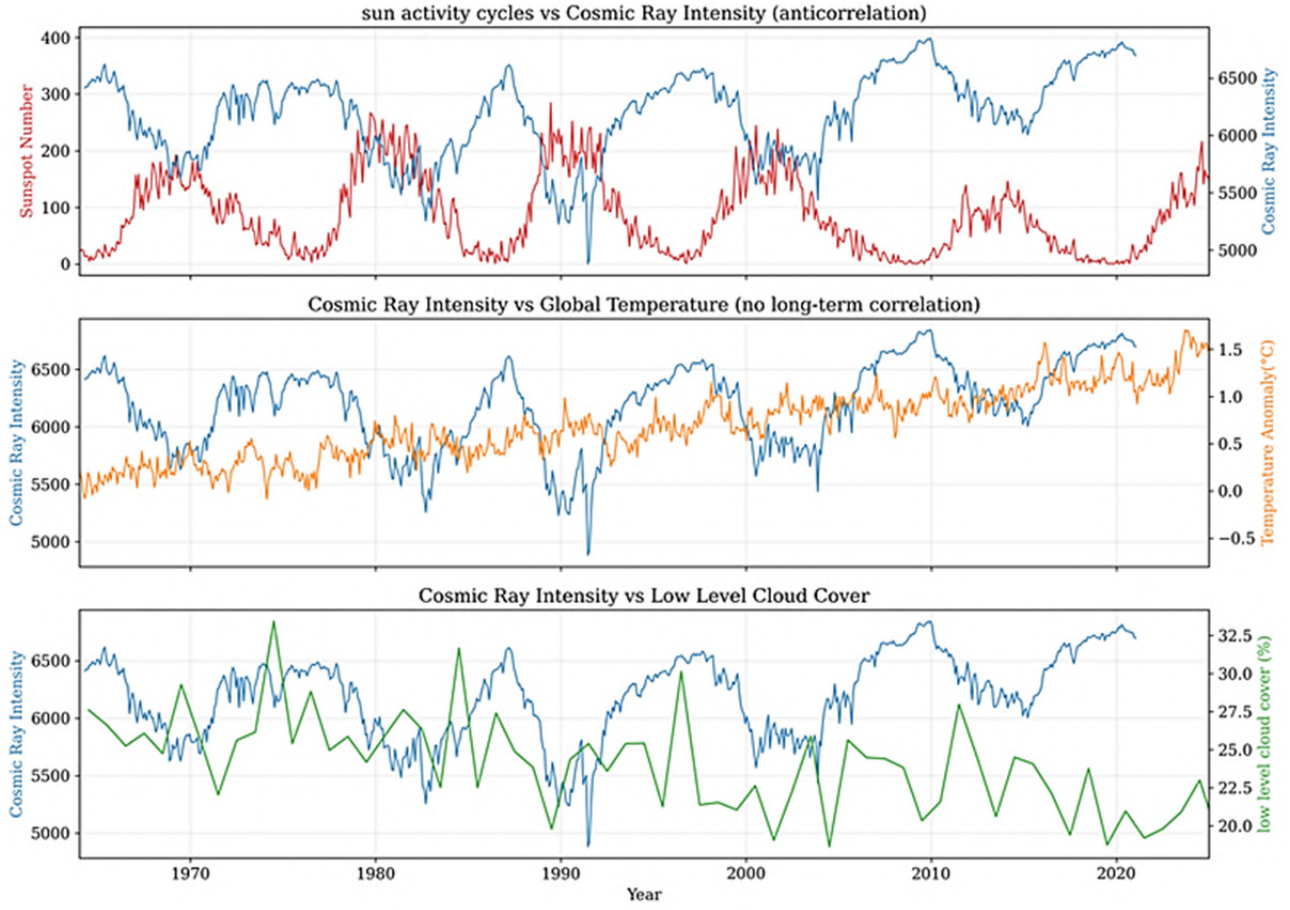



**Fig. 3.** Cosmic ray intensity (Oulu,1964-2020) compared with sunspot number, global temperature and low cloud cover over Tbilisi.

In quiet periods coherence is almost absent, confirming that cosmic rays at Tbilisi respond to large interplanetary structures rather than to small fluctuations of the field. Over five solar cycles, cosmic rays and solar activity behave as near-perfect mirror images (annual r = −0.87). Every solar maximum (1968, 1979, 1989, 2001, 2014) brings a deep cosmic-ray minimum a few months later, as the strengthened solar wind shields Earth more effectively. The cosmic-ray maxima alternate in shape, sharp in 1965, 1987 and 2009 and flat-topped in 1976, 1997 and 2020. This is a direct imprint of the Sun's magnetic field reversing every 11 years (the 22-year Hale cycle).

The record also captures the highest cosmic-ray flux of the space age during the deep solar minimum of 2009, as well as sharp storm-driven dips such as June 1991 and October 2003. The figure also tests the much-debated idea that cosmic rays influence climate through clouds. Global temperature rises steadily by about 1.2 °C while cosmic rays show no comparable trend; after removing long-term trends their correlation is only r = −0.12. Low cloud cover over Tbilisi decreases from about 27 % to 21 % with no matching change in cosmic rays (r = −0.14). The Sun therefore strongly controls the cosmic-ray flux reaching Earth, while recent warming and cloud changes over Tbilisi are driven by other factors.

## Conclusion

Cosmic rays measured at the Earth carry a clear imprint of the Sun on every time scale studied. During the G5 geomagnetic storm of May 2024, wavelet coherence directly linked the 7.5 % Forbush decrease observed in Tbilisi to the magnetic field of the coronal mass ejection. The two signals were strongly coherent ($R^2 > 0.8$) only during the disturbance, and the cosmic-ray depression lasted long after the field enhancement had passed. Over five solar cycles, cosmic rays mirror the sunspot number (r = −0.87) and reveal the 22-year magnetic cycle of the Sun through alternating peaked and flat-topped maxima. In contrast, neither global temperature nor low cloud cover over Tbilisi follows the cosmic rays, so recent warming and cloud changes are driven by other factors. A superposition of four known solar cycles reproduces three centuries of sunspot

observations and points to the late 2040s as the next period of strongly enhanced solar activity and reduced cosmic-ray flux. Together, these results show that long-term neutron-monitor observations, including those in Tbilisi, are a valuable tool for space-weather research and for testing proposed links between the Sun, cosmic rays and climate.

## References


1. Pikelner S., Physics of Interstellar Space.
2. Artsimovich L., Lukyanov S. Motion of charged particles in electric and magnetic fields.
3. Tsulukidze L. K., Kharshiladze O. A., Ghurchumelia A. P., Sorriso-Valvo L., Elbakidze K. Z., & Matiashvili T. G., Coherent Analysis of Intense Geomagnetic Disturbances Using Dusheti Observatory Data and the DST Index. // Journals of Georgian Geophysical Society, 27(2), 2024.
4. García-Farieta J. E., & Hurtado A., Simulation of charged particles in Earth's magnetosphere: An approach to the Van Allen belts, 2024.
5. https://cosmicrays.epizy.com/index.php?opt=home&i=1
6. https://omniweb.gsfc.nasa.gov/cgi/nx1.cgi
7. Webber, Charles & Marwan N., Recurrence Quantification Analysis, Theory and Best Practices, 2015. Doi: 10.1007/978-3-319-07155-8.

2nd International Scientific Conference "Modern Problems in Geophysics", Proceedings,
ISBN 978-9941-36-562-1, ISSN 3088-4349, Tbilisi, Georgia, October 29-31, 2026

# INTERMITTENCY IN THE GEOSPACE DURING THE 2024 MOTHER'S DAY STORM

[*,**]Kharshiladze O., [*,**]Martiashvili M., [***,****]Sorriso-Valvo L., [**]Zilpimiani D., [*,**]Mchedlishvili G.

[*]*Ivane Javakhishvili Tbilisi State University, Tbilisi, Georgia.*
[**]*Mikheil Nodia Institute of Geophysics of Ivane Javakhishvili Tbilisi State University, Tbilisi, Georgia.*
[***]*Department ofElectromagnetics and Plasma Physics, School of Electrical Engineering and Computer Science, KTH Royal Institute of Technology, Stockholm, Sweden,*
[****]*Institute for Plasma Science and Technology (ISTP), National Research Council (CNR), Rende, Italy*
*mariam.martiashvili971@ens.tsu.edu.ge*

***Abstract.*** *We analyzed L1 Lagrange point solar wind data from the OMNI database using the Local Intermittency Measure (LIM). The main phase of the geomagnetic storm showed a sharp rise in turbulence and intermittency (FF > 3). These nonlinear dynamics directly correlate with fluctuations in the magnetospheric Dst and AL indices the very drivers behind the May 2024 aurora borealis observed over Georgia.*

***Key words:*** *Geomagnetic storm, Solar wind, Intermittency, Turbulence, Wavelet transform.*

## Introduction

The Sun's hot coronal plasma routinely escapes gravitational pull, expanding into space as the solar wind. At solar maximum, frequent magnetic reconnection triggers coronal mass ejections (CMEs) and powerful flares. When this energetic plasma hits Earth's magnetosphere, severe space weather follows. Specifically, high dynamic pressure combined with a strong southward interplanetary magnetic field ($B_z < 0$) compresses the magnetosphere and drives powerful electric currents.

Scientists track these storms using the Dst and AL indices. During extreme events ($Dst < -250\,nT$), energetic particles stream along magnetic field lines into the upper atmosphere, exciting ambient gas to form auroras. On May 10-13, 2024, Earth experienced an extraordinary G5-class storm. A severe drop in the Dst index pushed the auroral oval far southward, bringing visible northern lights even to mid-latitude regions like Georgia.

## Theoretical Foundations and Methodology (LIM Technique)

Multiscale and intermittent processes play a central role in space plasma dynamics and plasma sheet turbulence (Vörös et al., 2004). Intermittency itself reflects an uneven energy dissipation across space and time periods of relative calm punctuated by sudden, high-energy bursts. In the turbulent solar wind and interplanetary magnetic field, this behavior takes on a multifractal character (Burlaga, 1991). At smaller timescales, magnetic field and velocity fluctuations stray sharply from standard Gaussian statistics (Marsch & Tu, 1994, 1997; Sorriso-Valvo et al., 1999).

To track this non-Gaussian behavior during geomagnetic storms, we applied the Local Intermittency Measure (LIM) technique (Bruno et al., 2001). Comparing the probability density function (PDF) of the interplanetary magnetic field $B_z$ component against a theoretical Gaussian curve showed clear discrepancies, marking both non-Gaussian dynamics and the formation of localized coherent structures. Crucially, the distribution's "heavy tails" confirm that extreme plasma fluctuations stem from nonlinear processes rather than random background noise.

Mathematically, we compute the wavelet coefficients $w(\tau, t)$ from the time-domain signal $f(t)$ by integrating the signal with a transformed wavelet function $\psi$, shifted in time $(t)$ and scaled by $(\tau)$ (Arancibia Riveros, K., M., 2008):

$$w(\tau, t) = \int f(t') \frac{1}{\sqrt{\tau}} \psi \left( \frac{t' - t}{\tau} \right) dt'$$

In this analysis, the Morlet wavelet was used as the basis:

$$\psi(t) = \pi^{-\frac{1}{4}} e^{i \omega_0 t} e^{-\frac{t^2}{2}}$$

According to Parseval's theorem, the squared wavelet coefficient $|w(\tau, t)|^2$ quantifies the fluctuation energy at a specific scale $\tau$ and time t. Farge (1990) leveraged this property to define the Local Intermittency Measure (LIM) as the ratio between local energy and its temporal mean:

$$LIM(\tau, t) = \frac{|w(\tau, t)|^2}{\langle |w(\tau, t)|^2 \rangle_t}$$

A value of $LIM(\tau, t) = 1$ indicates that the energy is uniformly distributed across time and the system exhibits no intermittency, whereas $LIM(\tau, t) > 1$ (Fig. 1).

Following Meneveau and Sreenivasan (1991), one can extract the flatness factor $FF(\tau)$ or kurtosis of the wavelet coefficients directly from the mean square of the $LIM(\tau, t)$:

$$FF(\tau) = \langle LIM^2(\tau, t) \rangle_t$$

Crucially, Meneveau (1991) showed that the flatness of wavelet coefficients at scale $\tau$ mirrors the flatness of the raw data at that exact scale. For a standard Gaussian distribution, the flatness factor caps at $FF = 3$. Any departure above this threshold ($FF > 3$) breaks Gaussian expectations, pointing directly to strong turbulence intermittency and coherent structure formation in the plasma (Fig. 2).

## Data Analysis and Results (OMNI Database)

For our analysis of the May 11-12, 2024 geomagnetic storm, we downloaded high-resolution solar wind parameters from NASA's OMNI database. The dataset combines L1 (Lagrange point, approximately 1.5 million kilometers from Earth) orbit measurements from ACE, WIND, and DSCOVR at a 1-minute time resolution. Specifically, we extracted the interplanetary magnetic field components ($B_x, B_y, B_z$), solar wind speed ($V_{sw}$), z-component of velocity ($V_z$), and dynamic pressure ($P_{sw}$). To assess the geomagnetic response, we paired these solar wind inputs with the 1-hour Dst index [1]. Prior to calculating intermittency, we checked the time series for missing values and removed quiet-time baselines to isolate storm-time fluctuations.

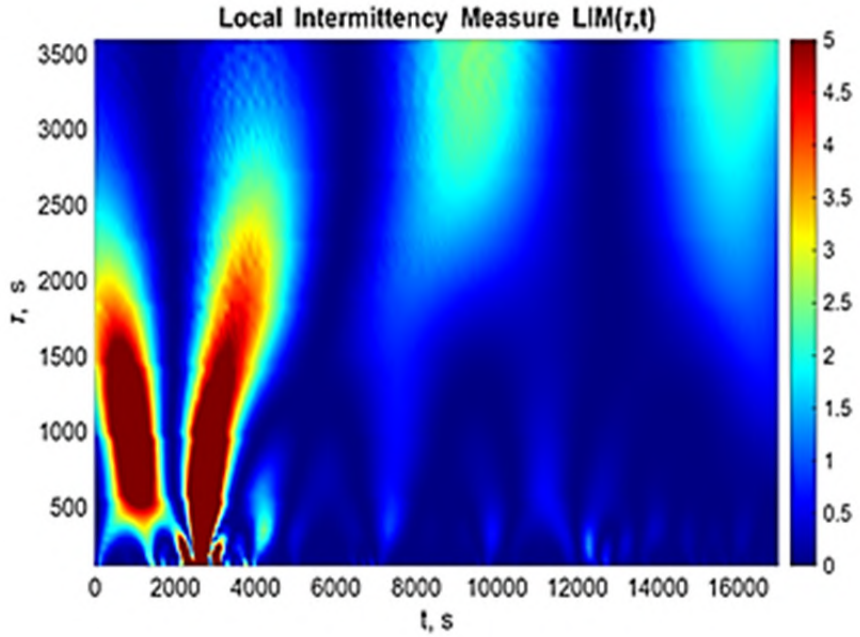



**Fig. 1.** Example of the Local Intermittency Measure LIM ($\tau$, $t$).

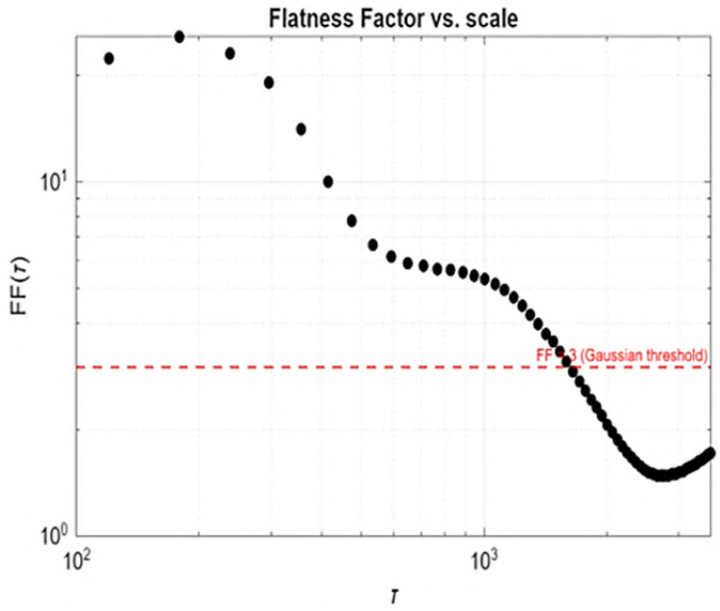



**Fig. 2.** Example of Flatness Factor, obtained frome LIM ($\tau$, $t$).

The analysis revealed that during the initial phase of the storm ($t < 500$ min), the negative peaks of the $B_z$ component ($-40$ nT), the increase in $P_{sw}(> 50\,nPa)$, and the rise in $V_{sw}$ up to (1000 km/s) directly induce a sharp depression in the Dst index and the excitation of the ring current (Fig. 3).

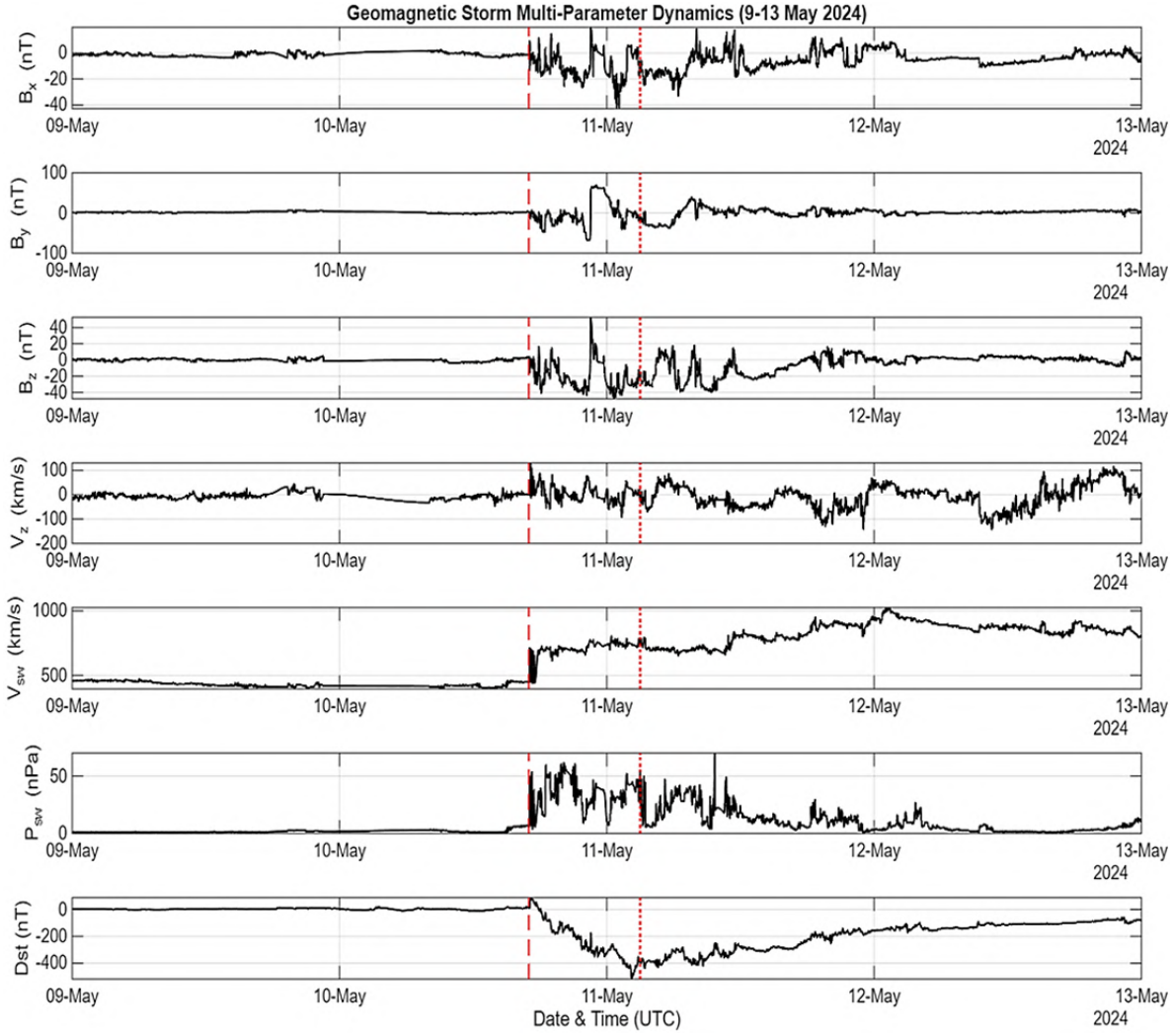



**Fig. 3.** Time dynamics of solar wind and geomagnetic parameters obtained from the OMNI database (May 9-13, 2024).

Look at Fig. 4. Here, $B_z$ and $V_{sw}$ shift away from stationary, random Gaussian rules during the storm. This non-Gaussian behavior shows up alongside a multimodal probability density function (PDF). Together, these features show that storm-time solar wind and interplanetary magnetic fields form an intertwined, nonlinear, turbulent setup.

In physical terms, plasma dynamics under storm conditions are not simple background noise. The heavy tails and multimodal PDF show something else. They mark the presence of intermittent, high-amplitude bursts and coherent structures. These structures include current sheets and magnetic flux tubes inside the flow. Energy does not release in a smooth manner. Instead, it comes out in short, localized bursts. This intermittent pattern boosts energy transfer across the magnetopause way above what standard linear models predict. In the end, this bursty energy input sustains the full geomagnetic storm.

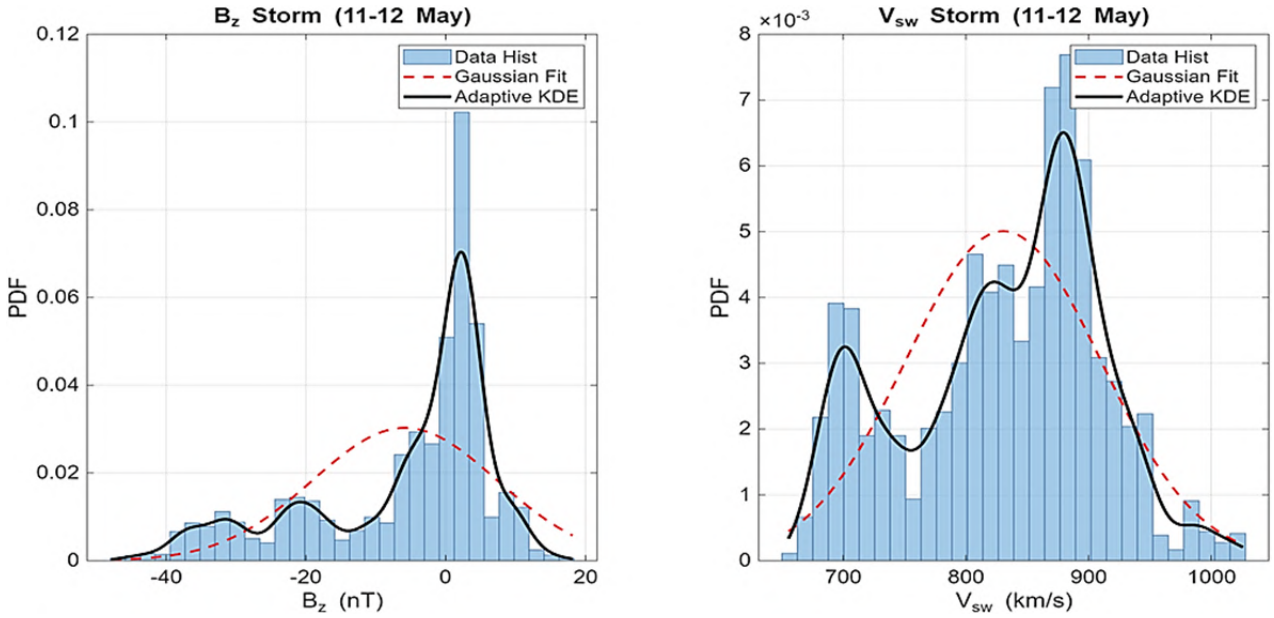



**Fig. 4.** Probability density function (PDF) of $B_z$ and $V_{sw}$ parameters.

## Conclusion

Intermittency marks specific time intervals with strong spatial and temporal correlations. These coherent structures dominate small-scale fluctuation statistics. Also, they outlive the surrounding background noise. Put simply, intermittency stems directly from non-Gaussian structures forming inside an otherwise stochastic Gaussian background.

By applying the LIM methodology to OMNI data, we showed how intermittent solar wind turbulence drives efficient energy transfer into Earth's magnetosphere. This process triggers sharp drops in geomagnetic indices like Dst and AL. During the May 2024 event, these nonlinear solar wind dynamics excited the magnetosphere so intensely that the auroral oval stretched far south. As a result, the aurora borealis became visible even over mid-latitudes like Georgia.

**Acknowledgement:** The Research was supported by Shota Rustaveli National Science Foundation of Georgia Grant FOR-25-1725.

## References

1. Kharshiladze O. A., Tsulukidze L. K., & Martiashvili M. J., Wavelet Coherence Analysis of Magnetic Declination During Quiet and Disturbed Geomagnetic Activity. // Journals of Georgian Geophysical Society, 28(1), 2025. https://ggs.openjournals.ge/index.php/GGS/article/view/9252
2. Arancibia Riveros K., Stepanova M., Bosqued J. and Antonova E., Study of the turbulence in the central plasma sheet during August 24-28 geomagnetic storm using the CLUSTER satellite data. // Geofísica Internacional, 47(3), 2008, pp. 265-271.

3. Bruno R., Carbone V., Veltri P., Pietropaolo E., & Bavassano B., Identifying coherent structures in the solar wind turbulence. // Planetary and Space Science, 49(12), 2001, pp. 1201–1210.
4. Burlaga L. F., Multifractal structure of the interplanetary magnetic field: 1 to 5 AU. // Journal of Geophysical Research: Space Physics, 96(A4), 1991, pp. 5847–5851.
5. Farge M., Wavelet transforms and their applications to turbulence. // Annual Review of Fluid Mechanics, 24(1), 1992, pp. 395–458.
6. Marsch E., & Tu C. Y., Non-Gaussian probability distributions of solar wind fluctuations. // Annales Geophysical, 12(12), 1994, pp. 1127–1138.
7. Meneveau C., & Sreenivasan K. R., The multifractal nature of turbulent trajectories and energy dissipation. // Journal of Fluid Mechanics, 224, 1991, pp. 429–484.
8. Sorriso-Valvo L., Carbone V., Veltri P., Consolini G., & Bruno R., Intermittency in the solar wind turbulence through probability distribution functions of magnetic field fluctuations. Geophysical Research Letters, 26(13), 1999, pp. 1801–1804.
9. Vörös Z., Jankovičová D., & Kovács P., Scaling and intermittency in solar wind–magnetosphere coupling. // Space Science Reviews, 111(1), 2004, pp. 123–143.

2nd International Scientific Conference "Modern Problems in Geophysics", Proceedings,
ISBN 978-9941-36-562-1, ISSN 3088-4349, Tbilisi, Georgia, October 29-31, 2026

# STUDY OF THE FORBUSH EFFECT OF COSMIC RAYS ON JANUARY 18-27, 2026

[*,**]Vanishvili G., [*]Alania E., [*]Bakradze T., [*]Ghlonti N., [*]Kiria J.,[*]Erkomaishvili T., [*]Kavlashvili V., [*]Takadze G., [*]Demurishvili Z., [*]Barbakadze P., [*]Peikrishvili M.,[*]Tinikashvili A., [*]Aslamazishvili M.

[*]*Ivane.Javakhishvili Tbilisi State University, Micheil Nodia Institute of Geophysics, Tbilisi, Georgia*
[**]*Sokhumi State University, Tbilisi, Georgia*
*g.vanishvili@sou.edu.ge*

***Abstract.*** *The article discusses the neutron component intensity data of 15 stations of the World Wide Web of Cosmic Rays operating from January 18 to January 27, 2026, for the following stations: Apatity, Inuvik, Kerguelen, Newark, Oulu, Terre-Adélie, Yakutsk, Moscow, Irkutsk, JungFrauJoch, Kiel, Lomnicky Shtit, Athens, Rome, Tbilisi.*

***Key Words:*** *Coupling Coefficient, Energy Spectrum, Primary and Secondary Cosmic Rays, Forbush decrease*

## Introduction

On January 18, 2026 Sun erupted with a powerful X1.9 class solar flare that launched a fast full-halo coronal mass ejection (CME) toward Earth. This CME's shockwave arrived on January 19, 2026, triggering a severe geomagnetic storm and a sudden, sharp global Forbush decrease in galactic cosmic ray intensity (https://www.irap.omp.eu/en/2026/01/all-about-the-solar-flare-of-january-18-2026/).

## Materials and Methods

Galactic Cosmic Rays energy Spectrum during January 18-27 2026 Forbush decrease was calculated by method developed by Prof. Alania M. V. [1-6, 8-10]. Method of intensity ratio calculates the energy spectrum of cosmic rays from graph relations between function **M** and its argument **γ: M = M( γ) ,** where **M** is the ratio of intensities at two distinct points, registered by the Neutron Monitors of The World Wide network of Cosmic Rays and M( γ) is the ratio of two integrals, corresponding to the theoretical value of Cosmic ray intensity for the selected pair of Cosmic Ray Stations. The theoretical value of Cosmic ray intensity for each station is calculated by the following formula :

$$\int_{R}^{\infty} R^{-\gamma} W dR,$$

where W is the coupling coefficient. Coupling Coefficients used in the method were calculated by method proposed by Xaplanteris [7].

The set of selected stations is divided into three groups; high latitude, mid latitude, and low latitude stations.The high-latitude station group includes 7 stations: Apatity, Inuvik, Kerguelen, Newark, Oulu, Terre-Adelie, Yakutsk; The middle-latitude station group includes 5 stations: Moscow, Irkutsk, Jungfrau-joch, Kiel, Lomncky Stit; The low-latitude station group includes 3 stations: Athens, Rome, Tbilisi.

Fig.1 Shows the amplitudes of the change in the intensity of the neutron component of the global cosmic ray network during the Forbush decrease January 18-27, 2026, for stations in all three groups and 15 stations: Apatity, Inuvik,Kerguelen, Newark, Oulu, Terre-Adélie, Yakutsk, Moscow, Irkutsk, JungFrauJoch, Kiel, Lom-nicky Shtit, Athens, Rome, Tbilisi.

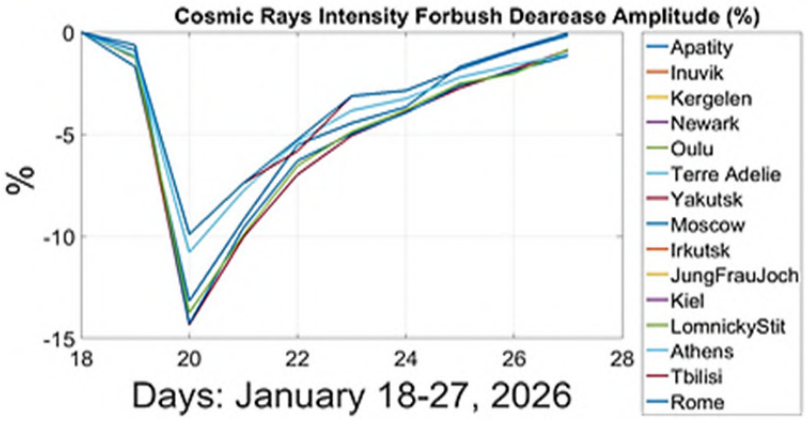



**Fig. 1.** January 18-27, 20206 Forbush decrease amplitudes for Cosmic Ray intensity changes.

Fig 2. Shows dependence M = M(γ) for Cosmic Ray Intensity ratio on the energy spectrum index for Athens/Tbilisi and Athens/Rome, at low latitudes.

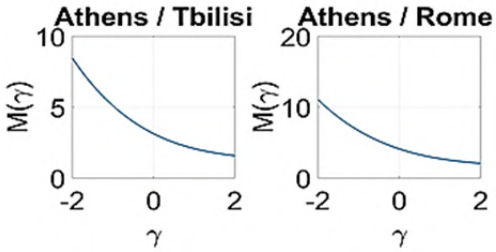



**Fig. 2.** M = M(γ) for lower latitudes.

Fig. 3 Shows the dependence of Cosmic Rays Intensity ratios on the energy spectrum index for two pair of stations at the lower latitudes: Athens/Tbilisi and Athens/Rome, at low latitudes, and energy spectrum index changes in the range: **0.9264 < γ < 1.5509**

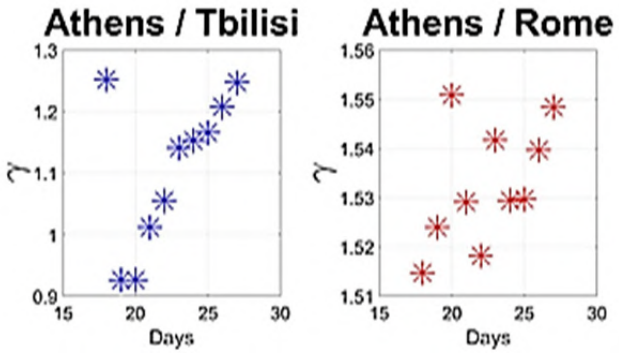



**Fig. 3.** Energy spectrum index γ, lower latitudes.

Fig. 4 Shows Dependence M = M(γ) for Cosmic Ray Intensity ratio on the energy spectrum index, for Moscow/Irkutsk, Moscow/Jungfraujoch, Moscow/Kiel, Moscow/Lomnicky Stit, at middle latitudes

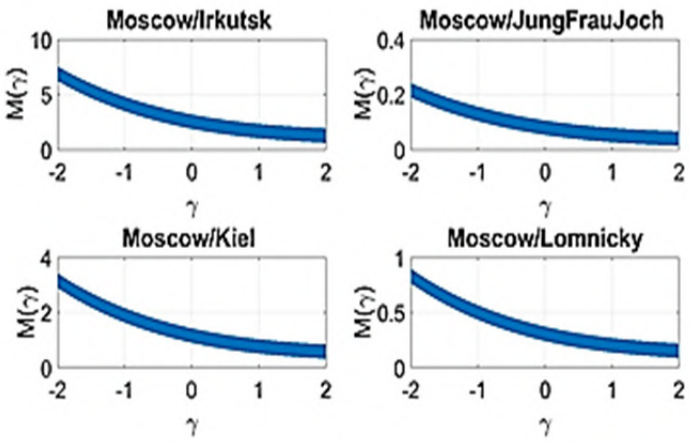



**Fig. 4.** M = M(γ) for middle latitudes.

Fig. 5. Shows Cosmic Rays energy spectrum index γ for two pair of stations, Moscow/Irkutsk, Moscow/ Jungfraujoch, Moscow/Kiel, Moscow/Lomnicky Stit. at middle latitudes, and energy spectrum index changes in the range: **-0.1010 < γ < 0.082200.**

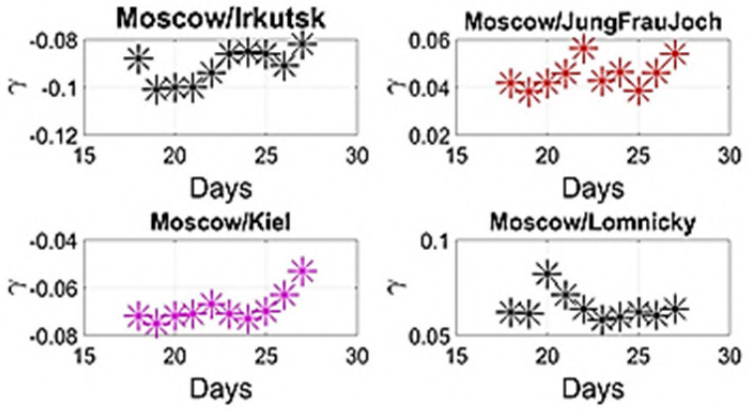



**Fig. 5.** Energy spectrum index γ, middle latitudes.

Fig. 6. Dependence M = M(γ) for Cosmic Ray Intensity ratio on the energy spectrum index γ for Apatity/Inuvik, Apatity/Kergelen, Apatity/Newark, Apatity/Oulu, Apatity/ TerreAdélie, Apatity/Yakutsk, at higher latitudes during January 18-27, 2026 Forbush-effect.

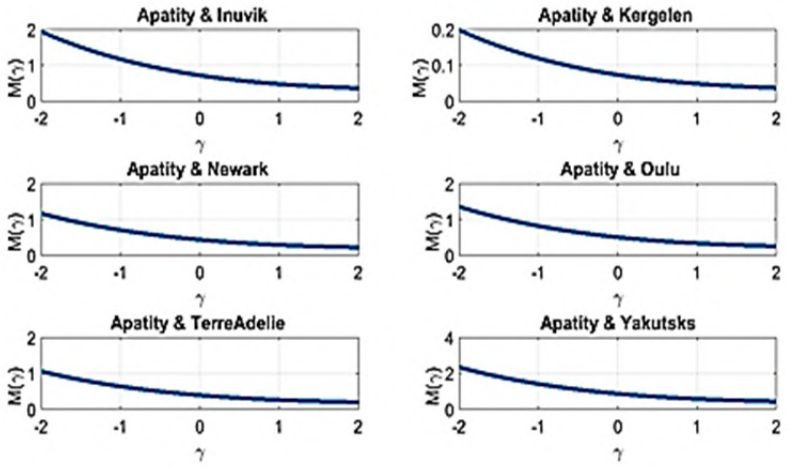



**Fig. 6.** M = M(γ) for higher latitudes.

Fig. 7. Shows Cosmic Rays energy spectrum index γ for two pair of stations, Apatity/Inuvik, Apatity/ Kergelen, Apatity/Newark, Apatity/Oulu,Apatity/ Terre-Adélie, Apatity/Yakutsk,at higher latitudes. and energy spectrum index changes in the range: **-1.8230 < γ < -1.0720 .**

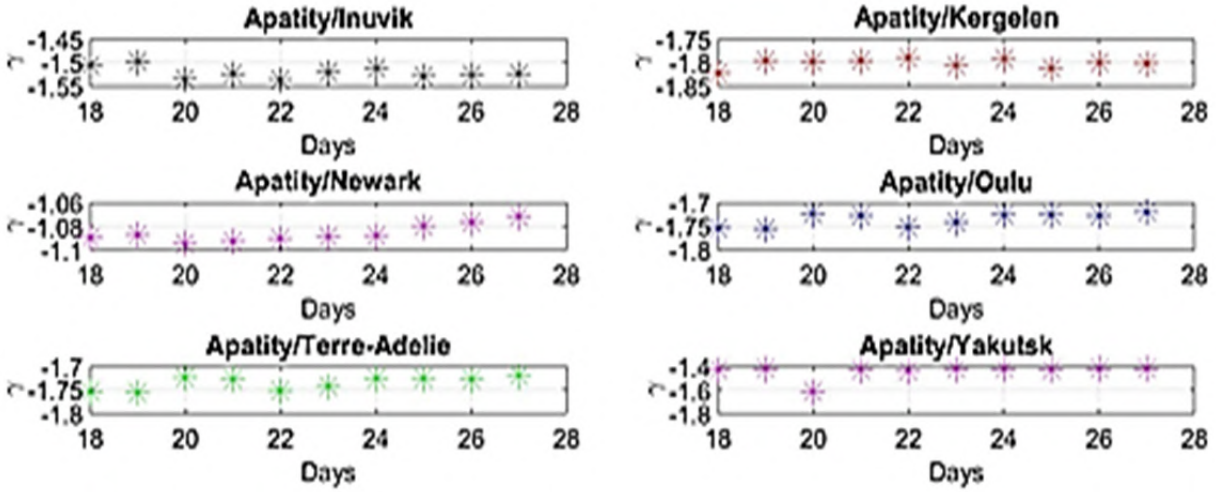



**Fig. 7.** Energy spectrum index γ, higher latitudes.

Table 1 shows the range of change of the cosmic rays energy spectrum index γ during January 18-27, 2026 Forbush effect

**Table 1.** The range of cosmic rays energy spectrum index, during January 18-27, 2026 Forbush Effect.

| Location | Low latitudes | Middle latitudes | High latitudes |
|---|---|---|---|
| Cut of rigidity range | R>6 GV | 2GV < R < 6 GV | 0 GV< R< 2GV |
| $\gamma_{max}$ | 1.5509 | 0.082200 | -1.0720 |
| $\gamma_{min}$ | 0.9264 | -0.1010 | -1.8230 |

## Conclusion

The energy spectrum of the Forbush effects of cosmic rays according to the data of the Neutron Monitor data with the lower CutOff Rigidity is softer than that of the second group Neutron Monitor Data with the higher CutOff Rigidity.

## References


1. Alania M.V., Dorman L.I., Aslamazashvili R.G., Gushchina R.T., Dzhapiashvili T.V., Modulation of galactic cosmic rays by the solar wind. // Tbilisi, "Metsniereba", 1987. (in Russian)
2. Alania M.V., and Wawrzynczak A., On the Relationship of the Interplanetary Magnetic Field Turbulence and the Energy Spectrum of The Forbush Effects. // 29-th International Cosmic Rays Conference Pune 1, 2005, pp. 371-374.
3. Alania M.V., Iskra K., Siluszyk M., New index of The galactic cosmic ray intensity variations. // Advances in Space Research, 41, 2006, pp. 267–274. https://events.lip.pt/2006/ecrs/proc/ecrs06-s2-44.pdf
4. Bochorishvili T., Experimental and model studies of the energy spectrum of long-term variations of cosmic rays. // Tbilisi, 1990. (in Russian)
5. Dorman L. I., Variations of Cosmic Rays. // Moscow, "Main Publishing House of Technical Literature," 1957. (in Russian)
6. Siluszyk M., Alania M.V., Iskra K. and Miernicki S., Interplanetary Magnetic Field Turbulence and Rigidity Spectrum of the Galactic Cosmic Rays Variations (1969 – 2011). // Journal of Geophysical research: Space physics, 2018, pp. 30-38.
7. Xaplanteris L., LivadaM., Mavromichalak H., "Cosmic ray spectral index by two coupling functions using data from the neutron monitor network". https://register-as.oma.be/esww16/contributions/public/S3-P1/S3-P1-20-KsaplanterisLoukas/ESWW16S3P20XAPLANTERISetal.pdf
8. Alania E., Bochorishvili T., Aslamazashvili R., Bakradze T., Glonti N., Kiria J., Erkomaishvili T., Belov A., Yanke V., Gushchina R., Eroshenko E., Wawrzynczak A., Vanishvili G., Energy Spectrum of the March 1989 Forbush Decrease. // JOURNAL OF THE GEORGIAN GEOPHYSICAL SOCIETY, Physics of Solid Earth, Atmosphere, Ocean and Space Plasma Vol. 28 , № 1, 2025, pp. 96-105
9. Alania E., Bochorishvili T., Aslamazashvili R., Bakradze T., Glonti N., Kiria J., Erkomaishvili T., Vanishvili G., "ENERGY SPECTRUM OF THE JUNE 2025 FORBUSH DECREASE", 2025.
10. 1st International Scientific Conference "Modern problems in Geophysics". // Proceedings, ISBN 978-9941-36-434-1, ISSN 3088-4349, Tbilisi, Georgia, November 6-8, 2025, pp. 268 – 270.
11. Vanishvili G., Bakradze T., Alania E., Erkomaishvili T., Kavlashvili V., Gugunashvili M., Iluridze N., "10 October 20 – November 10, 2003 Forbush Decrease Energy Spectrum" submitted to "Bulletin of Georgian National Academy of Sciences" on June 2026.

2nd International Scientific Conference "Modern Problems in Geophysics", Proceedings,
ISBN 978-9941-36-562-1, ISSN 3088-4349, Tbilisi, Georgia, October 29-31, 2026

# CORRELATION BETWEEN DAILY SUNSPOT NUMBERS, COSMIC RAYS, AND MORTALITY DURING JUNE 23-30 FORBUSH DECREASE

**[*,**]Vanishvili G., [*]Alania E., [*]Amiranashvili A., [*]Bakradze T., [*]Ghlonti N., [*]Kiria J., [*]Erkomaishvili T., [*]Kavlashvili V., [*]Takadze G., [*]Demurishvili Z., [*]Barbakadze P., [*]Peikrishvili M., [*]Tinikashvili A., [*]Aslamazishvili M.**

*[*]Ivane.Javakhishvili Tbilisi State University, Micheil Nodia Institute of Geophysics, Tbilisi, Georgia*
*[**]Sokhumi State University, Tbilisi, Georgia*
*g.vanishvili@sou.edu.ge*

***Abstract.*** *The article discusses the correlation between the intensity of the neutron component of cosmic rays, the number of sunspots, and mortality based on Tbilisi data, for two different cases, throughout 1980, and during the Forbush effect of June 1980.*

***Key Words:*** *Correlation coefficient, cosmic rays, sunspot numbers, Forbush-effext.*

## Introduction

Based on the Tbilisi Mortality Data, correlation with Cosmic Ray Intensity and Daily Sunspot Numbers has been studied. Tbilisi Mortality data, Moscow Neutron Monitor data and Daily Sunspot data for the whole 1980 period (Fig 1) and only for 1980 June Forbush period (Fig.2) were studied. The correlation coefficient between mortality and cosmic ray intensity, mortality and Sunspot Numbers, and cosmic ray intensity and Sunspot Numbers were calculated using the formula for the correlation function [1,2].

Cosmic rays and sunspots are highly anti-correlated during the Forbush effect (Table 1), and there is no correlation between cosmic rays and sunspots throughout the year (Table 2).

There is a low correlation between cosmic rays and mortality during the Forbush effect (Table 1), and there is no correlation between cosmic rays and mortality throughout the year (Table 2).

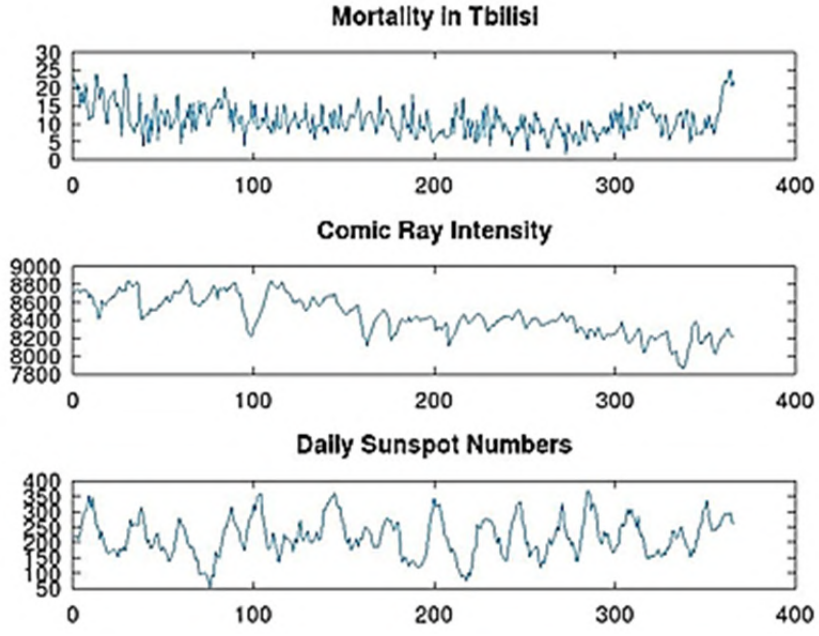



**Fig. 1.** Mortality in Tbilisi, Cosmic Ray intensity and Sunspot numbers during whole year 1980.

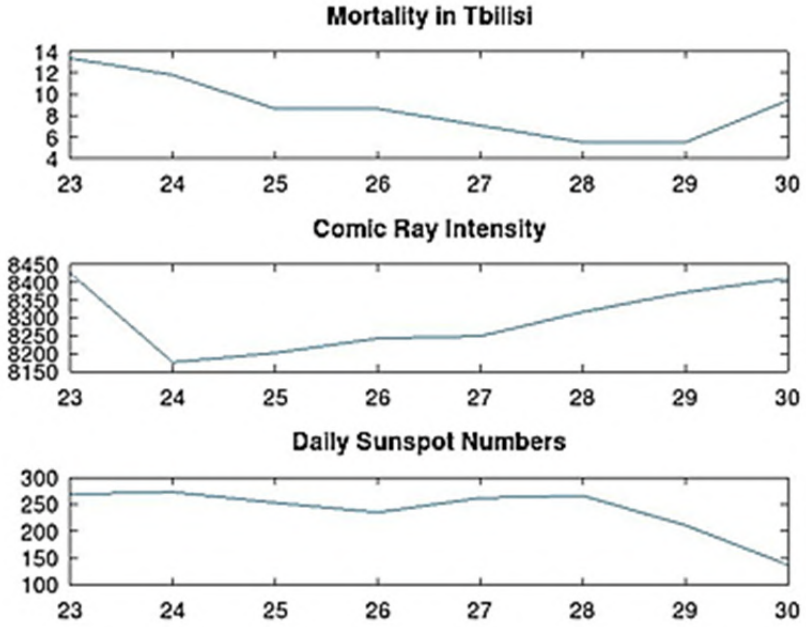



**Fig. 2.** Mortality in Tbilisi, Cosmic Ray intensity and Sunspot numbers during 1980 June 23-30 Forbush effect.

There is no correlation between sunspots and mortality during the Forbush effect(Table 1), and there is a low correlation between sunspots and mortality throughout the year (Table 2).

**Table 1.** Correlation between Mortality in Tbilisi, Cosmic Ray intensity and Sunspot numbers during whole year 1980.

| Correlation for the entire period of 1980 | | |
|---|---|---|
| Correlation criterion | Correlation coefficient | Correlation estimation |
| Mortality and Cosmic Rays | 0.1993 | Low correlation |
| Mortality & Sunspot Numbers | -0.0026 | No correlation |
| Cosmic Rays & Sunspot numbers | -0.0637 | No correlation |

**Table 2.** Correlation between Mortality in Tbilisi, Cosmic Ray intensity and Sunspot numbers during 1980 June 23-30 Forbush effect.

| Correlation during June 23-30, 1980 during Forbush-effect | | |
|---|---|---|
| Correlation criterion | Correlation coefficient | Correlation estimation |
| Mortality and Cosmic Rays | 0.0491 | No correlation |
| Mortality & Sunspot Numbers | 0.1511 | Low correlation |
| Cosmic Rays & Sunspot numbers | -0.5076 | High anti-correlation |

## Conclusion

Thus, there is no correlation between cosmic rays and mortality throughout the year, and between sunspots and mortality during the Forbush effect, and between cosmic rays and sunspots throughout the year. Thus, there is a low correlation between cosmic rays and mortality during the Forbush effect, and between sunspots and mortality throughout the year. Thus, cosmic rays and sunspots are highly anti-correlated with each other during the Forbush effect.

## References

1. Shiriaev A., Probability – 1., // Tbilisi State University Publishing House", Tbilisi, 405, 2018, 82 p.
2. Dorman L.I., Experimental and Theoretical Foundations of Cosmic Ray Astrophysics. // "Science", Moscow, 1975, 333 p.

# Content


| N | Autors – Paper | pp. |
|---|---|---|
| 1 | Kereselidze Z., Varamashvili N. – COMPARATIVE ANALYSIS OF THE 2023 SHOVI AND 2026 NEPAL CATASTROPHES | 3 |
| 2 | Nazaretyan S., Igityan H., Kazarian H., Harutyunyan R., Mirzoyan L., Bakunts S., Petrosyan V. – SOME REASONS FOR THE INCREASE IN SEISMIC RISK OF RESIDENTIAL BUILDINGS IN ARMENIA IN 1920-2020 | 6 |
| 3 | Tsereteli N. – NEW APPROACHES TO SEISMIC HAZARD ASSESSMENT IN SECOND-GENERATION EUROCODE 8: FROM PGA TO SPECTRAL REPRESENTATION | 11 |
| 4 | Amilakhvari D., Davitashvili T. – MODELLING THE EVOLUTION OF MAIN CHARACTERISTIC PARAMETERS OF THE BUBA, TBILISA, AND CHANCHAKHI GLACIERS UNDER CURRENT CLIMATE CHANGE CONDITIONS | 15 |
| 5 | Amiranashvili A., Chikhladze V., Samkharadze I., Pipia M. – MUDFLOW IN TELAVI (GEORGIA) ON JULY 12, 2026 | 19 |
| 6 | Huseynov H. – BUILDING BACK BETTER AFTER FLOODS: LESSONS FOR THE KURA RIVER BASIN | 23 |
| 7 | Gergokova Z. – UAV TECHNOLOGIES AS AN ADVANCED TOOL FOR GEOECOLOGICAL MONITORING IN HIGH-MOUNTAIN AREAS | 26 |
| 8 | Marrazzo R., Astorri F. – SAFETY EVALUATION OF OFFSHORE CO2 STORAGE IN DEPLETED LEVELS OF HYDROCARBON CULTIVATION FIELDS | 29 |
| 9 | Samkharadze I., Davitashvili T., Pipia M. – THERMODYNAMIC ASSESSMENT OF SOME EXTREME CONVECTION EVENTS IN EASTERN GEORGIA | 34 |
| 10 | Sherkhov A. – CALCULATED ASSESSMENT OF THE PARAMETERS OF VULNERABLE SECTIONS OF THE HYDRAULIC STRUCTURES OF THE TYRNYAUZ TAILINGS STORAGE FACILITY | 39 |
| 11 | Amiranashvili A., Chelidze T., Elizbarashvili I., Kiria T., Tsamalashvili T., Varamashvili N. – STATISTICAL ANALYSIS OF ANNUAL PRECIPITATION SUM WITH DIFFERENT PROVISIONS IN GEORGIA | 42 |
| 12 | Amiranashvili A., Chelidze T., Kiria T., Tsamalashvili T., Varamashvili N. – ESTIMATION OF THE ANNUAL DAMAGE LANDSLIDES NUMBER IN GEORGIA IN RELATION TO AVERAGE ANNUAL EXTREME PRECIPITATION SUMS OF DIFFERENT PROVISION | 48 |
| 13 | Chelidze T., Amiranashvili A., Brocca L., Kiria T., Svanadze D., Tsamalashvili T., Varamashvili N. – MAIN RESEARCH RESULTS OF THE PROJECT “MACHINE LEARNING APPROACH TO THE LANDSLIDE ACTIVATION PREDICTION IN GEORGIA” (2023-2026) | 52 |
| 14 | Amiranashvili A.,Chikhladze V., Pipia M. – UNPRECEDENTED PRECIPITATION IN BATUMI ON SEPTEMBER 19, 2026 | 58 |
| 15 | Amiranashvili A., Chikhladze V., Jamrishvili N., Tavidashvili Kh. – WATERSPOUT IN KOBULETI (GEORGIA) AND PENSACOLA (FLORIDA, USA) ON SEPTEMBER 07, 2026 | 62 |
| 16 | Kereselidze Z., Khvedelidze I., Chkhitunidze M. – ANALYSIS OF THE DESTRUCTIVE EFFECT OF THE KAKHETI HURRICANE BASED ON REAL DATA ON THE DIMENSIONS OF THE ALAVERDI CATHEDRAL | 66 |
| 17 | Bliadze T., Beglarashvili N., Janelidze I., Mepharidze E., Tchankvetadze A. – ANGSTROM FIRE INDEX FOR BOLNISI (GEORGIA) | 70 |
| 18 | Hajiyeva S., Mustafayev I., Aliyeva T., Huseynov E. – INVESTIGATION OF AROMATIC HYDROCARBON POLLUTION IN SOILS NEAR LAKE BOYUKSHOR ABSHERON PENINSULA | 74 |
| 19 | Aliyeva T. – HYDROECOLOGICAL ASSESSMENT OF HYDROCARBON CONTAMINATION IN BOTTOM SEDIMENTS OF LAKE GU, ABSHERON PENINSULA | 77 |
| 20 | Atabieva F., Selina V. – COMPOUNDS OF MANGANESE, COPPER, AND MOLYBDENUM IN THE BOTTOM SEDIMENTS OF THE TEREK RIVER | 80 |
| 21 | Chikviladze E., Ortega L., Watson A., Miller J., Birkel C., Melikadze G., Bong H., Kralisch S. – SENSITIVITY OF AN ISOTOPE-ENABLED WATER BALANCE MODEL TO GLOBAL INPUT DATA IN THE DATA-SCARCE ALAZANI RIVER BASIN, EASTERN GEORGIA | 84 |
| 22 | Dakhova O., Kerefova Z., Khuchunaeva L. – CURRENT STATE OF THE SOIL COVER | 89 |
| 23 | Demetrashvili D., Kukhalashvili V., Kvaratskhelia D. – NUMERICAL MODELING OF WIND WAVES BASED ON THE SPECTRAL MODEL SWAN IN THE GEORGIAN COASTAL ZONE OF THE BLACK SEA | 93 |

| | | |
|---|---|---|
| 24 | Kiria J., Dovgali N., Davitashvili L., Tsaguria T., Sakvarelidze E. – PRECIPITATION EFFECTS ON A BRANCH OF THE INGIRISHI MAIN FAULT AND RELATED HYDROLOGICAL AND GEODYNAMIC PROCESSES | 97 |
| 25 | Jandieri G., Janelidze I., Zivzivadze O. – INTEGRATED GEOPHYSICAL AND MICROBIAL BIOMONITORING OF METALLURGICAL CONTAMINATION IN SOIL AND GROUNDWATER | 101 |
| 26 | Kobzev G., Melikadze G., Jimsheladze T., Chelidze T., Tchankvetadze A., Goguadze N., Kiria T. – WATER REACTION INTO ONI WELL ON EARTHQUAKES IN 2026 | 106 |
| 27 | Kapanadze N., Melikadze G., Tsutskiridze E., Todadze M., Chikviladze E., Tchankvetadze A. – REVISITING THE TBILISI GEOTHERMAL SYSTEM: HYDROCHEMICAL AND STABLE-ISOTOPE EVIDENCE AND THE NEED FOR A MULTI-TRACER APPROACH | 110 |
| 28 | Kiknadze N., Gvarishvili N., Tavdgiridze G., Khakhutaishvili A., Kharazi N. – ASSESSMENT OF WATER QUALITY AND ECOLOGICAL STATUS OF SOME SMALL RIVERS IN THE COASTAL ZONE OF ADJARA | 114 |
| 29 | Shavliashvili L., Kuchava G., Shubladze E., Rikadze Z., Gavardashvili G., Tabatadze M. – RESULTS OF SOIL RESEARCH IN CHIATURA MUNICIPALITY AND MAP OF SOIL MANGANESE CONTAMINATION | 119 |
| 30 | Shavliashvili L., Kuchava G., Shubladze E., Rikadze Z., Gavardashvili G., Mdivani S. – ASSESSMENT OF HEAVY METAL CONTAMINATION RISKS IN THE SOILS OF CHIATURA MUNICIPALITY | 126 |
| 31 | Makalatia I., Darbaidze S., Kandashvili Z., Melia S. – DEVELOPMENT PROSPECTS OF GEORGIA'S BLACK SEA PORTS AND THE STRATEGIC IMPORTANCE OF THE ANAKLIA DEEP-SEA PORT | 131 |
| 32 | Sborshchikovi A., Mepharidze E., Tepnadze D., Laliashvili L., Chikviladze E. – ANALYSIS OF CHANGES IN THE DYNAMIC BEHAVIOR OF THE ENGURI ARCH DAM | 135 |
| 33 | Sborshchikovi A., Mepharidze E., Chelidze T. – TEMPORAL AND DYNAMIC ANALYSIS OF ENGURI DAM MONITORING DATASETS | 141 |
| 34 | Seidishvili N., Chkhartishvili I., Papunidze S, Kiknadze N., Abuladze D., Putkaradze N. – INNOVATIVE PRODUCTION OF FUNCTIONAL CANDIED PRODUCTS FROM LOCAL PLANT RAW MATERIALS AND PROSPECTS FOR RATIONAL RESOURCE UTILIZATION | 146 |
| 35 | Basilashvili Ts., Janelidze M., Basilashvili Kh. – LONG-TERM (1919-2023) AND EXPECTED CHANGES IN THE WATER AVAILABILITY OF GEORGIAN RIVERS | 151 |
| 36 | Boynagryan V., Ayriyants A. – MAP OF QUATERNARY LOOSE DEPOSITS OF THE REPUBLIC OF ARMENIA | 155 |
| 37 | Kharshiladze O., Kezua L., Tsulukidze L., Zilpimiani D. – MAGNETIC FIELD REVERSALS IN MODIFIED BULLARD'S MODEL | 159 |
| 38 | Kharebava N., Nikolaishvili D. – ANCIENT ACCOUNTS OF THE FOREST GREEN COVER OF TBILISI | 164 |
| 39 | Kurasheva O. – HEAVY METAL CONTENT IN THE SEASONAL SNOW COVER AT TERSKOL PEAK (ELBRUS REGION, KABARDINO-BALKARIAN REPUBLIC) | 168 |
| 40 | Salukvadze E. – SHIDA KARTLI ENVIRONMENTAL SITUATION CONDITIONED BY ANTHROPOGENIC FACTORS AND NATURAL EXODYNAMIC PROCESSES | 172 |
| 41 | Samkharadze I., Tatishvili M., Zotikishvili N. – VALIDATION OF ERA5 REANALYSIS AIR TEMPERATURE DATA IN THE KAKHETI REGION BASED ON DATA FROM THE TELAVI UNIVERSITY METEOROLOGICAL STATION | 176 |
| 42 | Sborshchikovi A. – STATISTICAL ESTIMATION OF QUANTILE FUNCTIONS IN THE TEMPORAL STUDY OF SEISMICITY | 181 |
| 43 | Shengelia L., Kordzakhia G., Tvauri G., Dzadzamia M., Shengelia M. – ELIMINATION OF PROBLEMS IDENTIFIED DURING THE COMPLEX STUDY OF GEORGIAN GLACIERS | 185 |
| 44 | Zaalishvili V., Revazov M., Melkov D., Burdzieva O. – GEOECOLOGICAL ZONING OF THE KARMADON GORGE BASED ON A SET OF FACTORS AND EXPERT ASSESSMENTS | 189 |
| 45 | Amiranashvili A., Bolashvili N., Chikhladze V., Japaridze N., Kartvelishvili L., Kereselidze Z., Khazaradze K., Matzarakis A., Megrelidze L., Melikadze G., Revishvili A., Sanikidze E., Tabidze M., Tatishvili M., Tsikarishvili K. – UTILIZATION OF GEORGIA'S NATURAL RESOURCES IN THE COMPREHENSIVE TREATMENT OF DISEASES AND THE DEVELOPMENT OF MEDICAL TOURISM | 193 |

| | | |
|---|---|---|
| 46 | Avalishvili A., Gunia N., Uchaneishvili S., Kalmakhelidze S., Ivanishvili N., Gogebashvili M. – EFFECT OF ENVIRONMENTAL HUMIDITY ON POST-IRRADIATION RECOVERY OF SOIL MICROORGANISMS | 197 |
| 47 | Japaridze N., Kartvelishvili L., Khazaradze K., Chkhitunidze M., Nikolaishvili M., Revishvili A. – DISTRIBUTION THE DAILY NUMBER OF AIR EFFECTIVE TEMPERATURE ACCORDING TO MISSENARD IN BOLNISI BY MONTH | 200 |
| 48 | Burdzenidze M., Tchitchaghua E., Elizbarashvili N. – ANTHROPOGENIC IMPACT ON ECOSYSTEM CONDITIONS: A LANDSCAPE-ECOLOGICAL APPROACH | 204 |
| 49 | Gairabekov U., Gunya A., Makhmudova L. – ANALYSIS OF THE CONDITIONS OF NATURAL-TERRITORIAL COMPLEXES OF KEY SITES OF THE CARBON RANGE OF THE CHECHEN REPUBLIC "WAY CARBON" | 207 |
| 50 | Ismayilova N. – DYNAMICS OF OAK AND BEECH FOREST DEGRADATION ON THE SOUTHERN SLOPES OF THE GREATER CAUCASUS UNDER THE INFLUENCE OF CLIMATIC FACTORS: A CASE STUDY OF THE ISMAYILLI DISTRICT | 210 |
| 51 | Kordzakhia M., Matchavariani V., Vekua Z., Arghvliani I.,Samadashvili N., Kutchava G., Bejanidze V., Pataraia G., Ketchakmadze Z., Sidamonidze E. – INNOVATIVE MONITORING SYSTEM FOR THE BLACK SEA COASTAL ZONE | 214 |
| 52 | Kutaladze N., Mikeladze Z., Gogolishvili T., Bolkvadze Ts., Kilasonia G., Gorgiladze T. – USE OF BIO-FERTILIZERS IN A TANGERINE PLANTATION AGAINST PESTS AND DISEASES | 218 |
| 53 | Gakhokidze R., Beruashvili M., Markarashvili E. – EFFECT OF THE BIOREGULATOR "BIORAG" ON SEED GERMINATION AND EARLY GROWTH OF TOMATO AND BASIL | 222 |
| 54 | Meladze M., Meladze G., Japiashvili N. – ASSESSMENT OF MAIZE CULTIVATION POTENTIAL AND HARVEST FORECAST IN THE AGROCLIMATIC CONDITIONS OF TSALKA-DMANISI | 225 |
| 55 | Osmanova S. – ECOLOGICAL ASSESSMENT OF "GREEN INFRASTRUCTURE" AND THE ANTHROPOGENIC LOAD OF SUSTAINABLE TOURISM IN THE COASTAL ZONES OF THE CASPIAN SEA | 230 |
| 56 | Papunidze G., Chkhartishvili I., Papunidze S., Seidishvili N., Mikeladze Z., Abuladze D. – REDUCING ANTHROPOGENIC IMPACT BY UTILIZING MANDARIN PROCESSING WASTE AS A RESOURCE | 234 |
| 57 | Gabibov F. – EXSPERIMENTAL STUDIES OF THE STRUCTURAL STRENGTH EFFECT ON THE SWELLING OF CLAY SOILS | 237 |
| 58 | Tsereteli G., Aftsiauri B., Tiginashvili Z., Merabishvili M., Kakhadze R. – BIOMASS AND CARBON STOCKS OF ALDER FORESTS IN WESTERN GEORGIA BY TREE FRACTIONS AND GEOPHYSICAL MONITORING PERSPECTIVES WITH AI INTEGRATION | 241 |
| 59 | Uchaneishvili S., Gunia N., Avalishvili A., Kalmakhelidze S., Ivanishvili N., Gogebashvili M. – FROM SOIL VARIABILITY TO FOOD-CHAIN ASSESSMENT: A FRAMEWORK FOR $^{137}$Cs RESEARCH IN GEORGIA | 244 |
| 60 | Burdzieva O. G., Kanukov A. S., Korbesova K. V., Arkhireeva I. G., Dadteeva E. V. – DEVELOPMENT OF AN ATMOSPHERIC AIR POLLUTION MAP FOR VLADIKAVKAZ USING GIS TECHNOLOGIES | 248 |
| 61 | Aliyev V., Amiranashvili A., Davitashvili T., Matchavariani L., Samkharadze I., Zotikishvili N. – COMPARATIVE ANALYSIS OF THE VARIABILITY OF MEAN MAX ANNUAL AND SEMI-ANNUAL AIR TEMPERATURE AND PRECIPITATION SUMS IN TBILISI AND PASANAURI IN 1980 – 2025 | 253 |
| 62 | Amiranashvili A., Bliadze T., Davitashvili M., Kirkitadze D., Zuroshvili L., Sukhitashvili G. – CHANGEABILITY OF ATMOSPHERIC PRECIPITATION IN KAKHETI (GEORGIA) IN 1936-2023 AGAINST THE BACKDROP OF CLIMATE CHANGE | 258 |
| 63 | Amiranashvili A., Bliadze T., Chikhladze V., Kereselidze Z. – 90 YEARS OF SCIENTIFIC RESEARCH IN THE FIELDS OF ATMOSPHERIC PHYSICS AND CLIMATOLOGY AT THE M. NODIA INSTITUTE OF GEOPHYSICS OF I. JAVAKHISHVILI TBILISI STATE UNIVERSITY | 263 |
| 64 | Aliyev V., Amiranashvili A., Kartvelishvili L., Matzarakis A., Tatishvili M, Kapanadze N. – VARIABILITY OF TEMPERATURE AND PRECIPITATION IN TBILISI AND BAKU IN 2005-2024 | 267 |
| 65 | Bolashvili N., Chichinadze T. , Gulashvili Z. , Suknidze N. , Tatishvii M. – SPATIAL PATTERNS OF LONG-TERM CLIMATE CHANGE: A GIS-BASED AND GEOSTATISTICAL ANALYSIS | 271 |
| 66 | Budaev A. – LABORATORY STUDIES OF ICE-FORMING PROPERTIES OF PYROTECHNIC COMPOSITION BASED ON SILVER IODIDE AND ZINC | 274 |

| | | |
|---|---|---|
| 67 | Elbakidze Kh. – EXPERIMENTAL DATA ANALYSIS OF SHORTWAVE-INFRARED RADIANCE USING MACHINE LEARNING METHODS | 278 |
| 68 | Elizbarashvili M., Elizbarashvili E., Chikhradze N. – CLIMATE AND METEOROLOGICAL HAZARDS OF THE KINTRISHI RIVER BASIN | 283 |
| 69 | Tavartkiladze K., Karalashvili T. – CHANGES IN PRECIPITATION AMOUNT AND INTENSITY IN GEORGIA UNDER GLOBAL WARMING | 288 |
| 70 | Gekkieva S. – REVIEW OF ICE-FORMING REAGENTS FOR PRECIPITATION MANAGEMENT FROM CONVECTIVE CLOUDS | 294 |
| 71 | Gekkieva S., Budaev A. – LABORATORY MODELING OF THE EFFECT OF CLOUD ELECTRICAL CHARACTERISTICS ON WATER VAPOR CRYSTALLIZATION PROCESSES ON ZINC OXIDE PARTICLES | 298 |
| 72 | Surmava A., Kukhalashvili V., Gigauri N., Intskirveli L., Dumbadze G. – PM10 SPATIAL DISTRIBUTION IN THE ATMOSPHERE OF BATUMI CITY IN SUMMER DURING BACKGROUND LIGHT AIR | 302 |
| 73 | Kagermazov A. – APPLICATION OF THE MOS CONCEPT FOR STATISTICAL FORECASTING OF SEVERE CONVECTIVE HAZARDS AND FLASH FLOODS IN THE SOUTHERN REGION OF RUSSIA | 306 |
| 74 | Kazakova S. – SEASONAL VARIATIONS IN THE DIURNAL COURSE OF THE EARTH'S ATMOSPHERIC ELECTRIC FIELD STRENGTH | 309 |
| 75 | Kerefova Z., Dakhova O. – APPLICATION OF MODERN TECHNOLOGIES FOR STUDYING THUNDERSTORM ACTIVITY | 312 |
| 76 | Kerefova Z., Adzhiev A. – SPATIOTEMPORAL DYNAMICS OF CLOUD LIGHTNING DISCHARGES | 317 |
| 77 | Khomasuridze G., Lagidze L. – THE IMPACT OF CLIMATE CHANGE ON THE DYNAMICS OF CLOUDINESS IN TBILISI | 321 |
| 78 | Matiashvili S. – PROSPECTS FOR THE USE OF SUNFLOWER (HELIANTHUS ANNUUS L.) IN THE PHYTOREMEDIATION OF MINING-IMPACTED SOILS IN GEORGIA: A REVIEW AND PRACTICAL RECOMMENDATIONS | 325 |
| 79 | Sozaeva L., Kagermazov A. – APPROBATION OF AN AUTOMATED METHOD FOR HAIL FORECASTING BASED ON THE OUTPUT PRODUCT OF THE GFS NCEP MODEL | 329 |
| 80 | Sozaeva L. – MODELING OF C-BAND RADAR BACKSCATTERING CHARACTERISTICS BY DEFORMABLE DROPLETS IN STRONG ELECTRIC FIELDS | 332 |
| 81 | Tatishvili M., Kapanadze N., Megrelidze L., Palavandishvili A., Mkurnalidze I. – WIND FIELD VARIABILITY FOR SELECTED LOCATIONS OF GEORGIA | 335 |
| 82 | Zhaboeva M. – INFORMATIVENESS OF CONVECTIVE CLOUD AND ATMOSPHERIC PARAMETERS IN HAIL FORECASTING BASED ON OPTIMIZED ENSEMBLES OF THE GFS NCEP MODEL | 339 |
| 83 | Kiria T., Nikolaishvili M., Chkhaidze T. – MULTI-YEAR TEMPORAL AND SPECTRAL ANALYSIS OF GEOMAGNETIC VARIATIONS AT DUSHETI OBSERVATORY | 342 |
| 84 | Odilavadze D., Chelidze T., Yavolovskaya O. – THREE-DIMENSIONAL REPRESENTATION OF THE GEORADIOLOCATION STUDY OF THE INTERNAL SPACE OF THE GEORGIAN CATHEDRAL SVETITSKHOVELI AND THE NEARBY TERRITORY | 348 |
| 85 | Kharshiladze O., Tsulukidze L., Sorriso-Valvo L., Kezua L., Elbakidze K., Zilpimiani D. – LOW-ORDER MODELS OF THE GEODYNAMO | 352 |
| 86 | Tatishvili M., Elbakidze-Chargazia Kh, Palavandishvili A., Khutsishvili E., Chelidze N. – TEMPERATURE VARIABILITY AND GEO-STORMS | 356 |
| 87 | Kharshiladze O., Aslamazishvili M. – SOLAR ACTIVITY AND COSMIC RAYS: FROM THE MAY 2024 STORM TO CENTURIES OF SOLAR CYCLES | 360 |
| 88 | Kharshiladze O., Martiashvili M., Sorriso-Valvo L., Zilpimiani D., Mchedlishvili G. – INTERMITTENCY IN THE GEOSPACE DURING THE 2024 MOTHER'S DAY STORM | 364 |
| 89 | Vanishvili G., Alania E., Bakradze T., Ghlonti N., Kiria J., Erkomaishvili T., Kavlashvili V., Takadze G., Demurishvili Z., Barbakadze P., Peikrishvili M.,Tinikashvili A., Aslamazishvili M. – STUDY OF THE FORBUSH EFFECT OF COSMIC RAYS ON JANUARY 18-27, 2026 | 369 |
| 90 | Vanishvili G., Alania E., Amiranashvili A., Bakradze T., Ghlonti N., Kiria J., Erkomaishvili T., Kavlashvili V., Takadze G., Demurishvili Z., Barbakadze P., Peikrishvili M.,Tinikashvili A., Aslamazishvili M. – CORRELATION BETWEEN DAILY SUNSPOT NUMBERS, COSMIC RAYS, AND MORTALITY DURING JUNE 23-30 FORBUSH DECREASE | 373 |

**IVANE JAVAKHISHVILI TBILISI STATE UNIVERSITY**
**Mikheil Nodia Institute of Geophysics**
**Georgian Geophysical Association**

**TECHNICAL UNIVERSITY OF GEORGIA**
**Institute of Hydrometeorology**

# 2nd INTERNATIONAL SCIENTIFIC CONFERENCE "Modern Problems in Geophysics"

## Tbilisi, Georgia, October 29-31, 2026

## PROCEEDINGS

Circulation 70 copy.

ISBN 978-9941-36-562-1
ISSN 3088-4349ISSN

E-mail: geophysics@tsu.ge
http://dspace.gela.org.ge/handle/123456789/254

2026 – Tbilisi

Typesetter Lali Kurdghelashvili
Cover Designer Mariam Ebralidze

1, Ilia Tchavtchavadze Ave., Tbilisi 0128
Tel 995(32) 225 04 84, 6284/6279
https://www.tsu.ge/ka/publishing-house